DISSERTATION

IMPLEMENTING A TREATED WASTEWATER RECHARGE TECHNIQUE AND REVERSE OSMOSIS UNIT SYSTEM FOR WATER SUSTAINABILITY

Submitted by

EMAD HUSSAIN ALALI

Civil Engineering Department

In partial fulfillment of the requirements

for the Degree of Doctor of Philosophy

Colorado State University

Fort Collins, Colorado

Spring 2004

COLORADO STATE UNIVERSITY

December 04, 2003

WE HEREBY RECOMMEND THAT THE DISSERTATION PREPARED UNDER OUR SUPERVISION BY EMAD HUSSAIN ALALI ENTITELED IMPLEMENTING A TREATED WASTEWATER RECHARGE TECHNIQUE AND REVERSE OSMOSIS UNIT SYSTEM FOR WATER SUSTAINBILITY BE ACCEPTED AS FULFILLING IN PART REQUIREMRNTS FOR THE DEGREE OF DOCTOR OF PHILOSOPHY.

Committee on Graduate Work

Ramchand Oad

Freeman M. Smith

R. Narvaez

Jan W. Warner

Adviser

Sandra Woods

Department Head/Director

ABSTRACT OF DISSERTATION

IMPLEMENTING A TREATED WASTEWATER RECHARGE TECHNIQUE AND REVERSE OSMOSIS UNIT SYSTEM FOR WATER SUSTAINABILITY

The aim of this dissertation was to design a conceptual system to provide a sustainable water source at a feasible cost. The conceptual design system was developed to address the problem of water scarcity and sustainability in general, and specifically to represent the Kuwaiti water quality and quantity limitation problem. The conceptual design system consists primarily of utilizing brackish groundwater in conjunction with treated wastewater augmentation and a reverse osmosis unit. The dissertation considered two types of simulation models for the conceptual design system approach. These models are the lump model approach and the areal distribution model approach. The lump model approach was carried out through the construction of a simplified model approach utilizing the Visual Basic model. On the other hand, the areal distribution model approach was carried out through the utilization of the Visual MODFLOW and MT3D simulation model approach.

To test the sensitivity and the durability of the conceptual design system, the lump model simulation approach was simulated for different ranges of hydrologic, hydrogeologic, and climatic parameters to determine the total power and treated wastewater consumption. Moreover, to valuate the robustness of the general conceptual design system by performing different operational scenarios, four perturbed scenarios of the general conceptual design system utilizing the lump model approach were performed and compared with the base case simulation of the general conceptual design system utilizing a lump model approach. The base case simulation was chosen to represent the quasi-Kuwaiti environment data. In addition, the areal distribution model simulation approach of the general conceptual model design was simulated for three orientation layouts and compared to the lump model simulation approach of the general conceptual design system to determine the total cost of operating the system.

The economical feasibility of the base case of the general conception design system was analyzed for the lump model simulation approach and for the three orientation layouts of the areal distribution model approach. The economical analysis was based on the calculations of the net present worth value of the cash flows for the capital cost, the operation and maintenance costs, and the revenues of the crop yields for the 40 years of operation. The benefit-cost ratios for the base case of the general conceptual design system using the lump model approach and the areal distribution model for the three orientation layouts were calculated for ranges of different interest rates. The benefit-cost ratios were feasible for the Middle East condition in general and to the GCC countries in particular, especially at low interest rates.

Emad Hussain AlAli
Civil Engineering Department
Colorado State University
Fort Collins, CO 80523
Spring 2004

ACKNOWLEDGEMENTS

I would like to express special thanks to my committee chairman, Dr. James W. Warner, who has gone beyond the duties of his advisory role to give me a great deal of encouragement and support. Thanks to my committee members, Dr. Freeman Smith, Dr. Ramchand Oad and Dr. Reza Namvargolian, for their ideas and contributions. I also would like to extend my thanks to my editor Ms. Nancy Berry for her help and time. Finally, special thanks and gratitude to my father Hussain and mother Makyya for their prayers, support and encouragement, to my lovely wife Mashael for her love and understanding, to my sons and daughter Mohammed, Ali, and Fatimah, respectively, for their inspiration and understanding, and to my brothers and sisters for their support.

Emad H. AlAli

DEDICATION

To almighty God (Allah) and to his miracle, the prophet Mohammed Ibn Abdullah (P.B.U.H.). To the caliph and successor of the prophet Mohammed, Emam Ali Ibn Aby Talib (P.B.U.H.). To the prophet Mohammed's chaste and virtuous daughter, Fatimah Bint Mohammed (P.B.U.H.). To Fatimah's sons, the caliphs and successors Emam Hassan and Emam Hussain (P.B.U.T.). To the nine caliphs and successors after Emam Hussain, Emam Ali Ibn Al-Hussain (P.B.U.T.), Emam Mohammed Ibn Ali (P.B.U.T.), Emam Jafar Ibn Mohammed (P.B.U.T.), Emam Mousa Ibn Jafar (P.B.U.T.), Emam Ali Ibn Mousa (P.B.U.T.), Emam Mohammed Ibn Ali (P.B.U.T.), Emam Ali Ibn Mohammed (P.B.U.T.), Emam Al Hassan Ibn Ali (P.B.U.T.), Emam Mohammed Ibn Al Hassan, the guider, (P.B.U.T.), and finally, Abo-Elfathl Al-Abbas and his mother Um-Al baneen (P.B.U.T).

TABLE Of CONTENTS

Chapter **Page**

Chapter **Page**

LIST OF TABLES

Table		Page

LIST OF FIGURES

Figure		Page

Figure		Page

Figure		Page
4.27	Sum of total power required by the system for 40-year of simulations for ranges of different porosity, $\boldsymbol{\Phi}$, values..................	157
4.28	Sum of treated wastewater injected into the native groundwater for 40-year of simulations for ranges of different porosity, $\boldsymbol{\Phi}$, values..	157
4.29	Total power required by the system for ranges of different hydraulic conductivity, ***K***, input values vs. simulation period............	160
4.30	Power required by the reverse osmosis unit for ranges of different hydraulic conductivity, ***K***, input values vs. simulation period...........	161
4.31	Total power required by the well pump system for ranges of different hydraulic conductivity, ***K***, input values vs. simulation period..........	161
4.32	Amount of treated wastewater injected into the native groundwater for ranges of different hydraulic conductivity, ***K***, input values vs. simulation period...	162
4.33	Initial groundwater salt concentrations for ranges of different hydraulic conductivity, ***K***, input values vs. simulation period..........	162
4.34	Hydraulic conductivity vs. irrigated farm area...........................	164
4.35	Sum of total power required by the system for 40-year of simulations for ranges of different hydraulic conductivity, ***K***, values..	165
4.36	Sum of treated wastewater injected into the native groundwater for 40-year of simulations for ranges of different hydraulic conductivity, ***K***, values..	165
4.37	Total power required by the system for ranges of different initial water table hydraulic head elevations, $\boldsymbol{h_o}$, input values vs. simulation period...	167
4.38	Power required by the reverse osmosis unit for ranges of different initial water table hydraulic head elevations, $\boldsymbol{h_o}$, input values vs. simulation period...	168
4.39	Power required by the well pump system for ranges of different initial water table hydraulic head elevations, $\boldsymbol{h_o}$, input values vs. simulation period...	168

Figure		Page
5.13	Sum of total power consumption comparison for 40-year of simulations between the off planting season scenario and the base case of the general conceptual design system simulation………	203
5.14	Sum of treated wastewater quantity injected comparison, over 40-year, between the off planting season scenario and the base case of the general conceptual design system simulation……	204
5.15	Obstacle scenario (1) salt mass balance and water balance of the groundwater system………………………………………..	208
5.16	Obstacle scenarios (1) of the general conceptual design system governing equations………………………………	211
5.17	Total power consumption comparison between the obstacle scenario (1) and the base case of the general conceptual design system simulation…………………………………………..	212
5.18	Reverse osmosis power consumption comparison between the obstacle scenario (1) and the base case of the general conceptual design system simulation………………………………	212
5.19	Well pump power consumption comparison between the obstacle scenario (1) and the base case of the general conceptual design system simulation………………………………	213
5.20	Initial groundwater salt concentration comparison between the obstacle scenario (1) and the base case of the general conceptual design system simulation………………………………	213
5.21	Sum of total power consumption comparison for 40-year of simulations between the obstacle scenario (1) and the base case of the general conceptual design system simulation……….	216
5.22	Obstacle scenario (2) salt mass balance and water balance of the groundwater system………………………………………………..	219
5.23	Obstacle scenario (2) of the general conceptual design system governing equations…………………………..…...	222
5.24	Total power (equals to pump well power only) consumed by obstacle scenario (2) simulation……………………………………..	224
5.25	Treated wastewater consumed by obstacle scenario (2) simulation…	225

Figure		Page

Figure | **Page**

Figure		Page

Figure		Page

Figure		Page

Figure		**Page**

LIST OF SYMBOLS

$Q_{irr(permeate)}$	Irrigation (permeate) water requirement for the period be considered [L^3/T].
Q_{ET_c}	Total water used by actual crop evapotranspiration [L^3/T].
$Q_{Precipitation}$	Effective rainfall (≥ 0.0254 cm) [L^3/T].
Q_{DP}	Water loss out of the root zone by deep percolation [L^3/T].
Q_{CR}	Upward capillary rise from the groundwater table [L^3/T].
Q_{Runoff}	Water runoff from the soil surface [L^3/T].
$Q_{irr(permeate)}$	Portion of the feed water that passes through the reverse osmosis membrane and is collected for irrigation use [L^3/T].
Q_{Feed}	Total water entering the reverse osmosis unit (pumped well water fed to reverse osmosis unit), (Thus, $Q_{pump} = Q_{Feed}$) [L^3/T]
Q_{Brine}	Portion of the feed water that does not pass through the reverse osmosis membrane, which exists as a separate stream containing concentrated impurities and is usually discharged to a drain [L^3/T].
Q_{inj}	Total treated wastewater injection to the native groundwater zone [L^3 / T].
Q_{waste}	Amount of treated wastewater fed to the reverse osmosis unit directly [L^3 / T].
$Q_{irr(permeate)(max)}$	Maximum irrigation (permeate) water capacity rate [m^3/day].
$Q_{pump\ (max)}$	Maximum allowable pumping capacity of the groundwater [m^3/season].
$Q_{Feed\ (max)}$	Maximum allowable pumping capacity rate ($Q_{pump\ (max)} = Q_{Feed\ (max)}$) for maximum allowable drawdown [m^3/day].
$Q_{g.w.(Brine)}$	Inward groundwater flow movement from the adjacent immediate vicinity of the groundwater under consideration.
Q	flow rate of water through the porous media [L^3/T].
q	Darcy's velocity [L/T].
q_s	The volumetric flow rate per unit volume of aquifer representing fluid sources (positive) and sinks (negative) [1/T].
W	Volumetric flux per unit volume and represents source/or sinks of water [1/T]. Where Q_{inj}, Q_{DP} are source terms, and Q_{Feed} is a sink term,
ET_o	Reference evapotranspiration [mm/day].

$ET_{c(max)}$	Maximum actual crop evapotranspiration amount per day during the farming season [m/day].
$M_{irr(permeate)}$	Salt mass flow of the irrigation (permeate) water [(m^3* mg)/ (l*season)].
M_{ET_c}	Salt mass flow of the evapotranspiration water [(m^3* mg)/ (l*season)].
M_{DP}	Salt mass flow of the deep percolation water [(m^3* mg)/ (l*season)].
M_{Feed}	Salt mass flow of the groundwater pump which will be fed to the reverse osmosis unit ($M_{pump} = M_{Feed}$) [(m^3* mg)/ (l*season)].
M_{inj}	Salt mass of the injected treated wastewater [M/ T].
M_{Brine}	Salt mass flow of the brine (rejected) water [(m^3* mg)/ (l*season)].
$C_{irr(permeat)}$	Irrigation (permeate) water salt concentration [mg/l].
C_{ET_c}	Evapotranspiration water salt concentration [mg/l].
C_{RZ}	Root zone salt concentration tolerance [mg/l].
C_{Feed}	Feed water to reverse osmosis salt concentration (**note**: because the pumped groundwater is fed to the reverse osmosis unit ,therefore, $C_{Feed} = C_{pump}$) [mg/l].
C_{inj}	Injected treated wastewater salt concentration [mg/l].
C_{Brine}	Reverse osmosis brine salt concentration (rejected salt concentration from the reverse osmosis unit) [mg/l].
C_{waste}	Treated wastewater that fed to the reverse osmosis salt concentration [mg/l].
$C_{g.w.}$	Groundwater salt concentration [mg/l].
$C_{g.w.(Brine)}$	The salt concentration of an inward groundwater flow movement from the adjacent immediate vicinity of the groundwater under consideration.
Cs	The ionic salt concentration within the reverse osmosis unit.
Cs_{Feed}	Ionic molar concentration of the feed water to the reverse osmosis unit [mole / liter].
$Cs_{irr\ (permeate)}$	Ionic molar salt concentration of the reverse osmosis permeate water [mole / liter].
C^k	The dissolved concentration of species k, [M/L].
D_{ij}	The hydrodynamic dispersion coefficient tensor, [L^2/ T], which is the sum of the mechanical mixing dispersion and the molecular diffusion ($D = \alpha\, v^* + D^*$).
D^*	The molecular diffusion.
α	The dynamic dispersivity.
Recovery % (δ)	Ratio of the permeate (product) water volume to the total feed water volume.
n	The salt concentration percentage in the permeating water through the reverse osmosis membrane.

V_o	The saltwater volume within the reverse osmosis unit.
V	The volume of permeate (desalinated) water [L^3].
ΔV	Small volume of permeate water flows through the reverse osmosis membrane.
$V_{g.w.}$	Groundwater volume [L^3].
R	Gas constant (= 0.082 (liter bar / ^oK mole)).
T	Absolute temperature in Kelvin of the water, (^oC + 273.15), [^oK].
Ps	Osmotic pressure within the reverse osmosis unit [bar].
Ps_{Feed}	The osmotic pressure of the feed water [bar].
$Ps_{(permeate)}$	The osmotic pressure of the permeate water [bar].
ϖ	Molecular weight of salt per mole of water [gm/mole].
TDS	Total dissolved salt [mg/liter].
Ψ	Number of ions per salt molecules of dissolved salt.
$Power_{(R.O.)}$	Power consumed by reverse osmosis unit pump [Kjoules / season].
$Power_{well}$	Power consumed by the groundwater pump [Kjoules / season].
Total Power	Sum of the power consumed by the reverse osmosis unit pump plus the power consumed by the groundwater pump [Kjoules / season].
$\eta_{R..O.}$	Reverse osmosis electrical pump efficiency, for electrical pump, ($\eta_{R.O}$ = 85 – 92 %), [percentage].
$\eta_{(well)}$	Groundwater electrical well pump efficiency, for electrical pump $\eta_{(well)}$ = 50 – 80 %.
$\dfrac{\Delta m_{g.w.}}{\Delta t}$	Time rate change of mass in the groundwater zone [M /T].
$\dfrac{\Delta V_{g.w.}}{\Delta t}$	Time rate change of the water volume in the groundwater zone [M^3/T].
Δt	Simulation time [season].
t	Present time cycle.
$t-1$	Initial or previous time cycle.
x	Time rate change.
x_i	The distance along the respective Cartesian coordinate axis [L].
γ	Specific weight of water ($\gamma = \rho * g$) [kg / m^2 sec.].
γ'	Psychrometric constant [KPa /°C].
H_{lift}	The height of water to be lifted to the ground surface [L].
h	Water table height from the aquifer bed [L].
$h_{surface}$	The height of ground surface from the bedrock [L].
h_o	Water table hydraulic head prior to pumping or water table hydraulic head at zero drawdown [L].
$h_{o\,(max)}$	Maximum allowable water table height.
h_w	Hydraulic water head at the well [L].
$h_{w\,(min)}$	Minimum allowable hydraulic water head at the pumping well (minimum saturated thickness) for maximum allowable drawdown [L].

$\boldsymbol{\Phi}$	Porosity [m^3/m^3].
$\boldsymbol{\theta}$	The porosity of the subsurface medium, [dimensionless], which is the ratio of volume of voids to the bulk volume of the porous material.
$\boldsymbol{S_w}$	Steady state drawdown of water hydraulic head at the well [L].
$\boldsymbol{S'_w}$	The transit drawdown of water hydraulic head at the well [L].
$\boldsymbol{S_s}$	Specific storage of the porous material [1/L], which is the volume of water released per unit volume of aquifer per unit change in head due to the compressibility of the water and the compressibility of the aquifer.
$\boldsymbol{S_y}$	Specific yield [dimensionless], which is the volume of water drained from a unit volume of aquifer due to the force of gravity, applied to unconfined aquifer only, typical range $0.10 \leq \boldsymbol{S_y} \leq 0.3$. Moreover, specific yield ≈ effective porosity, where, effective porosity is the part of the porosity (void space) through which the mobile fluid (groundwater) flows.
$\boldsymbol{A}$	Cross section area, perpendicular to the flow [L^2].
$\boldsymbol{A_F}$	Estimated field area [m^2].
$\boldsymbol{K}$	Hydraulic conductivity of the aquifer [L/T].
$\boldsymbol{K_{xx}}$, $\boldsymbol{K_{yy}}$, and $\boldsymbol{K_{zz}}$	Values of hydraulic conductivity along x, y, z coordinate axes, which are assumed to be parallel to the major axes of the hydraulic conductivity [L/T].
$\boldsymbol{T}$	transmissivity [L^2/T], which is the product of hydraulic conductivity (K) and the saturated thickness (B), or (h), where, (B) for the confined aquifer and (h) for the unconfined aquifer.
$\boldsymbol{K_c}$	Crop coefficient [dimensionless].
$\boldsymbol{K_{cb}}$	Basal crop coefficient [dimensionless], which represents the transpiration component of the crop evapotranspiration.
$\boldsymbol{K_e}$	Soil evaporation coefficient [dimensionless], which represents the soil evaporation component of the crop evapotranspiration.
$\boldsymbol{\frac{dh}{dr}}$	Hydraulic gradient [dimensionless].
$\boldsymbol{2\pi rh}$	Surface area [L^2].
$\boldsymbol{r}$	Radius [L].
$\boldsymbol{r_o}$	Intercept of distance drawdown line with zero drawdown axis [L].
$\boldsymbol{r_w}$	Pumping well radius [L].
$\boldsymbol{R_n}$	Net radiation at the crop surface [MJ/ (m^2- day)].
$\boldsymbol{G}$	Soil heat flux density [MJ/ (m^2- day)].
$\boldsymbol{T}$	Mean air temperature at 2 m height [°C].
$\boldsymbol{u_2}$	Wind speed at 2 m height [m /s].
$\boldsymbol{e_s}$	Saturation vapor pressure [KPa].
$\boldsymbol{e_a}$	Actual vapor pressure [KPa].
$\boldsymbol{e_s - e_a}$	Saturation vapor pressure deficit [KPa].
$\boldsymbol{\Delta}$	Slope vapor pressure curve [KPa /°C].
$\boldsymbol{v^*}$	The average linier groundwater velocity.

v_i	The seepage or linear pore water velocity; [L/T], it is related to the specific discharge or Darcy flux through the relationship, $v_i = q_i / \theta$.
$\sum R_n$	The chemical reaction term, [M/ (L^3T)].
GPD	Gallons per day.
NPWCV	Net present worth cost value of the system,
NPWRV	Net present worth revenue value.
N	Number of years.
i	Interest rate per period (%).

CHAPTER 1

INTRODUCTION

1.1 General Water Problems

Water scarcity is the predominant issue in the arid and semi arid countries. In particular, most Middle East countries and the Gulf Cooperation Council (GCC) countries (Kuwait, Saudi Arabia, Bahrain, Qatar, United Arab Emirates, and Oman), in particular, are characterized by extremely arid climate and limited surface water supplies. The major water resource for these countries is groundwater (91%) and desalination of seawater (7.2%). The lack of freshwater resources in these regions constitutes a major deterrent to their sustainable development.

Growing population, rising standards of living and expanding opportunities have exerted increasing demands for varied needs for water. The Middle East, as an example, has seen rapid economic development caused by sudden increases in oil revenues. This, in turn, has led to a significant increase in the standard of living of the population, resulting in population growth rates that are among the highest in the world. In GCC countries, the total annual water demand increased from 6 Billion cubic meters (Bm^3) in 1980 to 26 Bm^3 in 1995, and may reach 49 Bm^3 in 2025 (Al-Alawi and Abdulrazzak, 1994).

Food self-sufficiency has been the major political goal for the GCC countries and they have traded oil wealth for food. Hence, the agricultural sector has become the main water consumer (85%). However, water demand in various other sectors has been increasing at an alarming rate. Therefore, measures to control demand have become increasingly important to water-resource planners and decision makers in balancing the needs of agricultural development against the depletion of groundwater resources, and in developing strategic parameters for self-sufficiency in food.

The GCC countries depend primarily on groundwater to meet their agricultural water requirements. In Saudi Arabia, for example, mining groundwater used mainly for growing wheat, with a total yield of 741,000 tons per year. The unit water requirement is calculated to be 10.8 m^3 per kilogram of wheat (Akkad, 1990).

Groundwater is divided into two parts in the GCC countries. The first part is the shallow aquifers, developed in the alluvial deposits along the main wadi channels and the flood plains of drainage basins. Shallow aquifers are the most vital water resources in the GCC countries, with an approximate annual recharge of 3.5 Bm^3. A total combined groundwater reserve for the Arabian Peninsula in the shallow aquifers is estimated at 131 Bm^3 (Al-Alawi and Abdulrazzak, 1994). In addition, groundwater occurs in the deep sedimentary aquifers. Deep groundwater reserves are estimated at about 2,175 Bm^3, with the major part (1,919 Bm^3) located in Saudi Arabia. Annual recharge to deep aquifers is estimated at 2.7 Bm^3/year, with most of the water from these deep aquifers used for agricultural purposes.

At present, annual groundwater abstraction in GCC countries is about 21 (Bm^3), with annual groundwater recharge of about 6.2 (Bm^3), resulting in a groundwater overdraft of about 15 (Bm^3/yr) (Table 1.1). Al- Turback and Al-Dhowalia (1996) estimated that as of 1995, about 35% of the groundwater resources in Saudi Arabia have been depleted. Mining of groundwater has resulted in a continuous and sharp decline in groundwater levels, and furthermore, severe water quality deterioration due to seawater and surrounding brine water intrusion.

Table 1.1 Groundwater recharge and storage balance in the GCC countries (Al-Alawi and Abdulrazzak, 1994).

Shallow Aquifers	**Recharge**	**Storage**	**Pumped**	**Remarks**
	3.5 Bm^3/yr	131 Bm^3/yr		
Deep Aquifers	**Recharge**	**Storage**		
	2.7 Bm^3/yr	2,175 Bm^3/yr		
Combined Aquifers	Recharge	Storage		
	6.2 Bm^3/yr	2,306 Bm^3/yr	21 Bm^3/yr	Groundwater over draft by 15.2 Bm^3/yr

Currently GCC countries are suffering from an enormous deficit in water resources reaching about 15 Bm^3 annually. This deficit is met mainly by the over drafting of the groundwater resources. Unless trends reverse, the GCC countries are headed for a future major water crisis.

The increasing population and higher standard of living in most of the GCC countries have resulted in increasing water demands for industrial, urban and agricultural needs. Typically, increased desalinization of seawater has met growing urban demands. Because seawater desalination is very costly for agricultural water demand utilization, at

US$ 2-3 per m^3 of water, mining of groundwater has been used to meet increasing agricultural demands.

Much of the groundwater in the Middle East is of marginal and brackish quality. The excessive use of groundwater in arid regions, especially if groundwater is the only water source, results in the decline of groundwater levels and / or the deterioration of groundwater quality. Another result of mining groundwater will be the abandonment of agricultural lands due to either insufficient groundwater remaining or poor quality groundwater. In other words, the groundwater will become unsuitable for irrigation. Due to groundwater mining, irrigated agriculture faces the challenge of using less water or, in many cases, using poor quality water to provide food for the expanding population.

1.2 General Water Shortages and Recycled Water

Water shortages have already become commonplace in many parts of the world, including those that are not arid or semi-arid. In many areas of the world, water shortages have caused planners to look upon recycled water as an important water resource rather than as only a means of wastewater disposal. As population and wastewater flows increase, effluent is being increasingly considered for use in agricultural and urban irrigation. In general, treated wastewater is the most unused water source in the world and in the GCC countries, specifically. Therefore, wastewater treatment in the GCC countries constitutes an increasing water source. Now, almost all of the GCC countries are using modern treatment facilities with tertiary and advance treatment facilities.

In the GCC countries, total treated wastewater in 1995 was about 0.9 Bm^3/year. Reused treated wastewater is approximately 0.4 Bm^3/year, i.e., about 45% of the total was treated and the remaining 55% was dumped back to the sea. Consequently, this treated wastewater is a vital source of water that can be used directly in surface irrigation or indirectly by aquifer recharge. The latter will endorse the benefit of groundwater augmentation and public acceptance. Additionally, some GCC countries offer cheap treated wastewater delivered to farmers for $US 0.007/$m^3$ (FAO 1997).

1.3 Illustration Case Problem

In Kuwait, one of the GCC countries, natural resources of fresh water are very limited. Kuwait is situated in an arid coastal region characterized by high temperatures, low humidity, sparse precipitation rates, and high evaporation and evapotranspiration rates with no rivers or lakes. Therefore, Kuwait has always relied on other sources to secure freshwater to meet its growing demands. The water supply in Kuwait can be obtained from three main sources: brackish groundwater, water reuse (treated wastewater), and seawater desalination.

There are three classes of groundwater in Kuwait: fresh water with salinity below 1000 ppm, which is used for drinking and domestic purposes, slightly saline water with salinity ranging between 1000 and 10000 ppm, which is used for irrigation, and highly saline water with salinity exceeding 10 000 ppm. In general, groundwater quality and quantity are deteriorating due to the continuous mining of groundwater. On the Al-Wafra farms, in the south, 50% of the wells pumped water with a salinity level higher than 7,500 ppm in 1989. This figure is expected to reach 75-80% and 85-90% in the years 1997 and 2003 respectively. On the Al-Abdally farms, in the north, 55% of the deep drilled wells pumped water with a salinity level higher than 7,500 ppm in 1989. This is expected to reach 75% and 90% after 5 and 10 years of operation respectively.

Brackish groundwater exists in reasonable quantities. During 1999, the daily production of brackish groundwater was around 400 million imperial gallons per day (MIGD), which is almost 3 times the annual groundwater inflow (MEW, 2000). Thus, the production of brackish groundwater is exhausting the one and only vital natural water source. What is more, there are no water charges or limits on groundwater use by farmers. Additionally, brackish groundwater mining will have severe and serious consequences on the quality and quantity of scatters lenses of brackish water in the future due to saltwater intrusion of more saline (brine) surrounding water.

In Kuwait, treated wastewater is an almost unused water source. Urban wastewater is collected, treated and returned to the sea; limited quantities are utilized for landscaping purposes. In Kuwait, wastewater effluent is treated to a secondary or tertiary level. The relatively low salinity of the treated wastewater (1000 mg/l) compared with brackish water of 4000-10000 mg/l makes it a potentially excellent source of good quality water. Moreover, over 100 million imperial gallons per day (MIGD) of treated wastewater production in Kuwait will have a great potential to supplement/ replace the brackish water supplies.

Food self-sufficiency has been the major political goal for Kuwait. Water is the main limiting factor for the expansion of agriculture in Kuwait. Therefore, agricultural production in Kuwait is facing great challenges due to the lack of sustainable quantity and quality of water, and soil deterioration by increasing salinity. Hence, achieving continuous agricultural lands productivity potential requires sustainable good irrigation water quality and adequate drainage.

1.4 Objective

The objective of this dissertation is to evaluate the feasibility of a conceptual design system utilizing brackish groundwater in conjunction with treated wastewater augmentation and a reverse osmosis unit to achieve water sustainability. To fulfill this objective, two main approach models will be utilized (lump and areal distribution model) and compared for the most economic feasibility. This objective will result in achieving a sustainable water strategy (quantity and quality) and the relief and restoration of the aquifer after years of human over mining and uneconomical practices of brackish groundwater utilization for irrigation purposes (Figures 1.1, and 1.2).

In order to meet this dissertation objective, the approach was to:

- Construct a simplified lump model for the general conception design system, which will calculate the overall steady state groundwater heads, the salt concentrations, the amount of groundwater pumped, the treated wastewater injected, the deep percolation water, and the total operation power requirements, within the unconfined saturated aquifer.

Figure 1.1 Conceptual design system of implementing a treated wastewater recharge technique and R.O. unit system for water sustainability.

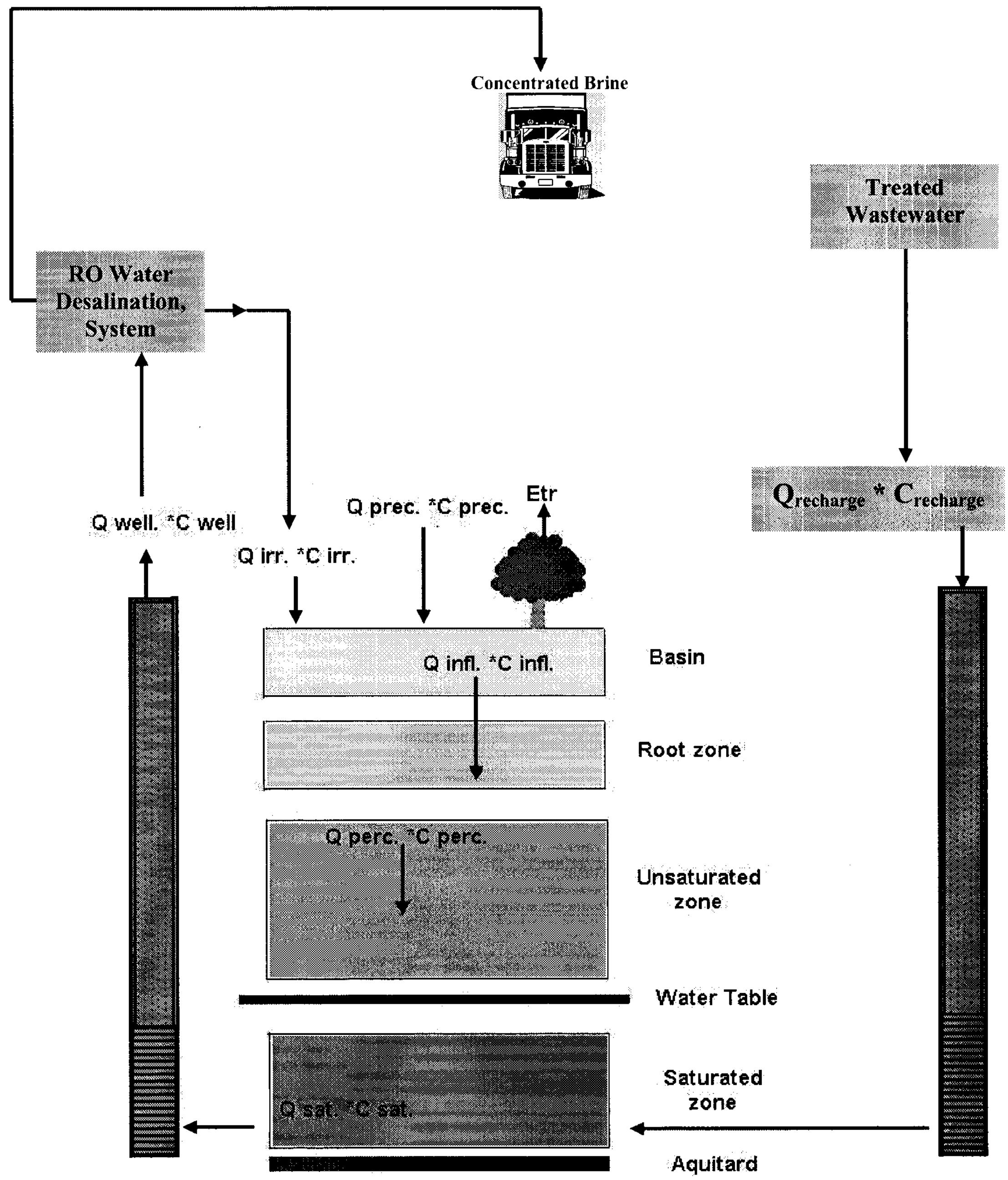

Figure 1.2 Detailed conceptual design system of implementing a treated wastewater recharge technique and R.O. unit system for water sustainability.

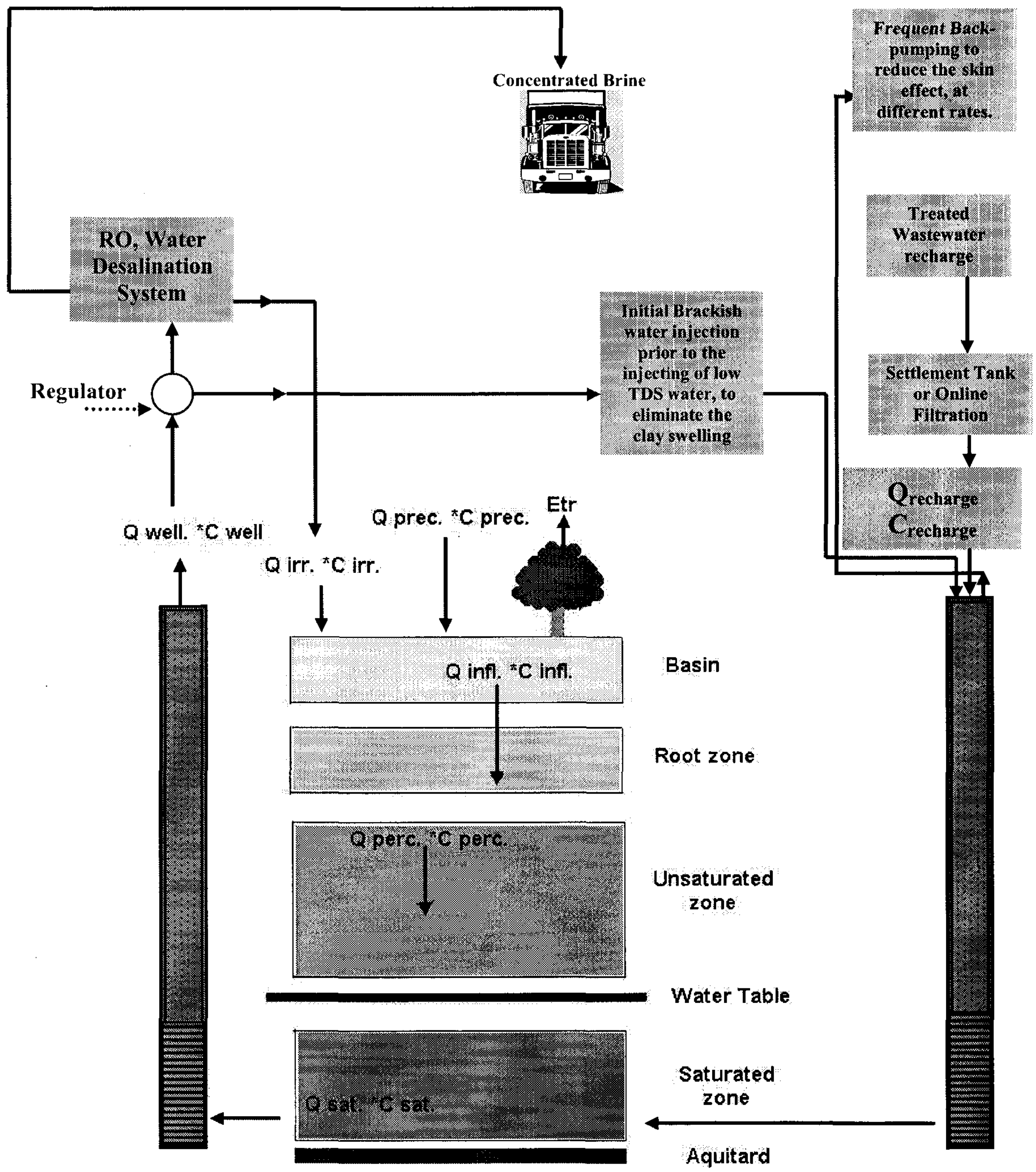

- Simulate the base case using the lump model. This base case will be analogous or representative of quasi-Kuwaiti ecosystem and environment data, where the conceptual design system initial roots were developed.

- Evaluate the sensitivity of the general conceptual design system while using the lump model simulation. The sensitivity of the conceptual design system will be executed by implementing different ranges of hydrologic, hydrogeologic, and climatic parameters: 1) evapotranspiration, 2) initial groundwater salt concentration, 3) wastewater salt concentration, 3) root zone salt concentration tolerance, 4) initial groundwater table hydraulic head, 5) hydraulic conductivity, and 6) porosity.

- Evaluate the robustness of the general conceptual design system by performing different operational scenarios. The goal will consist of four perturbed scenarios of the general conceptual design system utilizing the lump model approach and comparing their performance with the base case simulation of the general conceptual design system utilizing a lump model approach. The first scenario will be practiced during the off planting season to help acceleration and improvement of groundwater quality and water table height, thus, reducing the total power consumption. The other three scenarios will present most possible obstacles or lateral reduction in the operation system due to emergencies or cost effects.

- Utilize the areal distribution model, Visual MODFLOW and MT3D model, for three orientation layouts. These orientation layouts represent the orientation of the pump and injection well location, and in addition, the location of the hypothetical area relative to the groundwater salt concentration. The areal distribution orientation layouts will be simulated for the base case of the general conceptual design system. Therefore, by calculating the transit areal distribution groundwater heads, transit drawdown, and salt distribution within the unconfined saturated aquifer, total operation power requirements can be calculated.

- Analyze and compare the economic feasibility of the general conceptual design system for costs of setting up and operating the base case of the general conceptual design system utilizing the lump model and the areal distribution model (orientation layouts).

1.5 Dissertation Layout

- Chapter 1: Introduction.
- Chapter 2: Literature Review.
- Chapter 3: Methodology (Lump Model).
- Chapter 4: Methodology (Sensitivity Analysis).
- Chapter 5: Methodology (Scenarios)

- Chapter 6: Methodology (Areal Distribution Model)
- Chapter 7: System Economic Feasibility Analysis
- Chapter 8: Conclusion and Recommendations.
- Appendix I: Reverse Osmosis Desalination.
- Appendix II: Background.
- Appendix III: Depletion Figures.
- Appendix IV: TDS Contours Figures.
- Appendix V: Evapotranspiration.
- Appendix VI: Hydraulic Head, Groundwater Concentration, and Brine Water Concentration Figures.

CHAPTER 2

LITERATURE REVIEW

This dissertation considers reference information in two categories: (1) - wastewater, reverse osmosis (RO), irrigation and artificial recharge; (2) – salinity, water levels and drainage. The following review organizes bibliographic sources in these categories.

2.1 Wastewater, Reverse Osmosis (RO), Artificial Recharge and Irrigation

The aims of a study carried out by Abdel-Jawad et al., (2002) are to assess the technical viability of implementing Reverse Osmosis (RO) membrane technology to renovate Kuwait's tertiary-level treated wastewater effluent and to find solutions for problems encountered in wastewater renovation by Reverse Osmosis (RO), thus satisfying the increase in agricultural, industrial and demotic demand for good quality water that is free from viruses and bacteria and other microbial present. Therefore, in preserving the natural strategic water resources, the environmental pollution resulting from direct discharge of secondary/tertiary municipal effluent to the sea is reduced. This help in meeting unexpected emergency demands of fresh water shortages. Abdel-Jawad et al. (2002) conclude that wastewater can be treated to produce an excellent permeate quality almost devoid of salt and pollutants. They recommended that membrane fouling is the most important obstacle to be overcome in the implementation of the RO process. This is manifested in a reduction of permeate production rate and/or an increase in salt passage over time. Accordingly, the complexity of the fouling phenomenon makes mathematical modeling extremely difficult to predict the correlation of flux decline with time. Therefore, two empirical parameters have become wildly accepted, i.e., the silt density index (SDI) and the permanganate demand (PD). They have been studied to predict the performance of flux correlation with time and the quality effect of the feed water on the performance of RO membrane. Furthermore, Abdel-Jawad et al., (2002) relate the cases of fouling to numerous phenomenon including concentration polarization, gel formation, scaling, plugging of membrane pores by suspended matter, biological fouling, and degradation of the membrane itself. However, for wastewater desalination by R.O., all sources rely on the value of the turbidity in the feed water as measure of quality. Others rely on other parameters such as color, total organic carbon (TOC), chemical oxygen demand (COD), and suspended solids (SS). Finally Abdel-Jawad et al., (2002) suggested the following values of parameters as an acceptable level for operating RO plants using treated sewage effluent:

Parameter	Value
Turbidity, NTU	1-5
Color-Cu (at 408 mm)	9-15
Total Organic Carbon (TOC), (mg/l)	10-20

Suspended Solids (SS), (mg/l)	1-5
Chemical Oxygen Demand (COD), (mg/l)	5-10

A pilot study carried out by the Kuwait Institute for Scientific Research (KISR) to desalinate the subsurface water, used the reverse osmosis (R.O.) technique. The subsurface water feed was withdrawn from a 50 m deep well at the Kifan site, hence, assessing the viability and the economic feasibility of using RO technology. Al-Wazzan et al., (2002) outlined the results of over 8000 operating hours performance data of an RO plant utilizing spiral-wound membranes, SW, (Toray, SU810M) (Table 2.1), (which was used in a previous seawater desalination project (1994-1996) then was preserved in formaldehyde for future use) to desalinate subsurface water with total dissolved solids (TDS) of about 11000 mg/l. Moreover, the measured silt density index (SDI) of the feed water showed that no extensive chemical pretreatment is required.

Table 2.1 Operation parameters for the toray, SU810M membrane (after Al-Wazzan et al., 2002).

Parameter	Recommended values
Operating pressure, Kg/cm^2 (psi)	<70 (1000)
Feed water temperature, °C (°F)	<35 (95)
Silt Density Index (SDI)	<4
pH range, continuous operation	3-9
pH range, chemical cleaning	2-10
Feed flow rate per vessel, l/min (gpm)	<50 (13.2)
Brine flow rate per vessel, l/min (gpm)	>10 (2.6)
Brine permeate flow ratio	>6
Pressure drop per vessel, kg/ cm^2 (psi)	<2 (29)
Pressure drop per element, kg/ cm^2 (psi)	<1 (14)

The R.O. desalination plant at the Kifan system consists of one well pump, two transfer pumps, one high pressure pump (21 bar), one RO train, a cartridge filter, a complete pretreatment, buffer tank, break tanks, and two product tanks, one that can be used for membrane cleaning. Total plant capacity is $19m^3$/day (Figure 2.1).

The results indicate that spiral-wound membranes, SW, (Toray, SU810M) reverse osmosis system is a viable technique to desalinate subsurface water. In addition, the result showed an improvement in water quality total dissolved solids (TDS), chemical oxygen demand (COD) and biochemical oxygen demand (BOD) of 99%, 96%, and 42%, respectively. The economic feasibility evaluation of the spiral-wound membranes, SW, (Toray, SU810M) reverse osmosis system indicates that the unit cost of desalting subsurface water by RO is 0.235 KD/m^3 (0.775 US$/ m^3). This is based on 18fils/kWh of electricity cost with no government subsidy (2fils/kWh is the actual cost of subsidized electricity), (1KD = 1000fils = 3.3 US$). The unit cost is feasible for a small–scale plant, and will be more feasible as the capacity of desalination increases.

Finally, Al-Wazzan et al., (2002) conclude that the desalination of subsurface water, using the R.O. desalination system, will consume a reasonably low amount energy that can reduce the moderately high salinity of the water. In addition, the spiral-wound membranes, SW, (Toray, SU810M) used in this experiment produced water of excellent quality that can be reused for irrigation and greenery purposes, reducing the over stressed usage of brackish groundwater.

Figure 2.1 Schematic diagram of the RO plant utilizing spiral-wound membranes, SW, (toray, SU810M) (after Al-Wazzan et al., 2002).

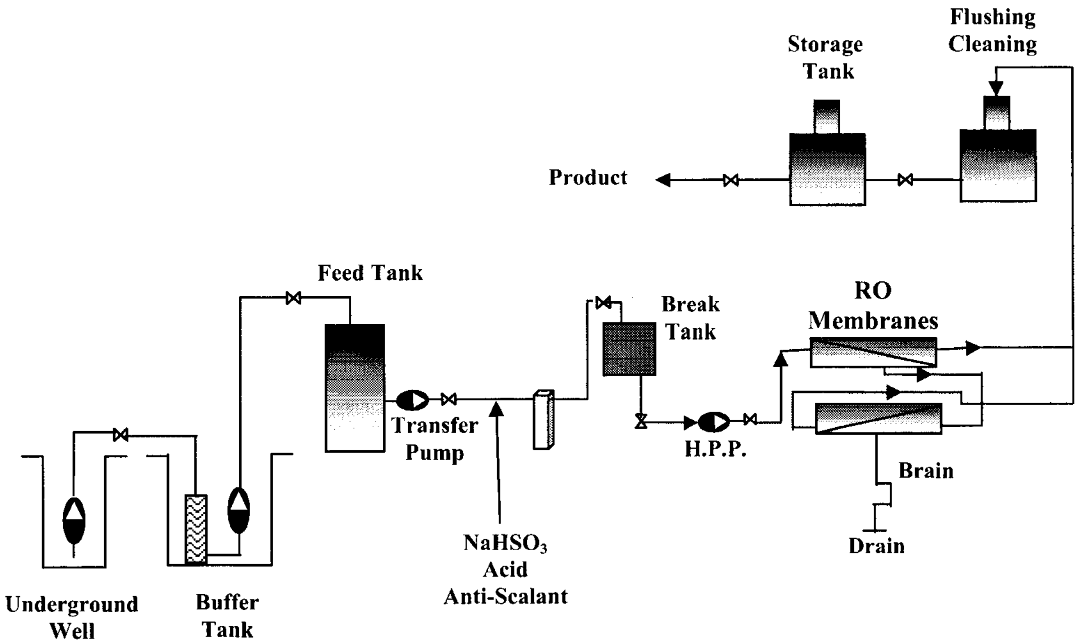

As a consequence of continued growth in population, in standard of life and industrial development, stress on water supplies is progressively increasing in the areas with water stress. Therefore, a need to use raw water of low quality has developed. Hence, some countries in the Middle East and in the Mediterranean regions initiated new strategical programs to recover and reuse treated municipal water, desalinated brackish water and other difficult raw water from marginal sources. Redondo, J.A., (2002) presented trends for such treatments and discussed alternatives and problems seen in implementing some of the possibilities. Moreover, benefits and problems encountered in real life application of modern membrane technologies were presented. Three example case histories on industrial size and pilot plants for reverse osmosis (RO) or nanofiltration (NF) treatment were discussed. (1) industrial effluent treatment; (2) secondary municipal and agricultural effluent application; and (3) high salinity "brackish" well water treatment. I will only focus on high salinity "brackish" well water treatment, as the other two cases are out of my scope of interest.

When water resources are scarce, marginal waters with a high fouling tendency or seawater can be used. Marginal waters are difficult to treat due to fouling problems that can occur with insufficient pretreatment in the membrane plant. Some large installations use integrated membrane systems (IMS), combining microfiltration (MF) or ultrafiltration (UF) with reverse osmosis (RO) or nanofiltration (NF) to achieve better quality for the RO/NF. This quality is in terms of turbidity, silt density index (SDI) and microbiology control, providing water with low fouling potential RO/NF membranes. Therefore, this results in an operation with substantially better plant availability and lower unit cost. But expensive pretreatment, as achieved with IMS, tends to increase pretreatment costs.

The high-salinity "brackish" well water treatment case history illustrates the membrane treatment of high salinity well water for potable water and agricultural irrigation, using the "regular" seawater reverse osmosis FILMTEC SW30-8040 elements. This case history plant is located in southern Spain, where, the water to treat contains agricultural run-off and aquifer water with substantial seawater penetration. The water is extracted from deep wells (up to 200 m) and the TDS is between 8,000 and 35,000 mg/l.

The first plant of their study had 2x1200 m^3 capacity and a TDS of 4,000 mg/l at the early 1990s. The plant was equipped with FILMTEC brackish water membrane type BW30-330. The wells were contaminated with agricultural run off water, quaternary amines and organo-halougenated compounds including iodine. The membranes suffered a severe flux reduction and had to undergo a Dow proprietary treatment to recover flow. The recovery was excellent; from a fouling factor of 0.55, the plant came back to a fouling factor of 0.9.

A new well was built, since in the meantime; the wells had experienced a strong salinity increase from 4,000 to about 18,000 and in some cases up to 33,000 mg/l. New R.O. plants were equipped with SWRO elements, of the non-high-rejection type. In the case study, the plant had five trains, seven elements per pressure vessels, type FILMTEC SW30-8040, and 1120 elements in total. In general, evaluation of operation and economical data from the literature, case histories, and studies involving FILMTEC membrane elements showed that the treatment of marginal water is feasible and economical.

A study carried out by the Kuwait Institute for Scientific Research (KISR) recommended drainage by deep wells to lower and maintain the subsurface water at desirable levels. A large quantity of water needed to be permanently pumped from over-stressed and practically slightly renewable natural groundwater resource. Since the quality of pumped water is likely to prohibit any direct use, it is proposed to reduce its salt content using reverse osmosis (RO) technology. The desalinated water could then be used for irrigation and urban gardening, thus saving the use of brackish groundwater supply from other sources. Ebrahim et al., (2000) studied the result of a pilot plant study carried out by KISR to investigate the viability and technical feasibility of using two small-size pilot plants of R.O. configuration systems.

(1) Spiral–Wound (SW) membrane (Fluid system, 4820XR).

(2) Dupont Hollow Fine Fiber (HFF) membrane (SW-M-8540); and

(3) Compared with an old Spiral-Wound (SW) membrane (Toray, SU-810m)

Utilizing water pumped from the Al-Shamia and Al-Kifan residential areas (Figure 2.2), the SW membrane is designed for desalinating high salinity brackish water (TDS >10,000 ppm), whereas the H.F.F. membrane is used for desalinating seawater (TDS >35,000 ppm), (Table 2.2).

Their techno-economic assessment, carried out by the Economics Studies Department of the Techno-economics Division at KISR, showed the following:

(1) The average cost of extracting and treating subsurface groundwater is KD 0.211 /m^3 (1Kuwaiti Dinnar (KD) = 1000 fils = US$ 3.3).

(2) The operation cost accounts for 51% of the total cost, followed by the capital cost, which accounts for 39%.

(3) Substantial variation in cost exists across the different R.O. units under operation, which is attributed to different electricity and chemical costs.

(4) The unit costs show that H.F.F., with a unit cost of KD 0.189/m^3, is the most efficient among the three R.O. units, and the Toray, with a unit cost of

KD 0.235/m^3 is the least cost effective.

(5) The unit costs of treating subsurface groundwater is found to be less than half of the cost of treating desalinating seawater, indicating that use of surface groundwater is a viable option.

(6) The unit cost of operation of large scale R.O. treatment plants, commercial R.O. plants, is likely to be less than the operation of small-size R.O. treatment plants.

Figure 2.2 Schematic diagram of S.W. and H.F.F. R.O. units, (after Ebrahim et al., 2000).

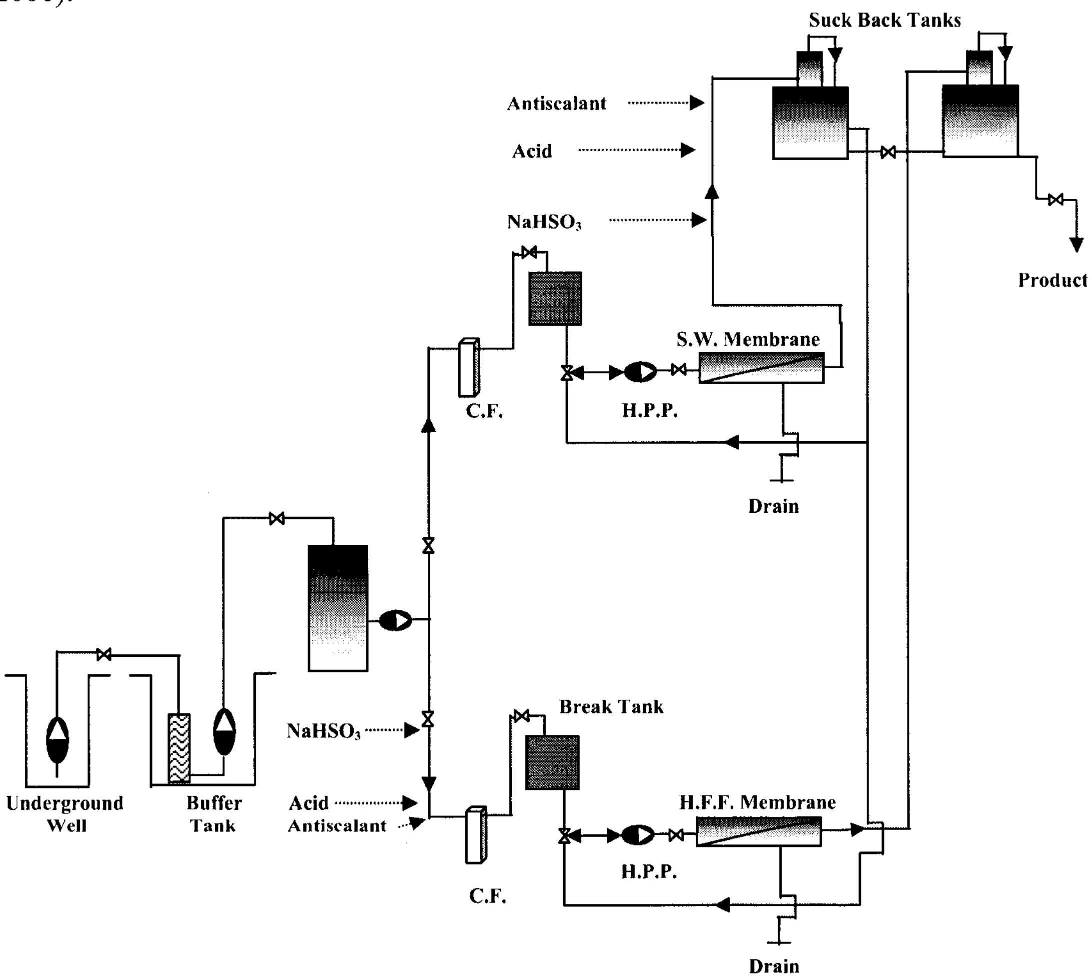

Emad H. AlAli

Table 2.2 Average water chemistry data for SW and HFF membranes at Al-Kifan city site (after Ebrahim et al., 2000).

ANALUTICAL PARAMETER	RAW	PRODUCT SW (Fluid system, 4820XR)	HFF (SW-M-8540)
PH	7.15	5.88	6.25
TDS, mg/l	10,786.60	152.00	139.32
T. alkalinity, mg/l	143.30	8.96	17.24
CO_3^{-2}, mg/l	< 0.10	< 0.01	< 0.10
HCO_3^-, mg/l	143.30	8.96	17.24
CO_2, mg/l	7.72	6.68	6.02
Na^+, mg/l	3045.00	34.80	28.00
K^+, mg/l	55.15	0.37	0.27
Mg^+, mg/l	432.40	0.67	0.10
Ca^{+2}, mg/l	869.87	1.18	0.18
Al^{+3}, mg/l	1.55	< 0.05	< 0.05
Pb^+, mg/l	< 0.03	< 0.03	< 0.03
Mn^+, mg/l	< 0.05	< 0.05	< 0.05
F^-, mg/l	1.95	0.16	0.10
Cl^-, mg/l	3983.80	43.20	30.60
SO_4^{-2}, mg/l	3018.90	30.30	20.72
Tot. Fe, mg/l	< 0.05	< 0.05	< 0.05
Silica, mg/l	5.45	2.10	1.94
Ba^{+2}, mg/l	< 0.05	< 0.05	< 0.05
Zn^{+2}, mg/l	< 0.05	< 0.05	< 0.05
PO_4^{-3}, mg/l	< 0.05	< 0.05	< 0.05
COD, mg/l	32.33	9.67	2.33
BOD, mg/l	1.60	0.80	0.73

The results showed that both systems, SW membrane (Fluid system, 4820XR) and H.F.F. membrane (SW-M-8540), have technical and economical merits and can produce fresh water of high quality for agriculture, lawns and emergencies at comparatively low cost (Table 2.3).

Table 2.3 Unit cost of extracting and treating surface water (after Ebrahim et al., 2000).

	--------RO unit--------			
	Toray (SU-810M)	Fluid system (4820XR)	HFF (SW-M-8540)	Average
Capacity, m^3/d	19	18	21	
Period	22/9/98-28/8/99	19/9/99-24/4/00	27/9/99-24/4/00	
Running hours	8025	5177.10	4625	
Production: treated water, m^3.	5531.78	3832.91	3922.16	
Electricity consumed, KWh.	22,705.71	16,091.52	15,232.11	
A. Capital cost (depreciation)	0.08418	0.08886	0.07615	0.08306
. Machinery	0.07282	0.07687	0.06588	0.07185
. Civil Work	0.01136	0.01199	0.01027	0.01120
B. Operation cost.	0.13094	0.09906	0.09264	0.10754
. Manpower	0.013	0.013	0.013	0.013
. Electricity	0.08213	0.07557	0.06991	0.07587
. Chemicals	0.03186	0.0094	0.0084	0.01655
. Filters	0.00395	0.00109	0.00133	0.00212
C. Maintenance and spares.	0.02	0.02	0.02	0.02
Total unit cost (A+B+C), KD/m^3	0.23512	0.20792	0.18879	0.21061

1Kuwaiti Dinnar (KD) = 1000 fils = US$ 3.3

A study was conducted by Bouchaib El Hamouri et al., (1996) using and comparing three types of water quality applications (raw wastewater, treated wastewater, and groundwater) for crop production under arid and saline conditions without any chemical fertilization. Four irrigation methods were used namely, surface irrigation, drip irrigation (with two systems "Bas Rhone" and "Rain bird") and sprinkler irrigation. The results after a three year experimentation period were: 1) the treated wastewater application instead of groundwater attenuated the effect of water salinity on the crop yields; 2) the drip irrigation system showed the highest irrigation performance and crop yield; 3) the morphology and the way the crop was conducted were found to play an important role in determining its final bacteriological quality; 4) treated wastewater irrigated crops and soils did not show any helminthes eggs contamination and 5) soil contamination by faecal coliforms were not isolated from the treated wastewater irrigated soil beyond the limit of 0.25 m (Table 2.4). Furthermore, irrigation with raw wastewater showed a higher attenuate effect on salt built up in the soil than the other two applications. Moreover, the usage of treated wastewater instead of groundwater for irrigation had a great impact on the attenuation of the detrimental effect of the salt on crop growth and yield, prevention of using groundwater, and reducing soil salinization.

Table 2.4 Crop yield obtained with the three types of water (groundwater, GW, treated wastewater, TW, and raw wastewater, RW) and with the four methods of irrigation tested: surface, drip (2 systems) and sprinkler irrigation in (tons/ha), (after Bouchaib El Hamouri et al., 1996).

IRRIGATION METHOD	WATER TYPE	ALF-ALFA (1)	CORN (2)	COURG-ETTES (3)	BEANS (4)	TOMA-TOES (5)	TURNIPS (6)	CUCUM-BER (7)
Surface irrigation	GW TW RW	158.3 252.6 293.4 S	02.3 04.4 04.5 S	03.0 10.1 13.7 S	05.8 11.5 12.8 S	11.0 26.6 34.8 S	04.0 25.9 36.4 S	00.0 22.5 41.5 S
Drip "Rain bird"	GW TW	276.7 269.1 S	01.1 01.2 N.S	13.0 15.9 S	02.2 05.2 S	17.3 36.5 S	15.2 47.0 S	00.0 27.3 S
Drip " Bas Rhone"	GW TW	264.1 315.9 S	03.5 05.0 S	09.6 21.6 S	08.3 16.2 S	08.2 12.9 N.S	15.5 43.3 S	07.1 32.7 S
Sprinkler irrigation	GW TW	263.7 276.4 N.S	03.0 01.6 N.S	11.1 19.8 S	11.1 13.2 N.S	02.3 23.7 S	17.9 34.1 S	09.88 32.18 S

S: statistically significant difference; **N.S:** not significant difference, (1) Total 3 years, (2) Spring/Summer, (3) Autumn, (4) Winter/Spring, (5) Spring/Summer, (6) Winter, (7) Summer.

Injection experiments through existing wells were carried out with Mukhopadhyay et al., (1995) to evaluate the feasibility of artificial recharge of aquifers in Kuwait. Clogging from suspended solids and air entrapment, non-uniform mixing of tracer, difficulty in maintaining stable injection rates, and well redevelopment efforts ,through acidization and pump surging, were required to restore the injection capacity of clastic aquifer were the operational problems that researchers encountered. Noteworthy recommendations and an optimistic conclusion were reached regarding the feasibility of future implementation of artificial recharge of aquifers in Kuwait. Despite the operational problems, the artificial recharge of aquifers through injection wells was technically and economically feasible in Kuwait. Furthermore, they recommended some preparation and troubleshooting procedures prior and through the injection to insure the optimum results, as follows:

(1) The injected water may by pass through settlement tanks prior to injection, for the low to moderate injection rates, to get rid of the suspended solids in the injected water, thus reducing the possibility of clogging phenomena, skin effect, in the injection face (on an average of 5 mg/l of suspended solids in the injected water may cause turbid yellowish brown water leading to future clogging).

(2) For high injection rates the suspended solids from the injected water are to be removed through online filtration, prior to injection.

(3) To avoid collection of the corrosion products from the water conveyance system, the supply network may be made of non-corrosive materials like PVC, catholically protected pipes, or pipes with internal cement or epoxy coating.

(4) Frequent back pumping of the well at high rates is required to eliminate the clogging phenomena. Airlifting, instead of backpumping, may also be practice by completing the well with an airlift pipe connected to a compressor.

(5) To avoid air clogging, the injection pipeline system should be made airtight as far as possible and positive pressure should always be maintained in the surface network. Air release valves will purge air entering the system during well injection. In addition, the bottom end of the injection pipe in the well bore should be under the water level all through the injection period to ensure that no air enters the pipe through this end and no cascading occurs. An alternative approach is to design the injection pipe to maintain a solid column of water without cascading, hence, eliminating the vacuum either by using one or more small pipes or through a throttling valve at the bottom of the injection pipe.

Other guidelines that Mukhopadhyay et al., (1995) derived from the results of their experiments and other hydrological data available for Kuwait are as follows:

(1) The aquifer transmissivity should be moderate (in the range of 150-400 m^2/d). Very high transmissivity, although allowing high injection rates, causes large-scale mixing with the native groundwater, thus, reducing the recovery efficiency (the pumping rate of the aquifer to the rate of injecting). In contrast, very low transmissivity limits the injection rates.

(2) To avoid lowering the recovery efficiency through mixing and from the effect of boundary, the salinity of the native groundwater should be as low as possible due to the association of H_2S (hydrogen sulfate) with high salinity (10,000 mg/l)

water in the region. Consequently, from overall considerations, the salinity of the target aquifer should not exceed 7000 mg/l.

(3) The lateral hydraulic gradient in the targeted aquifer at the injection site should not be too large to limit the conveyance of the injected water down gradient away from the injection well.

Mukhopadhyay et al., (1994a) conducted an experiment to assess the technical feasibility of artificial recharge in the carbonate Dammam formation and the clastic Kuwait Group aquifers. In the absence of any pre-treatment of the injected water and measures for maintenance of line pressure, clogging from suspended solids and air entrapment occurred in the experiment. Injection of water and subsequent withdrawal were carried out in three existing water wells. The injected water duration of one month was established in two wells (in the Sulaibya field and in the Shigaya field) perforating the Dammam Aquifer. On the other hand, clogging problems, due to injection, were significant in the third well (in the Sulaibya field) perforating the Kuwait Group aquifer that caused a temporary termination of the experiment. The multi-aquifer flow model and transport model were used to analyze the injection/withdrawal data. The main aim of using these models was: (1) to understand the flow behavior of the injected water during injection and withdrawal, and its influence on the recovery efficiency (defined as the percentage volume of water of acceptable quality recovered from the aquifer with respect to the volume of water injected); (2) to track the development of clogging with time on a quantitative basis; and (3) to estimate the dispersivity parameter of the aquifer. Thus, the experiment suggested that the artificial recharge of the Dammam and Kuwait Group aquifer was technically feasible. The problem of clogging was, however, more severe for the Kuwait Group aquifer. Furthermore, Mukhopadhyay et al., (1994a) results showed that it is technically feasible to artificially recharge the aquifer through wells and later recovery of the water injected through the same well. The problem of clogging, caused by entrapped air and suspended solids in the injection water leading to the skin phenomena, can be removed by simple back-pumping (pumping and injection must be done interchangeably) and acidization followed by pump surging. Finally, for the Kuwait Group aquifer, Mukhopadhyay et al., (1994a) suggested initial injection with poor quality, brackish water, followed by better quality water to avoid possible damage to the aquifer from clay swelling.

2.2 Salinity, Water levels and Drainage

Patel et al., (1999) investigated the effect of sub-irrigation methods with brackish water in saline soils for vegetable production, for yield and tuber grade, in arid regions using two varieties of potatoes, Atlantic and Russet Burbank. Sub-irrigated water with salinity levels of 1.5 or 9 dS/m was applied 13 days after planting. Moreover, water table levels were maintained at 40 and 80 cm below the soil surface. They concluded that water table depths or sub-irrigation water salinity levels had no significant effect on the total tuber weight of either cultivar. However, the yield of grade A Russet Burbank tuber was greater when the water table was maintained at 40 cm and the same trend but with less significance was observed for the Atlantic tubers. Sub-irrigation with brackish water in saline soil resulted in a yield 59% above the global average, thus demonstrating its utility for agriculture in dry areas.

Salama et al., (1999) investigated the process of soil and water salinization as they occur in different geological, hydrogeomorphological (interaction between soil, geology, surface, and groundwater), agricultural, and climatic settings. Their objective was to characterize and describe the groundwater condition contributing to existing salinity problems. Examples illustrating different settings, processes and modes of development of salinity were discussed for central Sudan, North America, and South and Western Australia. Through their studies, four mechanisms of water uptake and salt concentration are recognized: evaporation, evapotranspiration, hydrolysis, and leakage. Salt accumulates when mineralized groundwater at or near the ground surface continually evaporates causing minerals to precipitate. Evapotranspiration occurs where infiltrating recharge water is continually taken up by plants leaving behind the concentrating salts in the unsaturated zone. Hydrolysis is the process where water is taken up to the formation of new minerals in the weathering processes. The leakage process occurs between aquifers through confining beds layers.

Salama et al., (1999) studies showed that groundwater plays a major role in the mobilization, accumulation, and discharge of salt into the landscape. Salinity increases along the ground flow paths from catchments dividers and areas of recharge to the valley floors and areas of groundwater discharge. This pattern was similar in all three continents, North America, Australia, and Africa.

In South Australia, saline groundwater discharge activates the soil processes of oxidation, reduction, solinization, sulfidization, and sulfuricization, which cause the soil to lose structure and fertility and become susceptible to waterlogging and erosion.

In the North Great Plains region (NGPR), of the USA and Canada, the localized recharge and discharge scenarios caused salinization to occur mainly in depressions, resulting in the formation of saline soil and seepages, where, Na and SO4 dominate the shallow groundwater and soil solution. Moreover, groundwater from shallow aquifers mixes with groundwater from the deep bedrock aquifer in the groundwater discharge area, yielding a range of intermediate chemical compositions.

In Western Australia, recharge prior to clearing (replacement of the native vegetation with shallow rooted crops) was less than 1mm/yr. With this low rate of recharge, most of the total soluble salts (TSS) infiltrating with the recharging water are concentrated in the unsaturated zone, as water is distributed by one or more of the four mechanisms (evaporation, evapotranspiration, soluble salts hydrolysis, and leakage between aquifers). After clearing, rates of recharge increased 10-200 times, causing a new aquifer to develop within the former unsaturated zone. Consequently, water tables have risen and groundwater gradient and velocities have increased, thus, causing the TSS stored in the unsaturated zone to be mobile. As a result, salinity increased in the groundwater and soil surface, thus increasing the salinity of streams and lakes.

In the regional aquifers of the rift basins of Sudan, salinity increases along the groundwater flow paths and forms saline zones at the distal ends. The saline body or bodies were formed by evaporation, coupled with alkaline earth carbonate precipitation and dissolution of capillary salts.

Al-Ruwaih et al., (1998) to assess water quality of the Kuwait group aquifer, collected one hundred and sixty seven ground water samples from different water well fields. They outlined the geological processes factors and the substructure surface structure on controlling the trend in water quality as discharges-recharge relation. Field p^H, temperature and content of Ca^{2+}, Mg^{2+}, K^+, Na^+, Cl^-, $SO4^{2+}$, and HCO_3^- were determined for all the groundwater samples. Al-Ruwaih et al., (1998) found that the brackish NaCl and $CaSO_4$ water type, mainly occupies the Kuwait Group aquifer. Fresh water of Na_2SO_4, $Ca(HCO_3)_2$ and $NaHCO_3$ water types occurred in the upper part of the Dibdibba formation of the Kuwait Group. In addition, saline-brine groundwater was found in the residential areas located east of the Ahmadi anticline structure, where total dissolved solids, TDS, ranges from 10,000- 115,000 mg/l.

A computer program, WATEQ, was utilized to compute the saturation indices of minerals with respect to a given water composition. They found that the groundwater is supersaturated with respect to calcite ($CaCO_3$), aragonite ($CaCO_3$), and dolomite ($CaMg(CO_3)_2$), and it is under saturated with respect to anhydrite ($CaSO_4$), gypsum ($CaSO_42H_2O$) and halite (NaCl). Moreover, the increase in TDS of the aquifer from southwest toward northeast (the direction of groundwater flow), and north direction may attribute to the increased saturation thickness of the aquifer in this direction.

Calculated mean values of PCO_2 (partial pressure of carbon dioxide) for the fresh and brackish water fields were $4x10^{-3}$ and $5x10^{-3}$ (atm), respectively. This indicates that the groundwater becomes charged with CO_2 during infiltration processes. Generally, the salinity increased from 3000-100,000 mg/l in the direction of regional flow.

Al-Rashed et al., (1998) investigated the effect of extensive utilization of brackish water for landscaping and agriculture in Kuwait and the problems associated with this practice. They found several problems. These are: (1) declining groundwater levels by as much as 50 m in certain locations; (2) deterioration of groundwater quality in agriculture areas due to the return of irrigation water, in that the TDS of groundwater increased to about 8000 p.p.m. at selected sites; (3) excessive use of groundwater for landscaping and gardening in the urban areas resulted in the rise of groundwater levels by about 3 m. Furthermore, they suggested more studies to be conducted for some possible solutions to these problems as follows: (1) replacing the use of groundwater with artificial recharge, as much as possible, and stored wastewater in the aquifer; (2) usage of reverse osmosis treated groundwater for urban and irrigation at an appropriate price; and (3) elimination of the over usage of brackish groundwater for irrigation by a better understanding of soil salinity build up in the root zone, and better irrigation design and practices.

Nativ et al., (1997) conducted a study in Negev desert, Palestine, to depict the processes affecting salinization of all the components of the hydrological cycle in arid zones, namely, precipitation, surface water, vadose water and groundwater, spanning 18 years. They concluded that dissolved carbonate dust and evaporation of the falling raindrops results in $Ca(HCO_3)_2$ facies and increased ion concentration of the rainwater. The variable mixing with low salinity, isotopically depleted water percolating from the fractures, accounts for the depleted isotropic composition of the groundwater. However, the low solute content of the water percolating through the fracture cannot modify the ground water NaCl facies. Consequently, the preferentially flowing water reduces groundwater salinity in the chalk aquitard (most of the vadose zone water moves through preferential pathways and is typically not exposed to evaporation). But the $Ca(HCO_3)_2$ facies prevailing in the rainwater and floodwater disappears, and the NaCl effect from the vadose zone prevails.

A paper was introduced by Manguerra et al., (1997) concerning a new numerical approach for modeling a subsurface system that is based on the objectives of both crop productivity and water quality protection. They introduced a new modified linked approach to solve the governing partial differential equations for subsurface flow and salt transport by finite difference. As a consequence, this new approach will not only adopt the irrigating-drainage system to agricultural objectives of maintaining crop productivity ,but it will adopt the water quality of agricultural drainage as well, by using one dimensional (1D), two-dimensional (2D), and three-dimensional (3D) flow and salt transport problems, where they used the governing equation of the general flow system in three-dimensions (3D) as:

$$\nabla \cdot (K \cdot \nabla h) \pm Q_S = (\eta \cdot S_s + C)\frac{\partial h}{\partial t}$$

and the governing equation for salt transport in the subsurface as:

$$\frac{\partial(\Theta \cdot c)}{\partial t} = -\nabla \cdot (cq - \Theta D \cdot \nabla c) \pm c'$$

where,

$h = h(x,y,z,t)$ = the total head that describes the state of the system (L).

$K = K_r * K$, the hydraulic conductivity tensor (L/T) with K_r as the relative hydraulic conductivity and saturated hydraulic conductivity (L/T), respectively.

$C = \frac{d\Theta}{d\psi}$ = the specific soil moisture capacity (1/L) with Θ and ψ as the volumetric moisture content and capillary pressure head (L), respectively.

$\eta = \frac{\Theta}{\Theta_S}$ = the liquid saturation with Θ_S as the soil porosity.

$S_S = \rho g(n\beta + \alpha)$, the specific storage (1/L) with ρ, g, α, and β as the fluid density, gravitational constant, (L/T^2), solid matrix compressibility (LT^2/M), and fluid compressibility (LT^2/M), respectively.

Q_S = the source or sink term (1/T).

$\boldsymbol{t}$ = time (T), x, y, and z = orthogonal components of the Cartesian coordinates system (L).

$\boldsymbol{c}$ = salt concentration (M/L^3).

$\boldsymbol{q}$ = Darcy flux (L/T).

$\boldsymbol{D}$ = hydrodynamic dispersion tensor coefficient (L^2/T).

$\boldsymbol{c'}$ = salt concentration source or sink (M/L^3-T).

Manguerra et al., (1997) results showed that the modified formulation used in the modified approach reduced the computational requirements. The model is used to evaluate the effectiveness of the drains to intercept soil water from shallow layers (< 2m deep) as affected by drain spacing, drain depth, surface recharge, and depth to impermeable layers. The results of these evaluations provide useful insights for developing design and management strategies to improve water quality of the drainage effluent.

Yurtsever (1997) investigated the use of natural isotopes to study the sources and processes involved in the groundwater salinization, for verification of site-specific dynamic models of salt-water intrusion and identification of the geochemical evolution of groundwater. The most commonly used natural isotopes for applications in water sciences, including salinization processes identification and seawater intrusion dynamics, are the heavy isotopes of the elements oxygen (^{18}O), hydrogen (^{2}H-deuterium, ^{3}H – tritium), and carbon (^{13}C, ^{14}C – radiocarbon). Of these, ^{18}O, ^{2}H and ^{13}C are stable isotopes, whereas ^{3}H and ^{14}C are radioactive, with half-life values of 12.43 and 5730 years, respectively. Furthermore, because during the processes of leaching salt formation (mineral dissolution), the stable isotopes content of the water is not affected while the salinity of water increases. Thus, this is a unique feature which will enable identification of such processes based on isotropic and chemical data, where, the stable isotopes ^{18}O, and ^{2}H are the most conservative tracers during their transport in the hydrological systems and their relationship with salinity changes are univocal. On the other hand, since the concentration of the ^{3}H (tritium), and ^{14}C (radiocarbon) isotopes are removed from the system through radioactive decay and changes that may be induced by complex geochemical reactions in the case of radiocarbon, radioactive isotopes are used to estimate the travel time (transit time) of a component flow. Consequently, the identification of saltwater intrusion could be made through the use of ^{3}H (tritium) and ^{14}C (radiocarbon) concentrations.

Quality degradation of groundwater resources, particularly in arid and semi arid regions, due to rising salinity is an increasingly encountered problem. The case of groundwater salinization in these water scarce regions is, in many cases, stress imposed on the system by overexploitation (including seawater encroachment in coastal aquifers), irrigation water applications, mixing of freshwater with saline formation water (often underlying the upper freshwater aquifer) or leaching of salt formation causing increased mineralization. Yurtsever (1997) investigation, related to causes and resources of increasing salinity of groundwater, was concentrated in a part of the Middle East region. The salinity range in major aquifer units of the Middle East are given in (Table 2.5). Yurtsever (1997) concluded that the regional Umm er Rhaduma aquifer in Saudi Arabia and neogene limestone aquifers in Saudi Arabia and Kuwait exhibit characteristic features of Paleaowaters replenished during an earlier pluvial period.

Table 2.5 Present salinity levels in major aquifers in the Middle East region, (after Yurtsever, 1997).

COUNTRY	BRACKISH WATER LOCATION	AQUIFERS	DEPTH TO AQUIFERS FROM GROUND (m)	TOTAL DISSOLVED SOLIDS (TDS-ppm)
Bahrain	Main Island of Bahrain	Khober	30-39	2200-8400
Egypt	Bahar El Baqar Sinai	Nubian Sandstone	200-300	1000-7000
Lebanon	Coastal regions	Recent Alluvium	5-10	1000-3000
Jordan	Jordan Valley Azraq W. Dhuleil Wadi Araba	Alluvium Belqa-B2 Basalt Alluvium	0-100 10-50 10-60 30-70	> 5000
Kuwait	Sulaibya Shagayah Wafra Abdali	Kuwait Group Dammam Umm er-Rhaduma	30-100	2800-5300
Qatar	Northren prov. Southren prov.	Rusait Umm er-Rhaduma	20-80	2000-2500
Saudi Arabia	Al-Qatif Hufuf Wadi Al-Mish Al-Quawayah Rus-south	Dammam Umm er-Rhaduma Saq Khuff Wadi Alluvium	130 240-350 170-325 90-170 40-70	2450 2500-10000 2000-10000 10000 2000-57000

Groundwater ages are greater than 30000 years in the Umm er Rhaduma formation and in the range of 12000 to 26000 years in the neogene aquifers of Kuwait. The stable isotopes data together with the salinity values available for Umm er Rhaduma formation indicate mineral dissolution to be the main cause of salinity in the regional aquifer (since the salinity has increased along the flow path across the aquifer while the stable isotopes content remains unchanged). Groundwater salinity observed in the neogene aquifer of Kuwait is mainly caused by mixing of seawater due to earlier marine transgression that is being flushed out by lateral inflow to the aquifer from Saudi Arabia's western border. The salinity of the upper shallow aquifer in Qatar has been identified to be due to both seawater intrusion and upward leakage from the underlying Umm er Rhaduma aquifer.

Al-Sulaimi, et al., (1996) conducted a study on the Al-Abdally farms, north of Kuwait, to evaluate the impact of brackish groundwater mining for irrigation purposes on salinity and groundwater levels using two numerical models. They concluded that the groundwater extraction for irrigation has increased gradually since the 1960's and reached about 200 Ml /day (million litters per day) in 1989. About 30% of the irrigated water was lost as evapotranspiration and 70% infiltrated back to the aquifer. As a result, total dissolved solids, TDS, of ground water at several locations within the farming region increased to about 8000 - 9000 p.p.m (part per million) in 1989 compared with 5000 p.p.m in the 1963. Furthermore, the maximum decline in the groundwater levels, due to pumping, was about 3–5 m in the central farming region. Thus, if the pumping and irrigation level were to be continued at 1989 rates, only 10 – 25 % of the existing wells will have a TDS level less than 7500 p.p.m. within the next 10 years.

A study of hydrochemical facies, zonation, genesis and the trend in groundwater quality of the Al-Sulaibiya field was conducted by Al-Ruwaih (1996) 120 Km south of Kuwait Bay. The Al-Sulaibiya field is the oldest and largest water well field in Kuwait, where brackish groundwater is produced mainly for irrigation and domestic uses. The aquifer system of the study area is a part of the extensive Dammam limestone aquifer that underlies the whole State of Kuwait. More than 1000 groundwater sample have been analyzed during the period of 1980-1990 for the study purpose. Their results concluded that the aquifer salinity ranges between 3500-7500 mg/l, showing an insignificant increase in the salinity along the flow path toward the northeastern part of the aquifer (8000 mg/l). Moreover, the study revealed that there are four water types NaCl, $CaSO_4$, $CaCl_2$, and Na_2SO_4. The two major water types found during the study period were mainly the CaSO4 type, located primarily in the southwestern part of the aquifer, and the NaCl type located along the eastern part of the aquifer. Two genetic water types were recognized as mainly SO_4^{-2}-Na of continental origin and Cl-Mg of marine origin. Thus, this suggests that the native marine groundwater of the carbonate aquifer has mixed with meteoric water during the process of infiltration. Additionally, the dominant ions of the groundwater are Na^+, Ca^{2+}, Cl^- and SO_4^{-2}, while Mg^+ and HCO_3^- are the non-dominant ions.

Also, the groundwater analyses showed that water passed through simple dissolution processes and reverse ion exchange of Na^+- Cl^- water. This causes an increase of the total dissolved solids in the aquifer and a decrease of SO_4^{-2} – Cl^- values in the direction of the flow. Moreover, the developed hydrochemical cation facies calcium–

sodium and the anion facies chloride – sulphate show that the area is a discharge area and the fresh recharge area is excluded due to the depletion of HCO_3^- ions.

The groundwater of the Dammam limestone aquifer, under the study area, is classified as very hard water; the total hardness of CaCO3 ranges between 1500-3500 mg/l. Finally, Al-Ruwaih (1996) concluded that salinity and the total hardness of the aquifer have increased slightly over the period under investigation. Freeze and Cherry (1979) defined water hardness as water content of metallic ions which react with sodium soap to produce solid soaps or scummy residue which react with negative ions, (as when water evaporate in boilers) to produce solid boiler scale (carbon mineral precipitation). Hardness is expressed as the total concentration of Ca^{2+} and Mg^{2+} as milligrams per liter equivalent CaCO3. Thus, it can be determined by substituting the concentration of Ca^{2+} and Mg^{2+}, expressed in mg/l, in the expression

$$T.H. = \left(fw(CaCO_3) \big/ aw(Ca^{2+}) \right) * (Ca^{2+}) + \left(fw(CaCO_3) \big/ aw(Mg^{2+}) \right) * (Mg^{2+})$$

where,

T.H. = Total Hardness.

fw(CaCO₃) = Formula weight of $CaCO_3$.

aw(Ca²⁺) = Atomic weight of Ca^{2+}.

$aw(Mg^{2+})$ = Atomic weight of Mg^{2+}.

(Ca^{2+}) = Concentration of (Ca^{2+}).

(Mg^{2+}) = Concentration of (Mg^{2+}).

or,

$$T.H. = 2.5 * (Ca^{2+}) + 4.1 * (Mg^{2+})$$

Hence, the factors 2.5 and 4.1 represent the ratio of formula weight of $CaCO_3$ to the atomic weight of the ion. Water with hardness values greater than 150 mg/l is designated as being very hard, whereas; soft water has values less than 60 mg/l.

Drainage is necessary to maintain crop productivity in intensely irrigated areas where there is a presence of a highly saline, shallow water table. However, current environmental constraints demand that drainage should be controlled and minimized. A new design and management system that introduces the concepts of drainage and no-drainage cycles was presented by Manguerra et al., (1996) and applied to a hypothetical farm representative of field conditions in the San Joaquin Valley of California over eight growing seasons. The objective of this design was to reduce the subsurface drainage while maintaining an acceptable salt balance. The no-drainage cycle is an extended period that may span several growing seasons in which drains are not operated and no drainage releases are allowed. On the other hand, the drainage cycle is a limited period during the off season in which drains are opened to relieve excessive water table and salinity buildups and restore the suitability of the soil for growing crops. Furthermore, their main objection was to offer an alternative irrigation-drainage system design and management for semi-arid agricultural areas with saline groundwater. A computer simulation model is used to determine the effectiveness of alternative irrigation-drainage system design. The results of the simulation are compared with a traditional irrigation-drainage system using the same assumed disposal technologies and costs. In addition, the proposed management scheme is based on the assumption that disposal technologies are available to receive drainage water.

The advantages of Manguerra et al., (1996) operational system of cyclical periods of no-drainage and drainage cycles, as they stated, are:

1) The problem of disposing drainage water is nonexistent for an extended period of time.
2) Drainage releases can be easily scheduled to be consistent with the requirements of the drainage collection technologies.
3) The effectiveness of the drains to remove salt during the drainage cycle is enhanced naturally because of the evapoconcentration of the soil water during the no-drainage cycle.
4) With no-drainage cycles, farmers are forced to be more careful with their irrigation management, thereby improving water use efficiency because, theoretically, no water is lost through drainage during the growing season.

5) Farmers can adopt more uniform water management practices over the irrigation area since the drains, which are not operated during the no-drainage cycle, cannot cause uneven water table mounds.

Parameters that influenced the performance of the irrigation-drainage system during the drainage and no-drainage cycles are analyzed using a finite difference model. Hence, this allowed solving the governing flow and salt transport equations in both the unsaturated and saturated zones. The model uses a modified formulation of numerical implementation of the flow and salt transport equations by the Colorado State University Irrigation and Drainage (CSUID) Model. The performance parameters that are analyzed for the no-drainage cycle are (1) irrigation rate and duration; (2) irrigation application depth; and (3) salinity of irrigation water. Additionally, for the drainage cycle, the parameters are (1) drain spacing; (2) drain depth; (3) surface water recharge (irrigation applied during drainage cycle); and (4) depth to impermeable layer.

Manguerra et al., (1996) results showed that the new system reduced drainage approximately 50 to 58% compared to the traditionally managed system. Furthermore, the corresponding reduction in salt load was approximately 15 to 29%, indicating improvement in the efficiency of the drains to intercept more salt per unit volume of water. Despite the significant reduction in drainage volume, the new system was able to approximate the salt balance of the traditionally managed system. Manguerra et al., (1996) implied that shifting from the traditional system to the new system requires changing in drainage design parameters, i.e. drainage spacing, to prevent an unacceptable salt balance in the water table aquifer. Thus, the irrigation requirement was reduced by about 145 mm/growing season without any reduction in crop yield, using cotton as their crop. Also, Manguerra et al., (1996) results suggested that crop yield in area with shallow water tables is not significantly affected by matric stress, due to upward water movement from the water table to the rooting zone, but, only if irrigation is scheduled to prevent excessive osmotic stress buildup, due to upward movement of higher saline water that will cause resalinization of the root zone and lead to excessive osmotic stress.

A regional numerical model, calibrated under both steady and transit conditions, has been used by Mukhopadhyay et al., (1994b). This model investigates the hydrodynamic impacts of different groundwater management options on the potentiometry of the aquifers in Kuwait because recharge rates from lateral inflows and infiltration of rainwater are much less than the combined rate of extraction from the established water fields and natural discharge. The results indicate that there is real danger of either dewatering the aquifers, or deteriorating water quality by upconing of saline water and seawater intrusion, if the present trend of increased pumping withdrawal rates continues unchecked and unregulated. Moreover, the study suggested that even if the withdrawal were completely stopped in the near future, the aquifer water levels would not be restored to their pre-1960 conditions by the year 2010. Thus, more consideration and studies are needed on the implementation of future artificial water recharge of the aquifer and its beneficial effects on the potentiometric surface and deterioration levels.

A two- dimensional finite element model of solute transport in a tile-drained soil –aquifer system was applied by Kamra et al., (1994). They investigated the effect of depth of impervious layer and adsorption on salt distribution in the soil and groundwater, and salinity of the drainage effluent. The model was designed for steady state water flow in the unsaturated zone (from ground surface to water table) and saturated zone (from water table to impervious layer) (Figure 2.3). In addition, the effect of convection (advection) transport, dispersion and linear adsorption is

$$S = K_d * C^{\alpha}$$

where,

S = Isothermal.

K_d = Distribution coefficient.

C = Concentration, and

α = Coefficient depending on solute species, for linear isothermal, thus, $\alpha = 1$.

Figure 2.3 Domain for solute transport in a tile-drained soil-aquifer system.

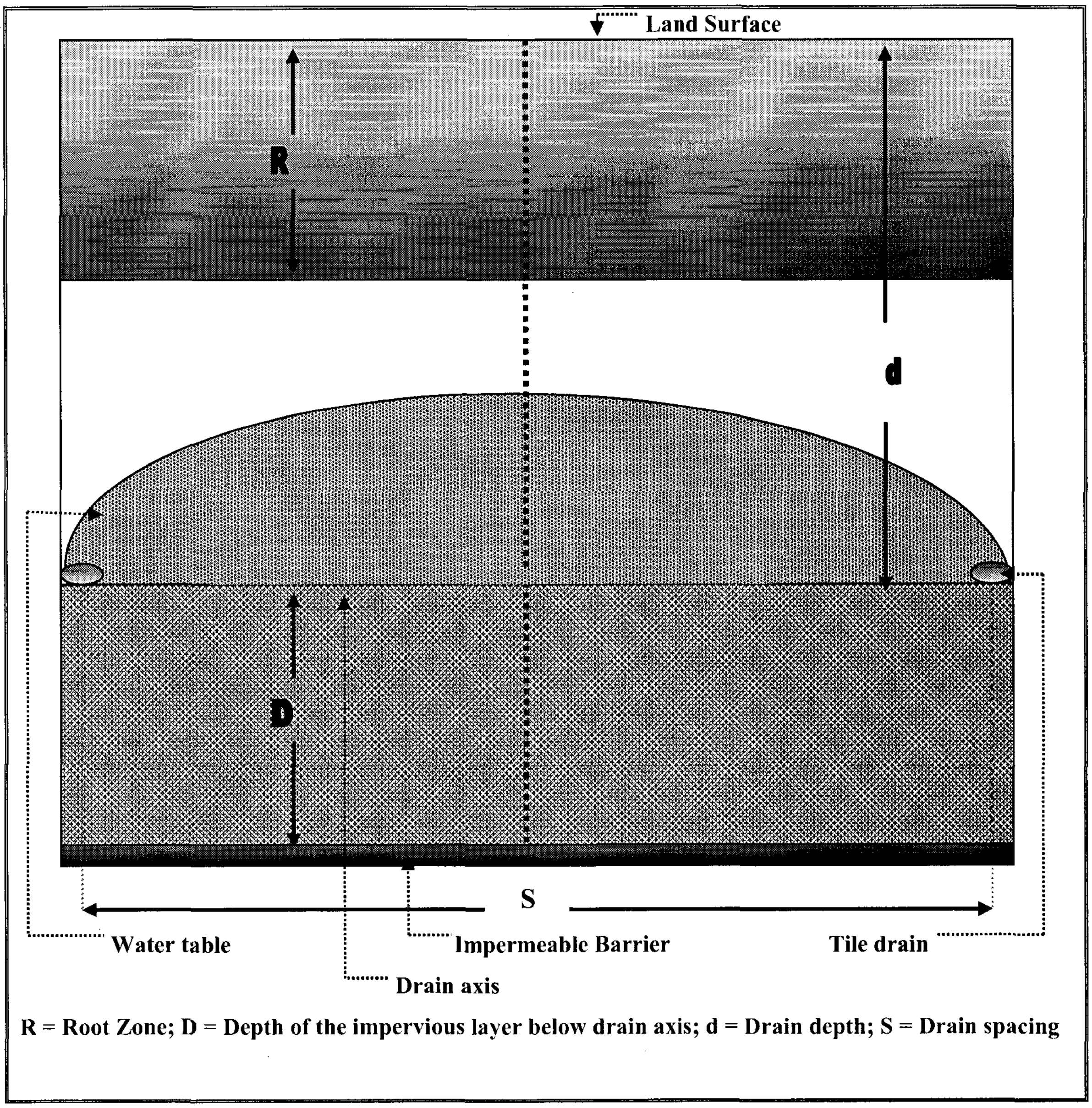

Kamra et al., (1994) results indicated that the depth of impervious layer (D) has a slight effect on the salt distribution in the unsaturated zone. Thus, their result is in agreement with the result of Childs (1943) which indicated that at a certain time, about

75% of the total flow to a field drain in deep homogeneous soil takes place within a depth equal to 1/20th of the drain spacing from the drain axis. In addition, Van Deemter (1950) and Childs (1969) also observed that no more than about 10% of the surface precipitation ever flows in a path any part of which penetrates to a depth greater than 1/6th of the drain spacing from the drain axis, even though the actual impervious layer is deeper than these depths. These results suggest that in deep homogenous soils the hydraulic conductivity of the soil layers just above and below the drain level is of paramount importance for the hydraulics of water and salt movement to drains. On the other hand, Kamra et al., (1994) found that the depth of impervious layer (D) had significantly influenced the quality of the drainage effluent, where the salinity of drainage water (electrical conductivity of the drained water, EC_d) increased with increasing impervious layer depth (D), due to the increase in groundwater domain. Further, it was found that during the initial years of reclamation of a highly saline soil with subsurface drainage, the effect of adsorption (chemical reaction of the solute in the groundwater with the soil porous media, leading to retardation of mobility of the groundwater in the porous media) is more pronounced in the unsaturated zone than in the saturated zone. And, the transport of the adsorbing solute species is retarded for a longer time in the groundwater than in the soil.

Thus, for unsaturated flow

$$R = 1 + \left(\rho_B / \theta \right) * K_d \ ,$$

And, for saturated flow

$$R = 1 + \left(\rho_B / \Phi \right) * K_d,$$

where,

R = retardation factor of solute front.

ρ_B = Bulk density of the porous media.

θ = Volumetric water content, for unsaturated soil.

Φ = Porosity of the saturated soil.

Consequently, the retardation factor is inversely proportional to volumetric water content, θ, (in unsaturated soils) or to the porosity, Φ, (in saturated soils). Therefore, the porosity has a higher magnitude in the saturated soils than volumetric water content in the unsaturated domain, causing stronger retardation of the advance rate of the leaching front towards the drains in the unsaturated zone. Moreover, the sorptive capacity of a soil tends to increase with the increase of fluid concentration, Freeze and Cherry (1979). Therefore, adsorption will be stronger in the surface layers of the soil profile which were initially more saline.

Kamra et al., (1994) investigation showed that the electrical conductivity of the drained water, EC_d, increased with increasing distribution coefficient, K_d, which is contrary to the expectation of decreasing EC_d with increasing K_d, causes less effective leaching from the soil and slower movement of an adsorbing solute in the groundwater. However, their explanation of this contradictory result was due to the availability of highly concentrated soil and groundwater in the immediate vicinity of the drain in comparison with the concentration elsewhere in the domain, which, contributed significantly to the salt load of drainage effluent.

A study was presented by Al-Ruwaih, F.M., (1994) to assess the water quality of the Kuwait Group aquifer presented by Al-Rawdhatain and Umm Al-Aish as fresh water well fields and Al-Abdali and Al-Wafra as brackish water well fields. Hydrochemical facies was correlated with the topography and groundwater flow path. A computer model, WATERQ, was utilized to compute the saturation indices of minerals with respect to a given water composition. The groundwater was classified as brackish to saline based on the total mineralization, and salinity increased from 4000-18000 mg/l in the direction of flow from a southwest to northeast direction.

The saturated indices are an indication of the saturated state of a mineral with respect to a given water composition (Table 2.6). The saturation index is defined as (Chapell, 1993):

$$SI = \log_{10}\left({IAP}/{K_{sp}} \right)$$

where,

SI = the saturation index.

IAP = the ion-activity product.

$\boldsymbol{K_{sp}}$ = the solubility product constant for the mineral.

If $SI < 0$, the mineral is undersaturated with respect to the solution and the mineral can dissolve. If $SI > 0$, the mineral is supersaturated and it can precipitate but not dissolve, and if SI is close to zero, the mineral may not be reacting at all or may be reacting reversibly.

Hosseinipour, Z., and Ghobadian, A., (1990) investigated the intensive hydrologic, erosion, salinity, and water resources in an arid region of the central province of Yazd within an area of 60,000 Km^2 for two years. Yazd is pronounced with very limited water resources, mainly groundwater, with high groundwater mining mainly utilized for irrigation practices (groundwater tables have dropped more than 50 m in the last 30 years) and with low precipitation (60 mm/year) and high evaporation (3500 mm/yr). They reached to a noteworthy conclusion and they presented various recommendations as result of their investigation.

Salinity levels of groundwater and soils are on the rise continuously in the region. Salinity of the soil and desertification are due to upward movement of water and the associated soluble salts in the soil layers. This is caused by the evaporation process, which extracts the water and leaves the salt in the soil top horizons (impeding the plant functions), and by insufficient precipitation and available soil moisture in the upper layer.

Hosseinipour, Z., and Ghobadian, A., (1990) concluded that salts movement mechanisms are of three types:

1) Movement from deep zone to the surface layer by capillarity.
2) Horizontal movement in the direction of natural gradient to the soil flats by surface and subsurface flows.
3) Movement by winds.

Table 2.6 Summary of saturated indices of the studies area (after Al-Ruwaih, F.M., 1994).

MINERALS	CHEMICAL FORMULA	SATURATED INDICES: MEAN AB	R	U	W	STANDERD DEVIATION AB	R	U	W	COEFFICIENT OF VARIATION AB	R	U	W
Anhydrite	$CaSO_4$	-0.30	-1.49	-1.42	-0.29	0.12	0.30	0.52	0.09	-0.40	-0.20	-0.37	-0.31
Aragonite	$CaCO_3$	0.11	0.15	0.26	0.32	0.18	0.26	0.09	0.29	1.64	1.37	0.35	0.91
Calcite	$CaCO_3$	0.25	0.29	0.41	0.46	0.18	0.26	0.09	0.28	0.72	0.90	0.22	0.61
Dolomite	$CaMg(CO_3)_2$	0.33	0.11	0.42	0.80	0.26	0.51	0.21	0.61	0.79	4.64	0.50	0.76
Gypsum	$CaSO_4 2H_2O$	-0.14	-1.28	-1.12	-0.15	0.12	0.29	0.52	0.09	-0.86	-0.23	-0.46	-0.06
Halite	NaCl	-4.19	-6.11	-6.31	-4.24	0.18	0.55	1.05	0.22	-0.04	-0.09	-0.17	-0.52
Huntite	$CaMg_3(CO_3)_4$	-3.24	-4.04	-3.35	-2.26	0.47	1.02	0.50	1.27	-0.15	-0.25	-0.15	-0.56
Magnesite	$MgCO_3$	-0.28	-0.55	-0.35	-0.04	0.11	0.25	0.14	0.32	-0.39	-0.45	-0.40	-8.00

AB = AL-ABDALI R = AL-RAWDHATAIHN U = UMM AL-ALISH W = AL-WAFRA

The majority salts content in the groundwater are in the form of anions (Cl^-, SO_4^{2-}, HCO_3^-, and CO_3^{2-}) and cations (Na^+, Ca^{2+}, Mg^{2+}, and K^+). The soluble salts causing salinity were identified as Na_2SO_4, Cl_2Ca, $MgCl_2$, NaCl and $MgSO_4$ as well as $NaHCO_3$

on a smaller scale. The other groups are less soluble salts which don't cause salinity but bring about high osmotic pressure, which leads to physiological death in plants.

Thus, Hosseinipour, Z., and Ghobadian, A., (1990) can safely state that the salinity of groundwater in Yazd is in direct relationship with the depletion of the aquifer, and factors affecting the salinity of groundwater are: (1) gradual depletion of the aquifer, (2) evaporation increases in salt flats and salt marshes, (3) existence of saline underground aquifers, (4) salt layers embedded between and within aquifers, (5) existence of salt domes, (6) gradual establishment of shallow saline groundwater bearing formations, and (8) gradual existence of desert salt lakes and salt marshes.

Finally, Hosseinipour, Z., and Ghobadian, A., (1990) recommended the following steps for conservation, maintenance, and management of water resources in Yazd:

(1) Reducing and preventing evaporation to the extent possible.

(2) Preventing excessive percolation and water losses.

(3) Research on and selection of crops with low consumptive demand and high salt tolerance.

(4) Improving irrigation efficiencies using modern technologies.

(5) Limiting well contraction and recharging aquifers artificially, helping to restore the decline in groundwater tables.

(6) Reuse of irrigation return water and controlling saline aquifers.

(7) Soil and water conservation through expansion of desert forest.

(8) Limiting water demand industrial activities.

(9) Limiting or stopping grazing on the sparse desert range lands in order to preserve the valuable soil covers and encourage rangeland expansions.

(10) Application of groundwater flow and transport models and groundwater management models to better understand the regional flow patterns and quality changes, and study alternative management plans for aquifers.

CHAPTER 3

METHODOLOGY (LUMP MODEL)

3.1 Simulating the General Conceptual Design System using Lump Model

In this chapter of the dissertation, the simulation of the general conceptual design system will be executed while using a lump simulation model approach. The simulation will be carried out through the construction of a simplified model. This simulation will calculate, using the Visual Basic model, the overall steady state groundwater heads, salt concentrations (by way of uniform mixing scheme), steady state drawdown, and total operation power requirements, within the unconfined saturated aquifer. A lump model simulation is constructed for basic design purposes, where, the assumptions and the hypothesis of the conceptual design system are simplified to calculate the overall power consumed by the design conceptual model system. Likewise, a lump model simulation is used as a primary indication of the system durability and feasibility. The order of executing the lump model simulation will be governed by the following set of governing equations.

- Root (Vadose) Zone Governing Equations

- Reverse Osmosis (R.O.) System Governing Equations
- Groundwater Zone Governing Equations
- Field Area Estimation Governing Equations

The above governing equations will be looked upon in more detail in the following subdivisions of Section 3.1, thus:

3.1.1 Root (Vadose) Zone Governing Equations

The root (vadose) zone system is a vital part of the conceptual design system. Water content of the root zone determines how much and when water should be applied, depending on crop type. Thus, sufficient irrigation water application allows sufficient soil water content, and therefore, hopefully controls the leaching (deep percolation) response. If the amount of water applied were equal to or less than the amount evaporated or transpired, then water normally available for leaching would be delayed or depleted by evapotranspiration. Therefore, leaching water must come from additional applications of irrigation water to keep the root zone within an acceptable crop salt concentration tolerance level. In practice, when water is used for irrigation, plants consume most of the water and return a portion of the irrigated water to the atmosphere through transpiration and soil evaporation as pure water vapor. The salts remain behind in the soil of the root zone and, eventually, it will lead to a reduction in crop yield. In this dissertation, for simplicity and assurance of keeping the root zone at acceptable salt concentration levels and avoiding water shortages for crop consumption and providing sufficient water for leaching purposes, the calculation of the governing equations of the root (vadose) zone system will utilize the following approaches:

- Steady state water balance of the root zone.
- Steady state salt mass balance of the root zone.

<u>Steady state water balance of the root zone</u>

To avoid water shortages within the rooting zone consumed by the crop and to keep the root zone within the allowable crop salt concentration level, a steady state balance on the root zone approach will be implied in this section of the dissertation. Hence, taking in consideration the entire inward and outlet flow variables within the root zone controlled volume (Figure 3.1); the steady state soil water balance of the root zone will be as:

$$Q_{irr(\,permeate\,)} + Q_{Precipitation} + Q_{CR} - Q_{ET_c} - Q_{DP} - Q_{Runoff} = 0 \qquad \textbf{(3.1)}$$

where,

$Q_{irr(permeate)}$ = Irrigation (permeate) water requirement for the period being considered [L^3/T],

Q_{ET_c} = Total water used by actual crop evapotranspiration [L^3/T],

$Q_{Precipitation}$ = Effective rainfall (≥ 0.0254 cm) [L^3/T], in arid regions with scarce rainfall $Q_{Precipitation} \cong 0$,

Figure 3.1 Soil water balance in the root zone.

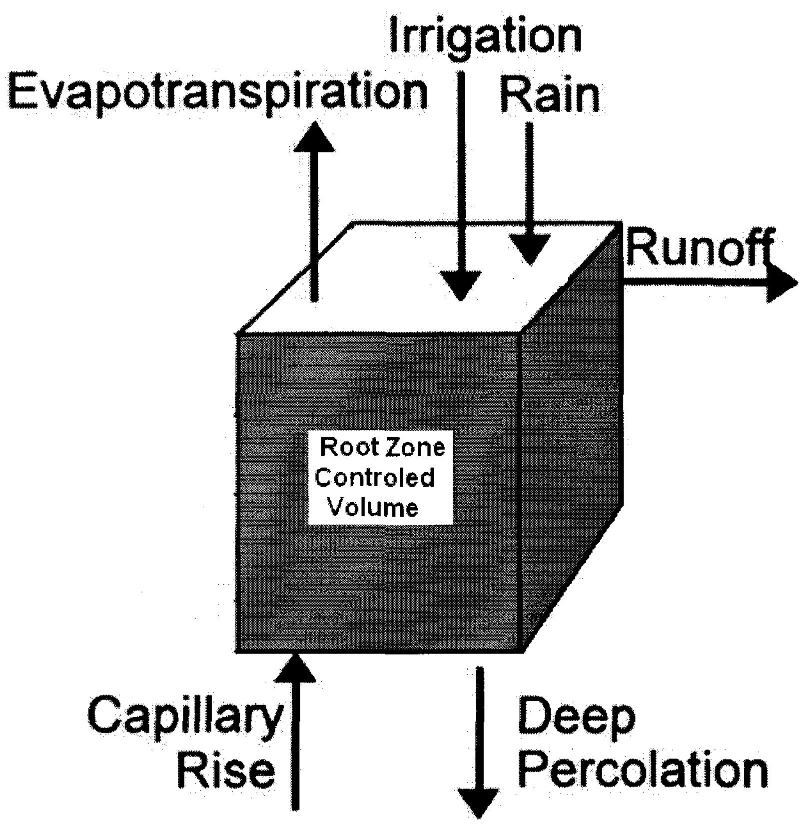

Q_{DP} = Water loss out of the root zone by deep percolation [L^3/T],

Q_{CR} = Upward capillary rise from the groundwater table [L^3/T], in arid regions with high hydraulic conductivity $\boldsymbol{Q_{CR} \cong 0}$, and

$\boldsymbol{Q_{Runoff}}$ = Water runoff from the soil surface [L^3/T], in arid regions with high hydraulic conductivity $\boldsymbol{Q_{Runoff} \cong 0}$.

Neglecting precipitation, runoff flow, and capillary rise flow from Equation (3.1),

$$Q_{irr\,(permeate)} - Q_{ET_c} - Q_{DP} = 0 \qquad \textbf{(3.2)}$$

rearrange,

$$Q_{irr\,(permeate)} = Q_{ET_c} + Q_{DP} \qquad \textbf{(3.3)}$$

As a result, Equation (3.3) represents the major governing equation of steady state water balance within the rooting zone.

Salt concentration in the rooting zone is a crucial and important decision variable in my design. To avoid crop yield reduction, the root zone salt concentration must be within a certain threshold tolerance value depending on the crop type. Therefore, salt mass balance within the rooting zone must be taken into consideration to keep the root within an acceptable salt tolerance. For that reason, a steady state salt mass balance in the root zone needs to be analyzed, thus:

Steady state salt mass balance of the root zone

To insure a salt balance tolerance within the root zone, the entire incoming and exiting mass flow variables within the root zone must be looked upon (Figure 3.2).

Figure 3.2 Steady state salt balance in the root zone.

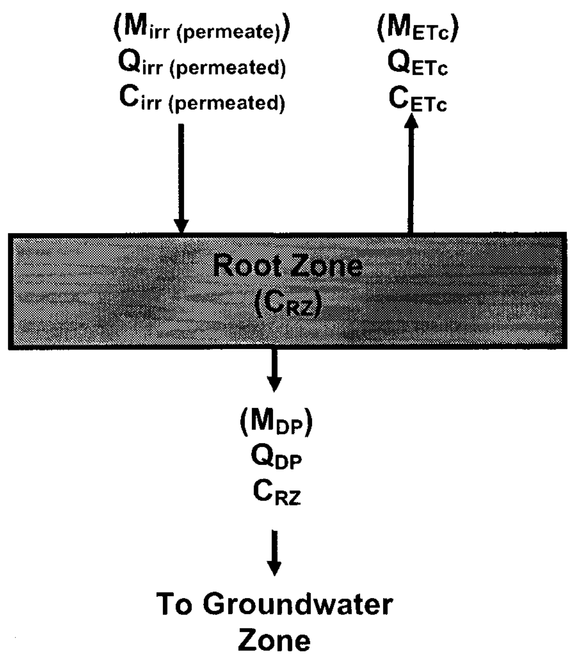

Therefore, from Figure 3.2, the steady state salt mass balance equation of the root zone will be as:

$$M_{irr(\,permeate\,)} - M_{ET_c} - M_{DP} = 0 \tag{3.4}$$

where,

$M_{irr(permeate)}$ = Salt mass flow of the irrigation (permeate) water

[(m^3* mg)/ (l*season)],

M_{ET_c} = Salt mass flow of the evapotranspiration water

[(m^3* mg)/ (l*season)], and

M_{DP} = Salt mass flow of the deep percolation water

[(m^3* mg)/ (l*season)].

Knowing that

$$M_{irr(permeate)} = Q_{irr(permeate)} * C_{irr(permeate)} \tag{3.5}$$

and,

$$M_{ET_c} = Q_{ET_c} * C_{ET_c} \tag{3.6}$$

and further that,

$$M_{DP} = Q_{DP} * C_{RZ} \tag{3.7}$$

where,

$C_{irr(permeat)}$ = Irrigation (permeate) water salt concentration [mg/l],

C_{ET_c} = Evapotranspiration water salt concentration [mg/l], Knowing that plants evapotranspirate pure water, therefore, $C_{ET_c} = 0$. (refer to Section 3.2, page 100, Equation 3.51), and

C_{RZ} = Root zone salt concentration tolerance [mg/l]. C_{RZ} is a decision variable, which depends on the crop type and its tolerance to salts.

Thus, by substituting Equations (3.5), (3.6), and (3.7) in Equation (3.4) and arranging as follows:

$$Q_{irr\,(permeate)} * C_{irr\,(permeate)} = Q_{ET_c} * C_{ET_c} + Q_{DP} * C_{RZ} \tag{3.8}$$

Equation (3.8) represents the main governing equation of steady state salt mass balance within the rooting zone.

3.1.2 Reverse Osmosis (R.O.) unit Governing Equations

The next critical system in the design is the reverse osmosis unit. This unit is the main significant low salt concentration water supplier, which dominates the quality and quantity of the product (permeate) water (Appendix I). The reverse osmosis unit has a very significant role in this conceptual design system. Moreover, depending on the unit design, the product (permeate) water quality and quantity are determined. In this conceptual design system, the reverse osmosis product (permeate) water will be utilized for irrigation purposes. Hence, product (permeate) water quantity, $Q_{irr(permeate)}$, and salt concentration in the product water, $C_{irr(permeate)}$, are major design variables that control the irrigation water quality and quantity and, as a consequence, manipulates the leaching (deep percolation) requirements demands. Therefore, implication of the steady state continuity equation of the reverse osmosis and the steady state salt mass equation will be implied for this purpose.

Power consumption by the reverse osmosis unit is another essential variable of this conceptual design system, which will influence the system feasibility. As a result, for a distinguished design system we aim to keep the power consumption to a minimum.

Therefore, the remainder of this section will be focused on the development of reverse osmosis unit system design variables and decision variables and their governing equations. The variables are:

- Reverse osmosis product (permeate) water quantity, $Q_{irr(permeate)}$.
- Reverse osmosis product (permeate) water salt concentration, $C_{irr(permeate)}$.
- Reverse osmosis brine (rejected) water quantity, Q_{Brine}.
- Reverse osmosis brine (rejected) water salt concentration, C_{Brine}.
- Reverse osmosis recovery percentage, δ.

- Reverse osmosis salt concentration percentage permeates capacity in the product (desalinated) water, ***n***.
- Power consumed by the reverse osmosis system, $\boldsymbol{Power}_{(R.O.)}$.

<u>Steady state water balance of the reverse osmosis unit</u>

The reverse osmosis unit is comprised of one inlet and two outlets. The first inlet is the feed water inlet (Q_{Feed}), which usually pervades the low quality of water to the reverse osmosis unit. Moreover, the source of this feed water is pumped groundwater (Q_{pump}); therefore, ($Q_{pump} = Q_{Feed}$). The first outlet is the product (permeate) water ($Q_{irr(permeate)}$) outlet, which guides the desalinated high-quality water. The second outlet is the concentrated salt (brine) water (Q_{Brine}) outlet, which contains highly concentrate impurities and is usually discharged to a drain (Figure 3.3).

Figure 3.3 Basic scheme of desalination by reverse osmosis unit.

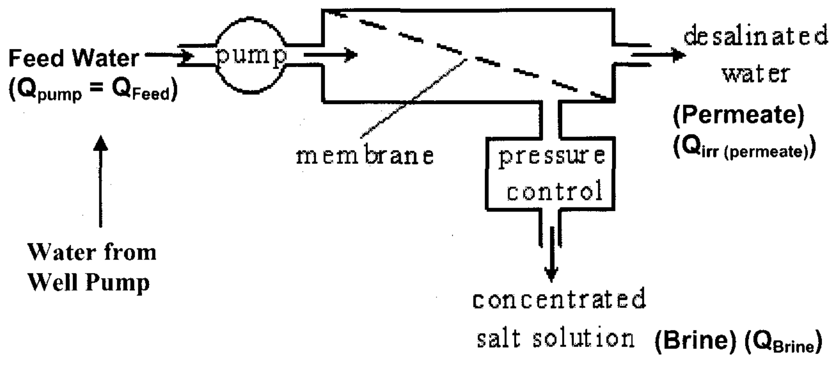

From the steady state water balance within the reverse osmosis system (Figure 3.3):

$$Q_{Feed} = Q_{irr\ (permeate)} + Q_{Brine} \tag{3.9}$$

where,

$Q_{irr(\ permeate\ )}$ = Portion of the feed water that passes through the reverse osmosis membrane and is collected for irrigation use $[L^3/T]$,

Q_{Feed} = Total water entering the reverse osmosis unit (pumped well water fed to reverse osmosis unit),
(Thus, $Q_{pump} = Q_{Feed}$) $[L^3/T]$, and

Q_{Brine} = Portion of the feed water that does not pass through the reverse osmosis membrane, which exists as a separate stream containing concentrated impurities and is usually discharged to a drain $[L^3/T]$.

Consequently, Equation (3.9) symbolizes the major governing equation of steady state water balance within the reverse osmosis unit.

The percentage of permeate water and salt concentration permeate through the reverse osmosis is controlled by two essential decision variables. These two decision variables are recovery (δ) and the membrane type. The former, controls the percent of permeate water through the reverse osmosis unit, and the latter controls the salt concentration percentage permeate capacity (***n***) in the product (desalinated) water. The commercial availability of reverse osmosis recovery percentage (δ) ranges from 40 % - 60 %, and membrane salt concentration percentage permeate capacity (***n***) ranges from 1 % – 15 % (personal communication). These wide selection ranges in (δ) and (***n***) are owed to the type of feed water to the reverse osmosis, quality and quantity, needed to be desalinated, (i.e. seawater, brine water, brackish water, reused tap water, wastewater, etc.).

First, consider the recovery percentage (decision variable), which dominates the product water (permeate) quantity. From the steady state water balance, recovery (δ) will be as:

$$\textit{Recovery\%}\ (\delta) = \frac{Q_{irr\ (permeated)}}{Q_{Feed}} \qquad \mathbf{(3.10)}$$

or,

$$\textit{Recovery\%}\ (\delta) = 1 - \left(\frac{Q_{Brine}}{Q_{Feed}} \right) \qquad \mathbf{(3.11)}$$

where,

Recovery % (δ) = Ratio of the permeate (product) water rate to the total feed water rate. Moreover, δ is a decision variable.

Consequently, Equation (3.10) corresponds to another main governing equation of steady state water balance within the reverse osmosis unit.

The second decision variable is membrane salt concentration percentage permeates capacity ($\boldsymbol{n}$), which dominates the product (permeate) water quality. The percent of salt concentration permeate through the reverse osmosis unit is controlled by membrane type and the steady state salt mass balance governing equation. Therefore, consider next the steady state salt balance within the reverse osmosis unit, thus:

Steady state salt mass balance of the reverse osmosis unit

From the reverse osmosis unit steady state salt mass balance (Figure 3.4),

$$M_{Feed} - M_{irr(\,permeate\,)} - M_{Brine} = 0 \tag{3.12}$$

where,

M_{Feed} = Salt mass flow of the groundwater pump which will be fed to the reverse osmosis unit ($M_{pump} = M_{Feed}$) [(m^3* mg)/ (l*season)],

$M_{irr(\,permeate\,)}$ = Salt mass flow of the irrigation (permeated) water [(m^3* mg)/ (l*season)], and

M_{Brine} = Salt mass flow of the brine (rejected) water

[(m^3* mg)/ (l*season)].

Figure 3.4 Steady state salt mass balance of the reverse osmosis system.

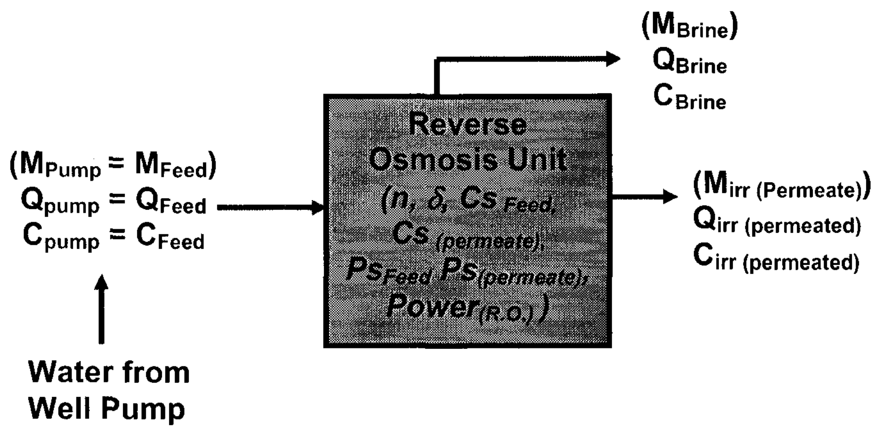

Knowing,

$$M_{Feed} = Q_{Feed} * C_{Feed} \tag{3.13}$$

and,

$$M_{irr(permeate)} = Q_{irr(permeate)} * C_{irr(permeate)} \tag{3.14}$$

and also,

$$M_{Brine} = Q_{Brine} * C_{Brine} \tag{3.15}$$

where,

C_{Feed} = Feed water to reverse osmosis salt concentration (**note**: because the pumped groundwater is fed to the reverse osmosis unit, therefore, $C_{Feed} = C_{pump}$) [mg/l], and

C_{Brine} = Reverse osmosis brine salt concentration (rejected salt concentration from the reverse osmosis unit) [mg/l].

Substitute Equations (3.13), (3.14), and (3.15) into Equation (3.12) and arrange, thus:

$$Q_{Feed} * C_{Feed} = Q_{irr\,(permeate)} * C_{irr\,(permeate)} + Q_{Brine} * C_{Brine} \qquad \textbf{(3.16)}$$

Afterwards, Equation (3.16) characterizes a main governing equation of steady state salt balance within the reverse osmosis unit.

In general, if C is the salt concentration in a volume of water (V), then the amount of salt in this volume is:

$$M = C * V$$

Now, let (Cs) be the ionic salt concentration within the reverse osmosis unit. When a small volume (ΔV) of permeate water flows through the membrane, it carries with it an amount of salt equal to $(n * Cs * \Delta V)$, where (n) is the salt concentration percentage permeating through the membrane. Therefore, if a volume ($V_{permeate}$) of permeate water is produced, the mass of salt in the permeate water will be:

$$\textit{The Mass of Salt in Permeate Water} = n * \int (Cs * \Delta V).$$

Consequently, the ionic salt concentration in the total permeates water, $Cs_{irr\,(permeate)}$, will be:

$$Cs_{irr\,(permeate)} = n * \frac{\int Cs * dV}{V} \tag{3.17}$$

where,

$Cs_{irr\,(permeate)}$ = Ionic molar salt concentration in the total reverse osmosis permeates water [mole/liter], and

V = The volume of permeate (desalinated) water [L^3].

Next consider the osmotic pressure within the reverse osmosis, which is the driving power behind the desalination process. The osmotic pressure is proportional to the salt concentration; thus, the higher the salt concentration of the water, the higher osmotic pressure is induced. The osmotic pressure, ***P***, is given by the Van't Hoff equation:

$$\boldsymbol{P = Cs * R * T} \tag{3.18}$$

where,

R = Gas constant (= 0.082 (liter bar / °K mole)),

T = Absolute temperature in Kelvin of the water, (°C + 273.15), [°K], and

Cs = Ionic molar salt concentration [mole / liter].

Thus, the osmotic pressure within the reverse osmosis unit will be:

$$\boldsymbol{Ps = Cs * R * T} \tag{3.19}$$

where,

Ps = Osmotic pressure within the reverse osmosis unit [bar].

Similarly, the feed water osmotic pressure will be:

$$Ps_{Feed} = Cs_{Feed} * R * T \qquad (3.20)$$

where,

Ps_{Feed} = The osmotic pressure of the feed water [bar],

Cs_{Feed} = Ionic molar concentration of the feed water to the reverse osmosis unit [mole / liter].

In addition, the permeate water osmotic pressure will be:

$$Ps_{(\,permeate\,)} = Cs_{irr(\,permeate\,)} * R * T \qquad (3.21)$$

where,

$Ps_{(permeate)}$ = The osmotic pressure of the permeate water [bar], and

$Cs_{irr\ (permeate)}$ = Ionic molar salt concentration of the reverse osmosis permeate water [mole / liter].

Dividing Equation (3.19) by Equation (3.20), and rearranging,

$$\left[\frac{Ps}{Ps_{Feed}}\right] = \left[\frac{Cs}{Cs_{Feed}}\right]$$

Also rearranging for the ionic salt concentration within the reverse osmosis:

$$Cs = \left[\frac{Cs_{Feed}}{Ps_{Feed}}\right] * Ps \qquad \textbf{(3.22)}$$

Moreover, from the steady state salt mass balance between the feed salt mass and the salt mass within the reverse osmosis unit, the salt concentration, ***Cs***, within the reverse osmosis unit will be:

$$Cs = Cs_{Feed} * \left[\frac{V + V_o}{V_o}\right] \qquad \textbf{(3.23)}$$

where,

V_o = The saltwater volume within the reverse osmosis unit, and

V = The volume of permeate (desalinated) water.

Since the osmotic pressure is proportional to the salt concentration as shown in Equation (3.22), similarly:

$$Ps = Ps_{Feed} * \left[\frac{V + V_o}{V_o} \right] \tag{3.24}$$

Substituting Equations (3.22) and (3.24) in Equation (3.17). Hence,

$$Cs_{irr(\,permeate\,)} = n * \left[\frac{\int \left[\frac{Cs_{Feed}}{Ps_{Feed}} \right] * \left[\frac{Ps_{Feed} * (V + V_o)}{V_o} \right] * dV}{V} \right]$$

where,

n = Salt concentration percentage in permeate water [%], which is a decision variable.

Rearrange,

$$Cs_{irr(\,permeate\,)} = n * Cs_{Feed} * \left[\frac{\int \left[\frac{(V + V_o)}{V_o} \right] * dV}{V} \right] \tag{3.25}$$

and by integrating Equation (3.25), then

$$Cs_{irr(permeate)} = n * Cs_{Feed} * \left[\frac{1-\frac{\delta}{2}}{1-\delta} \right] \quad \textbf{(Urila Lachish, 2002)} \quad \textbf{(3.26)}$$

and,

$$\delta = \left[\frac{V}{V+V_o} \right] \qquad \textbf{(3.27)}$$

where,

δ = Ratio of the permeate (product) water volume to the total feed water volume.

Next, convert Equation (3.25) from ionic molar concentration (mole / liter) to total dissolved salt concentration (milligram/ liter). Thus, starting with the number of salt moles in a liter of feed water:

$$\# \, Of \; Salt \; Moles \; in \; Feed \; Water = \left(\frac{\left(\frac{C_{Feed} \, (in TDS)}{1000} \right)}{\varpi} \right)$$

where,

ϖ = Molecular weight of salt per mole of water [gm/mole], and

TDS = Total dissolved salt [mg/liter].

Then, the ionic molar concentration of the salt ions of the feed water will be:

$$Cs_{(Feed)} = (\Psi) * \left(\frac{\left(\frac{C_{Feed}}{1000} \right)}{\varpi} \right) \quad \textbf{(Urila Lachish, 2000)} \qquad (3.28)$$

where,

Ψ = Number of ions per salt molecules of dissolved salt.

Similarly, the number of salt moles in a liter of the permeate water will be equal to:

$$\#\, Of\ Salt\ Moles\ in\ Permeate\ Water = \left(\frac{\left(\frac{C_{irr(permeate)}\ (in TDS)}{1000} \right)}{\varpi} \right)$$

Likewise, the ionic molar concentration of the salt ions of the permeate water will be:

$$Cs_{irr(permeate)} = (\Psi) * \left(\frac{\left(\frac{C_{irr(permeate)}}{1000} \right)}{\varpi} \right) \qquad \textbf{(3.29)}$$

Of note, Equations (3.28) and (3.29) are two significant governing equations converting the salt concentrations of feed water and irrigation water from ionic molar concentration (mole / liter) to total dissolved salt concentration (milligram/ liter) in the groundwater zone.

Likewise, substitute Equation (3.28) and Equation (3.29) in Equation (3.26), thus:

$$(\Psi) * \left(\frac{C_{irr(permeate)}}{\varpi} \right) = n * (\Psi) * \left(\frac{C_{Feed}}{\varpi} \right) * \left[\frac{1 - \frac{\delta}{2}}{1 - \delta} \right]$$

and rearrange,

$$C_{irr(permeate)} = n * C_{Feed} * \left[\frac{1 - \frac{\delta}{2}}{1 - \delta} \right] \qquad \textbf{(3.30)}$$

As a result, Equation (3.30) corresponds to another main governing equation for irrigation water salt concentration permeates from the reverse osmosis unit.

The aim of this section is to estimate the power exerted by the reverse osmosis. This power is required by the reverse osmosis pump in order to pump the high salt concentration feed water through the reverse osmosis membrane. Therefore, starting with the osmotic pressure of the feed and the permeated water, the reverse osmosis pumping pressure is equal to the difference between the osmotic pressure of the two sides of the membrane, feed pressure, Ps_{Feed}, and permeate pressure, $Ps_{(Permeate)}$, (neglecting the pressure drop across the membrane itself). Accordingly, if there is higher salt concentration in the permeate water, lower pump pressure and lower energy will be needed for the same flow rate. Therefore, power is the main deriving aspect of evaluating the system performance and its feasibility; hence, the power exerted by the reverse osmosis system pump will be:

$$Power_{(R.O.)} = \left[\frac{\left(Ps_{Feed} - Ps_{(permeate)}\right) * Q_{irr(permeate)}}{\eta_{R.O.}} \right] \qquad \textbf{(3.31)}$$

where,

$Power_{(R.O.)}$ = Power consumed by reverse osmosis unit pump [Kjoules / season], and

$\eta_{R..O.}$ = Reverse osmosis electrical pump efficiency, for electrical pump, ($\eta_{R.O.}$ = 85 – 92 %), [percentage].

Thus, Equation (3.31) characterizes another main governing equation for power consumed by the reverse osmosis unit.

Finally, in this dissertation, for all calculation purposes, the type of dominant salt concentration in the R.O. feed water will be assumed to be sodium chloride (NaCl). Keeping in mind that the source of this feed water is the groundwater, thus, sodium chloride will reflect the dominant salt contamination type within the groundwater. Moreover, Table 3.1 represents some of the assumed variable data inputs for the reverse osmosis unit that will be used in all future simulations of this dissertation.

Table 3.1 Reverse osmosis input data assumption variables for all simulations.

Variable	Value or Type	Remarks
R.O. Feed Water Temperature	**289.15 (°K)**	**°K=°C +273.15**
R	**0.082 (L-bar/°K-mole)**	**Gas constant**
R.O. Pumps Efficiency ($\eta_{R..O.}$)	**90 (%)**	**Average R.O. electrical pump efficiency 85 -92 %,**
Groundwater Dominant Salt Contamination Type (which will be fed to the R.O. unit)	**NaCl**	**NaCl chosen to illustrate the major salt contamination of the aquifer**

3.1.3 Groundwater Zone Governing Equations

The next decisive system in the conceptual design system is the unconfined groundwater zone. The importance of the unconfined groundwater came from its initiation in providing the primary source of water which will be fed to the reverse osmosis unit. Therefore, the initial salt concentration within the native groundwater, the unconfined aquifer maximum allowable pumping water capacity, the injected treated wastewater to the groundwater zone salt concentration, and the root zone salt concentration tolerance will manipulate the system capacity and performance in general.

The unconfined groundwater zone system is comprised of two inlet water sources and one outlet water source. The inlet water sources are the injection treated wastewater (Q_{inj}) and deep percolation water from the root zone (Q_{DP}). The outlet source is the pumped groundwater (Q_{pump}) which will be fed to the reverse osmosis unit (in other words, $Q_{pump} = Q_{Feed}$). These water sources are mixed with the native groundwater. In this section of the dissertation, for the lump model approach, uniform mixing of all inlet and outlet water sources with the native groundwater will be assumed. Furthermore, non-uniform mixing will be focused on in a later chapter of this dissertation when utilizing the areal distribution, Visual MODFLOW and MT3D, approach model. Thus, groundwater pumping, treated wastewater injection, deep percolation, and mixing within the groundwater will be acting simultaneously.

Additionally, to achieve long term water sustainability, which is one of the main goals of this dissertation, by either eliminating groundwater mining caused by well pumping, or by avoiding water logging due to water table rise caused by treated wastewater injection, a steady state water balance approach within the unconfined groundwater zone will be applied. Although, steady state water balance was assumed in the groundwater system zone, salt mass balance will be in the unsteady state (transit) form. This transit salt mass balance is due to the groundwater salt concentration variation by time as the mixing of the water sources with the native groundwater proceeds.

The remaining portion of this section will be focused on the development of groundwater design variables and their governing equations. The variables are:

- Groundwater pumped (feed to R.O. unit) water quantity, $\boldsymbol{Q_{pump} = Q_{Feed}}$
- Groundwater pumped (feed to R.O. unit) salt concentration, $\boldsymbol{C_{pump} = C_{Feed}}$
- Groundwater salt concentration, $\boldsymbol{C_{g.w.}}$
- Power consumed by the well pump system, ***Power*** $_{(well)}$

Next, to develop the governing equations for the groundwater zone system, the groundwater system will utilize the steady state water balance and transit salt mass balance approaches. Therefore, consider first the steady state water balance within the groundwater zone system, thus:

Steady state water balance of the groundwater zone

The aim of this section is to provide long term sustainable water quality and quantity by keeping the groundwater zone from mining and water logging. To do so, the pumped groundwater must be replaced by an equivalent amount of water by means of another source(s), hence, replacing the water depleted from the unconfined groundwater aquifer. The unconfined groundwater zone system is comprised of two inlet water sources and one outlet water source. The inlet water sources are the injection treated wastewater ($\boldsymbol{Q_{inj}}$) and deep percolation water from the root zone ($\boldsymbol{Q_{DP}}$). The outlet source is the pumped groundwater (Q_{pump}) which will be fed to the reverse osmosis unit (thus, $Q_{pump} = Q_{Feed}$) (Figure 3.5). From the steady state flow balance equation approach in the unconfined groundwater zone (Figure 3.5) assuming pumping and mixing with the groundwater is simultaneous, the groundwater governing equations can be calculated. Thus,

$$Q_{Feed} = Q_{inj} + Q_{DP} \tag{3.32}$$

Figure 3.5 The steady state water balance of the groundwater zone.

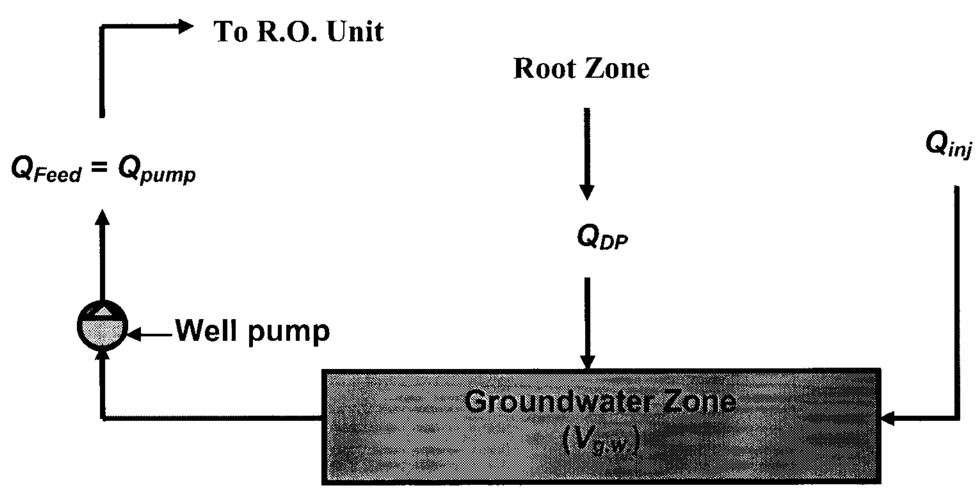

where,

Q_{inj} = Total treated wastewater injection to the native groundwater zone [L^3 / T].

Equation (3.32) represents one of the main steady state water balance governing equations of the groundwater zone.

Transit salt mass balance of the groundwater zone

To perform a mass balance within the groundwater zone, the unconfined groundwater zone system is comprised of two inlet salt mass sources and one outlet salt mass source. The inlet sources are the salt mass of the injection treated wastewater (M_{inj}) and the salt mass of deep percolation water from the rooting zone (M_{DP}). The outlet salt mass source is the mass of pumped groundwater (M_{pump}) which will be fed to the reverse osmosis unit ($M_{pump} = M_{Feed}$) (Figure 3.6).

From the transit salt mass balance equation approach of the groundwater zone (Figure 3.6). Hence:

$$M_{DP} + M_{inj} - M_{Feed} = \frac{\Delta m_{g.w.}}{\Delta t} \qquad \textbf{(3.33)}$$

where,

M_{DP} = Salt mass of deep percolation water from the root zone [M/ T],

M_{inj} = Salt mass of the injected treated wastewater [M/ T],

M_{Feed} = Salt mass of feed water (pumped well salt mass, $M_{pump} = M_{Feed}$) [M/ T], and

$\frac{\Delta m_{g.w.}}{\Delta t}$ = Time rate change of mass in the groundwater zone [M /T].

Figure 3.6 The transit salt mass balance of the groundwater system.

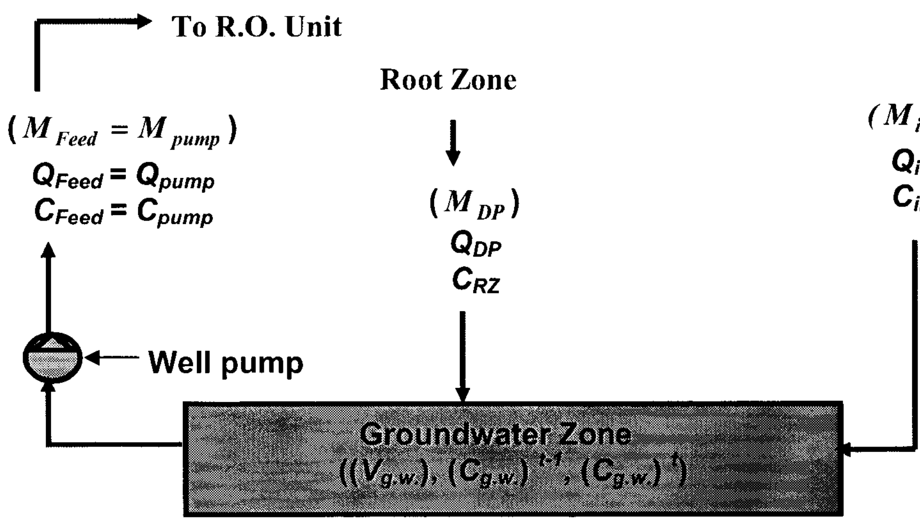

Knowing

$$M_{inj} = Q_{inj} * C_{inj} \qquad \textbf{(3.34)}$$

where,

Q_{inj} = Total treated wastewater injected into the groundwater zone [L^3/T],

C_{inj} = Injected treated wastewater salt concentration [mg/l].

Taking the rate of change of salt mass in the groundwater zone as the difference between the beginning time and ending time of the mixing period, time rate change of mass in the groundwater zone will be:

$$\frac{\Delta\, m_{g.w.}}{\Delta\, t} = \frac{V_{g.w.} * C^{t}_{g.w.} - V_{g.w.} * C^{t-1}_{g.w.}}{\Delta\, t} \tag{3.35}$$

where,

$V_{g.w.}$ = Groundwater volume [L^3],

$C_{g.w.}$ = Groundwater salt concentration [mg/l],

$\Delta\, t$ = Simulation time [season],

t = Present time cycle,

$t-1$ = Initial or previous time cycle.

Thus, substituting Equations (3.7), (3.13), (3.34), and (3.35) in Equation (3.33), Equation (3.33) will be:

$$(Q_{DP} * C_{RZ}) + (Q_{inj} * C_{inj}) - (Q_{Feed} * C_{Feed}) = \left(\frac{V_{g.w.} * C^{t}_{g.w.} - V_{g.w.} * C^{t-1}_{g.w.}}{\Delta t} \right) \quad (3.34)$$

Since the lump model is using a simplified approach, the groundwater zone will be assumed as one mixing cell. Therefore, the groundwater pumped salt concentration ($C_{pump} = C_{Feed}$) will be assumed to be the average of the initial time cycle (or previous time cycle) of the groundwater salt concentration ($C^{t-1}_{g.w.}$) and the end time cycle groundwater salt concentration ($C^{t}_{g.w.}$). In addition, the groundwater pumped salt concentration ($C_{pump} = C_{Feed}$) calculation will be implicitly iterated, using the Visual basic model, to represent the best representative C_{Feed} value within a certain tolerance value (tolerance value = 0.01). Thus,

$$C_{Feed} = \left(\frac{C^{t-1}_{g.w.} + C^{t}_{g.w.}}{2} \right) \quad (3.35)$$

where,

$C_{Feed} = C_{pump}$ = The pumped water salt concentration which will be fed to the reverse osmosis unit, [mg/l].

What is more, the treated wastewater salt concentration (C_{inj}) value is constant. Its value depends on the treatment stage level (tertiary or secondary level) that was treated for. Moreover, the root zone salt concentration tolerance (C_{RZ}) value is constant too, and its value depends on the crop type and its threshold tolerance level to salts. Additionally, deep percolation (Q_{DP}) quantities values during the simulation periods are minute compared to the irrigation ($Q_{irr(permeate)}$), evapotranspiration (Q_{ETc}), and groundwater pumping ($Q_{pump} = Q_{Feed}$) quality values and will not change significantly during the simulation periods. Finally, the groundwater volume ($V_{g.w.}$) will not change during simulation period, owing to the steady state water balance approach. For all the reasons above, the treated wastewater injection amount value (Q_{inj}) will not significantly change during the simulation periods. Therefore, the only significant changes occur in the groundwater zone is the salt concentration ($C_{g.w.}$) due to the groundwater mixing as the simulation proceeds. As a conclusion, steady state water balance was assumed for the entire inlet and outlet water sources (Q_{Feed}, Q_{DP}, and Q_{inj}) to the groundwater zone during simulation periods. But, due to the groundwater salt concentration ($C_{g.w.}$) variance from one simulation period to the other, individual water source quantity will slightly vary from one simulation period to the other while being under steady state water balance within any single simulation period. This slight variance in the inlet and outlet water sources will make these sources to be under transit flow condition, which contradict with the initial assumption of steady state flow. In other words, the water sources will behave in quasi steady state water balance from one simulation period to the other while behaving steadily within any single simulation period. Therefore, due to the slight variances in the individual water source quantity, the assumption of steady state will be implemented in driving the governing equation of the general conceptual design system, but a transit flow approach will be applied to all simulation calculations. Hence, Equation (3.33) will be as follows after substituting Equation (3.35):

$$\left(Q_{DP} * C_{RZ}\right) + \left(Q_{inj} * C_{inj}\right) - \left(Q_{Feed} * \left(\frac{C^{t-1}_{g.w.} + C^{t}_{g.w.}}{2}\right)\right) =$$

$$\left(\frac{V_{g.w.} * C^{t}_{g.w.} - V_{g.w.} * C^{t-1}_{g.w.}}{\Delta t}\right) \quad \textbf{(3.36)}$$

Rearranging Equation (3.36) for the groundwater salt concentration at present time ($C^{t}_{g.w.}$):

$$C^{t}_{g.w.} = \left(\frac{\left(Q_{Dp} * C_{RZ}\right) + \left(Q_{inj} * C_{inj}\right) - \left(\frac{Q_{Feed}}{2} * C^{t-1}_{g.w.}\right) + \left(\frac{V_{g.w.}}{\Delta t} * C^{t-1}_{g.w.}\right)}{\left(\frac{V_{g.w.}}{\Delta t} + \frac{Q_{Feed}}{2}\right)}\right) \quad \textbf{(3.37)}$$

Of note, Equation (3.37) represents another key governing equation for the groundwater salt concentration in the groundwater zone.

Power, a key design variable, will be considered next. Power is the main derive aspect of evaluating the system performance and its feasibility. Hence, the power exerted by pumping the groundwater to be used as feed water to the reverse osmosis system can be found as,

$$Power_{well} = \left[\left(\frac{\gamma * Q_{Feed} * H_{lift}}{\eta_{well}}\right)\right] \quad \textbf{(3.38)}$$

where,

$\boldsymbol{Power_{well}}$ = Power consumed by the groundwater pump [Kjoules / season].

$\boldsymbol{Q_{Feed}}$ = Pumped groundwater flow rate, which will be fed to the reverse osmosis system [L^3/T],

$\boldsymbol{H_{lift}}$ = The height of water to be lifted to the ground surface [L],

γ = Specific weight of water ($\gamma = \rho * g$) [kg / m^2 sec.], and

$\eta_{(well)}$ = Groundwater electrical well pump efficiency, for electrical pump $\eta_{(well)}$ = 50 – 80 %.

furthermore,

$$\boldsymbol{H_{lift} = \left(h_{surface} - h_o\right) + S_w} \qquad \textbf{(3.39)}$$

where,

$\boldsymbol{h_{surface}}$ = The height of ground surface from the bedrock [L],

h_o = Water table hydraulic head prior to pumping or water table hydraulic head at zero drawdown [L], and

S_w = Steady state drawdown of water hydraulic head at the well [L].

Substituting Equation (3.39) in Equation (3.38):

$$Power_{well} = \left[\left(\frac{\gamma * Q_{Feed} * (h_{surface} - h_o) + S_w}{\eta_{well}} \right) \right] \qquad \textbf{(3.40)}$$

Of note, Equation (3.40) characterizes the power consumed by the pumping well, and it is one of the major governing equations in the groundwater zone.

And,

$$S_w = h_o - h_w \qquad \textbf{(3.41)}$$

where,

h_w = Hydraulic water head at the well [L].

The next step is finding the pumping flow rate governing equation, which will be fed to the reverse osmosis unit ($Q_{pump} = Q_{Feed}$). Therefore, starting with the Darcy's law for the movement of water through a porous media:

$$Q = A * q \tag{3.42}$$

where,

$\boldsymbol{Q}$ = flow rate of water through the porous media [L^3/T],

$\boldsymbol{A}$ = Cross section area, perpendicular to the flow [L^2], and

$\boldsymbol{q}$ = Darcy's velocity [L/T].

From the steady state radial flow to a pump well equation in an unconfined saturated aquifer and a fully penetrated well, Darcy's velocity will be:

$$q = K * \frac{dh}{dr} \tag{3.43}$$

where,

$\boldsymbol{q}$ = Darcy's velocity [L/T],

$\boldsymbol{K}$ = Hydraulic conductivity of the aquifer [L/T], and

$\frac{dh}{dr}$ = Hydraulic gradient [dimensionless].

Substituting Equation (3.43) in Equation (3.42):

$$Q = (2\pi rh) * K * \frac{dh}{dr} \qquad (3.44)$$

where,

$2\pi rh$ = Surface area [L^2],

h = Water table height from the aquifer bed [L], and

r = Radius [L].

Separating Equation (3.44) variables and integrating for the water table hydraulic head between the well hydraulic head elevation (h_w) and the water table hydraulic head at zero drawdown (h_o), for the dissertation purpose, Q becomes ($Q_{pump} = Q_{Feed}$). Thus:

$$Q_{Feed} = \pi * K * \left(\frac{(h_o^2 - h_w^2)}{Ln(\frac{r_o}{r_w})} \right) \qquad (3.45)$$

where,

r_o = Intercept of distance drawdown line with zero drawdown axis [L], and

r_w = Pumping well radius [L].

Rearranging Equation (3.45) as follows,

$$h_w = \sqrt{\left(h_o^2 - \frac{Q_{Feed}}{\pi * K} * ln\left(\frac{r_o}{r_w}\right)\right)} \quad \textbf{(3.46)}$$

and substituting Equation (3.46) in Equation (3.41). Thus,

$$S_w = h_o - \sqrt{\left(h_o^2 - \frac{Q_{Feed}}{\pi * K} * ln\left(\frac{r_o}{r_w}\right)\right)} \quad \textbf{(3.47)}$$

In conclusion, Equation (3.47) represents another key governing equation of the groundwater zone, which symbolizes the pumping well steady state drawdown.

As a final point, Table 3.2 is the representation of the assumed groundwater input data variables that will be used for all future simulations calculation in this dissertation.

3.1.4 Field Area Estimation Governing Equations

Field area estimation and calculation is one of the main aspects in my model, which is directly related to the maximum actual evapotranspiration amount per day in the farming season and the maximum allowable drawdown of the water table adjacent to the pumping well. Moreover, from the reverse osmosis recovery Equation (3.10), the pumping flow rate Equation (3.45), and the maximum crop evapotranspiration amount per day (m/day) during the farming season, $ETc_{(max)}$, the field area can be estimated, assuming leaching will be practiced at the end of the irrigation season.

Table 3.2 Groundwater assumed input data variables for all simulations.

Variable	Value or Type	Remarks
Aquifer Type	Unconfined Aquifer	
Aquifer Thickness	60 (m)	
r_o	1500 (m)	Intercept of distance drawdown line with zero drawdown axis.
r_w	0.5 (m)	Pumping well radius.
Well Penetration	60 (m)	Fully penetrated well
Maximum Lift	55 (m)	
$h_{w(min)}$	5 (m)	Min. allowable hydraulic water at the pump well, for max. drawdown. (min. saturated thickness)
Well pump efficiency (η_{well})	75 (%)	Average electrical well pump efficiency 50 -80 %,

Therefore, Equation (3.10) can be used, substituting $Q_{irr(permeate)(max)}$ for $Q_{irr(permeate)}$, to denote the maximum irrigation (permeate) water rate that can be produced by the R.O. unit to meet the maximum actual crop evapotranspiration amount per day (m/day) during the farming season ($ETc_{(max)}$). Additionally, $Q_{Feed(max)}$ can be substituted for Q_{Feed} to denote for the maximum allowable pumping capacity rate to meet the maximum irrigation (permeate) water required (where, $Q_{pump\,(max)} = Q_{Feed\,(max)}$). Thus,

$$Q_{irr(\,permeate\,)\,(max)} = \delta * Q_{Feed\,(max)} \tag{3.48}$$

where,

$Q_{irr(permeate)(max)}$ = Maximum irrigation (permeate) water capacity rate [m^3/day], and

$Q_{Feed\,(max)}$ = Maximum allowable pumping rate ($Q_{pump\,(max)} = Q_{Feed\,(max)}$) for maximum allowable drawdown [m^3/day].

Next, it is necessary to find the maximum allowable pumping water rate which will be fed to the reverse osmosis unit ($Q_{pump\,(max)} = Q_{Feed\,(max)}$). Thus, Equation (3.45) can be used, substituting the minimum allowable hydraulic head at the well ($h_{w\,(min)}$) (minimum saturated thickness) instead of the hydraulic head at the well (h_w), to represent the maximum allowable pumping capacity ($Q_{pump(max)} = Q_{Feed\,(max)}$) for the maximum allowable drawdown (Figure 3.7). Therefore

$$Q_{Feed\,(max)} = \pi * K * \left[\frac{\left(h_o^2 - h_{w\,(min)}^2\right)}{ln\left(\frac{r_o}{r_w}\right)} \right] \tag{3.49}$$

where,

$Q_{Feed\ (max)}$ = Maximum allowable pumping rate capacity for maximum allowable drawdown [m^3/day], and

$h_{w\ (min)}$ = Minimum allowable hydraulic water head at the pumping well (minimum saturated thickness) for maximum allowable drawdown (Figure 3.7) [L].

Figure 3.7 General conceptual mode layout for maximum allowable drawdown and minimum allowable hydraulic water head at the pumping well.

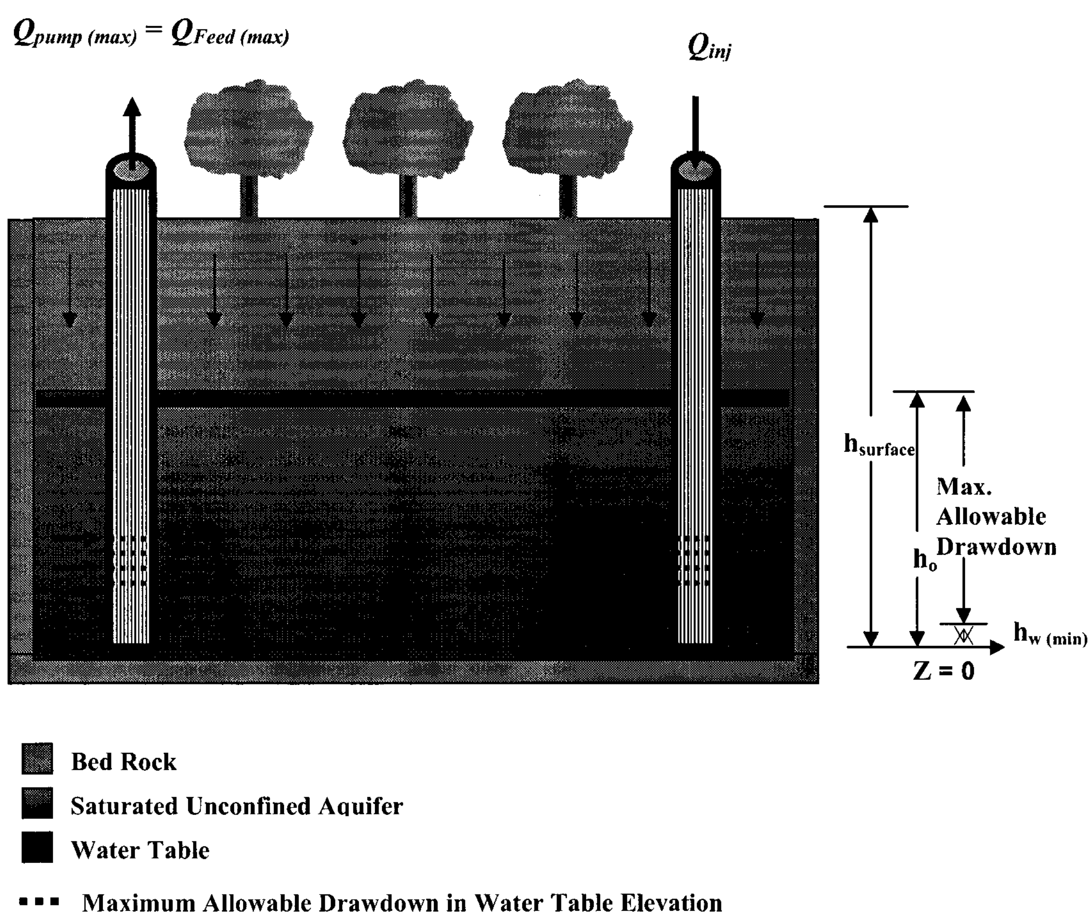

Knowing $Q_{Feed\,(max)}$ is the maximum allowable pumping rate for maximum allowable drawdown does not mean that the well will pump at maximum capacity, $Q_{Feed\,(max)}$, all the time, but, only to meet the maximum actual crop evapotranspiration (m/day), $ETc_{(max)}$, when it is required during the season.

Therefore, substitute Equation (3.49) in Equation (3.48) and divide by the maximum crop evapotranspiration amount per day during the farming season. The latter will insure sufficient water demand to meet the maximum evapotranspiration rate in the season. As a result, estimated field area will be:

$$A_F = \delta * \left[\frac{\dfrac{\pi * K * \left(h_o^2 - h_{w\,(min)}^2\right)}{ln\left(\dfrac{r_o}{r_w}\right)}}{ETc_{(max)}} \right] \tag{3.50}$$

where,

A_F = Estimated field area [m^2],

$ET_{c\,(max)}$ = Maximum actual crop evapotranspiration amount per day during the farming season [m/day], and

δ = Reverse osmosis recovery [-].

Finally, Equation (3.50) represents the main governing equation in estimating the field area size to cope with the maximum allowable pumping rate for maximum allowable drawdown to meet the maximum evapotranspiration when it is required during the season.

In conclusion, the conceptual design system is controlled by design system variables and decision variables, where the design system variables are used mostly for calculation purposes. On the other hand, the design decision variables control the performance of the system by means of power consumption. Table 3.3 and Figure 3.8 illustrate the conceptual design system variables and their types and the summary of the lump model governing equations, respectively.

Table 3.3 Conceptual design system variables and their types.

Variable	Variable Type	Variable	Variable Type
$Q_{irr\ (permeate)}$	Design System	C_{Feed}	Design System
Q_{Brine}	Design System	δ	Decision
Q_{ETc}	Design System	n	Decision
$ETc_{\ (max)}$	Design System	$C_{s(Feed)}$	Design System
Q_{inj}	Design System	$C_{s(Permeate)}$	Design System
Q_{DP}	Design System	Ps_{Feed}	Design System
$V_{g.w.}$	Design System	$Ps_{(permeted)}$	Design System
Q_{Feed}	Design System	A_{Field}	Design System
$C_{irr\ (permeate)}$	Design System	Δt	Design System
C_{Brine}	Design System	S_w	Design System
C_{ET}	Design System	$Power_{(R.O.)}$	Design System
C_{inj}	Design System	$Power_{\ (well)}$	Design System
C_{RZ}	Decision	$\eta_{(well)}$	Decision
$(C_{g.w.})^{t}$	Design System	$\eta_{(R.O.)}$	Decision

Figure 3.8 Summary of the general lump model governing equations.

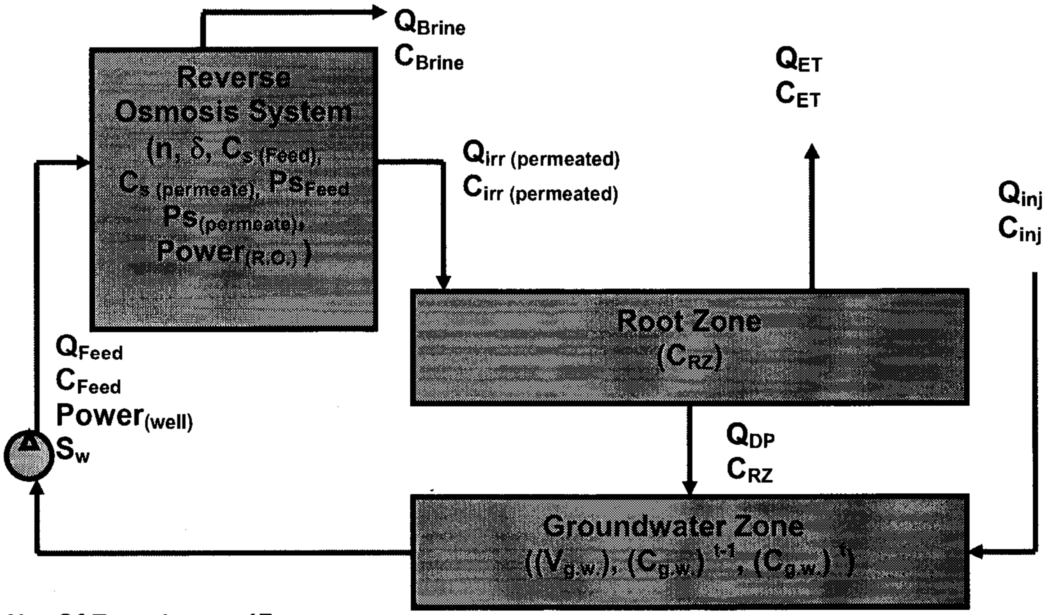

No. Of Equations = 17

Root (Vadose) Zone Governing Equations: **Equation No.**

1) $Q_{irr\,(permeate)} = Q_{ETc} + Q_{DP}$ (3.3)

2) $Q_{irr\,(permeate)} * C_{irr\,(permeate)} = Q_{ETc} * C_{ET} + Q_{DP} * C_{RZ}$ (3.8)

Reverse Osmosis Governing Equations:

3) $Q_{Feed} = Q_{irr\,(permeate)} + Q_{Brine}$ (3.9)

4) $\delta = (Q_{irr\,(permeate)}) / (Q_{Feed})$ (3.10)

5) $Q_{Feed} * C_{Feed} = Q_{irr\,(permeate)} * C_{irr\,(permeate)} + Q_{Brine} * C_{Brine}$ (3.16)

6) $Ps_{Feed} = C_{s\,(Feed.)} * R * T$ (3.20)

7) $Ps_{(permeate)} = C_{s\,(Permeate)} * R * T$ (3.21)

8) $C_{s\,(Feed)} = (\Psi) * (C_{Feed} / (1000 * \varpi))$ (3.28)

9) $C_{s\,(Permeate)} = (\Psi) * (C_{irr\,(permeate)} / (1000 * \varpi))$ (3.29)

10) $C_{irr\,(permeate)} = n * C_{Feed} * ((1 - (\delta / 2)) / (1 - \delta))$ (3.30)

11) $Power_{(R.O.)} = ((Ps_{Feed} - Ps_{permeate}) * Q_{irr\,(permeate)}) / (\eta_{(R.O.)})$ (3.31)

Groundwater Zone Governing Equations:

12) $Q_{Feed} = Q_{inj} + Q_{DP}$ (3.32)

13) $C_{Feed} = (((C_{g.w.})^{t-1} + (C_{g.w.})^{t}) / 2)$ (3.35)

14) $(C_{g.w.})^{t} = ((V_{g.w.} / \Delta t) * (C_{g.w.})^{t-1} + Q_{inj} * C_{inj} + Q_{DP} * C_{RZ} - (Q_{Feed} / 2) * (C_{g.w.})^{t-1}) / ((V_{g.w.} / \Delta t) + (Q_{Feed} / 2))$, (pumping and mixing are simultaneously). (3.37)

15) $Power_{(well)} = (\gamma * (Q_{Feed}) * H_{lift}) / \eta_{(well)} = (\gamma * Q_{Feed} * ((h_{surface} - h_o) + S_w)) / \eta_{(well)}$ (3.38), (3.40)

16) $S_w = h_o - [(h_o^2 - (Q_{Feed} / (\pi * K) * \ln (r_o / r_w))]^{0.5}$ (3.47)

Field Area Estimation Governing Equation:

17) $A_{Field} = (\delta) * (Q_{Feed} / ETc_{(max)}) = (\delta) * (\pi * K * (h_o^2 - h_{w\,(min)}^2) / (\ln (r_o / r_w))) / ETc_{(max)}$ (3.50)
(Note: for A_{Field} calculation, Q_{Feed} in (m^3/day) and $ETc_{(max)}$ in (m/day))

No. of Variables = 27

$Q_{irr\,(permeate)}$, Q_{Brine}, Q_{ETc}, $ETc_{(max)}$, Q_{inj}, Q_{DP}, $V_{g.w.}$, Q_{Feed}, $C_{irr\,(permeate)}$, C_{Brine}, C_{ET}, C_{inj}, C_{RZ}, $(C_{g.w.})^{t}$, $(C_{g.w.})^{t-1}$, C_{Feed}, δ, n, $C_{s(Feed)}$, $C_{s(Permeate)}$, Ps_{Feed}, $Ps_{(permeted)}$, A_{Field}, Δt, S_w, $Power_{(R.O.)}$, $Power_{(well)}$.

No. of Known Variables = 7

C_{ET}, C_{inj}, $(C_{g.w.})^{t-1}$, Q_{ETc}, $ETc_{(max)}$, $V_{g.w.}$, Δt.

No. of Decision Variables = 3

n, δ, C_{RZ}

3.2 General Conceptual Design System Simulation

Calculating and simulating the general simulation conceptual design system for the lump model will be conducted in the following order:

1. Calculating the estimated field area, A_F, from Equation (3.50). Thus,

$$A_F = \delta * \left[\frac{\dfrac{2 * \pi * K * \left(h_o^2 - h_{w\,(min)}^2\right)}{ln\left(\dfrac{r_o}{r_w}\right)}}{ETc_{(max)}} \right]$$

2. Calculating C_{Feed} while using an iteration approach. Thus, from Equation (3.35) C_{Feed} will be equal to

$$C_{Feed} = \left(\frac{C_{g.w.}^{t-1} + C_{g.w.}^{t}}{2} \right)$$

3. Calculating $C_{irr\,(permeate)}$, from Equation (3.30). Thus,

$$C_{irr(\,permeate\,)} = n * C_{Feed} * \left[\frac{1 - \dfrac{\delta}{2}}{1 - \delta} \right]$$

4. Calculating $Q_{irr\,(\mathrm{permeate})}$, from Equation (3.8). Thus,

$$Q_{irr\,(permeate)} * C_{irr\,(permeate)} = Q_{ET_c} * C_{ET} + Q_{DP} * C_{RZ}$$

Knowing that plants evapotranspirate pure water, therefore, $C_{ET_c} = 0$.

Consequently, Equation (3.8) will be:

$$Q_{irr\,(permeate)} * C_{irr\,(permeate)} = Q_{DP} * C_{RZ} \tag{3.51}$$

Rearranging Equation (3.51), therefore

$$Q_{DP} = Q_{irr\,(permeate)} * \left(\frac{C_{irr\,(permeate)}}{C_{RZ}} \right) \tag{3.52}$$

Now, substituting Equation (3.52) into Equation (3.2) and rearranging $Q_{irr\,(\mathrm{permeate})}$, Equation (3.2) is:

$$Q_{irr\,(permeate)} - Q_{ET_c} - Q_{DP} = 0 \tag{3.2}$$

As a result, the modified equation of calculating $Q_{irr\,(\mathrm{permeate})}$, which I will use in my simulation model, will be:

$$Q_{irr(permeate)} = \left(\frac{Q_{ET_C}}{1 - \left[\frac{C_{irr(permeate)}}{C_{RZ}} \right]} \right) \quad \textbf{(3.53)}$$

Of note, from the above Equation (3.53), it is obvious that there is proportional relationship between $C_{irr(permeate)}$ and $Q_{irr(permeate)}$. Additionally, there is an inverse proportionality relationship between C_{RZ} and $Q_{irr(permeate)}$. Table 3.4 and Figure 3.9 are illustration examples for these relationships.

5. Calculating Q_{Feed}, from Equation (3.10). Thus,

$$Recovery\%\ (\delta) = \frac{Q_{irr\ (permeated)}}{Q_{Feed}}$$

6. Calculating Q_{DP} from Equation (3.3). Thus,

$$Q_{irr(permeate)} = Q_{ET_c} + Q_{DP}$$

7. Calculating Q_{inj} from Equation (3.32). Thus,

$$Q_{Feed} = Q_{inj} + Q_{DP}$$

Table 3.4 Example of seasonal irrigation applied water requirement for irrigation system as irrigation water concentration (TDS) increases (assuming seasonal water requirement is 2m and keeping the root zone concentration at 2000 mg/l).

$C_{irr\ (permeate)}$ (mg/l)	Q_{DP} (%)	Q_{ETc} (%)	Total Applied Water (m)
50	2.5	97.5	2.05
100	5	95	2.11
200	10	90	2.22
300	15	85	2.35
400	20	80	2.50
500	25	75	2.67
600	30	70	2.86
700	35	65	3.08
800	40	60	3.33
900	45	55	3.64
1000	50	50	4.00
1100	55	45	4.44
1200	60	40	5.00
1300	65	35	5.71
1400	70	30	6.67
1500	75	25	8.00
1600	80	20	10.00
1700	85	15	13.33
1800	90	10	20.00
1900	95	5	40.00

Figure 3.9 Water movement and salt balance in the rooting zone.

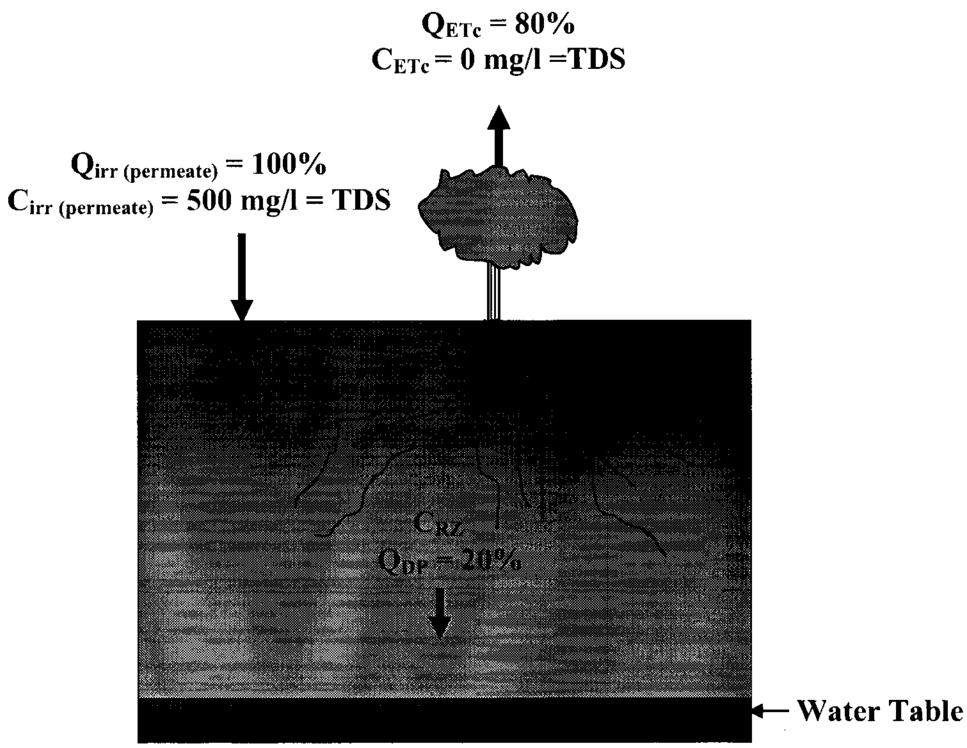

<u>Steady State Salt Balance in Root Zone:-</u>

$$C_{irr\ (permeate)}\ Q_{irr\ (permeate)} = C_{ETc}\ Q_{ETc} + C_{RZ}\ Q_{DP}$$

⇨ $C_{RZ} = (C_{irr\ (permeate)}\ Q_{irr\ (permeate)} - C_{ETc}\ Q_{ETc})\ /\ (Q_{DP})$

⇨ $C_{RZ} = (\ (500)\ (1) - (0)\ (0.8))/\ (0.2)$

⇨ $C_{RZ} = 2500$ mg/l (very High)

8. Calculating $C^{t}_{g.w.}$ from Equation (3.37), where

$$C^{t}_{g.w.} = \left(\frac{\left(Q_{Dp} * C_{RZ}\right) + \left(Q_{inj} * C_{inj}\right) - \left(\frac{Q_{Feed}}{2} * C^{t-1}_{g.w.}\right) + \left(\frac{V_{g.w.}}{\Delta t} * C^{t-1}_{g.w.}\right)}{\left(\frac{V_{g.w.}}{\Delta t} + \frac{Q_{Feed}}{2}\right)} \right)$$

9. Calculating Q_{Brine}, from Equation (3.9), where

$$Q_{Feed} = Q_{irr(permeate)} + Q_{Brine}$$

10. Calculating C_{Brine}, from Equation (3.16), where

$$Q_{Feed} * C_{Feed} = Q_{irr(permeate)} * C_{irr(permeate)} + Q_{Brine} * C_{Brine}$$

Rearranging Equation (3.16), the modified equation of calculating C_{Brine} (the reverse osmosis brine salt concentration), which I will use in my simulation model, will be:

$$C_{Brine} = \frac{(Q_{Feed} * C_{Feed}) - (Q_{irr(permeate)} * C_{irr(permeate)})}{Q_{Brine}} \qquad \textbf{(3.54)}$$

11. Calculating the osmotic pressure of feed water to the reverse osmosis unit (Ps_{Feed}), from Equation (3.20), where

$$Ps_{Feed} = Cs_{Feed} * R * T$$

Hence, from Equation (3.28), the ionic molar concentration of the feed water to the reverse osmosis unit is:

$$Cs_{Feed} = (\Psi) * \left(\frac{C_{Feed}}{\varpi} \right)$$

12. Calculating the osmotic pressure of the permeate water from the reverse osmosis, $Ps_{permeate}$, from Equation (3.21). Thus,

$$Ps_{permeate} = Cs_{irr(\,permeate\,)} * R * T$$

Hence, from Equation (3.29), the ionic molar concentration of the reverse osmosis unit permeates water is:

$$Cs_{irr(\,permeate\,)} = (\Psi) * \left(\frac{C_{irr(\,permeate\,)}}{\varpi} \right)$$

13. Calculating the power exerted by the reverse osmosis unit pump, $Power_{(R.O.)}$, from Equation (3.31). Thus,

$$Power_{(\,R.O.)} = \left[\frac{(Ps_{Feed} - Ps_{permeate}) * Q_{irr(\,permeate\,)}}{\eta_{R.O.}} \right]$$

14. Calculating the power exerted by pumping the groundwater, $Power_{well}$. By substituting Equations (3.38), (3.40), and (3.45) in Equation (3.37), the modified equation of calculating $Power_{well}$, which I will use in my simulation model, will be:

$$Power_{well} = \frac{\gamma * Q_{Feed} * \left(h_{surface} - \sqrt{h_o^2 - \frac{Q_{Feed}}{\pi * K} * ln\left(\frac{r_o}{r_w}\right)} \right)}{\eta_{(well)}} \quad (3.55)$$

15. Calculating The Total Power consumed by the system. Thus,

$$TotalPower = Power_{(R.O.)} + Power_{well} \quad (3.56)$$

3.3 The Base Case Simulation of the General Conceptual Design System

Base case simulation represents the main case of the conceptual design system simulation. The base case simulation will be analogous or representative of quasi-Kuwaiti ecosystem data. Therefore, the base case simulation input data will be similar to a semi- hypothetical case of the Wafra fields of Kuwait (Appendix II, III, and IV). Furthermore, all other diversions from the base case will be compared with the base case to evaluate the performance and durability of the system. Divergence from the base case will be looked on in the proceeding chapters, when evaluating the sensitivity and the robustness of the design conceptual system. Therefore, the base case simulation will be a mirror reflecting evaluation of the system's performance. The order of calculating the base case simulation of the general conceptual model, the 40-year simulation period, using the lump model, will be conducted in the following order:

1. The estimation of the reverse osmosis recovery percentage, $\boldsymbol{\delta}$, and the salt concentration percentage in the permeate water, $\boldsymbol{n}$, is a very crucial and critical element in this dissertation. The aim of this section is to find the most pronounced combination value of $\boldsymbol{\delta}$ and $\boldsymbol{n}$ which will result in the least power consumption system. An illustration example of the original conceptual design system was conducted with variable rational combination values of $\boldsymbol{\delta}$ and $\boldsymbol{n}$ (Table 3.5). This illustration example was simulated over a hypothetical area, 5 hectares. Simulation calculation procedures followed similar steps as in Section 3.2. The simulation was conducted over 40 years, which is the average life expectancy of the reverse osmosis unit and the pumping well system. Additionally, due to the commercial availability of the reverse osmosis recovery ranges and the salt concentration permeate membrane capacity ranges, the chosen range of $\boldsymbol{\delta}$ and $\boldsymbol{n}$ ($\boldsymbol{\delta}$ ranges from 40 % - 60 %, and $\boldsymbol{n}$ ranges from 1 – 15 %) was selected.

The results of 40-years simulation in estimating the $\boldsymbol{\delta}$ and $\boldsymbol{n}$**,** showed that the most pronounced combination value of $\boldsymbol{\delta}$ and $\boldsymbol{n}$**,** which resulted in the least power consumption, was the combination of $\boldsymbol{\delta}$ = **60 %** and $\boldsymbol{n}$ = **1%** (Figure3.10, and Table 3.6). Moreover, the result of the required amount of wastewater injection to the native groundwater showed that the combination of $\boldsymbol{\delta}$ = **60 %** and $\boldsymbol{n}$ = **1%** consumed the least amount required (Figure 3.11). As a consequence, this will reduce the wastewater costs. In conclusion, the combination of $\boldsymbol{\delta}$ = **60 %** and $\boldsymbol{n}$ = **1%** will be used in all future simulation calculations.

Table 3.5 Example data inputs for calculating the most pronounced combination values of δ and n, which will result in the least power consumption system.

Run No.	R.O. Recovery (δ) %	R.O. Salt Concentration permeate (n) %	ETc (m/se)	C_{RZ} (mg/l)	C_{inj} (mg/l)	Φ	K (m/d)	h_o (m)	$(C_{g.w.})^{t-1}$ (mg/l)
1	40	1	1.5	2000	1000	0.3	5	35	6000
2		5	1.5	2000	1000	0.3	5	35	6000
3		10	1.5	2000	1000	0.3	5	35	6000
4		15	1.5	2000	1000	0.3	5	35	6000
5	45	1	1.5	2000	1000	0.3	5	35	6000
6		5	1.5	2000	1000	0.3	5	35	6000
7		10	1.5	2000	1000	0.3	5	35	6000
8		15	1.5	2000	1000	0.3	5	35	6000
9	50	1	1.5	2000	1000	0.3	5	35	6000
10		5	1.5	2000	1000	0.3	5	35	6000
11		10	1.5	2000	1000	0.3	5	35	6000
12		15	1.5	2000	1000	0.3	5	35	6000
13	55	1	1.5	2000	1000	0.3	5	35	6000
14		5	1.5	2000	1000	0.3	5	35	6000
15		10	1.5	2000	1000	0.3	5	35	6000
16		15	1.5	2000	1000	0.3	5	35	6000
17	60	1	1.5	2000	1000	0.3	5	35	6000
18		5	1.5	2000	1000	0.3	5	35	6000
19		10	1.5	2000	1000	0.3	5	35	6000
20		15	1.5	2000	1000	0.3	5	35	6000

(m/se) = (m/season); (m/d) = (m/day).

Figure 3.10 Total power consumed in simulating the combination values of δ, n.

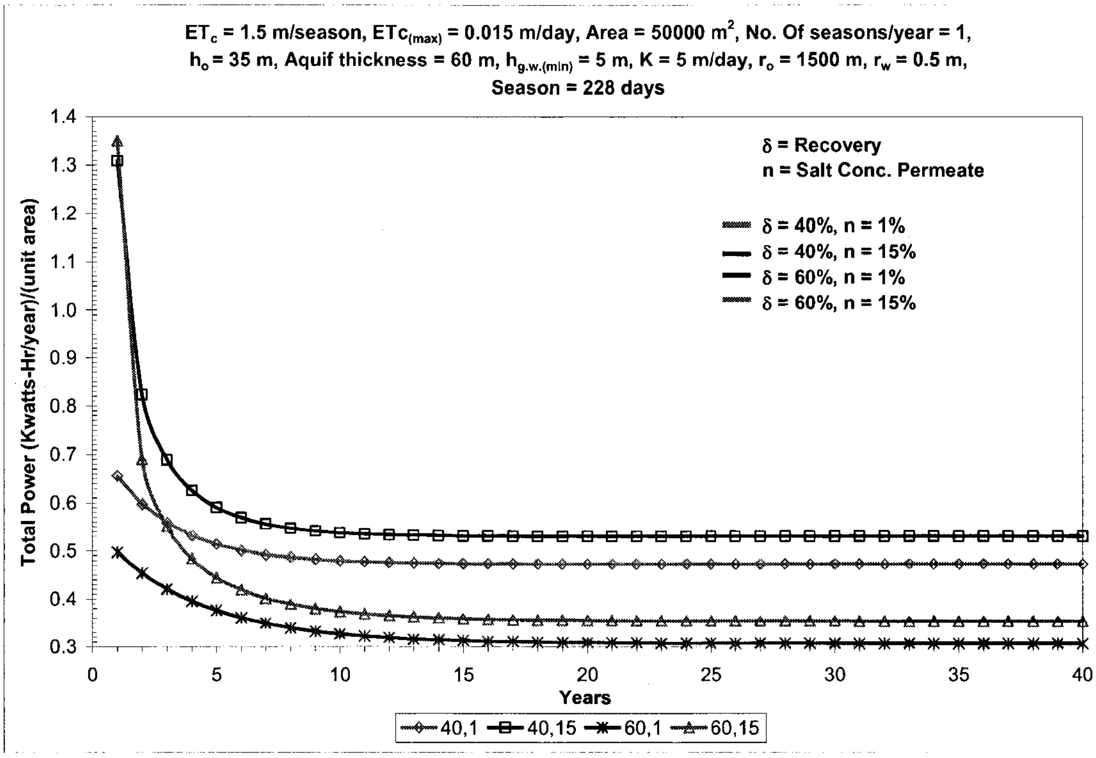

Table 3.6 Behavior of some of the design variables with regard to an increase in R.O. recovery (δ) or in R.O. salt concentration permeate %, (n).

Design Variables	Recovery, (δ) (↑)	Salt Concentration Permeate %, (n) (↑)
$C_{irr\ (permeate)}$	(↑)	(↑)
$Q_{irr\ (permeate)}$	(↑)	(↑)
Q_{Feed}	(↓)	(↑)
Q_{Brine}	(↓)	(↑)
Q_{DP}	(↑)	(↑)
Q_{inj}	(↓)	(↑)
$C_{g.w.}$	(↑)	(↓)
S_w	(↓)	(↑)
$Ps_{(permeate)}$	(↑)	(↓)
$Ps_{(Feed)}$	(↑)	(↑)
$Power_{(R.O.)}$	(↑)	(↓)
$Power_{(well)}$	(↓)	(↑)
Total Power	(↓)	(↑)

(↑) = increase; (↓) = decrease.

Figure 3.11 Required amount of treated wastewater injected in simulating the combination values of δ, n.

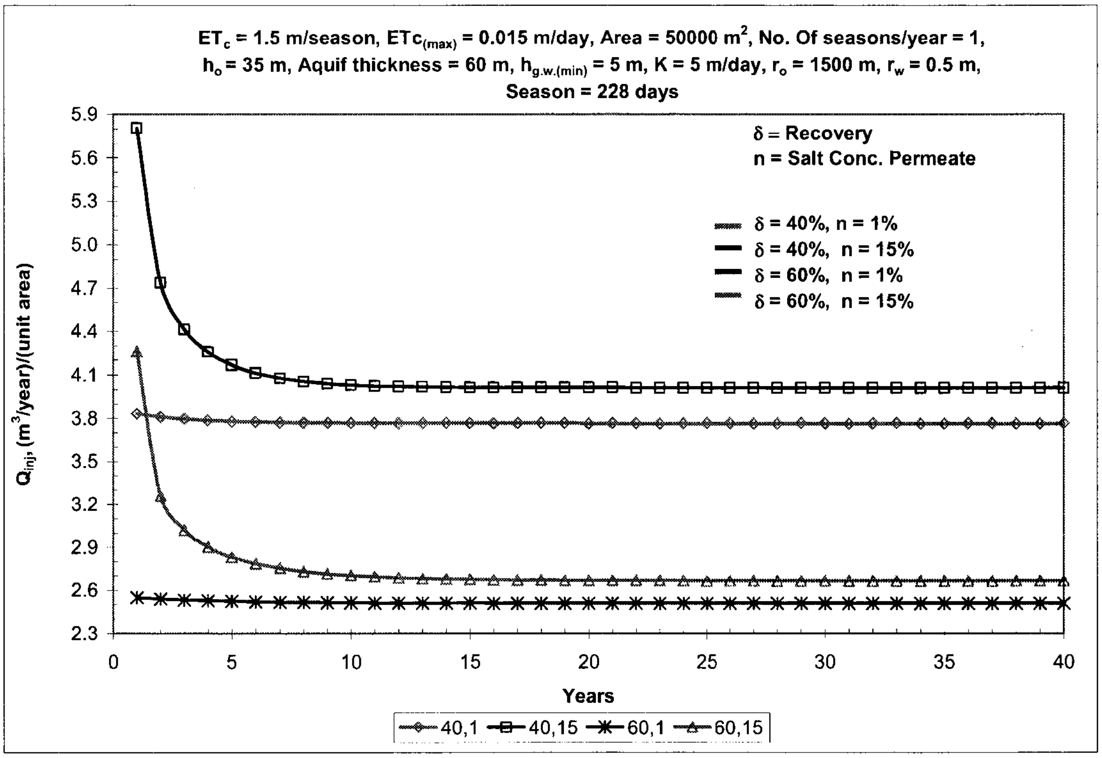

2. Actual evapotranspiration calculation for the base case simulation will be conducted while using the FAO Penman-Monteith method. Starting with the FAO Penman-Monteith method to estimate the reference evapotranspiration (***ET$_o$***). The panel of experts, organized by FAO (1998), recommended the adoption of the Penman-Monteith combination method as a new standard for reference evapotranspiration and advised on procedures for calculation of the various parameters. The FAO Penman-Monteith method was developed by defining the reference crop as a hypothetical crop with an assumed height of 0.12 m having a surface resistance of 70 s m^{-1} and an albedo of 0.23, closely resembling the evaporation of an extension surface of green grass of uniform

height, actively growing and adequately watered. Therefore, from the original Penman-Monteith equation (Appendix V) and the equations of the aerodynamic (Appendix V) and surface resistance (Appendix V), the FAO Penman-Monteith method was derived to estimate the reference evapotranspiration (ET_o). Thus,

$$ET_o = \frac{0.408 * \Delta * (R_n - G) + \gamma' * \dfrac{900}{T + 273} * u_2 (e_s - e_a)}{\Delta + \gamma' * (1 + 0.34 u_2)} \tag{3.57}$$

where,

ET_o = Reference evapotranspiration [mm/day].

R_n = Net radiation at the crop surface [MJ/ (m^2- day)],

G = Soil heat flux density [MJ/ (m^2- day)],

T = Mean air temperature at 2 m height [°C],

u_2 = Wind speed at 2 m height [m /s],

e_s = Saturation vapor pressure [KPa],

e_a = Actual vapor pressure [KPa],

$e_s - e_a$ = Saturation vapor pressure deficit [KPa],

Δ = Slope vapor pressure curve [KPa /°C], and

γ' = Psychrometric constant [KPa /°C].

The reference evapotranspiration, ET_o, provides a standard to which:

- Evapotranspiration at different periods of the year or in other regions can be compared, and
- Evapotranspiration of other crops can be related.

Apart from the site location, the FAO Penman-Monteith equation requires air temperature, humidity, radiation and wind speed data for daily, weekly, ten-day or monthly calculations. For more in depth information about evapotranspiration methods and calculations refer to Appendix V.

The next step is to calculate the actual crop evapotranspiration (ET_c). Thus, the crop evapotranspiration under standard conditions (ET_c) refers to crops grown in large fields under excellent agronomic and soil water conditions. The crop evapotranspiration differs distinctly from the reference evapotranspiration (ET_o) as the ground cover, canopy properties and aerodynamic resistance of the crop are different from grass. The effects of characteristics that distinguish field crops from grass are integrated into the crop coefficient (K_c). In the crop coefficient approach, crop evapotranspiration is calculated by multiplying ET_o by K_c.

Differences in evaporation and transpiration between field crops and the reference grass surface can be integrated in a single crop coefficient (K_c) or separated into two (dual) coefficients: a basal crop (K_{cb}) and a soil evaporation coefficient (K_e). Thus,

$$K_c = K_{cb} + K_e \tag{3.58}$$

where,

K_c = Crop coefficient [dimensionless],

K_{cb} = Basal crop coefficient [dimensionless], which represents the transpiration component of the crop evapotranspiration, and

K_e = Soil evaporation coefficient [dimensionless], which represents the soil evaporation component of the crop evapotranspiration.

In the crop coefficient approach the crop evapotranspiration, ET_c, is calculated by multiplying the reference crop evapotranspiration, ET_o, by a crop coefficient, K_c:

For single crop coefficient (Figure 3.12) ET_c equals to

$$ET_c = K_c * ET_o \tag{3.59}$$

For dual crop coefficient (Figure 3.13) ET_c equals to

$$ET_c = (K_{cb} + K_e) * ET_o \tag{4.7}$$

where,

ET_c = crop evapotranspiration [mm /day],

K_c = crop coefficient [dimensionless], and

Figure 3.12 Generalized crop coefficient curves for single crop coefficient approach (After FAO – 56).

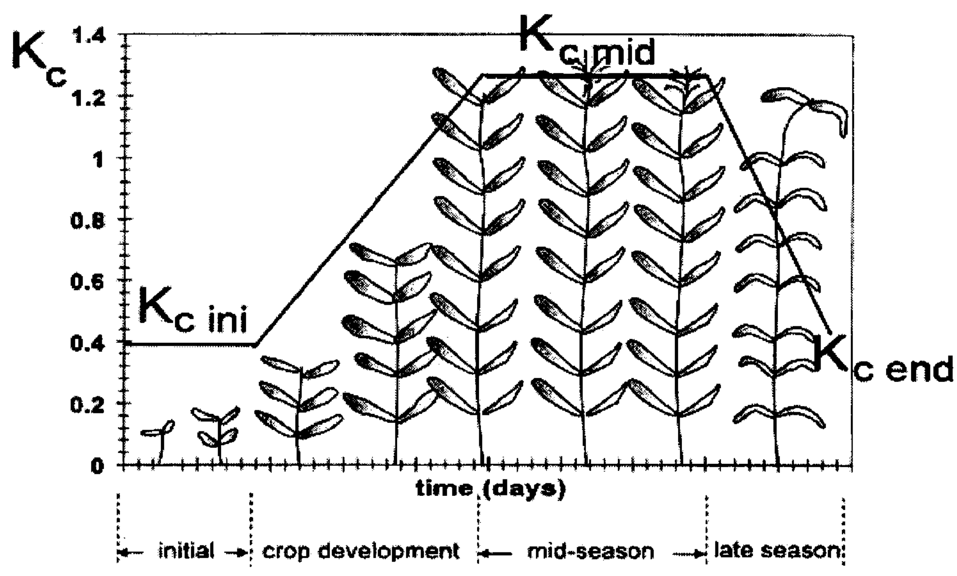

Figure 3.13 Crop coefficient curves showing the basal K_{cb} (thick line), soil evaporation *Ke* (thin line) and the corresponding single $K_c = K_{cb} + K_e$ curve (dashed) (After FAO – 56).

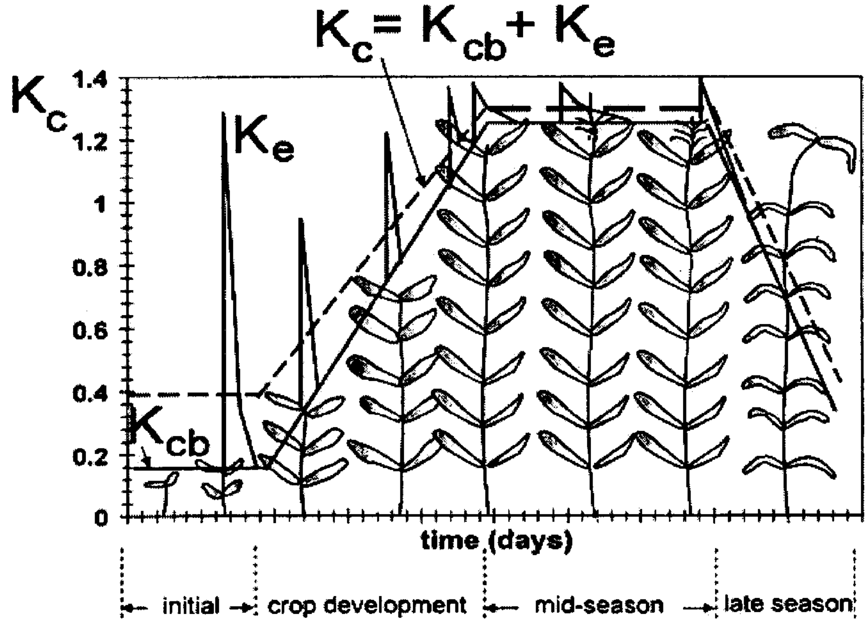

ET_o = reference crop evapotranspiration [mm /day].

The dual crop coefficient approach is more complicated and more computationally intensive than the single crop coefficient approach (K_c) (Figure 3.14). Moreover, FAO recommended that the dual crop coefficient approach be followed when improved estimation for K_c is needed, for example, to schedule irrigations for individual field on a daily basis. Therefore, the single crop coefficient approach will be utilized in this section to calculate the actual crop evapotranspirations (Figure 3.14).

Daily input data from Kuwait International Airport (30 Km from the proposed semi-hypothetical Wafra field area) was utilized to calculate the daily reference evapotranspiration (ET_o) using the FAO Penmen-Monteith method (Figure 3.15). In addition, a single crop coefficient approach was utilized to calculate the daily actual alfalfa crop evapotranspiration (ET_c). Although a seasonal actual evapotranspiration will be applied in all simulation calculations, the daily actual evapotranspiration calculations were chosen to predict and estimate the maximum crop evapotranspiration ($ETc_{(max)}$) amount per day (m/day) during the farming season. This $ETc_{(max)}$ will be the main data input to estimate and calculate the field area size (A_F) (refer to section 3.1.4). Figure 3.16 illustrates the seasonal actual crop evapotranspiration from year 1996 – 2002. Furthermore, the seasonal crop evapotranspiration is the sum of the daily (228 days) crop evapotranspiration of the planting season (the planting season starts September 1st and ends April 16th (228 days) in Kuwait). From Figure 3.16, the average seasonal crop evapotranspitation for the years of 1996 – 2002 is approximately 1.5 m/season.

Figure 3.14 Alfalfa crop coefficient curve for the single crop coefficient approach, with three cuts (After FAO – 56).

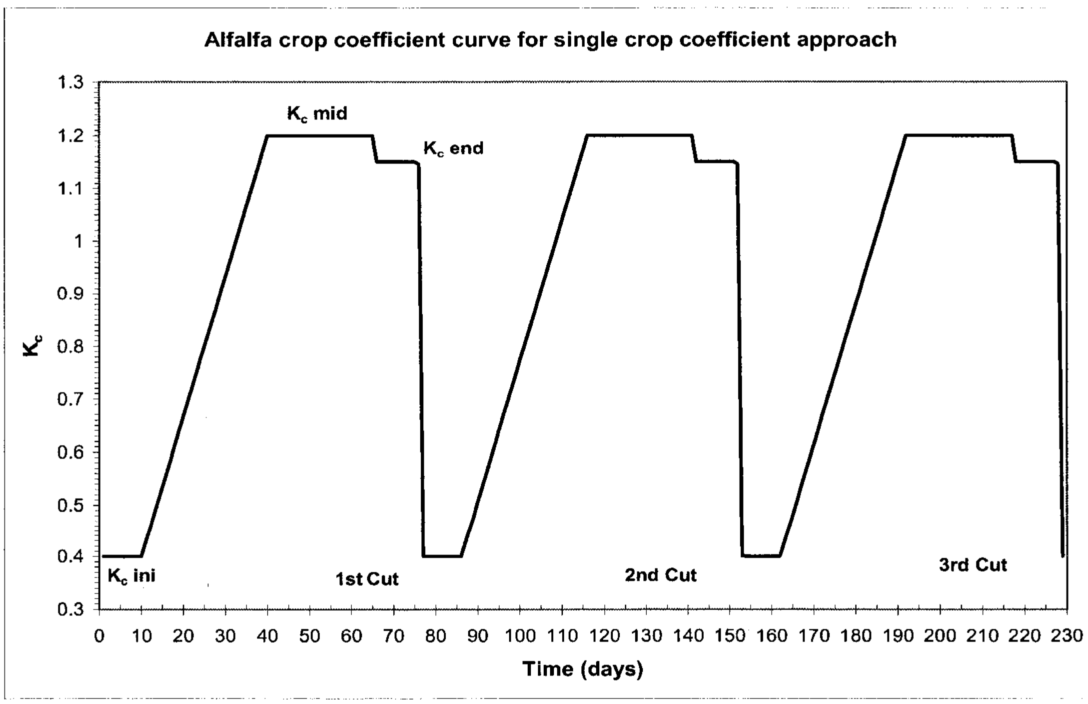

Figure 3.15 Reference evapotranspiration (*ET_o*) for Kuwait International Airport (1996 – 2002) and crop planting season dates.

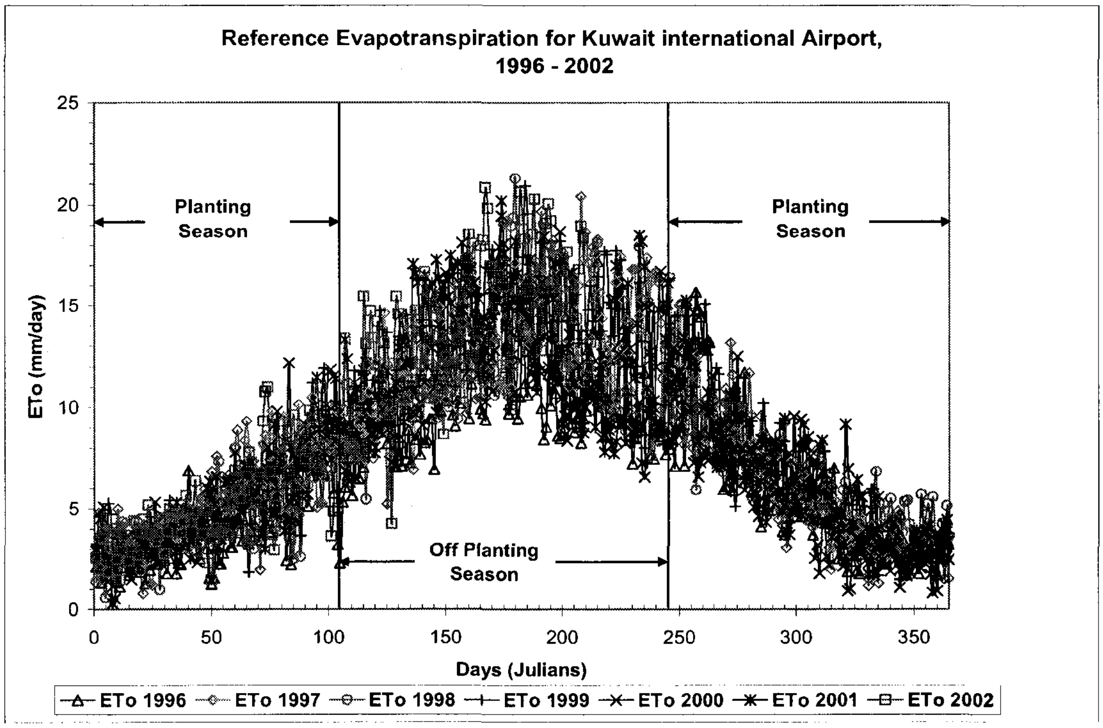

Figure 3.16 Actual alfalfa crop evapotranspiration (*ET_c*) for the planting season (228 days) in Kuwait (1996 – 2002).

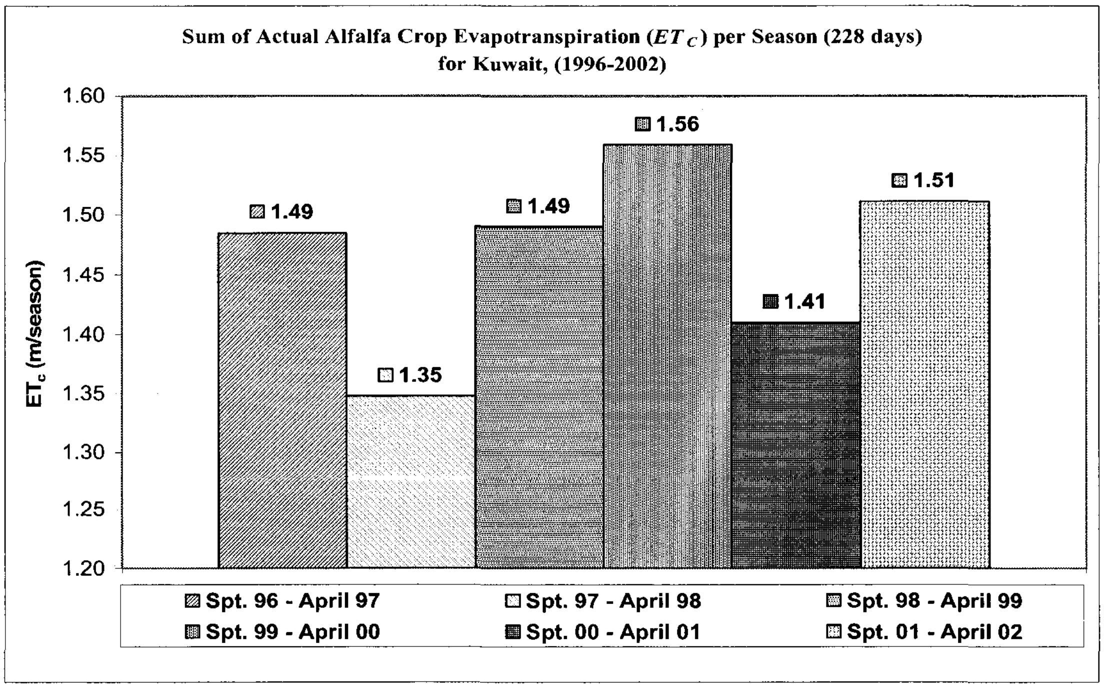

 Emad H. AlAli

Moreover, from the daily actual crop evapotranspiration calculations, the maximum actual crop evapotranspiration (***ETc*** $_{(max)}$) amount per day (m/day) during the farming season for the years of 1996 – 2002 was in the vicinity of 0.015 mm/day. As a result, the actual crop evapotranspiration (***ETc***) value of 1.5 m/season will be chosen to represent the seasonal actual crop evapotranspiration of the base case simulation. In reality, the actual crop evapotranspiration (***ETc***) value of 1.5 m/season must be adjusted (increased) to cope with the percentage losses in the water delivery system, thus increasing the amount of irrigation water required by the system. However, the value of 1.5 m/season will be considered to include these losses. In addition, the maximum actual crop evapotranspiration (***ETc*** $_{(max)}$) value of 0.015 mm/day will be chosen to represent the maximum actual crop evapotranspiration in all future simulations.

3. Field area estimation and calculation is one of the main aspects in my model, which is directly related to the maximum actual evapotranspiration amount per day in the farming season and the maximum allowable drawdown of the water table adjacent to the pumping well. Moreover, from the reverse osmosis recovery equation for maximum irrigation (permeate) water rate, Equation (3.48), the maximum pumping flow rate Equation (3.49), and the maximum crop evapotranspiration amount per day during the farming season, ***ETc*** $_{(max)}$, field area can be estimated, assuming leaching will be practiced at the end of the irrigation season. Thus,

$$A_F = \delta * \left[\frac{\frac{2 * \pi * K * \left(h_o^2 - h_{w\,(min)}^2\right)}{ln\left(\frac{r_o}{r_w}\right)}}{ETc_{(max)}} \right] \tag{3.50}$$

4. Calculating C_{Feed} while using an iteration approach method from Equation (3.35). Thus,

$$C_{Feed} = \left(\frac{C_{g.w.}^{t-1} + C_{g.w.}^{t}}{2} \right)$$

5. Calculating $C_{irr\,(permeate)}$, from Equation (3.30). Thus,

$$C_{irr(\,permeate\,)} = n * C_{Feed} * \left[\frac{1 - \frac{\delta}{2}}{1 - \delta} \right]$$

6. Calculating $Q_{irr\,\text{(permeate)}}$, from Equation (3.53). Thus,

$$Q_{irr(\,permeate\,)} = \left(\frac{Q_{ET_C}}{1 - \left[\frac{C_{irr(\,permeate\,)}}{C_{RZ}} \right]} \right)$$

7. Calculating Q_{Feed}, from Equation (3.10). Thus,

$$Recovery\%\ (\delta) = \frac{Q_{irr\ (permeated)}}{Q_{Feed}}$$

8. Calculating Q_{DP} from Equation (3.2). Thus,

$$Q_{irr(\,permeate\,)} = Q_{ET_c} + Q_{DP}$$

9. Calculating Q_{inj} from Equation (3.32). Thus,

$$Q_{Feed} = Q_{inj} + Q_{DP}$$

10. Calculating $C^{t}_{g.w.}$ from Equation (3.37). Thus,

$$C^{t}_{g.w.} = \left(\frac{\left(Q_{Dp} * C_{RZ}\right) + \left(Q_{inj} * C_{inj}\right) - \left(\frac{Q_{Feed}}{2} * C^{t-1}_{g.w.}\right) + \left(\frac{V_{g.w.}}{\Delta t} * C^{t-1}_{g.w.}\right)}{\left(\frac{V_{g.w.}}{\Delta t} + \frac{Q_{Feed}}{2}\right)} \right)$$

11. Calculating Q_{Brine} from Equation (3.9). Thus,

$$Q_{Feed} = Q_{irr(\,permeate\,)} + Q_{Brine}$$

12. Calculating C_{Brine} from Equation (3.54). Thus,

$$C_{Brine} = \frac{(Q_{Feed} * C_{Feed}) - (Q_{irr(permeate)} * C_{irr(permeate)})}{Q_{Brine}}$$

13. Calculating osmotic pressure of feed water to the reverse osmosis unit (Ps_{Feed}), from Equation (3.20). Thus,

$$Ps_{Feed} = Cs_{Feed} * R * T$$

Hence, from Equation (3.28), the ionic molar concentration of the feed water to the reverse osmosis unit is:

$$Cs_{Feed} = (\Psi) * \left(\frac{C_{Feed}}{\varpi} \right)$$

14. Calculating the osmotic pressure of the permeate water from the reverse osmosis unit ($Ps_{permeate}$) from Equation (3.21). Thus,

$$Ps_{permeate} = Cs_{irr(permeate)} * R * T$$

Hence, from Equation (3.29), the ionic molar concentration of the reverse osmosis unit permeates water is:

$$Cs_{irr(\,permeate\,)} = (\Psi) * \left(\frac{C_{irr(\,permeate\,)}}{\varpi} \right)$$

15. Calculating the power exerted by the reverse osmosis unit pump, $\boldsymbol{Power_{(R.O.)}}$, from Equation (3.31). Thus,

$$Power_{(\,R.O.)} = \left[\frac{\left(Ps_{Feed} - Ps_{permeate} \right) * Q_{irr(\,permeate\,)}}{\eta_{R.O.}} \right]$$

16. Calculating the power exerted by pumping the groundwater, $\boldsymbol{Power_{well}}$, from Equation (3.55). Thus,

$$Power_{well} = \frac{\gamma * Q_{Feed} * \left(h_{surface} - \sqrt{h_o^2 - \frac{Q_{Feed}}{\pi * K} * ln\left(\frac{r_o}{r_w} \right)} \right)}{\eta_{(\,well\,)}}$$

17. Calculating The Total Power consumed by the system, from Equation (3.56). Thus,

$$Total\,Power = Power_{(\,R.O.)} + Power_{well}$$

3.3.1 Input and Output Data of the Base Case Simulation of the General Conceptual Design System Using Lump model

The simulation of the base case of the general conceptual design system, using the Visual Basic model, was started with the data input required for the simulation of a 40-years period. Table 3.7 demonstrates all the essential input data required to simulate the base case simulation. Furthermore, Figure 3.17 illustrates the base case simulation layout. In contrast, Table 3.8 represents the major output data simulated for the base case of the general conceptual design system. In addition, Figure 3.18, Figure 3.19, and Figure 3.20 symbolize the total power consumed by the system, power consumed by the R.O. unit, and power consumed by the well pump, respectively. Finally, Figure 3.21 characterizes the required amount of injected treated wastewater to the native groundwater through the 40-years simulation period.

Table 3.7 Base case simulation of the general conceptual design system input data.

Variable	Value	Remarks
Field area	**10 (hectares)***	**Equation (3.50).**
ET_c	**1.5 (m/season)**	**Average actual evapotranspiration per season**
No. of Seasons Per year	**1**	
Season Length	**228 (days)**	
No. of Cutting Per Season	**3**	**In the 76th day of the season, 152nd day of the season, and 228th day of the season, respectively.**
$ETc_{(max)}$	**0.015 (m/day)**	**Maximum actual evapotranspiration amount per day in the farming season.**
C_{RZ}	**2000 (mg/l)**	**Maximum root salt concentration tolerance for Alfalfa crop without reduction in the yield. System management variable**
C_{inj}	**1000 (mg/l)**	**Average wastewater salt concentration after tertiary treatment.**
Φ	**0.30 (m^3/m^3)**	**Total Porosity**
$K= K_x= K_y =K_z$	**5.00 (m/day)**	**Hydraulic conductivity**
h_o	**35 (m)**	**Initial water table elevation**
$(C_{g.w.})^{t-1}$	**6000 (mg/l)**	**Initial groundwater salt concentration.**
δ	**60 (%)**	**R.O. decision variable**
n	**1 (%)**	**R.O. decision variable**
$Q_{Feed\ (max)}$	**2354.3 (m^3/day)**	**Maximum pumping flow rate per day in the farming season, Equation (3.49).**

* Area was rounded to 10 hectares.

Figure 3.17 Base case simulation of the general conceptual design system layout.

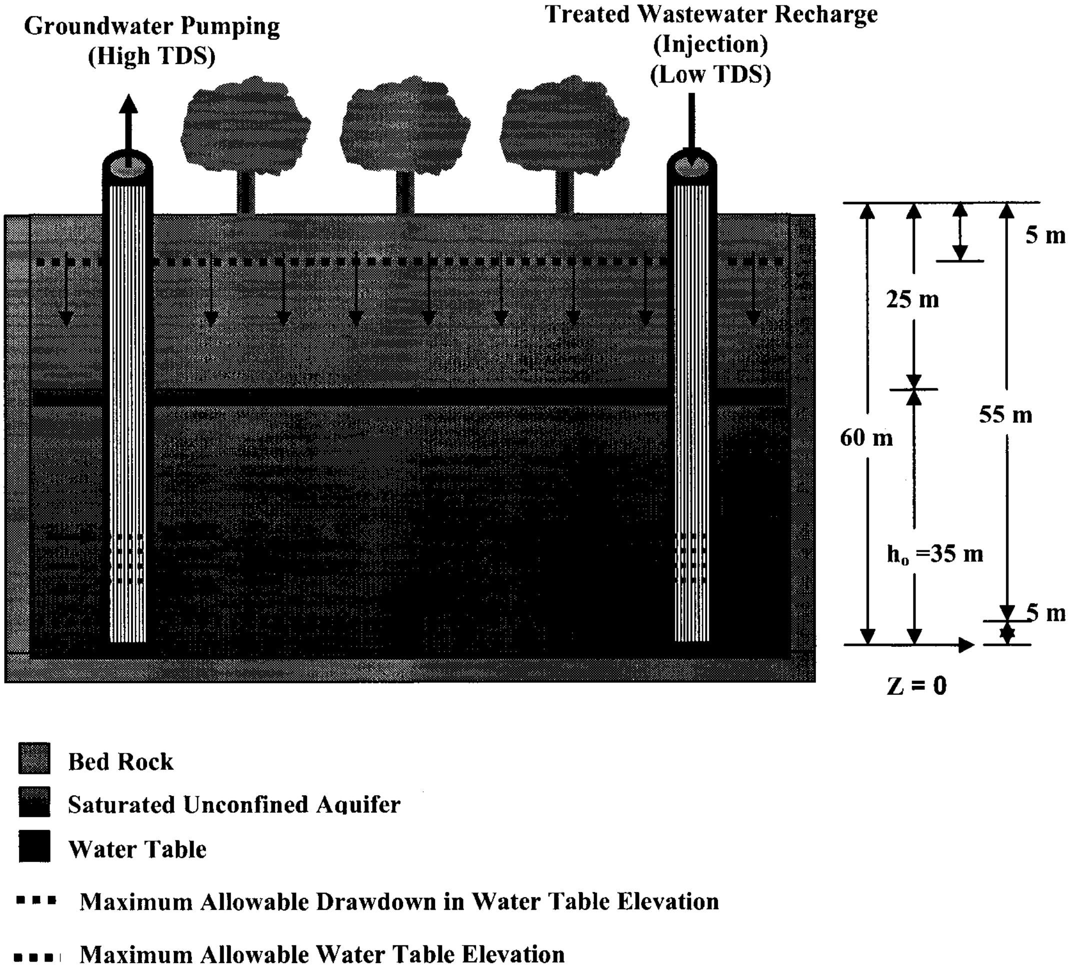

Table 3.8 Base case simulation of the general conceptual design system output data.

Year	Q_{Feed} (m^3/se)	Q_{inj} (m^3/se)	$Q_{irr(permeate)}$ (m^3/se)	Q_{DP} (m^3/se)	$Power_{(R.O.)}$ (KWH)/(ua)	$Power_{(well)}$ (KWH)/(ua)	*Total Power* (KWH)/(ua)
1	247216.0	240145.6	148329.6	7070.4	0.2164	0.3249	0.5412
2	245011.6	239263.9	147007.0	5747.8	0.1759	0.3211	0.4970
3	243332.3	238592.1	145999.4	4740.1	0.1451	0.3182	0.4633
4	242043.5	238076.6	145226.1	3966.8	0.1214	0.3160	0.4374
5	241048.9	237678.8	144629.3	3370.1	0.1031	0.3143	0.4174
6	240278.1	237370.5	144166.8	2907.6	0.0890	0.3130	0.4020
7	239678.8	237130.7	143807.3	2548.0	0.0780	0.3120	0.3899
8	239211.5	236943.9	143526.9	2267.7	0.0694	0.3112	0.3806
9	238846.7	236797.9	143308.0	2048.8	0.0627	0.3106	0.3733
10	238561.3	236683.8	143136.8	1877.5	0.0575	0.3101	0.3675
11	238337.8	236594.3	143002.7	1743.4	0.0534	0.3097	0.3631
12	238162.6	236524.3	142897.5	1638.3	0.0501	0.3094	0.3595
13	238025.1	236469.3	142815.1	1555.8	0.0476	0.3092	0.3568
14	237917.2	236426.1	142750.3	1491.1	0.0456	0.3090	0.3546
15	237832.5	236392.2	142699.5	1440.3	0.0441	0.3089	0.3529
16	237765.9	236365.6	142659.6	1400.3	0.0429	0.3087	0.3516
17	237713.6	236344.7	142628.2	1369.0	0.0419	0.3087	0.3505
18	237672.5	236328.3	142603.5	1344.3	0.0411	0.3086	0.3497
19	237640.2	236315.3	142584.1	1324.9	0.0405	0.3085	0.3491
20	237614.8	236305.2	142568.9	1309.7	0.0401	0.3085	0.3486
21	237594.9	236297.2	142556.9	1297.7	0.0397	0.3085	0.3482
22	237579.2	236290.9	142547.5	1288.3	0.0394	0.3084	0.3478
23	237566.8	236286.0	142540.1	1280.9	0.0392	0.3084	0.3476
24	237557.1	236282.1	142534.3	1275.0	0.0390	0.3084	0.3474
25	237549.5	236279.0	142529.7	1270.4	0.0389	0.3084	0.3473
26	237543.5	236276.6	142526.1	1266.8	0.0388	0.3084	0.3471
27	237538.7	236274.7	142523.2	1264.0	0.0387	0.3084	0.3470
28	237535.0	236273.2	142521.0	1261.8	0.0386	0.3083	0.3470
29	237532.1	236272.1	142519.3	1260.0	0.0386	0.3083	0.3469
30	237529.8	236271.2	142517.9	1258.6	0.0385	0.3083	0.3469
31	237528.0	236270.4	142516.8	1257.6	0.0385	0.3083	0.3468
32	237526.6	236269.9	142515.9	1256.7	0.0385	0.3083	0.3468
33	237525.5	236269.4	142515.3	1256.0	0.0384	0.3083	0.3468
34	237524.6	236269.1	142514.7	1255.5	0.0384	0.3083	0.3468
35	237523.9	236268.8	142514.3	1255.1	0.0384	0.3083	0.3467
36	237523.3	236268.6	142514.0	1254.8	0.0384	0.3083	0.3467
37	237522.9	236268.4	142513.7	1254.5	0.0384	0.3083	0.3467
38	237522.6	236268.3	142513.5	1254.3	0.0384	0.3083	0.3467
39	237522.3	236268.2	142513.4	1254.2	0.0384	0.3083	0.3467
40	237522.1	236268.1	142513.3	1254.0	0.0384	0.3083	0.3467

☐ = $Q_{irr\ (permete)\ (max)}$; (mm/se) = (mm/season); (m/d) = (m/day); (m^3/se) = (m^3/season); (KWH)/ (ua) = (Kwatts-Hr)/ (unit area)

Figure 3.18 Base case simulation output of the general conceptual design system for the total power consumed vs. simulation period.

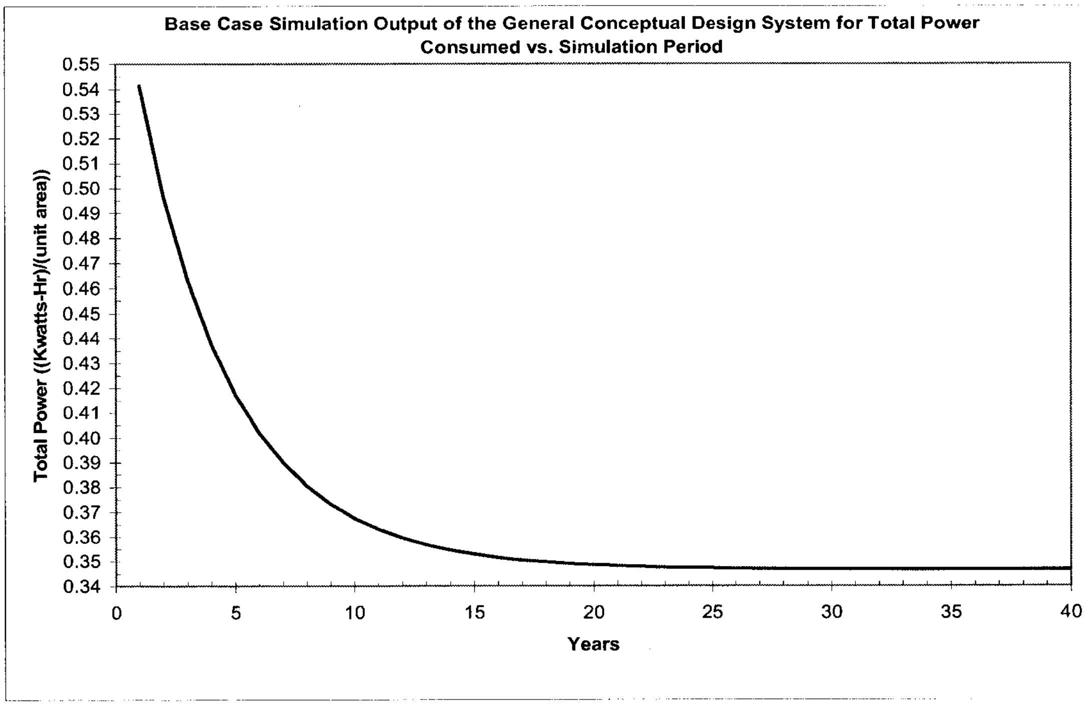

Figure 3.19 Base case simulation output of the general conceptual design system for the power consumed by reverse osmosis unit vs. simulation period.

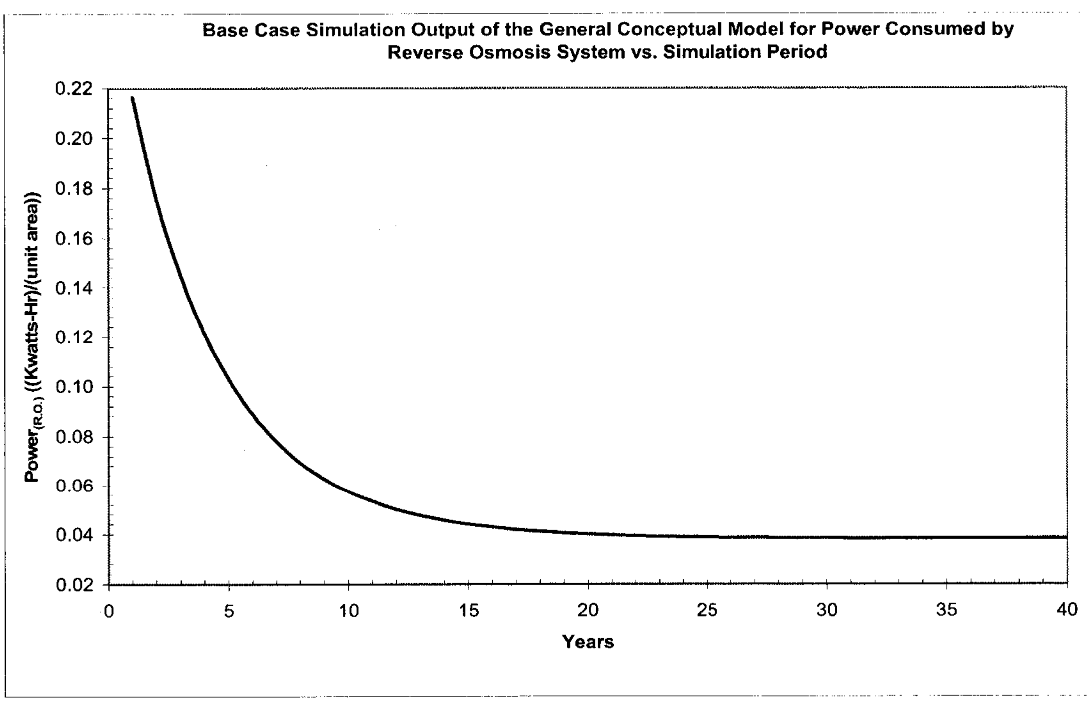

Figure 3.20 Base case simulation output of the general conceptual design system for the power consumed by well pump vs. simulation period.

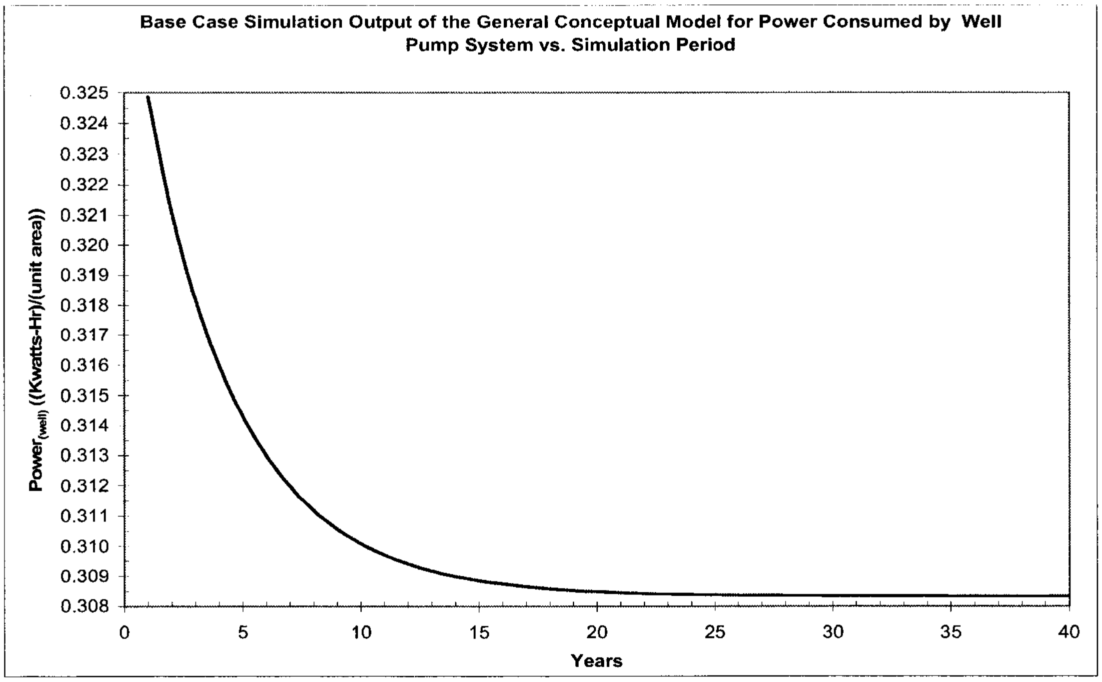

Figure 3.21 Base case simulation output of the general conceptual design system for the amount of wastewater injected to the native groundwater vs. simulation period.

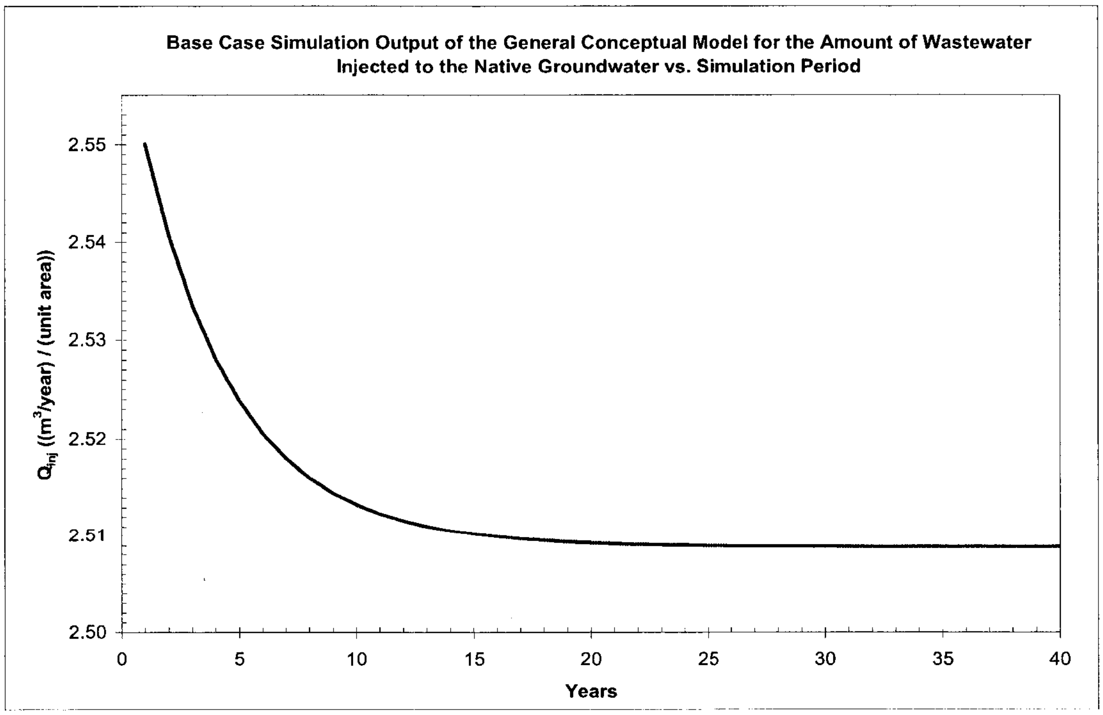

CHAPTER 4

METHODOLOGY (SENSITIVITY ANALYSIS)

4.1 Sensitivity and Performance Analysis of the General Conceptual Design System

In this chapter of the dissertation, the simulation of the general conceptual design system will be executed while using a lump simulation model approach. To test the sensitivity and performance of the general conceptual design system, the general conceptual design system will be studied for a range of input data for different variable inputs over a 40-year simulation period. These variable inputs are as follows:

- Actual crop evapotranspiration, ET_c.
- Root zone salt concentration tolerance, C_{RZ}.
- Wastewater salt concentration, C_{inj}.
- Porosity, Φ.
- Hydraulic conductivity, K.
- Initial groundwater table hydraulic head elevation, h_o.
- Initial groundwater salt concentration, $(C_{g.w.})^{t-1}$.

4.1.1 Actual Crop Evapotranspiration, ET_c

Actual crop evapotranspiration, ET_c, is one of the main variable input data in the simulation, as it corresponds to the amount of water lost to the ambient due to sensible and latent heat in general. Actual crop evapotranspiration data ranges (1 m/season – 2 m/season) were chosen to cope with and represent the semi-dry and dry climate conditions. Thus, to test the sensitivity and performance of the general conceptual design system the simulation will be executed five times, using five actual crop evapotranspiration values while keeping all other variables constant (Table 4.1). Simulation calculation procedures followed steps similar to those in Section 3.2. Moreover, all other required input data, except ET_c, will be the same as in Tables 3.1, 3.2, and 3.7.

Table 4.1 Test of the sensitivity and the performance of the general conceptual model by perturbing actual crop evapotranspiration, ET_c, values while keeping all other variables constant.

Run No.	ET_c *(m/season)*	$ET_{c\,(max)}$ *(m/day)*	C_{RZ} *(mg/l)*	C_{inj} *(mg/l)*	Φ *(m^3/m^3)*	K *(m/day)*	h_o *(m)*	$(C_{g.w.})^{t-1}$ *(mg/l)*
1	**1.00**	0.015	2000	1000	0.3	5	35	6000
2	**1.25**	0.015	2000	1000	0.3	5	35	6000
3*	**1.50**	0.015	2000	1000	0.3	5	35	6000
4	**1.75**	0.015	2000	1000	0.3	5	35	6000
5	**2.00**	0.015	2000	1000	0.3	5	35	6000

* Base case simulation.

Results for ET_c simulations of testing the sensitivity and performance of the general conceptual design system were captured in Figures 4.1, 4.2, 4.3, 4.4, and 4.5 respectively. These output result graphs were arranged by the total power required by the system, the power required by the reverse osmosis unit, the power required by the well pump system, the amount of wastewater injected into the native groundwater, and the initial groundwater salt concentrations respectively.

From Figures 4.1 and 4.4, it is obvious that as the actual evapotranspiration increases the higher the total power required by the system and the higher the amount of treated wastewater required to be injected into the groundwater zone. As the crop actual evapotranspiration increases the crop water requirement will increase. Thus, irrigation water demand will increase to meet this increase in the crop actual evapotranspiration. Moreover, to meet this increase in the irrigation water demand, a larger groundwater amount must be pumped and fed to the reverse osmosis unit to cope with the irrigation water requirement increases. Therefore, the higher the pumped groundwater amount required to be fed to the reverse osmosis unit the higher the amount of water needed to be desalinated and the higher the power will be consumed by the reverse osmosis unit (Figure 4.2). In addition, the higher the pumped groundwater requirement the higher the power consumption will be used by the pump (Figure 4.3). To cope with the increase in irrigation water demand, this leads to an increase in pumped groundwater, and to prevent the groundwater from mining, the higher the treated wastewater injection rate into the groundwater zone required to compensate for the higher water demand by the system (Figure 4.4). As evapotranspiration increases, more groundwater will be pumped and fed to the reverse osmosis unit. Thus, more groundwater will be desalinated and more treated wastewater of better quality than the native groundwater will be injected into the native groundwater. Therefore, the higher the evapotranspiration the more enhanced the groundwater quality will be in the long run (Figure 4.5).

Figure 4.1 Total power required by the system for ranges of different actual crop evapotranspiration, ET_c, input values vs. simulation period.

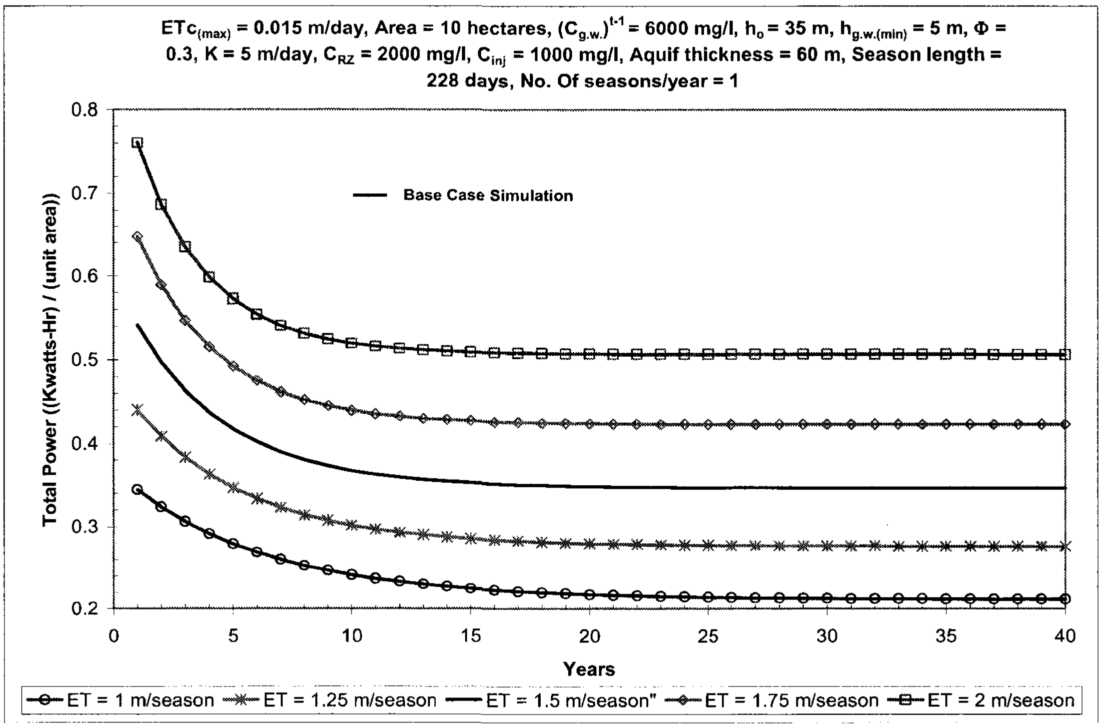

Figure 4.2 Power required by the reverse osmosis unit for ranges of different actual crop evapotranspiration, ET_c, input values vs. simulation period.

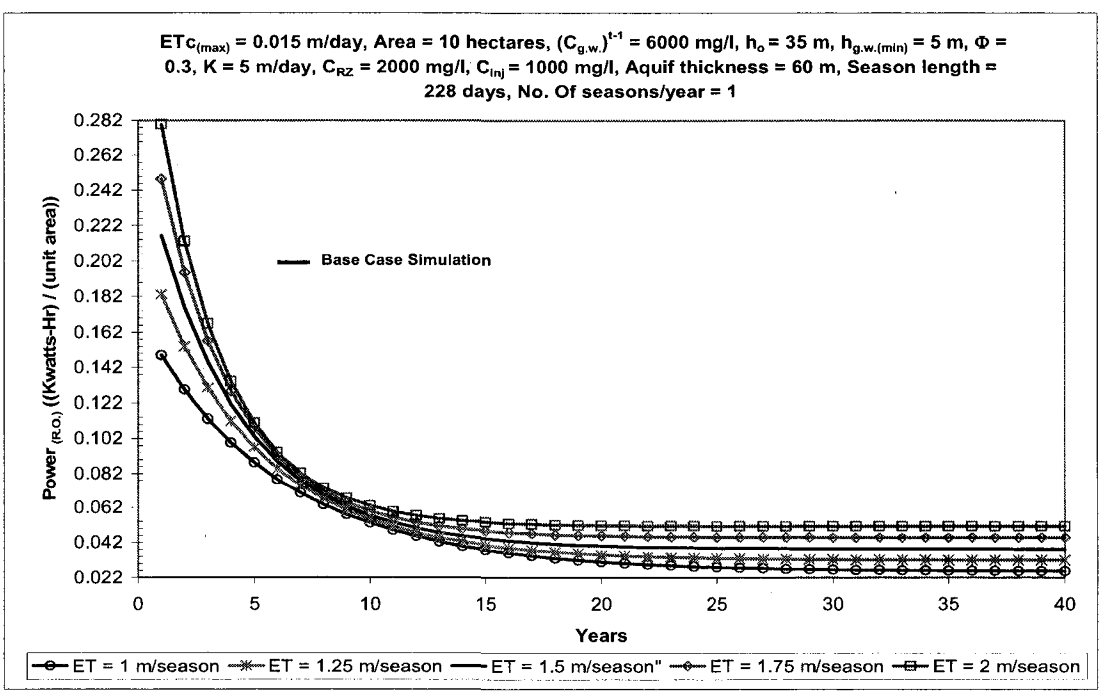

Figure 4.3 Power required by the well pump system for ranges of different actual crop evapotranspiration, ET_c, input values vs. simulation period.

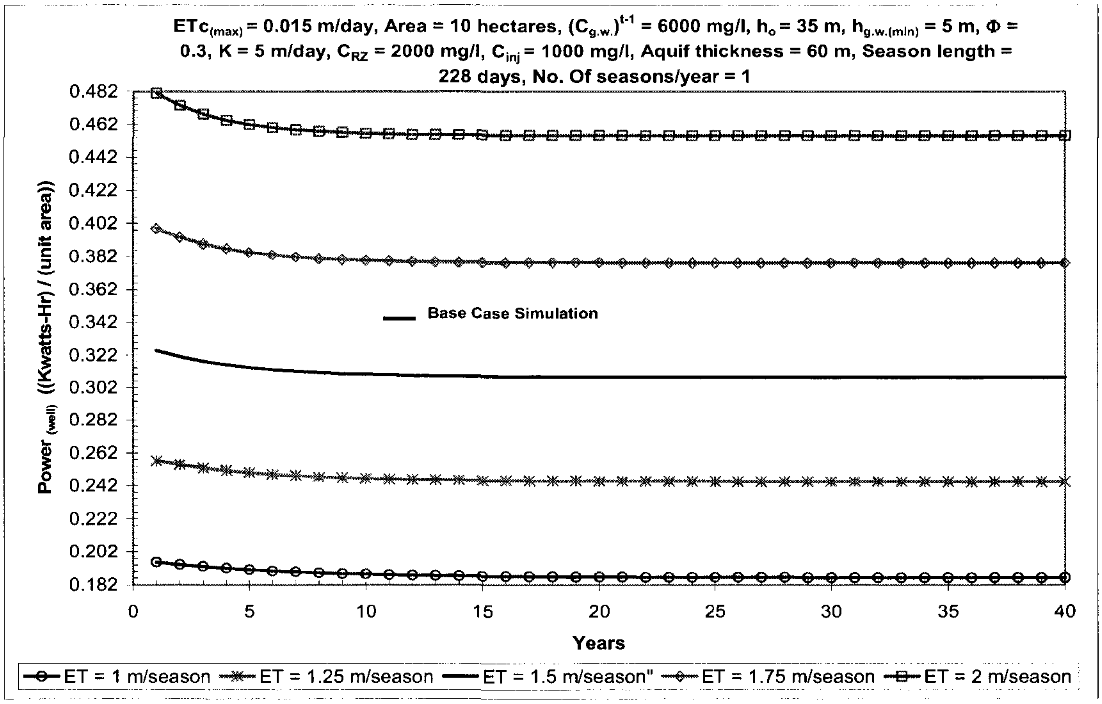

Figure 4.4 Amount of treated wastewater injected into the native groundwater for ranges of different actual crop evapotranspiration, ET_c, input values vs. simulation period.

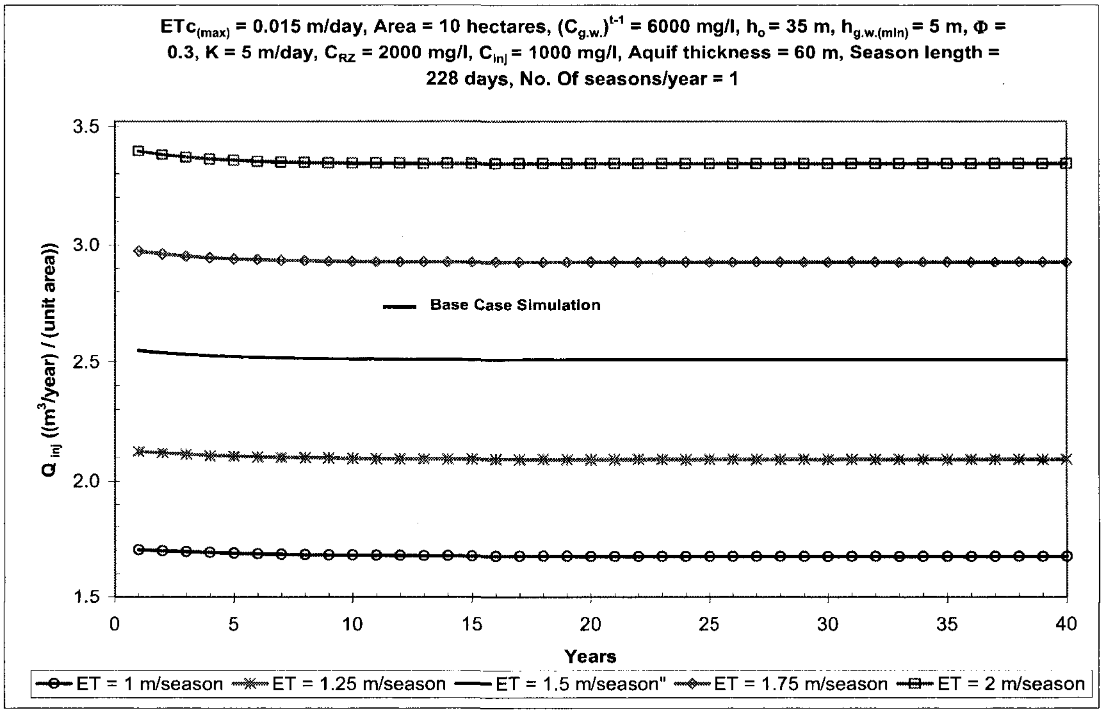

Figure 4.5 Initial groundwater salt concentrations for ranges of different actual crop evapotranspiration, $\boldsymbol{ET_c}$, input values vs. simulation period.

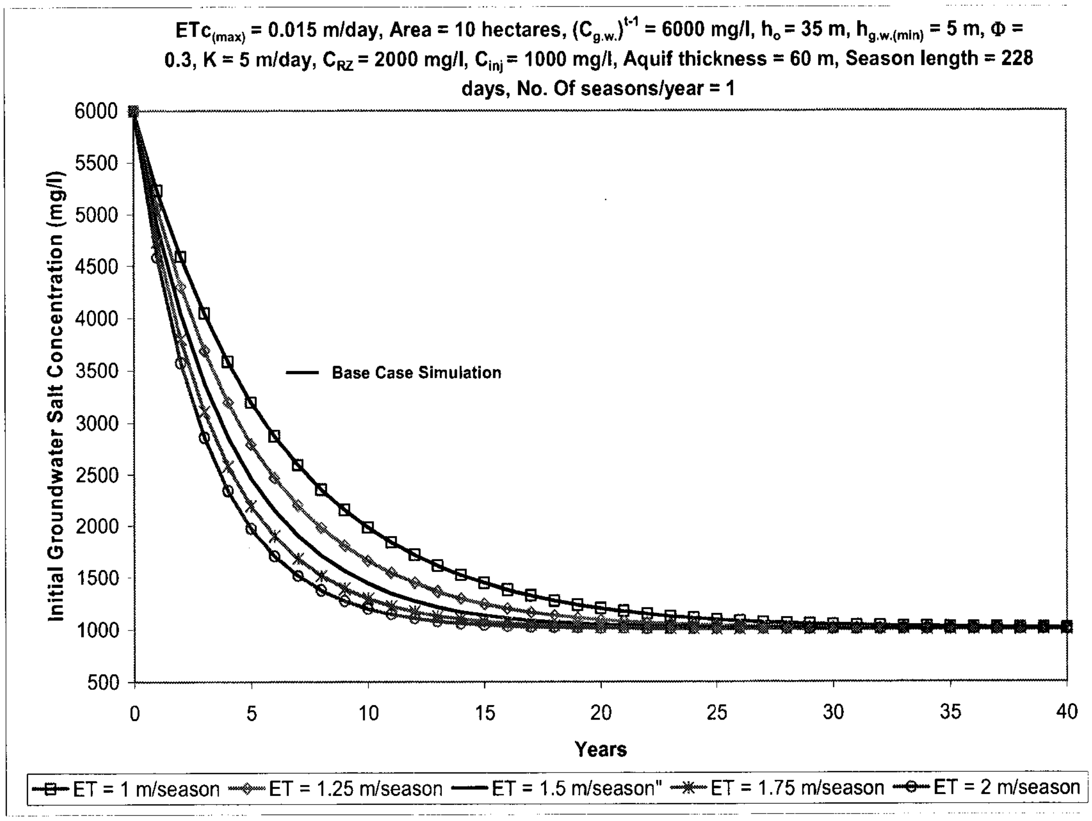

Figures 4.6 and 4.7 illustrate the sum of total power required by the system for 40-year simulations for ranges of different actual crop evapotranspiration ($\boldsymbol{ET_c}$) input values, and the sum of treated wastewater injected amounts into the native groundwater for 40-year simulations for ranges of different actual crop evapotranspiration ($\boldsymbol{ET_c}$) input values. Moreover, Table 4.2 demonstrates the percent increase in the total power consumption and the treated wastewater injection as the actual evapotranspiration increases.

Figure 4.6 The sum of total power required by the system for 40-year simulations for ranges of different actual crop evapotranspiration, ET_c, input values.

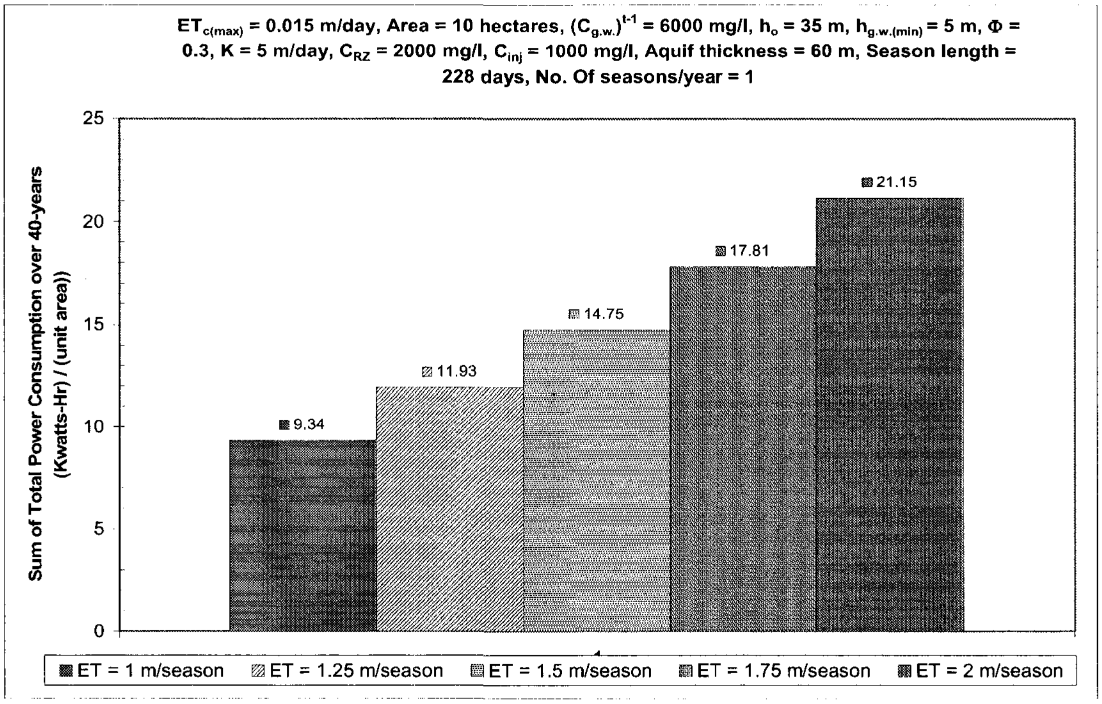

Figure 4.7 The sum of treated wastewater injected into the native groundwater for 40-year simulations for ranges of different actual crop evapotranspiration, *ETc*, input values.

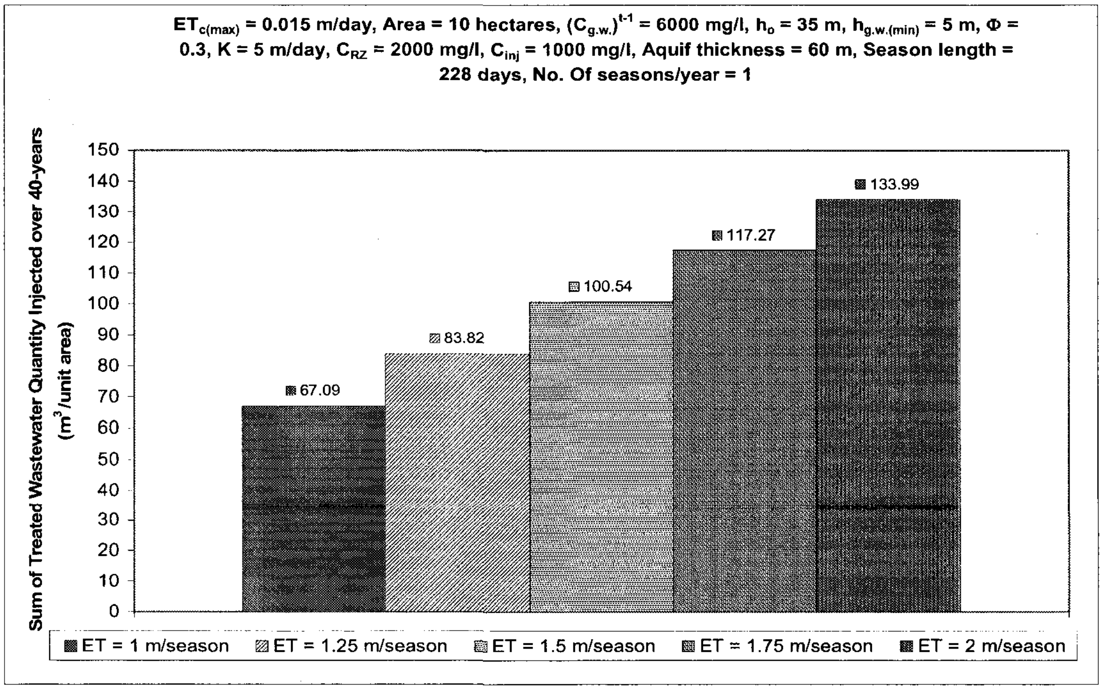

Table 4.2 Percent increase in the sum of the total power consumption and the sum of the treated wastewater injection as the actual evapotranspiration increases.

ET_c Changes (m/season)		% Change (increase) in ET_c	% Change (increase) in the Sum of the Total Power per Unit Area	% Change (increase) in the Sum of the Injected Treated Wastewater per Unit Area
From	To			
1	1.50	33.33	36.69	33.27
1.25	1.50	16.67	19.09	16.64
1.50	1.75	14.29	17.19	14.26
1.50	2.00	25.00	30.27	24.97

* Base case ET_c = 1.5 m/season

4.1.2 Root Zone Salt Concentration Tolerance, C_{RZ}

Root zone salt concentration tolerance, C_{RZ}, is one of the decision variable input data in the simulation, as it symbolizes the maximum root salt concentration tolerance for a crop without a reduction in the yield. Root zone salt concentration tolerance data ranges (1000 mg/l – 2000 mg/l) were chosen to cope with and characterize the wide varieties of plant root salt concentration tolerances (Table 4.3). Thus, to test the sensitivity and performance of the general conceptual design system, the simulation will be executed five times, using five root salt concentration tolerance values while keeping all other variables constant (Table 4.4). Simulation calculation procedures followed steps similar to those in Section 3.2. Moreover, all other required input data, except C_{RZ}, will be the same as Tables 3.1, 3.2, and 3.7.

Results for C_{RZ} simulations of testing the sensitivity and performance of the general conceptual design system were captured in Figures 4.8, 4.9, 4.10, 4.11, and 4.12 respectively. These output result graphs were arranged by the total power required by the system, the power required by the reverse osmosis unit, the power required by the well pump system, the amount of wastewater injected into the native groundwater, and the initial groundwater salt concentrations respectively.

Table 4.3 Crop root zone salt concentration tolerances threshold and crop rating (after FAO irrigation and drainage paper 56, 2000).

Crop	Root Zone Salt Concentration Tolerance Threshold (mg/l)	Rating
Date Palm	3500	T
Sweet Corn	1250	MS
Strawberry	1000	S
Alfalfa	2000	MS
Broccoli	1500	MS
Lettuce	1250	MS
Onion	1000	S
Cabbage	1250	MS
Tomato	1750	MS
Carrots	1000	S
Citrus	1750	MS
Cucumber	1750	MS
Cantaloupe	1500	MS
Rice	2000	MS
Spinach	1500	MS
Apricot	1000	S
Grape	1000	S

T = Tolerant; **MS** = Moderately Sensitive; **S** = Sensitive.

Table 4.4 Test of the sensitivity and the performance of the general conceptual model by perturbing root zone salt concentration tolerance values, C_{RZ}, while keeping all other variables constant.

Run No.	ET_c (m/season)	$ET_{c\,(max)}$ (m/day)	C_{RZ} (mg/l)	C_{inj} (mg/l)	Φ (m^3/m^3)	K (m/day)	h_o (m)	$(C_{g.w.})^{t-1}$ (mg/l)
1	1.50	0.015	**1000**	1000	0.3	5	35	6000
2	1.50	0.015	**1250**	1000	0.3	5	35	6000
3	1.50	0.015	**1500**	1000	0.3	5	35	6000
4	1.50	0.015	**1750**	1000	0.3	5	35	6000
5*	1.50	0.015	**2000**	1000	0.3	5	35	6000

* Base case simulation.

Figure 4.8 Total power required by the system for ranges of different root zone salt concentration tolerances, C_{RZ}, input values vs. simulation period.

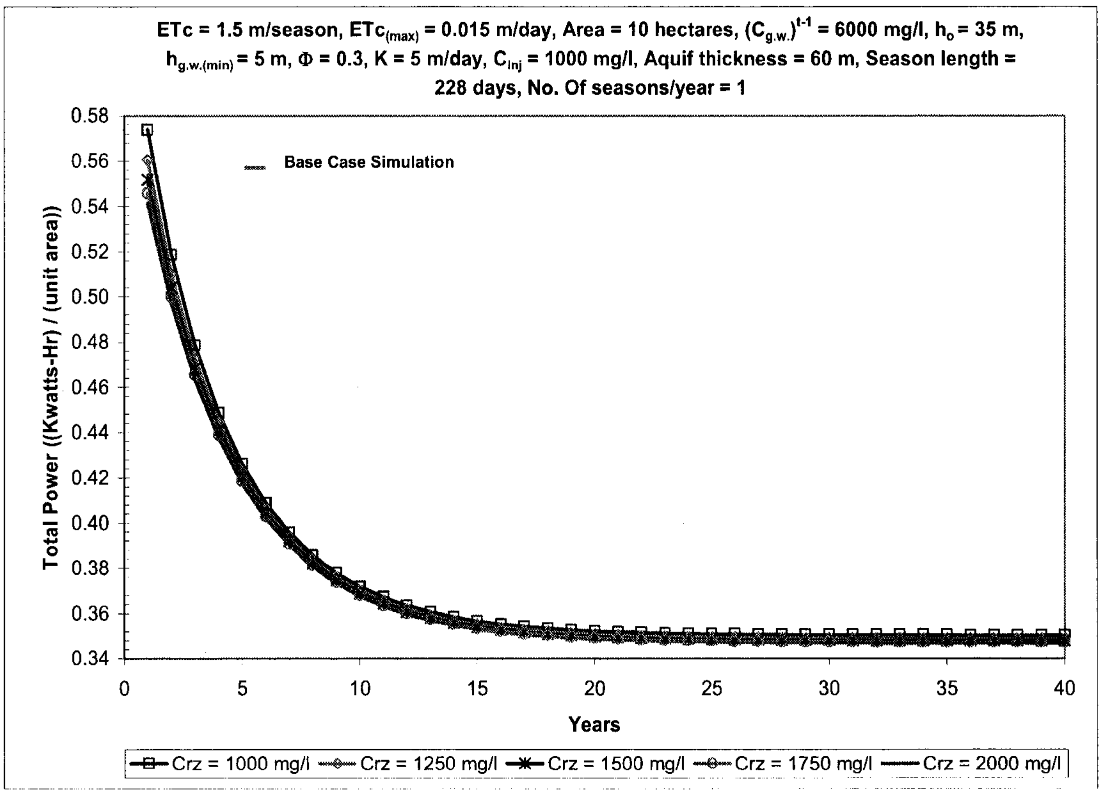

 Emad H. AlAli

Figure 4.9 Power required by the reverse osmosis unit for ranges of different root zone salt concentration tolerances, C_{RZ}, input values vs. simulation period.

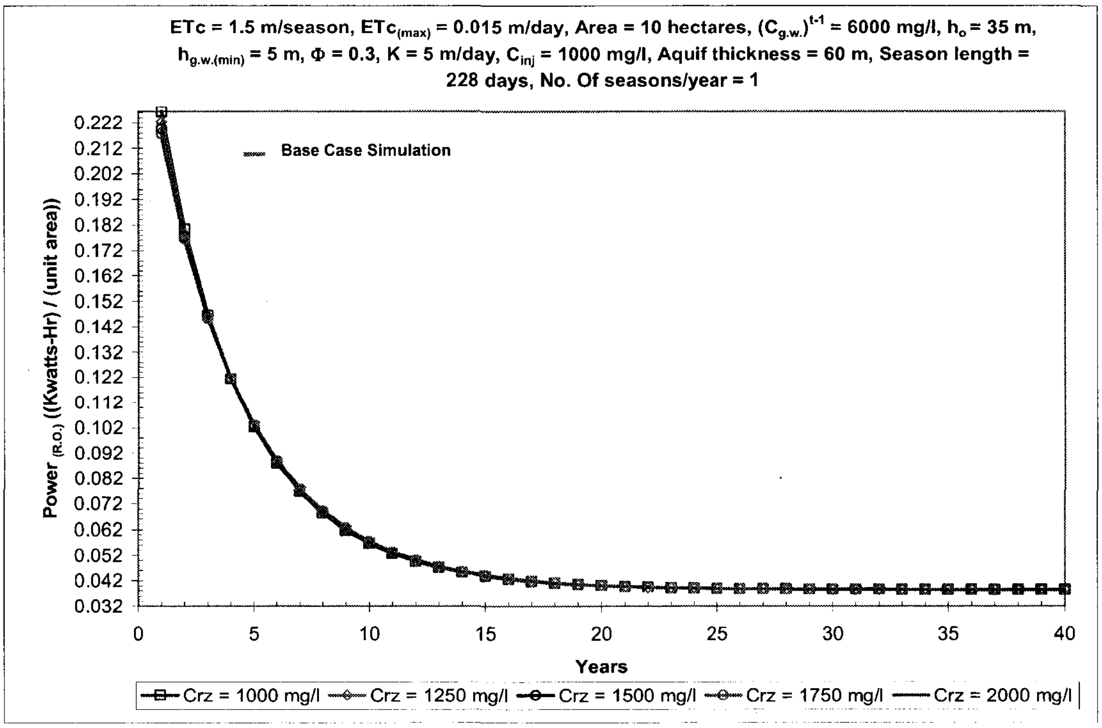

Figure 4.10 Power required by the well pump system for ranges of different root zone salt concentration tolerances, C_{RZ}, input values vs. simulation period.

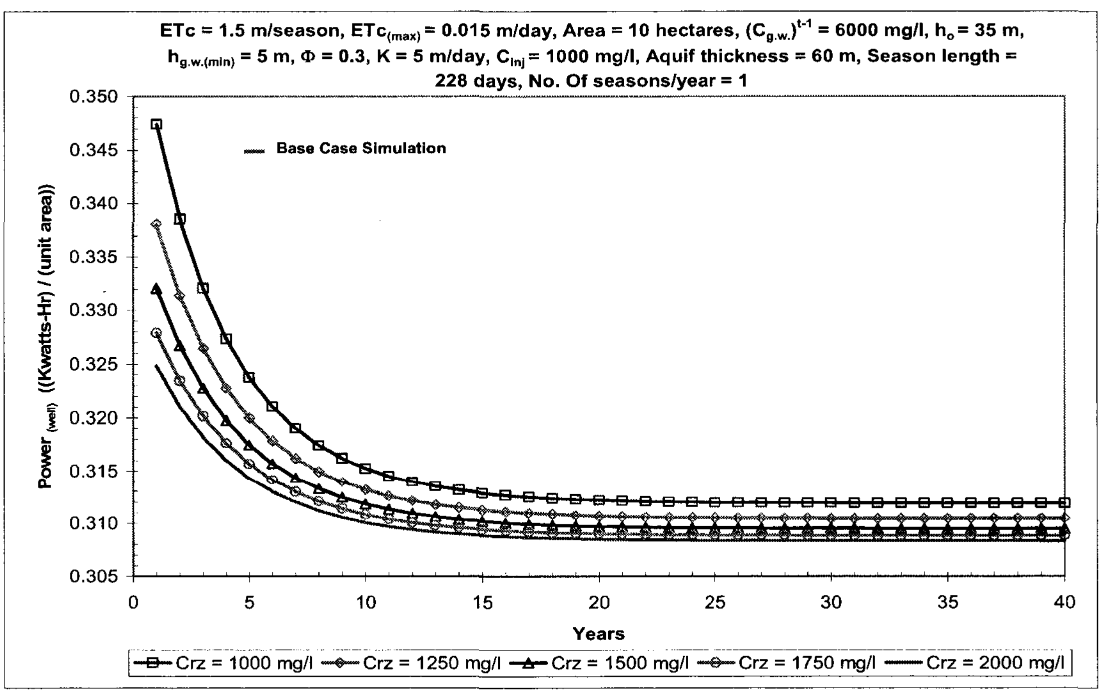

Figure 4.11 Amount of treated wastewater injected into the native groundwater for ranges of different root zone salt concentration tolerances, C_{RZ}, input values vs. simulation period.

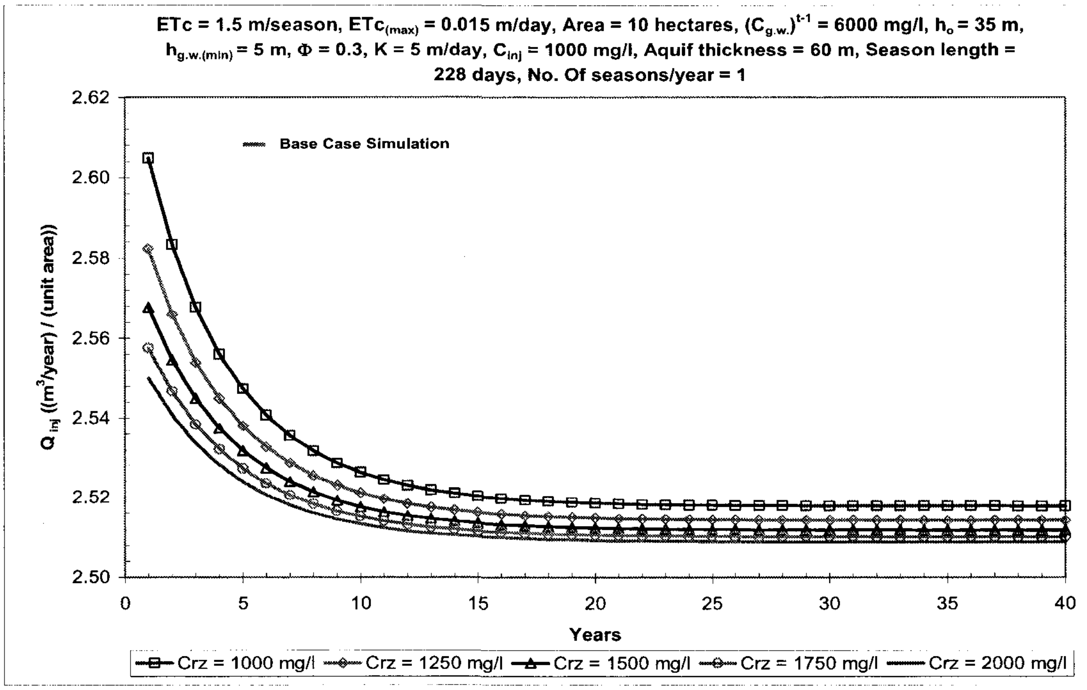

Figure 4.12 Initial groundwater salt concentrations for ranges of different root zone salt concentration tolerances, C_{RZ}, input values vs. simulation period.

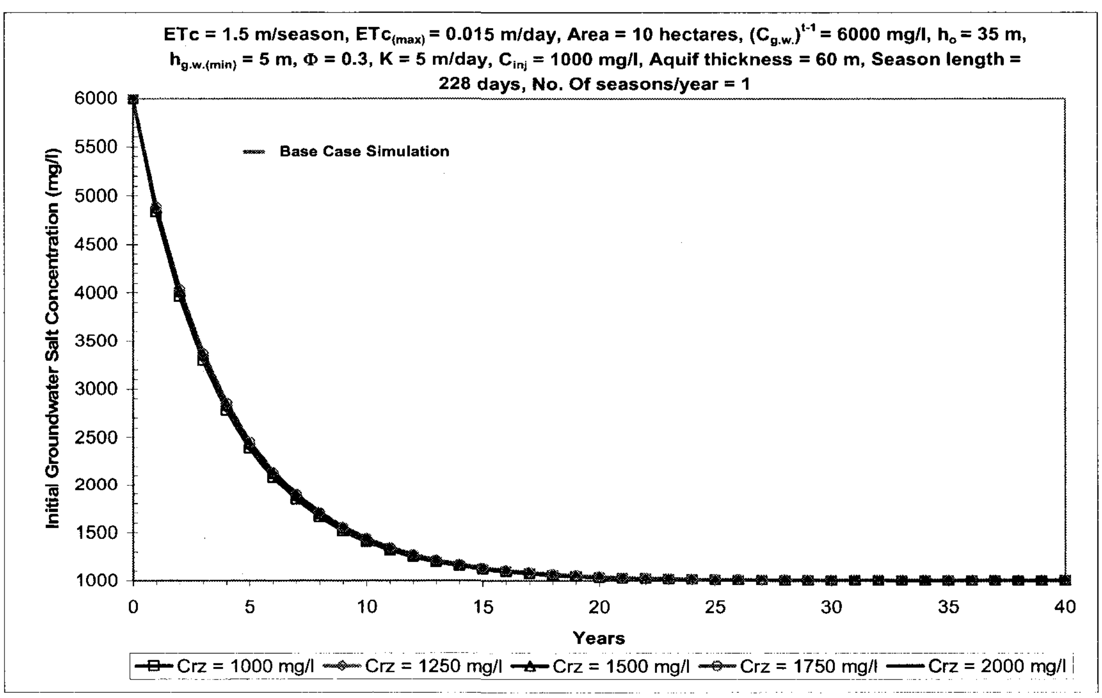

From Figures 4.8 and 4.11, it is obvious that as the root zone salt concentration tolerance decreases the higher the total power required by the system, and the higher amount of treated wastewater required to be injected into the groundwater zone. As the root zone salt concentration tolerance decreases the crop water requirement will increase to flush the excess salts from the root zone and to keep the salt concentration within the desirable root zone salt concentration tolerance level, thus, preventing crop yield reduction. Therefore, irrigation water demand will increase to meet this decrease in the root zone salt concentration tolerance. Moreover, to meet this increase in the irrigation water demand, a larger groundwater amount must be pumped and fed to the reverse osmosis unit to cope with the irrigation water requirement increases. Therefore, the higher the pumped groundwater amount required to be fed to the reverse osmosis unit the higher the amount of water needed to be desalinated and the more power will be consumed by the reverse osmosis unit (Figure 4.9). In addition, the higher the pumped groundwater requirement the higher the power consumption will be used by the pump (Figure 4.10). To cope with the increase in irrigation water demand, this leads to an increase in pumped groundwater, and to prevent groundwater from mining, the more treated wastewater injection rate into the groundwater zone is required to compensate for the higher water demand by the system (Figure 4.11). As the root zone salt concentration tolerance decreases, more groundwater will be pumped and fed to the reverse osmosis unit. Hence, more groundwater will be desalinated and more treated wastewater, of better quality than the native groundwater, will be injected into the native groundwater. Therefore, the lower the root zone salt concentration tolerance the more enhanced the groundwater quality will be in the long run (Figure 4.12). Comparing the groundwater pumped amount and injected treated wastewater amount to the deep percolation amount, the deep percolation amount is minute. Therefore, for the range of root zone salt concentration tolerance (1000 – 2000 mg/l), the amount of salt mass added to the groundwater system by the deep percolation is insignificant. Thus, the variances in the reverse osmosis power consumption, specifically, the variances of the total consumption power requirement by the system, the variances of the injected treated wastewater amount, and the variances in the groundwater salt concentration quality, in general, are minimal for the range of the root zone salt concentration tolerances.

Figures 4.13 and 4.14 illustrate the sum of the total power required by the system for 40-year simulations for ranges of different root zone salt concentration tolerances (C_{RZ}) inputs values and the sum of the treated wastewater injected amount into the native groundwater for 40-year simulations for ranges of different root zone salt concentration tolerances (C_{RZ}) inputs values.

Figure 4.13 Sum of total power required by the system for 40-year simulations for ranges of different root zone salt concentration tolerances, C_{RZ}, values.

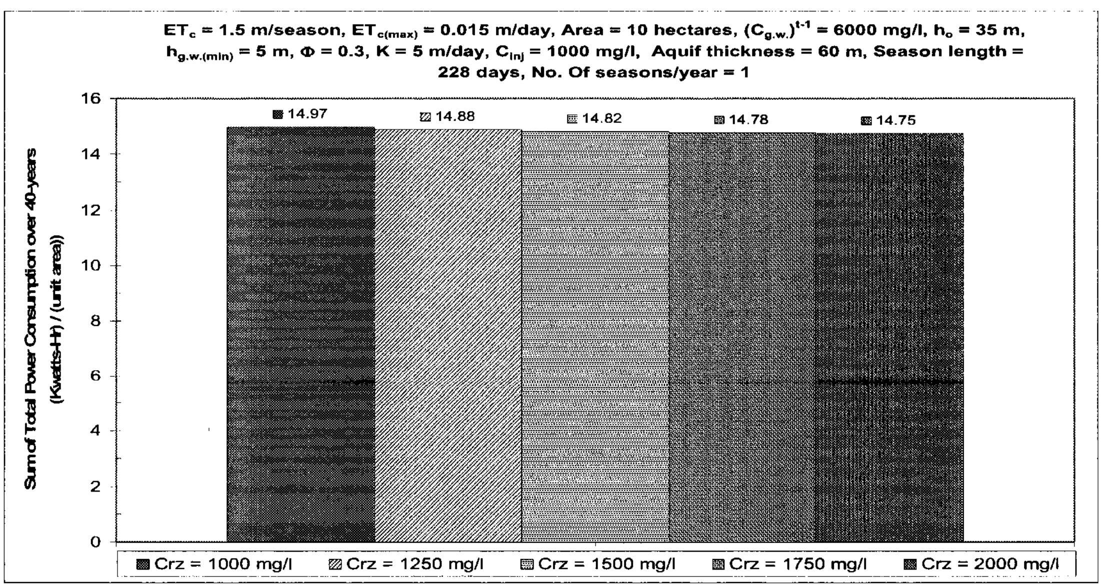

Moreover, Table 4.5 demonstrates the percent increase in the total power consumption and the treated wastewater injection as the root zone salt concentration tolerance (C_{RZ}) values increases.

Figure 4.14 Sum of treated wastewater injected to the native groundwater for 40-year simulations for ranges of different root zone salt concentration tolerances, C_{RZ}, values.

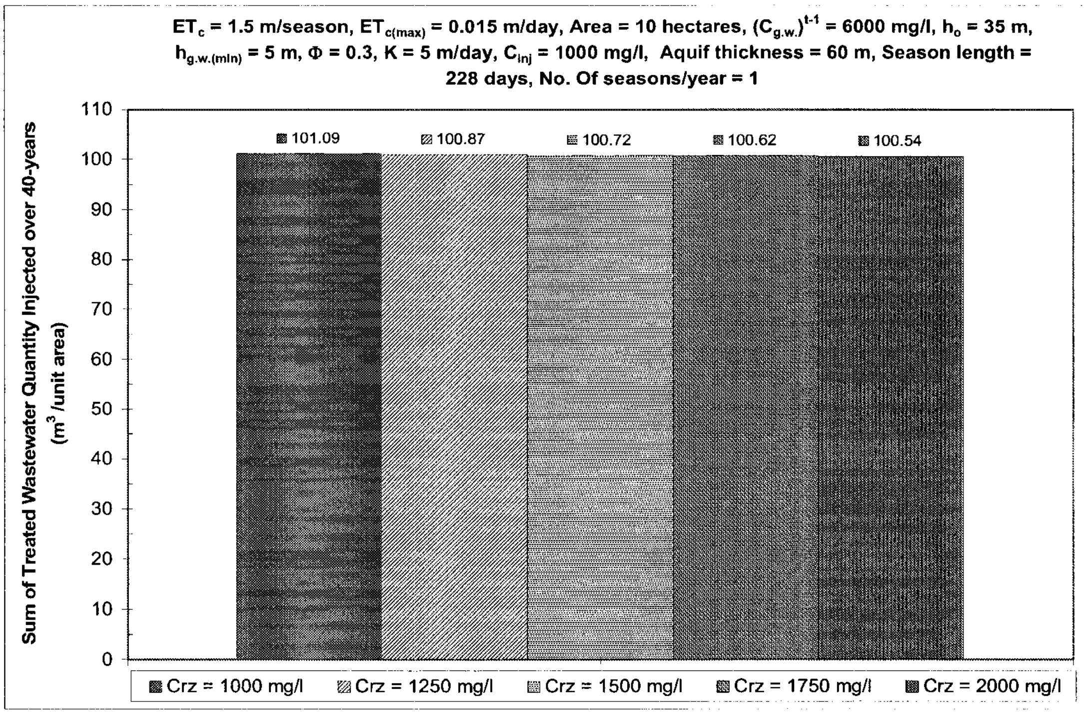

Table 4.5 Percent increase in the sum of the total power consumption and the sum of the treated wastewater injection as the root zone salt concentration tolerances decreases.

C_{RZ} Changes (mg /l)		% Change (decrease) in C_{RZ}	% Change (increase) in the Sum of the Total Power per Unit Area	% Change (increase) in the Sum of the Injected Treated Wastewater per Unit Area
From	To			
2000	1000	50.00	1.47	0.54
2000	1250	37.50	0.87	0.33
2000	1500	25.00	0.47	0.18
2000	1750	12.50	0.20	0.08

* Base case C_{RZ} = 2000 mg/l.

4.1.3 Treated Wastewater Salt Concentration, C_{inj}

Treated wastewater salt concentration, C_{inj}, is of crucial variable input data in the simulation, because it will control the amount of added salt concentration to the groundwater in the form of injection. Treated wastewater salt concentration data ranges (1000 mg/l – 2000 mg/l) were chosen to deal with and illustrate the range of salt concentration within most treated wastewater effluent available after tertiary or secondary treatment level. Thus, to test the sensitivity and performance of the general conceptual design system, the simulation will be executed five times, using five treated wastewater salt concentration values while keeping all other variables constant (Table 4.6). Simulation calculation procedures followed similar steps as shown in Section 3.2. Moreover, all other required input data, except C_{inj}, will be the same as in Tables 3.1, 3.2, and 3.7.

Table 4.6 Test of the sensitivity and the performance of the general conceptual model by perturbing wastewater salt concentration values, C_{inj}, while keeping all other variables constant.

Run No.	ET_c *(m/season)*	$ET_{c\,(max)}$ *(m/day)*	C_{RZ} *(mg/l)*	C_{inj} *(mg/l)*	Φ *(m^3/m^3)*	*K* *(m/day)*	h_o *(m)*	$(C_{g.w.})^{t-1}$ *(mg/l)*
1*	1.50	0.015	2000	**1000**	0.3	5	35	6000
2	1.50	0.015	2000	**1250**	0.3	5	35	6000
3	1.50	0.015	2000	**1500**	0.3	5	35	6000
4	1.50	0.015	2000	**1750**	0.3	5	35	6000
5	1.50	0.015	2000	**2000**	0.3	5	35	6000

* Base case simulation.

Results for C_{inj} simulations of testing the sensitivity and performance of the general conceptual design system were captured in Figures 4.15, 4.16, 4.17, 4.18, and 4.19 respectively. These output result graphs were arranged by the total power required by the system, the power required by the reverse osmosis unit, the power required by the well pump system, the amount of wastewater injected into the native groundwater, and the initial groundwater salt concentrations respectively.

Figure 4.15 Total power required by the system for ranges of different treated wastewater salt concentrations, C_{inj}, input values vs. simulation period.

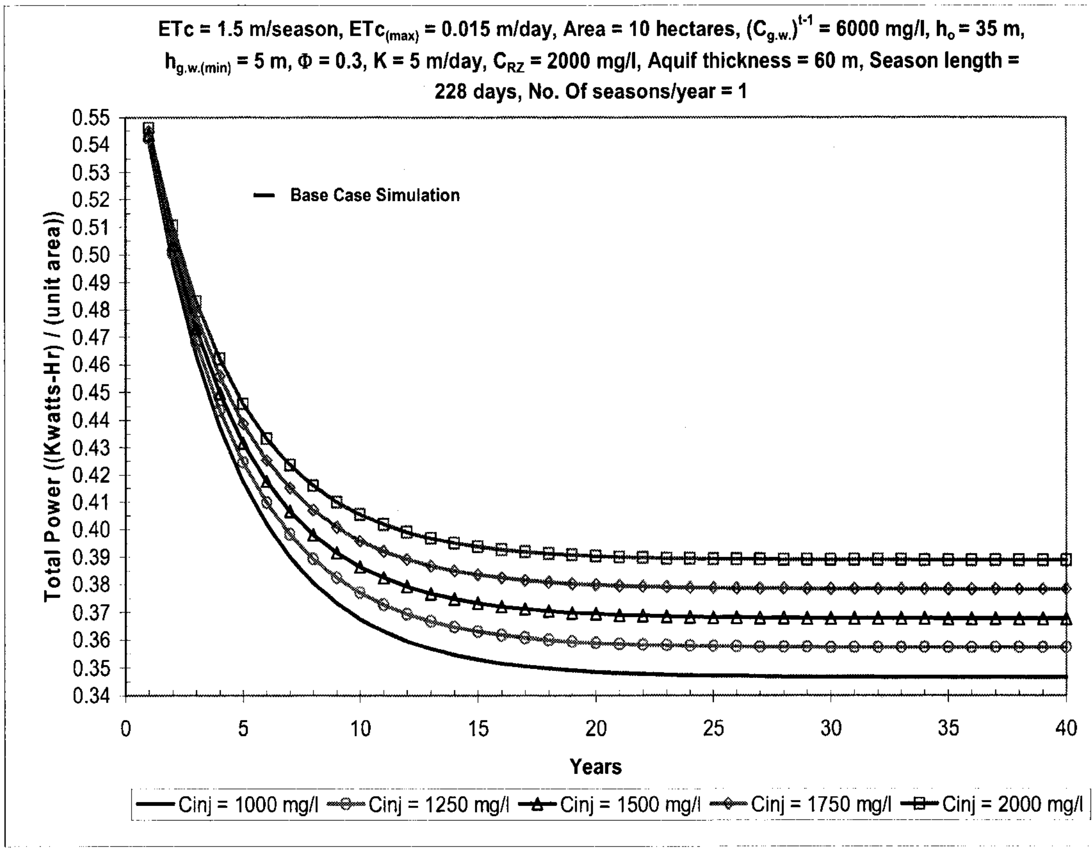

Figure 4.16 Power required by the reverse osmosis unit for ranges of different treated wastewater salt concentrations, C_{inj}, input values vs. simulation period.

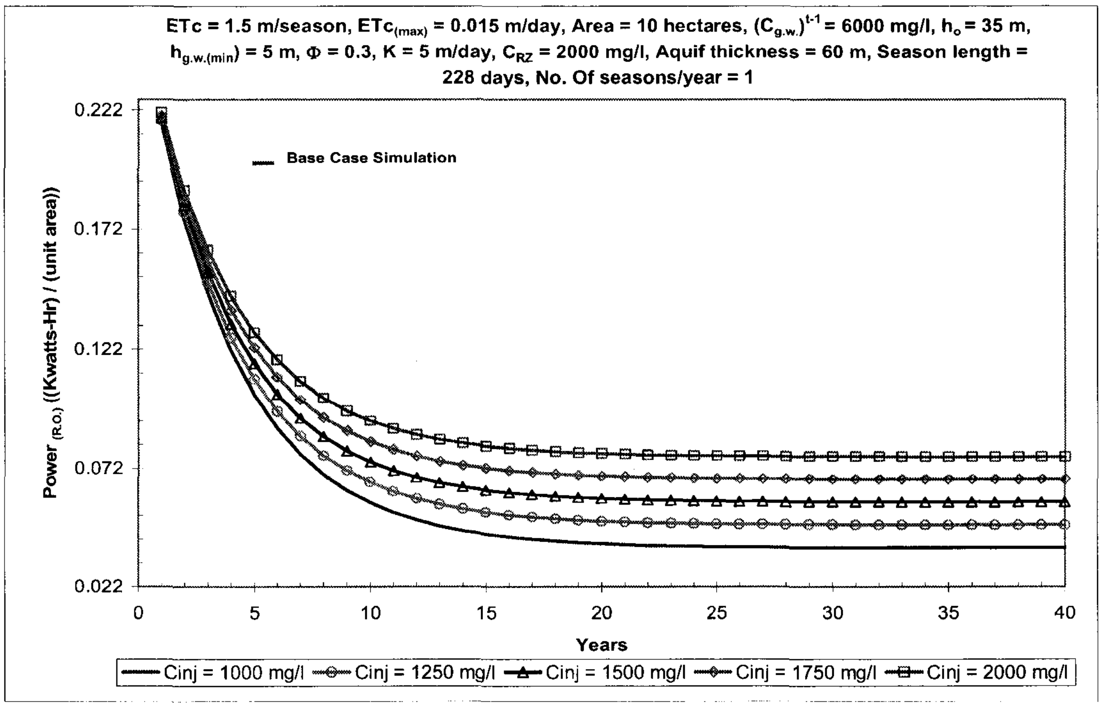

Figure 4.17 Power required by the well pump system for ranges of different treated wastewater salt concentrations, C_{inj}, input values vs. simulation period.

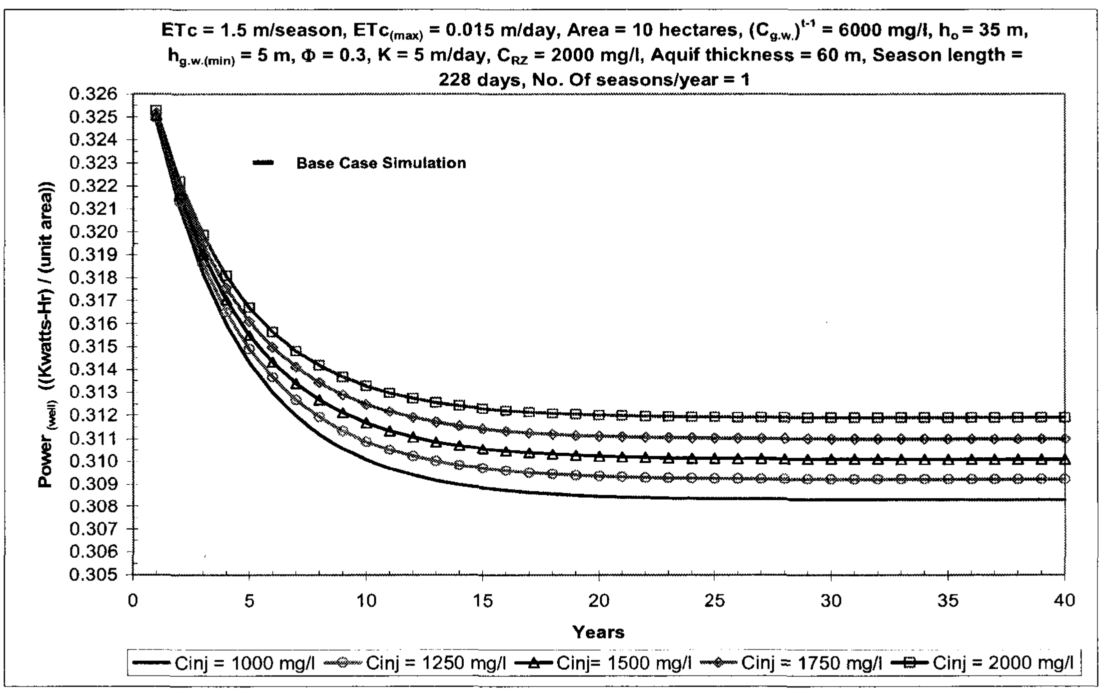

Figure 4.18 Amount of treated wastewater injected into the native groundwater for ranges of different treated wastewater salt concentrations, C_{inj}, input values vs. simulation period.

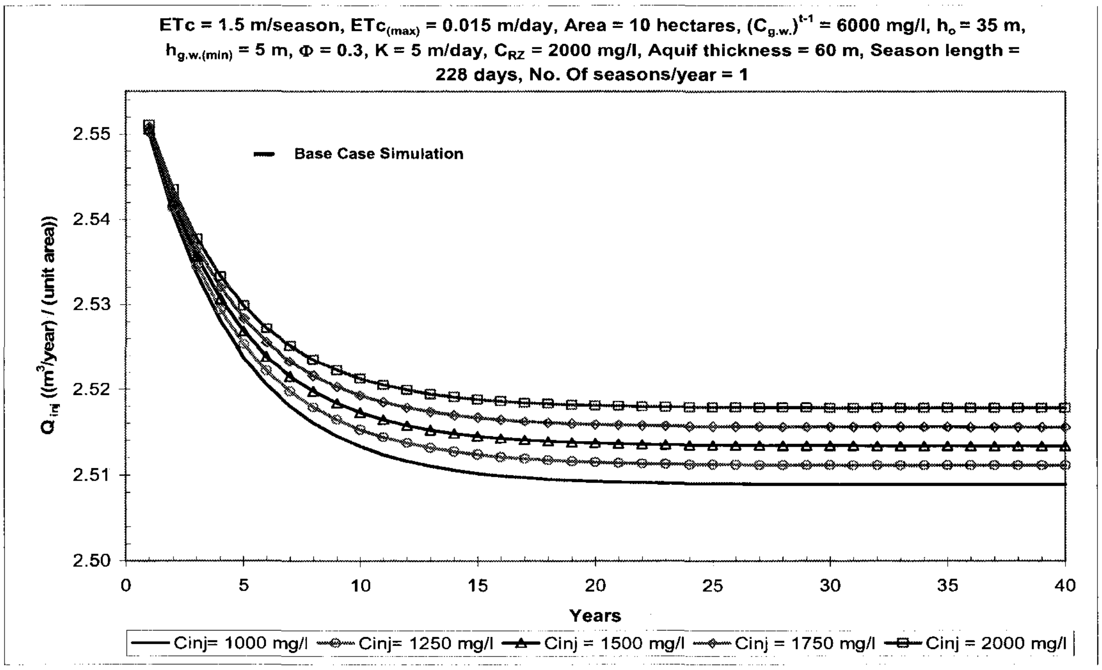

Figure 4.19 Initial groundwater salt concentrations for ranges of different wastewater salt concentrations, C_{inj}, input values vs. simulation period.

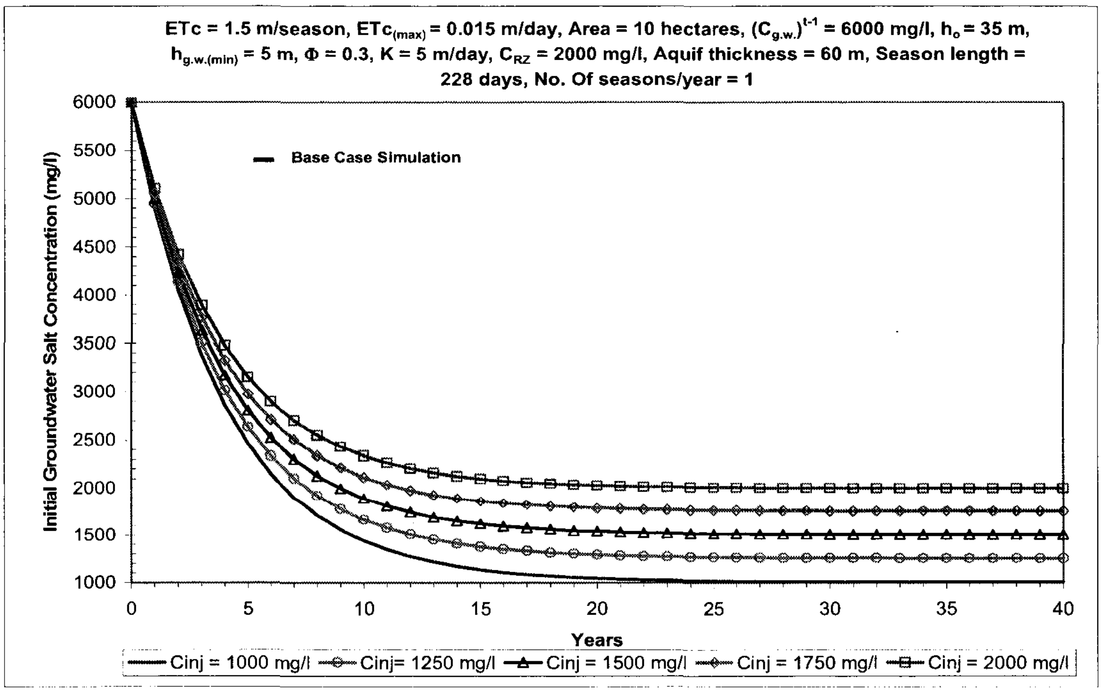

From Figures 4.15 and 4.18, it is obvious that as the injected treated wastewater salt concentration increases the higher the total power required by the system and the higher the amount of treated wastewater required to be injected into the groundwater zone. As the injected treated wastewater salt concentration increases, the groundwater salt concentration enhancement will be retarded. Thus, the pumped groundwater salt concentration will be relatively higher (Figure 4.19). Due to the increase in the pumped groundwater salt concentration, the feed water to the reverse osmosis unit will be at a relatively higher salt concentration. Thus, the water permeate from the reverse osmosis unit will be at a higher concentration, too. Therefore, the more permeate water is required (to be used as irrigation water) to cope with the irrigation efficiency, the higher the salt concentration in the irrigation water and the higher the amount of irrigation water needed to be applied to keep the root zone at the desirable salt concentration tolerance. Hence, irrigation water demand will increase to meet this increase in the injected treated wastewater salt concentration. Moreover, to meet this increase in the irrigation water demand, a larger groundwater amount must be pumped and fed to the reverse osmosis unit to cope with the irrigation water requirement increases. Therefore, the higher the pumped groundwater amount required to be fed to the reverse osmosis unit the higher the amount of water needed to be desalinated and the more power will be consumed by the reverse osmosis unit (Figure 4.16). In addition, the higher the pumped groundwater requirement the higher the power consumption will be used by the pump (Figure 4.17). To cope with the increase in irrigation water demand, this leads to an increase in pumped groundwater, and to prevent groundwater from mining, the more treated wastewater injection rate into the groundwater zone required to compensate for the higher water demand by the system (Figure 4.18). As the injected treated wastewater salt concentration increases, the higher the salt mass quantity will be added to the groundwater. Therefore, the higher the injected treated wastewater salt concentration, the more the enhancement of the groundwater quality will be retarded in the long run (Figure 4.19).

Figures 4.20 and 4.21 illustrate the sum of the total power required by the system for 40-year simulations for ranges of different injected treated wastewater salt concentrations (C_{inj}) input values and the sum of the treated wastewater injected amount into the native groundwater for 40-year simulations for ranges of different injected treated wastewater salt concentrations (C_{inj}) input values. Moreover, Table 4.7 demonstrates the percent increase in the total power consumption and the treated wastewater injection as the injected treated wastewater salt concentration (C_{inj}) increases.

Figure 4.20 Sum of total power required by the system for 40-year of simulations ranges of different treated wastewater salt concentrations, C_{inj}, values.

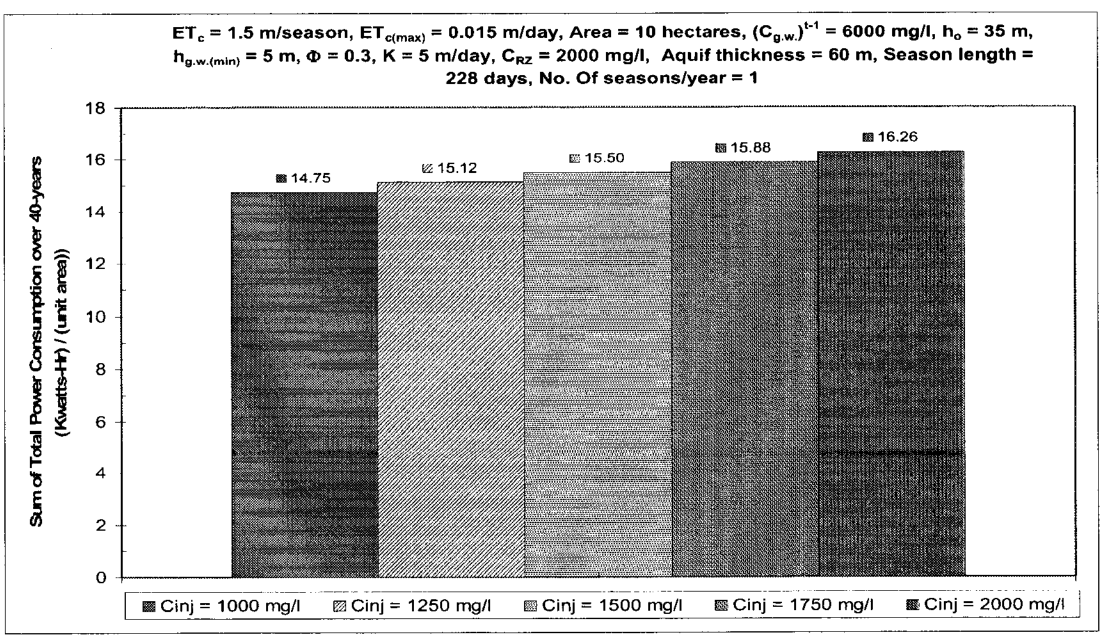

Figure 4.21 Sum of treated wastewater injected into the native groundwater for 40-year simulations for ranges of different treated wastewater salt concentrations, C_{inj}, values.

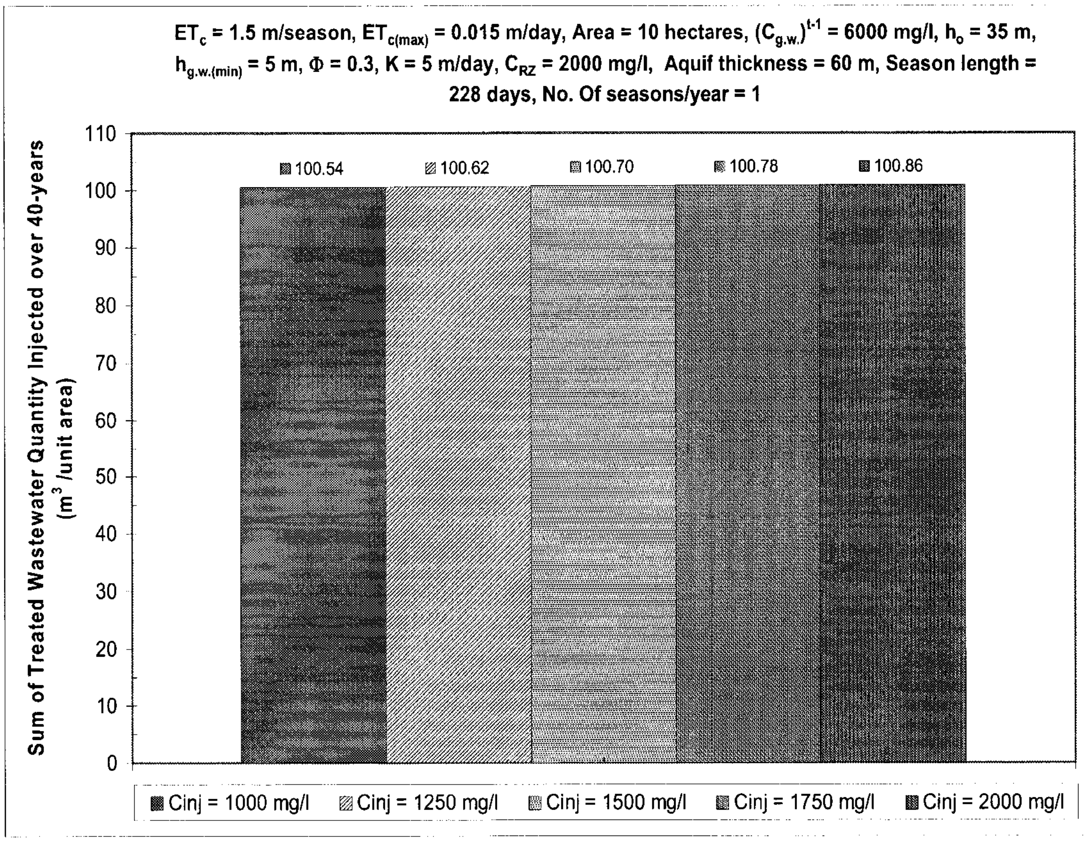

Table 4.7 Percent increase in the sum of the total power consumption, and the sum of the treated wastewater injection as the treated wastewater salt concentration increases.

C_{inj} Changes (mg /l)		% Change (increase) in C_{inj}	% Change (increase) in the Sum of the Total Power per Unit Area	% Change (increase) in the Sum of the Injected Treated Wastewater per Unit Area
From	To			
1000	1250	20.00	2.45	0.08
1000	1500	33.33	4.84	0.16
1000	1750	42.86	7.12	0.24
1000	2000	50.00	9.29	0.32

* Base case C_{inj} = 1000 mg/l.

4.1.4 Porosity, Φ

Porosity, Φ, is of fundamental importance to groundwater variable input data in the simulation, because it serves as water conduits. Porosity data ranges (0.3 – 0.45) were chosen to cope with and distinguish wide varieties of soil type (Table 4.8). Thus, to test the sensitivity and performance of the general conceptual design system, the simulation will be executed four times, using four porosity values while keeping all other variables constant (Table 4.9). Simulation calculation procedures followed similar steps as those outlined in Section 3.2. Moreover, all other required input data, except Φ, will be the same as in Tables 3.1, 3.2, and 3.7.

Table 4.8 Representative values of porosity (after Morris and Johnson, 1967).

Material	Porosity	Material	Porosity
Gravel, coarse	0.28*	Loess	0.49
Gravel, medium	0.32*	Peat	0.92
Gravel, fine	0.34*	Schist	0.38
Sand, coarse	0.39	Siltstone	0.35
Sand, medium	0.39	Claystone	0.43
Sand, fine	0.43	Shale	0.06
Silt	0.49	Till, Predominantly silt	0.34
Clay	0.42	Till, Predominantly sand	0.31
Sandstone, fine -grained	0.33	Tuff	0.41
Sandstone, medium- grained	0.37	Basalt	0.17
Limestone	0.30	Gabbro, weathered	0.43
Dolomite	0.26	Granite, weathered	0.45
Dune sand	0.45		

* These values are for repacked samples; all others are undisturbed.

Results for Φ simulations of testing the sensitivity and performance of the general conceptual design system were captured in Figures 4.22, 4.23, 4.24, 4.25, and 4.26 respectively. These output result graphs were arranged by the total power required by the system, the power required by the reverse osmosis unit, the power required by the well pump system, the amount of wastewater injected into the native groundwater, and the initial groundwater salt concentrations respectively.

Table 4.9 Test of the sensitivity and the performance of the general conceptual model by perturbing porosity values, Φ, while keeping all other variables constant.

Run No.	ET_c *(m/season)*	$ET_{c\,(max)}$ *(m/day)*	C_{RZ} *(mg/l)*	C_{inj} *(mg/l)*	Φ *(m^3/m^3)*	*K* *(m/day)*	h_o *(m)*	$(C_{g.w.})^{t-1}$ *(mg/l)*
1*	1.50	0.015	2000	1000	**0.30**	5	35	6000
2	1.50	0.015	2000	1000	**0.35**	5	35	6000
3	1.50	0.015	2000	1000	**0.40**	5	35	6000
4	1.50	0.015	2000	1000	**0.45**	5	35	6000

* Base case simulation.

Figure 4.22 Total power required by the system for ranges of different porosity, $\boldsymbol{\Phi}$, input values vs. simulation period.

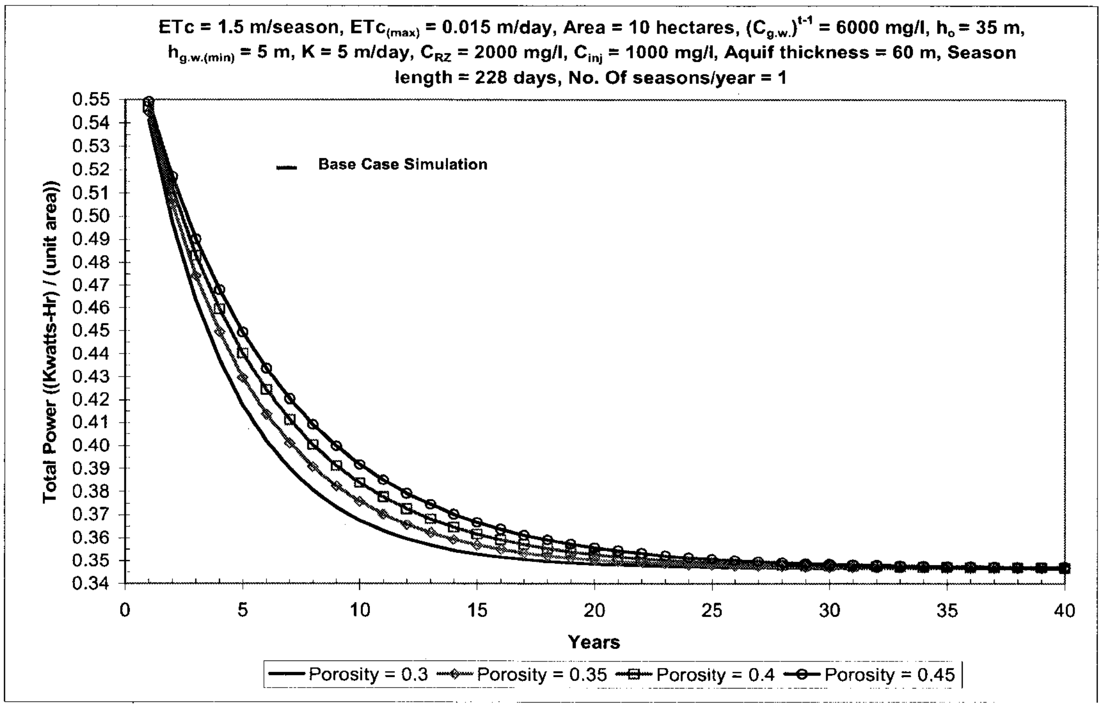

Figure 4.23 Power required by the reverse osmosis unit for ranges of different porosity, $\boldsymbol{\Phi}$, input values vs. simulation period.

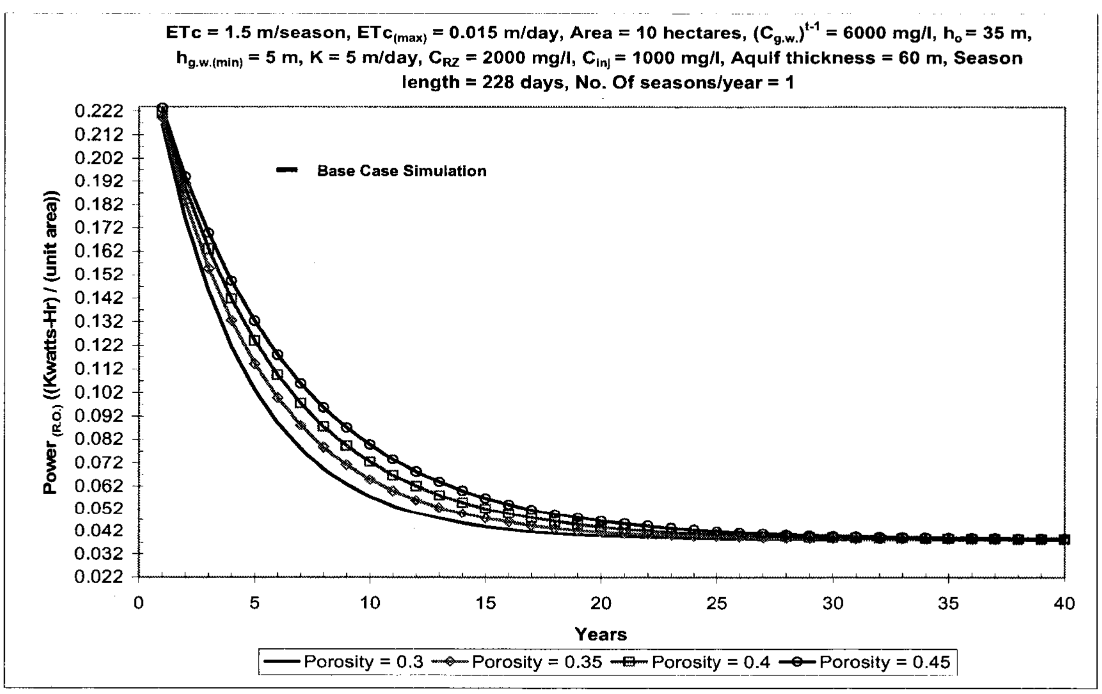

Figure 4.24 Power required by the well pump system for ranges of different porosity, Φ, input values vs. simulation period.

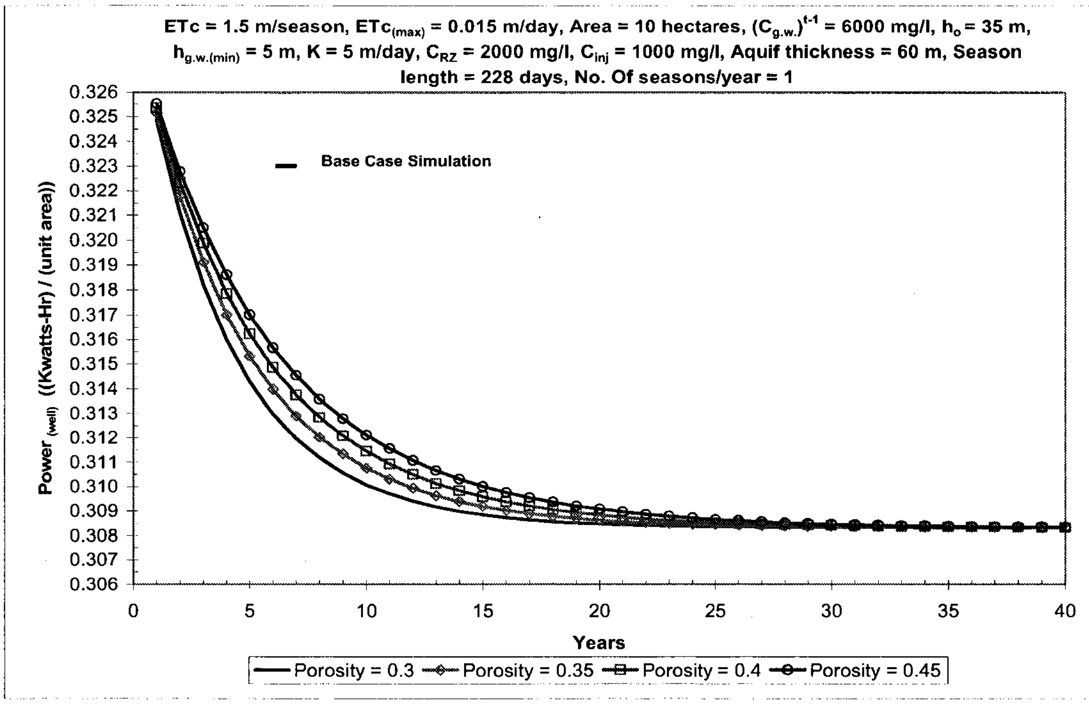

Figure 4.25 Amount of treated wastewater injected into the native groundwater for ranges of different porosity, Φ, input values vs. simulation period.

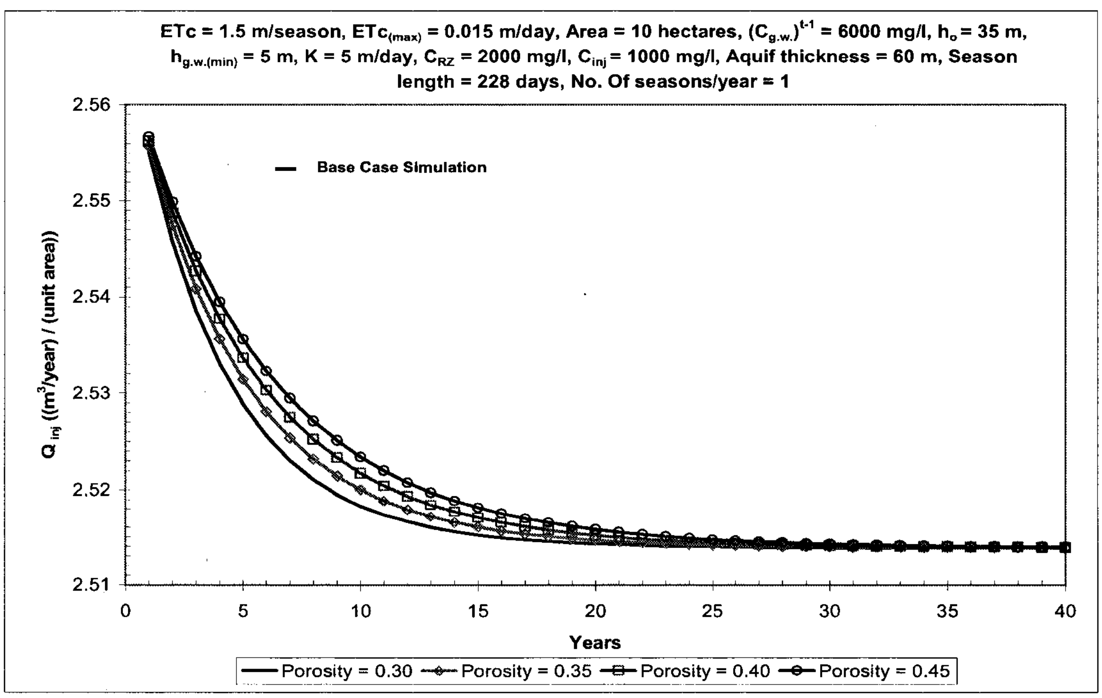

 Emad H. AlAli

Figure 4.26 Initial groundwater salt concentrations for ranges of different porosity, $\boldsymbol{\Phi}$, input values vs. simulation period.

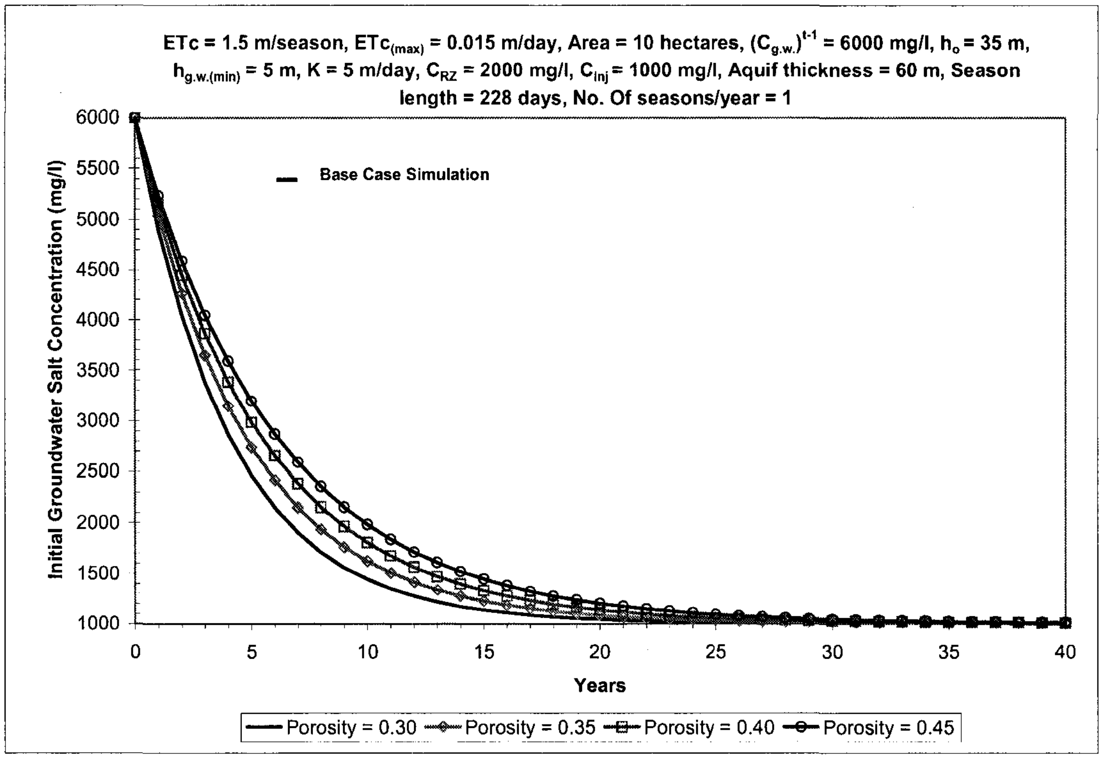

From Figures 4.22 and 4.25, it is obvious that as the porosity increases the higher the total power required by the system and the higher the amount of treated wastewater required to be injected into the groundwater. As the porosity increases, the initial volume of groundwater will increase. Thus, the initial salt mass quantity of the groundwater will increase. Moreover, due to larger initial groundwater volume, the enhancement of the salt concentration of the groundwater will be delayed compared with smaller porosity (where the groundwater volume is less) as the simulation progresses. Thus, the pumped groundwater initial salt concentration will be relatively higher as the initial groundwater volume increases, due to the increase in porosity (Figure 4.26). Due to the increase in the pumped groundwater salt concentration, the feed water to the reverse osmosis unit will be at a relatively higher salt concentration. Hence, the water permeate from the reverse osmosis unit will be at a higher concentration, too. Therefore, the more permeate water is required (to be used as irrigation water) to cope with the irrigation efficiency, the higher the salt concentration in the irrigation water and the higher the amount of irrigation water needed to be applied to keep the root zone at the desirable salt concentration tolerance. Hence, irrigation water demand will increase to meet this increase in the porosity. Moreover, to meet this increase in the irrigation water demand, a larger groundwater amount must be pumped and fed to the reverse osmosis unit to cope with the irrigation water requirement increases. Therefore, the higher the pumped groundwater amount required to be fed to the reverse osmosis unit the higher the amount of water needed to be desalinated and the more power will be consumed by the reverse osmosis unit (Figure 4.23). In addition, the higher the pumped groundwater requirement the higher the power consumption will be excreted by the pump (Figure 4.24). To cope with the increase in irrigation water demand, this leads to an increase in pumped groundwater, and to prevent the groundwater from mining, the higher the treated wastewater injection rate into the groundwater zone required to compensate for the higher water demand by the system (Figure 4.25). As the porosity increases, the higher the salt mass quantity will be present in the groundwater; therefore, the larger the porosity the more the enhancement of the groundwater quality will be retarded in the long run (Figure 4.26).

Figures 4.27 and 4.28 illustrate the sum of the total power required by the system for 40-year simulations for ranges of different porosity, $\boldsymbol{\Phi}$, input values, and the sum of the treated wastewater injected amount into the native groundwater for 40-year simulations for ranges of different porosity, $\boldsymbol{\Phi}$, input values. Moreover, Table 4.10 demonstrates the percent increase in the total power consumption and the treated wastewater injection into the groundwater zone as the porosity, $\boldsymbol{\Phi}$, increases.

Figure 4.27 Sum of total power required by the system for 40-year simulations for ranges of different porosity, $\boldsymbol{\Phi}$, values.

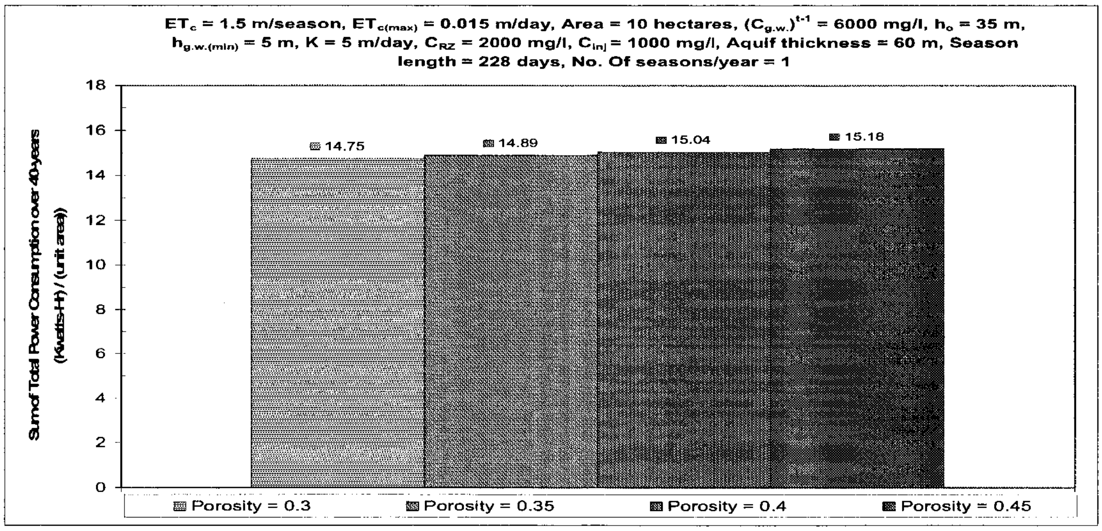

Figure 4.28 Sum of treated wastewater injected into the native groundwater for 40-year simulations for ranges of different porosity, $\boldsymbol{\Phi}$, values.

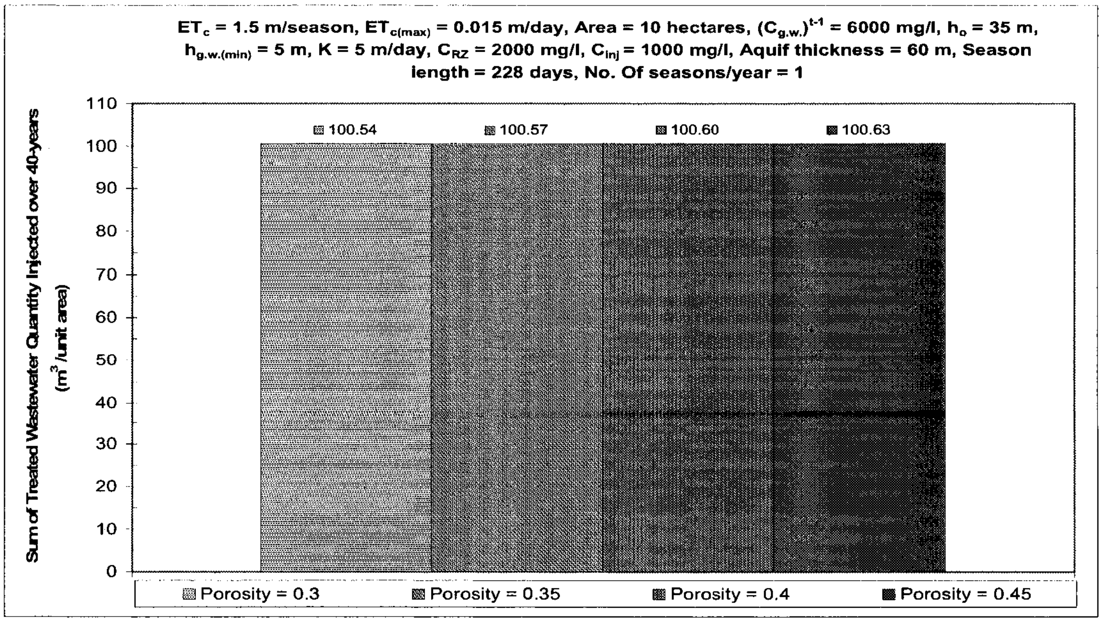

Table 4.10 Percent increase in the sum of the total power consumption and the sum of the treated wastewater injection as the porosity increases.

Φ Changes		% Change (increase) in Φ	% Change (increase) in the Sum of the Total Power per Unit Area	% Change (increase) in the Sum of the Injected Treated Wastewater per Unit Area
From	To			
0.30	0.35	14.29	0.94	0.03
0.30	0.40	25.00	1.93	0.06
0.30	0.45	33.33	2.83	0.09

* Base case Φ = 0.30.

4.1.5 Hydraulic Conductivity, *K*

Hydraulic conductivity, ***K***, is of essential significance to groundwater variable input data in the simulation, as it measures the ease with which a fluid (water) can be transmitted in the porous media. Hydraulic conductivity data ranges (3 m/day – 7 m/day) were chosen to handle and distinguish the moderate hydraulic conductivity (i.e. ***K*** = 1 – 10 m/day) of porous media (Table 4.11). Thus, to test the sensitivity and performance of the general conceptual design system, the simulation will be executed five times, using five hydraulic conductivity values while keeping all other variables constant (Table 4.12). Simulation calculation procedures followed similar steps as those presented in Section 3.2. Moreover, all other required input data, except ***K*** and field area, will be the same as in Tables 3.1, 3.2, and 3.7.

Results for ***K*** simulations of testing the sensitivity and performance of the general conceptual design system were captured in Figures 4.29, 4.30, 4.31, 4.32, and 4.33 respectively. These output result graphs were arranged by the total power required by the system, the power required by the reverse osmosis unit, the power required by the well pump system, the amount of wastewater injected into the native groundwater, and the initial groundwater salt concentrations respectively.

Table 4.11 Representative values of hydraulic conductivity (after Morris and Johnson, 1967).

Material	Hydraulic Conductivity, (m / day)	Material	Hydraulic Conductivity, (m / day)
Gravel, coarse	150	Dune sand	20
Gravel, medium	270	Loess	0.08
Gravel, fine	450	Peat	5.7
Sand, coarse	45	Schist	0.2
Sand, medium	12	Slate	0.00008
Sand, fine	2.5	Till, Predominantly silt	0.49
Silt	0.08	Till, Predominantly sand	30
Clay	0.0002	Tuff	0.2
Sandstone, fine -grained	0.2	Basalt	0.01
Sandstone, medium- grained	3.1	Gabbro, weathered	0.2
Limestone	0.94	Granite, weathered	1.4
Dolomite	0.001		

Table 4.12 Test of the sensitivity and the performance of the general conceptual model by perturbing hydraulic conductivity values, ***K***, while keeping all other variables constant.

Run No.	ET_c *(m/season)*	$ET_{c\,(max)}$ *(m/day)*	C_{RZ} *(mg/l)*	C_{inj} *(mg/l)*	Φ *(m^3/m^3)*	*K* *(m/day)*	h_o *(m)*	$(C_{g.w.})^{t-1}$ *(mg/l)*
1	1.50	0.015	2000	1000	0.3	3	35	6000
2	1.50	0.015	2000	1000	0.3	4	35	6000
3*	1.50	0.015	2000	1000	0.3	5	35	6000
4	1.50	0.015	2000	1000	0.3	6	35	6000
5	1.50	0.015	2000	1000	0.3	7	35	6000

* Base case simulation.

Figure 4.29 Total power required by the system for ranges of different hydraulic conductivity, ***K***, input values vs. simulation period.

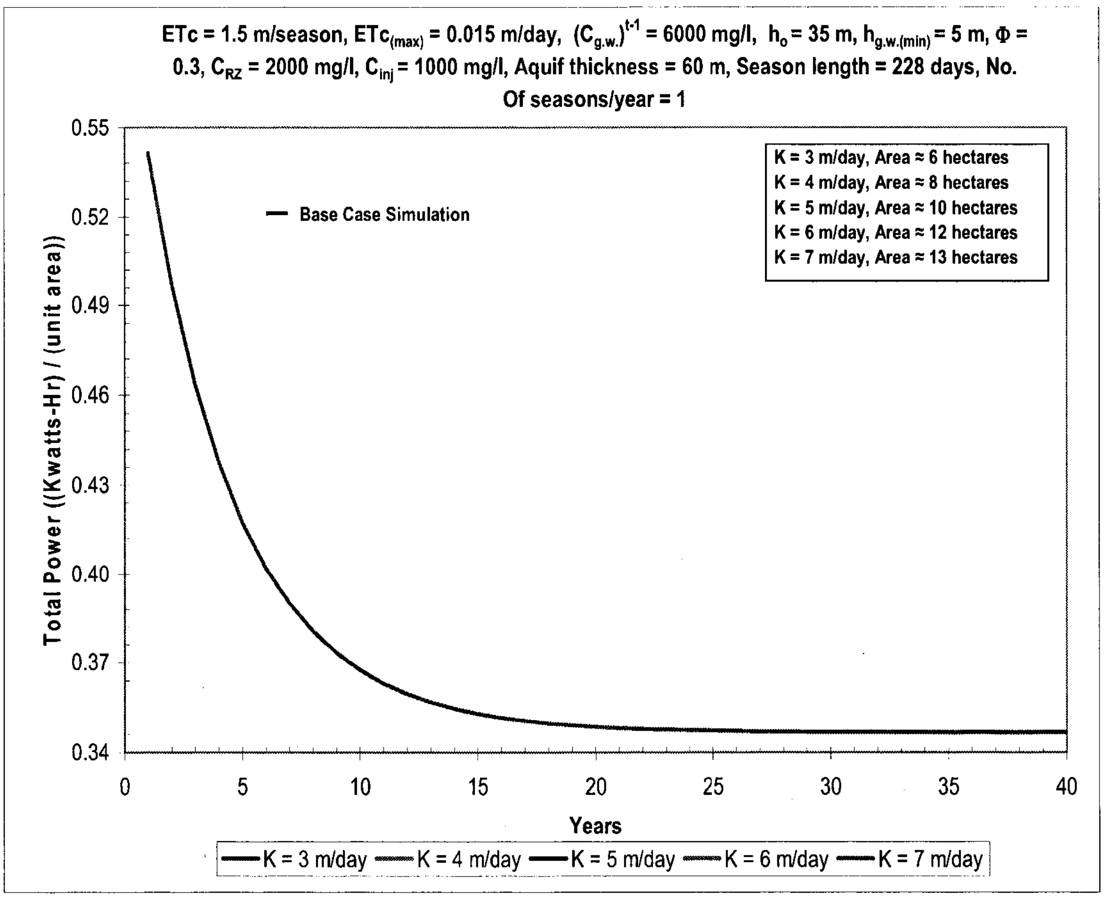

 Emad H. AlAli

Figure 4.30 Power required by the reverse osmosis unit for ranges of different hydraulic conductivity, ***K***, input values vs. simulation period.

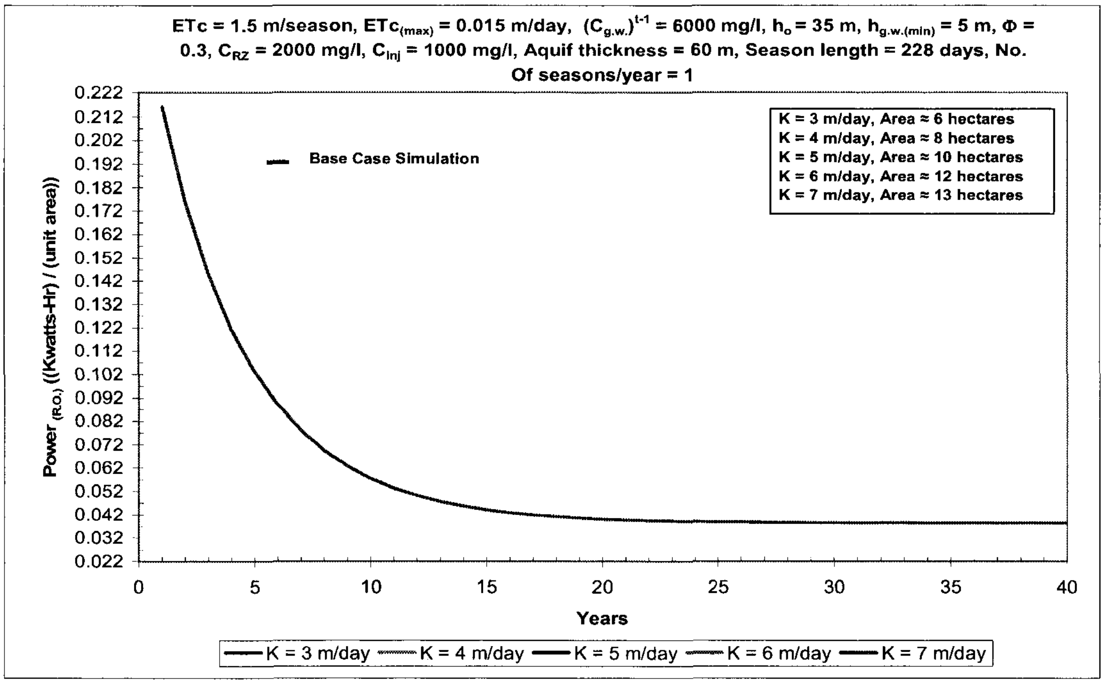

Figure 4.31 Power required by the well pump system for ranges of different hydraulic conductivity, ***K***, input values vs. simulation period.

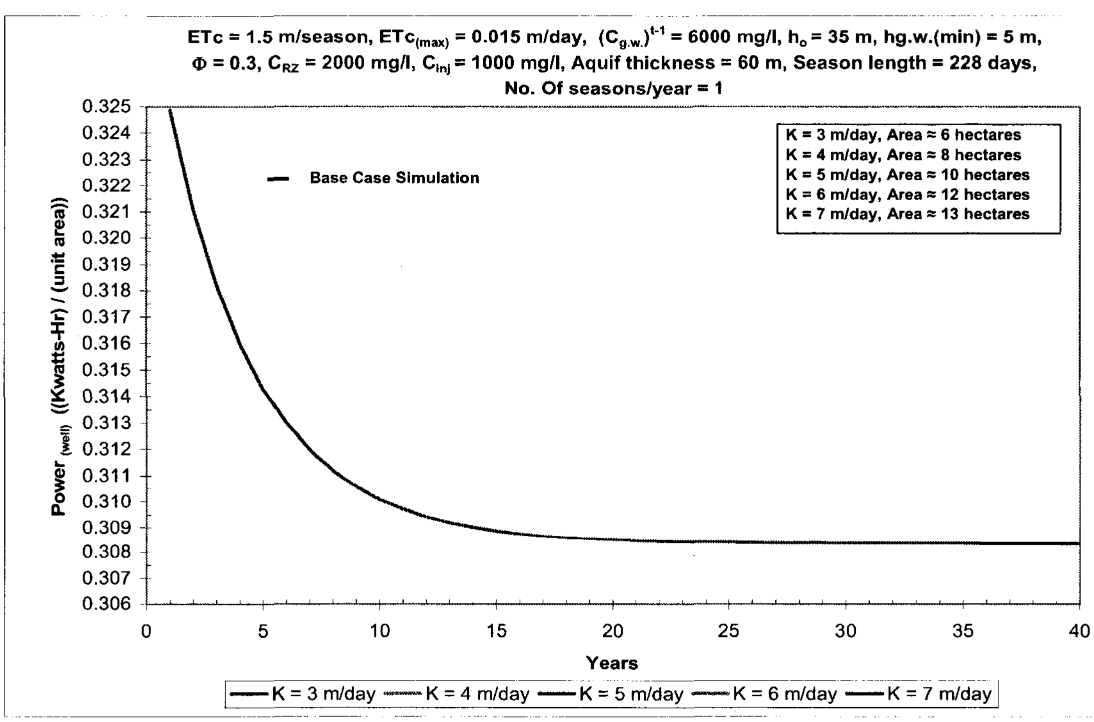

Figure 4.32 Amount of treated wastewater injected into the native groundwater for ranges of different hydraulic conductivity, ***K***, input values vs. simulation period.

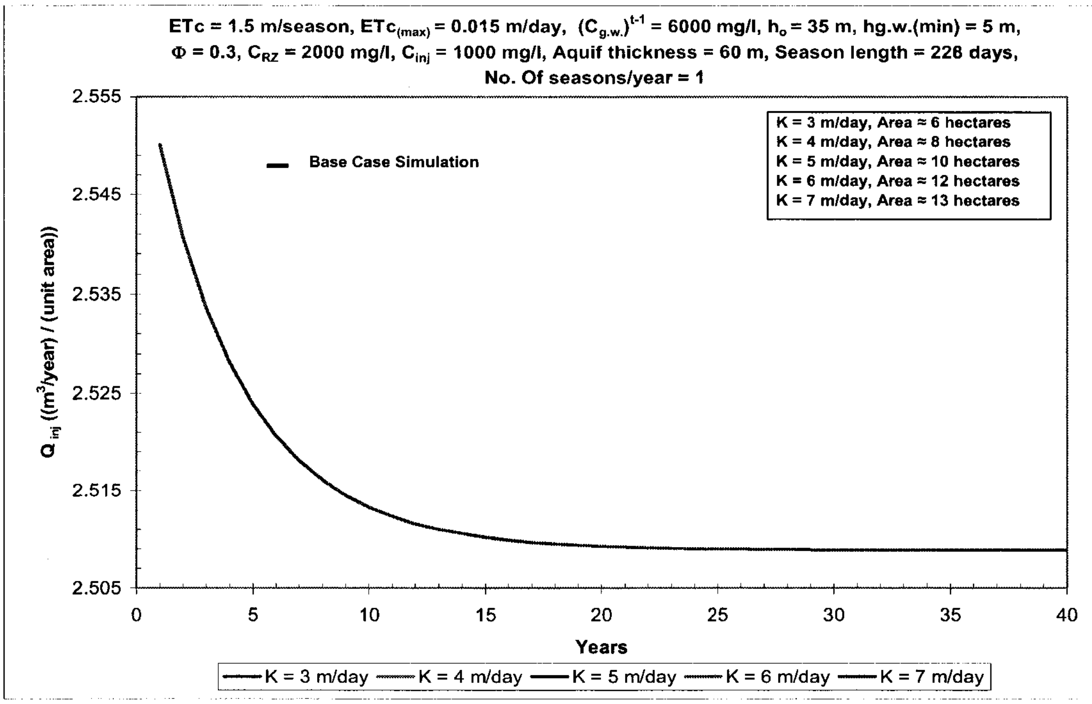

Figure 4.33 Initial groundwater salt concentrations for ranges of different hydraulic conductivity, ***K***, input values vs. simulation period.

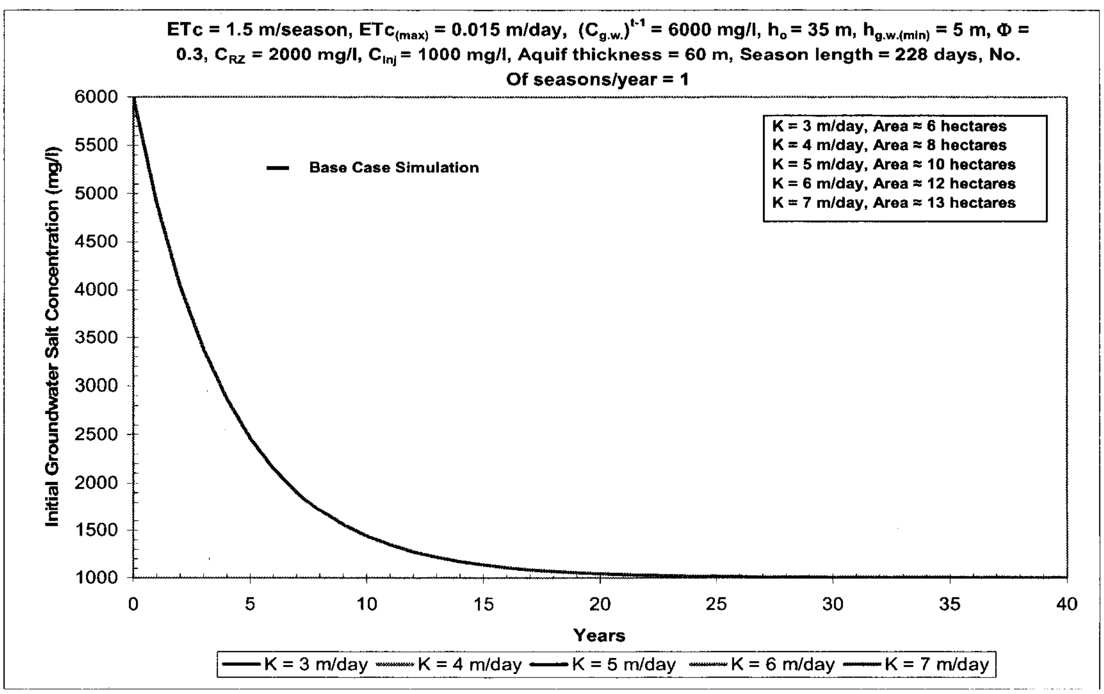

From Figures 4.29 and 4.32, it is obvious that as the hydraulic conductivity, ***K***, increases the total power required by the system per unit area, and the amount of treated wastewater required to be injected into the groundwater zone per unit area does not change for ranges of hydraulic conductivity values. The hydraulic conductivity measures the ease with which a fluid (water) can be transmitted in the porous media. Thus, the higher the hydraulic conductivity of the soil matrix of the aquifer the more groundwater can be pumped from the groundwater zone. The higher the hydraulic conductivity the higher the amount of water that can be yielded from the aquifer for the same maximum allowed drawdown (minimum unconfined aquifer thickness). Therefore, due to this higher groundwater pumping yield capacity from the groundwater zone, a larger irrigated farm area can be utilized (Figure 4.34). Thus, higher crop yield can be produced which will lead to higher crop revenues. Although increase in hydraulic conductivity has no direct impact on the total power requirement by the system per unit area and on the injected treated wastewater amount into the groundwater per unit area, the higher the hydraulic conductivity the larger irrigated farm area can be utilized. Therefore, to cope with the increase in irrigated area, the cost of well drilling and well construction completion, the cost of well pump and maintenance, and the cost of reverse osmosis unit and maintenance will be significantly higher as the irrigated area increases. In conclusion, the higher the hydraulic conductivity the larger the irrigated farm area the higher the crop revenue and the higher the capital cost of the system.

Figures 4.35 and 4.36 illustrate the sum of the total power required by the system for 40-year simulations for ranges of different hydraulic conductivity, ***K***, input values, and the sum of the treated wastewater injected amount into the native groundwater for

40-year simulations for ranges of different hydraulic conductivity, ***K***, input values. Moreover, Table 4.13 demonstrates the percent increase in the total power consumption, the treated wastewater injection into the groundwater zone, and the farm area as hydraulic conductivity, ***K***, increases.

Figure 4.34 Hydraulic conductivity vs. irrigated farm area.

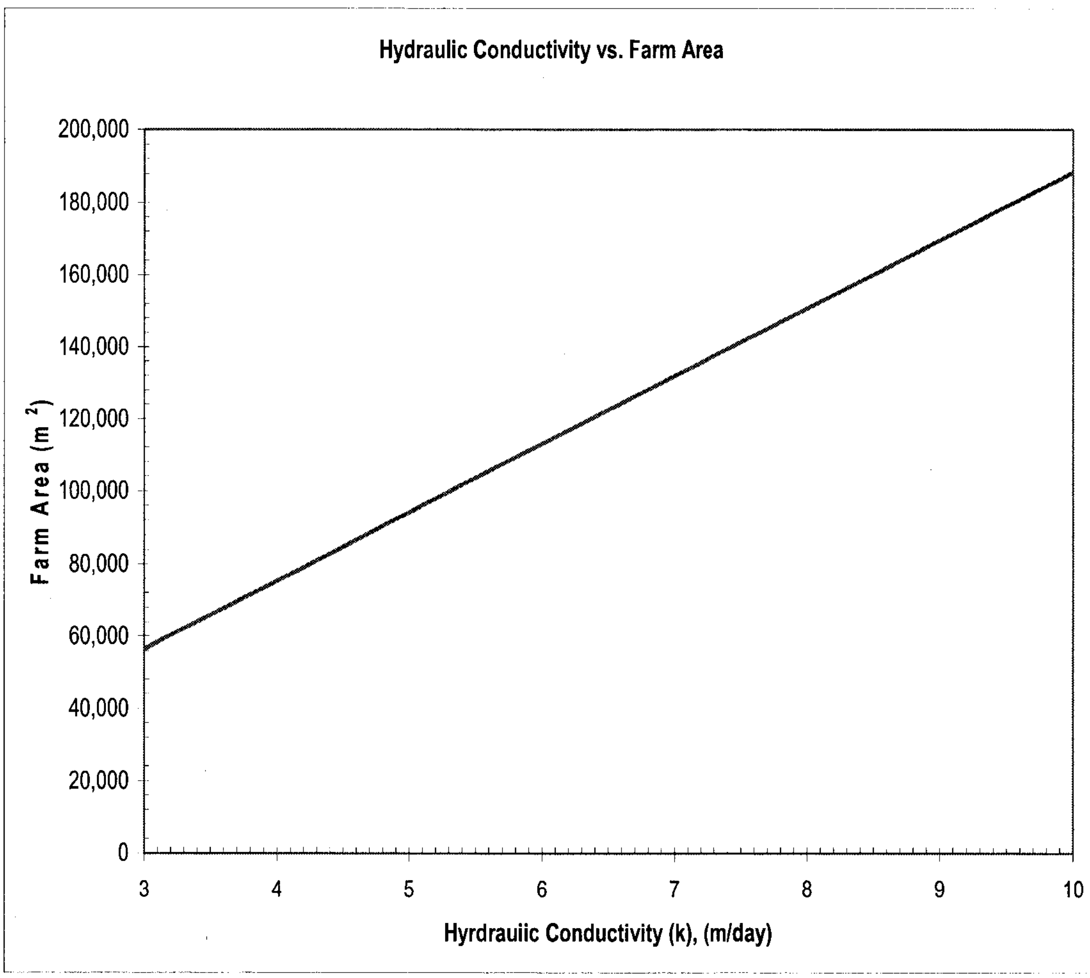

 Emad H. AlAli

Figure 4.35 Sum of the total power required by the system for 40-year simulations for ranges of different hydraulic conductivity, ***K***, values.

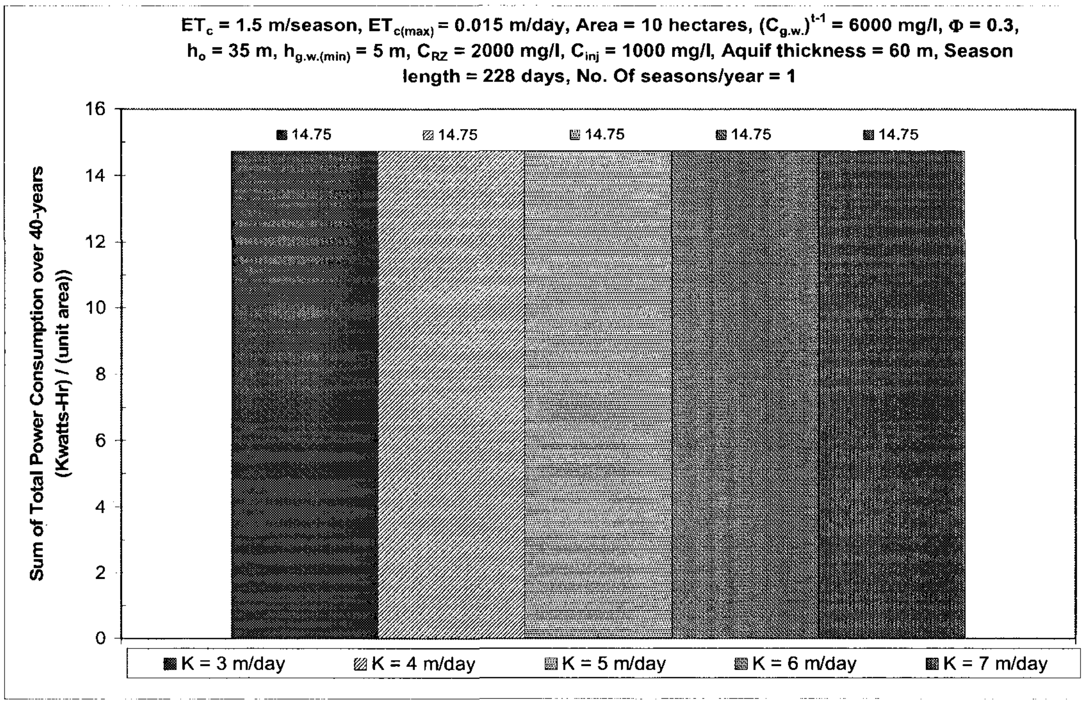

Figure 4.36 Sum of treated wastewater injected into the native groundwater for 40-year simulations for ranges of different hydraulic conductivity, ***K***, values.

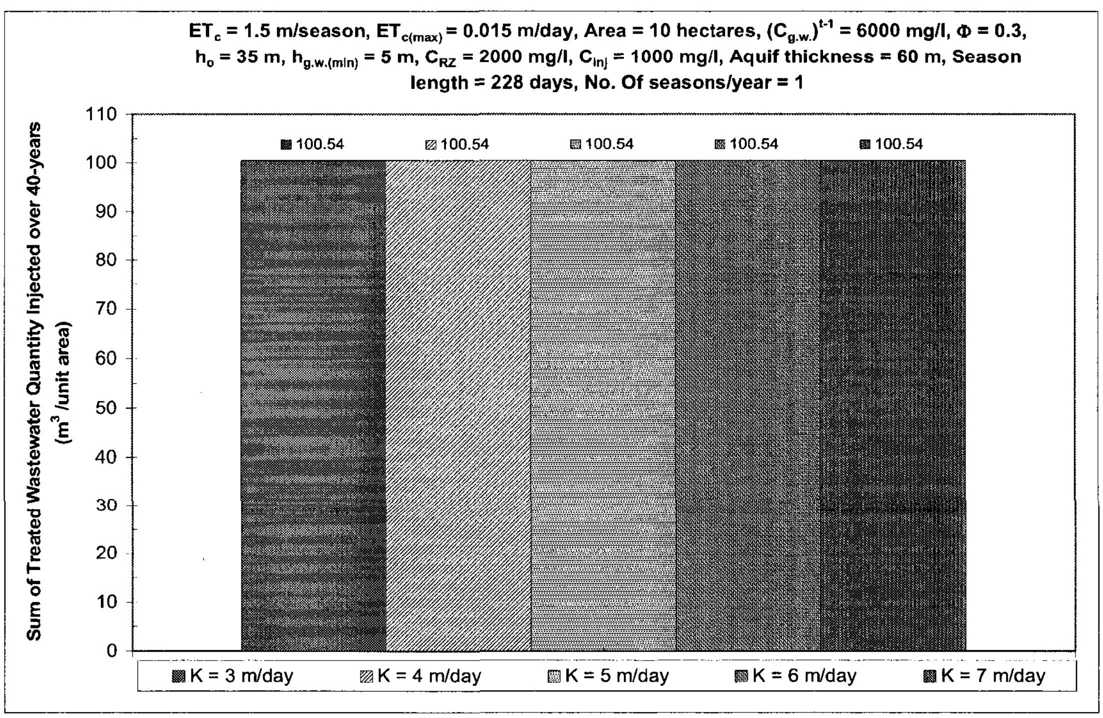

Table 4.13 Percent change in the sum of the total power consumption, the sum of the treated wastewater injection, and farm area as the hydraulic conductivity increases.

K Changes (m/day)		% Change (increase) in *K*	% Change (increase) in the Sum of the Total Power per Unit Area	% Change (increase) in the Sum of the Injected Treated Wastewater per Unit Area	% Change (increase) in Farm Area
From	To				
3	5	33.33	0	0	40.00
4	5	16.67	0	0	20.00
5	6	14.29	0	0	16.67
5	7	25.00	0	0	28.57

* Base case ***K*** = 5 m/day.

4.1.6 Initial Groundwater Table Hydraulic Head Elevation, h_o

Initial groundwater table hydraulic head elevation, h_o, is of vital importance to groundwater variable input data in the simulation, as it determines the amount of lift needed to be exerted by the well pump. Initial groundwater table hydraulic head elevation data ranges (30 m – 50 m/day) were chosen to embody the average groundwater table elevation in most semi-arid and arid regions. Thus, to test the sensitivity and performance of the general conceptual design system, the simulation will be executed five times, using five initial groundwater table hydraulic head elevation values while keeping all other variables constant (Table 4.14). Simulation calculation procedures followed similar steps as those outlined in Section 3.2. Moreover, all other required input data, except h_o and field area, will be the same as in Tables 3.1, 3.2, and 3.7.

Results for initial groundwater table hydraulic head elevation, h_o, simulations of testing the sensitivity and performance of the general conceptual design system were captured in Figures 4.26, 4.27, 4.28, 4.29, and 4.30 respectively. These output result graphs were arranged by the total power required by the system, the power required by the reverse osmosis unit, the power required by the well pump system, the amount of wastewater injected into the native groundwater, and the initial groundwater salt concentrations respectively.

Table 4.14 Test of the sensitivity and the performance of the general conceptual model by perturbing initial groundwater table hydraulic head values, h_o, while keeping all other variables constant.

Run No.	*ET_c (m/season)*	*$ET_{c\,(max)}$ (m/day)*	*C_{RZ} (mg/l)*	*C_{inj} (mg/l)*	*Φ (m^3/m^3)*	*K (m/day)*	*h_o (m)*	*$(C_{g.w.})^{t-1}$ (mg/l)*
1	1.50	0.015	2000	1000	0.3	5	**30**	6000
2*	1.50	0.015	2000	1000	0.3	5	**35**	6000
3	1.50	0.015	2000	1000	0.3	5	**40**	6000
4	1.50	0.015	2000	1000	0.3	5	**45**	6000
5	1.50	0.015	2000	1000	0.3	5	**50**	6000

* Base case simulation.

Figure 4.37 Total power required by the system for ranges of different initial water table hydraulic head elevations, h_o, input values vs. simulation period.

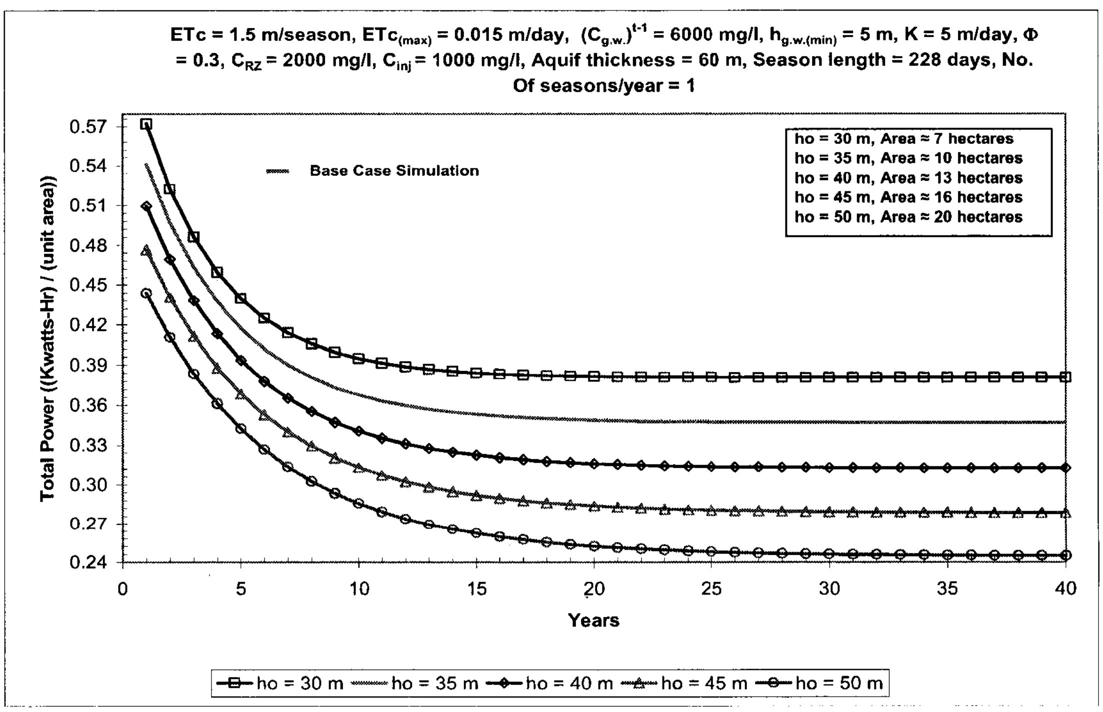

 Emad H. AlAli

Figure 4.38 Power required by the reverse osmosis unit for ranges of different initial water table hydraulic head elevations, $\boldsymbol{h_o}$, input values vs. simulation period.

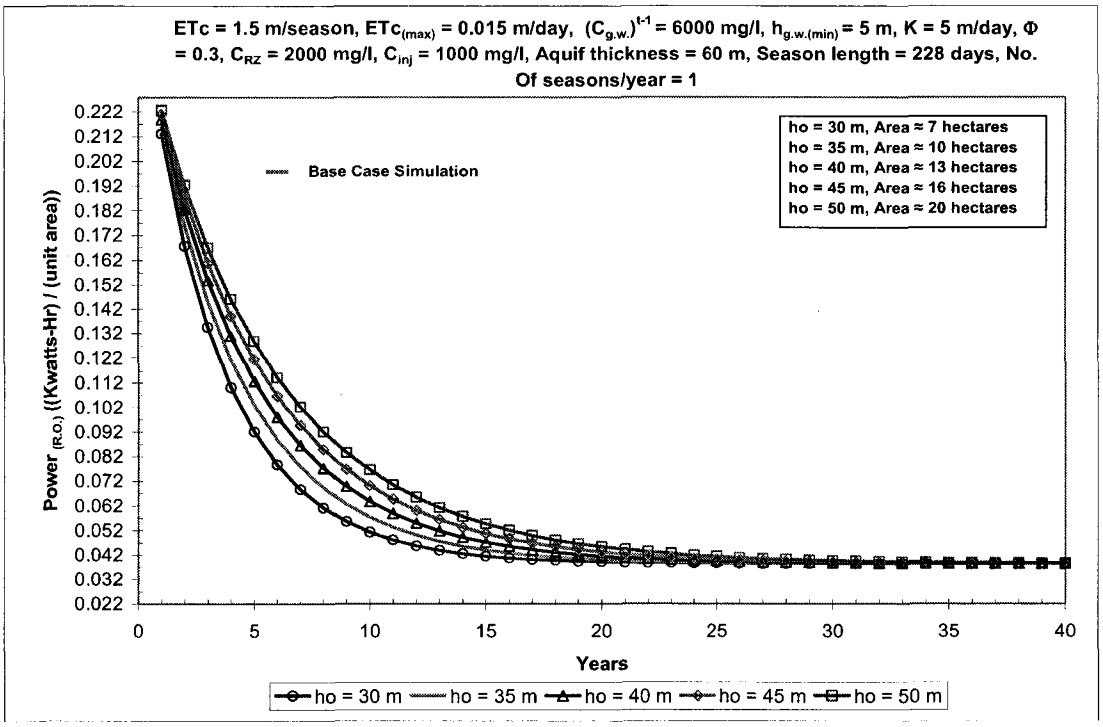

Figure 4.39 Power required by the well pump system for ranges of different initial water table hydraulic head elevations, $\boldsymbol{h_o}$, input values vs. simulation period.

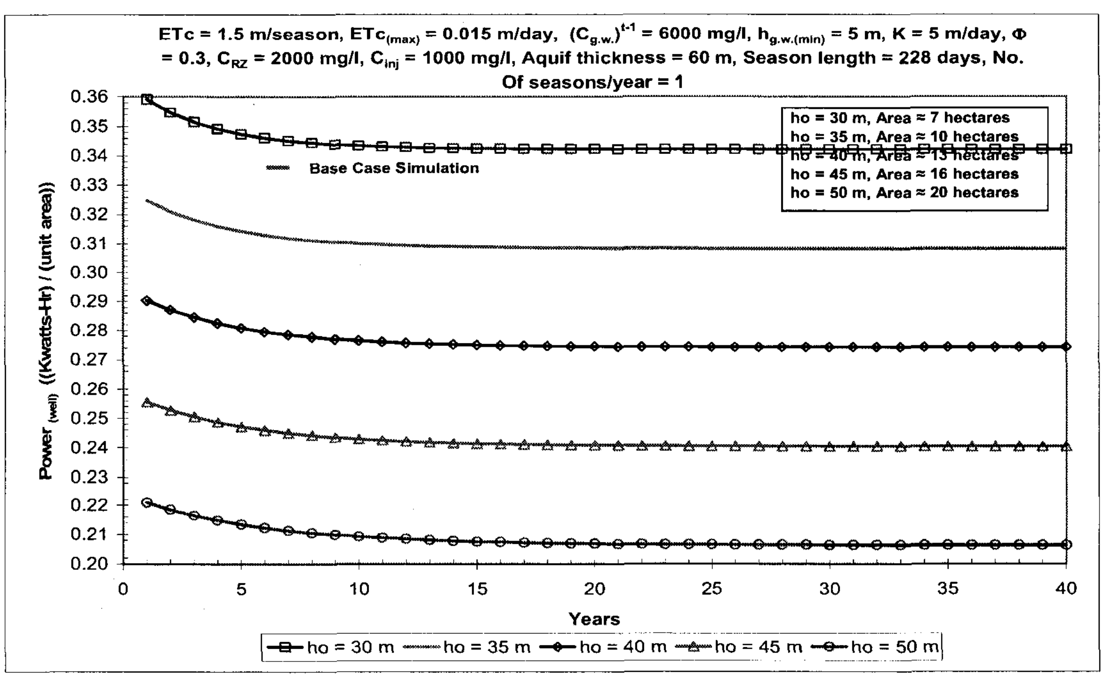

Figure 4.40 Amount of treated wastewater injected into the native groundwater for ranges of different initial water table hydraulic head elevations, $\boldsymbol{h_o}$, input values vs. simulation period.

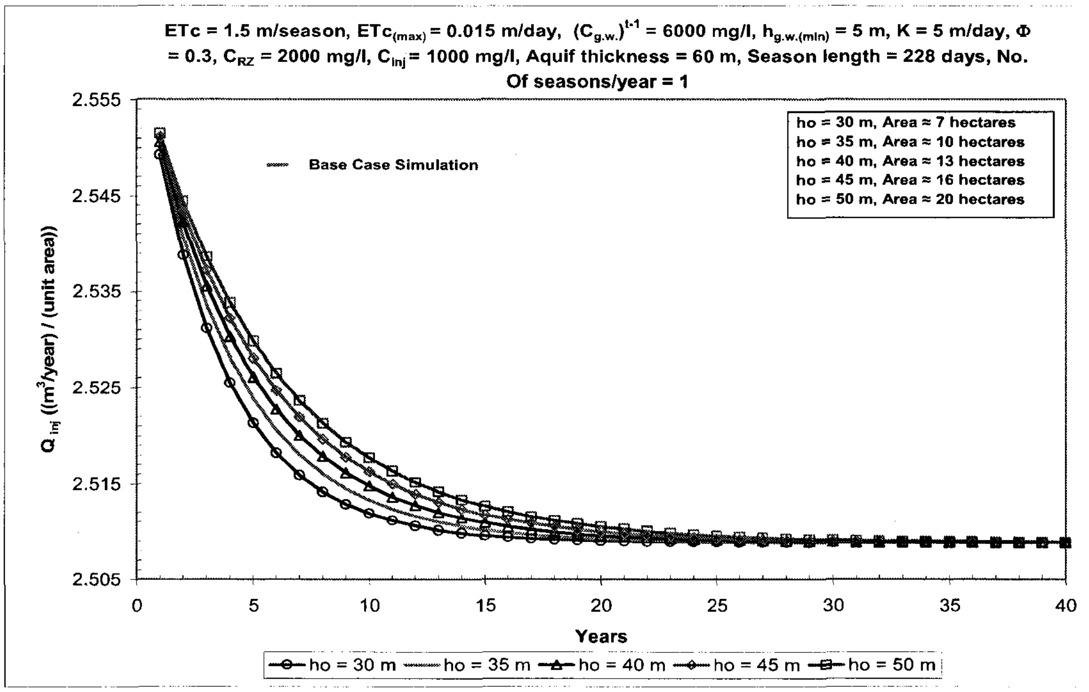

Figure 4.41 Initial groundwater salt concentrations for ranges of different initial water table hydraulic head elevations, $\boldsymbol{h_o}$, input values vs. simulation period.

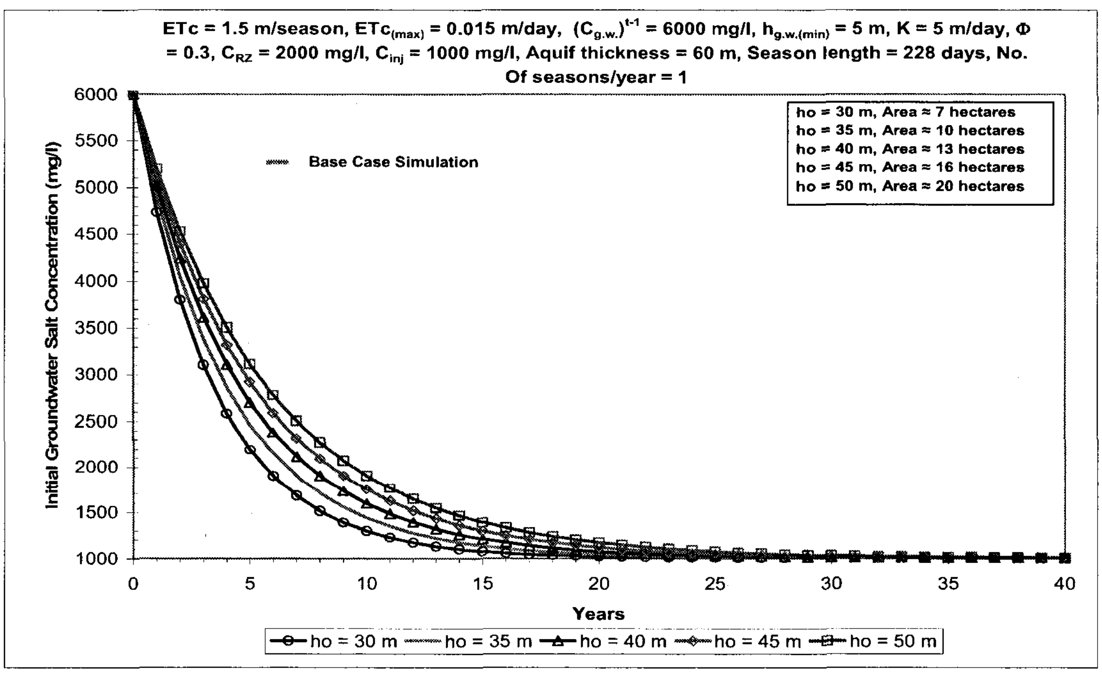

From Figures 4.37 and 4.40, it is obvious that as the initial water table hydraulic head elevations increase the lower the total power per unit area required by the system and the higher the amount of treated wastewater per unit area required to be injected into the groundwater zone. As the initial water table hydraulic head elevations increase, the initial volume of groundwater will increase. Thus, the initial salt mass quantity of the groundwater will increase. Moreover, due to the larger initial groundwater volume, the enhancement of the salt concentration of the groundwater will be delayed compared with the lower initial water table hydraulic head elevations (where the groundwater volume is less) as the simulation proceeds. Thus, the pumped groundwater initial salt concentration will be relatively higher as the initial groundwater volume increases due to the increase in initial water table hydraulic head elevations (Figure 4.41). Due to the increase in the pumped groundwater salt concentration, the feed water to the reverse osmosis unit will be at a relatively higher salt concentration. Hence, the water permeate from the reverse osmosis unit will be at a higher concentration, too. Therefore, the more permeate water required (to be used as irrigation water) to cope with the irrigation efficiency, the higher the salt concentration in the irrigation water and the higher the amount of irrigation water needed to be applied to keep the root zone at the desirable salt concentration tolerance. Hence, irrigation water demand will increase to meet this increase in the initial water table hydraulic head elevations. Moreover, to meet this increase in the irrigation water demand, a larger groundwater amount must be pumped and fed to the reverse osmosis unit to cope with the irrigation water requirement increases. Therefore, the higher the pumped groundwater amount required to be fed to the reverse osmosis unit the higher the amount of water needed to be desalinated and the more power will be consumed by the reverse osmosis unit (Figure 4.38). In addition, due to the increase in the initial water table hydraulic head elevations, the height of water to be lifted by the pump to the ground surface will be reduced, thus reducing the amount of power to be exerted by the pump. However, the power consumed by the reverse osmosis unit will increase as the initial water table hydraulic head elevations increase due to the increase in pumped groundwater salt concentration and the increase in the amount of the pumping water required. But, due to the pump power consumption reduction by reducing the left head, which is more dominant and influential (Figure 4.39), the total power exerted by the system will be reduced as the initial water table hydraulic head elevations increase. In other words, the reduction in power exerted by the pump is much higher than the power increase by the reverse osmosis system as the initial water table hydraulic head elevations increase. Thus, the total power of the system will be reduced. To cope with the increase in irrigation water demand, this leads to an increase in pumped groundwater, and to prevent the groundwater from mining, the higher the treated wastewater injection rate into the groundwater zone required to compensate for the higher water demand by the system (Figure 4.40). As the initial water table hydraulic head elevation increases, a higher salt mass quantity will be present in the groundwater; therefore, the higher the initial water table hydraulic head elevation the greater the enhancement of the groundwater quality will be retarded in the long run (Figure 4.41). Moreover, the higher the initial water table hydraulic head elevation the higher the amount of groundwater can be pumped from the aquifer for the same maximum allowed drawdown (minimum unconfined aquifer thickness). Therefore, due to this higher groundwater pumping yield capacity from the groundwater zone, a larger irrigated farm area can be utilized (Figure 4.42).

Figures 4.43 and 4.44 illustrate the sum of the total power required by the system for 40-year simulations for ranges of different initial water table hydraulic head elevations, h_o, input values, and the sum of the treated wastewater injected amount into the native groundwater for 40-year simulations for ranges of different initial water table hydraulic head elevations, h_o, input values. Moreover, Table 4.15 demonstrates the percent increase in the total power consumption, the treated wastewater injection into the groundwater zone, and the farm area as initial water table hydraulic head elevations, h_o, increases.

Figure 4.42 Water table hydraulic head elevation (***h₀***) vs. farm area.

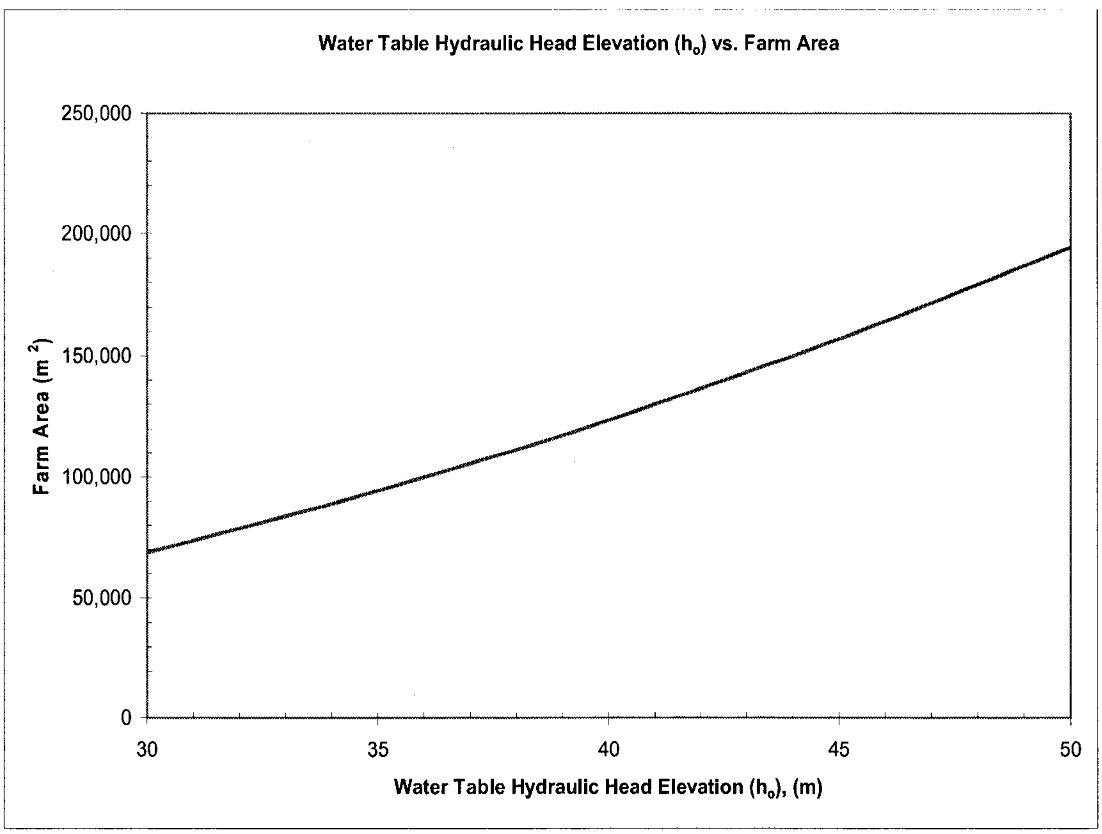

 Emad H. AlAli

Figure 4.43 Sum of total power required by the system for 40-year simulations for ranges of different initial water table hydraulic head elevations, h_o, values.

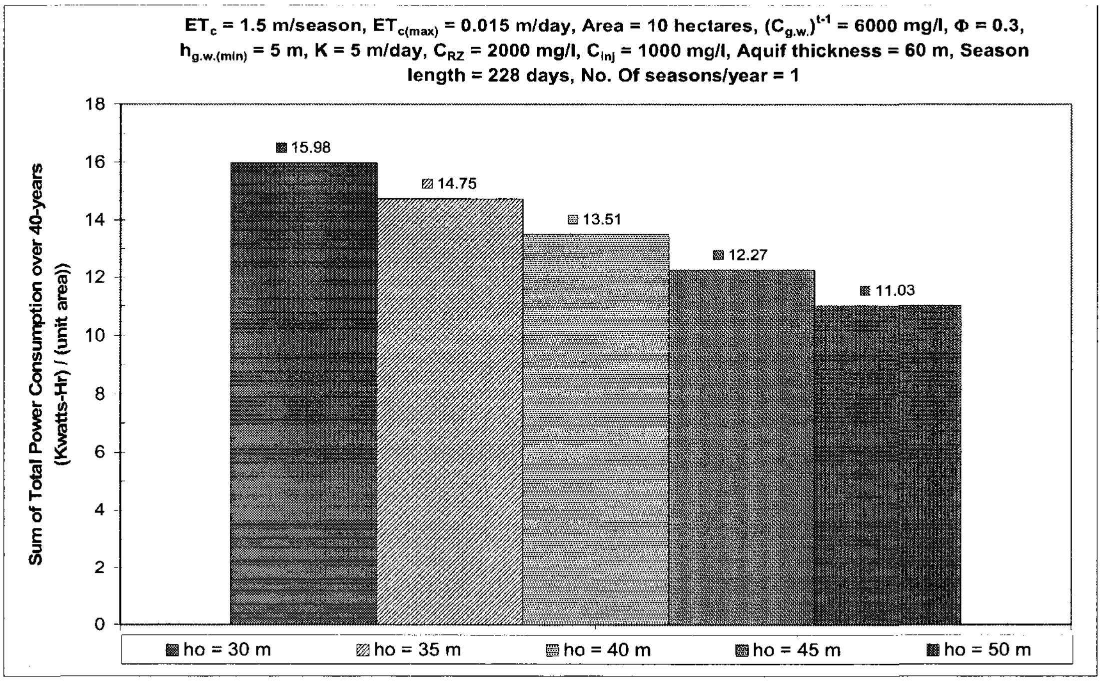

Figure 4.44 Sum of treated wastewater injected to the native groundwater for 40-year simulations for ranges of different initial water table hydraulic heads, h_o, values.

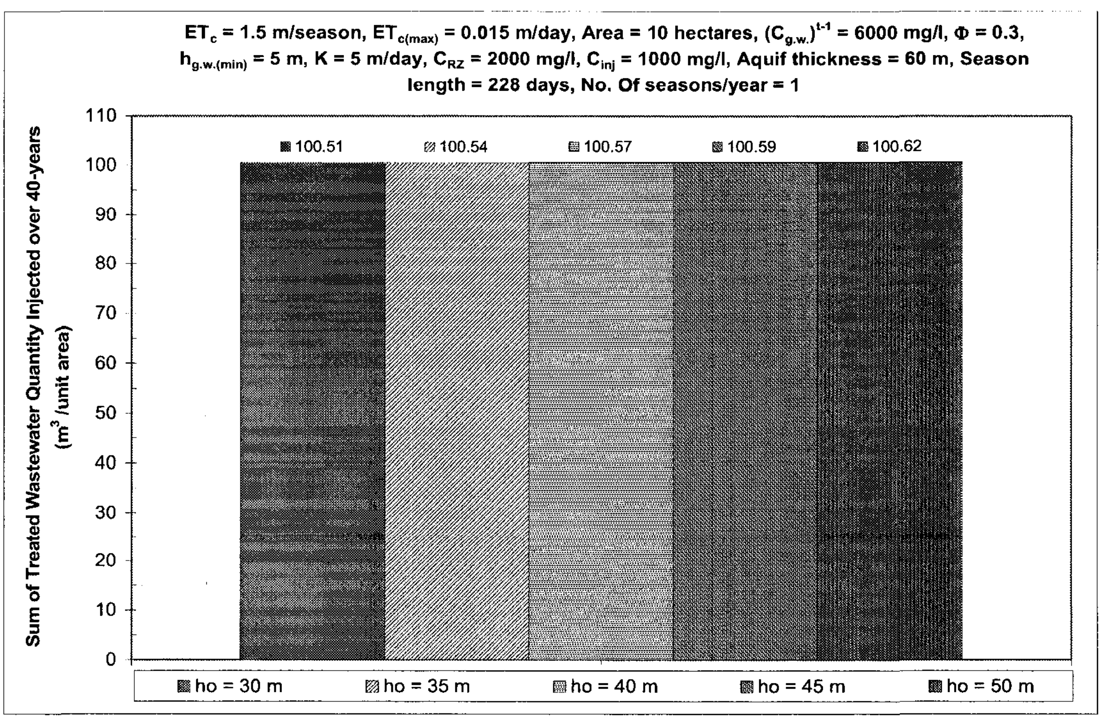

Table 4.15 Percent change in the sum of the total power consumption, the sum of the treated wastewater injection, and the farm area as the hydraulic initial water table hydraulic head elevation, h_o, increases.

h_o Changes (m)		% Change (increase) in h_o	% Change (decrease) in the Sum of the Total Power per Unit Area	% Change (increase) in the Sum of the Injected Treated Wastewater per Unit Area	% Change (increase) in the Farm Area
From	From				
30	35	14.29	7.70	0.03	27.08
35	40	12.50	8.41	0.03	23.81
35	45	22.22	16.81	0.05	40.00
35	50	30.00	25.22	0.08	51.52

* Base case h_o = 35 m.

4.1.7 Initial Groundwater Salt Concentration, $(C_{g.w.})^{t-1}$

Initial groundwater salt concentration of the native groundwater, $(C_{g.w.})^{t-1}$, is of crucial implication to groundwater variable input data in the simulation, as it determines the amount of distillation and power consumption needed to be exerted by the reverse osmosis unit. Initial groundwater salt concentration of the native groundwater data ranges (4000 mg/l – 12000 mg/l) were chosen to represent brackish to brine groundwater quality, which is incompatible for direct crop irrigation in general. Thus, to test the sensitivity and performance of the general conceptual design system, the simulation will be executed five times, using five initial groundwater salt concentration values while keeping all other variables constant (Table 4.16). Simulation calculation procedures followed steps similar to those in Section 3.2. Moreover, all other required input data, except $(C_{g.w.})^{t-1}$, will be the same as in Tables 3.1, 3.2, and 3.7.

Results for $(C_{g.w.})^{t-1}$ simulations of testing the sensitivity and performance of the general conceptual design system were captured in Figures 4.45, 4.46, 4.47, 4.48, and 4.49 respectively. These output result graphs were arranged by the total power required by the system, the power required by the reverse osmosis unit, the power required by the well pump system, the amount of wastewater injected to the native groundwater, and the initial groundwater salt concentrations respectively.

Table 4.16 Test of the sensitivity and the performance of the general conceptual model by perturbing initial groundwater salt concentration values, $(C_{g.w.})^{t-1}$, while keeping all other variables constant.

Run No.	ET_c (m/season)	$ET_{c\,(max)}$ (m/day)	C_{RZ} (mg/l)	C_{inj} (mg/l)	Φ (m^3/m^3)	K (m/day)	h_o (m)	$(C_{g.w.})^{t-1}$ (mg/l)
1	1.50	0.015	2000	1000	0.3	5	35	**4000**
2*	1.50	0.015	2000	1000	0.3	5	35	**6000**
3	1.50	0.015	2000	1000	0.3	5	35	**8000**
4	1.50	0.015	2000	1000	0.3	5	35	**10000**
5	1.50	0.015	2000	1000	0.3	5	35	**12000**

* Base case simulation.

Figure 4.45 Total power required by the system for ranges of different initial groundwater salt concentrations, $(C_{g.w.})^{t-1}$, input values vs. simulation period.

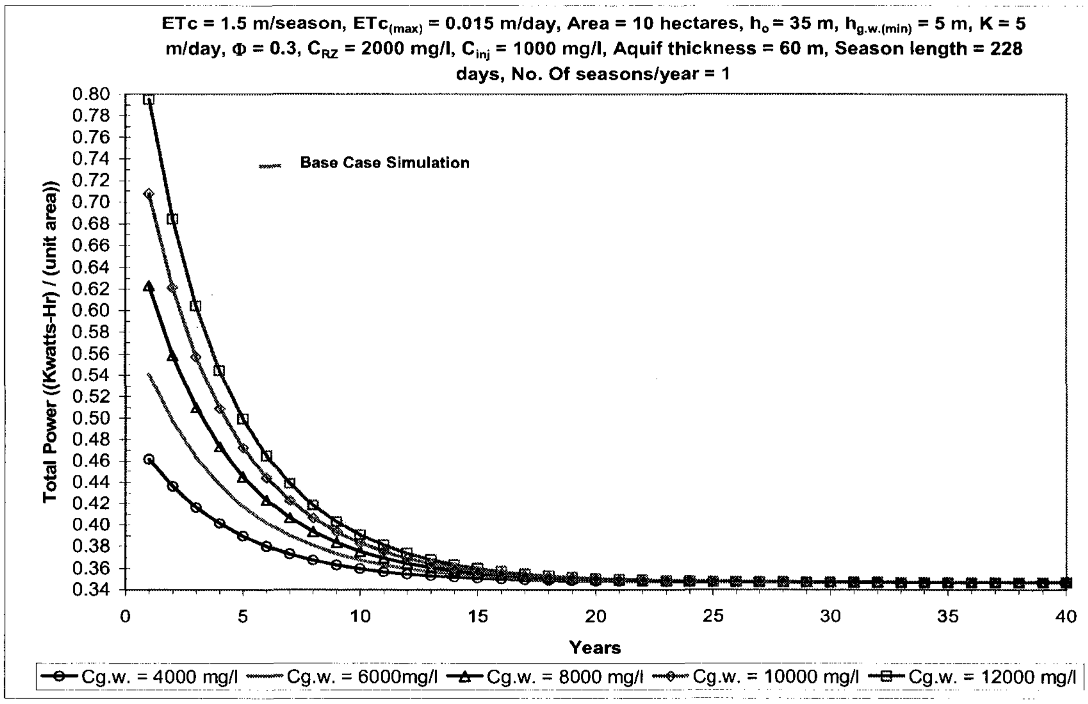

Figure 4.46 Power required by the reverse osmosis unit for ranges of different initial groundwater salt concentrations, $(C_{g.w.})^{t-1}$, input values vs. simulation period.

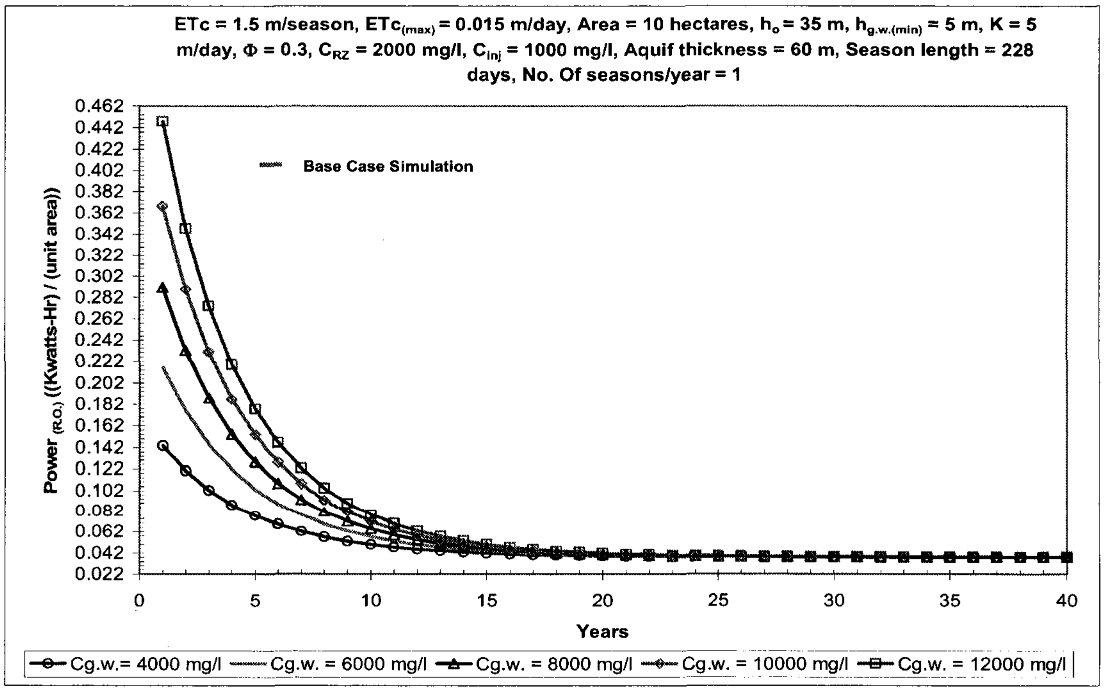

Figure 4.47 Power required by the well pump system for ranges of different initial groundwater salt concentrations, $(C_{g.w.})^{t-1}$, input values vs. simulation period.

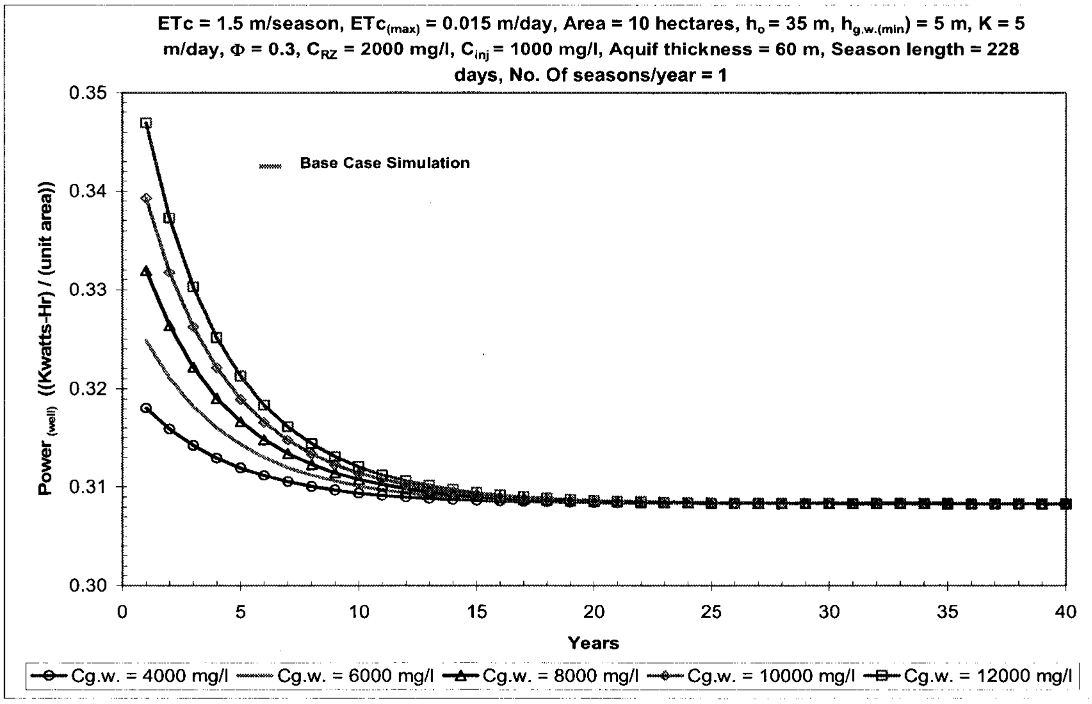

Figure 4.48 Amount of treated wastewater injected into the native groundwater for ranges of different initial groundwater salt concentrations, $(C_{g.w.})^{t-1}$, input values vs. simulation period.

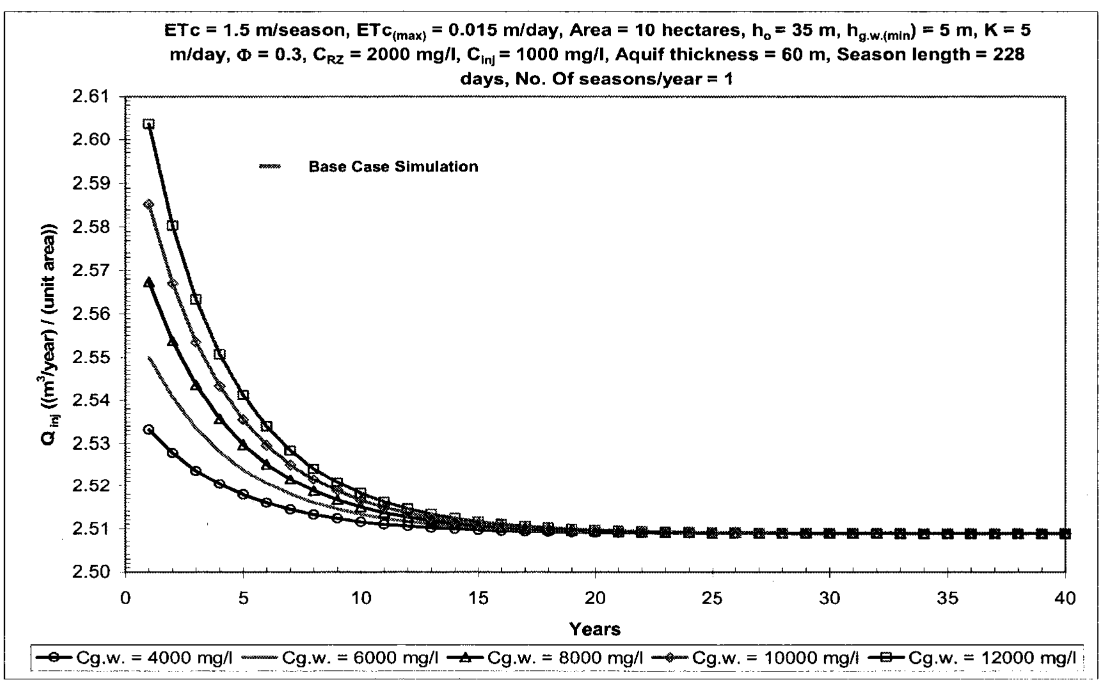

Figure 4.49 Initial groundwater salt concentrations for ranges of different initial groundwater salt concentrations, $(C_{g.w.})^{t-1}$, input values vs. simulation period.

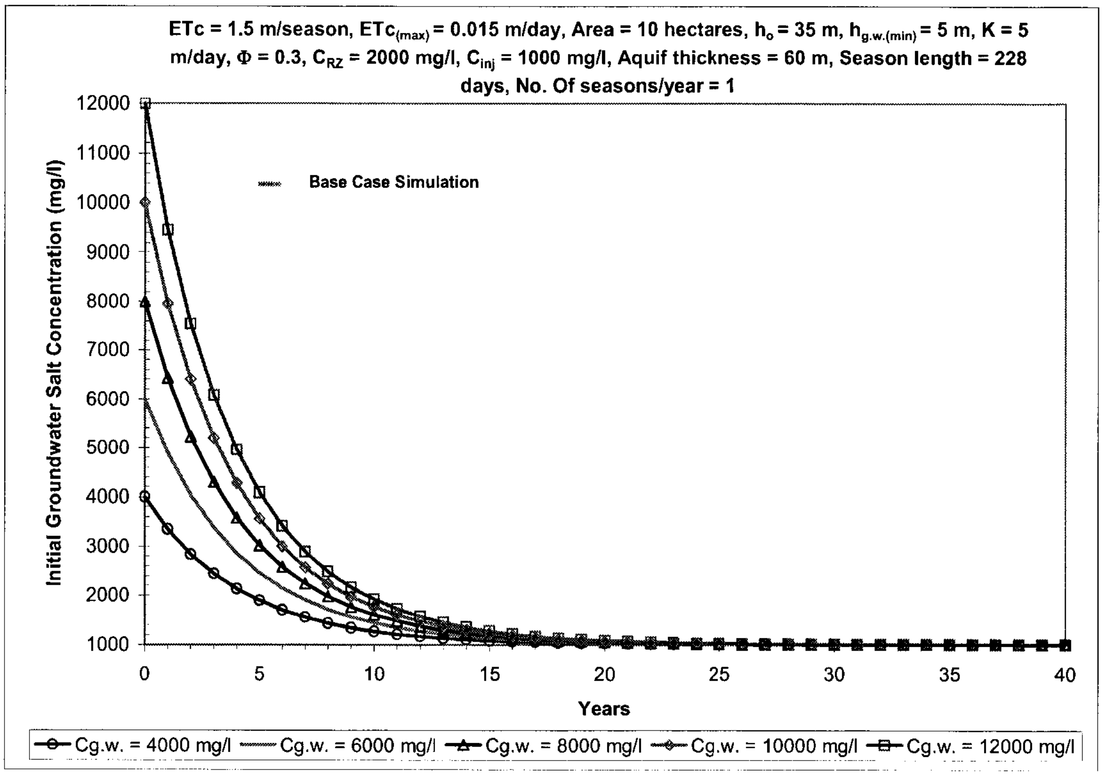

From Figures 4.45 and 4.48, it is obvious that as the initial groundwater salt concentration, $(C_{g.w.})^{t-1}$, increases the higher the total power required by the system, and the higher the amount of treated wastewater required to be injected into the groundwater zone. As the initial groundwater salt concentration increases the pumped groundwater salt concentration will be higher (Figure 4.49). Due to the increase in the pumped groundwater salt concentration, the feed water to the reverse osmosis unit will be at a higher salt concentration. Thus, the water permeate from the reverse osmosis unit will be at a higher concentration, too. Therefore, the more permeate water required (to be used as irrigation water) to cope with the irrigation efficiency, the higher the salt concentration in the irrigation water and the higher the amount of irrigation water needed to be applied to keep the root zone at the desirable salt concentration tolerance. Hence, irrigation water demand will increase to get by the increase in the groundwater salt concentration. Moreover, to meet this increase in the irrigation water demand, a larger groundwater amount must be pumped and fed to the reverse osmosis unit to cope with the irrigation water requirement increases. Therefore, the higher the pumped groundwater amount required to be fed to the reverse osmosis unit the higher the amount of water needed to be desalinated and the higher the power will be consumed by the reverse osmosis unit (Figure 4.46). In addition, the higher the pumped groundwater requirement the higher the power consumption will be used by the pump (Figure 4.47). To cope with the increase in irrigation water demand, this leads to an increase in pumped groundwater, and to prevent the groundwater from mining, the higher the treated wastewater injection rate into the groundwater zone required to compensate for the higher water demand by the system (Figure 4.48). As the initial groundwater salt concentration increases, a higher salt mass quantity will be present in the groundwater. Therefore, the higher the initial groundwater salt concentration the more the enhancement of the groundwater quality will be retarded in the long run (Figure 4.49).

Figures 4.50 and 4.51 illustrate the sum of the total power required by the system for 40-year simulations for ranges of initial groundwater salt concentrations, $(C_{g.w.})^{t-1}$, input values, and the sum of the treated wastewater injected amount into the native groundwater for 40-year simulations for ranges of different initial groundwater salt concentrations, $(C_{g.w.})^{t-1}$, input values. Moreover, Table 4.15 demonstrates the percent increase in the total power consumption and the treated wastewater injection into the groundwater zone, as initial groundwater salt concentration, $(C_{g.w.})^{t-1}$, increases.

Figure 4.50 Sum of total power required by the system for 40-year simulations for ranges of different initial groundwater salt concentrations, $(C_{g.w.})^{t-1}$, values.

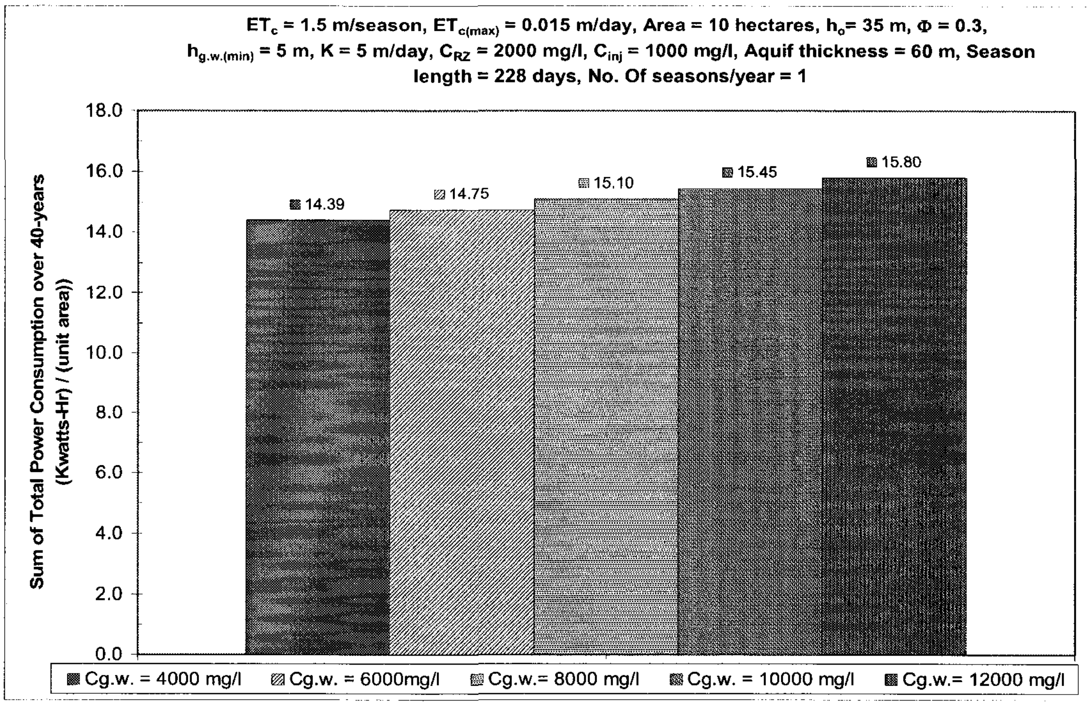

Figure 4.51 Sum of treated wastewater injected into the native groundwater for 40-year simulations for ranges of different initial groundwater salt concentrations values.

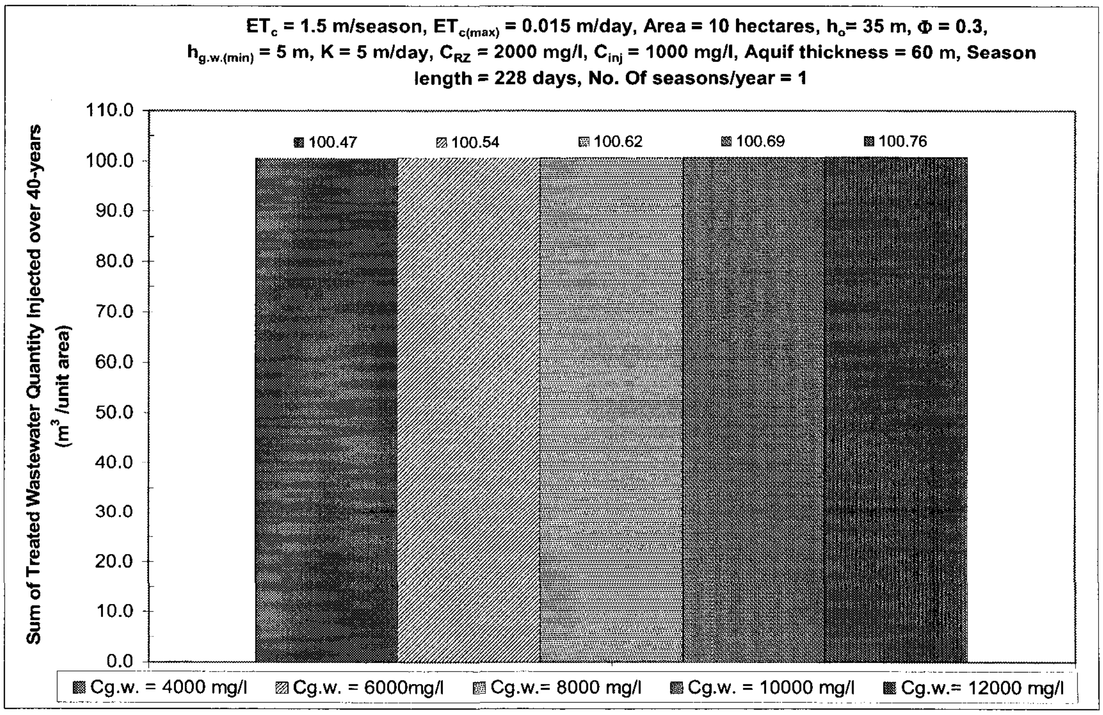

Table 4.17 Percent increase in the sum of the total power consumption and the sum of the treated wastewater injection as the hydraulic initial groundwater salt concentration, $(C_{g.w.})^{t-1}$, increases.

$(C_{g.w.})^{t-1}$ Changes (mg/l)		% Change (increase) in $(C_{g.w.})^{t-1}$	% Change (increase) in the Sum of the Total Power per Unit Area	% Change (increase) in the Sum of the Injected Treated Wastewater per Unit Area
From	**To**			
4000	**6000**	**33.33**	**2.44**	**0.07**
6000	**8000**	**25.00**	**2.32**	**0.08**
6000	**10000**	**40.00**	**4.53**	**0.15**
6000	**12000**	**50.00**	**6.65**	**0.22**

* Base case $(C_{g.w.})^{t-1}$ = 6000 mg/l.

CHAPTER 5

METHODOLOGY (SCENARIOS)

5.1 Scenarios

In this chapter of the dissertation, the simulation of the base case of the general conceptual design system will be executed while using a lump simulation model approach by using Visual Basic program. To examine the robustness and the viability of my system, the objective will consist of four perturbed scenarios of the general conceptual design system utilizing the lump model approach and comparing there performance with the base case simulation of the general conceptual design system utilizing a lump model approach. The first scenario will be practiced during the off planting season, to help acceleration and improvement of groundwater quality and water table height, thus, enhancing the power consumption of the system. The other three scenarios will assemble all possible obstacles or lateral reduction in the operation of the general conceptual design system due to emergencies or cost effects.

- **Off Planting Season Scenario.** In this scenario, treated wastewater will be augmented (injected) directly to the native groundwater during the off planting season. The groundwater pumping will cease during the off planting season compared to the original general conceptual design system (Figure 5.1).

Figure 5.1 Off planting season scenario of the general conceptual design system.

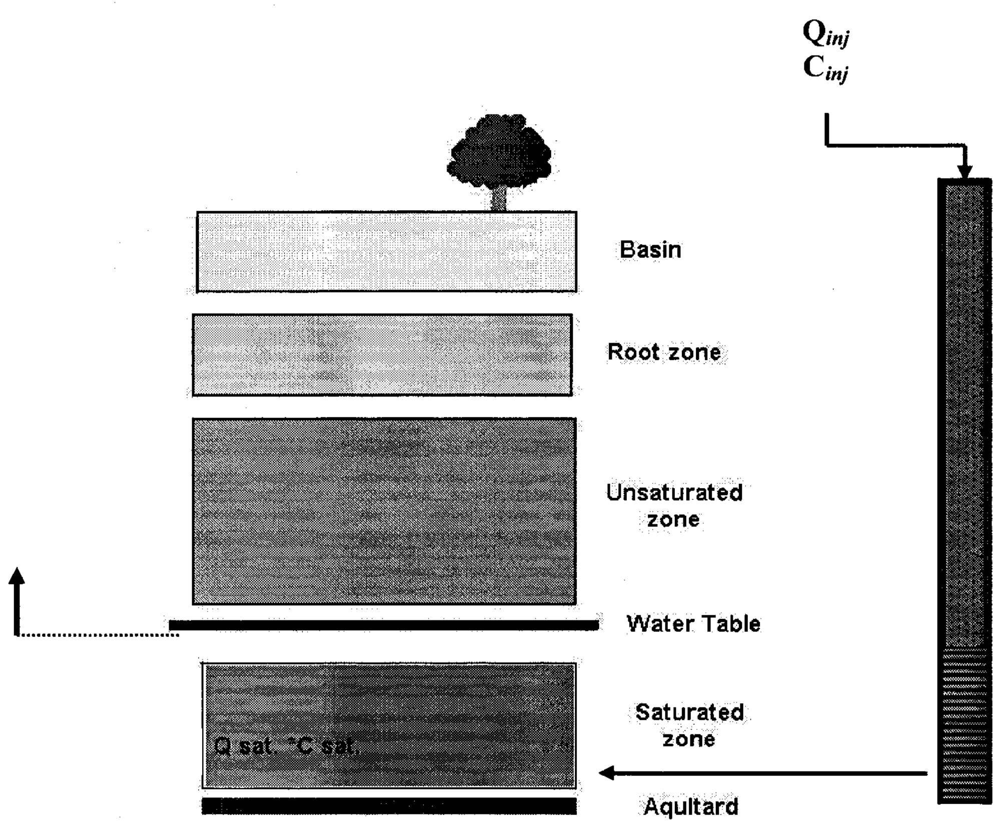

- **<u>Obstacle Scenario (1).</u>** In this scenario, treated wastewater augmentation (injection) to the native groundwater will cease during the planting season compared to the original general conceptual design system (Figure 5.2).

Figure 5.2 Obstacle scenario (1) of the general conceptual design system.

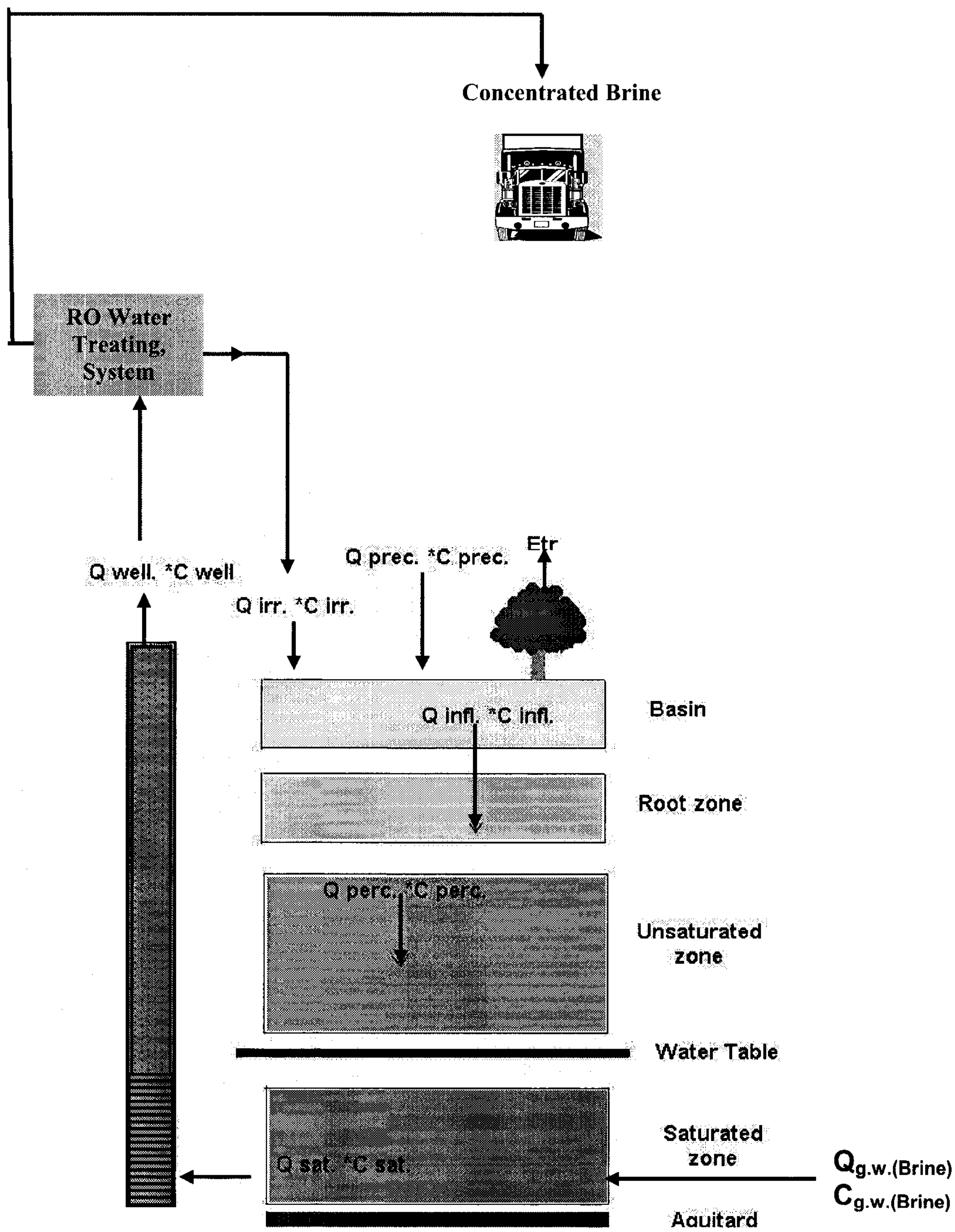

- **<u>Obstacle Scenario (2).</u>** In this scenario, the reverse osmosis system will be omitted from the original general conceptual design system (Figure 5.3).

Figure 5.3 Obstacle Scenario (2) of the general conceptual design system.

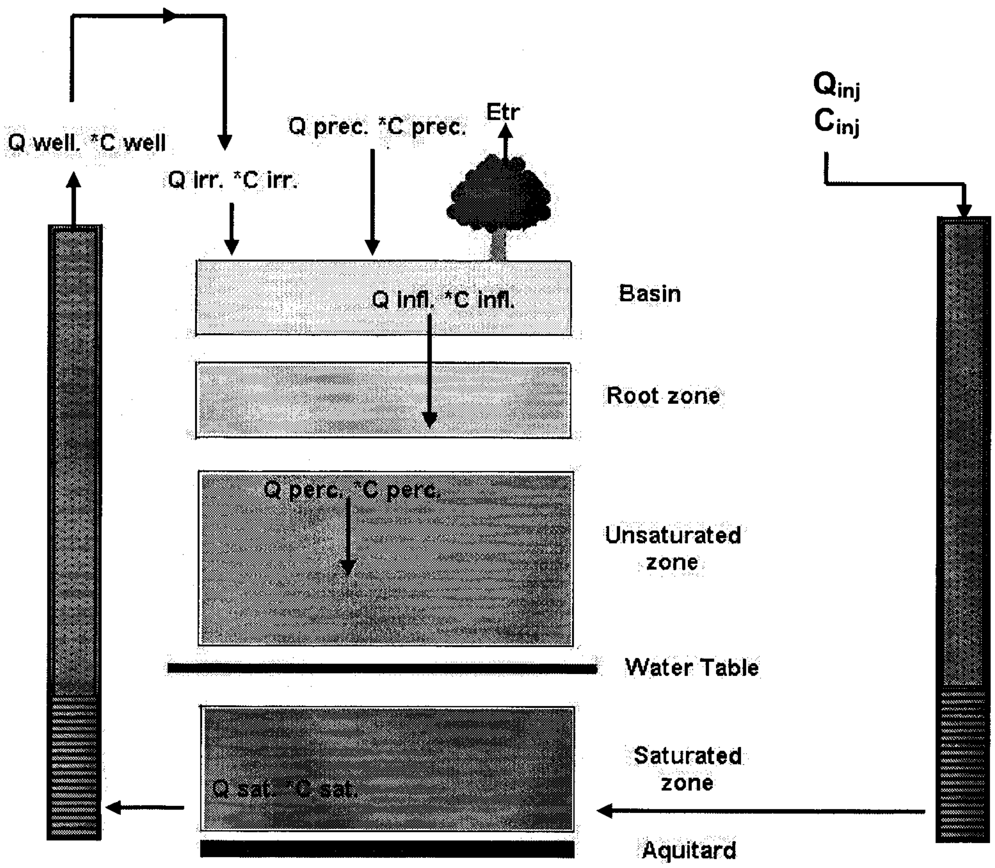

- **Obstacle Scenario (3).** In this scenario, treated wastewater augmentation will be re-routed through the reverse osmosis unit instead of direct injection to the native groundwater. The desalinated (permeate) water will be used for irrigation. Additionally, the groundwater pumping will be equal to the deep percolation recharge (Figure 5.4).

Figure 5.4 Obstacle Scenario (3) of the general conceptual design system.

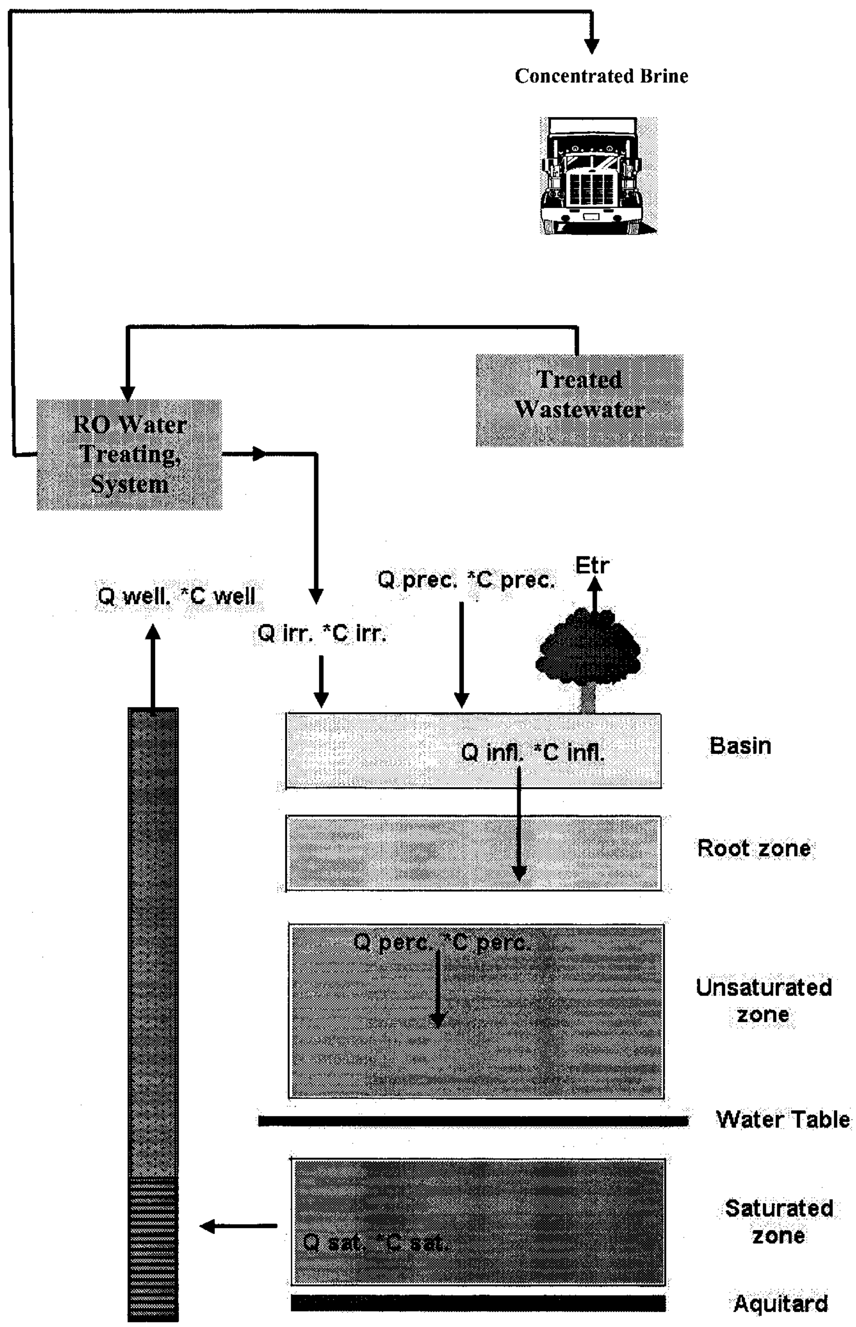

5.1.1 Off Planting Season Scenario Model Simulation

In this scenario, treated wastewater will be directly augmented (injected) to the native groundwater during the off planting season while ceasing the groundwater pumping (Figure 5.5). The order of simulating the off planting season scenario of the general conceptual design system, 40 year simulation period, will be performed in the same order as in Section 3.3, the base case simulation of the general conceptual design system, except in the off planting season scenario, treated wastewater augmentation to the native groundwater will be conducted through the off planting period. This might help the acceleration and improvement of groundwater quality and water table height, which might be an essential aspect in reducing the power consumption by the system. Of note, due to the off planting season treated wastewater augmentation, which makes the system flow to be transit, the steady state water balance assumptions will not hold true in this simulation. Hence, the calculation procedure will be analogous to Section 3.3, except the simulation will be carried for transit water balance and transit salt mass balance. Therefore, the calculation processors will be as follows:

1. Calculating C^{t}_{Feed} while using an iteration approach. Thus, for the transit approach, Equation (3.35) will be as

$$C^{t}_{Feed} = \left(\frac{C^{t}_{g.w.} + C^{t-1}_{g.w.}}{2} \right)$$

Figure 5.5 The off planting season scenario treated wastewater augmentation.

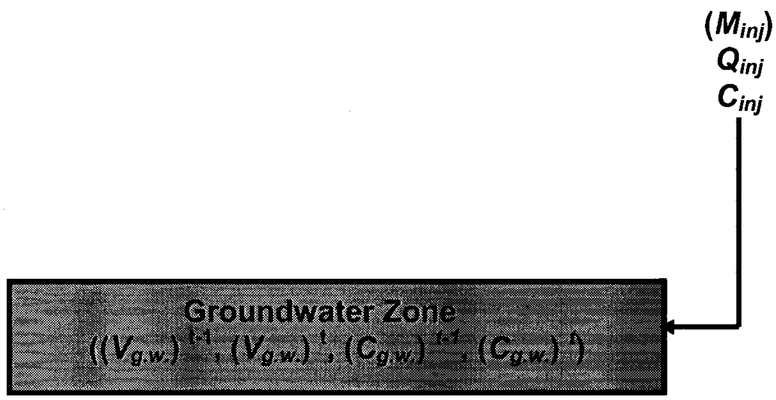

2. Calculating $C^t_{irr(permeate)}$. Thus, for the transit approach, Equation (3.30) will be as

$$C^t_{irr(permeate)} = n * C^t_{Feed} * \left[\frac{1-\dfrac{\delta}{2}}{1-\delta}\right]$$

3. Calculating $Q^t_{irr(permeate)}$. Thus, for the transit approach, Equation (3.53) will be as

$$Q^t_{irr(permeate)} = \left(\frac{Q^t_{ETc}}{1-\left[\dfrac{C^t_{irr(permeate)}}{C^t_{RZ}}\right]}\right)$$

where,

Q^t_{ETc} = Constant = ***1.5*** (m/season), and $Q^t_{ETc} = 0$ (m/off planting season) in this scenario.

C^t_{RZ} = Constant = ***2000*** mg/l, in this scenario.

4. Calculating Q^t_{Feed}. Thus, for the transit approach, Equation (3.10) will be as

$$Recovery\%\ (\delta) = \frac{Q^t_{Irr(permeate)}}{Q^t_{Feed}}$$

5. Calculating Q^t_{DP}. Thus, for the transit approach, Equation (3.3) will be as

$$Q^t_{irr(permeate)} = Q^t_{ETc} + Q^t_{DP}$$

6. Calculating Q^t_{inj}. Thus, for the transit approach, Equation (3.32) will be as

$$Q^t_{Feed} = Q^t_{inj} + Q^t_{DP}$$

7. Calculating $C^t_{g.w.}$. Thus, for the transit approach, Equation (3.37) will be as

$$C^t_{g.w.} = \left(\frac{\left(Q^t_{DP} * C^t_{RZ}\right) + \left(Q^t_{inj} * C^t_{inj}\right) - \left(\frac{Q^t_{Feed}}{2} * C^{t-1}_{g.w.}\right) + \left(\frac{V^t_{g.w.}}{\Delta t} * C^{t-1}_{g.w.}\right)}{\left(\frac{V^t_{g.w.}}{\Delta t} + \frac{Q^t_{Feed}}{2}\right)} \right)$$

where,

C^t_{inj} = Constant = ***1000*** mg/l, in this scenario.

8. Calculating Q^t_{Brine}. Thus, for the transit approach, Equation (3.9) will be as

$$Q^t_{Feed} = Q^t_{irr(permeate)} + Q^t_{Brine}$$

9. Calculating C^t_{Brine}. Thus, for the transit approach, Equation (3.54) will be as

$$C^t_{Brine} = \frac{(Q^t_{Feed} * C^t_{Feed}) - (Q^t_{irr(permeate)} * C^t_{Irr(permeate)})}{Q^t_{Brine}}$$

10. Calculating the osmotic pressure of feed water to the reverse osmosis unit (Ps_{Feed}). Thus, for the transit approach, Equation (3.20) will be as

$$Ps^t_{Feed} = Cs^t_{Feed} * R * T$$

Hence, from Equation (3.28), the ionic molar concentration of the feed water to the reverse osmosis unit for the transit approach will be as

$$Cs^{t}_{Feed} = (\Psi) * \left(\frac{C^{t}_{Feed}}{\varpi} \right)$$

11. Calculating the osmotic pressure of the permeate water from the reverse osmosis (***$Ps_{permeate}$***). Thus, for the transit approach, Equation (3.21) will be as

$$Ps^{t}_{permeate} = Cs^{t}_{irr(permeate)} * R * T$$

Hence, from Equation (3.29), the ionic molar concentration of the reverse osmosis permeate water for the transit approach will be

$$Cs^{t}_{irr(permeate)} = (\Psi) * \left(\frac{C^{t}_{irr(permeate)}}{\varpi} \right)$$

12. Calculating the power exerted by the reverse osmosis system pump, ***$Power_{(R.O.)}$***. Thus, for the transit approach, Equation (3.31) will be as

$$Power^{t}_{(R.O.)} = \left[\frac{\left(Ps^{t}_{Feed} - Ps^{t}_{permeate} \right) * Q^{t}_{irr(permeate)}}{\eta_{R.O.}} \right]$$

13. Calculating the power exerted by pumping the groundwater, $\boldsymbol{Power_{well}}$. Thus, for the transit approach, Equation (3.55) will be as

$$Power^{t}_{well} = \frac{\gamma * Q^{t}_{Feed} * \left(h_{surface} - \sqrt{(h_o^2)^t - \dfrac{Q^t_{Feed}}{\pi * K} * ln\left(\dfrac{r_o}{r_w}\right)} \right)}{\eta_{(well)}}$$

14. Calculating The Total Power consumed by the system. Thus, for the transit approach, Equation (3.56) will be as

$$(Total\,Power)^t = Power^t_{(R.O.)} + Power^t_{well}$$

15. During the off planting season (137 days) treated wastewater will added to the native groundwater. Therefore, the groundwater zone water volume will significantly vary through the simulation periods. Hence, the steady state flow balance approach will not hold true. Accordingly, from the transit flow balance equation of the groundwater zone approach, the volume of the groundwater at the end on the planting season will be:

$$\left(\frac{\Delta V_{g.w.}}{\Delta t}\right)^x = Q^t_{inj} + Q^t_{DP} - Q^t_{Feed} \qquad \textbf{(5.1)}$$

where,

$\frac{\Delta V_{g.w.}}{\Delta t}$ = Time rate change of the water volume in the groundwater zone

[M ^{3} /T], and

x = Time rate change.

And, taking the rate of change of the water volume in the groundwater zone as the difference between the beginning time and the ending time of the rate of change in groundwater volume, the time rate change of water volume in the groundwater zone will be:

$$\left(\frac{\Delta V_{g.w.}}{\Delta t}\right)^x = \frac{V^t_{g.w.} - V^{t-1}_{g.w.}}{\Delta t} \qquad \textbf{(5.2)}$$

Now, substituting Equation (5.2) in Equation (5.1) and rearrange, the rate of the volume change in the groundwater zone at time (t) will be

$$\left(\frac{V^t_{g.w.}}{\Delta t}\right) = \left(\frac{V^{t-1}_{g.w.}}{\Delta t}\right) + Q^t_{inj} + Q^t_{DP} - Q^t_{Feed} \qquad \textbf{(5.3)}$$

and knowing that,

$$\left(\frac{V^{t}_{g.w.}}{\Delta t}\right)=\left(\frac{A_F * h^{t}_{o} * \Phi}{\Delta t}\right) \tag{5.4}$$

and also,

$$\left(\frac{V^{t-1}_{g.w.}}{\Delta t}\right)=\left(\frac{A_F * h^{t-1}_{o} * \Phi}{\Delta t}\right) \tag{5.5}$$

where,

Φ = Porosity [m^3/m^3].

Hence, substituting Equation (5.4) and Equation (5.5) in Equation (5.3). Thus,

$$\left(\frac{A_F * h^{t}_{o} * \Phi}{\Delta t}\right)=\left(\left(\frac{A_F * h^{t-1}_{o} * \Phi}{\Delta t}\right)+Q^{t}_{inj}+Q^{t}_{DP}-Q^{t}_{Feed}\right) \tag{5.6}$$

Rearrange Equation (5.6), and as a result, the water table height at the end of the planting season will be:

$$h^{t}_{o}=\left[\frac{\left(\left(\frac{A_F * h^{t-1}_{o}}{\Delta t}\right)+Q^{t}_{inj}+Q^{t}_{DP}-Q^{t}_{Feed}\right)}{\left(\frac{A_F * \Phi}{\Delta t}\right)}\right] \tag{5.7}$$

However, the water table height during or at the end of the off planting season (137 days), after treated wastewater augmentation, must never exceed a prefixed maximum allowable water table height ($h_{o\,(max)}$). Maximum allowable water table height ($h_{o\,(max)}$) will be set for 55 m in this scenario, 5 m from the ground surface to prevent water logging in the root zone. Thus, treated wastewater augmentation will be reduced or stopped during the 40-year simulation, to cope with the prefixed maximum allowable water table height ($h_{o\,(max)}$) (Figure 5.6). Moreover, the amount of 5 m depth per off planting season per unit area of applied wastewater augmentation, Q_{inj}, will be applied to the native groundwater. The off planting season Q_{inj} = 5 (m /off season) was chosen to be coped with the maximum installation pipe size delivery capacity of the base case simulation of the general conceptual design system. Additionally, this maximum installation pipe size delivery capacity was designed to handle and deliver the maximum amount of treated wastewater to the injection site during the base case simulation. Hence, Q_{inj} can be calculated within the threshold of the prefixed maximum allowable water table height ($h_{o\,(max)}$) as:

$$\text{if } \left(\frac{Q^{t}_{inj} * \Delta t}{A_F * \Phi}\right) + h_o^{t-1} \geq h_{o\,(max)} \tag{5.8}$$

$$\text{Then } Q^{t}_{inj} = \frac{\left(h_{o\,(max)} - h_o^{t-1}\right) * A_F * \Phi}{\Delta t} \tag{5.9}$$

otherwise,

$$\text{if} \left(\frac{Q_{inj}^{t} * \Delta t}{A_F * \Phi} \right) + h_o^{t-1} \langle h_{o(max)} \qquad \textbf{(5.10)}$$

Then Q_{inj}^{t} = 5 m depth per off planting season per unit area. **(5.11)**

Figure 5.6 Off planting season scenario layout of the general conceptual design system.

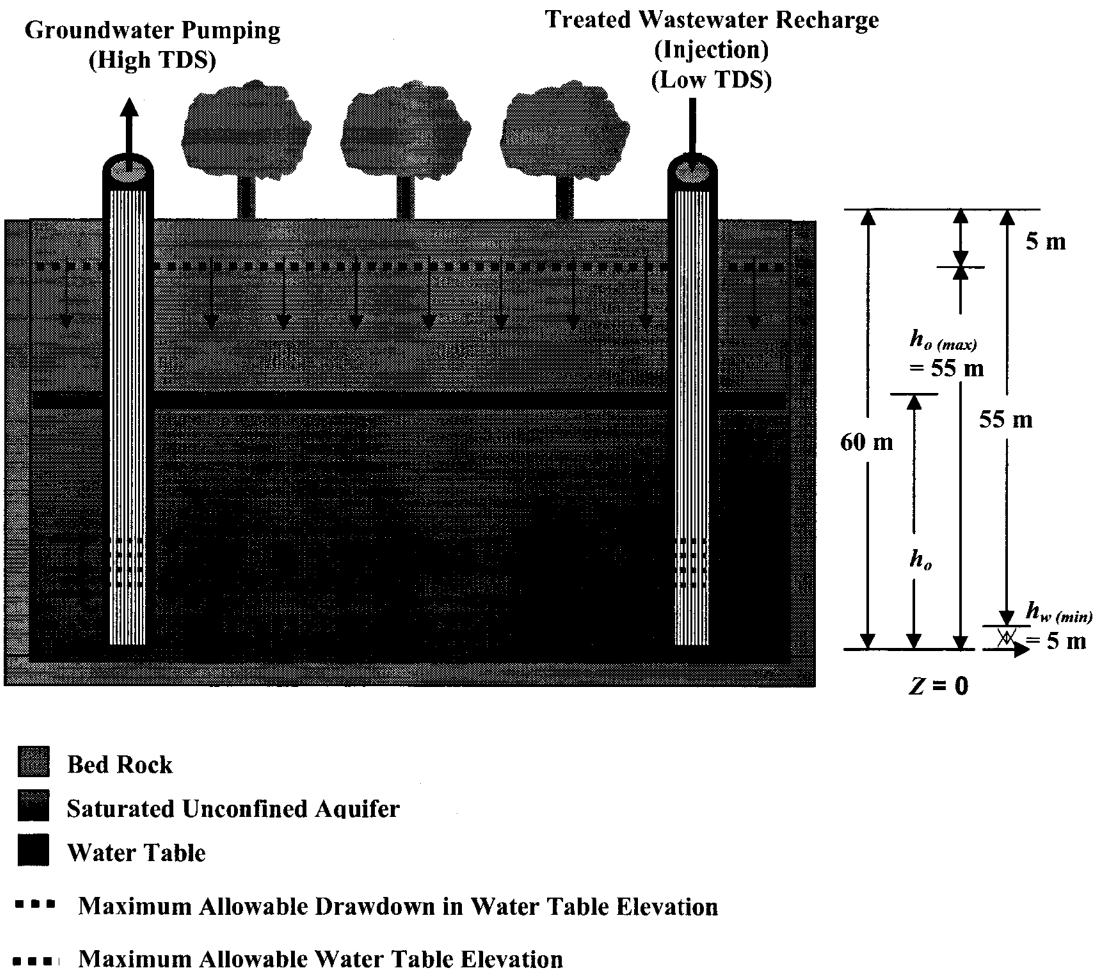

Finally, Figure 5.7 illustrates the governing equations of the off planting season scenario of the general conceptual design system.

Figure 5.7 Summary of the off planting season scenario of the general conceptual design system governing equations.

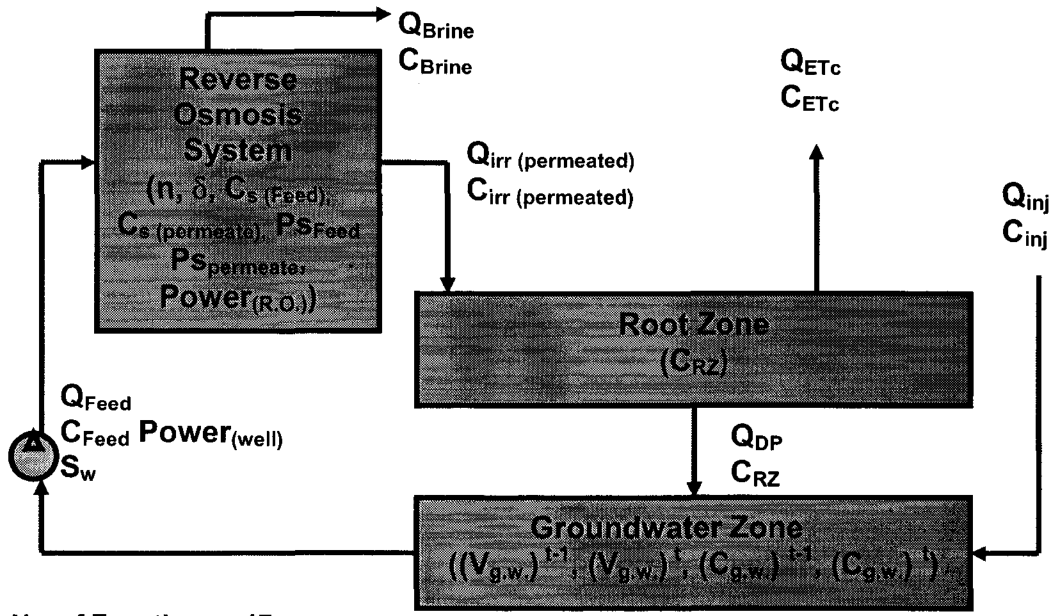

<u>**No. of Equations = 17**</u>

<u>**Root (Vadose) Zone Governing Equations:**</u>

1) $Q^{t}_{irr\,(permeated)} = Q^{t}_{ETc} + Q^{t}_{DP}$
2) $Q^{t}_{irr\,(permeate)} * C^{t}_{irr\,(permeate)} = Q^{t}_{ETc} * C^{t}_{ETc} + Q^{t}_{DP} * C^{t}_{RZ}$

<u>**Groundwater Zone Governing Equations:**</u>

3) $Q^{t}_{Feed} = Q^{t}_{inj} + Q^{t}_{DP}$
4) $C^{t}_{Feed} = (((C_{g.w})^{t-1} + (C_{g.w.})^{t}) / 2)$
5) $(C_{g.w.})^{t} = ((V_{g.w.} / \Delta t)^{t-1} * (C_{g.w})^{t-1} + Q^{t}_{inj} * C^{t}_{inj} + Q^{t}_{DP} * C^{t}_{RZ} - (Q^{t}_{Feed} / 2) * (C_{g.w})^{t-1}) / ((V_{g.w.} / \Delta t)^{t} + (Q^{t}_{Feed} / 2))$, (pumping and mixing are simultaneously).
6) $Power_{(well)} = (\gamma * Q^{t}_{Feed} * H^{t}_{lift}) / \eta_{(well)} = (\gamma * Q^{t}_{Feed} * ((h_{surface} - h^{t}_{o}) + S^{t}_{w})) / \eta_{(well)}$
7) $S^{t}_{w} = h^{t}_{o} - [((h^{t}_{o})^{2} - (Q^{t}_{Feed} / (\pi * K) * \ln(r_o / r_w))]^{0.5}$
8) $(V_{g.w.} / \Delta t)^{t} = ((A_F * h^{t}_{o} * \theta / \Delta t))^{t} = ((V_{g.w.} / \Delta t)^{t-1} + Q^{t}_{inj} + Q^{t}_{DP} - Q^{t}_{Feed})$

<u>**Reverse Osmosis Governing Equations:**</u>

9) $Q^{t}_{Feed} = Q^{t}_{irr\,(permeate)} + Q^{t}_{Brine}$
10) $Q^{t}_{Feed} * C^{t}_{Feed} = Q^{t}_{irr\,(permeate)} * C^{t}_{irr\,(permeate)} + Q^{t}_{Brine} * C^{t}_{Brine}$
11) $\delta = (Q^{t}_{irr\,(permeate)}) / (Q^{t}_{Feed})$
12) $C^{t}_{irr\,(permeate)} = n * C^{t}_{Feed} * ((1 - (\delta / 2)) / (1 - \delta))$
13) $Power^{t}_{(R.O.)} = ((Ps^{t}_{Feed} - Ps^{t}_{permeate}) * Q^{t}_{irr\,(permeate)}) / (\eta_{(R.O.)})$
14) $Ps^{t}_{Feed} = C_s{}^{t}_{(Feed.)} * R * T$
15) $Ps^{t}_{permeted} = C_s{}^{t}_{(Permeate)} * R * T$
16) $C_s{}^{t}_{(Feed)} = (\Psi) * (C^{t}_{Feed} / (1000 * \varpi))$
17) $C_s{}^{t}_{(Permeate)} = (\Psi) * (C^{t}_{irr\,(permeate)} / (1000 * \varpi))$

<u>**No. of Variables = 26**</u>

$Q^{t}_{irr\,(permeate)}$, Q^{t}_{Brine}, Q^{t}_{ETc}, Q^{t}_{inj}, Q^{t}_{DP}, $(V_{g.w.})^{t-1}$, $(V_{g.w.})^{t}$, Q^{t}_{Feed}, $C^{t}_{irr\,(permeate)}$, C^{t}_{Brine}, C^{t}_{ETc}, C^{t}_{inj}, C^{t}_{RZ}, $(C_{g.w.})^{t}$, $(C_{g.w.})^{t-1}$, C^{t}_{Feed}, δ, n, $C_s{}^{t}_{(Feed)}$, $C_s{}^{t}_{(Permeate)}$, Ps^{t}_{Feed}, $Ps^{t}_{permeted}$, Δt, S^{t}_{w}, $Power^{t}_{(R.O.)}$, $Power^{t}_{(well)}$.

<u>**No. of Known Variables = 6**</u>

C^{t}_{ETc}, C^{t}_{inj}, $(C_{g.w.})^{t-1}$, Q^{t}_{ETc} (Or from Penman-Monteith method), $(V_{g.w.})^{t-1}$, Δt.

<u>**No. of Decision Variables = 3**</u>

n, δ, C^{t}_{RZ}

The results for the off planting season scenario simulation were compared with the base case of the general conceptual model design system that was captured in Figures 5.8, 5.9, 5.10, 5.11, and 5.12 respectively. These output results graphs were arranged by the total power required by the system, the power required by the reverse osmosis unit, the power required by the well pump system, the amount of treated wastewater injected into the native groundwater, and the initial groundwater salt concentrations, respectively.

Figure 5.8 Total power consumption comparison between the off planting scenario and the base case of the general conceptual design system simulation.

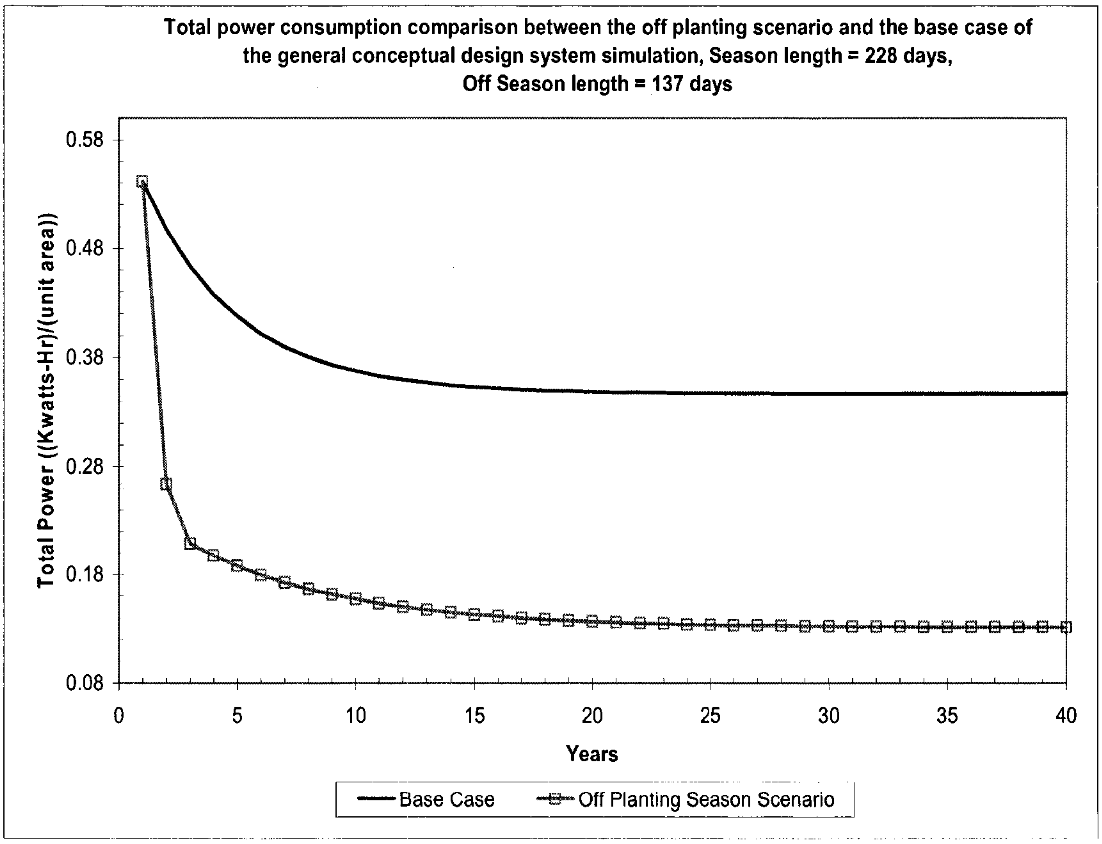

Figure 5.9 Reverse osmosis power consumption comparison between the off planting scenario and the base case of the general conceptual design system simulation.

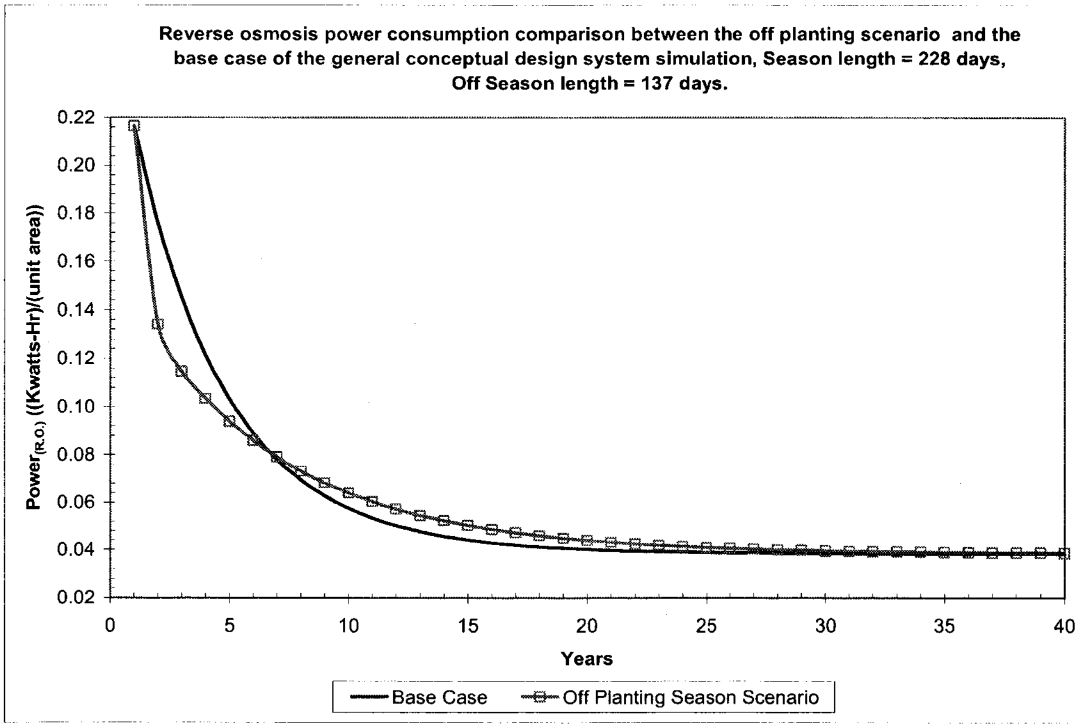

Figure 5.10 Well pump power consumption comparison between the off planting scenario and the base case of the general conceptual design system simulation.

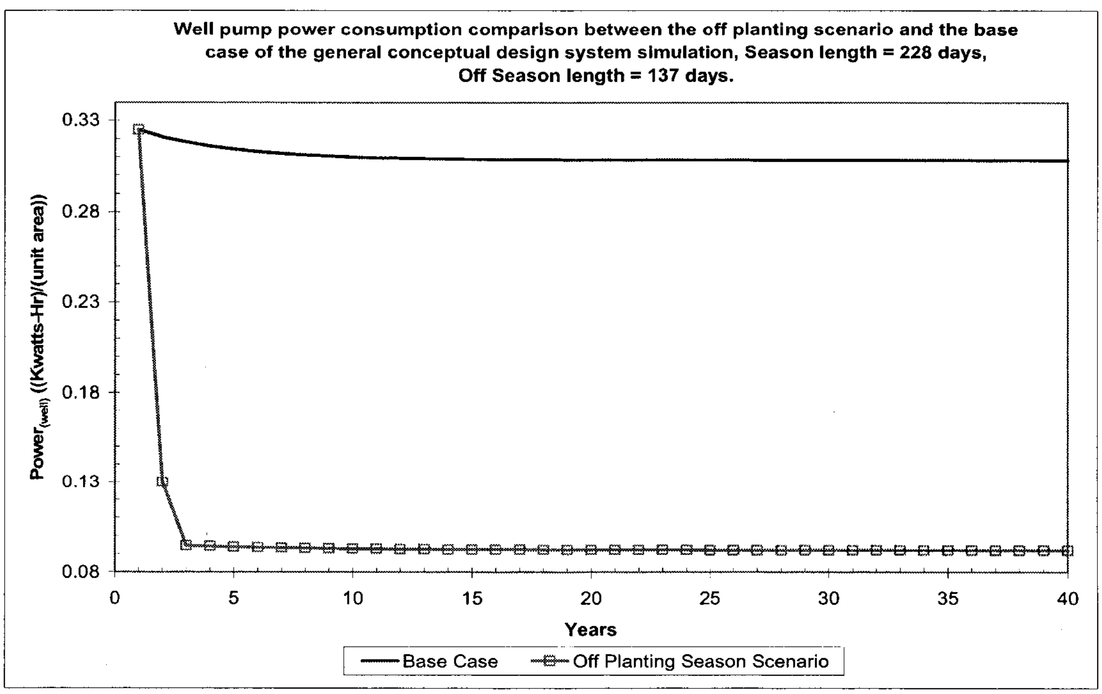

Figure 5.11 Treated wastewater consumption comparison between the off planting scenario and the base case of the general conceptual design system simulation.

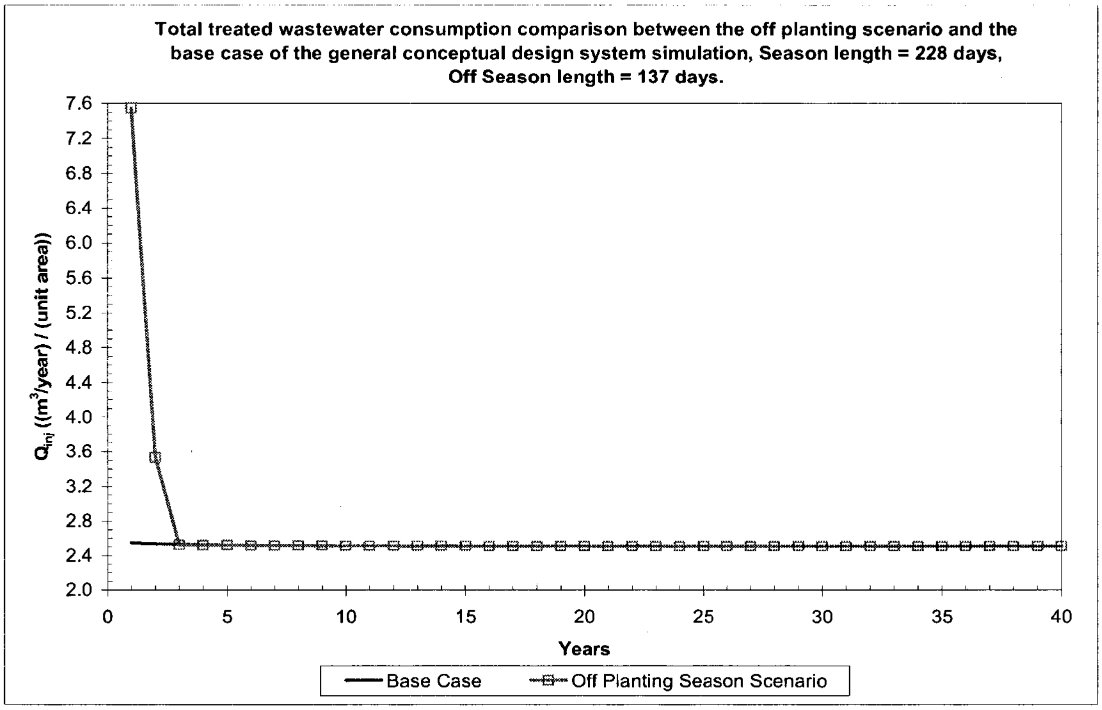

Figure 5.12 Initial groundwater salt concentration comparison between the off planting scenario and the base case of the general conceptual design system simulation.

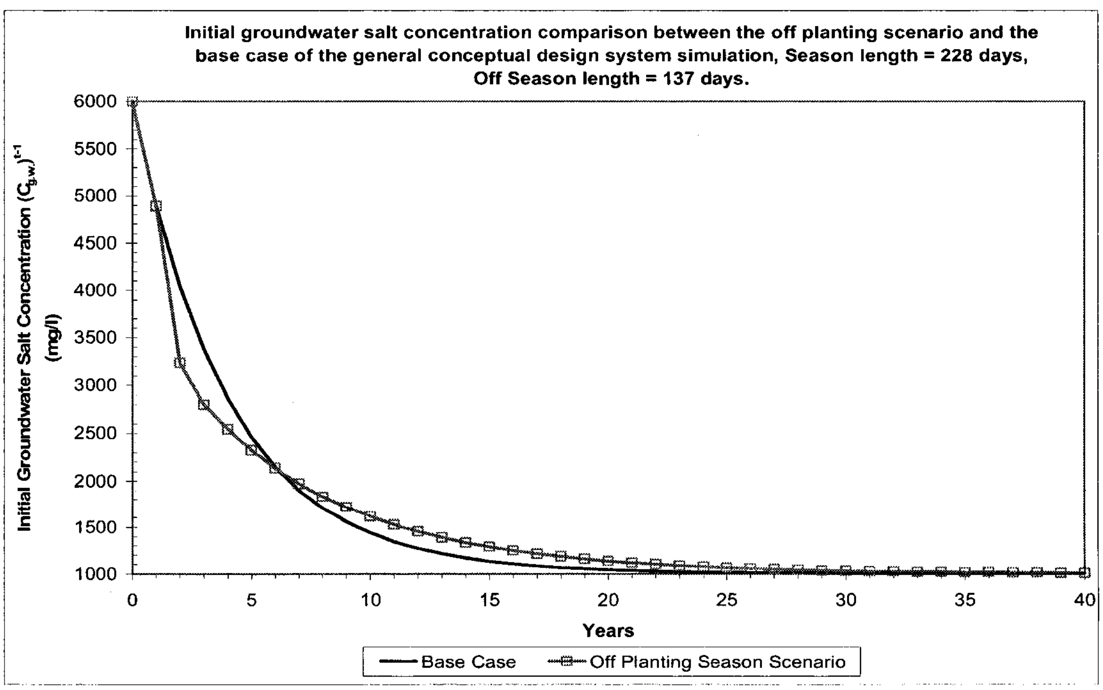

From Figures 5.8 and 5.11, it is noticeable that the off planting season scenario simulation total power per unit area required by the system is significantly lower than the base case simulation, and the base case simulation amount of treated wastewater per unit area required to be injected into the groundwater zone is lower than the off planting season scenario simulation. As the water table hydraulic head elevations increased, due to the off planting season wastewater injection of better quality water than the groundwater, the volume of groundwater increased and the salt concentration of the groundwater decreased. The groundwater salt concentration enhancement was caused by the dilution and mixing of the groundwater with better quality injected treated wastewater. Thus, the pumped groundwater salt concentration will be relatively lower due to the dilution and mixing with the better quality injected wastewater. Owing to the decrease in the pumped groundwater salt concentration, the feed water to the reverse osmosis unit will be at a relatively lower salt concentration. Thus, the water permeate from the reverse osmosis unit will be at lower concentration, too. Therefore, less permeate water is required (to be used as irrigation water) to cope with the irrigation efficiency. Hence, irrigation water demand will decrease due to the off planting season treated wastewater injection theme. Therefore, a lower amount of groundwater must be pumped and fed to the reverse osmosis unit due to the decrease in the irrigation water requirements. In view of that, the lower the pumped groundwater amount required to be fed to the reverse osmosis unit the lower the amount of water needed to be desalinated and less power will be consumed by the reverse osmosis unit. In addition, due to the increase in the water table hydraulic head elevations, caused by the off planting season treated wastewater injection, the height of water to be lifted by the pump to the ground surface will be reduced, thus reducing the amount of power to be exerted by the pump. The injected treated wastewater in the off planting season was reduced in the second year of simulation and was terminated in the third year of simulation to cope with the prefixed maximum allowable water table height ($h_{o\,(max)}$ = 55 m). The off planting treated wastewater injection was terminated when the water table hydraulic head elevation reached 55 m from the bed rock (5m from the ground surface). Due to the latter reason, the groundwater salt concentration dilution and mixing with the better quality treated wastewater was eliminated. Thus, after the 6th year of simulation, the groundwater salt concentration enhancement was retarded and exceeded the groundwater salt concentration of the base case simulation (Figure 5.12). Thus, as the groundwater salt concentration enhancement was retarded, the power consumption by the reverse osmosis will start to increase (after the 6th year) more than the base case simulation (Figure 5.9). On the other hand, owing to the increase in the water table hydraulic head elevation (from 35 to 55 m), the power exerted by the pump will be significantly reduced due to the reduction in the height of water lift by the pump to the ground surface (Figure 5.10). Consequently, the total power consumption by the system will be significantly reduced using the off planting season scenario (Figure 5.8). Alternatively, owing to the treated wastewater injection during the off planting season, the amount of water utilized by the off planting season scenario model simulation is higher than the base case model simulation (Figure 5.11). As a result, the percent of decrease in the sum of the total power consumption over the 40-year simulation was 57.22 %, and an increase in treated wastewater injection of 5.63 % was observed when using the off planting season scenario. Figures 5.13 and 5.14 illustrate the sum of the total power consumption comparison for 40-year simulations between the off planting season scenario and the base case of the general conceptual design system simulation, and the sum of treated wastewater quantity injected comparison, over 40 years, between the off planting scenario and the base case of the general conceptual design system simulation. Moreover, Table 5.1 demonstrates the percent change comparison in the sum of the total power consumption and the sum of the treated wastewater injection between the base case and off planting season scenario.

Figure 5.13 Sum of total power consumption comparison for 40-year simulations between the off planting season scenario and the base case of the general conceptual design system simulation.

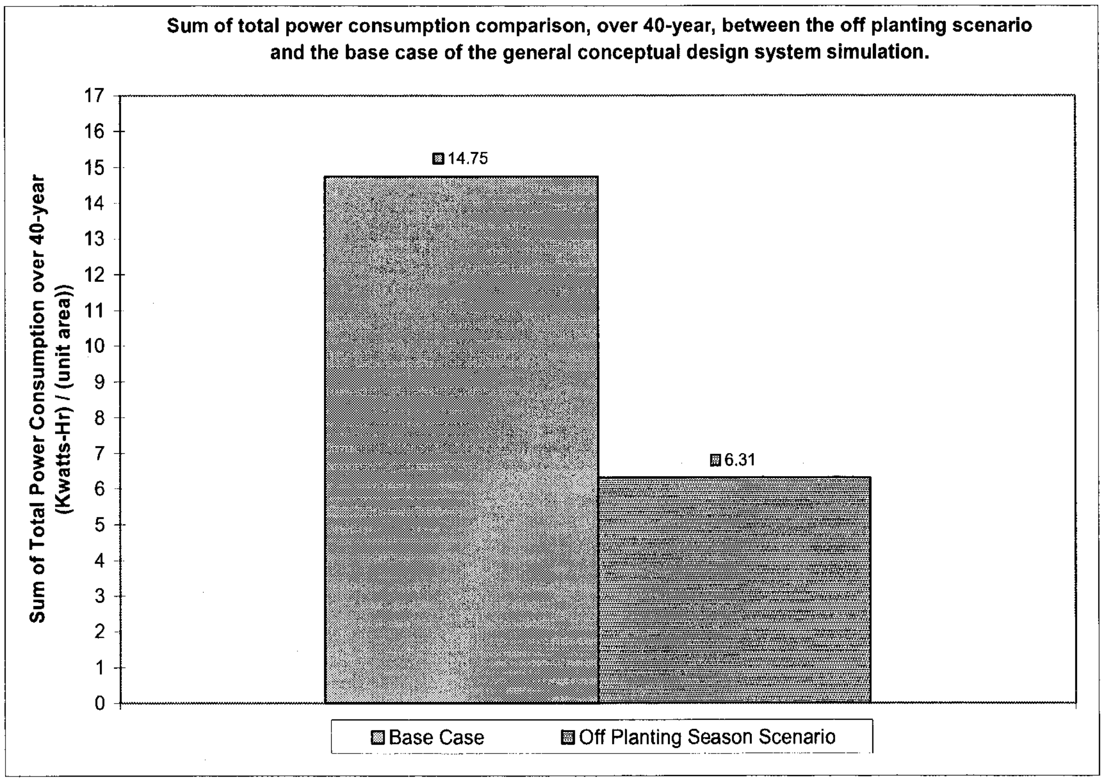

Figure 5.14 Sum of treated wastewater quantity injected comparison, over 40 years, between the off planting season scenario and the base case of the general conceptual design system simulation.

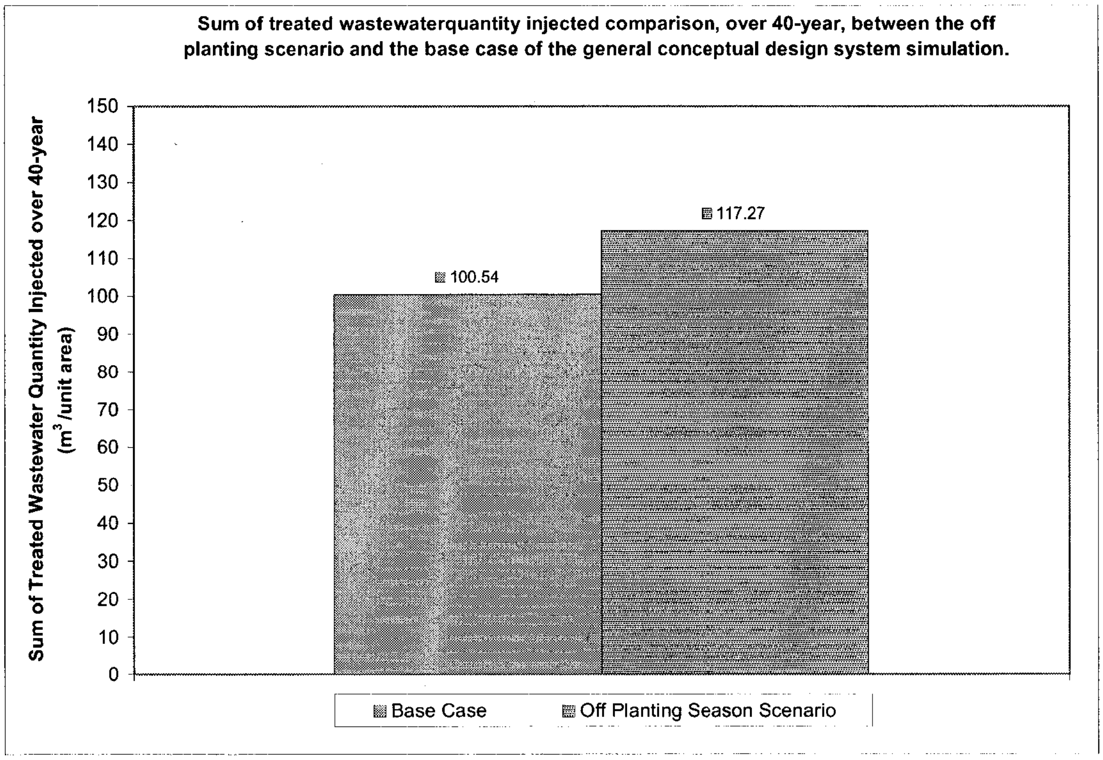

Table 5.1 Percent change comparison in sum of total power consumption and sum of treated wastewater injection between the base case and off planting season scenario.

From	To	% Change (decrease) in Sum of Total Power per Unit Area	% Change (increase) in Sum of Injected Treated Wastewater per Unit Area
Base Case	**Off Planting Season Scenario**	**57.22**	**5.63**

5.1.2 Obstacle Scenario (1) Model Simulation

In this scenario, treated wastewater augmentation will be stopped ($Q_{inj} = C_{inj} = 0$); hence, for the steady state flow balance equation approach in the unconfined groundwater to hold true, an inward groundwater flow movement from the adjacent immediate vicinity of the groundwater, $Q_{g.w.(Brine)}$ and $C_{g.w.(Brine)}$, will be induced. Moreover, due to the slight variances in the individual water source quantity from one simulation period to the other (as shown in Section 3.1.3) the assumption of steady state water balance will be implemented in driving the governing equations of the conceptual design system, but a transit flow approach will be applied to the simulation calculations. The order of simulating the obstacle scenario (1) of the conceptual design system, 40 year simulation period, will be performed in the same order as in Section 3.3 for the base case simulation of the general conceptual design system. Except in this scenario a new variables, $Q_{g.w.(Brine)}$ and $C_{g.w.(Brine)}$, will be introduced instead of treated wastewater augmentation to the native groundwater, Q_{inj} and C_{inj}. Thus, the calculation processors will be conducted in the following order:

1. Calculating C_{Feed} while using an iteration approach. Thus, from Equation (3.35), where

$$C_{Feed} = \left(\frac{C^{t}_{g.w.} + C^{t-1}_{g.w.}}{2} \right)$$

2. Calculating $C_{irr\ (permeate)}$ from Equation (3.30), where

$$C_{irr(permeate)} = n * C_{Feed} * \left[\frac{1-\frac{\delta}{2}}{1-\delta} \right]$$

3. Calculating Q_{irr} (permeate) from Equation (3.53), where

$$Q_{irr(permeate)} = \left(\frac{Q_{ET_c}}{1-\left[\frac{C_{irr(permeate)}}{C_{RZ}}\right]} \right)$$

4. Calculating Q_{Feed} from Equation (3.10), where

$$Recovery\%\ (\delta) = \frac{Q_{irr\ (permeated)}}{Q_{Feed}}$$

5. Calculating Q_{DP} from Equation (3.3), where

$$Q_{irr} = Q_{ET_c} + Q_{DP}$$

6. Calculating $Q_{g.w.(Brine)}$, because in this scenario the treated wastewater augmentation will be stopped, $Q_{inj} = 0$. Hence, for the steady state flow

balance equation approach in the unconfined groundwater to hold true(to keep the groundwater volume constant), an inward groundwater flow movement from the adjacent immediate vicinity of the groundwater, $Q_{g.w.(Brine)}$, will be induced (Figure 5.15), where

$$Q_{Feed} = Q_{g.w.(Brine)} + Q_{DP} \tag{5.12}$$

7. Calculating ($C^{t}_{g.w.}$) from Equation (3.37), and substituting $Q_{g.w.(Brine)}$ as a replacement for Q_{inj}, and $C_{g.w.(Brine)}$ as a replacement for C_{inj} (Figure 5.15), where

$$C^{t}_{g.w.} = \frac{\left(\left(\frac{V_{g.w}}{\Delta t}\right) * C^{t-1}_{g.w.}\right) + (Q_{g.w.(Brine)} * C_{g.w.(Brine)}) + (Q_{DP} * C_{RZ}) - \left(\left(\frac{Q_{Feed}}{2}\right) * C^{t-1}_{g.w}\right)}{\left(\left(\frac{V_{g.w.}}{\Delta t}\right) + \left(\frac{Q_{Feed}}{2}\right)\right)}$$

(5.13)

where,

$C_{g.w.(Brine)}$ = The salt concentration of an inward groundwater flow movement from the adjacent immediate vicinity of the groundwater. In this scenario simulation,

$C_{g.w.(Brine)} = C_{g.w.} = 6000$ mg/l.

Figure 5.15 Obstacle scenario (1) salt mass balance and water balance of the groundwater system.

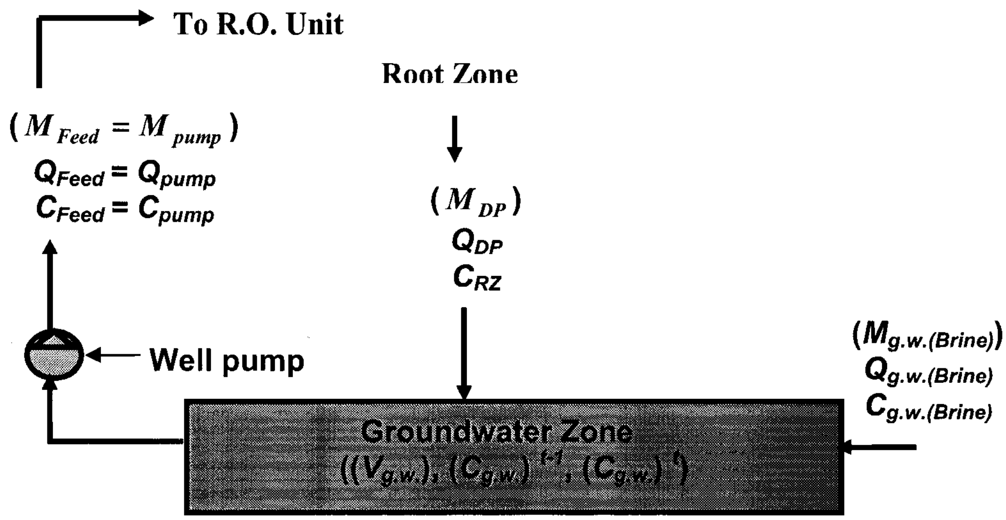

8. Calculating Q_{Brine} from Equation (3.9), where

$$Q_{Feed} = Q_{irr(permeate)} + Q_{Brine}$$

9. Calculating C_{Brine} from Equation (3.54), where

$$C_{Brine} = \frac{(Q_{Feed} * C_{Feed}) - (Q_{irr(permeate)} * C_{irr(permeate)})}{Q_{Brine}}$$

10. Calculating the feed water to the reverse osmosis osmotic pressure (Ps_{Feed}), from Equation (3.20), where

$$Ps_{Feed} = Cs_{Feed} * R * T$$

Hence, from Equation (3.28), the ionic molar concentration of the feed water to the reverse osmosis model is

$$Cs_{Feed} = (\Psi) * \left(\frac{C_{Feed}}{\varpi} \right)$$

11. Calculating the osmotic pressure of the permeate water from the reverse osmosis (***$Ps_{permeate}$***), from Equation (3.21), where

$$Ps_{permeate} = Cs_{irr(permeate)} * R * T$$

Hence, from Equation (3.29), the ionic molar concentration of the reverse osmosis permeates water is:

$$Cs_{irr(permeate)} = (\Psi) * \left(\frac{C_{irr(permeate)}}{\varpi} \right)$$

12. Calculating the power exerted by the reverse osmosis system pump, ***$Power_{(R.O.)}$***, from Equation (3.31), where

$$Power_{(R.O.)} = \left[\frac{(Ps_{Feed} - Ps_{permeate}) * Q_{irr(permeate)}}{\eta_{R.O.}} \right]$$

13. Calculating the power exerted by pumping the groundwater, $\boldsymbol{Power_{well}}$, from Equation (3.55), where

$$Power_{well} = \frac{\gamma * Q_{Feed} * \left(h_{surface} - \sqrt{h_o^2 - \frac{Q_{Feed}}{\pi * K} * ln\left(\frac{r_o}{r_w}\right)} \right)}{\eta_{(well)}}$$

14. Calculating the total power consumed by the system from Equation (3.56), where,

$$Total\,Power = Power_{(R.O.)} + Power_{well}$$

Finally, Figure 5.16 illustrates the governing equations of the obstacle scenario (1) of the general conceptual design system.

The results for the obstacle scenario (1) simulation were compared with the base case simulation of the general conceptual model design system and captured in Figures 5.17, 5.18, 5.19, and 5.20 respectively. These output results graphs were arranged by the total power required by the system, the power required by the reverse osmosis unit, the power required by the well pump system, and the initial groundwater salt concentrations, respectively.

Figure 5.16 Obstacle scenarios (1) of the general conceptual design system governing equations.

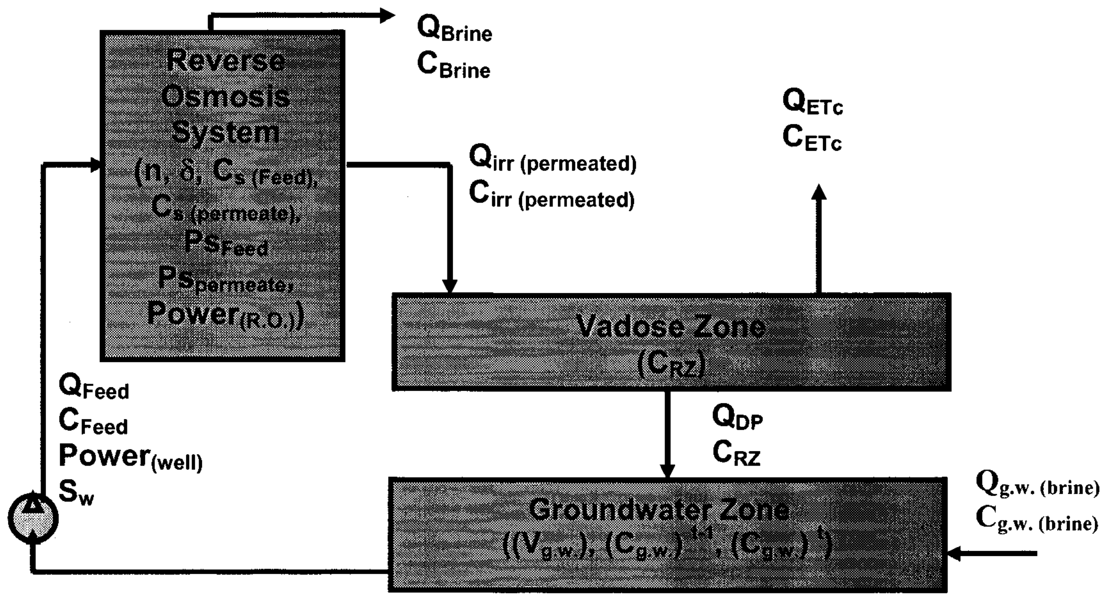

<u>**No. of Equations = 16**</u>

<u>**Vadose Zone Governing Equations:**</u>

1) $Q_{irr\ (permeate)} * C_{irr\ (permeate)} = Q_{ET} * C_{ETc} + Q_{DP} * C_{RZ}$

2) $Q_{irr\ (permeate)} = Q_{ETc} + Q_{DP}$

<u>**Groundwater Zone Governing Equations:**</u>

3) $Q_{Feed} = Q_{g.w.\ (Brine)} + Q_{DP}$

4) $C_{Feed} = (((C_{g.w})^{t-1} + (C_{g.w.})^{t}) / 2)$

5) $(C_{g.w.})^{t} = ((V_{g.w.} / \Delta t) * (C_{g.w})^{t-1} + Q_{g.w.\ (Brine)} * C_{g.w.\ (Brine)} + Q_{DP} * C_{RZ} - (Q_{Feed} / 2) * (C_{g.w})^{t-1}) / ((V_{g.w.} / \Delta t) + (Q_{Feed} / 2))$, (pumping and mixing are simultaneously).

6) $Power_{(well)} = (\gamma * Q_{Feed} * H_{lift}) / \eta_{(well)} = (\gamma * Q_{Feed} * ((h_{surface} - h_o) + S_w)) / \eta_{(well)}$

7) $S_w = h_o - [(h_o^2 - (Q_{Feed} / (\pi * K) * \ln(r_o / r_w))]^{0.5}$

<u>**Reverse Osmosis Governing Equations:**</u>

8) $Q_{Feed} = Q_{irr\ (permeate)} + Q_{Brine}$

9) $Q_{Feed} * C_{Feed} = Q_{irr\ (permeate)} * C_{irr\ (permeate)} + Q_{Brine} * C_{Brine}$

10) $\delta = (Q_{irr\ (permeate)}) / (Q_{Feed})$

11) $C_{irr\ (permeate)} = n * C_{Feed} * ((1 - (\delta / 2)) / (1 - \delta))$

12) $Power_{(R.O.)} = ((Ps_{Feed} - Ps_{permeate}) * Q_{irr\ (permeate)}) / \eta_{(R.O.)}$

13) $Ps_{Feed} = C_{s\ (Feed)} * R * T$

14) $Ps_{permeate} = C_{s\ (Permeate)} * R * T$

15) $C_{s\ (Feed)} = (\Psi) * (C_{Feed} / (1000 * \varpi))$

16) $C_{s\ (Permeate)} = Cs_{(Permeate)} = (\Psi) * (C_{irr\ (permeate)} / (1000 * \varpi))$

<u>**No. of Variables = 25**</u>

$Q_{irr\ (permeate)}$, Q_{Brine}, Q_{ETc}, $Q_{g.w.\ (Brine)}$, Q_{DP}, $(V_{g.w.})$, Q_{Feed}, $C_{irr\ (permeate)}$, C_{Brine}, C_{ETc}, $C_{g.w.\ (Brine)}$, C_{RZ}, $(C_{g.w.})^{t}$, $(C_{g.w.})^{t-1}$, C_{Feed}, δ, n, $C_{s(permeate)}$, $C_{s(Permeate)}$, Ps_{pump}, $Ps_{permeate}$, S_w, $Power_{(R.O.)}$, $Power_{(well)}$, Δt.

<u>**No. of Known Variables = 6**</u>

C_{ETc}, $C_{g.w.\ (Brine)}$, $(C_{g.w.})^{t-1}$, Q_{ETc} (Or from Penman-Monteith method), $(V_{g.w.})$, Δt.

<u>**No. of Decision Variables = 3**</u>

n, δ, C_{RZ}

Figure 5.17 Total power consumption comparison between the obstacle scenario (1) and the base case of the general conceptual design system simulation.

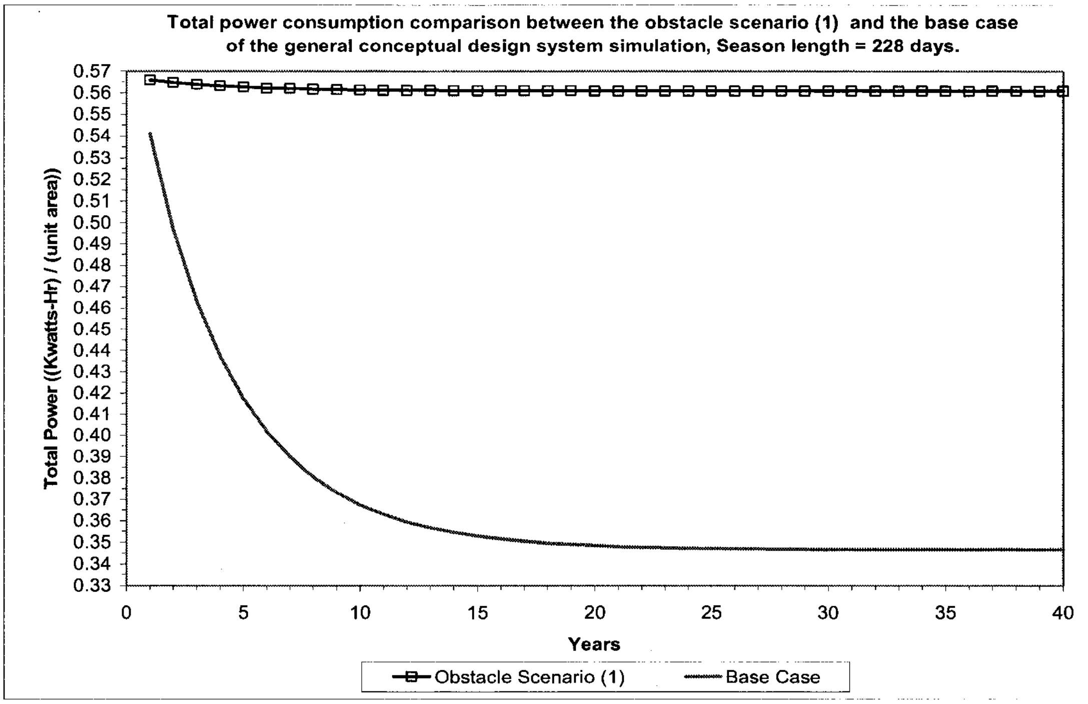

Figure 5.18 Reverse osmosis power consumption comparison between the obstacle scenario (1) and the base case of the general conceptual design system simulation.

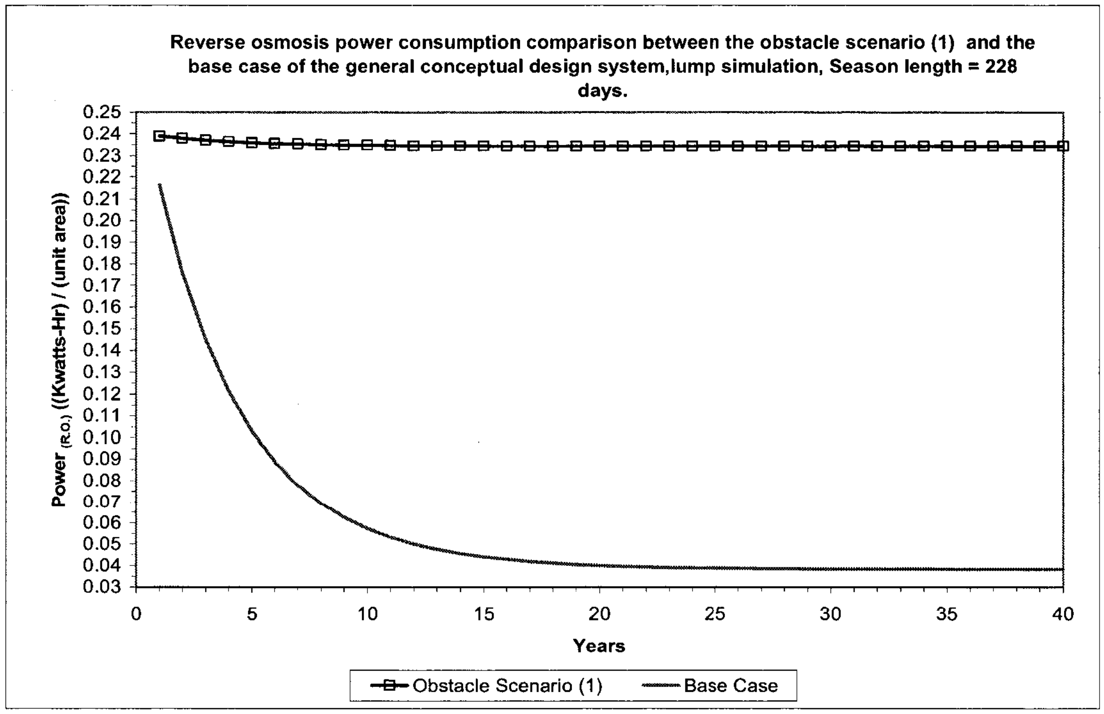

Figure 5.19 Well pump power consumption comparison between the obstacle scenario (1) and the base case of the general conceptual design system simulation.

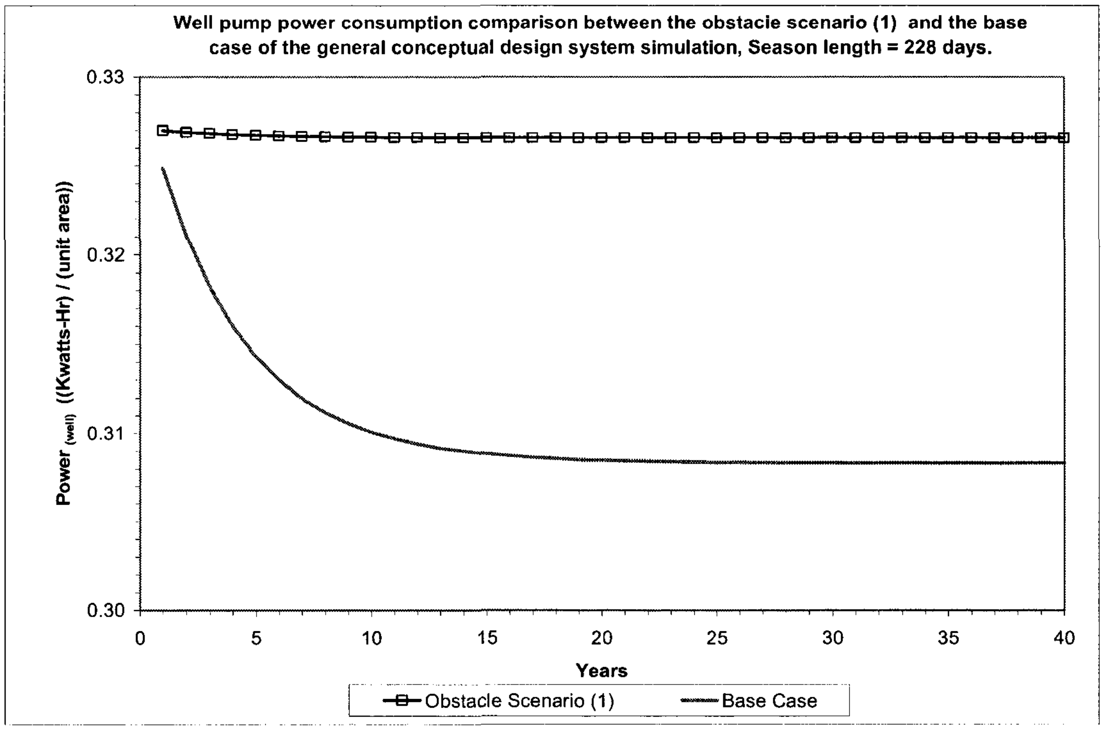

Figure 5.20 Initial groundwater salt concentration comparison between the obstacle scenario (1) and the base case of the general conceptual design system simulation.

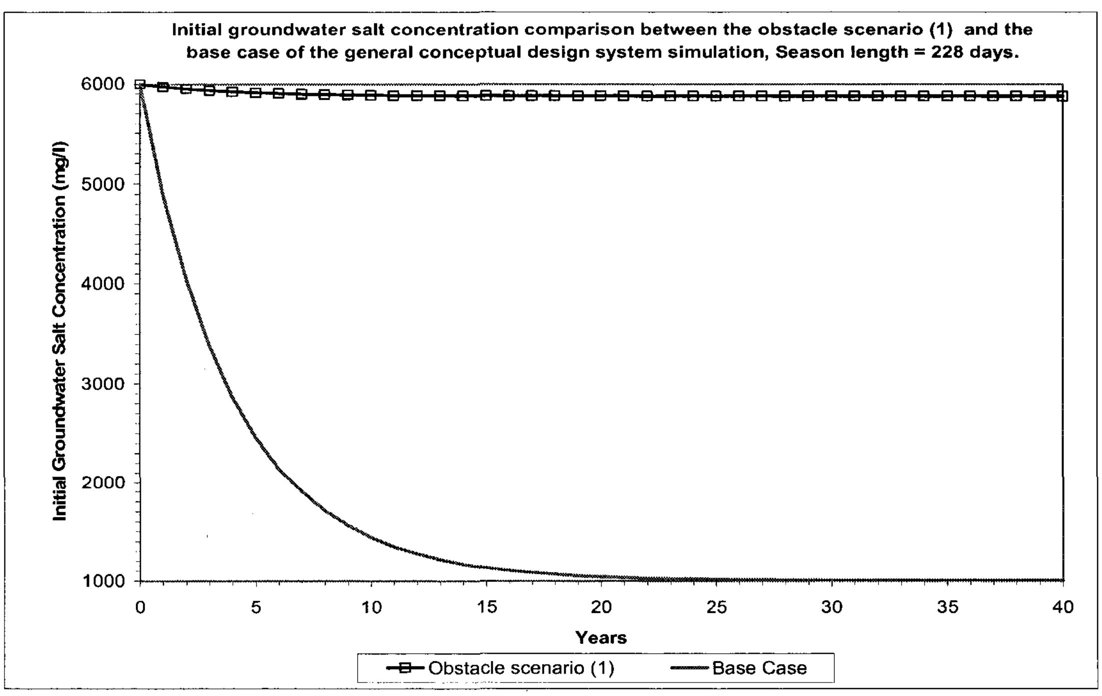

 Emad H. AlAli

From Figure 5.17, it is noticeable that the obstacle scenario (1) simulation total power per unit area required by the system is significantly higher than the base case simulation. In the obstacle scenario (1), the treated wastewater injection into the groundwater zone was eliminated. Moreover, an inward groundwater flow movement from the adjacent immediate vicinity of the groundwater, $Q_{g.w.(Brine)}$ and $C_{g.w.(Brine)}$, was induced. Due to the elimination of the better water quality treated wastewater injection to the groundwater zone, the enhancement of groundwater quality was retarded. Moreover, the only inlet sources of water to the groundwater zone are deep percolation water from the root zone and the inward groundwater flow movement from the adjacent immediate vicinity of the groundwater zone. The former water source quantity is minute compared to the amount of the latter source and the pumped groundwater. Furthermore, the salt concentration of the deep percolated water is relatively high (2000 mg/l). Thus, deep percolated water has no significant effect in enhancing the groundwater quality. In addition, the prevailing amount of the inward groundwater flow movement (with high salt concentration, 6000 mg/l) from the adjacent immediate vicinity of the groundwater zone will retard the enhancement of the groundwater salt concentration to a larger extent. For all the above reasons, the pumped groundwater salt concentration for the obstacle scenario (1) simulation will be much higher than the base case simulation. Owing to the increase in the pumped groundwater salt concentration in the obstacle scenario (1) simulation (Figure 5.20), the feed water to the reverse osmosis unit will be at a high salt concentration. Thus, the water permeate from the reverse osmosis unit will be at a higher concentration, too. Therefore, the more permeate water required (to be used as irrigation water) to cope with the irrigation efficiency, the higher the salt concentration in the irrigation water and the higher amount of irrigation water needed to be applied to keep the root zone at the desirable salt concentration tolerance. Hence, irrigation water demand will increase. Moreover, to meet this increase in the irrigation water demand, a larger groundwater amount must be pumped and fed to the reverse osmosis unit to cope with the irrigation water requirement increases. Therefore, the higher the pumped groundwater amount required to be fed to the reverse osmosis unit the higher the amount of water needed to be desalinated and the more the power will be consumed by the reverse osmosis unit (Figure 5.18). Moreover, to meet this increase in the irrigation water demand, a larger groundwater amount must be pumped and fed to the reverse osmosis unit to deal with the irrigation water requirement increases. Therefore, the pump power consumption will increase (Figure 5.19). As a result, the percent of increase in the sum of total power consumption over the 40-year simulation was 34.33 % when using the obstacle scenario (1). Even though the sum of total power consumption increased by 34.33 %, which increased the power utilization cost, the sum of the treated wastewater utilization was reduced by 100.54 m^3 per unit area, over the 40-year simulation, due to the elimination of the treated wastewater injection. This will cut the cost of the treated wastewater utilization by the system. Moreover, the most critical drawback of this obstacle scenario (1) is the retardation in enhancement of the groundwater salt concentration and the inward groundwater flow movement from the adjacent immediate vicinity of the groundwater. The latter will have a major negative effect on groundwater quality and quantity in the long run due to the intrusion of the adjacent higher salt concentration (brine) groundwater and consequently mining the groundwater, hence deteriorating the relatively better quality groundwater. Figures 5.21 illustrate the sum of the total power consumption comparison for 40-year simulations between the obstacle scenario (1) and the base case of the general conceptual design system simulation. Moreover, Table 5.2 demonstrates the percent change comparison in the sum of the total power consumption and the decrease in the sum of the treated wastewater injection between the base case and obstacle scenario (1) simulation.

Figure 5.21 Sum of the total power consumption comparison for 40-year simulations between the obstacle scenario (1) and the base case of the general conceptual design system simulation.

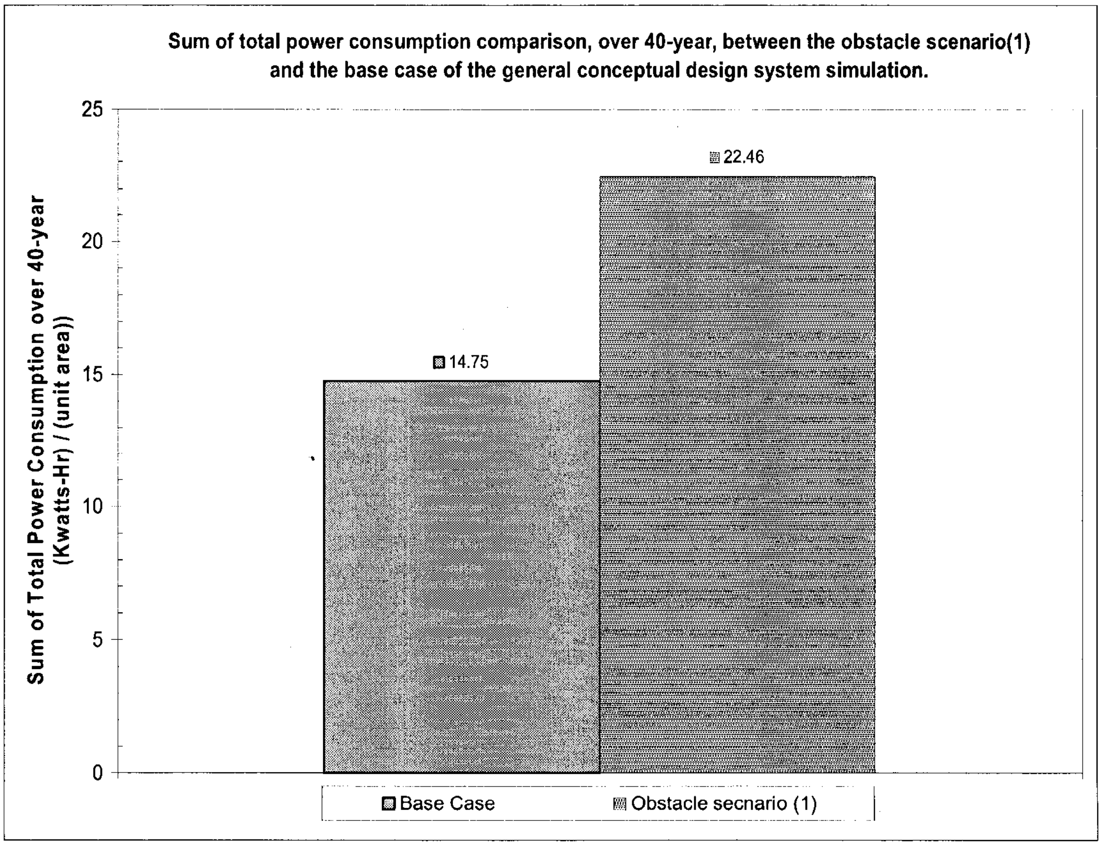

 Emad H. AlAli

Table 5.2 Percent increase in the sum of the total power consumption and the decrease in the amount of the injected treated wastewater (over a 40-year simulation) between the base case and the obstacle season scenario (1).

From	To	% Change (increase) in Sum of Total Power per Unit Area	Decrease in the sum of the Injected Treated Wastewater (m^3/unit area)
Base Case	**Obstacle Scenario (1)**	**34.33**	**100.54**

5.1.3 Obstacle Scenario (2) Model Simulation

In this scenario, the reverse osmosis system will be omitted; consequently, the Q_{Feed} from the groundwater pumping will be used directly to irrigate the field, $Q_{Feed} = Q_{irr}$. Moreover, the salt concentration of the irrigation water will be the same as the salt concentration of the pumped groundwater, feed water, $C_{Feed} = C_{irr}$. Moreover, due to the slight variances in the individual water source quantity from one simulation period to the other (as shown in Section 3.1.3) the assumption of steady state will be implemented in driving the governing equations of the conceptual design system, but a transit flow approach will be applied to the simulation calculations. The order of simulating the obstacle scenario (2) of the general conceptual design system, 40-year simulation period, will be performed in the same order as in Section 3.3 for the base case of the general conceptual design system simulation. However, in this scenario, the reverse osmosis unit governing equation and calculation will be ignored due to the omission of the reverse osmosis unit. Thus, the calculation processors will be conducted in the following order:

1. Calculating C_{Feed} while using an iteration approach. Thus, from Equation (3.35), where

$$C_{Feed} = \left(\frac{C^{t}_{g.w.} + C^{t-1}_{g.w.}}{2} \right)$$

2. Calculating $C_{irr\ (permeate)}$, due to the omission of the reverse osmosis system. The salt concentration of the irrigation water will be the same as the salt concentration of the pumped groundwater, feed water (Figure 5.22), where

$$C_{irr(\,permeate\,)} = C_{Feed} \qquad \textbf{(5.14)}$$

3. Calculating $Q_{irr\ (\mathrm{permeate})}$, from Equation (3.50), where

$$Q_{irr(\,permeate\,)} = \left(\frac{Q_{ET_C}}{1 - \left[\frac{C_{irr(\,permeate\,)}}{C_{RZ}} \right]} \right)$$

4. Calculating Q_{Feed}. Due to the omission of the reverse osmosis system Q_{Feed} from the groundwater will be used directly to irrigate the field (Figure 5.22).

Thus,

$$Q_{Feed} = Q_{irr(\,permeate\,)} \tag{5.15}$$

5. Calculating Q_{DP} from Equation (3.3), where

$$Q_{irr} = Q_{ET_c} + Q_{DP}$$

Figure 5.22 Obstacle scenario (2) salt mass balance and water balance of the groundwater system.

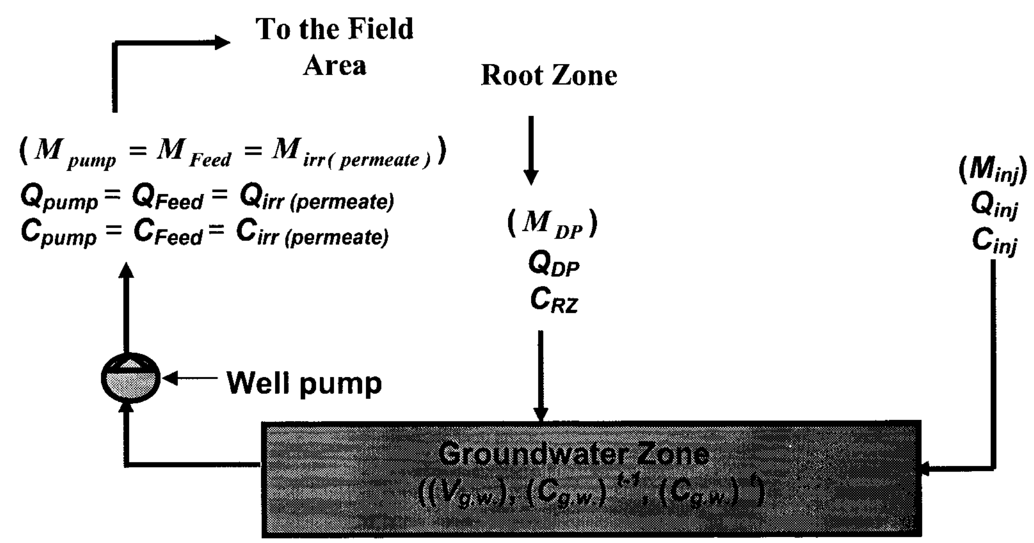

6. Calculating Q_{inj} from Equation (3.32), where

$$Q_{Feed} = Q_{inj} + Q_{DP}$$

7. Calculating $C^{t}_{g.w.}$ from Equation (3.37), where

$$C^{t}_{g.w.} = \frac{\left(\left(\frac{V_{g.w.}}{\Delta t}\right) * C^{t-1}_{g.w.}\right) + Q_{inj.} * C_{inj} + Q_{DP} * C_{RZ} - \left(\left(\frac{Q_{Feed}}{2}\right) * C^{t-1}_{g.w.}\right)}{\left(\left(\frac{V_{g.w.}}{\Delta t}\right) + \left(\frac{Q_{Feed}}{2}\right)\right)}$$

8. Calculating the power exerted by pumping the groundwater, $\boldsymbol{Power_{well}}$, from Equation (3.55), where

$$Power_{well} = \frac{\gamma * Q_{Feed} * \left(h_{surface} - \sqrt{h_o^2 - \frac{Q_{Feed}}{\pi * K} * \ln\left(\frac{r_o}{r_w}\right)}\right)}{\eta_{(well)}}$$

9. Calculating the total power consumed by the system. Due to the omission of the reverse osmosis system $\boldsymbol{Power_{(R.O.)} = 0}$, from Equation (3.56), where,

$$Total\,Power = Power_{well} \tag{5.16}$$

10. However, due to the omission of the reverse osmosis system, the groundwater pumped water, feed water, must never exceed the maximum allowable pumping capacity of the groundwater per season. Thus, the simulation will be terminated by the model during the 40-year simulation if the ($\boldsymbol{Q_{pump} = Q_{Feed}}$) requirement exceeds the maximum allowable pumping capacity of the

groundwater per season due to the increase in groundwater salt concentration. From Equation (3.49), maximum allowable pumping capacity of the groundwater can be calculated, where

$$Q_{Pump\ (max)} = \pi * K * \left(\frac{(h_o^2 - h_{w(min)}^2)}{Ln(\frac{r_o}{r_w})} \right)$$

Where, $Q_{pump\ (max)}$ is in m^3/season, and

$$\text{if } Q_{Feed} \rangle\ Q_{Pump\ (max)} \qquad \textbf{(5.17)}$$

then, the simulation will be terminated.

The increase in Q_{Feed} in the beginning of the simulation or within the simulation seasons is owed to the initial groundwater concentration or increase in the groundwater concentration as the simulation proceeds. This will induce an increase in the $Q_{irr(permeate)}$, to maintain the root zone, C_{RZ}, at the allowable salt concentration tolerance level. Furthermore, because $Q_{Feed} = Q_{irr(permeate)}$, this will cause an increase in the Q_{Feed} required to maintain the root zone within the desirable salt concentration, C_{RZ}, tolerance. Hence, as the groundwater salt concentration increases the Q_{Feed} will increase.

Finally, Figure 5.23 illustrates the governing equations of the obstacle scenario (2) of the general conceptual design system.

Figure 5.23 Obstacle scenario (2) of the general conceptual design system governing equations.

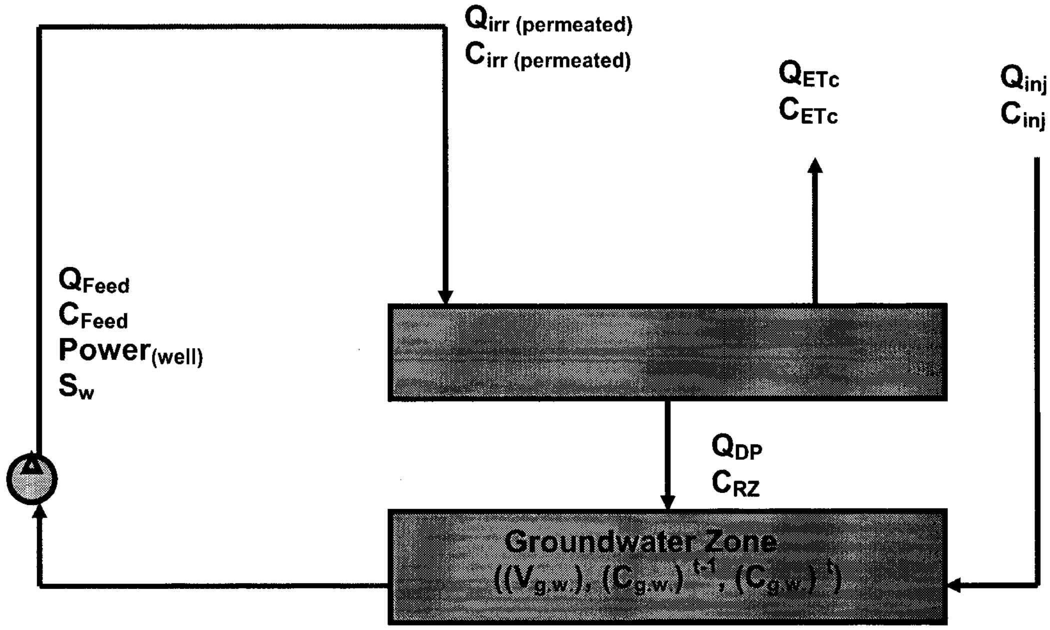

<u>**No. of Equations = 9**</u>

<u>**Vadose Zone Governing Equations:**</u>

1) $Q_{irr\ (permeate)} * C_{irr\ (permeate)} = Q_{ETc} * C_{ETc} + Q_{DP} * C_{RZ}$
2) $Q_{irr\ (permeate)} = Q_{ETc} + Q_{DP}$

<u>**Groundwater Zone Governing Equations:**</u>

3) $Q_{Feed} = Q_{irr\ (permeate)}$
4) $Q_{Feed} = Q_{inj} + Q_{DP}$
5) $C_{Feed} = (((C_{g.w})^{t-1} + (C_{g.w.})^{t}) / 2)$
6) $C_{Feed} = C_{irr\ (permeate)}$
7) $(C_{g.w.})^{t} = ((V_{g.w.} / \Delta t) * (C_{g.w})^{t-1} + Q_{inj} * C_{inj} + Q_{DP} * C_{RZ} - (Q_{Feed} / 2) * (C_{g.w})^{t-1}) / ((V_{g.w.} / \Delta t) + (Q_{Feed} / 2))$, **(Pumping and mixing are simultaneously).**
8) $Power_{(well)} = (\gamma * Q_{Feed} * H_{lift}) / \eta_{(well)} = (\gamma * Q_{Feed} * ((h_{surface} - h_o) + S_w)) / \eta_{(well)}$
9) $S_w = h_o - [(h_o^2 - (Q_{Feed} / ((\pi * K) * \ln (r_o / r_w))]^{0.5}$

<u>**No. of Variables = 16**</u>

$Q_{irr\ (permeate)}$, Q_{ETc}, Q_{inj}, Q_{DP}, $V_{g.w.}$, Q_{Feed}, $C_{irr\ (permeate)}$, C_{ETc}, C_{inj}, C_{RZ}, $(C_{g.w.})^{t}$, $(C_{g.w.})^{t-1}$, S_w, C_{Feed}, Δt, $Power_{(well)}$.

<u>**No. of Known Variables = 6**</u>

C_{ETc}, C_{inj}, $(C_{g.w.})^{t-1}$, Q_{ETc} **(Or from Penman-Montelth method)**, $V_{g.w.}$, Δt.

<u>**No. of Decision Variables = 1**</u>

C_{RZ}

The results for the obstacle scenario (2) simulation were captured in Figures 5.24, 5.25, and 5.26 respectively. Due to the elimination of the reverse osmosis unit the simulations failed to simulate when the initial groundwater salt concentration was larger than 1400 mg/l. Moreover, the simulation was terminated by the model after a one year period, 2 year period, and 3 year period of simulations for the initial ground salt concentration ranges of less than 1400 to 1300 mg/l, 1250 – 1150 mg/l, and 1100 – 1000 mg/ l respectively. The main cause of the system failure is caused by the initial groundwater concentration or increase in the groundwater concentration as the simulation proceeds. This will induce an increase in the irrigation water requirement, $Q_{irr(permeate)}$, to maintain the root zone salt concentration tolerance, C_{RZ}, at the allowable level. Owing to the elimination of the reverse osmosis unit, the pumped groundwater flow will be directly used as irrigation water ($Q_{pump} = Q_{Feed} = Q_{irr(permeate)}$); therefore, as $Q_{irr(permeate)}$ increases the Q_{pump} will increase, too. If Q_{pump} requirement exceeded the maximum allowable pumping capacity of the groundwater per season, due to the increase in groundwater salt concentration, the model will be terminated. Due to the simulation termination or failure, the obstacle scenario (2) simulation results were not compared with the base case simulation results of the general conceptual design system. Even though the utilization of this obstacle scenario (2) is limited to low initial groundwater salt concentration, the simulation will only proceed for 2 – 3 years. This obstacle scenario (2) can be an alternative (for 2-3 years only) for the base case simulation after almost 17 years of the base case simulation, where the groundwater salt concentration will be in the vicinity of 1100-100 mg/l (Figure 5.20, for the base case). Therefore, for illustration purposes, an initial groundwater salt concentration of 1000 mg/l was chosen to illustrate the results output. These output result graphs were arranged by the total power required by the system (which is equals to the power consumed by the pump well only due to the elimination of the R.O. unit), the amount of treated wastewater injected to the native groundwater, and the initial groundwater salt concentrations, respectively.

Figure 5.24 Total power (equal to pump well power only) consumed by obstacle scenario (2) simulation.

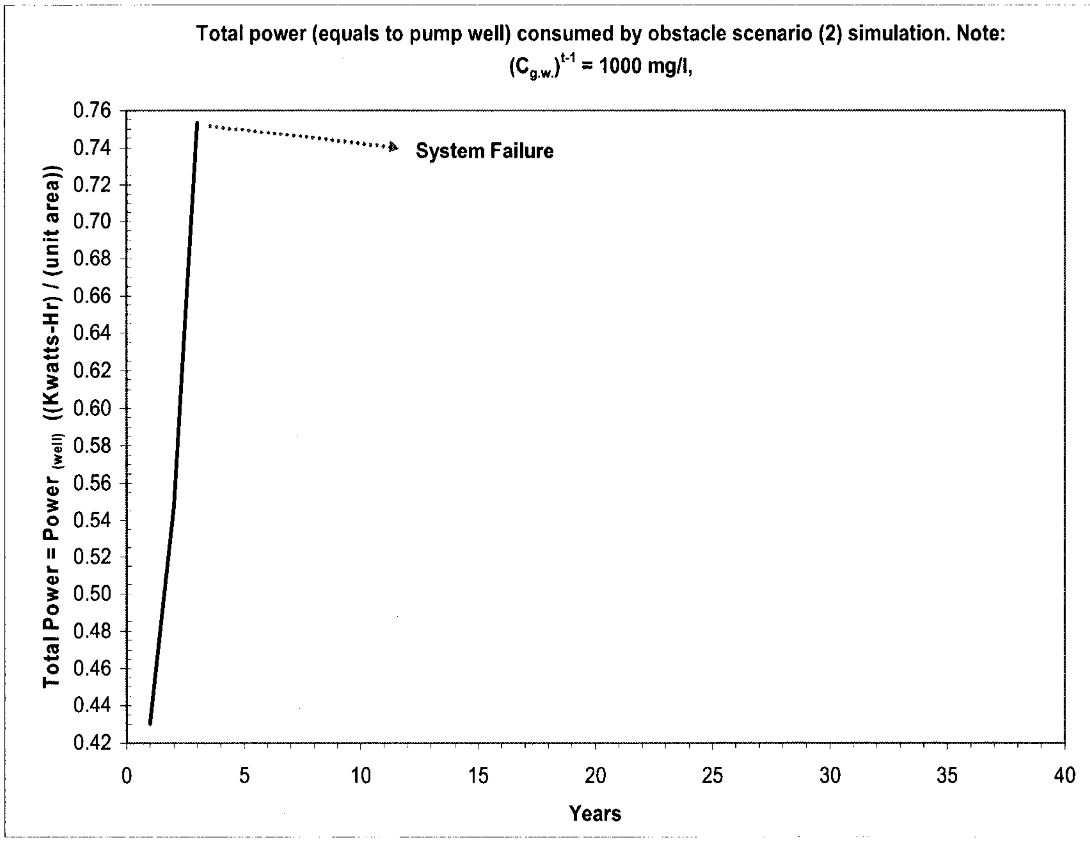

Figure 5.25 Treated wastewater consumed by obstacle scenario (2) simulation.

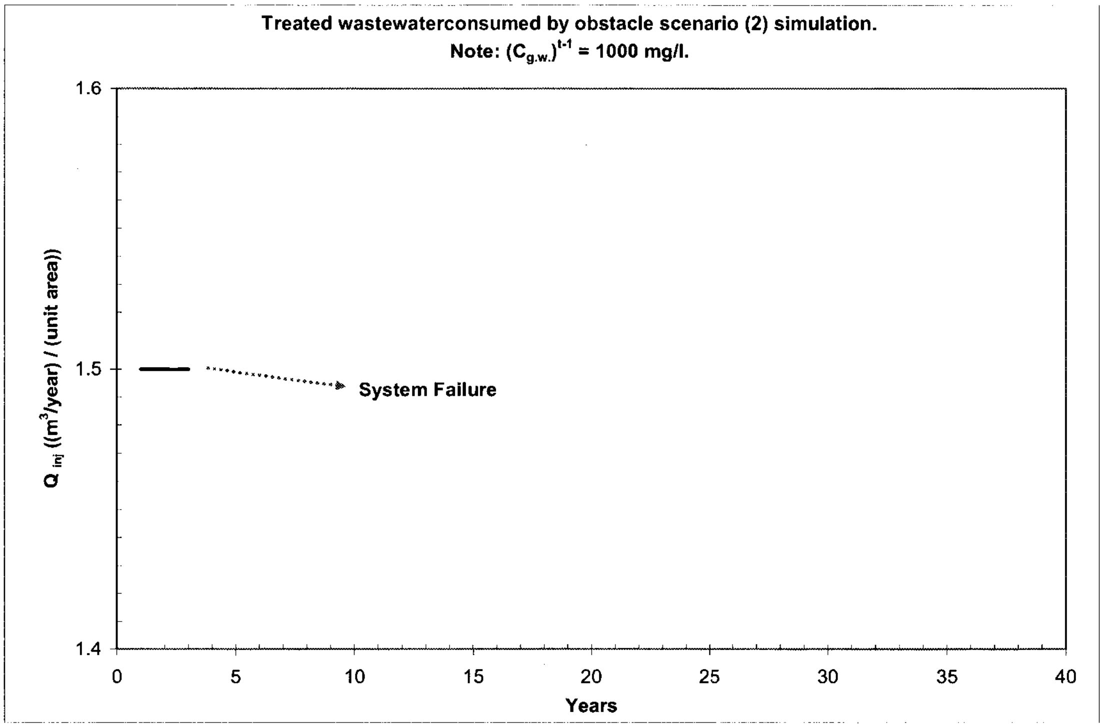

Figure 5.26 Initial groundwater salt concentration of obstacle scenario (2) simulation.

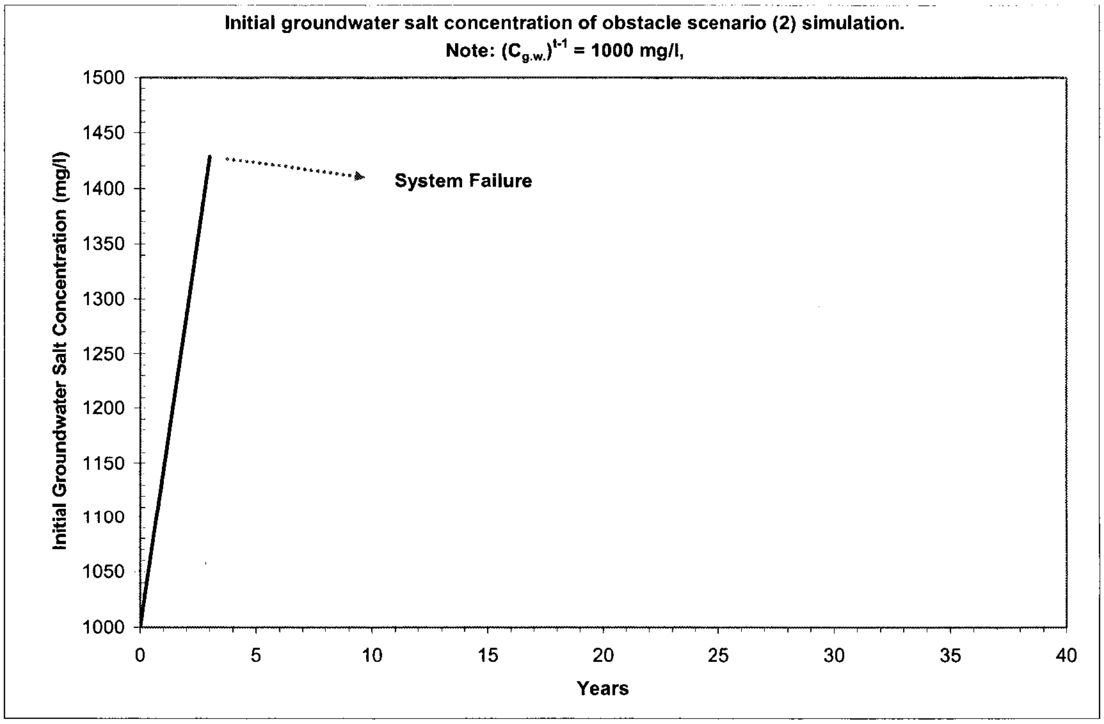

5.1.4 Obstacle Scenario (3) Model Simulation

In this scenario, treated wastewater augmentation will be re-routed through the reverse osmosis unit instead of direct injection to the native groundwater ($Q_{waste} = Q_{Feed}$, $C_{waste} = C_{Feed}$, and $Q_{inj} = C_{inj} = 0$) (Figure 5.27). The desalinated (permeate) water will be used for irrigation. Furthermore, to avoid a water table rise through the simulation period, the groundwater pumping, Q_{pump}, will be set equal to the deep percolation recharge, Q_{DP}. Moreover, this pumped water will be discarded away from the system, or it will be kept in evaporation ponds (Figure 5.28). Furthermore, due to the slight variances in the individual water source quantity from one simulation period to the other (as shown in Section 3.1.3) the assumption of a steady state flow will be implemented in driving the governing equations of the conceptual design system, but a transit flow approach will be applied to the simulation calculations. The order of simulating the obstacle scenario (3) of the general conceptual design system, 40 year simulation period, will be performed in the same order as in Section 3.3 for the base case of general conceptual design system simulation. However, in this scenario the treated wastewater will be diverted to the reverse osmosis unit instead of direct injection to the native groundwater. Therefore, the treated wastewater injection to the native groundwater will be omitted, hence $Q_{inj} = C_{inj} = 0$, $Q_{Feed} = Q_{waste}$, and $C_{Feed} = C_{waste}$. Moreover, groundwater pumping, Q_{pump}, will be set equal to the deep percolation recharge, Q_{DP}. Thus, $Q_{pump} = Q_{DP}$. Accordingly, the calculation processors of this scenario will be conducted in the following order:

1. Calculating C_{pump} while using an iteration approach. Thus, from Equation (3.35), using C_{pump} instead of C_{Feed}, where

$$C_{pump} = \left(\frac{C^{t}_{g.w.} + C^{t-1}_{g.w.}}{2} \right)$$

Figure 5.27 Steady state salt mass balance of the reverse osmosis system.

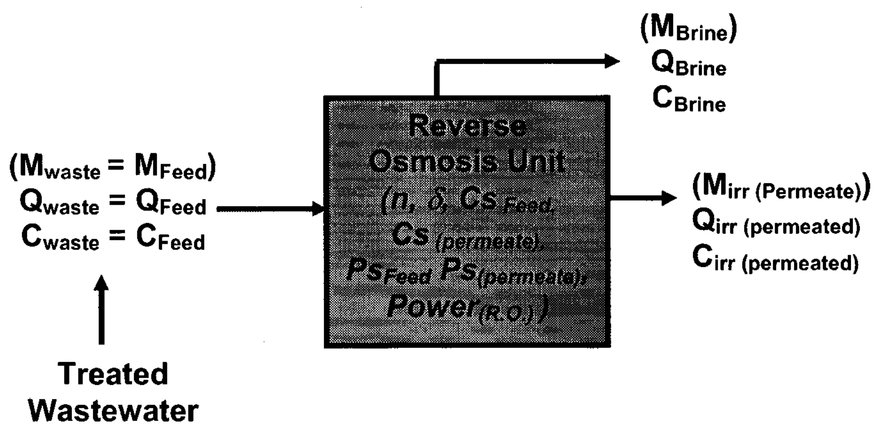

2. Calculating $C_{irr\,(permeate)}$, from Equation (3.30), using C_{waste} instead of C_{Feed} (Figure 5.27), where

$$C_{irr(\,permeate\,)} = n * C_{waste} * \left[\frac{1 - \frac{\delta}{2}}{1 - \delta} \right]$$

3. Calculating $Q_{irr\,\text{(permeate)}}$, from Equation (3.53), where

 Emad H. AlAli

$$Q_{irr(permeate)} = \left(\frac{Q_{ET_C}}{1 - \left[\frac{C_{irr(permeate)}}{C_{RZ}} \right]} \right)$$

Figure 5.28 Salt mass balance and water balance of the groundwater system.

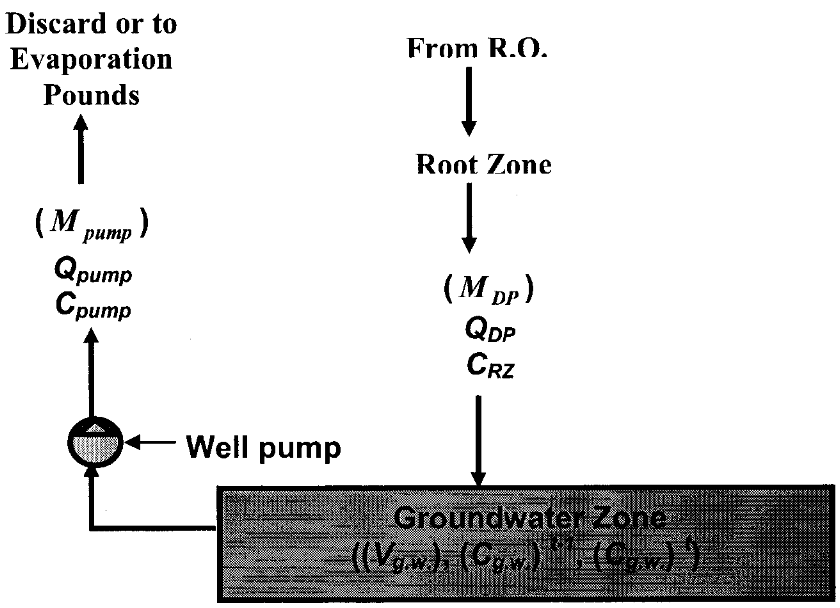

4. Calculating Q_{waste}, from Equation (3.10), using Q_{waste} instead of Q_{Feed}, where

$$Recovery\%\ (\delta) = \frac{Q_{irr\ (permeated)}}{Q_{waste}}$$

5. Calculating Q_{DP} from Equation (3.3), where

 Emad H. AlAli

$$Q_{irr} = Q_{ET_c} + Q_{DP}$$

6. Calculating $\boldsymbol{Q_{pump}}$, to avoid water table rise through the simulation period, the groundwater pumping, $\boldsymbol{Q_{pump}}$, will be set equal to the deep percolation recharge, $\boldsymbol{Q_{DP}}$. Thus,

$$Q_{pump} = Q_{DP} \tag{5.18}$$

7. Calculating $\boldsymbol{C^{t}_{g.w.}}$ from Equation (3.37), knowing that $\boldsymbol{Q_{inj}} = \boldsymbol{C_{inj}} = \boldsymbol{0}$ and using $\boldsymbol{Q_{pump}}$ instead of $\boldsymbol{Q_{Feed}}$, where

$$C^{t}_{g.w.} = \frac{\left(\left(\frac{V_{g.w.}}{\Delta t}\right) * C^{t-1}_{g.w.}\right) + (Q_{DP} * C_{RZ}) - \left(\left(\frac{Q_{pump}}{2}\right) * C^{t-1}_{g.w.}\right)}{\left(\left(\frac{V_{g.w.}}{\Delta t}\right) + \left(\frac{Q_{pump}}{2}\right)\right)} \tag{5.15}$$

8. Calculating $\boldsymbol{Q_{Brine}}$ from Equation (3.9), using $\boldsymbol{Q_{waste}}$ instead of $\boldsymbol{Q_{Feed}}$, where

$$Q_{waste} = Q_{irr(permeate)} + Q_{Brine}$$

9. Calculating $\boldsymbol{C_{Brine}}$ from Equation (3.54), using $\boldsymbol{Q_{waste}}$ instead of $\boldsymbol{Q_{Feed}}$ and $\boldsymbol{C_{waste}}$ instead of $\boldsymbol{C_{Feed}}$, where

$$C_{Brine} = \frac{(Q_{waste} * C_{waste}) - (Q_{irr(permeate)} * C_{irr(permeate)})}{Q_{Brine}} \quad \textbf{(5.19)}$$

10. Calculating the osmotic pressure of the feed wastewater to the reverse osmosis unit $\boldsymbol{Ps_{waste}}$, from Equation (3.20), and using $\boldsymbol{Ps_{waste}}$ instead of $\boldsymbol{Ps_{Feed}}$ and using $\boldsymbol{Cs_{waste}}$ instead of $\boldsymbol{Cs_{Feed}}$, where

$$Ps_{waste} = Cs_{waste} * R * T \quad \textbf{(5.20)}$$

Hence, from Equation (3.28), the ionic molar concentration of the feed wastewater to the reverse osmosis unit is

$$Cs_{waste} = (\Psi) * \left(\frac{C_{waste}}{\varpi} \right) \quad \textbf{(5.21)}$$

11. Calculating the osmotic pressure of the permeate water from the reverse Osmosis unit, $\boldsymbol{Ps_{permeate}}$, from Equation (3.21), where

$$Ps_{permeate} = Cs_{irr(permeate)} * R * T$$

Hence, from Equation (3.29), the ionic molar concentration of the reverse osmosis permeate water is

$$Cs_{irr(\,permeate\,)} = (\Psi) * \left(\frac{C_{irr(\,permeate\,)}}{\varpi} \right)$$

12. Calculating the power exerted by the reverse osmosis system pump, $\boldsymbol{Power_{(R.O.)}}$, from Equation (3.31), using $\boldsymbol{Ps_{waste}}$ instead of $\boldsymbol{Ps_{Feed}}$, where

$$Power_{(\,R.O.)} = \left[\frac{\left(Ps_{waste} - Ps_{permeate}\right) * Q_{irr(\,permeate\,)}}{\eta_{R.O.}} \right] \tag{5.22}$$

13. Calculating the power exerted by pumping the groundwater, $\boldsymbol{Power_{well}}$, from Equation (3.55), and using $\boldsymbol{Q_{pump}}$ instead of $\boldsymbol{Q_{Feed}}$, where

$$Power_{well} = \frac{\gamma * Q_{pump} * \left(h_{surface} - \sqrt{h_o^2 - \frac{Q_{pump}}{\pi * K} * ln\left(\frac{r_o}{r_w}\right)} \right)}{\eta_{(\,well\,)}} \tag{5.23}$$

14. Calculating the total power consumed by the system, from Equation (3.56), thus

$$Total\,Power = Power_{(\,R.O.)} + Power_{well}$$

Finally, Figure 5.29 illustrates the governing equations of the obstacle scenario (3) of the general conceptual design system.

Figure 5.29 Obstacle scenario (3) of the general conceptual design system governing equations.

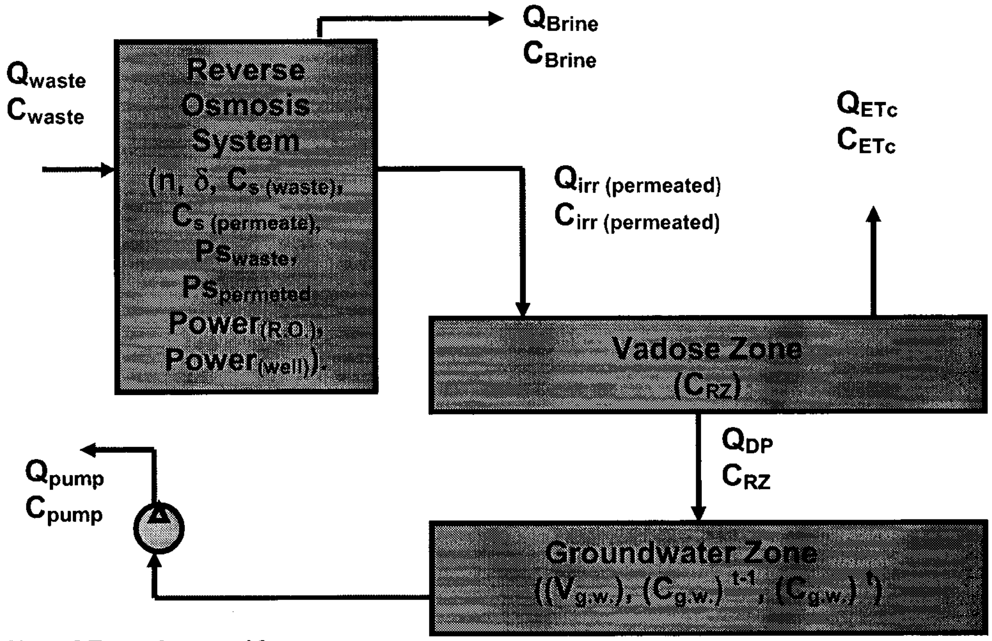

No. of Equations = 16

Root (Vadose) Zone Governing Equations:

1) $Q_{irr\,(permeate)} * C_{irr\,(permeate)} = Q_{ETc} * C_{ETc} + Q_{DP} * C_{RZ}$

2) $Q_{irr\,(permeated)} = Q_{ETc} + Q_{DP}$

Groundwater Zone Governing Equations:

3) $(C_{g.w.})^{t} = ((V_{g.w.}/\Delta t) * (C_{g.w})^{t-1} + Q_{DP} * C_{RZ} - (Q_{pump} / 2) * (C_{g.w})^{t-1}) / ((V_{g.w.}/\Delta t) + (Q_{pump} / 2))$

4) $Q_{pump} = Q_{DP}$

5) $C_{pump} = (((C_{g.w.})^{t-1} + (C_{g.w.})^{t}) / 2))$

6) $Power_{(well)} = (\gamma * (Q_{pump}) * H_{lift}) / \eta_{(well)} = (\gamma * Q_{pump} * ((h_{surface} - h_o) + S_w)) / \eta_{(well)}$

7) $S_w = h_o - [(h_o^2 - (Q_{pump} / (\pi * K) * \ln (r_o / r_w))]^{0.5}$

Reverse Osmosis Governing Equations:

8) $Q_{waste} = Q_{irr\,(permeate)} + Q_{Brine}$

9) $Q_{waste} * C_{waste} = Q_{irr\,(permeate)} * C_{irr\,(permeate)} + Q_{Brine} * C_{Brine}$

10) $\delta = (Q_{irr\,(permeate)}) / (Q_{waste})$

11) $C_{irr\,(permeate)} = n * C_{waste} * ((1 - (\delta / 2)) / (1 - \delta))$

12) $Power_{(R.O.)} = (Ps_{waste} - Ps_{(permeate)}) * Q_{irr\,(permeate)}$

13) $Ps_{waste} = C_{s\,(waste)} * R * T$

14) $Ps_{(permeate)} = C_{s\,(Permeate)} * R * T$

15) $C_{s\,(waste)} = (\Psi) * (C_{waste} / (1000 * \varpi))$

16) $C_{s\,(Permeate)} = (\Psi) * (C_{irr\,(permeate)} / (1000 * \varpi))$

No. of Variables = 25

$Q_{irr\,(permeate)}$, Q_{Brine}, Q_{ETc}, Q_{waste}, Q_{DP}, Q_{pump}, $V_{g.w.}$, $C_{irr\,(permeate)}$, C_{Brine}, C_{ETc}, C_{waste}, C_{RZ}, C_{pump}, $(C_{g.w.})^{t}$, $(C_{g.w.})^{t-1}$, δ, n, $C_{s\,(waste)}$, $C_{s\,(Permeate)}$, Ps_{waste}, $Ps_{permeted}$, Δt, S_w, $Power_{(R.O.)}$, $Power_{(well)}$.

No. of Known Variables = 6

C_{ETc}, C_{waste}, $(C_{g.w.})^{t-1}$, Q_{ETc} (Or from Penman-Monteith method), $V_{g.w.}$, Δt

No. of Decision Variables = 3

n, δ, C_{RZ}

The results for the obstacle scenario (3) simulation were compared with the base case of the general conceptual design system simulation captured in Figures 5.30, 5.31, 5.32, 5.33, and 5.34 respectively. These output result graphs were arranged by the total power required by the system, the power required by the reverse osmosis unit, the power required by the well pump system, the amount of treated wastewater consumed, and the initial groundwater salt concentrations, respectively.

Figure 5.30 Total power consumption comparison between the obstacle scenario (3) and the base case of the general conceptual design system simulation.

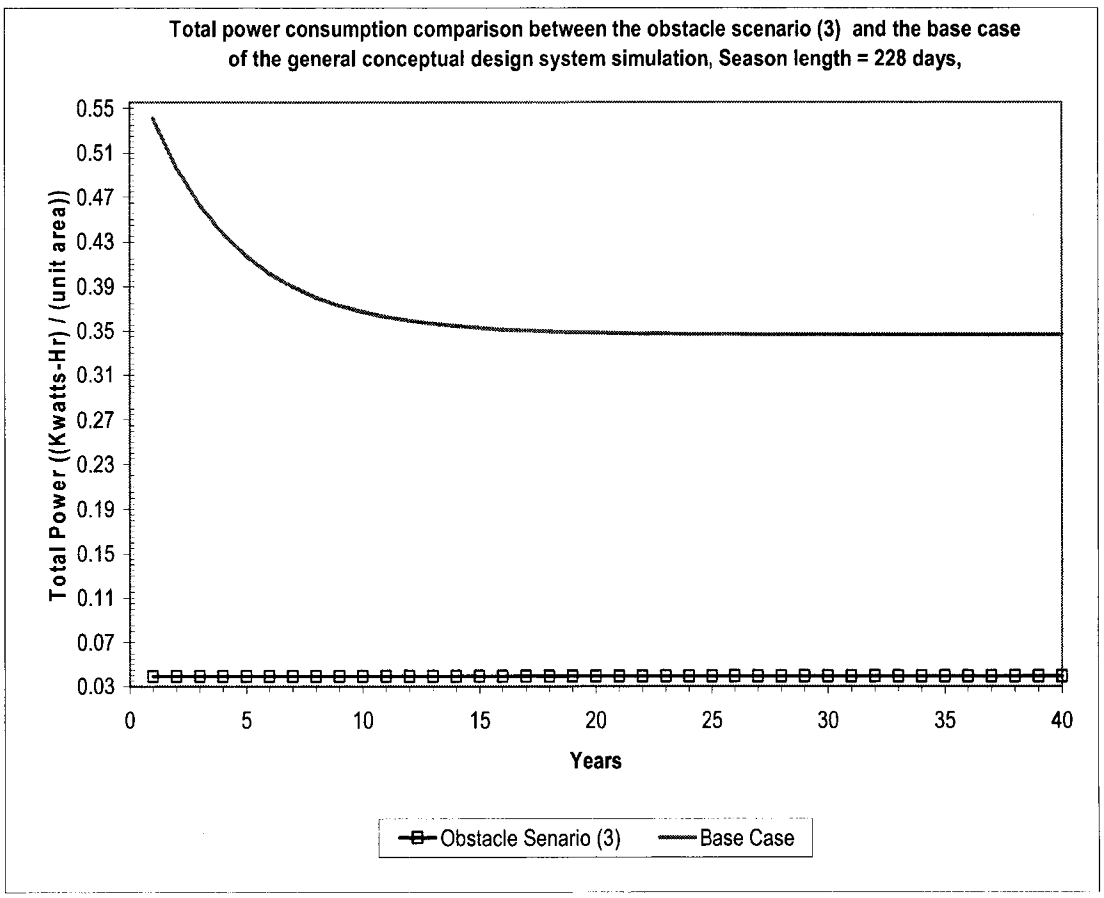

 Emad H. AlAli

Figure 5.31 Reverse osmosis power consumption comparison between the obstacle scenario (3) and the base case of the general conceptual design system simulation.

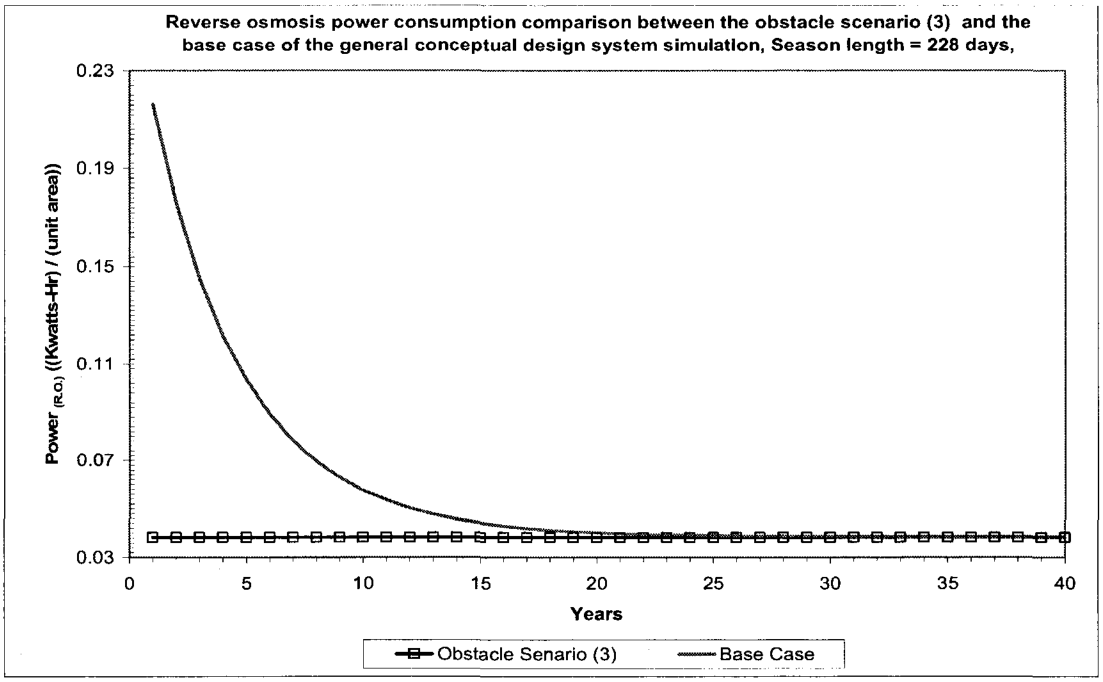

Figure 5.32 Well pump power consumption comparison between the obstacle scenario (3) and the base case of the general conceptual design system simulation.

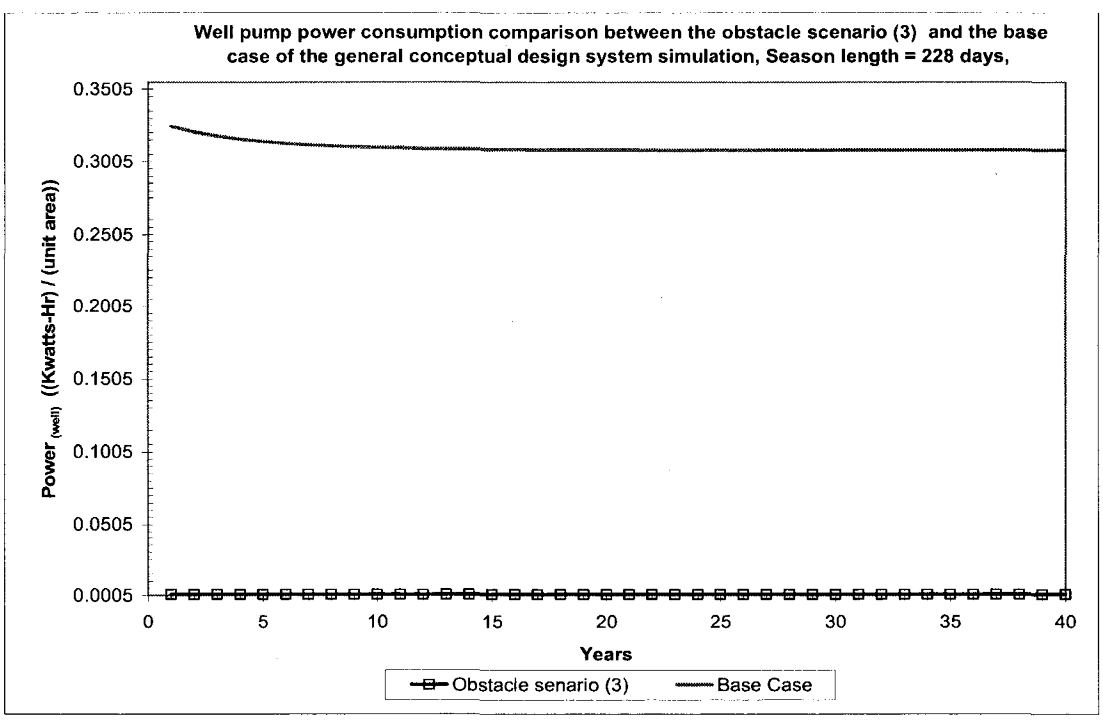

Figure 5.33 Treated wastewater power consumption comparison between the obstacle scenario (3) and the base case of the general conceptual design system simulation.

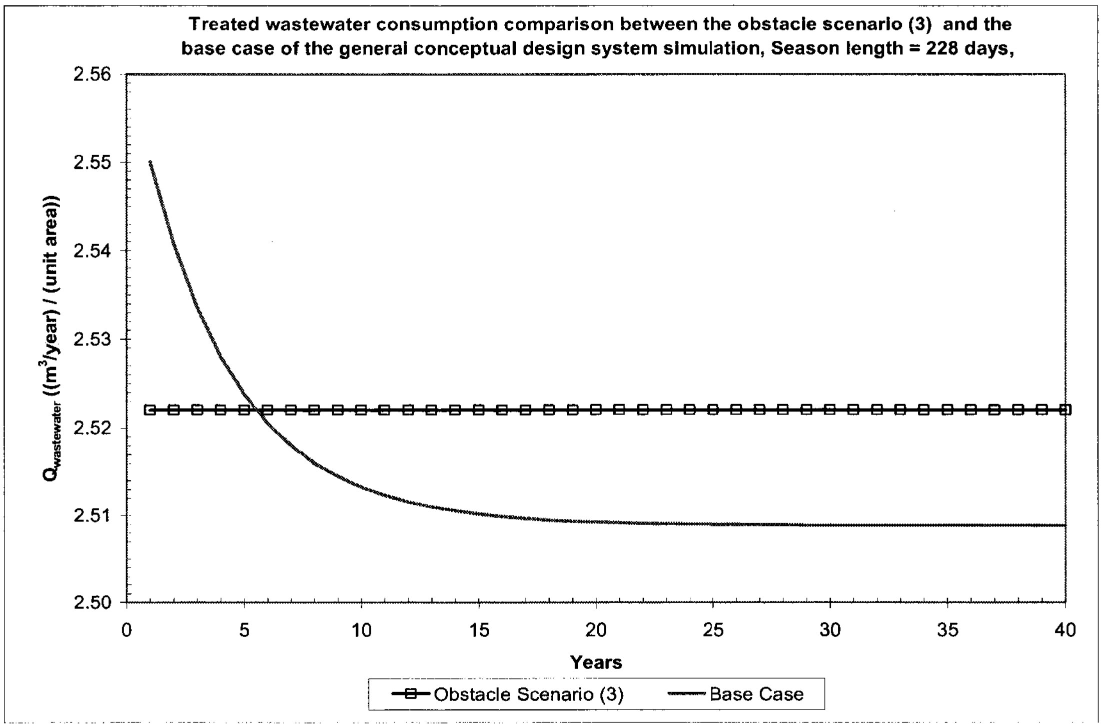

Figure 5.34 Initial groundwater salt concentration comparison between the obstacle scenario (3) and the base case of the general conceptual design system simulation.

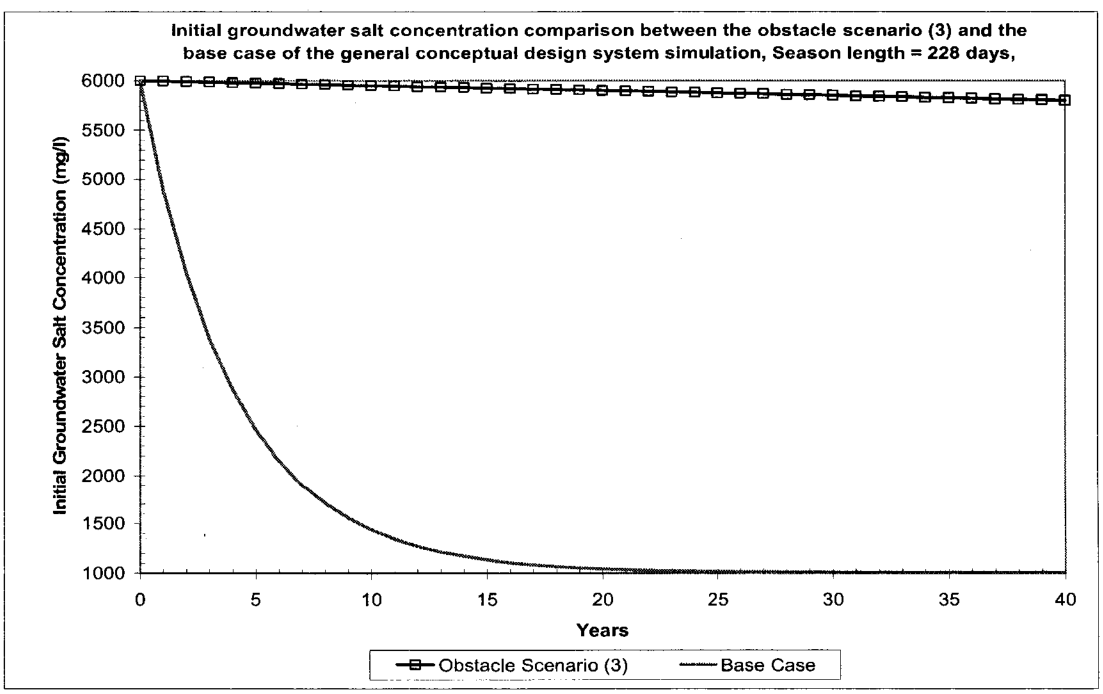

From Figures 5.30 and 5.33, it is manifest that the obstacle scenario (3) simulation total power per unit area required by the system is significantly lower than the base case simulation. Moreover, the base case simulation amount of treated wastewater per unit area required to be injected into the groundwater zone is slightly lower than the amount of the treated wastewater per unit area re-routed through reverse osmosis unit, instead of direct injection to the native groundwater, in obstacle scenario (3) simulation. As the treated wastewater re-routed is to be directly utilized by the reverse osmosis unit, the input treated wastewater salt concentration is constant and equal to 1000 mg/l. Therefore, the reverse osmosis permeate water (which will be used for irrigation) will be of a constant salt concentration, too. Due to the latter reason, the amount of water required by the system to be used for irrigation will be constant per season as well. Furthermore, to avoid water table hydraulic head elevation rise through the simulation period, due to the deep percolation water recharge to the groundwater zone, the groundwater pumping ($\boldsymbol{Q_{pump}}$) will be set equal to the deep percolation recharge ($\boldsymbol{Q_{DP}}$). The deep percolation water quantity is minute per unit area per season. Hence, the amount of pumped groundwater will be minimal as well, and as a result, the power required to be exerted by the pump will be minimal (Figure 5.32). The inflow treated wastewater salt concentration to the reverse osmosis unit is of a mild quality (1000 mg/l); therefore, the power exerted by the reverse osmosis unit for desalination will be minimal as well (Figure 5.31). Thus, the total power consumption by the system will be significantly reduced using the obstacle scenario (3) simulation (Figure 5.30). The treated wastewater utilization in obstacle scenario (3) simulation is slightly higher than the base case simulation theme because the obstacle scenario (3) simulation depends totally on treated wastewater as the main source of irrigation water. In addition, due to the mild quality (1000 mg/l) inflow of treated wastewater to the reverse osmosis unit, the reverse osmosis permeate water salt concentration will be very low. Due to the latter reason, less permeate water is required (to be used as irrigation water) to cope with the irrigation efficiency. Hence, irrigation water demand will decrease. In a conclusion, even though obstacle scenario (3) simulation depends totally on treated wastewater for irrigation, due to the mild salt concentration of the treated wastewater, the amount of treated wastewater utilized by the system was rational (Figure 5.33). As a result, the percent decrease in the sum of the total power consumption over a 40-year simulation was 89.36 % when using the obstacle scenario (3). On the other hand, the percent increase in the sum of the treated wastewater utilization over a 40-year simulation was 0.34 % when using the obstacle scenario (3). This will have a negligible effect on the increase of the cost of the treated wastewater utilized by the system. Owing to the large cutback in power consumption utilization and the negligible increase in the utilization amount of the treated wastewater, obstacle scenario (3) system can be one of the most operationally cost efficient system. However, the biggest drawback of the obstacle scenario (3) system is the public non-endorsement of utilizing treated wastewater as irrigation water, and the retardation in enhancement of the groundwater salt concentration in the long run (Figure 5.31). Figures 5.35 and 5.36 illustrate the sum of the total power consumption comparison for 40-year simulations between the obstacle scenario (3) and the base case of the general conceptual design system simulation, and the sum of treated wastewater quantity injected comparison, over 40 years, between the obstacle scenario (3) and the base case of the general conceptual design system simulation.

Figure 5.35 Sum of the total power consumption comparison for 40-year simulations between the obstacle scenario (3) and the base case of the general conceptual design system simulation.

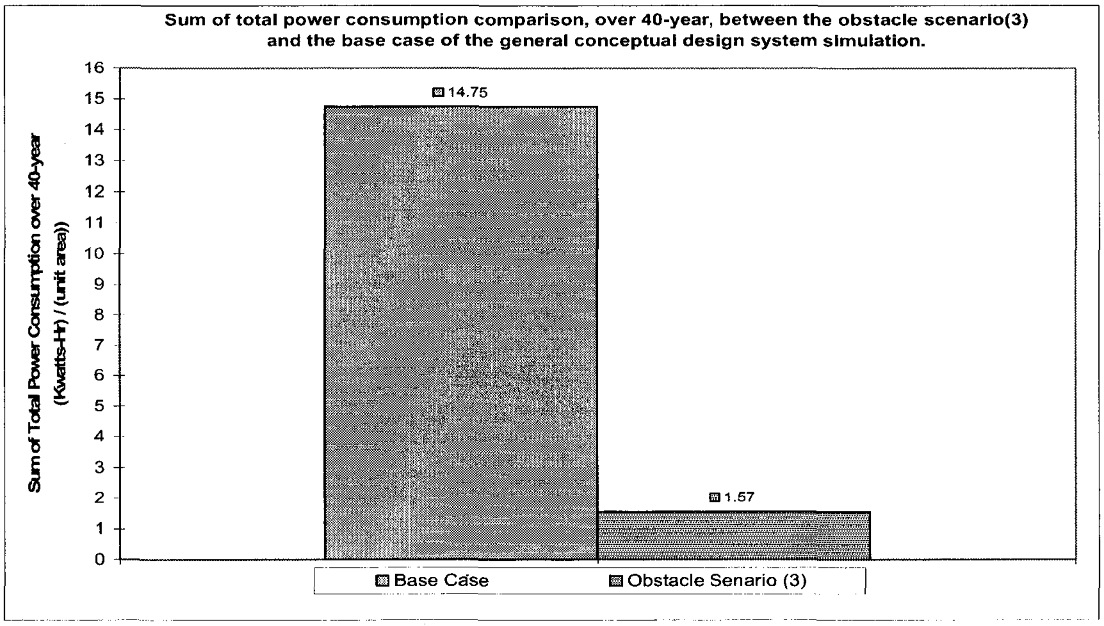

Figure 5.36 Sum of the treated wastewater quantity injected comparison, over 40 years, between the obstacle scenario (3) and the base case of the general conceptual design system simulation.

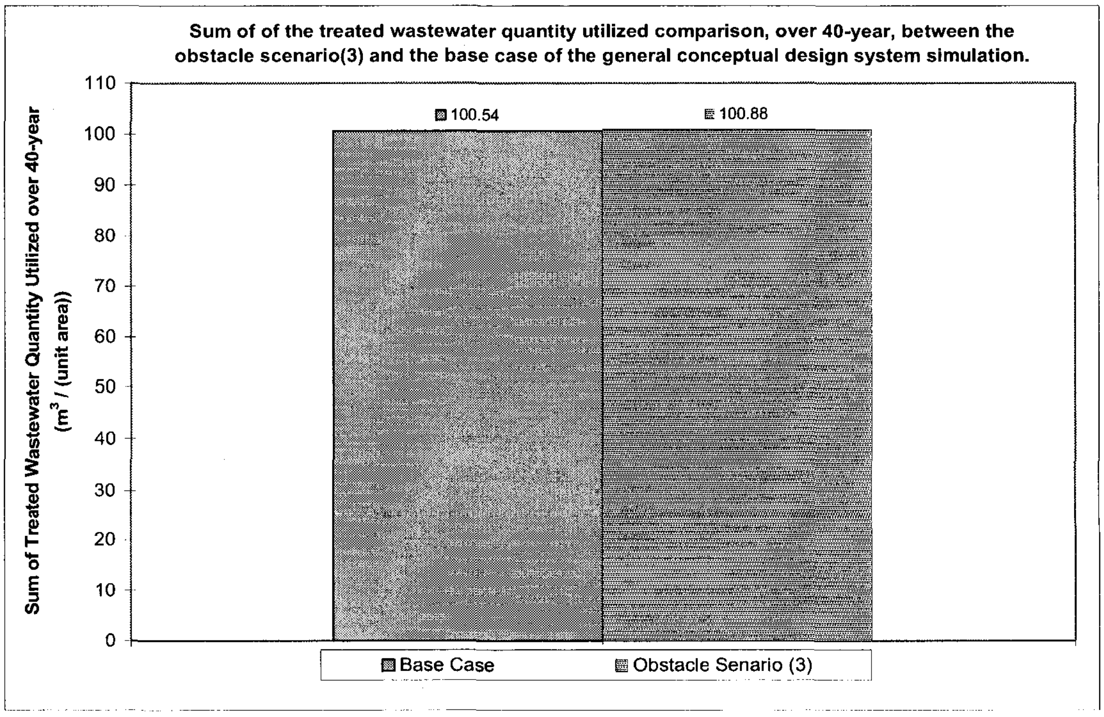

Moreover, Table 5.3 demonstrates the percent change comparison in the sum of the total power consumption and the sum of the treated wastewater injection between the base case and obstacle scenario (3) simulation.

Table 5.3 Percent change comparison in the sum of the total power consumption and the sum of the treated wastewater utilization between the base case simulation and obstacle scenario (3) simulation.

From	To	% Change (decrease) in Sum of the Total Power per Unit Area	% Change (increase) in Sum of the Utilization of the Treated Wastewater per Unit Area
Base Case	**Obstacle Scenario (3)**	**89.36**	**0.34**

CHAPTER 6

METHODOLOGY (AREAL DISTRIBUTION MODEL)

6.1 Simulating the General Conceptual Design System Using the Areal Distribution Model

In this chapter of the dissertation, the simulation of the general conceptual design system will be executed while using the areal distribution (Visual MODFLOW and MT3D) model approach. The areal distribution simulation model will be applied only to the base case of the general conceptual design system. In previous analysis of the base case of the general conceptual design system, a simplified model approach, the lump model approach, was utilized (Chapter 3). Moreover, complete uniform mixing in the space between all the water sources and the groundwater was assumed in the lump model simulation process. Hence, the groundwater zone was assumed to be as one mixing cell. In contrast, in this chapter of the dissertation, the groundwater mixing and the groundwater hydraulic heads will be non-uniform in space (spatially changing). Table 6.1 illustrates the main difference in the calculation approach between the lump model simulation and the areal distribution model simulation approaches. The simulation of the areal distribution model will be carried out through the Visual MODFLOW and MT3D simulation model approach. This model approach will calculate the transit areal distribution of the groundwater heads and the salt distribution and the transit drawdown within the unconfined saturated groundwater aquifer. After that, total operation power requirements will be calculated.

Table 6.1 Main difference in calculation between lump simulation model and areal distribution simulation model approaches.

NO.	Lump Simulation	Visual MODFLOW Simulation
1	Steady state drawdown	Transit drawdown calculated by partial differential equation
2	Aquifer groundwater salt concentration is considered constant in space, uniform in space. Groundwater salt concentration calculation by mixing approach.	Aquifer groundwater salt concentration is considered to be non-uniform in space, spatially changing. Groundwater salt concentration calculation by partial differential equation.
3	Groundwater hydraulic head is considered constant in space. Hydraulic head is uniform over the entire area.	Groundwater hydraulic head is considered non-uniform in space. Hydraulic head changes non- uniformly over the entire area.
4	Location of well pump(s) and injection well is not significant, due to the mix approach calculation of the groundwater salt concentration	Location of well pump(s) and injection well is significantly important, dominated by the groundwater salt concentration calculation.
5	Treated wastewater injection mound head effect on the pump well head is neglected, thus, overestimating the pump well drawdown	Treated wastewater injection mound head effect on the pump well head is applicable. Thus, pump well drawdown is more accurate.

The areal distribution (Visual MODFLOW and MT3D) simulation model approach is employed for more in depth analysis and more realistic prospect design. Thus, results of calculating the system overall costs of construction and operation will be more rational and feasible.

The outcome will compare and calculate the total cost of operating the system for the two approaches, the base case of the general conceptual design system simulation using lump model and the base case of the general conceptual design system simulation using areal distribution model. These calculations will consider electricity consumed costs, reverse osmosis system capital and maintenance costs, well construction cost, well pump capital and maintenance costs, and treated wastewater cost. More detailed cost analysis will be covered in the next chapter.

6.2 Base Case Layouts for the Areal Distribution Model Approach of the General Conceptual Design System

The orientation of the pump and injection well location in the areal distribution model (Visual MODFLOW and MT3D model) simulation is very essential. Moreover, the location of the hypothetical area relative to the groundwater salt concentration is another element of concern in designing the simulation of this model (Figures 6.1, 6.2, and 6.3). Furthermore, several layout combinations can be oriented between the pump well locations relative to the injection well location in the hypothetical area. Hence, the location of the pump well to the injection well and the location of the hypothetical field area relative to the groundwater concentration may cause a significant discrepancies in the overall power consumption and total costs of the conceptual design system. Therefore, in this dissertation, three orientation layouts for the areal distribution model (Visual MODFLOW and MT3D) simulation will be put under consideration. The simulation layout with the least power consumption and least total cost will be considered for design purposes.

The simulation of the three orientation layouts utilizing the areal distribution model approach (Visual MODFLOW and MT3D) of the general conceptual design system will be applied only to the base case of the general conceptual design system. Moreover, more variable input data will be added to the lump model approach base case input data variables (Table 3.7) to cope with the Visual MODFLOW and MT3D model input data requirements (Table 6.2).

The simulation of the areal distribution model will consist of three orientation layout, they are as follows: 1) orientation layout (1), 2) orientation layout (2), and 3) orientation layout (3). The first simulation layout, orientation layout (1), will be identically similar to the second layout, orientation layout (2), except for the location of the hypothetical field area relative to the groundwater salt concentration, as in Figures 6.2 and 6.3. Moreover, orientation layout (1) will be similar to orientation layout (3), except for the relative locations of the well pump to the location of the treated wastewater injection well. The orientation layout (1) and orientation layout (3) hypothetical farm area will be located entirely over the immediate vicinity of the brackish groundwater with groundwater salt concentration of $\boldsymbol{C_{g.w.}}$ = 6000 mg/l, as in Figure 6.2.

Figure 6.1 Areal distribution (Visual MODFLOW and MT3D) simulation of the base case of the general conceptual design system layout.

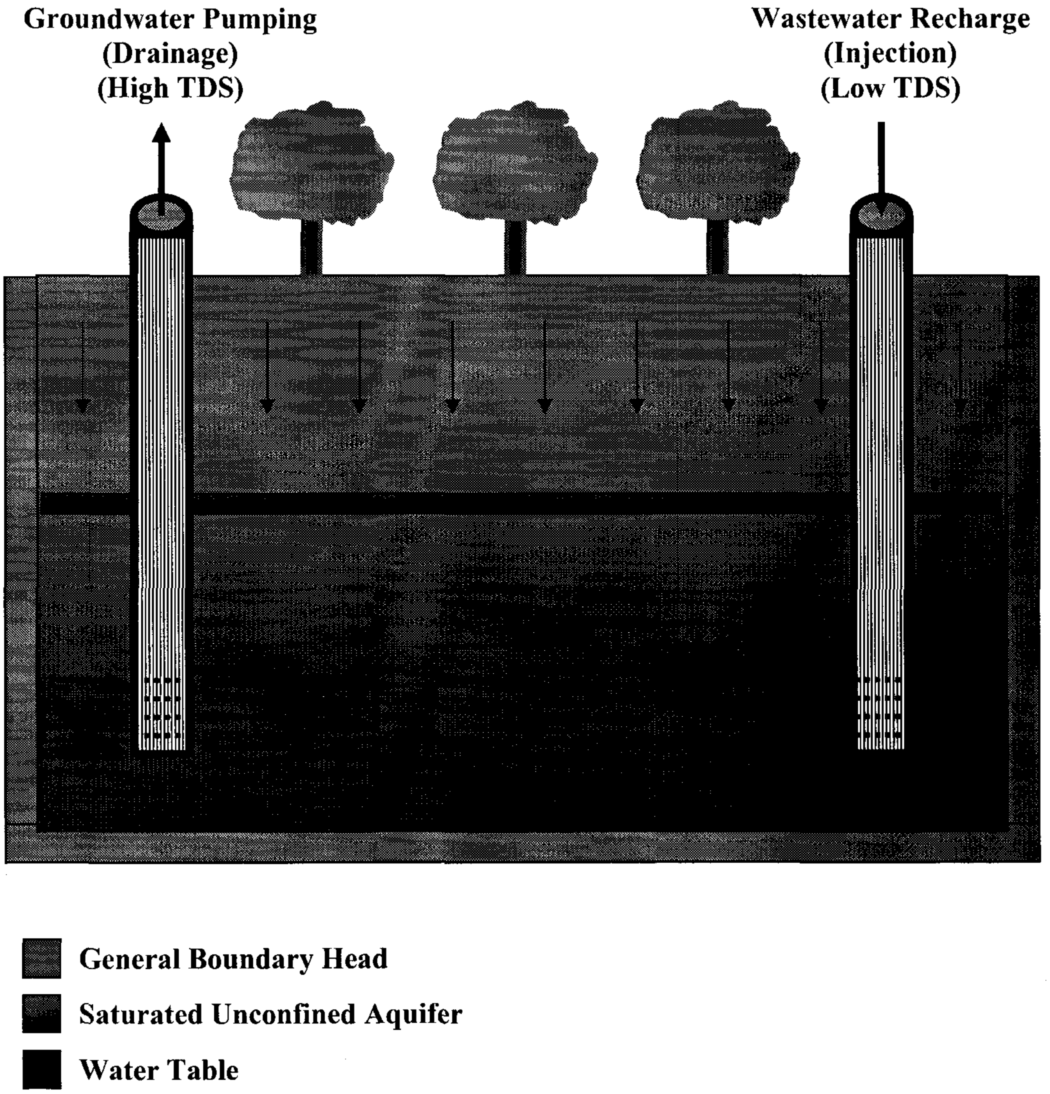

Figure 6.2 Aerial view of the location of the hypothetical field area relative to groundwater concentration.

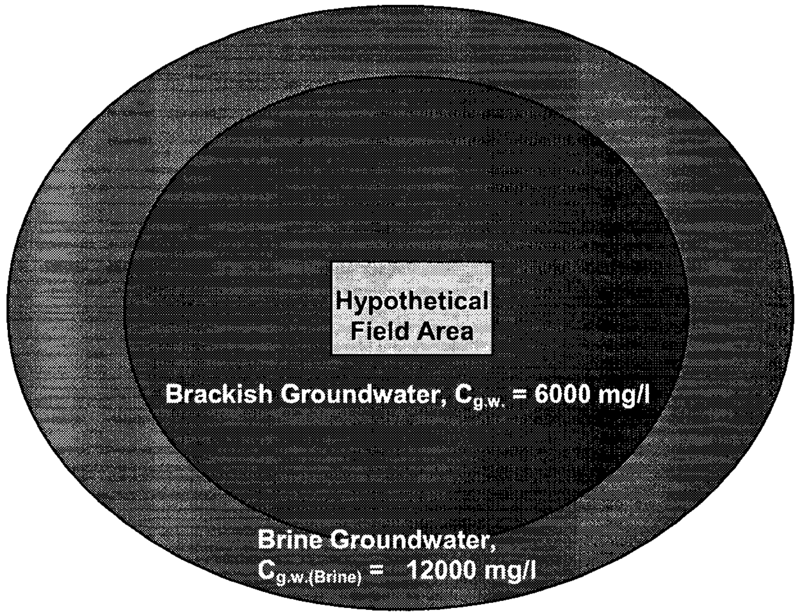

Figure 6.3 Aerial view of the location of the hypothetical field area relative to groundwater concentration.

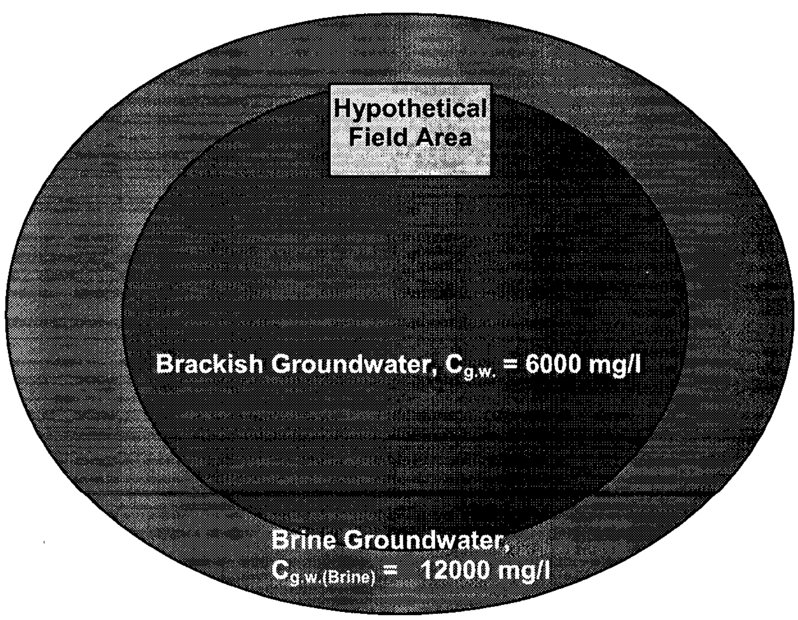

Table 6.2 Base case of the general conceptual design system input data for the areal distribution model approach.

Variable	Value	Remarks
Field Area	10 (hectares)*	Equation (3.50).
Aquifer Type	Unconfined Aquifer	
Simulation Period	40 (years)	Average life expectancy of R.O. unit and well pump system.
No. of Seasons Per Year	1	
Season Length	228 (days)	
ET_c	1.5 (m/season)	Average actual crop evapotranspiration per planting season
C_{RZ}	2000 (mg/l)	Maximum root salt concentration tolerance for Alfalfa crop without reduction in the yield.
C_{inj}	1000 (mg/l)	Average wastewater salt concentration after tertiary treatment.
Φ	0.30 (m^3/m^3)	Total Porosity
$K = K_x = K_y = K_z$	5.00 (m/day)	Hydraulic conductivity
h_o	35 (m)	Initial water table elevation
$(C_{g.w.})^{t-1}$	6000 (mg/l)	Initial groundwater salt concentration.
Aquifer Thickness	60 (m)	
Maximum Lift	55 (m)	
$h_{w(min)}$	5 (m)	Minimum saturated thickness
Well Penetration	60 (m)	Fully penetrated well
No. of Cell in X - Direction	51 (cell)	
No. of Cell in Y - Direction	51 (cell)	
Cell size	36 (m^2)	
Cell ΔX	6 (m)	
Cell ΔY	6 (m)	
Effective Porosity(Φ)	0.3 (m^3/m^3)	
Ss	0.0003 (m^{-1})	Specific storage
Sy	0.3 (m^3/m^3)	Specific Yield ≈ Effected Porosity
Boundary Type	General Head Boundary (G.H.B.)	
G.H.B. Conductance	0.702 (m2/day)	= (K/L) * (ho (or B))* ΔY), where, B = Aquifer thickness

* Area was rounded to 10 hectares.

On the other hand, the orientation layout (2) hypothetical field area will be located over the brackish groundwater with groundwater salt concentration of $C_{g.w}$ = 6000 mg/l and partially adjacent to the brine groundwater with groundwater salt concentration of $C_{g.w(Brine)}$ = 12000 mg/l, as in Figure 6.3. Moreover, the relatively high brine groundwater salt concentration of $C_{g.w.\ (Brine)}$ = 12000 mg/l was chosen to represent an extreme influence of the adjacent or surrounding lenses of higher salt concentration groundwater. As a result the performance of the three layout simulations will be evaluated with respect to power consumption variance and the significance of these variances. These three detailed simulation layouts will be as follows:

6.2.1 Orientation layout (1)

The orientation layout (1) will consist of one pumping groundwater well and one treated wastewater well. The separation distance between the groundwater pump well and the wastewater injection well is 210 m (Figure 6.4). This large separation distance between the two wells was chosen to resemble the longer time residing and mixing of the inlet and outlet sources salt mass concentration within the groundwater zone, which will result in wider mixing coverage area of the groundwater. Therefore, allowing longer time mixing performance of the injected treated wastewater and deep percolation water with the native groundwater. As a result, this longer time performance mixing will lower groundwater zone salt concentration in the long run. The advantage of this layout is the longer time mixing, which will lead to a less groundwater salt concentration in the long run for a larger coverage groundwater area. Hence, the direct utilization of groundwater will be more reliable in the face of all possible obstacles or lateral reduction in the operation system of the model due to emergences or cost effects. In contrast, the disadvantage of this layout is the power consumption. More power will be consumed by the pump and the reverse osmosis unit to desalinate the pumped groundwater due to the retardation of the enhancement of the groundwater salt concentration due to a wider mixing coverage area.

6.2.2 Orientation layout (2)

The orientation layout (2) is analogous to the orientation layer (1) except for the location of the hypothetical field area relative to the groundwater salt concentration (Figure 6.5). Due to the close locations of the groundwater pumping well and the treated wastewater injection well to the location of the field boundary, 48 m, the groundwater salt mass concentration on the adjacent immediate vicinity of the field area will have an affect (if it is different from the salt mass concentration under the field area) on the salt mass concentration of groundwater under the field area. This effect is caused by the mixing and the movement of the groundwater from the immediate adjacent vicinity of the field area to the groundwater under the field area and vise versa, due to pumping and injection practice. Therefore, this orientation layout was chosen to examine the significant effect of this phenomenon on the total power consumption of the system.

6.2.3 Orientation layout (3)

The orientation layout (3) will consist of one pumping groundwater well and one treated wastewater well. The separation distance between the groundwater pump well

Figure 6.4 Orientation layout (1) and the hypothetical area located as in Figure 6.2.

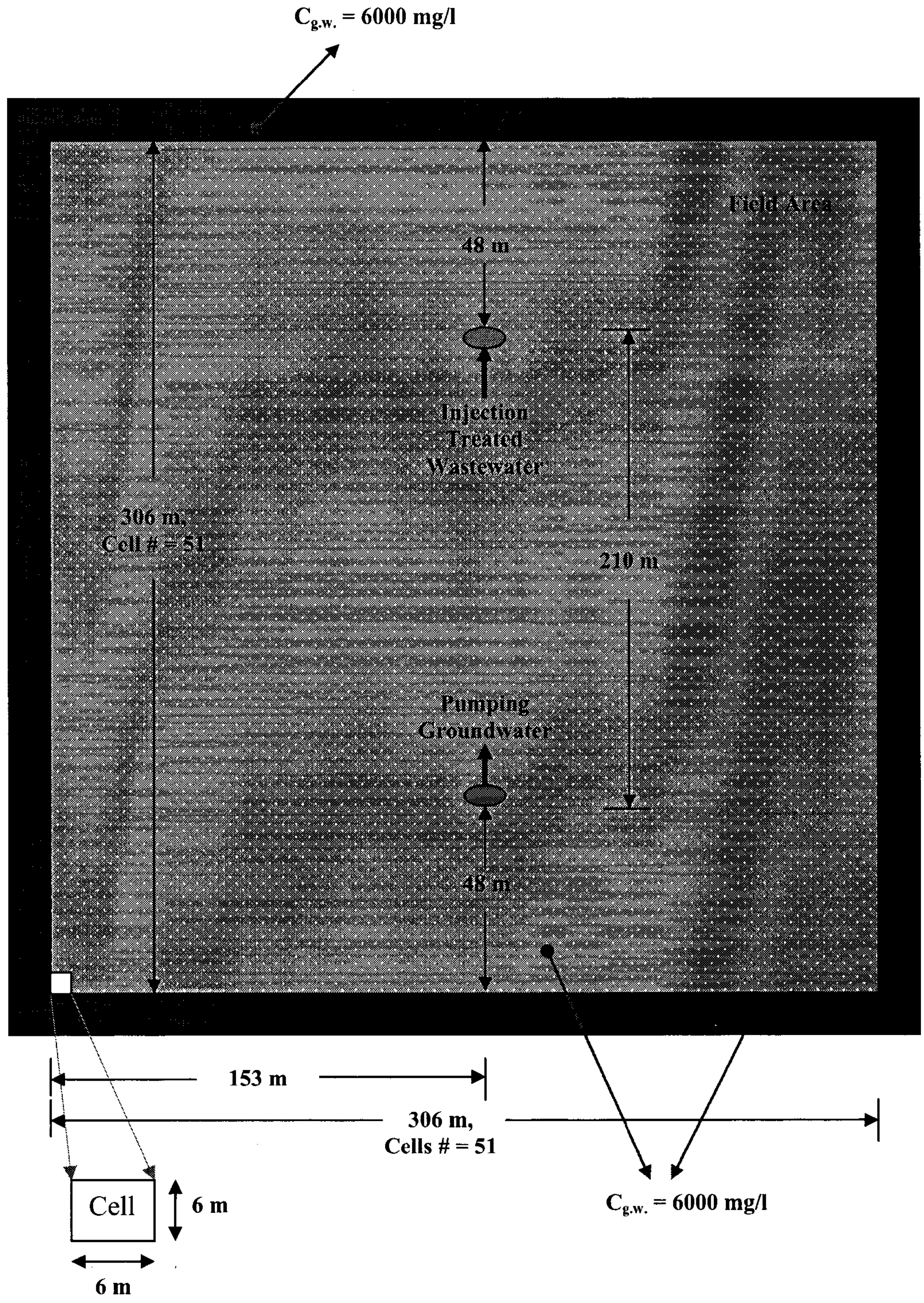

and the treated wastewater injection well is 20 m (Figure 6.4). This 20 m is the minimum separation distance between the two wells that will be accepted by the public with regard to practicing simultaneous treated wastewater injection and groundwater pumping. Moreover, due to this short separation distance, 20 m, the injected treated wastewater will have a shorter mixing time with the native groundwater, a limited mixing coverage area, and shorter travel time to reach the pumping well. As a result, due to this short mixing time with the native groundwater and the short travel time of the injected treated wastewater to reach the pumping well, the pumped groundwater salt concentration will be of a better quality than the native groundwater salt concentration; therefore, the power consumption required by the pump and by the reverse osmosis unit will be enhanced. In contrast, due to the short mixing time of the treated wastewater with the native groundwater and due to the limited mixing coverage area of the groundwater, the overall groundwater salt concentration enhancement will be retarded. Thus, the direct groundwater utilization will be less reliable in case of possible obstacles or any lateral reduction in the operation system of the model due to emergencies or cost effects.

6.3 Areal Distribution Model Simulation

The areal distribution simulation will consist of three parts. These parts are as follows:

- The root (vadose) zone simulation.
- The reverse osmosis unit simulation.
- The groundwater zone simulation.

Figure 6.5 Orientation layout (2) and the hypothetical area located as in Figure 6.3.

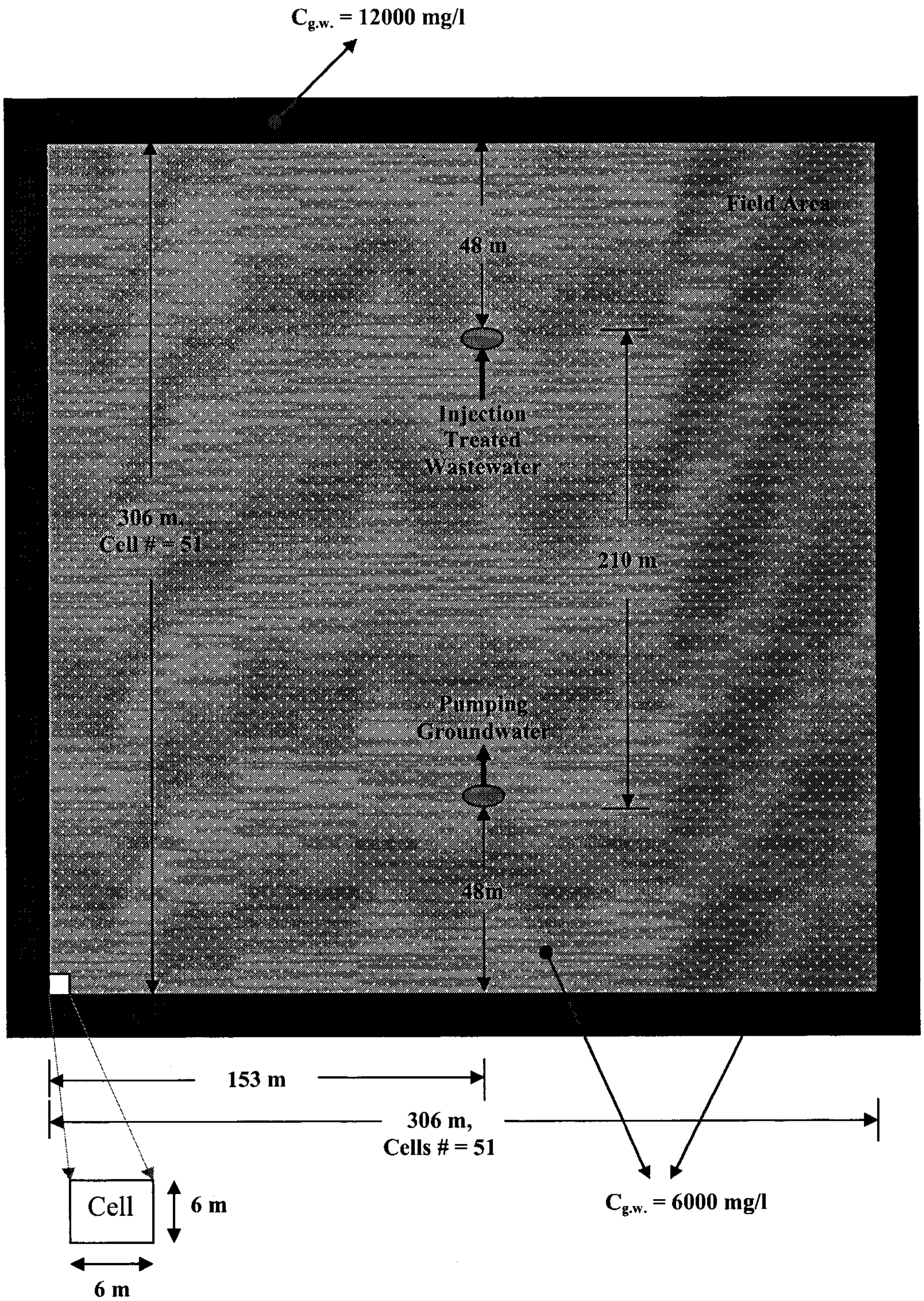

 Emad H. AlAli

Figure 6.6 Orientation layout (3) and the hypothetical area located as in Figure 6.2.

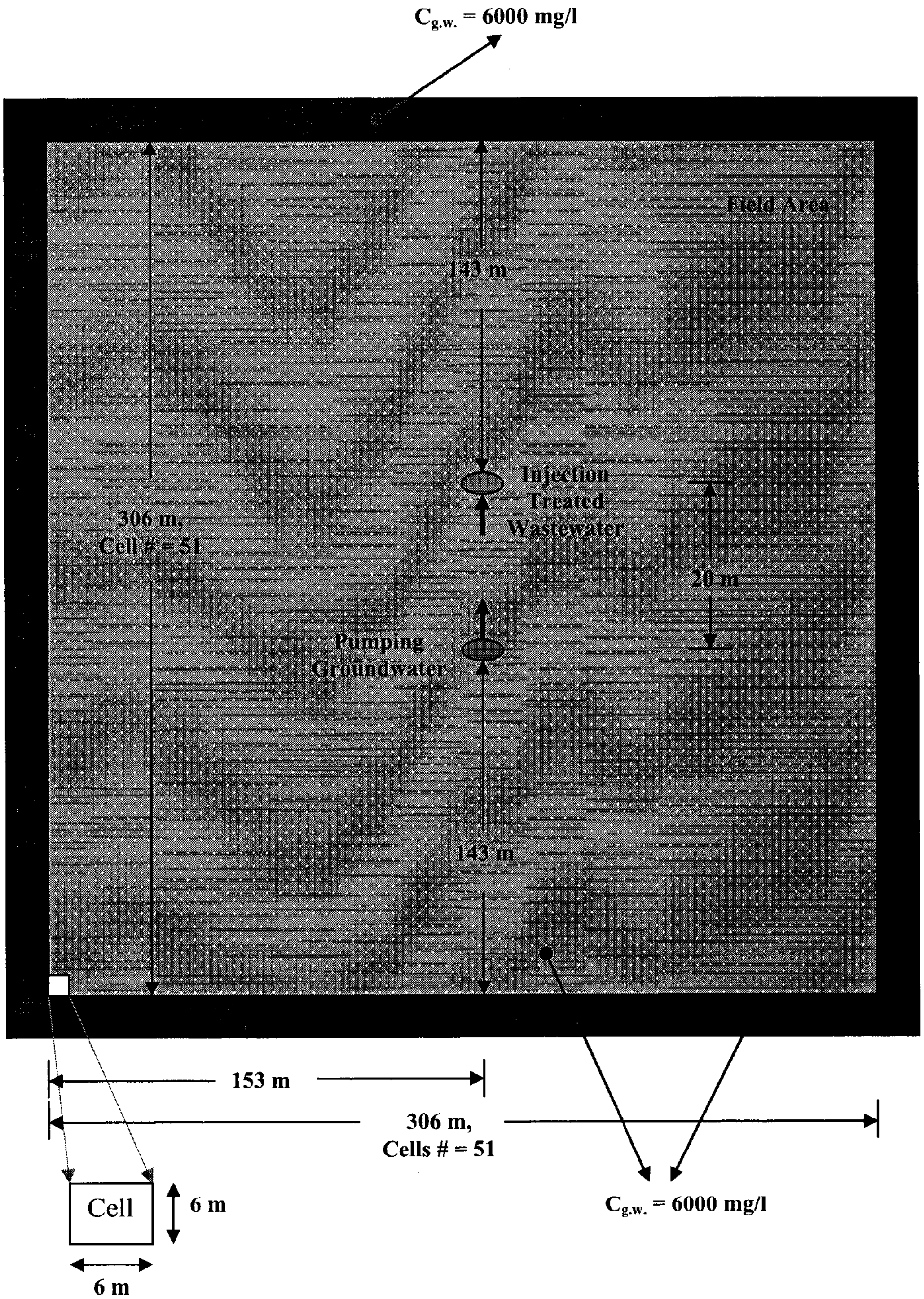

The simulation calculations of the root (vadose) zone and the reverse osmosis unit calculation will be analogous to the calculation of the lump model in Sections 3.1.1 and 3.1.2. Furthermore, the Visual MODFLOW and MT3D model will be employed for the simulation calculations of the groundwater zone. What is more, the areal distribution model simulation order of simulation will be in a different sequence than the lump model approach. The sequences of simulating the areal distribution model will be as follows:

1. The main purpose of simulating the areal distribution of the base case of the general conceptual design system is to compare it with the lump model simulation of the base case of the general conceptual design system and evaluate the power consumption variance between the two simulations, thus establishing a relationship between the lump model simulation and the areal distribution model simulation power consumption, in general, and the operation cost, specifically. To compare the performance of the areal distribution model simulation to the lump model simulation for the base case of the general conceptual design system, the water source output data from the base case simulation of the lump model will be used as input data in the MODFLOW and MT3D model. This input water source data (Table 6.3) is as follows:

- Deep percolation water, Q_{DP}.
- Injected treated wastewater, Q_{inj}.
- Pumped groundwater, which will be used as feed water to

the reverse osmosis unit, Q_{Feed}.

Table 6.3 Water source output data from the base case simulation of the lump model, which will be used as input data in the MODFLOW and MT3D model.

Year	Q_{Feed} (m^3/season)	Q_{inj} (m^3/season)	Q_{DP} (m^3/season)
1	247216.0	240145.6	7070.4
2	245011.6	239263.9	5747.8
3	243332.3	238592.1	4740.1
4	242043.5	238076.6	3966.8
5	241048.9	237678.8	3370.1
6	240278.1	237370.5	2907.6
7	239678.8	237130.7	2548.0
8	239211.5	236943.9	2267.7
9	238846.7	236797.9	2048.8
10	238561.3	236683.8	1877.5
11	238337.8	236594.3	1743.4
12	238162.6	236524.3	1638.3
13	238025.1	236469.3	1555.8
14	237917.2	236426.1	1491.1
15	237832.5	236392.2	1440.3
16	237765.9	236365.6	1400.3
17	237713.6	236344.7	1369.0
18	237672.5	236328.3	1344.3
19	237640.2	236315.3	1324.9
20	237614.8	236305.2	1309.7
21	237594.9	236297.2	1297.7
22	237579.2	236290.9	1288.3
23	237566.8	236286.0	1280.9
24	237557.1	236282.1	1275.0
25	237549.5	236279.0	1270.4
26	237543.5	236276.6	1266.8
27	237538.7	236274.7	1264.0
28	237535.0	236273.2	1261.8
29	237532.1	236272.1	1260.0
30	237529.8	236271.2	1258.6
31	237528.0	236270.4	1257.6
32	237526.6	236269.9	1256.7
33	237525.5	236269.4	1256.0
34	237524.6	236269.1	1255.5
35	237523.9	236268.8	1255.1
36	237523.3	236268.6	1254.8
37	237522.9	236268.4	1254.5
38	237522.6	236268.3	1254.3
39	237522.3	236268.2	1254.2
40	237522.1	236268.1	1254.0

The reason for utilizing the water source data from the lump model in the areal distribution model is to compare the effect of groundwater salt concentration at the well pump and the drawdown at the pump well for the same water sources utilized by the lump model. The groundwater with a salt concentration, which will be used as feed water to the reverse osmosis unit, will control the power consumed by the reverse osmosis, and the well drawdown will control the power consumed by the pumping well. Therefore, any variation in groundwater salt concentrations and pump well drawdown will be the main comparison criteria between the areal distribution and the lump model power consumption specifically, and the total operational costs, in general, for the same water resource quantities. What is more, the pump location relative to the injection well sources and the location of the hypothetical area relative to the groundwater salt concentration are other areal distribution model criteria for manipulating the power consumption and the total operation costs.

2. Next in the simulation of the groundwater zone, the MODFLOW and MT3D model will be employed, starting with the governing equations of the MODFLOW and MT3Dmodel. First, the MODFLOW model uses a finite difference equation mathematical model, a three-dimensional movement of groundwater of constant density through porous earth material. This movement is described in the Visual MODFLOW by the partial differential equation

$$\frac{\partial}{\partial x}\left(K_{xx} * \frac{\partial h}{\partial x}\right)+\frac{\partial}{\partial y}\left(K_{yy} * \frac{\partial h}{\partial y}\right)+\frac{\partial}{\partial z}\left(K_{zz} * \frac{\partial h}{\partial z}\right)-W = S_s * \frac{\partial h}{\partial t} \qquad \textbf{(6.1)}$$

where,

K_{xx}, K_{yy}, and K_{zz} = Values of hydraulic conductivity along x, y, and z coordinate axes, which are assumed to be parallel to the major axes of the hydraulic conductivity [L/T],

h = Potentiometric head [L],

W = Volumetric flux per unit volume and represents source/or sinks of water [1/T], where Q_{inj}, Q_{DP} are source terms, and Q_{Feed} is a sink term,

S_s = Specific storage of the porous material [1/L], which is the volume of water released per unit volume of aquifer per unit change in head due to the compressibility of the water and the compressibility of the aquifer, and

t = Time [T].

Furthermore, the Visual MODFLOW uses a1-D radial coordinate partial differential equation for an unconfined aquifer with a source / or sink of water (such as pumping, injection, and recharge). Thus, drawdown and water table elevation and locations can be calculated. Where,

$$\frac{1}{r}\frac{\partial}{\partial r}\left(Tr\frac{\partial h}{\partial r}\right) \pm W = S_y\frac{\partial h}{\partial t} \tag{6.2}$$

where,

$W = \dfrac{Q_i}{Surface \quad Area}$ = Sink or source term [L/T],

Q_i = Sink or source flow rate [L^3/T], (i.e. Q_{Feed}, Q_{inj}, Q_{DP}),

S_y = Specific yield [dimensionless], which is the volume of water drained from a unit volume of aquifer due to the force of gravity, applied to an unconfined aquifer only, with a typical range $0.10 \leq S_y \leq 0.3$. Moreover, specific yield ≈ effective porosity, where, effective porosity is the part of the porosity (void space) through which the mobile fluid (groundwater) flows.

r = radius [L],

T = transmissivity [L^2/T], which is the product of hydraulic conductivity (K) and the saturated thickness (B), or (h), with (B) for the confined aquifer and (h) for the unconfined aquifer, and

$\frac{\partial h}{\partial r}$ = Hydraulic gradient [dimensionless].

Next, the governing equation of the MT3D model, the Modular Three-Dimensional Multispecies Transport Model, utilizing the partial differential equation describing the fate and transport of contaminants of species k in three-dimensional, transient groundwater flow systems can be written as,

$$\frac{\partial}{\partial x_i}\left(\theta D_{ij}\frac{\partial C^k}{\partial x_i}\right)-\frac{\partial}{\partial x_i}\left(\theta v_i C^k\right)+q_s C_s^k+\sum R_n=\frac{\partial\left(\theta C^k\right)}{\partial t} \quad \textbf{(6.3)}$$

where,

C^k = The dissolved concentration of species k, [M/L],

θ = The porosity of the subsurface medium, [dimensionless], which is the ratio of the volume of voids to the bulk volume of the porous material,

t = Time, [T],

x_i = The distance along the respective Cartesian coordinate axis, [L],

D_{ij} = The hydrodynamic dispersion coefficient tensor, [L^2/ T], which is the sum of the mechanical mixing dispersion and the molecular diffusion ($D = \alpha v^* + D^*$), where, α = the dynamic dispersivity,

v^* = the average linear groundwater velocity, and D^* = the molecular diffusion,

v_i = The seepage or linear pore water velocity; [L/T], it is related to the specific discharge or Darcy flux through the relationship, $v_i = q_i / \theta$,

q_s = The volumetric flow rate per unit volume of aquifer representing fluid sources (positive) and sinks (negative), [1/T],

C_s^k = The concentration of the source or sink flux for species k

, [M/L], and

$\sum R_n$ = The chemical reaction term, [M/ (L^3T)].

MODFLOW and MT3D simulation will be simulated on yearly bases, but the pumping rate, the deep percolation rate, and the treated wastewater rate will be constant during the growing season and will vary slightly from one growing season to the another (Figure 6.3). In addition, the latent water sources will be applied only in the growing season (228 days) and then will cease during the off growing season (137 days). Of note, the MODFLOW and MT3D model simulation will be simulated for the complete year (365 days) over a 40-year simulation period. Thus, due to the yearly simulation (simulation of the growing season and the off growing season) by the MODFLOW and MT3D model, the groundwater salt concentration distribution, water table hydraulic head distributions, and well drawdown will be more realistically presented at the end of the year. The latent data will be utilized by the MODFLOW and MT3D model as input for the next year simulation and so on. In addition, the MODFLOW and MT3D model keeps a record for each simulation stress period at the end of the 40-year simulation for the well pump drawdown, distributed water table hydraulic elevation and location, and distributed salt concentrations and location.

3. From the yearly MODFLOW and MT3D data output, the amount of brine water produced by reverse osmosis unit, the brine water concentration, the power consumed by the reverse osmosis, and the power consumed by the well pump can be calculated on yearly bases. The order of calculating the brine water amount and concentration, the power consumed by the reverse osmosis unit, and the well pump will be as follows:

   1. From Equation (3.9), the amount of brine water (Q_{Brine}) produced by the reverse osmosis unit can be calculated thus:

$$Q_{Feed} = Q_{irr(permeate)} + Q_{Brine}$$

   2. From Equation (3.54), the brine salt concentration (C_{Brine}) produced by the reverse osmosis can be calculated, thus

$$C_{Brine} = \frac{(Q_{Feed} * C_{Feed}) - (Q_{irr(permeate)} * C_{irr(permeate)})}{Q_{Brine}}$$

where,

C_{Feed} = the pumped water salt concentration which will be fed to the reverse osmosis unit from the MODFLOW and MT3D output data [mg/l].

3. From Equation (3.30), the permeate salt concentration ($C_{irr(permeate)}$) from the reverse osmosis unit can be calculated thus:

$$C_{irr(permeate)} = n * C_{Feed} * \left[\frac{1 - \frac{\delta}{2}}{1 - \delta} \right]$$

where,

δ = 60 % as we concluded from Section 3.3, and

n = 1% as we concluded from Section 3.3.

4. From Equation (3.20), the osmotic pressure of feed water to the reverse osmosis unit (Ps_{Feed}), can be calculated thus:

$$Ps_{Feed} = Cs_{Feed} * R * T$$

And, from Equation (3.28), the ionic molar concentration of the feed water to the reverse osmosis unit is:

$$Cs_{Feed} = (\Psi) * \left(\frac{C_{Feed}}{\varpi} \right)$$

5. From Equation (3.21), the osmotic pressure of the permeate water from the reverse osmosis unit (***$Ps_{permeate}$***) can be calculated thus:

$$Ps_{permeate} = Cs_{irr(permeate)} * R * T$$

And also, from Equation (3.29), the ionic molar concentration of the reverse osmosis unit permeate water is:

$$Cs_{irr(permeate)} = (\Psi) * \left(\frac{C_{irr(permeate)}}{\varpi} \right)$$

6. From Equation (3.10), the amount of permeate water from the reverse osmosis unit, which will be used for irrigation can be calculated thus:

$$Recovery\% \ (\delta) = \frac{Q_{irr\ (permeated)}}{Q_{Feed}}$$

7. From Equation (3.31), the power exerted by the reverse osmosis unit (***$Power_{(R.O.)}$***) can be calculated thus:

$$Power_{(R.O.)} = \left[\frac{\left(Ps_{Feed} - Ps_{permeate}\right) * Q_{irr(permeate)}}{\eta_{R.O.}} \right]$$

8. From Equation (3.40), the power exerted by pumping the groundwater, ($\boldsymbol{Power_{well}}$) can be calculated thus:

$$Power_{well} = \left[\left(\frac{\gamma * Q_{Feed} * \left(h_{surface} - h_o\right) + S'_w}{\eta_{well}} \right) \right]$$

where,

$\boldsymbol{S'_w}$ = The transit drawdown of the water hydraulic head at the well [L] from the MODFLOW and MT3D output data. Of note, the treated wastewater injection mound head effect on the pump well drawdown is applicable in this drawdown calculation.

$\boldsymbol{h_{surface}}$ = The height of the ground surface from the bedrock [L], and

$\boldsymbol{h_o}$ = Water table hydraulic head prior to pumping or water table hydraulic head at zero drawdown [L].

9. From Equation (3.56) the total power consumed by the system can be calculated thus:

$$\textbf{\textit{Total Power}} = \textbf{\textit{Power}}_{(R.O.)} + \textbf{\textit{Power}}_{well}$$

6.4 Results of the Base Case Simulation of the General Conceptual Design System Using the Areal Distribution Model

The results of the base case of the general conceptual design system using the areal distribution model simulation for the three orientation layouts were compared with the base case of the general conceptual model design system using the lump model simulation and were captured in Figures 6.7, 6.8, 6.9, 6.10, 6.11, 6.12, 6.13, 6.14, and 6.15 respectively. These output comparison result graph were arranged by the total power required by the system, the power required by the reverse osmosis unit, and the power required by the well pump system, respectively, for the three orientation layouts.

From Figure 6.7, it is noticeable that the total power per unit area required by the system utilizing the areal distribution (orientation layout (1)) model simulation is lower than the total power per unit area required by the system utilizing the lump model simulation. Due to the non-uniform mixing of the inlet water sources with the groundwater, aquifer groundwater salt concentration is considered to be non-uniform in space. Furthermore, the pumped water salt concentration reflected the more realistic salt concentration level at the stress periods while utilizing the areal distribution model. From

Figure 6.8, the reverse osmosis power consumption by the areal distribution (orientation layout (1)) model simulation was higher than the lump model simulation. Because the inlet sources (Q_{inj} and Q_{DP}) mix non-uniformly with the native groundwater and due to the significantly large distance between the treated wastewater injection well and the groundwater pump well (210 m), the mixing coverage area of the groundwater will increase. Therefore, the enhancement of the groundwater will not be uniform and will be relatively retarded compared to the lump model simulation. Due to the latter reason, the reverse osmosis unit power consumption is higher in the areal distribution (orientation layout (1)) model simulation than the lump model simulation. Moreover, the pump power consumption by the areal distribution (orientation layout (1)) model simulation was significantly lower than the power consumption by the lump model simulation (Figure 6.9). Because the treated wastewater injection mound head effect is applicable to the pump well head while utilizing the areal distribution model, the pump well drawdown is more accurate. Furthermore, due to the transit drawdown caused mainly by frequent pumping and non-pumping during the planting and off planting season respectively, the drawdown at the pump well utilizing the areal distribution (orientation layout (1)) model simulation will be less than the lump model simulation. Moreover, the decrease in the pump power consumption is more influential in the areal distribution (orientation layout (1)) model simulation than the increase in the reverse osmosis power consumption in the areal distribution (orientation layout (1)) model simulation. In addition, the pump power consumption in the areal distribution (orientation layout (1)) model simulation is significantly lower than the lump model simulation. Therefore, the total power consumption by the areal distribution (orientation layout (1)) model simulation is lower than the lump model simulation. As a result, the percent decrease in the sum of total power consumption over the 40-year simulations was 9.29 % compared to the lump model simulation (Figure 6.10, and Table 6.4).

Figure 6.7 Total power consumption comparison for the base case of the general conceptual design system between the areal distribution **(orientation layout (1))** and the lump model simulation.

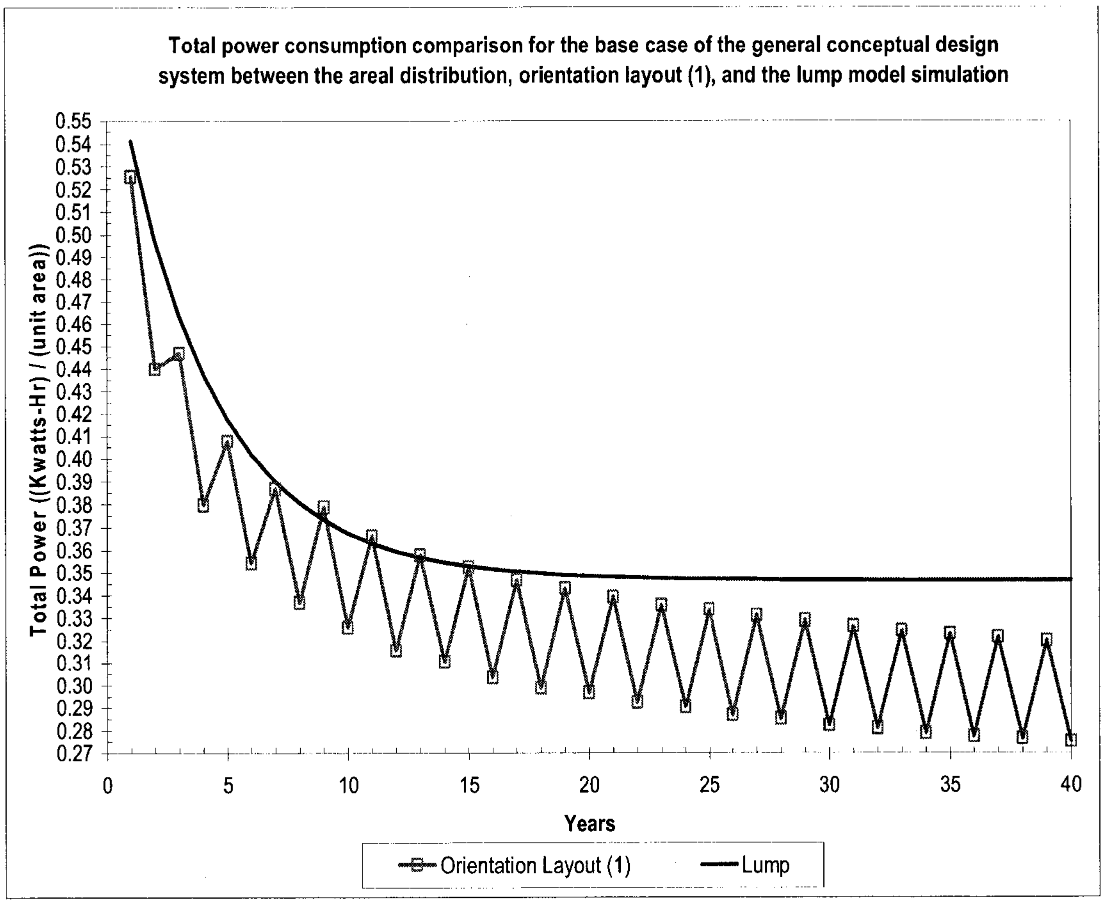

Emad H. AlAli

Figure 6.8 Reverse osmosis power consumption comparison for the base case of the general conceptual design system between the areal distribution **(orientation layout (1))** and the lump model simulation.

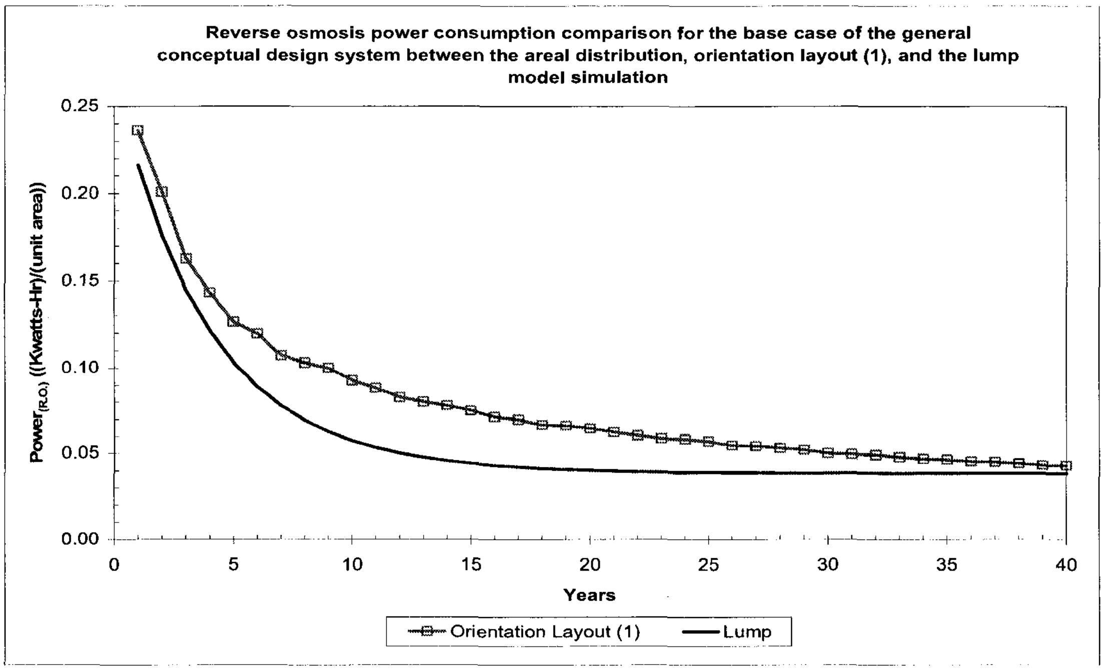

Figure 6.9 Well pump power consumption comparison for the base case of the general conceptual design system between the areal distribution **(orientation layout (1))** and the lump model simulation.

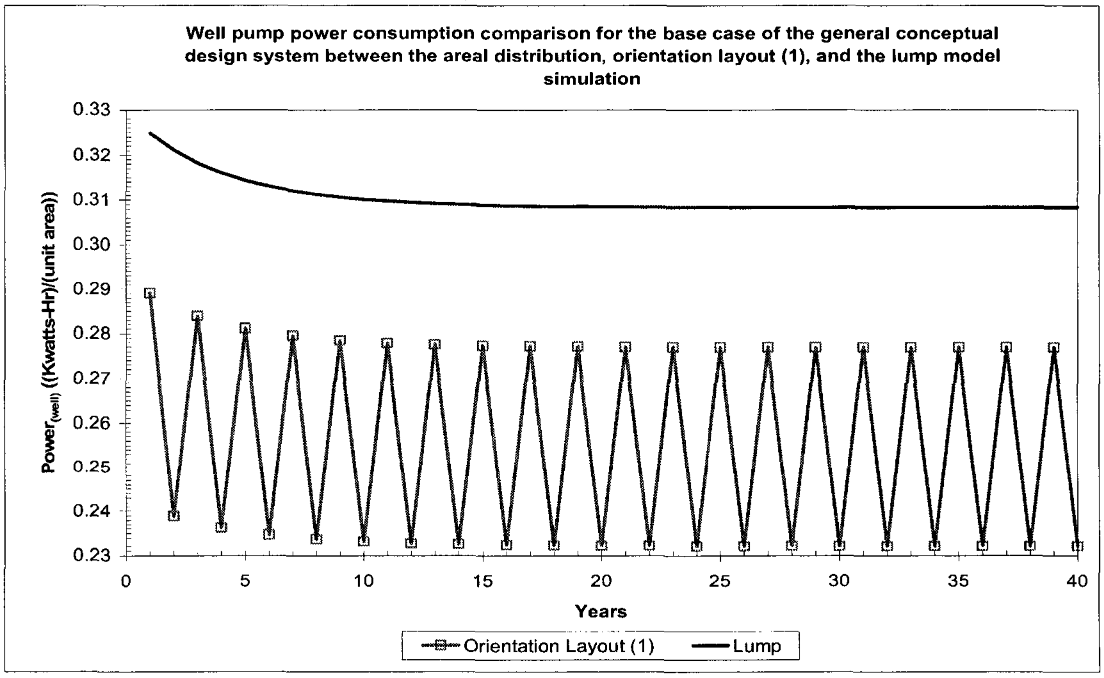

Figure 6.10 Sum of the total power consumption, 40-year simulation, comparison for the base case of the general conceptual design system between the areal distribution **(orientation layout (1))** and the lump model simulation.

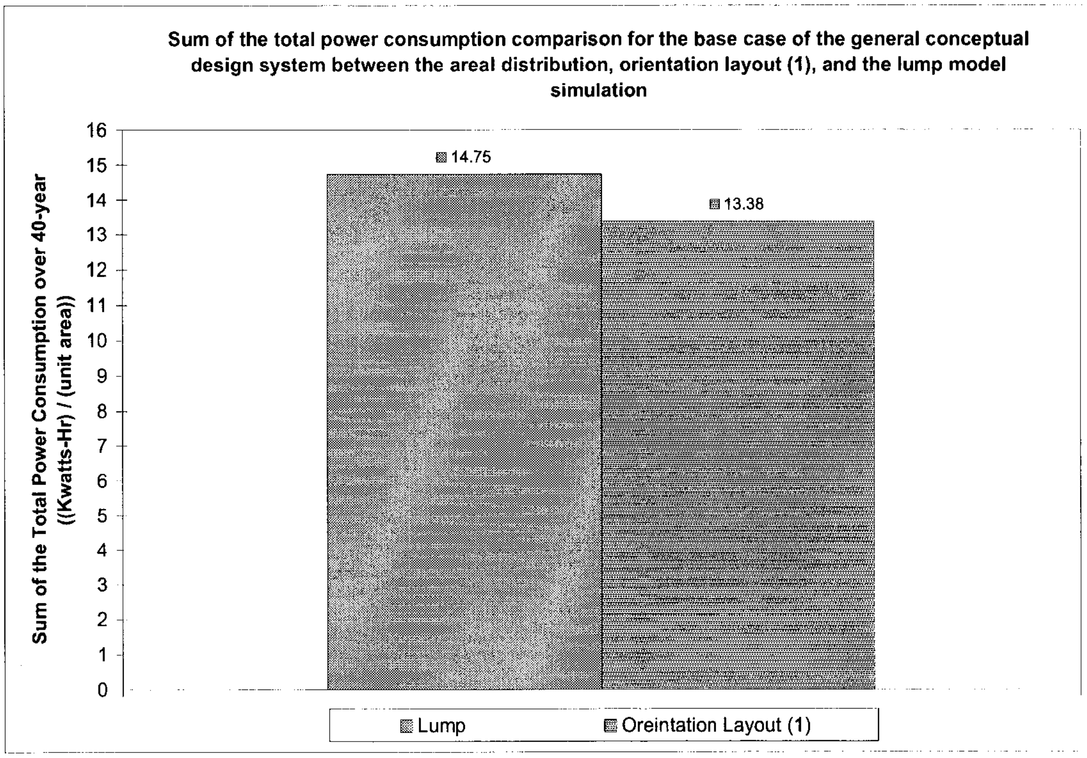

Table 6.4 Percent change comparison in the sum of the total power consumption between the areal distribution **(orientation layout (1))** and the lump model simulation.

.

From	To	% Change (decrease) in Sum of Total Power per Unit Area
Lump model	**Areal Distribution, Orientation Layout (1), Model**	**9.29**

From Figure 6.11, it is obvious that the total power per unit area required by the system utilizing the areal distribution (orientation layout (2)) model simulation is lower than the total power per unit area required by the system utilizing the lump model simulation. The areal distribution (orientation layout (2)) model simulation is analogous to the areal distribution (orientation layout (1)) model simulation except for the location of the hypothetical field area relative to the groundwater salt concentration, where the groundwater salt concentration of 12,000 mg/l is adjacent to the groundwater salt concentration of 6,000 mg/l under the field area. Furthermore, due to the close proximity of the groundwater pumping well and the treated wastewater injection well to the location of the field boundary, 48 m, the groundwater salt concentration (12,000 mg/l) in the adjacent immediate vicinity of the field area will have an effect on the salt mass concentration of groundwater under the field area. This effect is caused by the mixing and the movement of the groundwater from the adjacent immediate vicinity of the field area to the groundwater under the field area and vice versa, due to pumping and injection practice. Moreover, owing to the non-uniform mixing of the inlet water sources with the groundwater, aquifer groundwater salt concentration is considered to be non-uniform in space, and the pumped water salt concentration reflects a more realistic salt concentration level during the stress periods while utilizing the areal distribution model. From Figure 6.12, the reverse osmosis power consumption by the areal distribution (orientation layout (2)) model simulation was higher than the lump model simulation. Moreover, the reverse osmosis power consumption by the areal distribution (orientation layout (2)) model simulation is higher than the power consumption by the areal distribution (orientation layout (1)) model simulation. This increase in the reverse osmosis power consumption is caused by the movement of the higher salt concentration (12,000 mg/l) groundwater from the adjacent immediate vicinity of the field area to the groundwater under the field area. Because the inlet sources (Q_{inj} and Q_{DP}) mix non-uniformly with the native groundwater, and due to the significantly large distance between the treated wastewater injection well and the groundwater pump well (210 m), the mixing coverage area of the groundwater will increase. Therefore, the enhancement of the groundwater will not be uniform and will be relatively retarded compared to the lump model simulation. Due to latter reason, the reverse osmosis unit power consumption is higher in the areal distribution (orientation layout (2)) model simulation than in the lump model simulation. Moreover, the pump power consumption by the areal distribution (orientation layout (2)) model simulation was significantly lower than the power consumption by the lump model simulation (Figure 6.13). Because the treated wastewater injection mound head effect is applicable to the pump well head while utilizing the areal distribution model, the pump well drawdown is more accurate. Furthermore, due to the transit drawdown caused mainly by frequent pumping and non-pumping during the planting and off planting season respectively, the drawdown at the pump well utilizing the areal distribution (orientation layout (2)) model simulation will be less than the lump model simulation. Moreover, the decrease in the pump power consumption is more influential in the areal distribution (orientation layout (2)) model simulation than the increase in the reverse osmosis power consumption in the areal distribution (orientation layout (2)) model simulation. In addition, the pump power consumption in the areal distribution (orientation layout (2)) model simulation is significantly lower than the lump model simulation. Therefore, the total power consumption by the areal distribution (orientation layout (2)) model simulation is lower than the lump model simulation. Furthermore, the total power consumption of the areal distribution (orientation layout (2)) simulation model is higher than the areal distribution (orientation layout (1)) simulation model, owing to the adjacent higher groundwater salt concentration to the groundwater concentration under the field area. As a result, the percent decrease in the sum of the total power consumption over the 40-year simulation was 8.20 % compared to the lump model simulation (Figure 6.15, and Table 6.5).

Figure 6.11 Total power consumption comparison for the base case of the general conceptual design system between the areal distribution **(orientation layout (2))** and the lump model simulation.

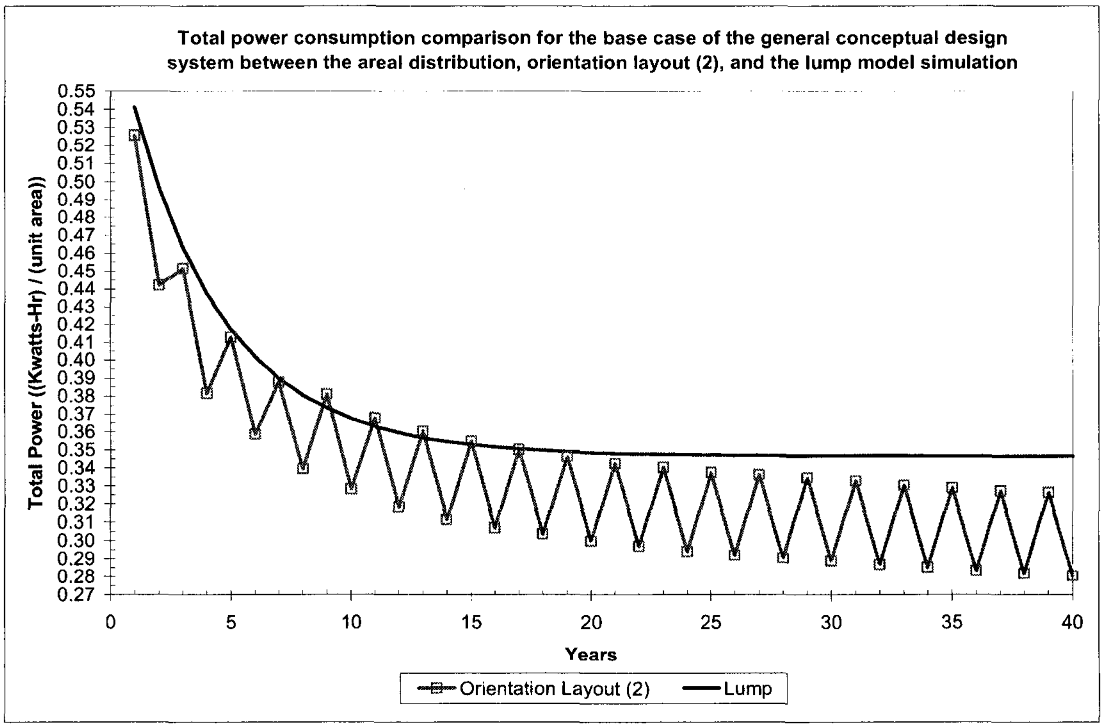

 Emad H. AlAli

Figure 6.12 Reverse osmosis power consumption comparison for the base case of the general conceptual design system between the areal distribution **(orientation layout (2))** and the lump model simulation.

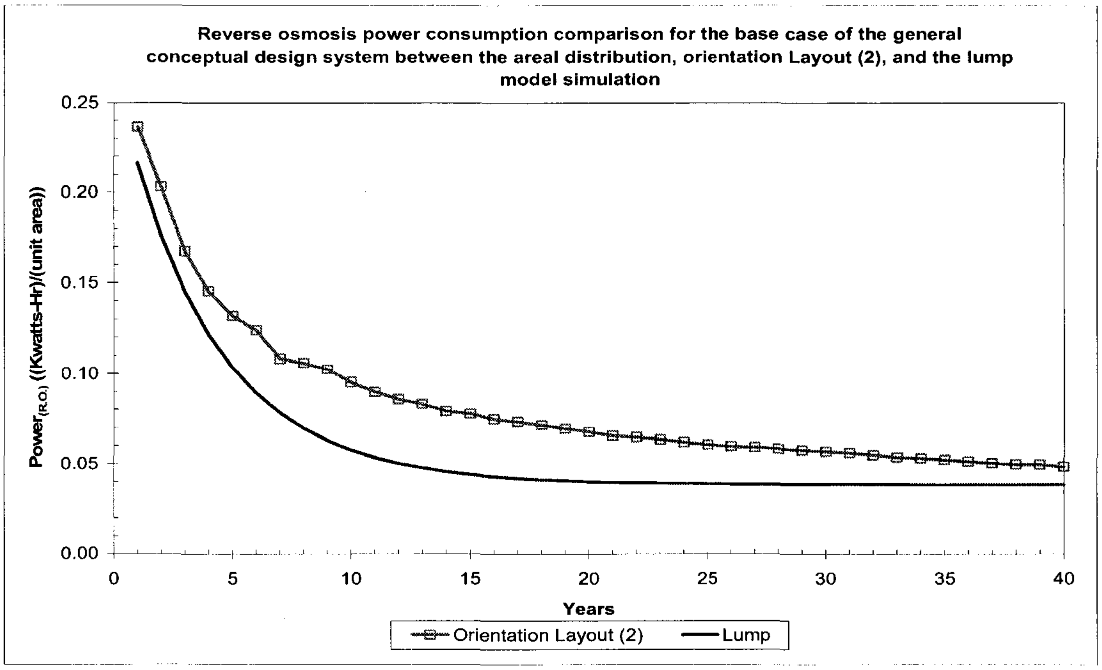

Figure 6.13 Well pump power consumption comparison for the base case of the general conceptual design system between the areal distribution **(orientation layout (2))** and the lump model simulation.

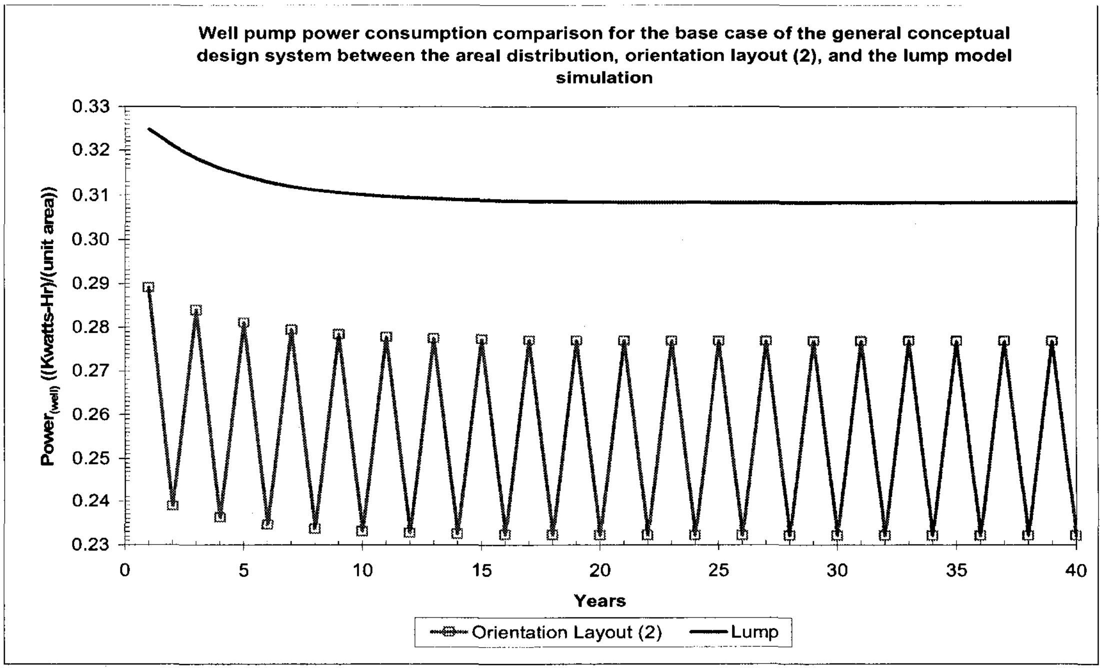

Figure 6.14 Sum of the total power consumption, 40-year simulation comparison for the base case of the general conceptual design system between the areal distribution **(orientation layout (2))** and the lump model simulation.

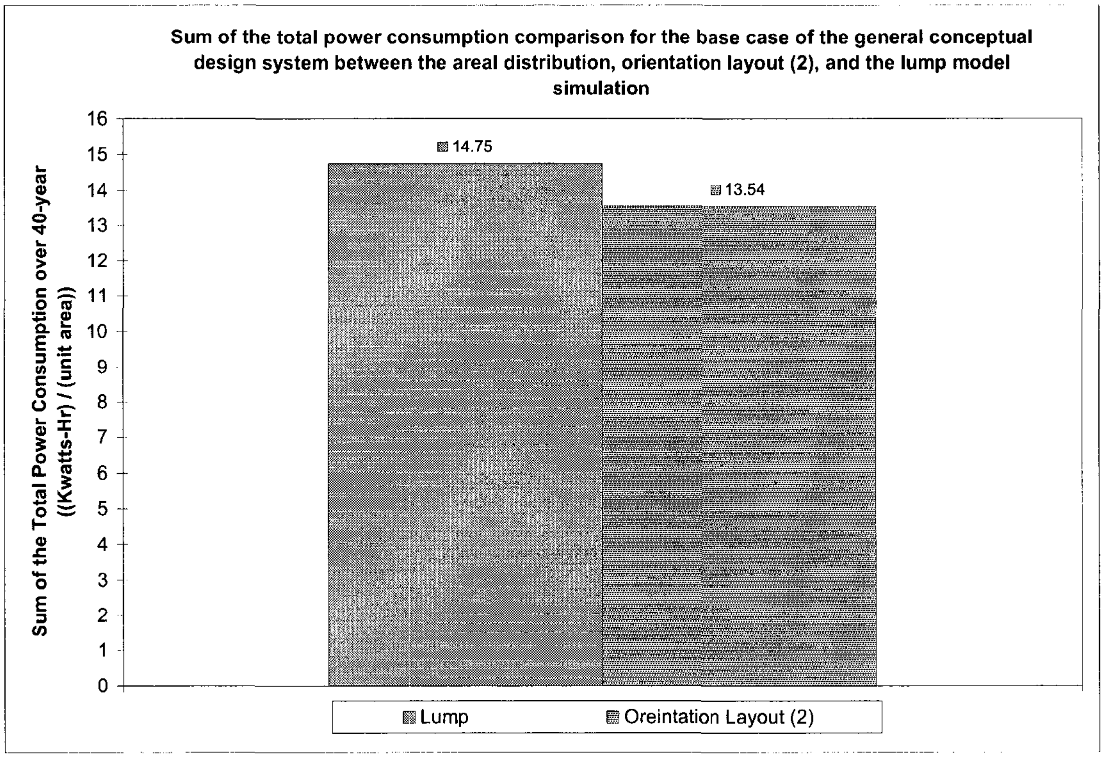

Table 6.5 Percent change comparison in the sum of the total power consumption between the areal distribution **(orientation layout (2))** and the lump model simulation.

From	To	% Change (decrease) in Sum of Total Power per Unit Area
Lump model	Areal Distribution, Orientation Layout (2), Model	8.20

From Figure 6.15, it is clear that the total power per unit area required by the system utilizing the areal distribution (orientation layout (3)) model simulation is notably lower than the total power per unit area required by the system utilizing the lump model simulation. From Figure 6.16, the reverse osmosis power consumption by the areal distribution (orientation layout (3)) model simulation was lower than the lump model simulation up through the first 10 years of simulation. Then, the reverse osmosis power consumption by the areal distribution (orientation layout (3)) model simulation was higher than the lump model simulation in the remaining simulation years. Due to the short separation distance, 20 m, between the injection well and the pump well, the injected treated wastewater will have a shorter mixing time with the native groundwater, limited mixing coverage area, and shorter travel time to reach the pumping well. As a result, due to this short mixing time with the native groundwater and short travel time of the injected treated wastewater to reach the pumping well, the pumped groundwater salt concentration will be of a more improved quality than the native groundwater salt concentration. Moreover, owing to the limited mixing coverage area of the treated wastewater with the native groundwater due to short travel time between the injection well and the pump well, the water quality of the pumped groundwater will be of better quality and will not vary significantly as the simulation proceeds. Therefore, reverse osmosis power consumption variation during the 40-year simulation is minute, especially after the first 10 years of simulation for the areal distribution (orientation layout (3)) model simulation (Figure 6.16). On the other hand, due to uniform mixing and wider mixing coverage area of the water sources (Q_{inj}, Q_{DP}, and $Q_{pump} = Q_{Feed}$) with the native groundwater in the lump model simulation, the groundwater salt concentration enhancement is steady and improves through the simulation period. As a result, the reverse osmosis power consumption of the lump model simulation was lower than the areal distribution (orientation layout (3)) model simulation after the 10^{th} year of simulation. Moreover, the pump power consumption by the areal distribution (orientation layout (3)) model simulation was significantly lower than the power consumption by the lump model simulation (Figure 6.17). Due to the short separation distance between the injection well and the pump well, the treated wastewater injection mound head effect is significantly applicable to the pump well head while utilizing the areal distribution model. Thus, the pump well drawdown will be lowered. Furthermore, due to the transit drawdown caused mainly by frequent pumping and non-pumping during the planting and off planting season respectively, the drawdown at the pump well utilizing the areal distribution (orientation layout (3)) model simulation will be less than the lump model simulation. What is more, the decrease in the pump power consumption is more influential in the areal distribution (orientation layout (3)) model simulation than the increase in the reverse osmosis power consumption in the areal distribution (orientation layout (3)) model simulation. In addition, the pump power consumption in the areal distribution (orientation layout (3)) model simulation is significantly lower than the lump model simulation. Accordingly, the total power consumption by the areal distribution (orientation layout (3)) model simulation is distinctly lower than the lump model simulation. As a result, the percent decrease in the sum of the total power consumption over the 40-year simulation was 19.25 % compared to the lump model simulation (Figure 6.18, and Table 6.6).

Figure 6.15 Total power consumption comparison for the base case of the general conceptual design system between the areal distribution **(orientation layout (3))** and the lump model simulation.

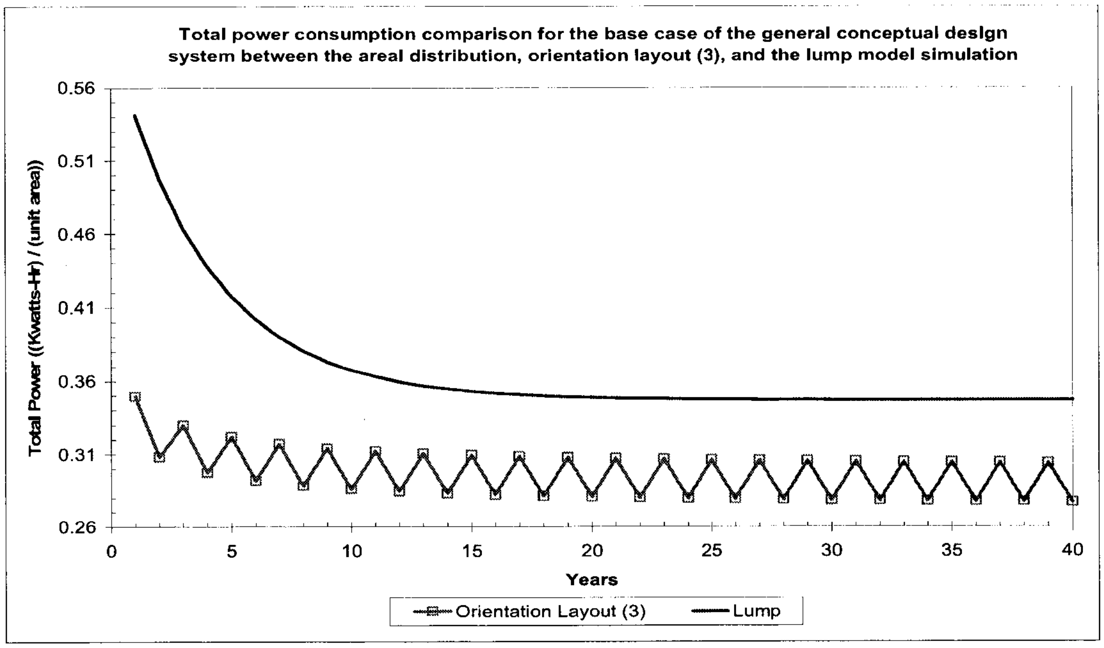

Figure 6.16 Reverse osmosis power consumption comparison for the base case of the general conceptual design system between the areal distribution **(orientation layout (3))** and the lump model simulation.

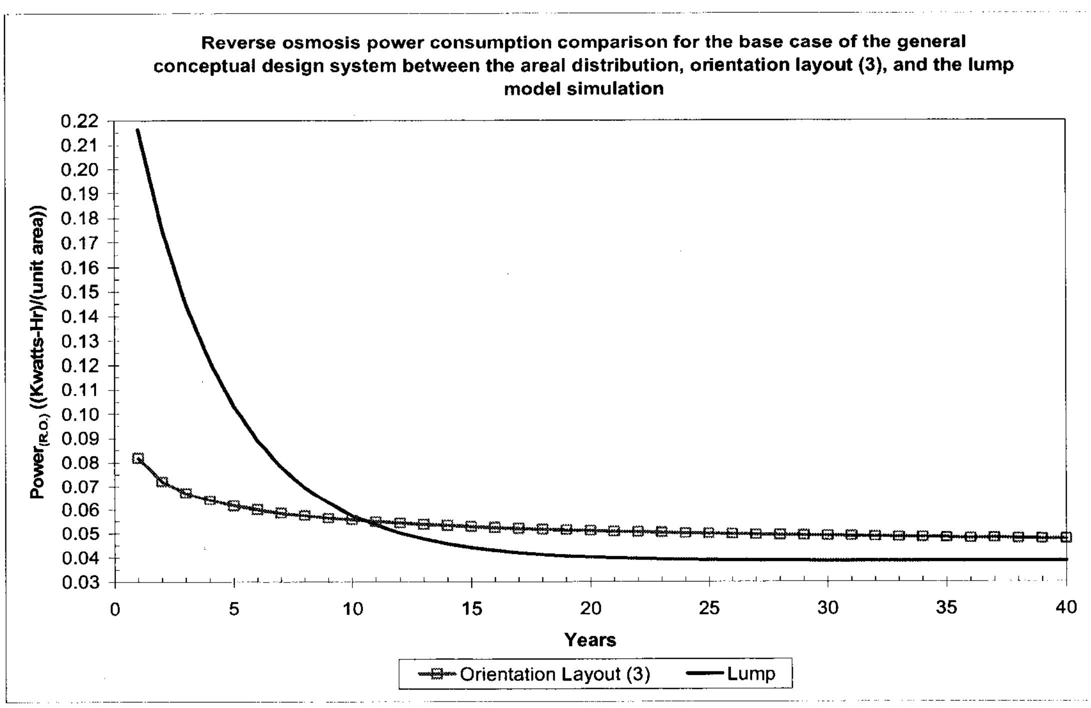

Figure 6.17 Well pump power consumption comparison for the base case of the general conceptual design system between the areal distribution **(orientation layout (3))** and the lump model simulation.

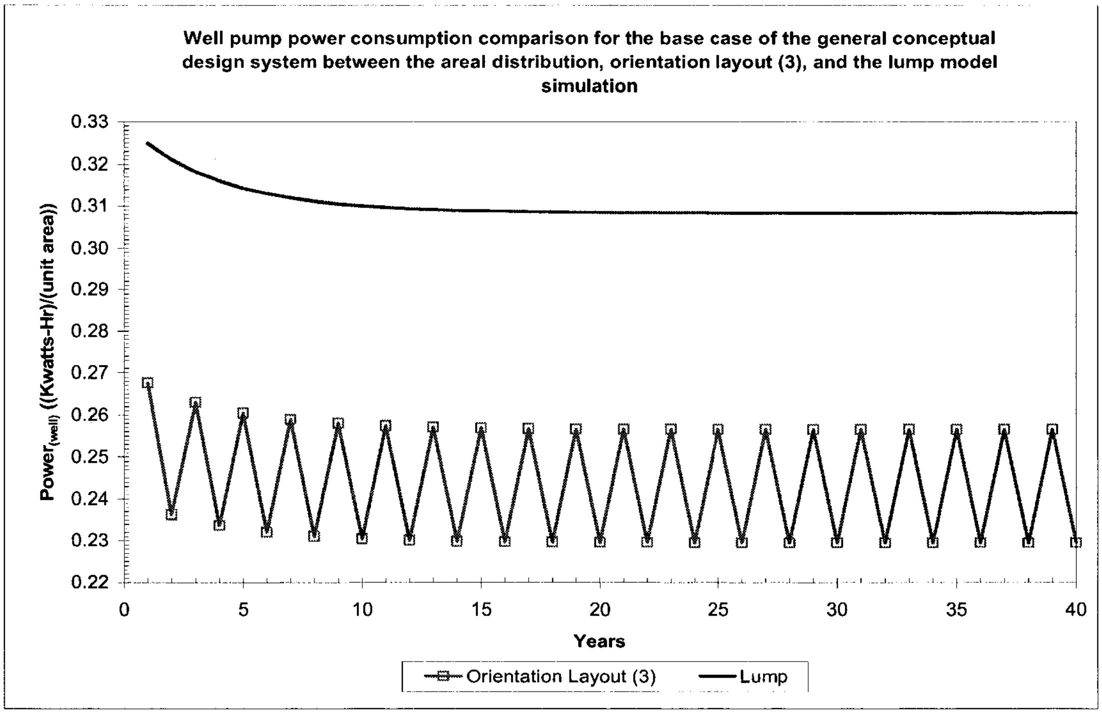

Figure 6.18 Sum of the total power consumption, 40-year simulation, comparison for the base case of the general conceptual design system between the areal distribution **(orientation layout (3))** and the lump model simulation.

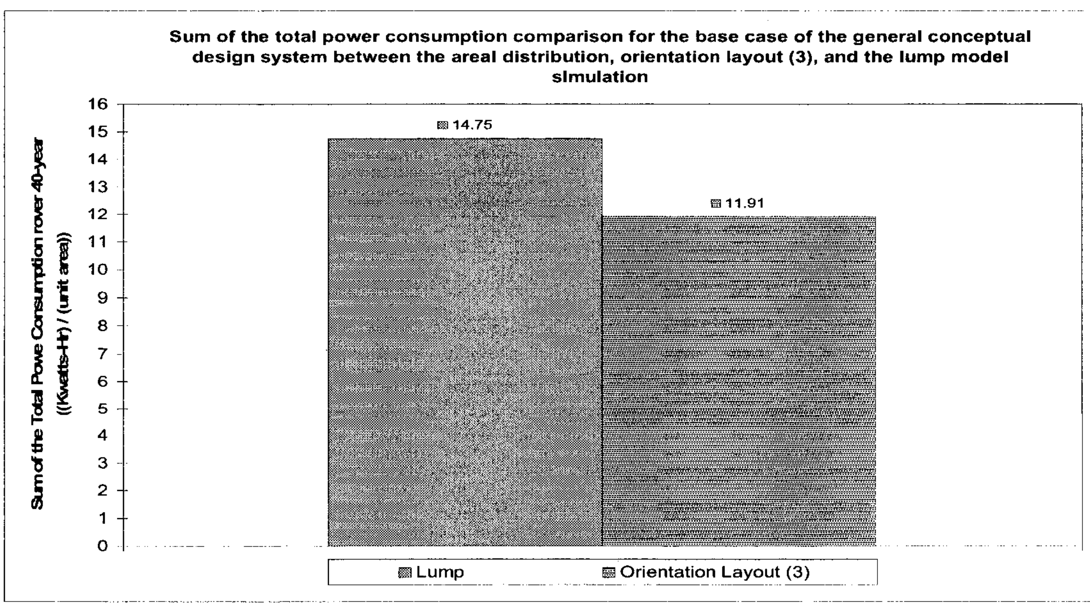

Table 6.6 Percent change comparison in the sum of the total power consumption between the areal distribution **(orientation layout (3))** and the lump model simulation.

From	To	% Change (decrease) in Sum of Total Power per Unit Area
Lump model	**Areal Distribution, Orientation Layout (3)**	**19.25**

In conclusion, Table 6.7 represents the percent change comparison in the sum of the total power consumption between the lump model simulation and the areal distribution model for the three orientation layouts. To compare the performance of the

Table 6.7 Percent change comparison in the sum of the total power consumption between the areal distribution orientation layouts and the lump model simulation.

From	To	% Change (decrease) in Sum of Total Power per Unit Area
Lump model	**Areal Distribution, Orientation Layout (1), Model**	**9.29**
Lump model	**Areal Distribution, Orientation Layout (2), Model**	**8.20**
Lump model	**Areal Distribution, Orientation Layout (3), Model**	**19.25**

areal distribution model to the lump model for the base case simulation, the water source output data (Q_{inj}, Q_{DP}, and $Q_{pump} = Q_{Feed}$) from the base case simulation of the lump model was used as input data in the areal distribution model simulation (Section 6.3, indent 1). In reality, the water source (Q_{inj}, Q_{DP}, and $Q_{pump} = Q_{Feed}$) assumption utilized in the areal distribution model simulation of the orientation layout (1) and orientation layout (2) will need a slight adjustment to adjust and cope with the increase in groundwater salt concentration. The groundwater salt concentration of the areal distribution while simulating orientation layout (1) and orientation layout (2) was higher than the lump model simulation. As a result, the power consumption by the reverse osmosis is higher in both orientation layout (1), and (2) than the lump model simulation (Figure 6.8, and 6.12). Because the water source data (Q_{inj}, Q_{DP}, and $Q_{pump} = Q_{Feed}$) is similar in the areal distribution model simulation and the lump model simulation, the only cause of the increase in the reverse osmosis unit power consumption is the increase in groundwater salt concentration. Therefore, as the groundwater salt concentration increases in the areal distribution simulation model for orientation layout (1), and (2) higher than the lump model simulation, slightly more groundwater will need to be pumped to be fed to the reverse osmosis unit to cope with irrigation water efficiency (Section 4.1.7). Therefore, as the pump water amount slightly increases, the injected treated wastewater amount will slightly increase, and the deep percolation water amount will slightly increase, too. Hence, the reverse osmosis power consumption and the pump power consumption will slightly increase. For that reason, the total power consumption will slightly increase. Accordingly, the percent change, over the 40-year simulation, in the sum of the total power consumption between the lump model simulation and the areal distribution model for orientation layout (1) and orientation layout (2) will decrease slightly down more than what is represented in Table 6.7. As a final conclusion, the orientation layout (1) and orientation layout (2) of the areal distribution simulation model are very rational representation of the lump model simulation. On the other hand, the areal distribution (orientation layout (3)) model simulation is the most efficient orientation layout in the power consumption, and hence, in the total operation cost. Personally, I recommend the utilization of the areal distribution's orientation layout (1) and/or orientation layout (2) over the orientation layout (3). Even though orientation layout (3) consumes the least total power, it provides the least groundwater salt concentration enhancement in general, which will reduce the vulnerability of possible lateral reduction of the operation system due to emergencies or cost effects.

Appendix VI illustrates figures for groundwater salt concentrations and groundwater hydraulic heads for the 5th, 10th, 20th, and 40th year of simulations for the three areal distribution simulation model orientation layouts (orientation layout (1), (2), and (3)). Moreover, figures of the brine salt concentration rejected from the reverse osmosis system vs. the simulation period for the three areal distribution simulation model orientation layouts (orientation layout (1), (2), and (3)) and the lump model are presented in Appendix VI as well.

CHAPTER 7

SYSTEM ECONOMIC FEASIBILITY ANALYSIS

7.1 System Costs Analysis

System cost analysis is one of the most essential measures of the system feasibility. The aim of the feasibility study is to see whether it is possible to develop a system at a reasonable cost. At the end of the feasibility study a decision is taken whether to proceed or not. The costs of setting and operating the general conceptual design system will be divided over several elements such as:

- Cost of reverse osmosis system and maintenance
- Cost of well drilling and well construction completion
- Cost of well pump and maintenance, and installation
- Cost of treated wastewater utilized by the system
- Cost of electrical power consumed by the system

7.1.1 Cost of Reverse Osmosis Unit and Maintenance

The reverse osmosis system costs are divided between the actual capital cost of the reverse osmosis unit and the maintenance costs of operating the reverse osmosis unit. For a reverse osmosis unit with water product capacity larger than 2000 gpd or/and the inlet feed water to the reverse osmosis unit, with a total dissolved salt concentration exceeding 2000 mg /l, the capital cost of the reverse osmosis unit without the pretreatment system will be in the vicinity of $1 per one gallon per day ($1 /gpd) of water produced (personal communications).

Or,

$$\boldsymbol{Cost\ of\ R.O.System} = \left(\frac{\boldsymbol{1\$}}{\boldsymbol{GPD}}\right) * \boldsymbol{Q_{irr(\,permeate\,)(max)}} \qquad \textbf{(7.1)}$$

where,

$\boldsymbol{Q_{irr(\,permeate\,)(max)}}$ = Maximum portion of the feed, during the simulation period that passes through the reverse osmosis membrane and is collected for use $[L^3/T]$, and

GPD = Gallons per day.

Moreover, the yearly maintenance cost of operating the reverse osmosis unit will be in the vicinity of 5% of the capital cost of the reverse osmosis unit (personal communications). Thus

$$R.O.\ System\ Maintenance\ Cost\ per\ year = \left(\frac{5}{100}\right) * \left(\left(\frac{1\$}{GPD}\right) * Q_{irr(\,permeate\,)(max)}\right)$$

(7.2)

7.1.2 Cost of Well Drilling and Well Construction Completion

The cost of drilling a well will vary in cost. The cost variance is mainly due to the soil type. The general average drilling cost in the USA ranges in the vicinity of \$13 – \$22 per foot (\$43 – \$66 per meter) for almost all types of soil (personal communications) (Table 7.1). Moreover, the cost of well construction can be more expensive than the latter price range. The well construction completion prices can vary mainly due to the soil type, depth of the drilling, well borehole size, casing size, casing type, well screening, drop pipe length and size, and well packing. Moreover, additional expenses are required to cover the pump insulation and well development, the latter being the cleaning and pump testing prior to pump initiation cost. Table 7.2 illustrates the average cost of the well construction (personal communications). Moreover, Figure 7.1 illustrates a well construction layout.

Table 7.1 Average cost of well drilling only, for 10 - 12 inch borehole diameter.

Cost of Well Drilling	Average Cost (\$/foot)	Average Cost (\$/meter)
Colorado	13 - 15	43 – 50
USA	12 - 22	40 – 73
In General	9 - 30	30 – 100

Table 7.2 Average cost of well completion construction.

	Borehole Size (inch)	Casing Size (inch)	Well Depth (ft)	Cost ($/ft)*	Drop Pipe Cost ($/ft)**	Development (lump sum) Cost ($)***	Total Cost ($)
Drilling & Completion	18	12	50	100	5	1500	6,750
			100	150	5	2000	17,500
			200	200	5	2500	43,500
	24	16	50	150	5	1500	9,250
			100	250	5	2000	27,500
			200	300	5	2500	63,500
	30	20	50	200	5	1500	11,750
			100	300	5	2000	32,500
			200	400	5	2500	83,500
	36	24	50	250	5	1500	14,250
			100	350	5	2000	37,500
			200	500	5	2500	103,500

* Includes drilling the borehole, galvanized well casing (for stainless steel casing add $10-$20 per foot), gravel packing, well screening, and sanitary surface seal; ** PVC pipe (6"), schedule 40; *** Well cleaning and pumping test cost.

	Borehole Size (m)	Casing Size (m)	Well Depth (m)	Cost ($/m)*	Drop Pipe Cost ($/m)**	Development (lump sum) Cost ($)***	Total Cost ($)
Drilling & Completion	0.5	0.3	15	333	16	1500	6,750
			31	500	16	2000	17,500
			61	667	16	2500	43,500
	0.6	0.4	15	500	16	1500	9,250
			31	833	16	2000	27,500
			61	1000	16	2500	63,500
	0.8	0.5	15	667	16	1500	11,750
			31	1000	16	2000	32,500
			61	1333	16	2500	83,500
	0.9	0.6	15	833	16	1500	14,250
			31	1167	16	2000	37,500
			61	1667	16	2500	103,500

* Includes drilling the borehole, galvanized well casing (for stainless steel casing add $33-$67 per meter), gravel packing, well screening, and sanitary surface seal; ** PVC pipe (6"), schedule 40; *** Well cleaning and pumping test cost.

Figure 7.1 Well construction layout.

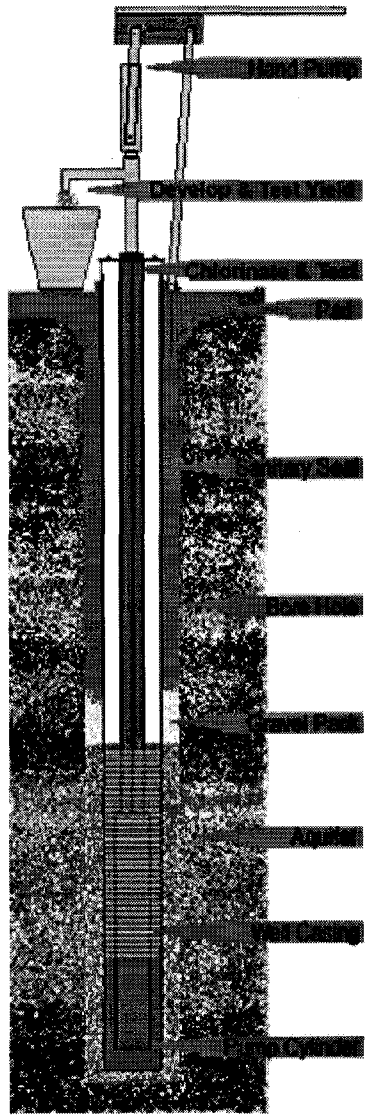

7.1.3 Cost of Well Pump and Maintenance, and Installation

The cost of the well pump will consists of the cost of the pump impeller and suction shafts (turbine style bowls), the cost of the pump motor, and the cost of installing the pump. Depending on the pump capacity, head lift, and the pump efficiency, the power consumed by the pump well can be calculated. Moreover, from the power consumed by the pump well, the price of the well pump can be estimated (Table 7.3). The groundwater pump power can be found from:

$$\textit{Pump Power (Kwatts)} = \frac{\gamma * Q_{pump} * H_{lift}}{(1000 * \eta_{pump})} \qquad \textbf{(7.3)}$$

$$\textit{Pump Power (Horse Power)} = \frac{\textit{Pump Power (Kwatts)}}{0.7457} \qquad \textbf{(7.4)}$$

where,

Pump Power = Power consumed by the groundwater pump [Kwatts] or [Horse Power],

Q_{pump} = Pumped groundwater flow rate [m^3/sec],

H_{lift} = The height of water to be lifted to the ground surface [m],

γ = Specific weight of water ($\gamma = \rho * g$) [kg / (m^2 -sec.)], and

$\eta_{(pump)}$ = Groundwater electrical well pump efficiency, for electrical pump $\eta_{(pump)}$ = 50 – 80 %.

Table 7. 3 Example of well pumps and pump shaft type and cost (Flint & Walling, Inc.).

200 GPM Series Pump Ends (Turbine Style Bowls), Most Efficient Operation Range (125 – 250 GPM)*				
Horse Power				**Price ($)**
5 hp				**597**
7.5 hp				**787**
10 hp				**1001**
15 hp				**1222**
20 hp				**1665**
25 hp				**1881**
30 hp				**2382**
40 hp				**3061**
50 hp				**3792**
Franklin 6" Motors*				
Phase	**Horse Power**	**Lift (ft)**	**Lift (m)**	**Price ($)**
Single Phase	**5 hp**	**50**	**15**	**1034**
Single Phase	**7.5 hp**	**100**	**31**	**1215**
Single Phase	**10 hp**	**150**	**46**	**1363**
Single Phase	**15 hp**	**200**	**62**	**1771**
Three Phase	**5 hp**	**50**	**15**	**983**
Three Phase	**7.5 hp**	**100**	**31**	**1145**
Three Phase	**10 hp**	**150**	**46**	**1283**
Three Phase	**15 hp**	**200**	**62**	**1479**
Three Phase	**20 hp**	**300**	**92**	**1818**
Three Phase	**25 hp**	**350**	**107**	**2114**
Three Phase	**30 hp**	**450**	**137**	**2453**
Three Phase	**40 hp**	**600**	**183**	**2949**
Three Phase	**50 hp**	**750**	**229**	**3757**

* Note: the total pump price = (Turbine Style Bowls price) + (Motors price).
Example: the total price of 7.5 hp for three phase electricity well pump = $787+$1145 = $1932.

In addition, the average cost for pump installation is in the vicinity of $60 / hr. Furthermore, 9 – 10 hrs is the usual average installation time required for setting up the pump. Moreover, the yearly maintenance cost of operating the well pump will be in the vicinity of 3% of the capital cost of the well construction cost (personal communications). Thus,

$$\textit{Well Pump Maintenance Cost per year} = \left(\frac{3}{100}\right) * (\textit{Well Construction Cost})$$

(7.5)

7.1.4 Cost of Wastewater

The average cost of wastewater in the USA is in the vicinity of \$21.5 - \$24 per acre-foot (\$0.017 – \$0.019 per cubic meter) (Ringskog, K. (2000), and personal communication) (Table 7.4). In this dissertation, the average treated wastewater value of \$0.018 per m^3 will be assumed for treated wastewater consumption cost calculation purposes in the USA. Moreover, the base case simulation will be analogous or representative of a quasi-Kuwaiti ecosystem and environment data (as assumed in Chapter 3). Therefore, the average cost of treated wastewater in Kuwait is in the vicinity of \$0.007 /m^3 (FAO 1997) and will be used to represent the cost of treated wastewater in all base case simulations.

7.1.5 Cost of Electrical Power

The average cost of electricity in the USA is in the vicinity of \$0.05- 0.10 per Kwatts-hr (personal communication). In this dissertation, the average electricity value of \$0.06 per Kwatts-hr will be assumed for power consumption cost calculation purposes in the USA. Moreover, the base case simulation will be analogous or representative of a quasi-Kuwaiti ecosystem and environment data (as assumed in Chapter 3). Therefore, the average cost of subsidized electricity in Kuwait is in the vicinity of $0.0066 per Kwatts-hr and $0.0594 per Kwatts-hr for non-subsidized electricity (personal communication). The cost of $0.0066 per Kwatts-hr will be used to represent the cost of subsidized electricity per Kwatts-hr and the cost of $0.0594 per Kwatts-hr will be used for non-subsidized electricity in all base case simulations representing Kuwait.

Table 7.4 Average cost of water type in the USA (Ringskog, K. (2000), and personal communications).

Water Type	Average Cost in USA ($/acre-foot)	Average Cost in USA ($/m^3)
Desalinated freshwater	**600 - 700**	**0.49-0.57**
Surface water	**35 - 85**	**0.028-0.069**
Wastewater	**21.5 - 24**	**0.017-0.019**
Water Right Leasing per year	**10 - 30**	**0.008-0.024**

7.1.6 System Crop Yield Revenue

The general conceptual design system base case simulation was designed for alfalfa crop production. Alfalfa hay crop production will be used mainly as animal feed for dairy and meat production purposes. The recorded yield of an alfalfa hay crop of one acre of alfalfa is 10 tons/acre per year (24.7 tons/hectares) without irrigation and 24 tons/acre per year (59.3/hectares) with irrigation. The estimated value of alfalfa hay is $102.50 per ton (1998 USDA Agriculture

Statistics, last updated: Feb. 8th, 2000). In this dissertation, the average value of 24.7 tons/hectares (10 tons/acre) of alfalfa hay yield and an estimated value of $102.5 per ton for alfalfa will be assumed for calculation purposes. Thus, the revenue value of the alfalfa crop yield will be $2,531.75 per hectare per year for the base case simulation of the general conceptual design system.

7.2 Economical Feasibility of the Base Case of the General Conceptual Design System:

The total cost of the base case of the general conceptual design system will be the sum of all the costs of the capital, operation, and construction expenditures for the following: 1) reverse osmosis unit capital cost, 2) the well pump capital cost, 3) the reverse osmosis unit maintenance cost, 4) the well pump maintenance cost, 5) total electrical power cost exerted by the reverse osmosis unit and the well pump, 6) the cost of the treated wastewater utilized, and 7) the cost of well completion construction cost. In this section and the subsequent sub-sections, the detailed costs of the base case of the general conceptual design system will be shown for both the lump model approach and the areal distribution approach. Moreover, the detailed costs for the areal distribution approach will be shown for the three layout orientations. Of note, the capital costs for both the lump model and areal distribution (including all layouts orientations) approaches will be the same, and the only difference in costs will be in the operation aspect. Thus,

Table 7.5 illustrates the detailed capital costs for the base case for all simulation approaches, lump model and/or areal distribution model.

Table 7.5 Detailed capital cost prices for the base case of the general conceptual design system for the lump model and areal distribution simulations approaches.

	Item	Cost	Remarks
Capital Costs	Price of R.O.	$171,813	(1$/GPD), equation (7.1)
	Pump Well Construction Completion	$43,500	For 18 inch (0.5 m) borehoie, 12 inch (0.3 m) casing, and 197 foot (60 m) depth. Table (7.2)
	Injection Well Construction Completion	$43,500	For 18 inch (0.5 m) borehole, 12 inch (0.3 m) casing, and 197 foot (60 m) depth. Table (7.2)
	Well Pump	$2692	For 200 GPM, 15 hp pump (Max GPM = 198.86, lift = 34.31 m, efficiency = 75%, 3 phases), equation (7.3), (7.4), and manufacture graphs and tables (i.e. Figure 7.3)
	Well Pump Installation	$540	Well insulation ($60/ hr for 9 hrs)
Total Cost		$262,045	

7.2.1 Economical Feasibility of the Base Case of the General Conceptual Design System Using the Lump Model

The cost analysis for the base case of the general conceptual design system using the lump model approach will be investigated. The cost analysis of the electrical power and treated wastewater will be based on USA electrical power costs and the treated wastewater cost, and based on Kuwait electrical power costs and treated wastewater costs. The economical feasibility of the base case of the general conceptual design system using the lump model approach will be based on the calculations of the net present worth value of the cash flows and the benefit-cost ratio theme for the capital cost, the operation and maintenance costs, and the revenues of the crop yields for the 40 years of operation. Based on the benefit-cost ratio, the economical feasibility of the system using the lump model approach can be considered, thus, the benefit-cost ratio for the present cash flows can be calculated as follows:

1. Calculating the present worth cost value of the system which is equal to:

$$NPWCV = Initial\ Capital\ Cost\ of\ the\ System + \sum_{j=1}^{N} \frac{Total\ Cost\ per\ Year}{(1+i)^j} \tag{7.6}$$

where,

NPWCV = Net present worth cost value of the system,

N = Number of years, and

i = Interest rate per period (%).

2. Calculating the present worth revenue value of the system which is equal to:

$$NPWRV = \sum_{j=1}^{N} \frac{Total\ Revenue\ per\ Year}{(1+i)^j} \quad (7.7)$$

where,

$NPWRV$ = Net present worth revenue value.

3. From Equation (7.6) and Equation (7.7) the benefit-cost ratio for the present cash flow can be calculated as:

$$Cost - Benefit\ Ratio = \frac{NPWRV}{NPWCV} \quad (7.8)$$

Tables 7.6 and 7.7 illustrate detailed operation and maintenance cost prices, over 40 years, for the base case of the general conceptual design system using the lump model for the USA and Kuwait, respectively. Moreover, Figures 7.2 and 7.3 illustrate a detailed cash flow diagram, over 40 years, for the base case simulation of the general conceptual design system using the lump model for the USA and Kuwait respectively.

Table 7.6 Detailed operation and maintenance cost prices, over 40 years, for the base case simulation of the general conceptual design system using the lump model, for the USA.

Year	Operation & Maintenance Cost ($/year)				
	R.O. Maintenance	Pump Maintenance	Total Power consumed (a)	Treated wastewater (b)	Sum
1	$8,590	$1,305	$3,058	$4,323	$17,276
2	$8,590	$1,305	$2,808	$4,307	$17,010
3	$8,590	$1,305	$2,618	$4,295	$16,807
4	$8,590	$1,305	$2,471	$4,285	$16,652
5	$8,590	$1,305	$2,359	$4,278	$16,532
6	$8,590	$1,305	$2,271	$4,273	$16,439
7	$8,590	$1,305	$2,203	$4,268	$16,367
8	$8,590	$1,305	$2,150	$4,265	$16,310
9	$8,590	$1,305	$2,109	$4,262	$16,266
10	$8,590	$1,305	$2,077	$4,260	$16,232
11	$8,590	$1,305	$2,051	$4,259	$16,205
12	$8,590	$1,305	$2,032	$4,257	$16,184
13	$8,590	$1,305	$2,016	$4,256	$16,167
14	$8,590	$1,305	$2,004	$4,256	$16,154
15	$8,590	$1,305	$1,994	$4,255	$16,144
16	$8,590	$1,305	$1,987	$4,255	$16,136
17	$8,590	$1,305	$1,981	$4,254	$16,130
18	$8,590	$1,305	$1,976	$4,254	$16,125
19	$8,590	$1,305	$1,972	$4,254	$16,121
20	$8,590	$1,305	$1,970	$4,254	$16,118
21	$8,590	$1,305	$1,967	$4,253	$16,116
22	$8,590	$1,305	$1,965	$4,253	$16,114
23	$8,590	$1,305	$1,964	$4,253	$16,112
24	$8,590	$1,305	$1,963	$4,253	$16,111
25	$8,590	$1,305	$1,962	$4,253	$16,110
26	$8,590	$1,305	$1,961	$4,253	$16,109
27	$8,590	$1,305	$1,961	$4,253	$16,109
28	$8,590	$1,305	$1,960	$4,253	$16,108
29	$8,590	$1,305	$1,960	$4,253	$16,108
30	$8,590	$1,305	$1,960	$4,253	$16,108
31	$8,590	$1,305	$1,960	$4,253	$16,108
32	$8,590	$1,305	$1,960	$4,253	$16,107
33	$8,590	$1,305	$1,959	$4,253	$16,107
34	$8,590	$1,305	$1,959	$4,253	$16,107
35	$8,590	$1,305	$1,959	$4,253	$16,107
36	$8,590	$1,305	$1,959	$4,253	$16,107
37	$8,590	$1,305	$1,959	$4,253	$16,107
38	$8,590	$1,305	$1,959	$4,253	$16,107
39	$8,590	$1,305	$1,959	$4,253	$16,107
40	$8,590	$1,305	$1,959	$4,253	$16,107

(a) Electricity cost based on $0.06 per Kwatts-hr; Treated wastewater cost based on $0.018 pre m^3.

Table 7.7 Detailed operation and maintenance cost prices, over 40 years, for the base case simulation of the general conceptual design system using the lump model, for Kuwait.

Year	Operation & Maintenance Cost ($ /year)				
	R.O. Maintenance	Pump Maintenance	Total Power consumed (a)	Treated wastewater (b)	Sum
1	$8,590	$1,305	$336	$1,681	$11,912
2	$8,590	$1,305	$309	$1,675	$11,879
3	$8,590	$1,305	$288	$1,670	$11,853
4	$8,590	$1,305	$272	$1,667	$11,833
5	$8,590	$1,305	$259	$1,664	$11,818
6	$8,590	$1,305	$250	$1,662	$11,806
7	$8,590	$1,305	$242	$1,660	$11,797
8	$8,590	$1,305	$237	$1,659	$11,790
9	$8,590	$1,305	$232	$1,658	$11,785
10	$8,590	$1,305	$228	$1,657	$11,780
11	$8,590	$1,305	$226	$1,656	$11,777
12	$8,590	$1,305	$223	$1,656	$11,774
13	$8,590	$1,305	$222	$1,655	$11,772
14	$8,590	$1,305	$220	$1,655	$11,770
15	$8,590	$1,305	$219	$1,655	$11,769
16	$8,590	$1,305	$219	$1,655	$11,768
17	$8,590	$1,305	$218	$1,654	$11,767
18	$8,590	$1,305	$217	$1,654	$11,767
19	$8,590	$1,305	$217	$1,654	$11,766
20	$8,590	$1,305	$217	$1,654	$11,766
21	$8,590	$1,305	$216	$1,654	$11,765
22	$8,590	$1,305	$216	$1,654	$11,765
23	$8,590	$1,305	$216	$1,654	$11,765
24	$8,590	$1,305	$216	$1,654	$11,765
25	$8,590	$1,305	$216	$1,654	$11,765
26	$8,590	$1,305	$216	$1,654	$11,765
27	$8,590	$1,305	$216	$1,654	$11,765
28	$8,590	$1,305	$216	$1,654	$11,765
29	$8,590	$1,305	$216	$1,654	$11,765
30	$8,590	$1,305	$216	$1,654	$11,764
31	$8,590	$1,305	$216	$1,654	$11,764
32	$8,590	$1,305	$216	$1,654	$11,764
33	$8,590	$1,305	$216	$1,654	$11,764
34	$8,590	$1,305	$216	$1,654	$11,764
35	$8,590	$1,305	$216	$1,654	$11,764
36	$8,590	$1,305	$216	$1,654	$11,764
37	$8,590	$1,305	$216	$1,654	$11,764
38	$8,590	$1,305	$215	$1,654	$11,764
39	$8,590	$1,305	$215	$1,654	$11,764
40	$8,590	$1,305	$215	$1,654	$11,764

(a) Electricity cost based on $0.0066 per Kwatts-hr; Treated wastewater cost based on $0.007 pre m^3.

Figure 7.2 Detailed cash flow diagram, over 40 years, for the base case simulation of the general conceptual design system using the lump model for the USA.

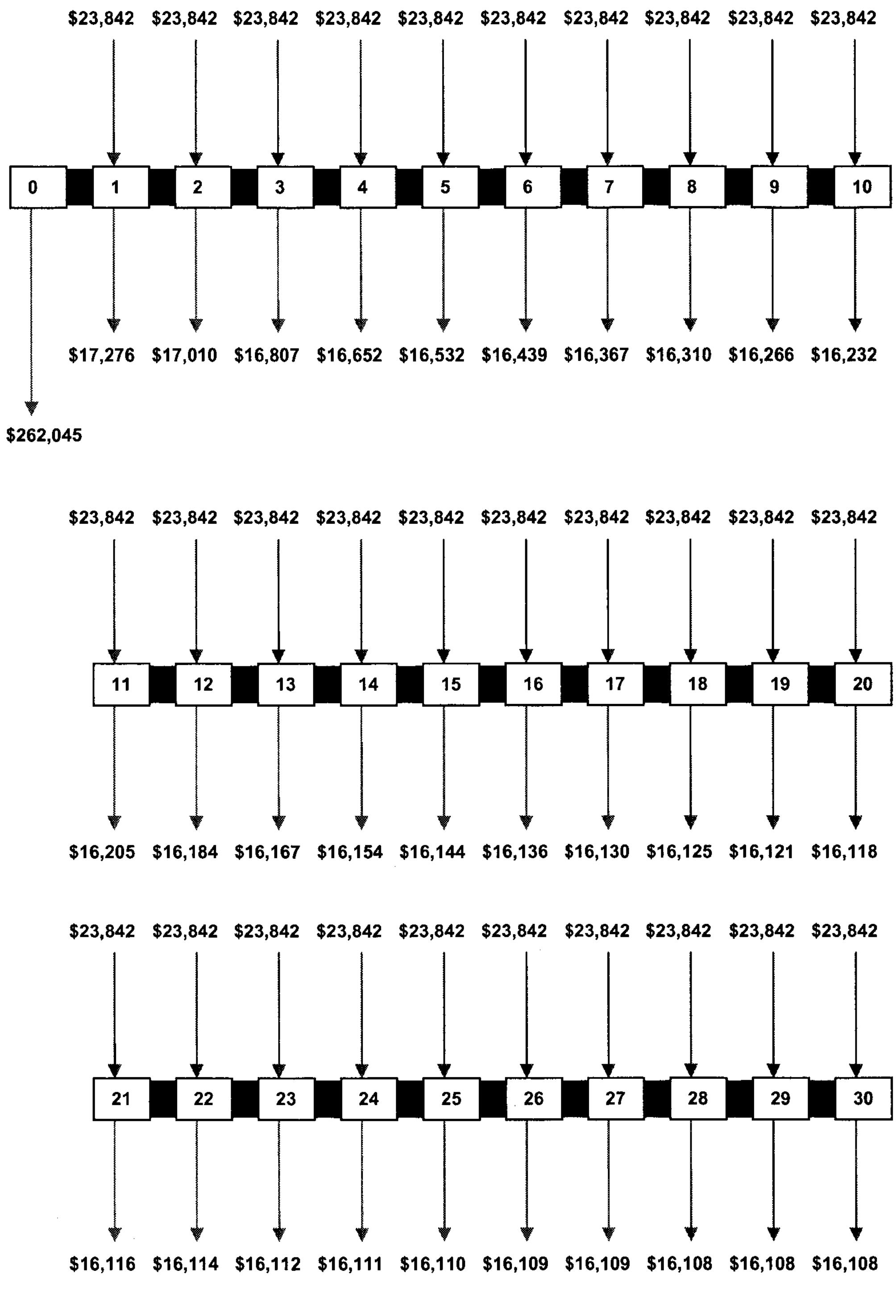

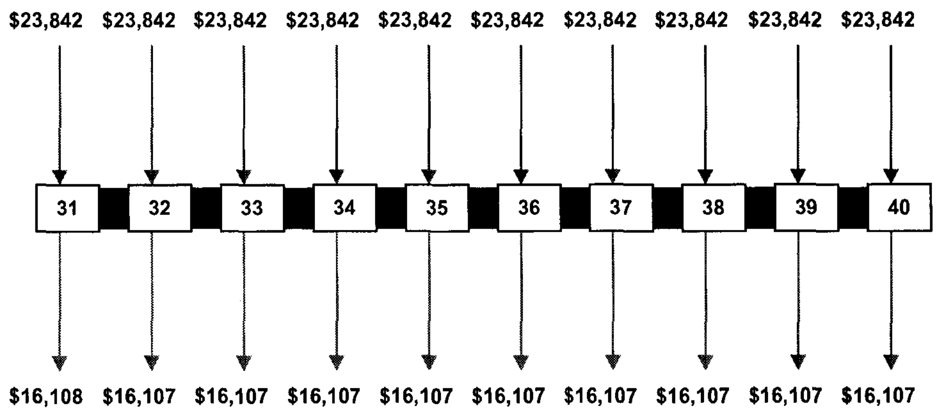

Figure 7.3 Detailed cash flow diagram, over 40 years, for the base case simulation of the general conceptual design system using the lump model for Kuwait.

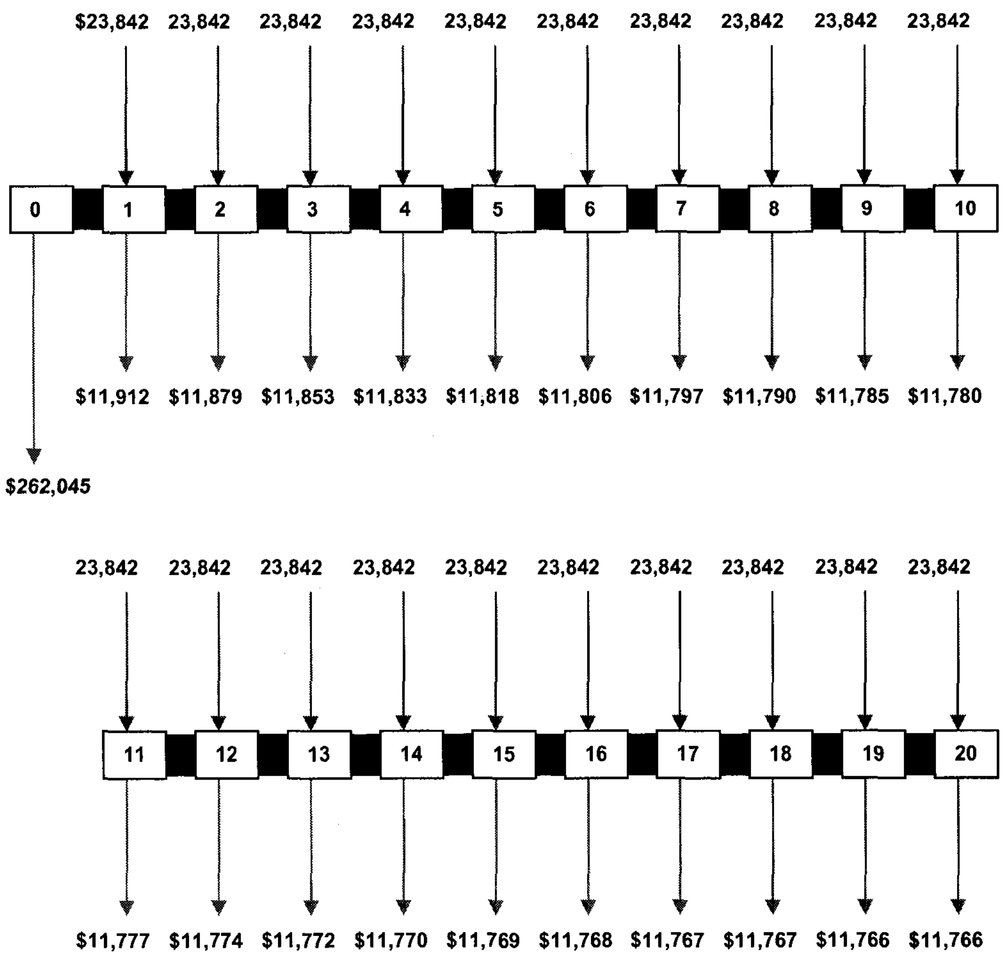

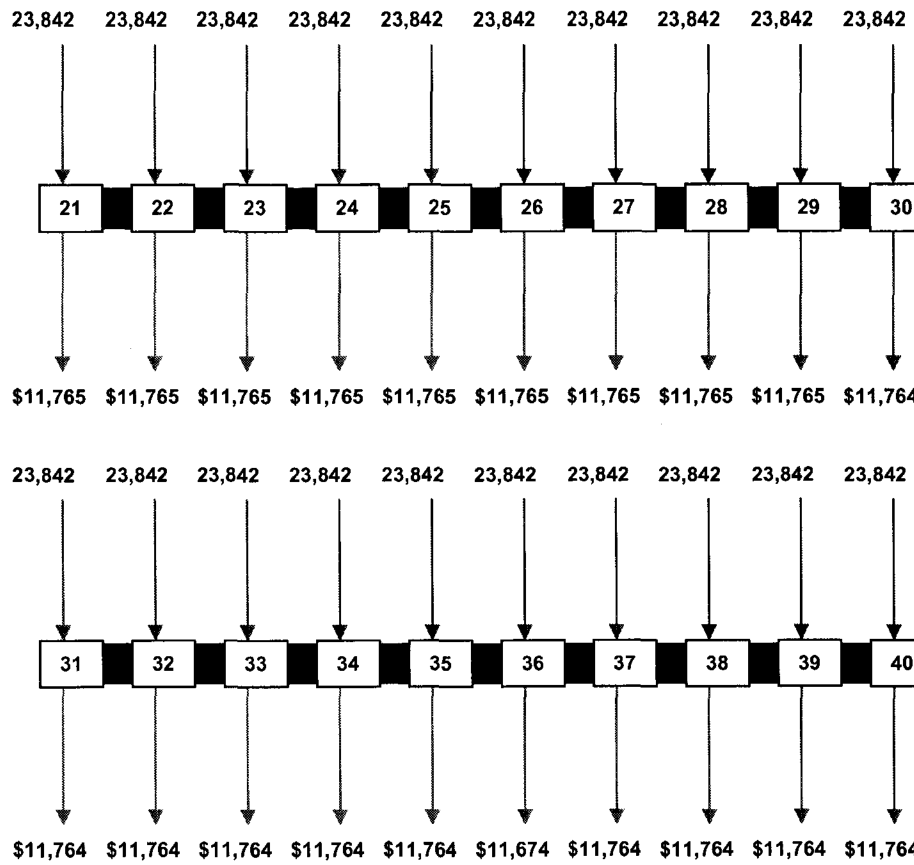

7.2.2 Economical Feasibility of the Base Case of the General Conceptual Design System Using the Areal Distribution Model

The cost analysis for the base case of the general conceptual design system using the areal distribution approach will be investigated for the three orientation layers (orientation layer (1), orientation layer (2), and orientation layer (3)). The cost analysis of the electrical power and treated wastewater will be based on USA electrical power costs and the treated wastewater cost, and based on Kuwait electrical power costs and treated wastewater costs. The economical feasibility of the base case of the general conceptual design system using the areal distribution approach will be based on the calculations of the net present worth value of the cash flow values and the cost-benefit ratio theme for the capital cost, the operation and maintenance costs, and the revenues of the crop yields for the 40 years of operation. Based on the benefit-cost ratio (Equation 7.8) the most feasible economical orientation layout can be selected.

Tables 7.8, 7.9, 7.10, 7.11, 7.12, and 7.13 illustrate detailed operation and maintenance cost prices, over 40 years, for the base case of the general conceptual design system using the areal distribution model for the three orientation layouts for the USA and Kuwait respectively. Moreover, Figures 7.4, 7.5, 7.6, 7.7, 7.8, and 7.9 illustrate detailed cash flow diagram, over 40 years, for the base case simulation of the general conceptual design system using the areal distribution model for the three orientation layouts for the USA and Kuwait respectively.

Table 7.8 Detailed operation and maintenance cost prices, over 40 years, for the base case simulation of the general conceptual design system using the areal distribution, **orientation layout (1)**, approach model for the USA.

Year	Operation & Maintenance Cost ($/year)				
	R.O. Maintenance	Pump Maintenance	Total Power consumed (a)	Treated wastewater (b)	Sum
1	$8,590	$1,305	$2,969	$4,323	$17,187
2	$8,590	$1,305	$2,485	$4,307	$16,687
3	$8,590	$1,305	$2,525	$4,295	$16,715
4	$8,590	$1,305	$2,145	$4,285	$16,325
5	$8,590	$1,305	$2,303	$4,278	$16,476
6	$8,590	$1,305	$2,002	$4,273	$16,170
7	$8,590	$1,305	$2,184	$4,268	$16,348
8	$8,590	$1,305	$1,904	$4,265	$16,064
9	$8,590	$1,305	$2,139	$4,262	$16,297
10	$8,590	$1,305	$1,842	$4,260	$15,997
11	$8,590	$1,305	$2,069	$4,259	$16,223
12	$8,590	$1,305	$1,783	$4,257	$15,935
13	$8,590	$1,305	$2,022	$4,256	$16,173
14	$8,590	$1,305	$1,755	$4,256	$15,906
15	$8,590	$1,305	$1,991	$4,255	$16,141
16	$8,590	$1,305	$1,716	$4,255	$15,866
17	$8,590	$1,305	$1,959	$4,254	$16,108
18	$8,590	$1,305	$1,689	$4,254	$15,838
19	$8,590	$1,305	$1,939	$4,254	$16,088
20	$8,590	$1,305	$1,677	$4,254	$15,826
21	$8,590	$1,305	$1,917	$4,253	$16,066
22	$8,590	$1,305	$1,653	$4,253	$15,801
23	$8,590	$1,305	$1,897	$4,253	$16,045
24	$8,590	$1,305	$1,641	$4,253	$15,789
25	$8,590	$1,305	$1,886	$4,253	$16,034
26	$8,590	$1,305	$1,621	$4,253	$15,769
27	$8,590	$1,305	$1,871	$4,253	$16,019
28	$8,590	$1,305	$1,611	$4,253	$15,759
29	$8,590	$1,305	$1,859	$4,253	$16,007
30	$8,590	$1,305	$1,595	$4,253	$15,743
31	$8,590	$1,305	$1,844	$4,253	$15,992
32	$8,590	$1,305	$1,589	$4,253	$15,737
33	$8,590	$1,305	$1,834	$4,253	$15,982
34	$8,590	$1,305	$1,576	$4,253	$15,723
35	$8,590	$1,305	$1,826	$4,253	$15,974
36	$8,590	$1,305	$1,567	$4,253	$15,715
37	$8,590	$1,305	$1,819	$4,253	$15,966
38	$8,590	$1,305	$1,561	$4,253	$15,709
39	$8,590	$1,305	$1,809	$4,253	$15,957
40	$8,590	$1,305	$1,554	$4,253	$15,702

(a) Electricity cost based on $0.06 per Kwatts-hr; Treated wastewater cost based on $0.018 pre m^3.

Table 7.9 Detailed operation and maintenance cost prices, over 40 years, for the base case simulation of the general conceptual design system using the areal distribution, **orientation layout (1)**, approach model for Kuwait.

Year	Operation & Maintenance Cost ($ /year)				
	R.O. Maintenance	Pump Maintenance	Total Power consumed (a)	Treated wastewater (b)	Sum
1	$8,590	$1,305	$327	$1,681	$11,903
2	$8,590	$1,305	$273	$1,675	$11,843
3	$8,590	$1,305	$278	$1,670	$11,843
4	$8,590	$1,305	$236	$1,667	$11,797
5	$8,590	$1,305	$253	$1,664	$11,812
6	$8,590	$1,305	$220	$1,662	$11,777
7	$8,590	$1,305	$240	$1,660	$11,795
8	$8,590	$1,305	$209	$1,659	$11,763
9	$8,590	$1,305	$235	$1,658	$11,788
10	$8,590	$1,305	$203	$1,657	$11,754
11	$8,590	$1,305	$228	$1,656	$11,779
12	$8,590	$1,305	$196	$1,656	$11,747
13	$8,590	$1,305	$222	$1,655	$11,773
14	$8,590	$1,305	$193	$1,655	$11,743
15	$8,590	$1,305	$219	$1,655	$11,769
16	$8,590	$1,305	$189	$1,655	$11,738
17	$8,590	$1,305	$215	$1,654	$11,765
18	$8,590	$1,305	$186	$1,654	$11,735
19	$8,590	$1,305	$213	$1,654	$11,763
20	$8,590	$1,305	$185	$1,654	$11,734
21	$8,590	$1,305	$211	$1,654	$11,760
22	$8,590	$1,305	$182	$1,654	$11,731
23	$8,590	$1,305	$209	$1,654	$11,758
24	$8,590	$1,305	$180	$1,654	$11,729
25	$8,590	$1,305	$207	$1,654	$11,756
26	$8,590	$1,305	$178	$1,654	$11,727
27	$8,590	$1,305	$206	$1,654	$11,755
28	$8,590	$1,305	$177	$1,654	$11,726
29	$8,590	$1,305	$204	$1,654	$11,753
30	$8,590	$1,305	$175	$1,654	$11,724
31	$8,590	$1,305	$203	$1,654	$11,752
32	$8,590	$1,305	$175	$1,654	$11,724
33	$8,590	$1,305	$202	$1,654	$11,751
34	$8,590	$1,305	$173	$1,654	$11,722
35	$8,590	$1,305	$201	$1,654	$11,750
36	$8,590	$1,305	$172	$1,654	$11,721
37	$8,590	$1,305	$200	$1,654	$11,749
38	$8,590	$1,305	$172	$1,654	$11,721
39	$8,590	$1,305	$199	$1,654	$11,748
40	$8,590	$1,305	$171	$1,654	$11,720

(a) Electricity cost based on $0.0066 per Kwatts-hr; Treated wastewater cost based on $0.007 pre m^3.

Figure 7.4 Detailed cash flow diagram, over 40 years, for the base case simulation of the general conceptual design system using the areal distribution model, **orientation layout (1)**, approach for the USA.

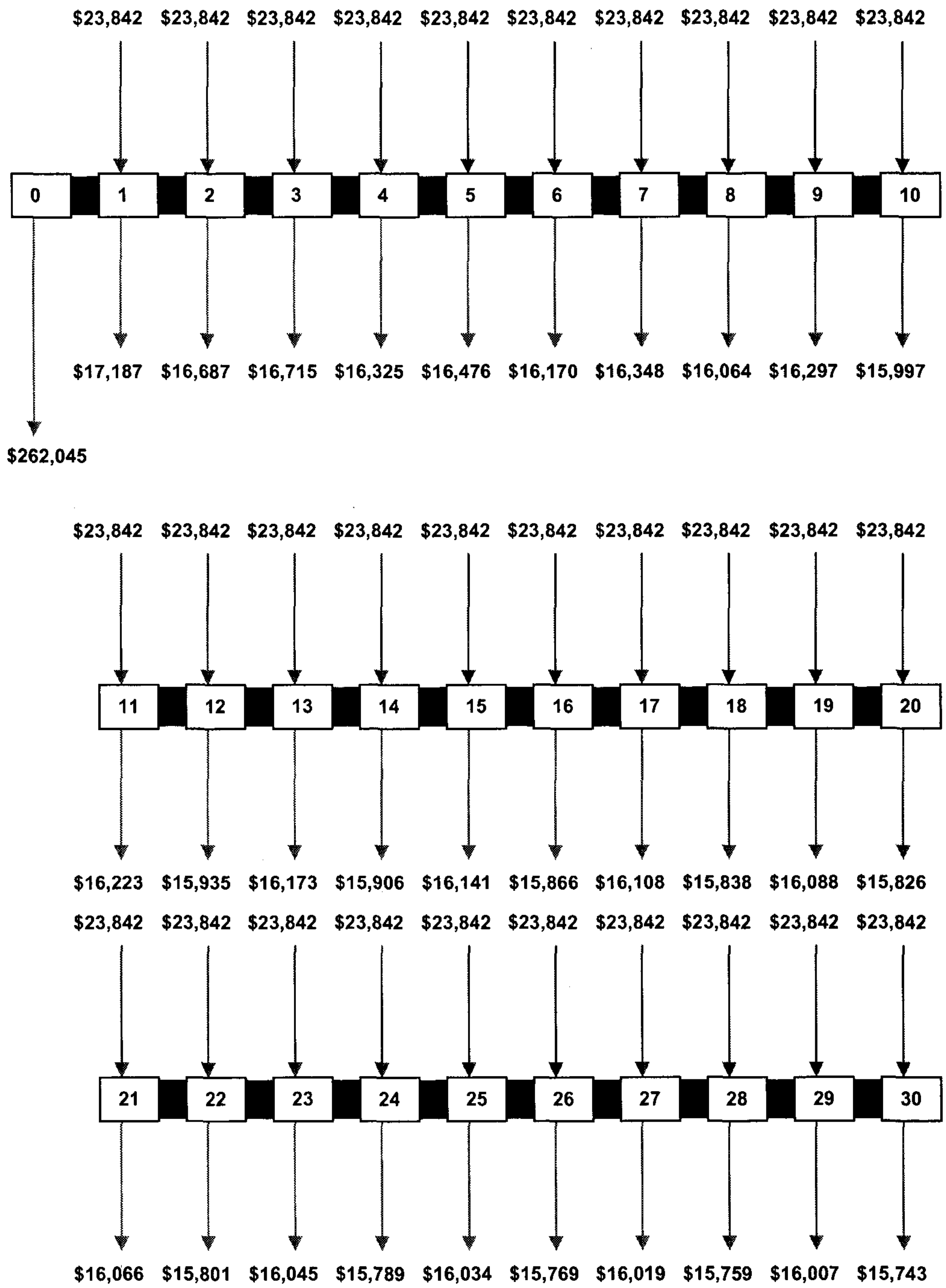

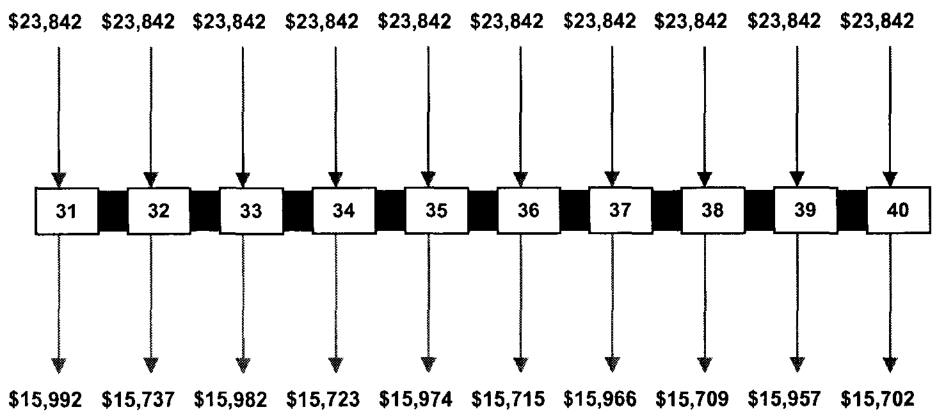

Figure 7.5 Detailed cash flow diagram, over 40 years, for the base case simulation of the general conceptual design system using the areal distribution model, **orientation layout (1)**, approach, for Kuwait.

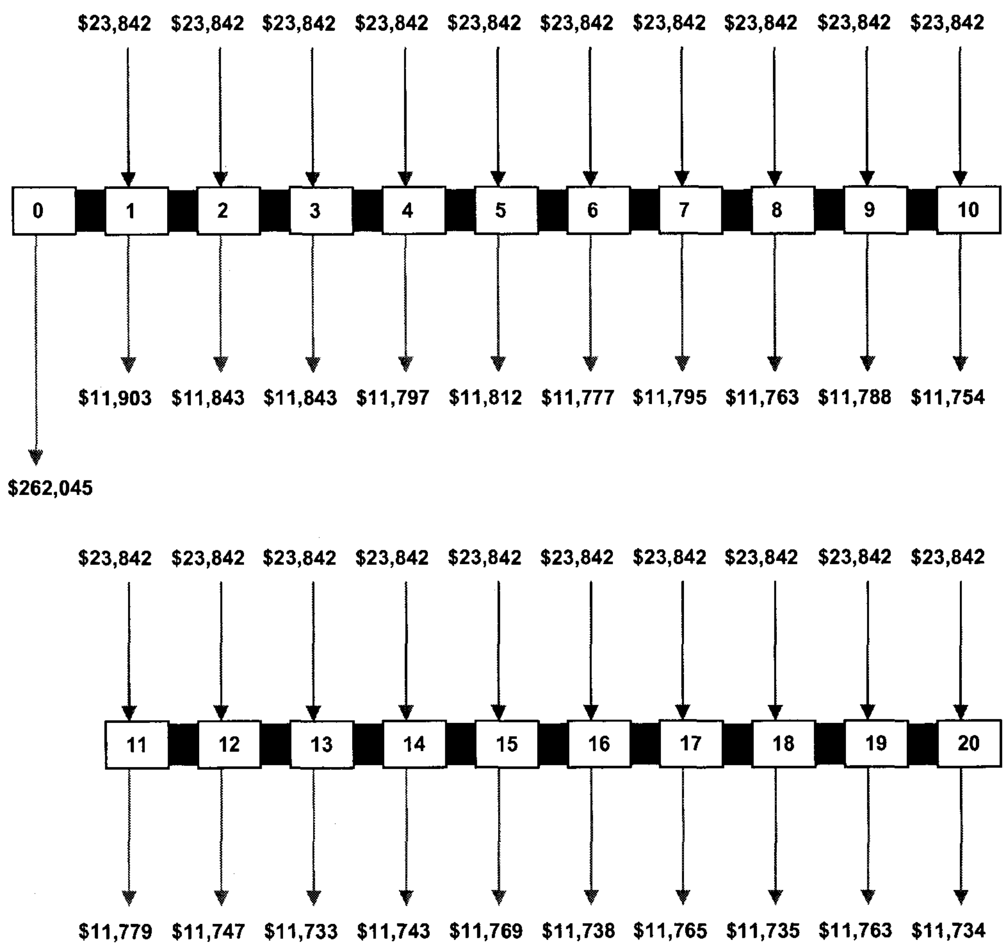

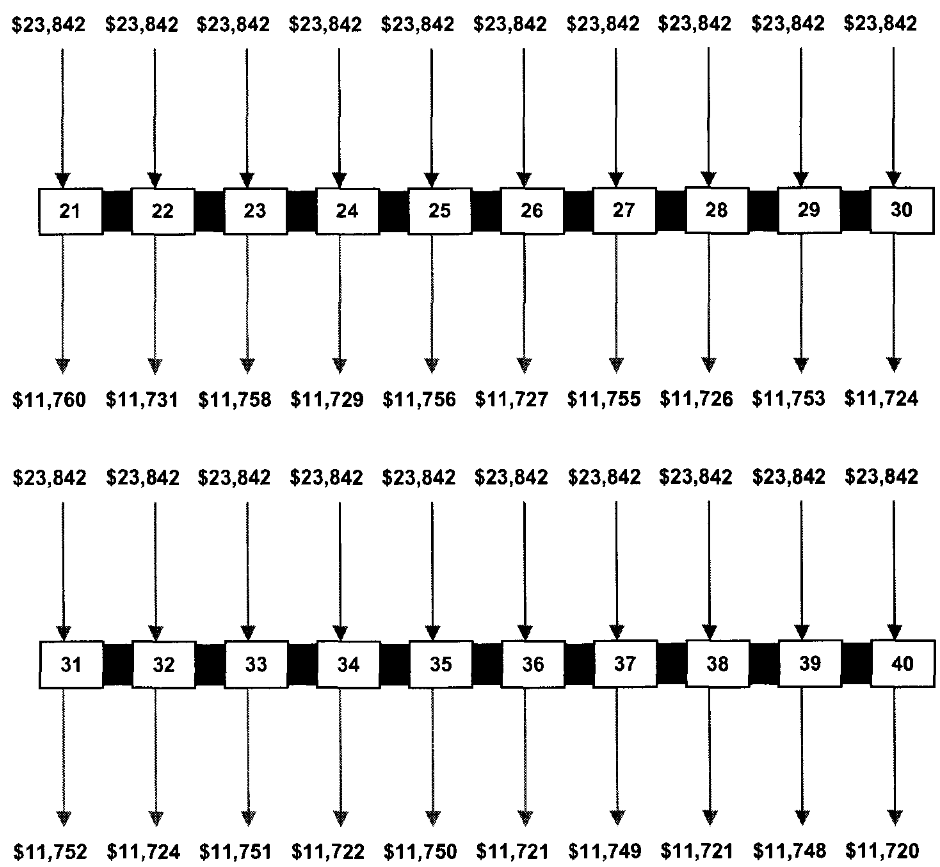
$23,842 $23,842 $23,842 $23,842 $23,842 $23,842 $23,842 $23,842 $23,842 $23,842
21 22 23 24 25 26 27 28 29 30
$11,760 $11,731 $11,758 $11,729 $11,756 $11,727 $11,755 $11,726 $11,753 $11,724
$23,842 $23,842 $23,842 $23,842 $23,842 $23,842 $23,842 $23,842 $23,842 $23,842
31 32 33 34 35 36 37 38 39 40
$11,752 $11,724 $11,751 $11,722 $11,750 $11,721 $11,749 $11,721 $11,748 $11,720

Table 7.10 Detailed operation and maintenance cost prices, over 40 years, for the base case simulation of the general conceptual design system using the areal distribution, **orientation layout (2)**, approach model for the USA.

Year	Operation & Maintenance Cost ($/year)				
	R.O. Maintenance	Pump Maintenance	Total Power consumed (a)	Treated wastewater (b)	Sum
1	$8,590	$1,305	$2,969	$4,323	$17,187
2	$8,590	$1,305	$2,498	$4,307	$16,700
3	$8,590	$1,305	$2,552	$4,295	$16,742
4	$8,590	$1,305	$2,156	$4,285	$16,336
5	$8,590	$1,305	$2,334	$4,278	$16,507
6	$8,590	$1,305	$2,027	$4,273	$16,195
7	$8,590	$1,305	$2,192	$4,268	$16,355
8	$8,590	$1,305	$1,918	$4,265	$16,078
9	$8,590	$1,305	$2,153	$4,262	$16,310
10	$8,590	$1,305	$1,855	$4,260	$16,010
11	$8,590	$1,305	$2,078	$4,259	$16,232
12	$8,590	$1,305	$1,799	$4,257	$15,951
13	$8,590	$1,305	$2,037	$4,256	$16,189
14	$8,590	$1,305	$1,760	$4,256	$15,911
15	$8,590	$1,305	$2,005	$4,255	$16,155
16	$8,590	$1,305	$1,734	$4,255	$15,883
17	$8,590	$1,305	$1,979	$4,254	$16,128
18	$8,590	$1,305	$1,715	$4,254	$15,864
19	$8,590	$1,305	$1,957	$4,254	$16,106
20	$8,590	$1,305	$1,694	$4,254	$15,842
21	$8,590	$1,305	$1,935	$4,253	$16,083
22	$8,590	$1,305	$1,677	$4,253	$15,825
23	$8,590	$1,305	$1,923	$4,253	$16,072
24	$8,590	$1,305	$1,661	$4,253	$15,809
25	$8,590	$1,305	$1,906	$4,253	$16,054
26	$8,590	$1,305	$1,648	$4,253	$15,796
27	$8,590	$1,305	$1,899	$4,253	$16,047
28	$8,590	$1,305	$1,641	$4,253	$15,789
29	$8,590	$1,305	$1,890	$4,253	$16,037
30	$8,590	$1,305	$1,632	$4,253	$15,779
31	$8,590	$1,305	$1,880	$4,253	$16,028
32	$8,590	$1,305	$1,621	$4,253	$15,769
33	$8,590	$1,305	$1,867	$4,253	$16,015
34	$8,590	$1,305	$1,611	$4,253	$15,758
35	$8,590	$1,305	$1,859	$4,253	$16,006
36	$8,590	$1,305	$1,600	$4,253	$15,748
37	$8,590	$1,305	$1,848	$4,253	$15,996
38	$8,590	$1,305	$1,592	$4,253	$15,739
39	$8,590	$1,305	$1,843	$4,253	$15,991
40	$8,590	$1,305	$1,585	$4,253	$15,733

(a) Electricity cost based on $0.06 per Kwatts-hr; Treated wastewater cost based on $0.018 pre m^3.

Table 7.11 Detailed operation and maintenance cost prices, over 40 years, for the base case simulation of the general conceptual design system using the areal distribution, **orientation layout (2)**, approach model for Kuwait.

Year	Operation & Maintenance Cost ($ /year)				
	R.O. Maintenance	Pump Maintenance	Total Power consumed (a)	Treated wastewater (b)	Sum
1	$8,590	$1,305	$327	$1,681	$11,903
2	$8,590	$1,305	$275	$1,675	$11,845
3	$8,590	$1,305	$281	$1,670	$11,846
4	$8,590	$1,305	$237	$1,667	$11,799
5	$8,590	$1,305	$257	$1,664	$11,815
6	$8,590	$1,305	$223	$1,662	$11,780
7	$8,590	$1,305	$241	$1,660	$11,796
8	$8,590	$1,305	$211	$1,659	$11,765
9	$8,590	$1,305	$237	$1,658	$11,789
10	$8,590	$1,305	$204	$1,657	$11,756
11	$8,590	$1,305	$229	$1,656	$11,780
12	$8,590	$1,305	$198	$1,656	$11,749
13	$8,590	$1,305	$224	$1,655	$11,774
14	$8,590	$1,305	$194	$1,655	$11,744
15	$8,590	$1,305	$221	$1,655	$11,770
16	$8,590	$1,305	$191	$1,655	$11,740
17	$8,590	$1,305	$218	$1,654	$11,767
18	$8,590	$1,305	$189	$1,654	$11,738
19	$8,590	$1,305	$215	$1,654	$11,764
20	$8,590	$1,305	$186	$1,654	$11,735
21	$8,590	$1,305	$213	$1,654	$11,762
22	$8,590	$1,305	$184	$1,654	$11,733
23	$8,590	$1,305	$212	$1,654	$11,761
24	$8,590	$1,305	$183	$1,654	$11,732
25	$8,590	$1,305	$210	$1,654	$11,759
26	$8,590	$1,305	$181	$1,654	$11,730
27	$8,590	$1,305	$209	$1,654	$11,758
28	$8,590	$1,305	$180	$1,654	$11,729
29	$8,590	$1,305	$208	$1,654	$11,757
30	$8,590	$1,305	$179	$1,654	$11,728
31	$8,590	$1,305	$207	$1,654	$11,756
32	$8,590	$1,305	$178	$1,654	$11,727
33	$8,590	$1,305	$205	$1,654	$11,754
34	$8,590	$1,305	$177	$1,654	$11,726
35	$8,590	$1,305	$204	$1,654	$11,753
36	$8,590	$1,305	$176	$1,654	$11,725
37	$8,590	$1,305	$203	$1,654	$11,752
38	$8,590	$1,305	$175	$1,654	$11,724
39	$8,590	$1,305	$203	$1,654	$11,752
40	$8,590	$1,305	$174	$1,654	$11,723

(a) Electricity cost based on $0.0066 per Kwatts-hr; Treated wastewater cost based on $0.007 pre m^3.

Figure 7.6 Detailed cash flow diagram, over 40 years, for the base case simulation of the general conceptual design system using the areal distribution model, **orientation layout (2)**, approach for the USA.

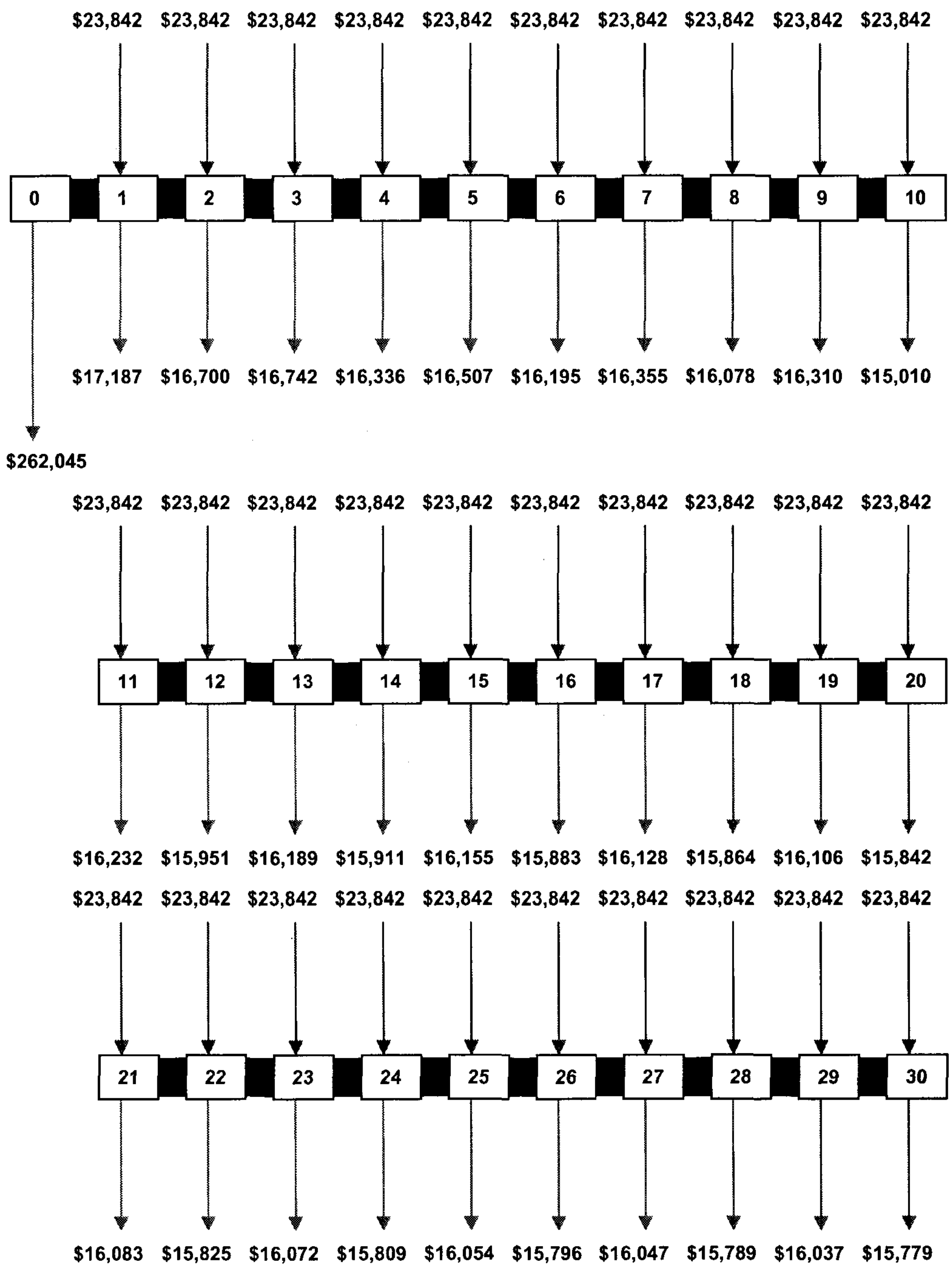

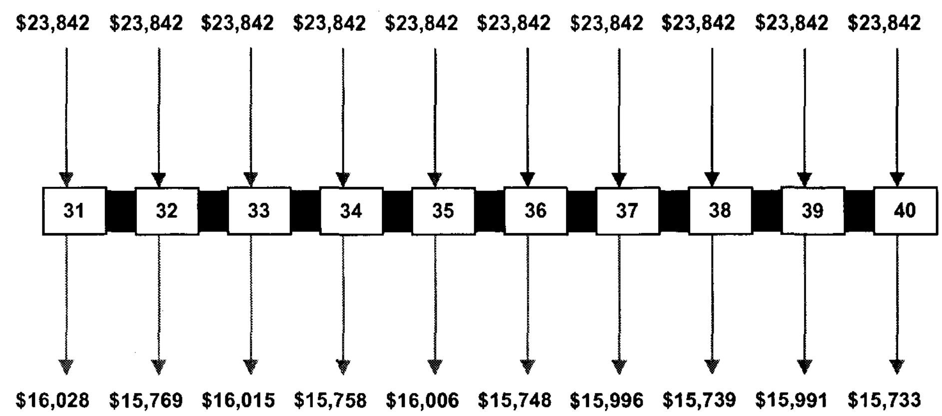

Figure 7.7 Detailed cash flow diagram, over 40 years, for the base case simulation of the general conceptual design system using the areal distribution model, **orientation layout (2)**, approach, for Kuwait.

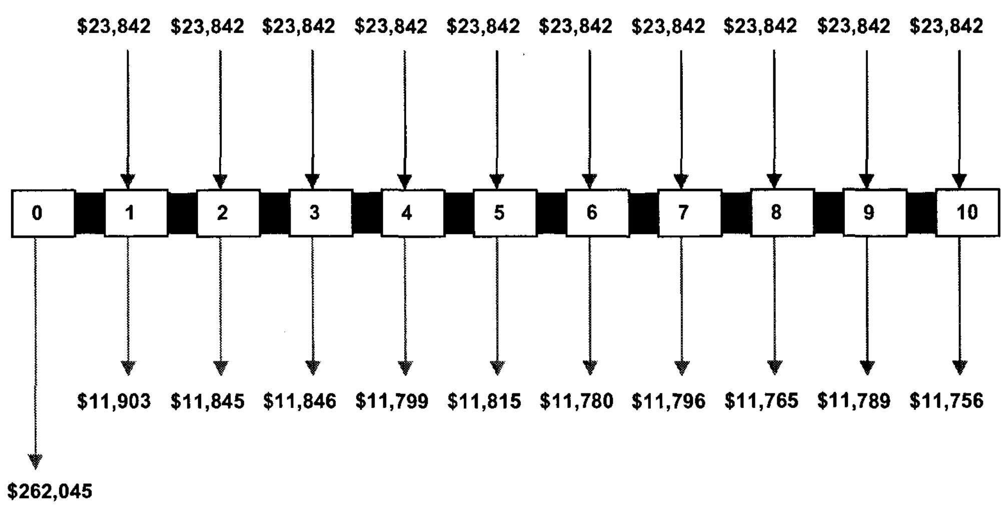

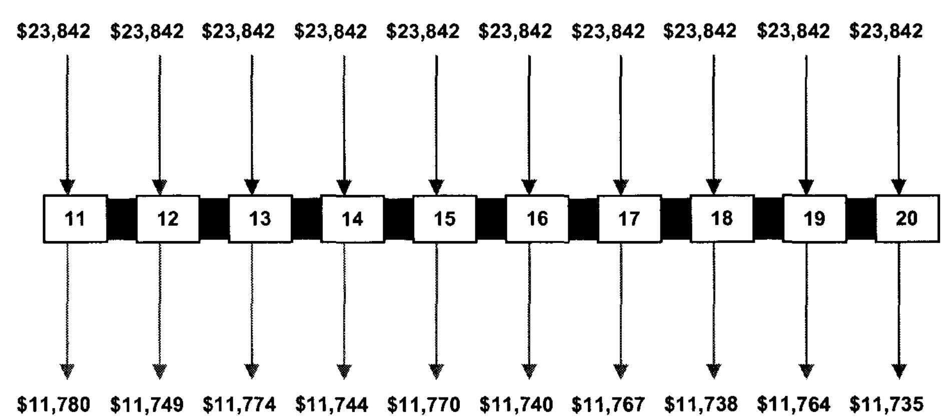

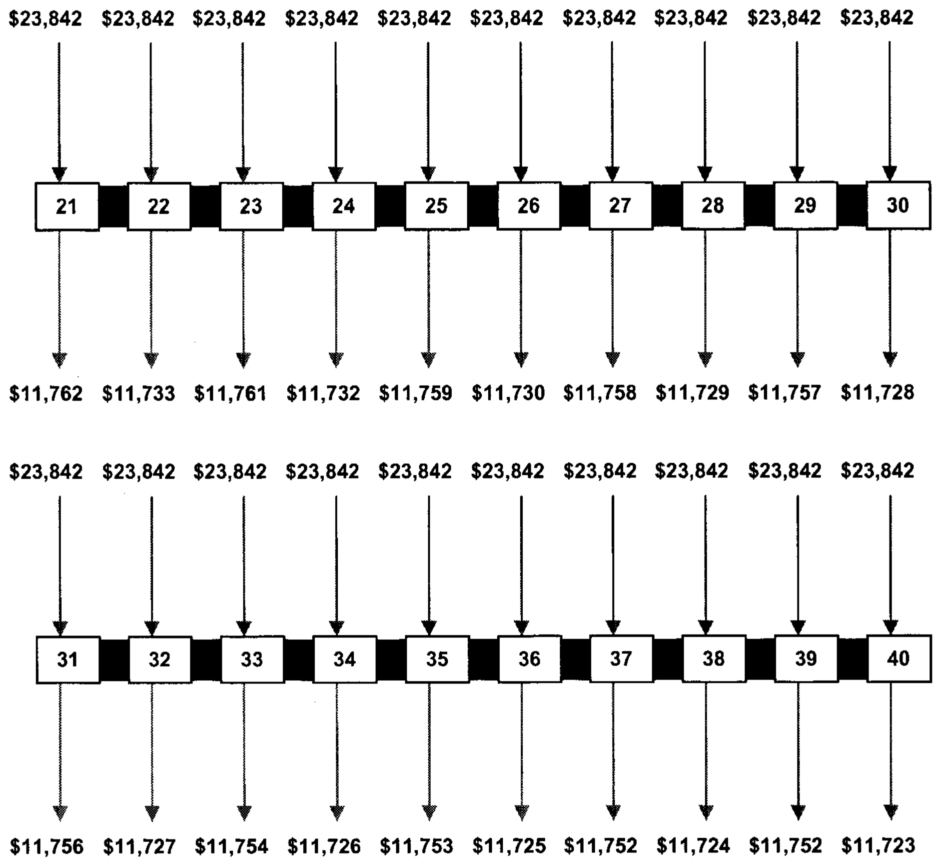
$23,842 $23,842 $23,842 $23,842 $23,842 $23,842 $23,842 $23,842 $23,842 $23,842
21 22 23 24 25 26 27 28 29 30
$11,762 $11,733 $11,761 $11,732 $11,759 $11,730 $11,758 $11,729 $11,757 $11,728
$23,842 $23,842 $23,842 $23,842 $23,842 $23,842 $23,842 $23,842 $23,842 $23,842
31 32 33 34 35 36 37 38 39 40
$11,756 $11,727 $11,754 $11,726 $11,753 $11,725 $11,752 $11,724 $11,752 $11,723

Table 7.12 Detailed operation and maintenance cost prices, over 40 years, for the base case simulation of the general conceptual design system using the areal distribution, **orientation layout (3)**, approach model for the USA.

Year	Operation & Maintenance Cost ($/year)				
	R.O. Maintenance	Pump Maintenance	Total Power consumed (a)	Treated wastewater (b)	Sum
1	$8,590	$1,305	$1,975	$4,323	$16,193
2	$8,590	$1,305	$1,742	$4,307	$15,944
3	$8,590	$1,305	$1,865	$4,295	$16,055
4	$8,590	$1,305	$1,681	$4,285	$15,862
5	$8,590	$1,305	$1,820	$4,278	$15,993
6	$8,590	$1,305	$1,650	$4,273	$15,817
7	$8,590	$1,305	$1,793	$4,268	$15,957
8	$8,590	$1,305	$1,630	$4,265	$15,790
9	$8,590	$1,305	$1,776	$4,262	$15,934
10	$8,590	$1,305	$1,616	$4,260	$15,772
11	$8,590	$1,305	$1,765	$4,259	$15,918
12	$8,590	$1,305	$1,607	$4,257	$15,759
13	$8,590	$1,305	$1,756	$4,256	$15,908
14	$8,590	$1,305	$1,600	$4,256	$15,750
15	$8,590	$1,305	$1,750	$4,255	$15,900
16	$8,590	$1,305	$1,594	$4,255	$15,744
17	$8,590	$1,305	$1,745	$4,254	$15,894
18	$8,590	$1,305	$1,590	$4,254	$15,739
19	$8,590	$1,305	$1,741	$4,254	$15,889
20	$8,590	$1,305	$1,586	$4,254	$15,734
21	$8,590	$1,305	$1,737	$4,253	$15,885
22	$8,590	$1,305	$1,583	$4,253	$15,731
23	$8,590	$1,305	$1,734	$4,253	$15,882
24	$8,590	$1,305	$1,580	$4,253	$15,728
25	$8,590	$1,305	$1,732	$4,253	$15,880
26	$8,590	$1,305	$1,578	$4,253	$15,726
27	$8,590	$1,305	$1,729	$4,253	$15,877
28	$8,590	$1,305	$1,575	$4,253	$15,723
29	$8,590	$1,305	$1,727	$4,253	$15,875
30	$8,590	$1,305	$1,573	$4,253	$15,721
31	$8,590	$1,305	$1,725	$4,253	$15,873
32	$8,590	$1,305	$1,572	$4,253	$15,719
33	$8,590	$1,305	$1,724	$4,253	$15,871
34	$8,590	$1,305	$1,570	$4,253	$15,718
35	$8,590	$1,305	$1,722	$4,253	$15,870
36	$8,590	$1,305	$1,568	$4,253	$15,716
37	$8,590	$1,305	$1,721	$4,253	$15,869
38	$8,590	$1,305	$1,567	$4,253	$15,715
39	$8,590	$1,305	$1,719	$4,253	$15,867
40	$8,590	$1,305	$1,566	$4,253	$15,714

(a) Electricity cost based on $0.06 per Kwatts-hr; Treated wastewater cost based on $0.018 pre m^3.

Table 7.13 Detailed operation and maintenance cost prices, over 40 years, for the base case simulation of the general conceptual design system using the areal distribution, **orientation layout (3)**, approach model for Kuwait.

Year	Operation & Maintenance Cost ($ /year)				
	R.O. Maintenance	Pump Maintenance	Total Power consumed (a)	Treated wastewater (b)	Sum
1	$8,590	$1,305	$217	$1,681	$11,793
2	$8,590	$1,305	$192	$1,675	$11,761
3	$8,590	$1,305	$205	$1,670	$11,770
4	$8,590	$1,305	$185	$1,667	$11,746
5	$8,590	$1,305	$200	$1,664	$11,759
6	$8,590	$1,305	$181	$1,662	$11,738
7	$8,590	$1,305	$197	$1,660	$11,752
8	$8,590	$1,305	$179	$1,659	$11,733
9	$8,590	$1,305	$195	$1,658	$11,748
10	$8,590	$1,305	$178	$1,657	$11,730
11	$8,590	$1,305	$194	$1,656	$11,745
12	$8,590	$1,305	$177	$1,656	$11,727
13	$8,590	$1,305	$193	$1,655	$11,743
14	$8,590	$1,305	$176	$1,655	$11,726
15	$8,590	$1,305	$192	$1,655	$11,742
16	$8,590	$1,305	$175	$1,655	$11,725
17	$8,590	$1,305	$192	$1,654	$11,741
18	$8,590	$1,305	$175	$1,654	$11,724
19	$8,590	$1,305	$191	$1,654	$11,741
20	$8,590	$1,305	$174	$1,654	$11,724
21	$8,590	$1,305	$191	$1,654	$11,740
22	$8,590	$1,305	$174	$1,654	$11,723
23	$8,590	$1,305	$191	$1,654	$11,740
24	$8,590	$1,305	$174	$1,654	$11,723
25	$8,590	$1,305	$190	$1,654	$11,739
26	$8,590	$1,305	$174	$1,654	$11,722
27	$8,590	$1,305	$190	$1,654	$11,739
28	$8,590	$1,305	$173	$1,654	$11,722
29	$8,590	$1,305	$190	$1,654	$11,739
30	$8,590	$1,305	$173	$1,654	$11,722
31	$8,590	$1,305	$190	$1,654	$11,739
32	$8,590	$1,305	$173	$1,654	$11,722
33	$8,590	$1,305	$190	$1,654	$11,738
34	$8,590	$1,305	$173	$1,654	$11,722
35	$8,590	$1,305	$189	$1,654	$11,738
36	$8,590	$1,305	$172	$1,654	$11,721
37	$8,590	$1,305	$189	$1,654	$11,738
38	$8,590	$1,305	$172	$1,654	$11,721
39	$8,590	$1,305	$189	$1,654	$11,738
40	$8,590	$1,305	$172	$1,654	$11,721

(a) Electricity cost based on $0.0066 per Kwatts-hr; Treated wastewater cost based on $0.007 pre m^3.

Figure 7.8 Detailed cash flow diagram, over 40 years, for the base case simulation of the general conceptual design system using areal distribution model, **orientation layout (3)**, approach, for the USA.

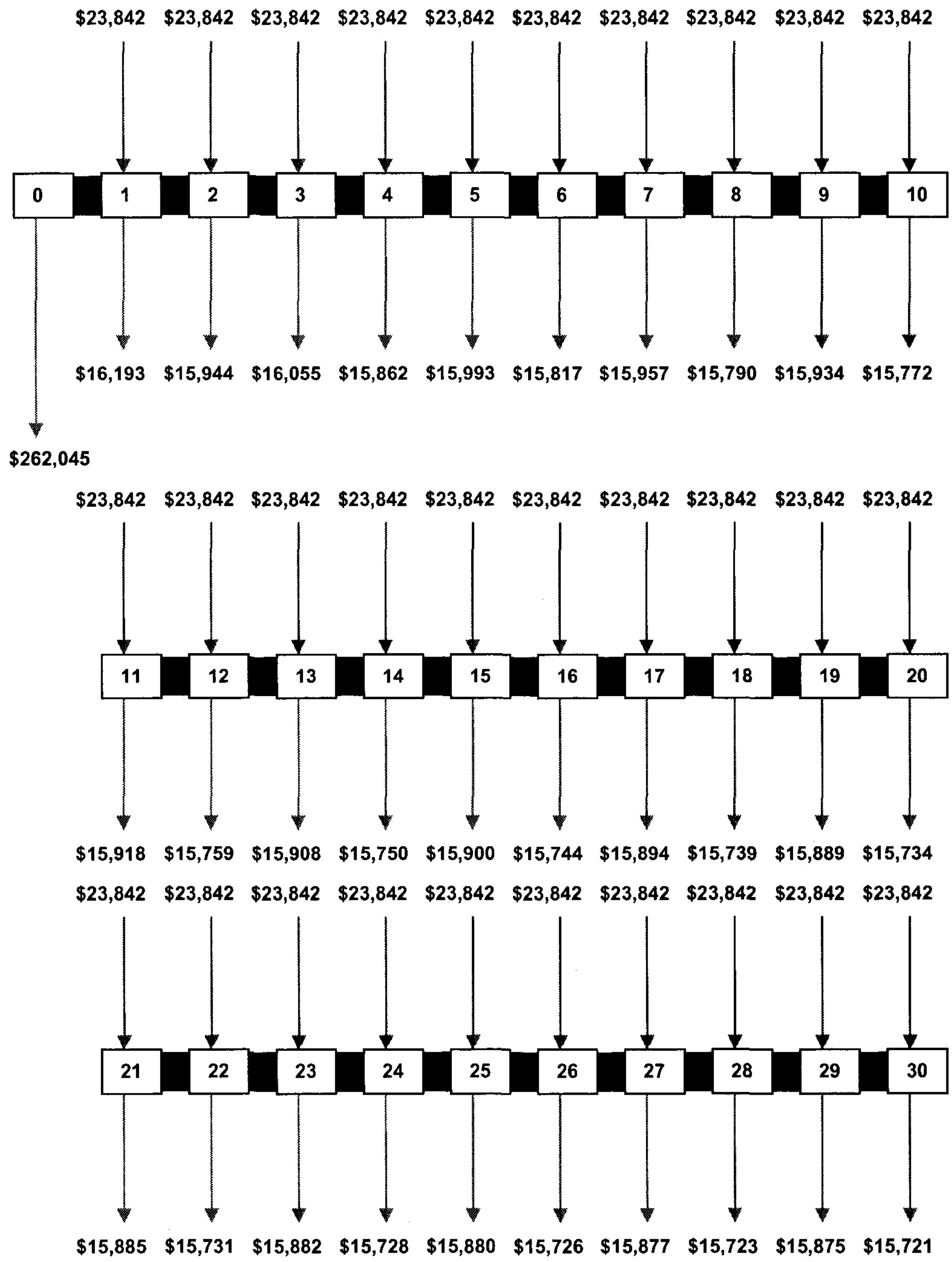

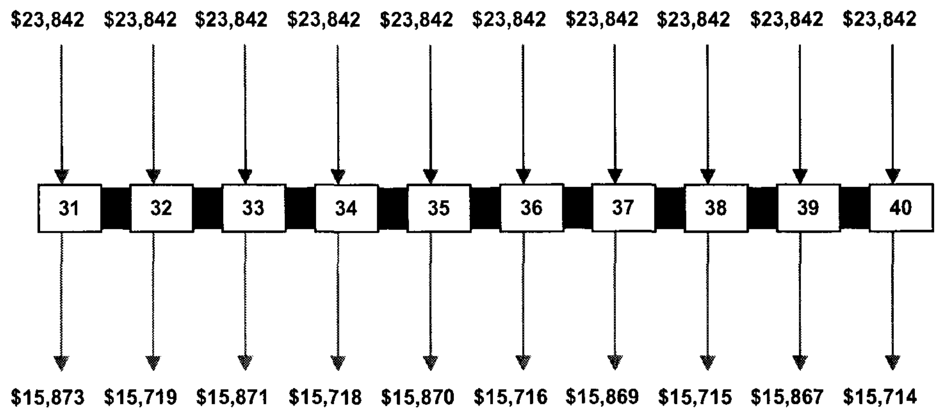

Figure 7.9 Detailed cash flow diagram, over 40 years, for the base case simulation of the general conceptual design system using the areal distribution model, **orientation layout (3)**, approach, for Kuwait.

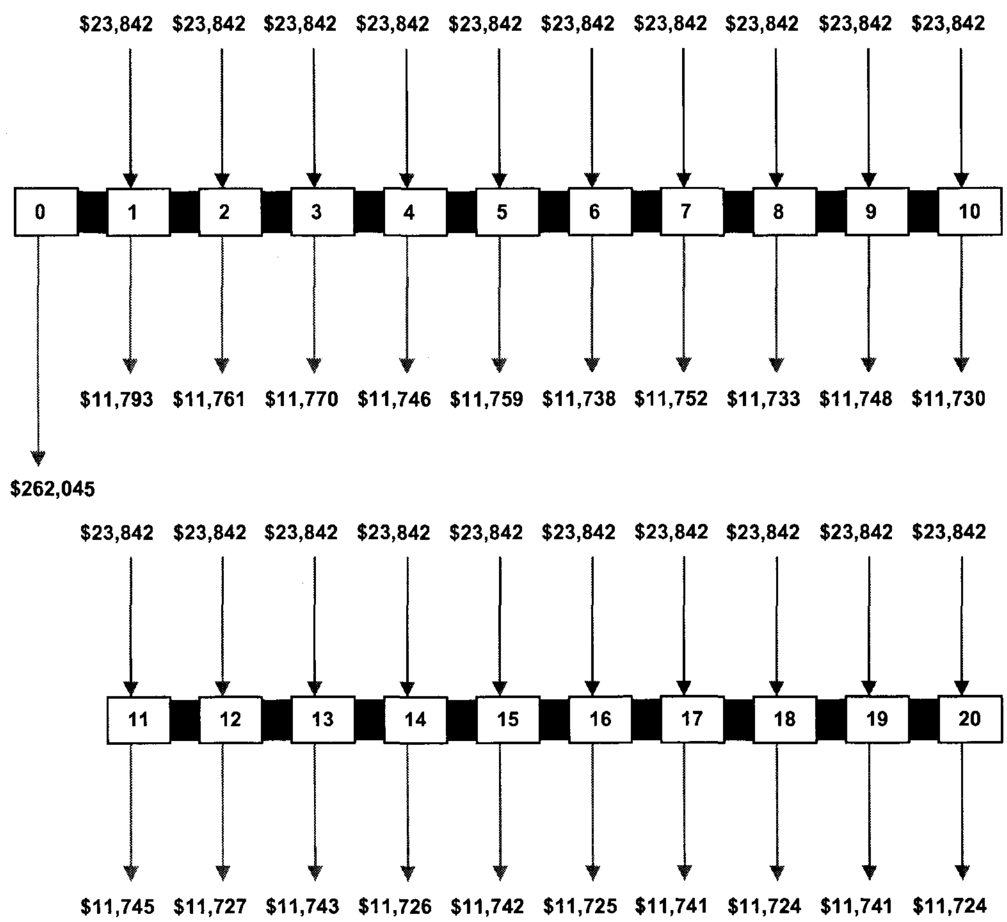

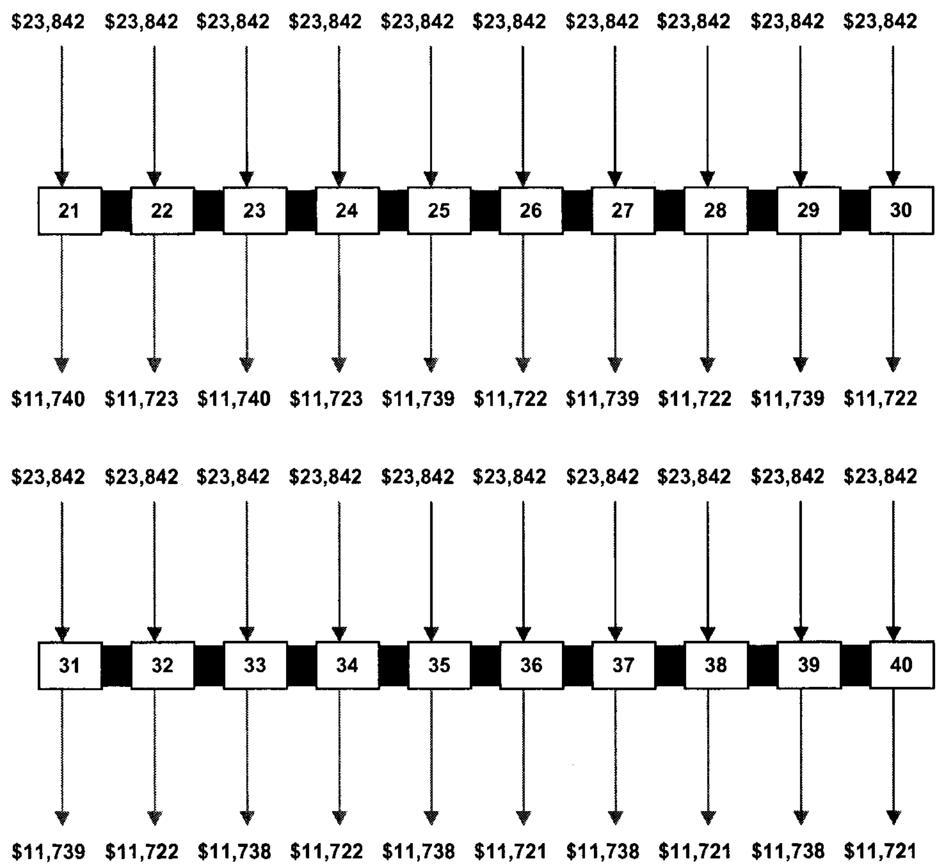

The benefit-cost ratio for the base case of the general conceptual design system using the lump model approach and the areal distribution model for the three orientation layouts were calculated for ranges of different interest rates (2%, 4%, 6%, and 8%). These benefit-cost ratios values were calculated for USA and Kuwait conditions. Moreover, calculation of the Kuwait benefit-cost ratio was calculated for electrical power consumption with and without the government electrical power subsidy (Table 7.14, and Figures 7.10, 7.11, and 7.12).

Table 7.14 Benefit-Cost ratios for ranges of different interest rates.

Method	Interest Rate %	Benefit –Cost Ratio		
		USA	Kuwait [a]	Kuwait [b]
Lump Model	2	0.9219	1.1159	1.0261
Lump Model	4	0.8063	0.9525	0.8849
Lump Model	6	0.7054	0.8161	0.7650
Lump Model	8	0.6208	0.7058	0.6665
Areal Distribution Model, Orientation Layout (1)	2	0.9284	1.1169	1.0341
Areal Distribution Model, Orientation Layout (1)	4	0.8110	0.9532	0.8906
Areal Distribution Model, Orientation Layout (1)	6	0.7090	0.8166	0.7691
Areal Distribution Model, Orientation Layout (1)	8	0.6235	0.7062	0.6696
Areal Distribution Model, Orientation Layout (2)	2	0.9277	1.1168	1.0332
Areal Distribution Model, Orientation Layout (2)	4	0.8105	0.9531	0.8900
Areal Distribution Model, Orientation Layout (2)	6	0.7086	0.8166	0.7687
Areal Distribution Model, Orientation Layout (2)	8	0.6232	0.7061	0.6692
Areal Distribution Model, Orientation Layout (3)	2	0.9375	1.1184	1.0453
Areal Distribution Model, Orientation Layout (3)	4	0.8192	0.9544	0.9004
Areal Distribution Model, Orientation Layout (3)	6	0.7161	0.8176	0.7774
Areal Distribution Model, Orientation Layout (3)	8	0.6296	0.7070	0.6766

[a] With electrical power cost subsidy ($0.0066 per Kwatts-Hr); [b] Without electrical power cost subsidy ($0.0595 per Kwatts-Hr).

Figure 7.10 Benefit-Cost ratios for ranges of different interest rates for the USA.

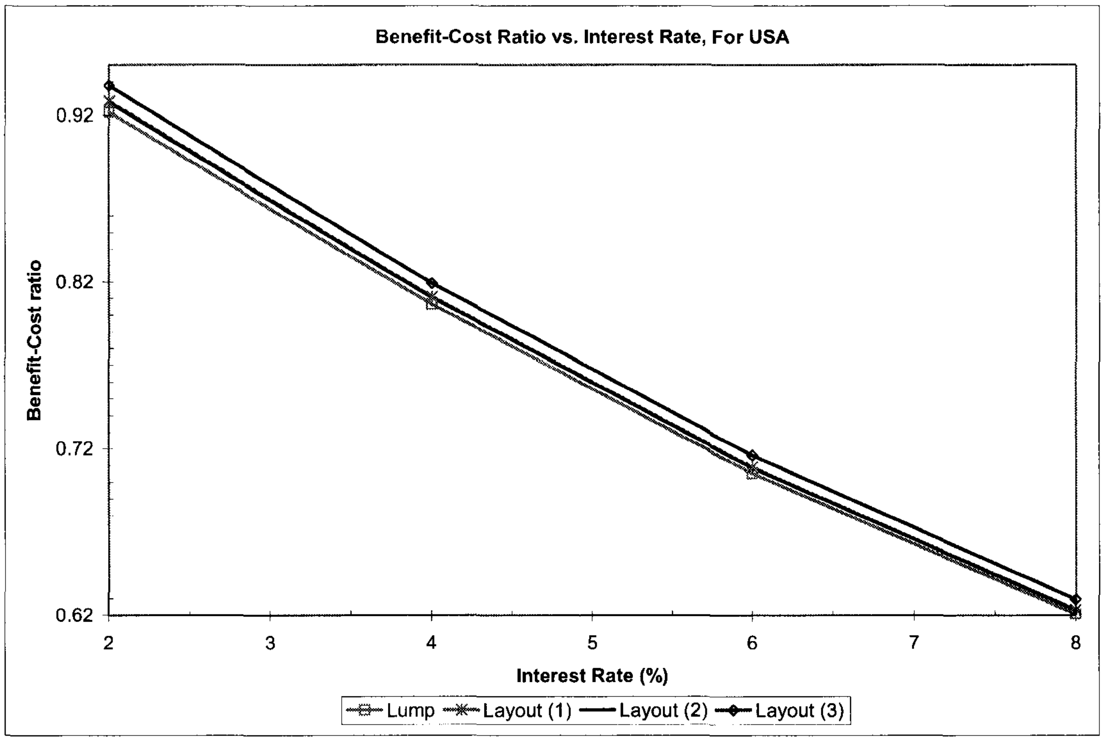

Figure 7.11 Benefit-Cost ratios for ranges of different interest rates for Kuwait with electrical subsidy.

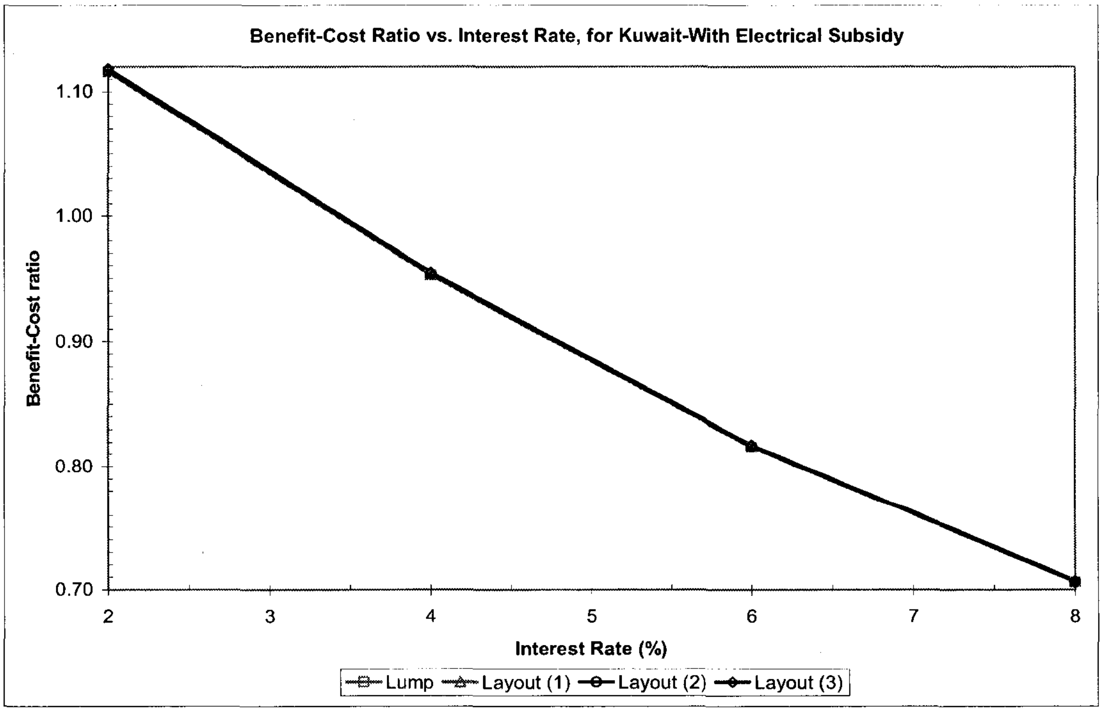

Figure 7.12 Benefit-Cost ratios for ranges of different interest rates for Kuwait without electrical subsidy.

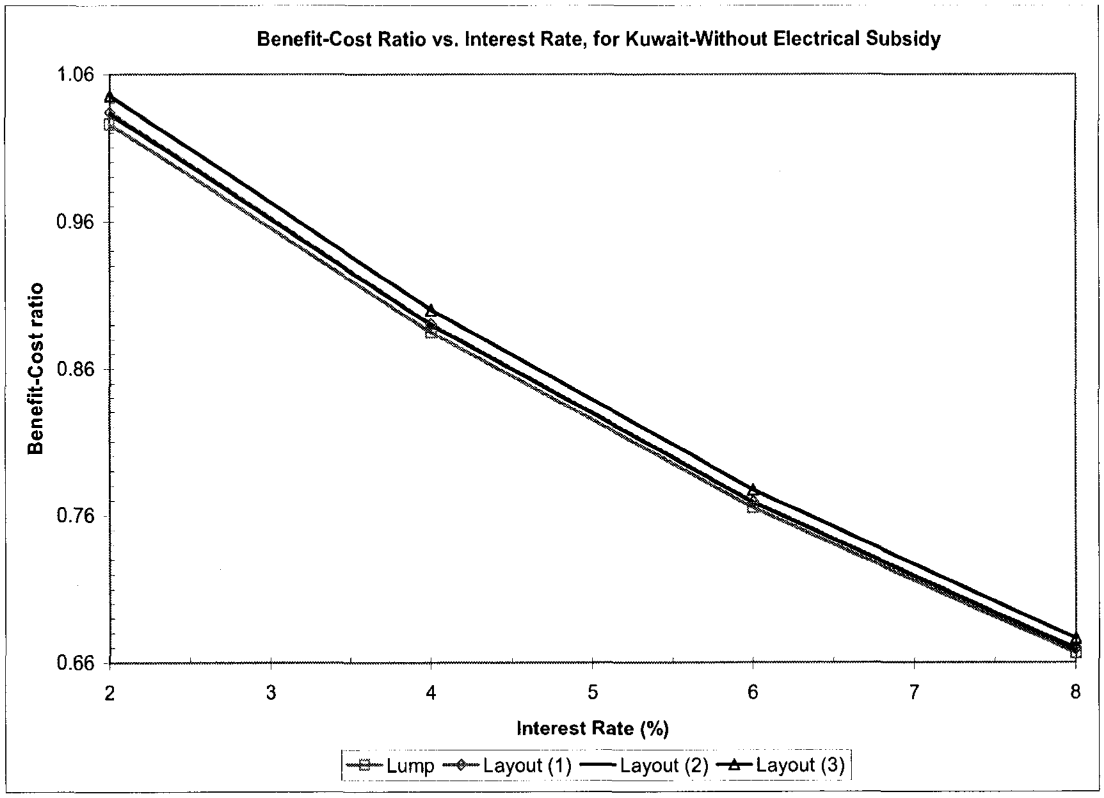

From Table 7.14, it is obvious that the areal distribution model (orientation layout (3)) simulation approach was the most benefit-cost ratio efficient for all possible ranges of interest rates. Moreover, the second most efficient benefit-cost ratio is the areal distribution model (orientation layout (1)), then, the areal distribution model (orientation layout (2)), and finally the lump model for all possible ranges of interest rates. The benefit-cost ratio was almost equal for both the areal distribution model's orientation layout (1) and orientation layout (2) for the ranges of interest rates. The percent decrease in benefit-cost ratios for the USA condition between the lump model and the areal distribution model orientation layout (1) is 0.70%, 0.58%, 0.51%, and 0.43% for the interest rates of 2%, 4%, 6%, and 8% respectively. Moreover, the percent decrease in benefit cost ratios for Kuwait with the electrical power subsidy condition between lump model and the areal distribution model orientation layout (1) is 0.0.09%, 0.07%, 0.06%, and 0.06% for the interest rates of 2%, 4%, 6%, and 8% respectively. Furthermore, the percent decrease in benefit-cost ratios for Kuwait without the electrical power subsidy condition between the lump model and the areal distribution model orientation layout (1) is 0.80%, 0.64%, 0.53%, and 0.46% for the interest rates of 2%, 4%, 6%, and 8% respectively. Therefore, the variation difference between the areal distribution orientation layout (1) model and the lump model benefit-cost ratio is minute for all the interest rate ranges. In a conclusion, the lump model approach can safely be substituted for the areal distribution orientation layout (1) and/or orientation layout (2).

The benefit-cost ratios for all the simulation approaches methods were less than 1, except for the Kuwait condition at interest rate of 2%. As an initial conclusion, from the benefit-cost ratio results, the general conceptual design system is unfeasible for most of the simulation method approaches when the interest rate is higher than 2%. The conceptual design system for the base case approach simulations may not be feasible in the United State of America due to the benefit-cost ratio (less than 1). But for Kuwait, specifically, and the Middle East, in general, food-self efficiency is one of the main aspects of the government's higher political strategy. For that reason, oil wealth is used as a highly valuable commodity traded for food. Thus, the general conceptual design model for the base case simulation can be strongly economically feasible, especially if utilizing the orientation layout (3) design with the 2% interest rate and the electrical power subsidy, where the benefit-cost ratio = 1.1184. Of note, now a day, the government of Kuwait provides long period loans (up to 50 years) with 2% interest rates for small to medium size projects (Industrial Bank of Kuwait). Personally, I strongly recommend the utilization of the orientation layout (1) design, particularly for the low interest rate, where the benefit-cost ratio for 2% is equal to 1.1169. The utilization of orientation layout (1) will give us the benefit, to a larger extent, of enhancing the groundwater salt concentration, which will reduce the vulnerability of possible lateral reduction of the operation system due to emergencies or cost effects. Furthermore, the enhancement of groundwater salt concentration will have a positive impact on the ecosystem and the environment.

CHAPTER 8

CONCLUSIONS AND RECOMMENDATIONS

8.1 Conclusions

Water scarcity is the predominant issue in the arid and semi arid countries. Moreover, growing population, rising standard of living and expanding opportunities have exerted increasing demands for varied needs for water all over the world. The Middle East, specifically, has seen rapid economic development caused by sudden increases in oil revenues. In addition to water scarcity, much of the groundwater in the Middle East is of marginal and brackish quality, which puts more burdens on utilizing the groundwater as a water supply for crop production. Therefore, water sustainability, quality and quantity, is an essential element for food self-sufficiency.

The aim of this dissertation was to design a conceptual system to provide a sustainable water source at a feasible cost. The conceptual design system was developed to address the problem of water scarcity and sustainability in general, and specifically to represent the Kuwaiti water quality and quantity limitation problem. The conceptual design system consists primarily of utilizing brackish groundwater in conjunction with treated wastewater augmentation and a reverse osmosis unit. Therefore, the treated wastewater augmentation was utilized to help relieve and restore the aquifer from over mining. Moreover, the reverse osmosis unit was utilized as a main source of good quality water to be used for irrigation purposes. The dissertation considered two types of simulation models for the conceptual design system approach. These models are the lump model approach and the areal distribution model approach. The lump model approach was carried out through the construction of a simplified model approach utilizing the Visual Basic model. On the other hand, the areal distribution model approach was carried out through the utilization of the Visual MODFLOW and MT3D simulation model approach. The areal distribution simulation model approach was employed for more in depth analysis and a more realistic project design.

To test the sensitivity and the durability of the conceptual design system, the lump model simulation approach was simulated for different ranges of hydrologic, hydrogeologic, and climatic parameters to determine the total power and treated wastewater consumption. From the sensitivity test results, the increase in evapotranspiration had the highest increase effect on the system total power consumption per unit area and the highest increase effect on the treated wastewater consumption per unit area. On the other hand, the increase in the aquifer porosity had the least increase effect on both the total power consumption and the treated wastewater consumption by the system. In contrast, the hydraulic conductivity increase had no direct effect on either the total power consumption or on the treated wastewater consumption per unit area.

To evaluate the robustness of the general conceptual design system by performing different operational scenarios, four perturbed scenarios of the general conceptual design system utilizing the lump model approach were performed and compared with the base case simulation of the general conceptual design system utilizing a lump model approach. The base case simulation was chosen to represent the quasi-Kuwaiti environment data.

The first scenario was chosen to study the effect of the treated wastewater augmentation during the off planting season on the total power consumption and the treated wastewater consumption by the system. Moreover, the other three scenarios were chosen mainly to study the effect of any possible obstacles or lateral reduction in the operation system, due to emergencies or cost effects, on the total power and treated wastewater consumption. As demonstrated by the results of the four scenarios, the obstacle scenario (3) simulation performed the most feasible power consumption reduction compared to the base case simulation of the general conceptual design system. The percent decrease in the sum of the total power consumption over a 40-year simulation was 89.36 % when using the obstacle scenario (3) simulation system instead of the base case simulation system. Moreover, the percent increase in the sum of the treated wastewater utilization over a 40-year simulation was 0.34 % when using the obstacle scenario (3) simulation system instead of the base case simulation system. However, the biggest drawback of the obstacle scenario (3) of the general conceptual design system is the public non-endorsement of utilizing treated wastewater as irrigation water, and the retardation in enhancement of the groundwater salt concentration in the long run. The second most reasonable scenario compared to the base case simulation of the general conceptual design system was the off planting season scenario of the general conceptual design system. The percent decrease in the sum of the total power consumption over a 40-year simulation was 57.22 % when using the off planting season scenario simulation system instead of the base case simulation system. Moreover, the percent increase in the sum of the treated wastewater utilization over a 40-year simulation was 5.63 % when using the off planting season scenario simulation system instead of the base case simulation system.

The percent increase in the sum of the total power consumption over a 40-year simulation was 34.33% when using the obstacle scenario (1) simulation system instead of the base case simulation system. Moreover, the sum of the treated wastewater utilization was reduced by 100.54 m^3 per unit area, over the 40-year simulation, due to the elimination of the treated wastewater injection. This will cut the cost of the treated wastewater utilization by the system. However, the most critical drawback of this obstacle scenario (1) is the retardation in enhancement of the groundwater salt concentration. On the other hand, the obstacle scenario (2) simulation failed to simulate when the initial groundwater salt concentration was higher than 1400 mg/l. In addition, the simulation was terminated by the model after a one year period, 2 year period, and 3 year period of simulation for initial ground salt concentration ranges of less than 1400 to 1300 mg/l, 1250 – 1150 mg/l, and 1100 – 1000 mg/ l respectively. Even though the utilization of this obstacle scenario (2) is limited to low initial groundwater salt concentration, the simulation will only proceed for 2 – 3 years. Therefore, this obstacle scenario (2) can be an alternative (for 2-3 years only) for the base case simulation after almost 17 years of the base case simulation, where the groundwater salt concentration will be in the vicinity of 1100-100 mg/l. In conclusion, all the scenarios can be good alternatives for the base case of the general conceptual design system, except obstacle scenario (2). Moreover, the off planting season scenario can be the best alternative choice for substituting the base case simulation, after the obstacle scenario (3), for the reduction in total operation expenses.

The areal distribution model simulation approach of the general conceptual model design was simulated for three orientation layouts and compared to the lump model simulation approach of the general conceptual design system to determine the total cost of operating the system. Three orientation layouts were used in the areal distribution simulation model to represent the different orientations of the location of the pump well to the injection well and the location of the hypothetical field area relative to the groundwater concentration, thus, resulting in possible discrepancies in the overall power consumption and the total costs of the conceptual design system. The results of the three orientation layout simulations for the areal distribution model were compared with the lump model simulation. The percent decrease in the sum of the total power consumption compared to the lump model simulation over the 40-year simulation was 9.29, 8.20, and 19.25 for orientation layout (1), orientation layout (2), and orientation layout (3) respectively. Accordingly, due to the low percent decrease in the sum of the total power consumption between the lump model simulation and the areal distribution model for orientation layout (1) and orientation layout (2), it can be concluded that the orientation layout (1) and orientation layout (2) of the areal distribution simulation model is a very rational representation of the lump model simulation. On the other hand, the areal distribution (orientation layout (3)) model simulation is the most efficient orientation layout in power consumption, hence, in the total operation cost.

The economical feasibility of the base case of the general conception design system was analyzed for the lump model simulation approach and for the three orientation layouts of the areal distribution model approach. The economical analysis was based on the calculations of the net present worth value of the cash flows and the benefit-cost ratio theme for the capital cost, the operation and maintenance costs, and the revenues of the crop yields for the 40 years of operation. The benefit-cost ratio for the base case of the general conceptual design system using the lump model approach and the areal distribution model for the three orientation layouts was calculated for ranges of different interest rates (2%, 4%, 6%, and 8%). These benefit-cost ratio values were calculated for the USA and Kuwait conditions. Moreover, the cost analysis of the electrical power and treated wastewater was based on the USA electrical power cost and the treated wastewater cost, and based on the Kuwait electrical power cost and treated wastewater cost. In addition, the calculation of the Kuwait benefit-cost ratio was calculated for electrical power consumption with and without government electrical power subsidies. The results of the benefit-cost ratio economical analysis showed that the areal distribution model (orientation layout (3)) simulation approach was the most benefit-cost ratio efficient for all possible ranges of interest rates. Moreover, the second most benefit-cost ratio efficient model is the areal distribution model (orientation layout (1)), then, the areal distribution model (orientation layout (2)), and finally, the lump model for all possible ranges of interest rates. The benefit-cost ratio was almost equal for both the areal distribution model's orientation layout (1) and orientation layout (2) for the ranges of interest rates. What is more, the variation differences between the areal distribution orientation layout (1) model and the lump model benefit-cost ratio are minute for all the interest rate ranges. In conclusion, the lump model approach can safely represent the areal distribution orientation layout (1) and/or orientation layout (2).

The benefit-cost ratios for all the simulation approach methods was less than 1, except for the Kuwait condition at an interest rate of 2%. As an initial conclusion, from the benefit-cost ratio results, the general conceptual design system is unfeasible for most of the simulation method approaches when the interest rate higher than 2%. The conceptual design system for the base case approach simulations may not be feasible in the United State of America due to the benefit-cost ratio (less than 1). But for Kuwait, specifically, and the Middle East, in general, food self-sufficiency is one of the main aspects of government higher political strategy. For that reason, oil wealth is used as a highly valuable commodity traded for food. Furthermore, the GCC countries, as an example, provide long period loans (up to 50 years) with 2% interest rates for small to medium size projects (Industrial Bank of Kuwait) to create more job and work activities for small investors, thus, helping to reduce the unemployment phenomena and create more job opportunities. In addition, the GCC governments adapted a strong trend in encouraging the establishment of private sectors, which in return, will help provide more job opportunities, where 90% of the GCC citizens are now employed by the government. Therefore, this will reduce the burden from the government shoulders.

8.2 Recommendations for future study

Recommendations for future studies that might improve the efficiency of the general conceptual design system are as follows:

- Selecting higher salt concentration tolerance growing crops, which will require less total power consumption and lower treated wastewater utilization, thus, lowering the operational cost of the system.

- Planting higher crop cash value crops, which will have higher crop cash return revenue, therefore, increasing the income profits.
- Utilizing higher salt concentration irrigation water as the crop matures and less salt concentration irrigation water at the critical stages of growth, thus reducing the total power consumption consumed by the reverse osmosis unit and the well pump and reducing the consumption of treated wastewater.

- Studying the possibility of utilizing the off planting season scenario as the main general conceptual design system, where treated wastewater augmentation is practiced during the off planting season.

- Studying the possibility of utilizing obstacle scenario (3) as the main general conceptual design system, where treated wastewater augmentation will be re-routed through the reverse osmosis unit instead of direct injection to the native groundwater. The desalinated (permeate) water will be used for irrigation and the groundwater pumping will be equal to the deep percolation recharge.

REFERENCES

Abd Elhafez, S. 1990. Major problems and constrains of soil and water Management in Kuwait. Soil and Water Division, Public Authority for Agriculture and Fish Resources, Kuwait.

Abdel-Jawad, M., Al-Shammari, S., and Al-Sulaimi, J. 2002. Non-Conventional Treated Municipal Wastewater for Reverse Osmosis. Desalination Vol.142, pp. 11- 18.

Abdel-Jawad, M. 1998. Training Course on Sea Water Desalination by Reverse Osmosis. KFAS.

Abdulrazzak, M. J. 1994. Review and Assessment of Water Resources in Gulf Cooperation Council Countries, Water Resources Development, 10(1), pp. 23-27.

Akkad, A. A. 1990. Conservation in the Arabian Gulf Countries. Management and Operations, journal of the American Water Works Association, May, pp. 40-50.

Al-Alawi, J., and M. Abdulrazzak. 1994. Water in the Arabian Peninsula: problems and Perspectives. In water in the Arab world, perspective and prognoses, Rogers, P, and Lydon, p (eds.) Division of Applied Science, Harvard University.

Allen, R. G., M. E. Jensen, J. L. Wright, and R. D. Burman. 1989. Operational estimates of evapotranspiration. Agron. J., 81:650-662.

Al-Nakshabandi, G. A., and F. T. El-Robee. 1988. Aeolian deposits in relation to climatic conditions, soil characteristics system. Professional Paper 964, Reston, VA.

Al-Rashed, M., M. N. Al-Senafy, M. N. Viswanathan, and A. Sumait. 1998. Groundwater Utilization in Kuwait: Some Problems and Solutions. Water Resource Development, Vol 14, N0. 1, pp. 91-105.

Al-Ruwaih, F.M., S. Sayed, and M. Al-Rashed. 1998. Geological Controls on Water Quality in Arid Kuwait. Journal of Arid Environments, Vol. 38, pp. 187-204.

Al-Ruwaih, F. M. 1996. Hydrogeochemical Variation of Carbonate Aquifer, Al-Sulaibiya, Kuwait. Water, Air, and Soil Pollution, Vol. 90, pp. 489-505.

Al-Ruwaih, F. M. 1994. Patterns of Groundwater Chemistry, Kuwait Group Aquifer, Kuwait. Journal of Environmental Hydrology, Vol. 2, No. 1, pp. 24-35.

ASCE. 1990. Evaporation and Irrigation Water Requirements. ASCE Manuals and Reports on Engineering Practice No. 70. Published by ASCE, New York.

Al-Sulaimi, J. et al. 1993. Assessment of Groundwater Quality at Al-abdally and Al-Wafra Farms. KISR Project. WH-004. Kuwait Institute for scientific research, Kuwait.

Al-Sulaimi, J., M. N. Viswanathan, M. Naji, and A. Sumait. 1996. Impact of Irrigation on Brackish Groundwater Lenses in Northern Kuwait. Agricultural water management, vol. 31, pp. 75-90.

Al-Turbak, A. S., and K. H. Al-Dhowalia. 1996. Contribution of treated Wastewater in solving water shortage problem in Saudi Arabia. Proc. Symposium on wastewater Treatment Technology and Reuse, King Saud University, Saudi Arabia, pp. 14-33 (in Arabic).

Al-Wazzan, Y., M. Safae, S. Ebrahim, N. Burney, and A. Mesri. 2002. Desalting of Surface Water Using Spiral-Wound Reveres Osmosis (RO) System: Technical and Economic Assessment. Desalination Vol. 142, pp. 21-28.

Akbar, A., and K. Puskas. 1992. Water Availability. Sub-task 2b. In Development Study for the Agricultural Sector in Kuwait. Progress Report. Kuwait Institute for Scientific Research, Kuwait.

ASTM. 1993. The Annual Book of ASTM Standard, Designation: D4516-85.

AWWA (American Water Works Association). 1989a. Theme Introduction: Membrane Processes. Management and Operations, Nov., p. 29.

Balachandran, C. S., and P. E. Fisher. 1990. DESERT: A prototype expert system to advise on land degradation control. Land Degradation & Rehabilitation, 5, 27-41.

Barrat, J., F. Z. Siddeek, and A. Al-Yaqubi. 1990. Assessment of Groundwater Resources in Kuwait using Remote Sensing Technology. Kuwait Institute for scientific research, Final Report. KISR, Kuwait.

Barrat, J. M., A. Amer, F. Z. Sideek, and A. Al-Yaqubi. 1990a. Draft Final Report. Assessment of Groundwater Resources in Kuwait Using Remote Sensing technology. Vol. 5. Hydrogeology. Kuwait Institute for Scientific Research.

Bergstorm, R. E., and R. E. Aten. 1964. Natural Recharge and Localization of Fresh Groundwater in Kuwait. J. Hydrol., 2: 213-231.

Blaney, H. F., and W. D. Criddle. 1945. Determining water requirements in irrigated areas from climatological data. (processed). 17 pp.

Blaney, H. F., and W. D. Criddle. 1950. Determining water requirements in irrigated areas from climatological and irrigation data. USDA Soil Conserv. Serv. SCS-TP 96. (Processed). 49 pp.

Blaney, H. F., and W. D. Criddle. 1962. Report in irrigation requirements for West Pakistan. Tipton-Kalmbach, Inc., Denver.

Blaney, H. F., and K. Harris. 1952. Consumptive use of water rates in the lower Colorado River Basin. USDA Soil Conserv. Serv. (processed). 8pp.

Bouchaib El Hamouri, Abderrahim Handouf, Mohamed Mekrane, Mohamed Touzani, Addi Khana, Khalid Khallayoune and Taieb Benchokroun. 1996. Use of Wastewater for Crop Production under Arid and Saline Conditions: Yield and Hygienic Quality of the Crop and Soil Contaminations. Wat. Sci. Tech. Vol. 33, No. 10-11, pp. 327-334.

Burman, R. D., R. H. Cuenca, and A. Weiss. 1983. Techniques for Estimating Irrigation Water Requirements. 335-394. In Hillel, D. (ed), Advance in Irrigation, Vol. 2, Academic Press, New York.

Burman, R. D., P. R. Nixon, J. L. Wright, and W. O. Pruitt. 1980. Water Requirements. 189-232. In Jensen, M. E. (ed), Design and operation of farm irrigation system. Amer. Soc. Agric. Engr., St. Joseph, Mich.

Buros, O. K. 1989. Desalting Practices in the United States. Management and Operations, journal of the American Water Works Association, Nov., pp. 38-42.

Bushnak, A. A. 1990. Water Supply Challenge in the Gulf Region. Desalination, 78, pp. 133-145.

Chakravorty, B., and A. Layson. 1997. Ideal Feed Pretreatment for Reverse Osmosis by Continuous Microfiltration. Presented at the International Symposium on Pretreatment of Feedwater for Reverse Osmosis Desalination Plants, March 31 – April 2, 1997, Kuwait.

Chapell, F. H. 1993. Groundwater Microbiology and Geochemistry. Published by John Wiley and Sons, Inc., pp. 424.

Childs, E. C. 1943. The Water Table, Equipotentials and Streamlines in Drained Lands. Soil Sci., Vol. 56, pp. 317-330.

Childs, E. C. 1969. An Introduction to Physical Basis of Soil Water Phenomena. Wiley, London, 493 pp.

Christiansen, J. E. 1968. Pan evaporation and evapotranspiration from climatic data. J. Irrigation and Drainage Div., ASCE, 94: 243-265.

Christiansen, J. E., and G. H. Hargreaves. 1969. Irrigation requirements from evaporation. Tran, Int. Comm. on Irrig. And Drain., Vol.III, 23.569-23.596.

Darwish, M. A., and A. M. Jawad. 1989a. Technical comparison between large capacity MSF and RO desalting plants. Proceedings of the Fourth World Congress on Desalination and Water Reuse, Kuwait. International Desalination Association. Desalination 76 (4): 281-304.

Doorenbos, J., and W. O. Pruitt. 1975. Guidelines for predicting crop water requirements. FAO Irrig. And Drain. Paper No. 24, FAO Roma, Italy. 179 pp.

Doorenbos, J., and W. O. Pruitt. 1977. Guidelines for predicting crop water requirements. FAO Irrig. And Drain. Paper No. 24, 2nd ed., FAO Roma, Italy. 156 pp.

Dykes, G. M., and W. J. Colon. 1989. Use of Membrane Technology in Florida. Management and Operations, journal of the American Water Works Association, Nov., pp. 43-46.

Ebrahim, S., Y. Al-Wazzan, M. Safar, N. Burney, and A. Al-Mesri. 2000. Pilot Study on Renovation of Subsurface Water using a Reverse Osmosis Desalting System. Desalination, Vol. 131, pp. 315-324.

FAO, 1997. Irrigation in the near east region in figures. Food and Agriculture Org. of United Nations, Roma.

FAO-56. 1989. Crop evapotranspiration - Guidelines for computing crop water requirements - FAO Irrigation and drainage paper 56. Food and Agriculture Organization of the United Nations Rome.

Freeze, R. A., and J. A. 1979. Groundwater. Prentice Hall, Inc, Upper Saddle River, NJ 07458, 213 pp.

Frére, M., and G. F. Popov. 1979. Agrometeorological crop monitoring and forecasting. FAO Plant Production and Protection Paper 17. FAO, Roma, Italy. 38-43.

Frevert, D. K., R. W. Hill, and B. C. Braaten. 1983. Estimation of FAO evapotranspiration coefficient. J. Irrig. And Drain., ASCE, 109(IR2): 265-270.

Fuches, W., T. E. Gattinger, and H. F. Holzer. 1968. Explanatory Test to the Synoptic Geology Map of Kuwait. A surface Geology of Kuwait and the Natural Zone. Vienna: Geological Survey of Austria. 87 pp.

Hanbury, W. T., T. Hodgkiess, and R. Morris. 1992. Desalination Technology, Porthan LTd, U.K.

Hargreaves, G. H. 1975. Moisture availability and crop production. Trans. Am. Soc.Agric. Engrs., 18(5): 980-984.

Hargreaves, G. H., and Z. A. Samani. 1982. Estimating potential evapotranspiration. Tech. Note, J. Irrig. And Drain. Engrg., ASCE, 108(3): 225-230.

Hargreaves, G. H., and A. Z. Samani. 1985. Reference crop evapotranspiration from temperature. Applied Engrg. In Agric., 1(2): 96-99.

Helfferich, F. 1959. Ionenaustaustausther (ED. 1, Grundlagen) Verlag Chemie, Winheim.

Hosseinipour, Z., and A. Ghobadian. 1990. Groundwater Depletion and Salinity in Yazd, Iran. In: Hydraulics/Hydrology of Arid Lands (H2AL). American Society of Civil Engineering, New York, pp. 465-471.

Jensen, M. E. 1966b. Empirical methods of estimating or predicting evapotranspiration using radiation." 57-61, 64. Proc. Conf. On Evapotranspiration, Am. Soc. Of Agric. Engrs., Chicago, III. Dec.

Jensen, M. E., and H. R. Haise. 1963. Estimating evaportanspiration from solar radiation. J. Irrig. And Drain. Div., ASCE, 93(IR3): 209-231.

Jensen, M. E., and L. J. Erie. 1971. Irrigation and water management. 189-222. In Johnson, R. T., et al. (eds). Advances in sugar beet production, Iowa State University Press, Ames, Iowa.

Jensen, M. E., D. C. N. Robb, and C. E. Franzoy, C. E. 1970. Scheduling irrigations using climate-crop-soil data. J. Irrig. And Drain. Div., ASCE, 96:25-28.

Kamra, S. K., S. R. Singh, and K. V. G. K. Rao. 1994. Effect of Impervious Layer and Adsorption on Solute Transport in Tile-Drained Irrigation Lands. Journal of Hydrology, Vol. 155, pp. 251-264.

KISR. 1987. Water Resources for Greenery Aspects in Kuwait, The Greenery master plan of Kuwait, Kuwait Institute for scientific research, Kuwait.

KISR. 1994. Geohydrological Studies of Al-Wafra and Al-Abdally Farm Area, Vol. 1. WH-004 Hydrology Department, Water resources Division, Kuwait Institute for scientific research, Kuwait.

Makkink, G. F. 1957. Testing the Penman formula by means of lysimeters. J. Inst. Water Engng., 11(3): 277-288.

Manguerra, H. B., L. A. Garcia. 1997. Modeling Flow and Transport in Drainage Areas with Shallow Ground Water. Journal of Irrigation and Drainage Engineering, Vol. 123, No. 3, pp.185-193. May/June, 1997.

Manguerra, H. B., L. A. Garcia. 1996. Drainage and No-Drainage Cycles for Salinity Management in Irrigated Areas. Transaction of ASAE, Vol. 39, No. 6, pp. 2039-2049.

MEW. 1989. Statistical Year Book, Water, ed. 16B, Ministry of Electricity and Water, Kuwait.

MEW. 2000. Water Statistical Year Book. Ministry of Electricity and Water, Kuwait, 2000.

Monteith, J. L. 1981. Evaporation and surface temperature. Quart. J. Ray. Meteorol. Soc., 107: 1-27.

Morris, D. A., and A. I. Johnson. 1967. Summary of the hydrologic and physical properties of rock and soil materials, as analyzed by the Hydrologic Laboratory of the U.S. Geological Survey 1948-1960, U.S. Geological Survey Water-Supply Paper 1839-D, 42 pp.

Mukhopadhyay, A., J. Al-Sulaimi, and A. Al-Sumait. 1995. Lessons from Recharge Experiments in Kuwait. Int'l Symposium on Artificial Recharge of Groundwater Proceedings, ASCE, USA, pp. 790-799.

Mukhopadhyay, A., F. Szekely, and Y. Senay. 1994a. Artificial Groundwater Recharge Experiment in Carbonate and Clastic Aquifer of Kuwait. Water Resource Bulletin, American Water Resources Association. Vol 30, No. 6. pp. 1091-1107.

Mukhopadhyay, A., J. Al-Sulaimi, and J. M. Barrat. 1994b. Numerical Modeling of Groundwater Resource Management Options in Kuwait. Ground Water, Vol. 32, No. 6, Nov. – Dec. 1994, pp. 917-928.

Murakami, M. 1993a. Hydro-powered Reverse Osmosis (RO) Desalination for Co-generation: A Middle East Case Study. Proceedings of the IDA and WRPC World Congress on Desalination and Water Treatment, 2: 37-44.

Murakami, M. 1991. Arid Zone Water Resources Planning Study with Applications of Non-conventional Alternatives. Doctoral thesis, University of Tokyo, Japan.

Nativ, R., E. Adar, O. Dahan, and I. Nissim. 1997. Water Salinization in Arid Regions, Observed from Negev Desert. Journal of Hydrology, Vol. 196, pp. 271-296.

Omar, S., A. Al-Yaqubi, and Y. Senay. 1981. Geology and Groundwater Hydrology of the State of Kuwait. Ministry of Electricity and Water, Kuwait.

Omar, S. A., I. El-Bagouri, Y. Anwar, F. Khalaf, M. Hashash, and A. Nassef. 1988. Measures to Control Mobile Sand in Kuwait. Vol. 1. Environmental Assessment and Control Measures, EES-78, Kuwait Institute for scientific research, Report No. KISR2760, Kuwait.

Patel, R. M., S. O. Prasher, D. Donnelly, R. B. Bonnell, and R. S. Broughton. 1999. Subirrigation with Brackish Water for Vegetable Production in Arid Regions. Bioresource Technology, Vol. 70, pp. 33-37.

Penman, H. L. 1948. Natural evaporation from open water, bare soil grass. Proc. Roy. Soc. London, A193: 120-146.

Penman, H. L. 1963. Vegetation and hydrology. Tech. Comm. No. 53, Commonwealth Bureau of Soil, Harpenden, England. 125 pp.

Powell, J. H., and M. E. Guild. 1961. Salinity Problems in the Arid Zones: Field Operation of Electric Membrane Equipment for Water Desalinating. Proceedings of the Teheran Symposium. Unesco. Pp. 363-70.

Priestly, C. H. B., and R. J. Taylor. 1972. On assessment of surface heat flux and evaporation using large scale parameter. Mon. Weath. Rev., 100: 81-92.

Ringskog, K. 2000. International Trends in Water Pricing and Use, Website: http://www.worldbank.org.

Salama, R. B., C. J. Otto, R. W. Fitzpatrick. 1999. Contribution of Groundwater Conditions to Soil and Water Salinization. Hydrology Journal, Vol. 7, pp. 46-64.

Stockle, C. O., L. G. James, D. L. Bassett, and K. E. Saxton. 1991. Effect of evapotranspiration underprediction on irrigation scheduling and yield of corn: a simulation study. Agriculture water management, v. 19, N. 2, 167-179. Elsevier Science Publishers B. V., Amsterdam.

Tanner, C. B. 1967. Measurement of evapotranspiration. 534-574. In Irrigation of Agricultural lands. Mono No. 11, Am. Soc. Agron., Madison, Wis.

Thornthwaite, C. W. 1948. An approach toward a rational classification of climate. Geograph. Rev., 38, 55.

Turc, L. 1961. Estimation of irrigation water requirements, potential evapotranspiration: A simple climatic formula evolved up to date. Ann. Agron., 12: 13-49.

USDA. 1998. United State Department of Agriculture, National Agricultural Statistics Service. US Agriculture Statistics at the website http://www.usda.gov/nass/pubs/agr98/acro98.htm.

Urila, L. 2000. Energy of Seawater Desalination, http://urila.tripod.com/desalination.htm, April (2000).

Urila, L. 2002. Optimizing the Efficiency of Reverse Osmosis Seawater Desalination, http://urila.tripod.com/Seawater.htm, May (2002).

Van Deemter, J. J. 1950. Bijdragen tot de Kennis Van Enige Natuurkundige Grootheden Van de Grond. 11, Theoretische en numerieke behandeling van ontwatering-en infiltratie-stromingsproblemen. Veersl. Landbouwk. Onderz., 56(7): 7-46.

Van't Hoff, J. H. 1887. The Role of Osmotic Pressure in the Analogy between Solutions and Gases, Zeitschrift fur physikalische Chemie, vol 1, pp. 481-508.

Wright, J. L. 1982. New evapotranspiration crop coefficients. J. of the Irrig. And Drain. Div., ASCE, 108(IR2): 57-74.

Wright, J. L., and M. E. Jensen. 1972. Peak water requirement of crop in south Idaho. J. of the Irrig. And Drain. Div., ASCE, 96(IR1): 193-201.

Yurtsever, Y. 1997. Role and Contribution of Environmental Traces for Study of Sources and Processes of Groundwater Salinization. Hydrochemistry (Proceeding of the Rabat Symposium, April 1997). IAHS Publ. No. 244, 1997.

APPENDIX I

REVERSE OSMOSIS DESALINATION

I.1 Background

Desalting techniques are primarily intended for the removal of dissolved salts that generally cannot be removed by conventional treatment processes. Distillation units have been used on some American ships for more than 100 years. Desalting was used on a limited scale for municipal water treatment in the late 1960s. The development of desalting can be divided into three phases: the 1950s were a time of discovery; the 1960s were concerned with research; and the 1970s and 1980s were the time of commercialization. Beginning in the 1970s, the industry began to concentrate on commercially viable desalination applications and processes (Burgs 1989).

The first commercial plant for the production of potable water from a saline source using electro-dialysis (ED) and ion-exchange membranes was put into operation in 1954 (Powell and Guild 1961). In 1968, use of membranes for brackish-water treatment started with the construction of an ED plant in Florida, in the United States. This process was not favorably received in view of its inability to adequately reduce dissolved solids. The first reverse osmosis (RO) water treatment plant was constructed in 1970 for a condominium project on Longboat Key, Florida (Dykes and Colon 1989). Significant advances in membrane technologies in the last 20 years have improved the cost effectiveness and performance capabilities of the processes. RO membrane processes are increasingly used worldwide to solve a variety of water treatment problems.

I.2 World Desalination

Arid regions, with their very limited fresh-water potential, have generally used high-salinity waters, such as seawater, as major water supply sources. More than two-thirds of the world's desalting capacity is located in the arid, oil-rich areas of the Middle East, North Africa and Western Asia (Burgs 1989):

- Western Asia (Middle East), 63%
- North America, 11%
- North Africa, 7%
- Europe, 7%
- Pacific, 4%
- Caribbean, 2%
- (former) USSR, 2%
- Others, 4%

I.2.1 Desalinating Technology and Processes

The major desalting technologies used today are distillation (several types of evaporative processes), reverse-osmosis (RO), electro-dialysis (ED), electro-dialysis reversal (EDR), and ion-exchange demineralization. The typical concentration ranges of total dissolved solids (TDS) in the feed water for distillation, RO, ED, and EDR demineralization are between 5,000 and 100,000 mg/l. For thermal distillation (non-membrane) processes, TDS concentration (seawater concentrations) limits are up to about 35,000-45,000 mg/l. For RO membrane, TDS concentration limits are up to approximately 12,000 mg/l, using ED or EDR membrane (AWWA 1989) (Figure I.1). Ion exchange, in which anion and cation resins are used to exchange ions for hydrogen and hydroxide, is primarily used in industrial applications, for which very pure water is required and the feed-water TDS is relatively low. Distillation and other thermal processes are used primarily for seawater conversion and special industrial applications, such as brine concentration.

I.2.2 Economics and Environment

The cost of desalination has generally decreased from more than US$3/m^3 to as low as US$0.50/m^3 over time as a result of both technological advances and market processes (Burgs 1989), (Figure I.2). Improvements in RO membranes have been the main technological change in desalination in recent years. The United States and Japan are the world's leading countries in innovative research to develop the membrane industry. A high level of competition on both a national and international basis has also played a significant role in containing prices for capital equipment. The following percentages illustrate the distribution of overall costs for the operation of a brackish-water desalting plant (Dykes and Colon 1989):

- Capital-cost recovery, 41%

- Membranes, 12%
- Energy, 26%

Figure I.1 Typical feed-water TDS operating ranges for desalting processes (AWWA, 1989).

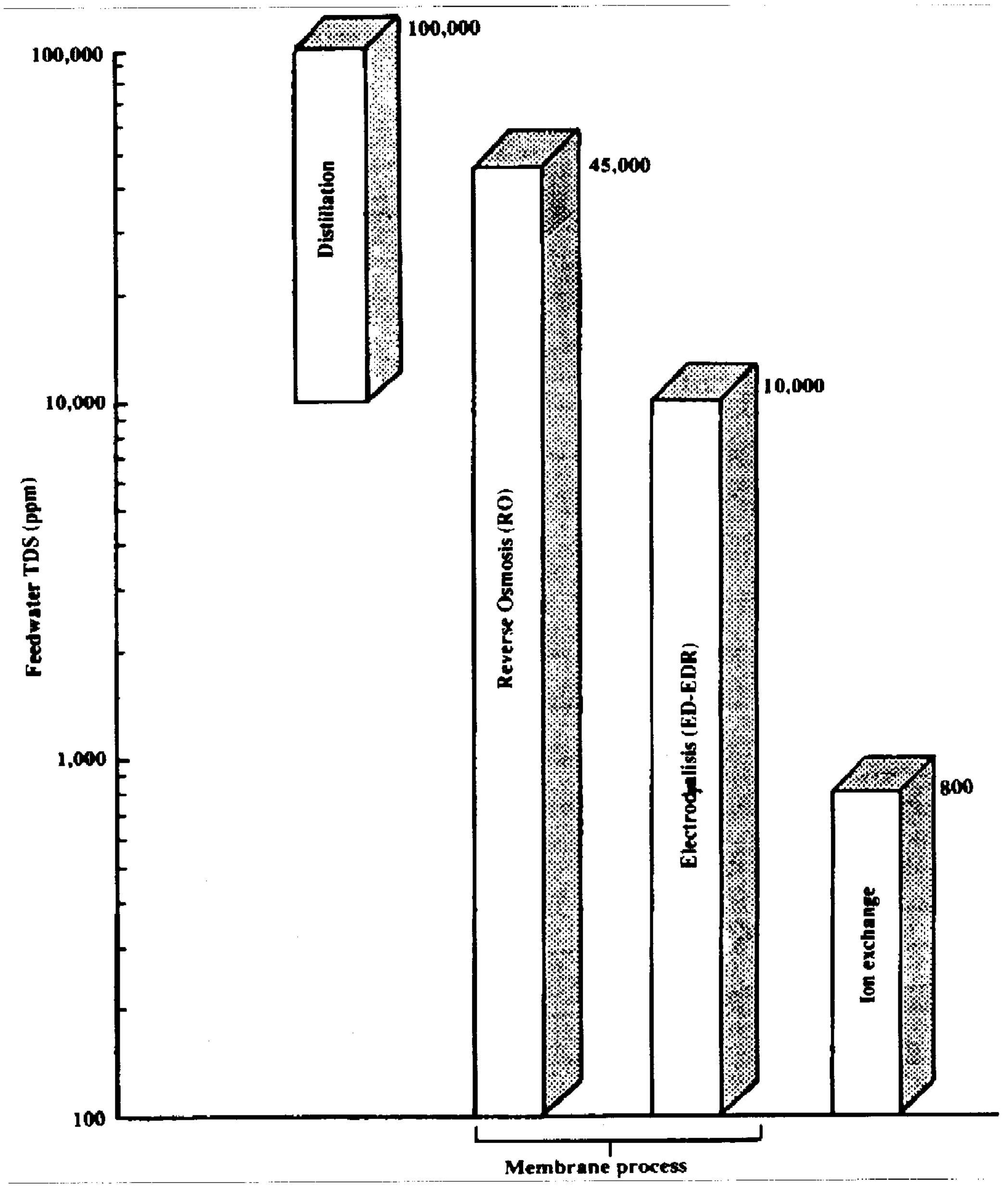

 Emad H. AlAli

- Labor, 11%,
- Chemicals, 7%
- Other expendable items, 3%

Thus, the main item of cost is capital recovery, which represents almost half of the overall cost. The next most significant cost items are energy, membranes, and labor. The dominant cost element in seawater RO desalination is the energy, or electricity, which accounts for 50% or more. Substantial cost reduction can be achieved by taking into account the following:

- Technology improvement and research to increase membrane life- from three years to up to five to seven years.
- The development of low-pressure-type or low-energy-requirement membranes, and
- The development of a pumped-storage-type RO desalination system using off-peak cheap electricity from nuclear power plants or other thermal power plants; hydro-powered RO desalination is another option (Murakami 1991,1993a).

Generally seen as benign, desalination is not without environmental concerns of its own. From a regulatory standpoint, the big advantage to desalination is that it takes out water that is unusable, leaving fresh water available for other uses. But there is some question about how to dispose of the concentrated brine that is the by-product of desalination. The very highly concentrated brine from distilling plants poses a major

Figure I.2. Desalination cost ranges over time. Cost of producing potable water, by distillation or reverse osmosis, including both capital and operating cost (1985 prices) for plants producing 3,700-18, 000 m^3/day. The increasing cost of distillation from early 1970's reflects international crude oil prices (Buros, 1989).

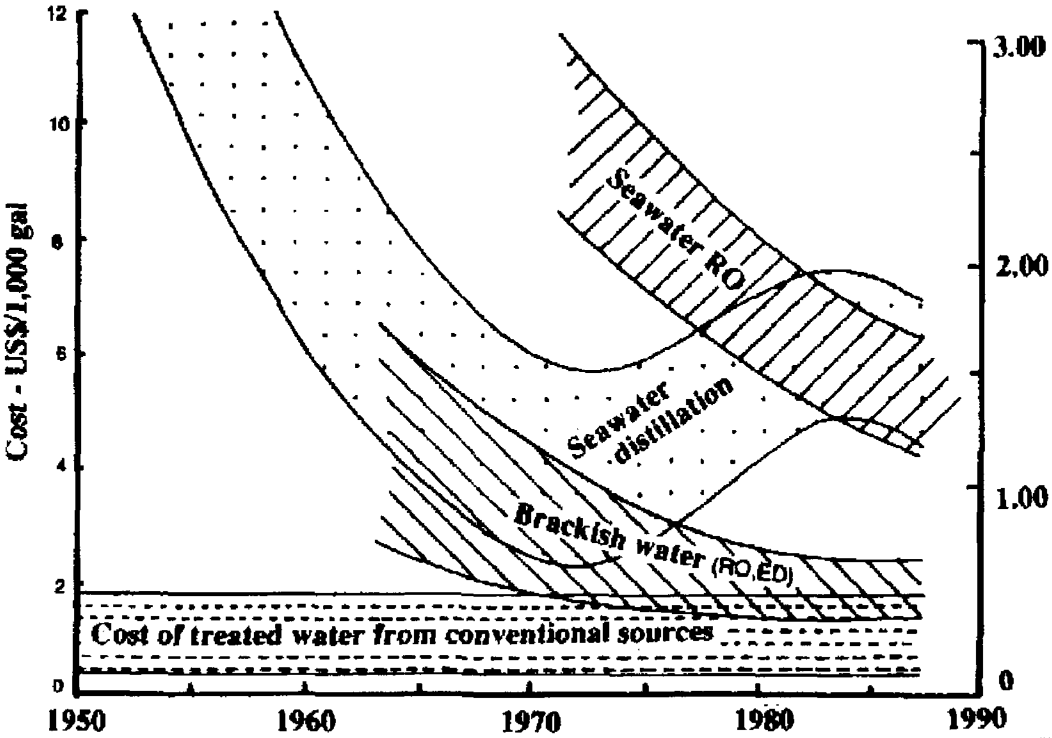

problem to be solved, including a sufficient analysis of the potential impact on the marine environment, while less saline brine from RO plants may have a relatively minor adverse impact on the marine ecology.

I.3 Seawater desalination in the Arabian Gulf Countries

In extremely arid countries, where good-quality water is not available, seawater desalination is commonly used to supply water for municipal and industrial uses. In spite of the high cost of desalinated water, a vast quantity is produced to meet the demand for domestic water in the Gulf countries.

I.3.1 Installed capacity of desalination plants

The installed capacity of desalination plants in Saudi Arabia, Kuwait, the United Arab Emirates, Qatar, Bahrain, and Oman is estimated at 5.08 million m^3 per day in total, including 2.4 million m^3 per day in Saudi Arabia, which is approximately half of the total for the Gulf countries. Dual-purpose multi-stage flash (MSF) is the most commonly used technique to desalt seawater, representing 97% of the total installed capacity, (Table I.1.) (Akkad 1990).

Table I.1. Installed capacity of desalination plants in Arabian Gulf countries (million m^3 per day), (Akkad 1990).

	MSF	RO	Other	Total
Saudi Arabia	2,316	77	2	2,395
Kuwait	1,409	-	-	1,409
U.A.E.	709	-	-	709
Qatar	295	-	-	295
Bahrain	115	45	-	160
Oman	105	1	1	107
TOTAL	4,949	123	3	5,075

I.3.2 Remakes on Seawater distillation

The problem with seawater distillation is the high cost of producing fresh water by the MSF process, which is the most prevalent type of thermal distillation in the Middle

East. The process is largely dependent on the rate of energy consumption, which is high and influenced by the unstable world market price of crude oil (Figure I.2.).

I.4 Reverse Osmosis Desalination

The membrane processes will probably be the key technological approach to the desalination of brackish water and seawater in future years. Although the RO, ED, and EDR membrane processes are used worldwide to solve a variety of water treatment problems, it is likely that RO will continue to have the greatest market share. Where fresh water supplies are limited or must be imported over long distances, RO desalting of nearby brackish water can be cost-effective. Most of the countries in the Middle East and North Africa have rather long sea coasts, with a total length of about 25,000 km. Seawater desalination will continue to increase in these countries, either by distillation or RO, depending on site-specific conditions and technology development.

I.4.1 Brackish Water

Good-quality water is neither abundant nor available to meet the growing demand in most of the coastal areas in arid to semi-arid countries. However, sufficient brackish water is normally available on site to support development. Since the early 1970s, advances in desalination have mostly been directed towards improving the abundant sources of brackish water rather than towards the comparatively expensive conversion of seawater. Significant advances in membrane technologies in the last twenty years have improved the cost effectiveness and performance capabilities of the RO process. Brackish water desalination usually costs only one-fifth to one-third as much as seawater desalting (Burgs 1989).

I.4.2 Seawater

For environmental reasons, thermal distillation plants, which are largely dependent on high specific energy consumption, are likely to be replaced progressively by low-specific-energy-consumption types of RO desalination plants. At the end of 1989, the world's largest seawater RO desalination plant, with an installed capacity of 56,500 m^3 /day was constructed at Jeddah, on the west coast of Saudi Arabia, to replace a 20 year old Dual-purpose multi-stage flash (MSF) distilling plant that was being phased out. It should be noted that a case study on the Doha desalination plant in Kuwait in 1989 estimated the unit cost of seawater desalination at US$2.70/$m^3$ by MSF and US$1.70/$m^3$ by the RO membrane process (Darwish et al. 1989).

I.4.3 Reclamation of Treated Wastewater

The application of membrane-separation technology to salvage treated waste water includes three alternative processes: (1) micro-filtration, (2) ultra-filtration, and (3) loose reverse osmosis. Both the micro-filter and ultra-filter are used to better control water quality in the tertiary treatment process and/or the final water purification process. Another application is being tested to be used directly in the primary or secondary wastewater treatment process. The loose RO process is being developed to reclaim treated waste water for strategic reuse in the agricultural and/or industrial sector.

Although it is clear that membrane desalting is a cost-effective alternative to importing fresh water over long distances, the use of the membrane process to remove turbidity, organic matter, and hardness has typically been more expensive than conventional treatment. However, with the continuing improvements in membrane-separation technology, increasing competition among manufacturers of capital equipment, and the ever-escalating cost of meeting increasingly stringent water quality standards by conventional approaches, the cost gap is decreasing (AWWA 1989).

I.4.4 Membrane Technologies Applications

Membrane-separation technology, using low-energy and/or energy saving types of membrane, are expected to continue to be popular in arid coastal regions and other areas wherever saline waters are available but good-quality fresh water is limited or not available. Application of the membrane-separation technology in the arid countries will be mainly for seawater and brackish water desalination. Reverse osmosis, ultra-filter, and micro-filter membranes are being used to reclaim either saline water or waste water for reuse, which could indeed be the technology to take the drinking-water and sanitation industries gradually into the twenty-first century.

I.5. Principles, Methods, and Processes of Reverse Osmosis

I.5.1 Principles

Osmosis is a natural process whereby a solvent (water) diffuses through a semi-permeable membrane from a solution of lower concentration to one of higher concentration (Part A, Figure I.3.). The membrane readily passes the solvent but acts as a barrier to the solutes (dissolved solids). At equilibrium conditions, the pressure differential across the membrane is called the osmotic pressure (Part B, Figure I.3.). For example, the osmotic pressure of brackish water containing about 2,000 p.p.m. TDS at a typical water temperature of 25°C is only about 1.6 kg/cm², whereas it is 27.7 kg/cm² for standard seawater of 35,000 p.p.m. TDS at 25°C. In reverse osmosis, a pressure greater than the osmotic pressure is applied to the concentrated solution (saline water), and a dilute permeate (product water) is produced (Part C, Figure I.3).

Figure I.4, is a flow schematic of a simplified schematic RO unit. The pressure of the feed water, pre-treated to meet certain established RO membrane feed-water quality guidelines, is boosted before the water enters the RO membranes. Two flows exit the membranes: (1) the combined product (permeate), and (2) the combined concentrate (reject). The fraction of the resulting feed water which is permeate is called the recovery and is usually expressed as a percentage. The maximum allowable ratio of permeate to reject depends on the water's scaling potential, which is a function of the feed-water quality.

This ratio is maintained by the use of a control valve on the reject piping, which controls the flow rate of the reject, thus forcing the permeate flow rate to the desired value.

Figure I.3 Simplified concept of osmosis, osmotic pressure and reverse osmosis.

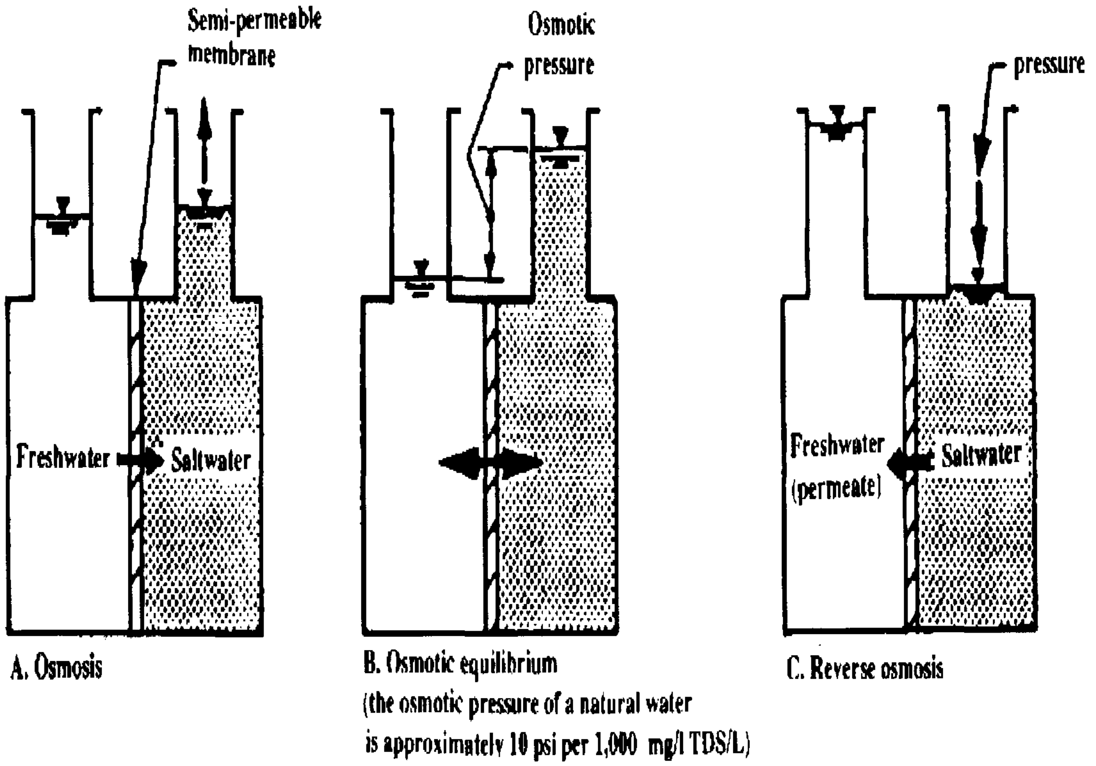

I.5.2 Reverse Osmosis Membrane

The first commercially available membranes, developed in the mid 1960s, were made of cellulose acetate (CA) manufactured in flat sheets. Modern CA membranes are modifications of the cellulose acetate structure, including blends and different surface

Figure I.4 Flow Diagram and Schematic of Typical Reverse Osmosis system.

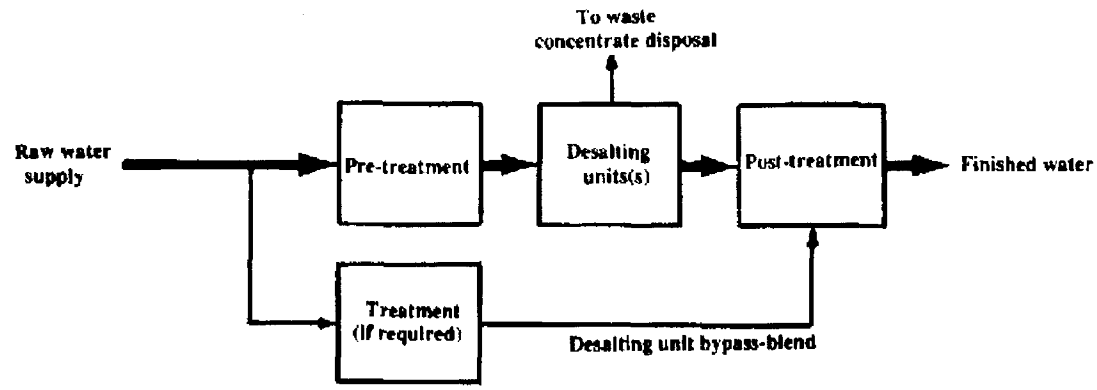

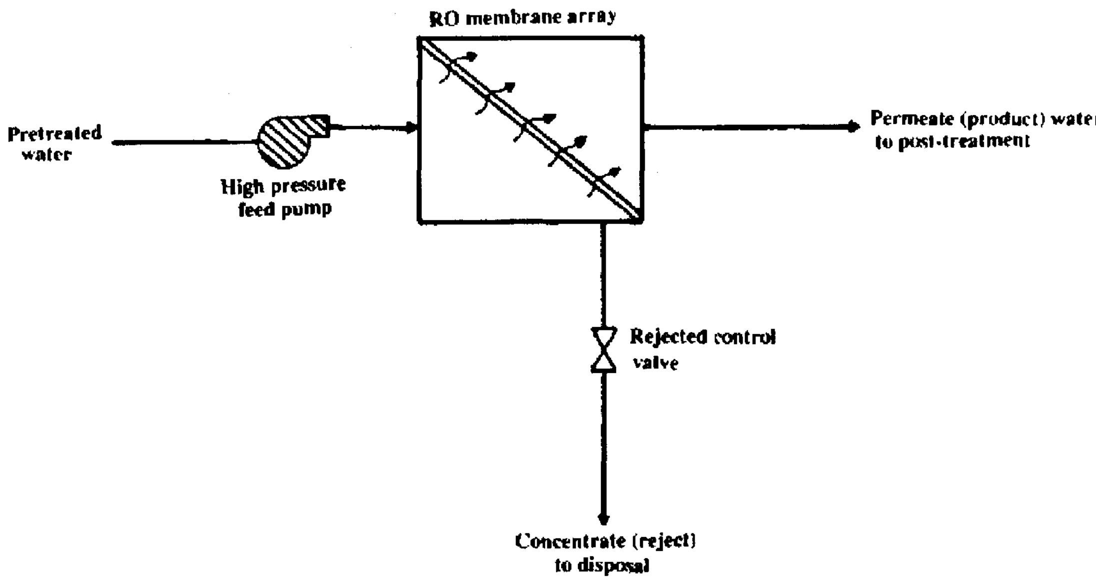

treatments, and are called cellulosic or symmetric membranes. Non-cellulosic membranes, called thin-film composite membranes, have been developed since the 1970s. These include polyamide membranes with relatively thick asymmetric polyamide support structures and composite membranes with thin-film polyamide or other membrane materials on a porous support structure.

Each membrane material has advantages and disadvantages. The CA-based membranes are now generally the least expensive per gallon of installed capacity (first cost). The price difference between CA and composites is decreasing, however, as the number of manufacturers supplying the composite-type membranes increases and with new developments in the manufacturing process. Use of CA membranes generally requires chlorinated feed water and higher operating pressures than those needed by the composite membranes. Composite membranes generally operate over wider p^H and temperature ranges than CA membranes. In some cases, these operating characteristics of composite membranes result in savings in electric power and chemical costs. Their greater p^H tolerance provides additional advantages in cleaning for some applications. Sensitivity to chlorine and other strong oxidants in the feed water is a disadvantage of polyamide-based membranes. New developments in membrane research to produce chlorine-tolerant composite membranes are overcoming this limitation.

I.5.3 Membrane Elements and Reverse Osmosis Units

RO membranes are placed inside pressure vessels in several different configurations: (1) hollow-fiber, (2) spiral-wound, (3) tubular, and (4) plate and frame (Table I.2). In the past years, hollow-fiber and spiral-wound configurations have become the industry standard for RO water treatment (Figures I.5 and I.6). The spiral wound (SW) membrane is designed for low to high salinity brackish water (TDS > 10,000 ppm), whereas the hollow-fiber (HFF) membrane is used for seawater (TDS > 35,000 ppm) (Ebrahim et al., 2000). The predominance of the spiral-wound configuration has resulted from recent advances in membrane technology. Thus, this has been more easily translated into commercial flat-sheet membranes than into the hollow-fiber configuration.

Figure I.5 Typical hollow-fiber reverse osmosis element.

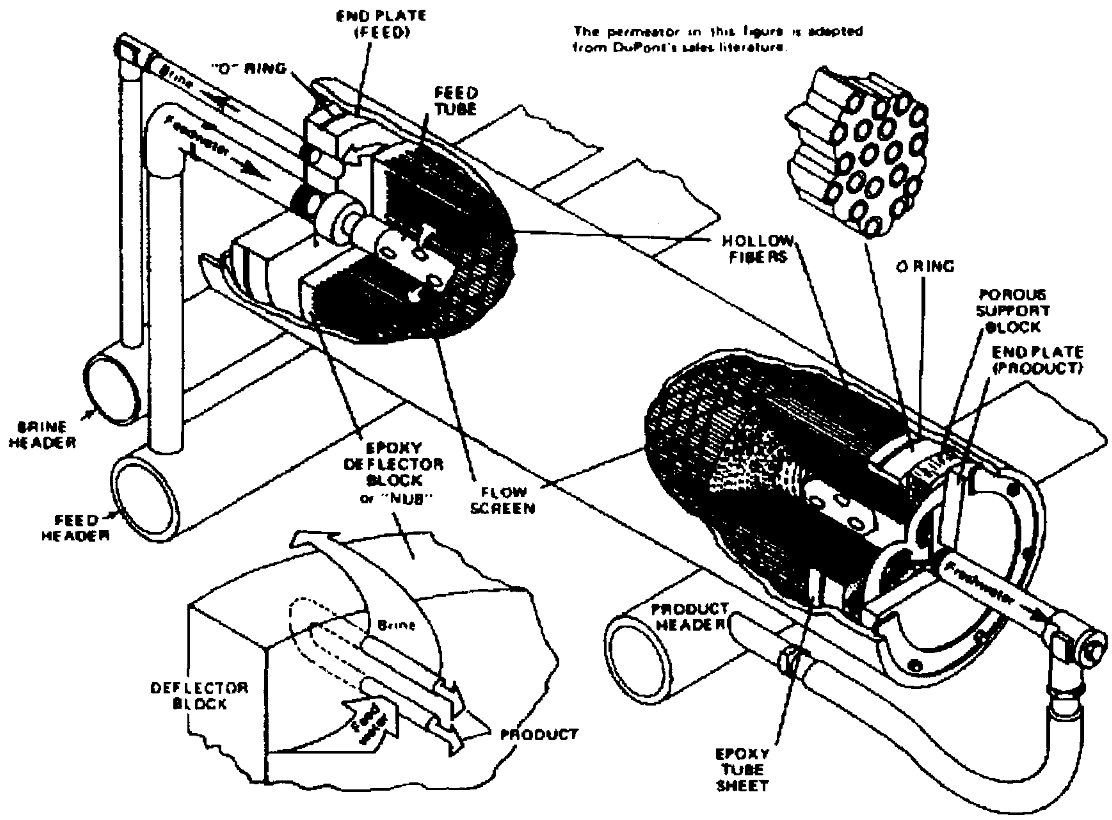

 Emad H. AlAli

Figure I.6 Typical spiral-wound reverse osmosis membrane element, pressure vessel and configuration.

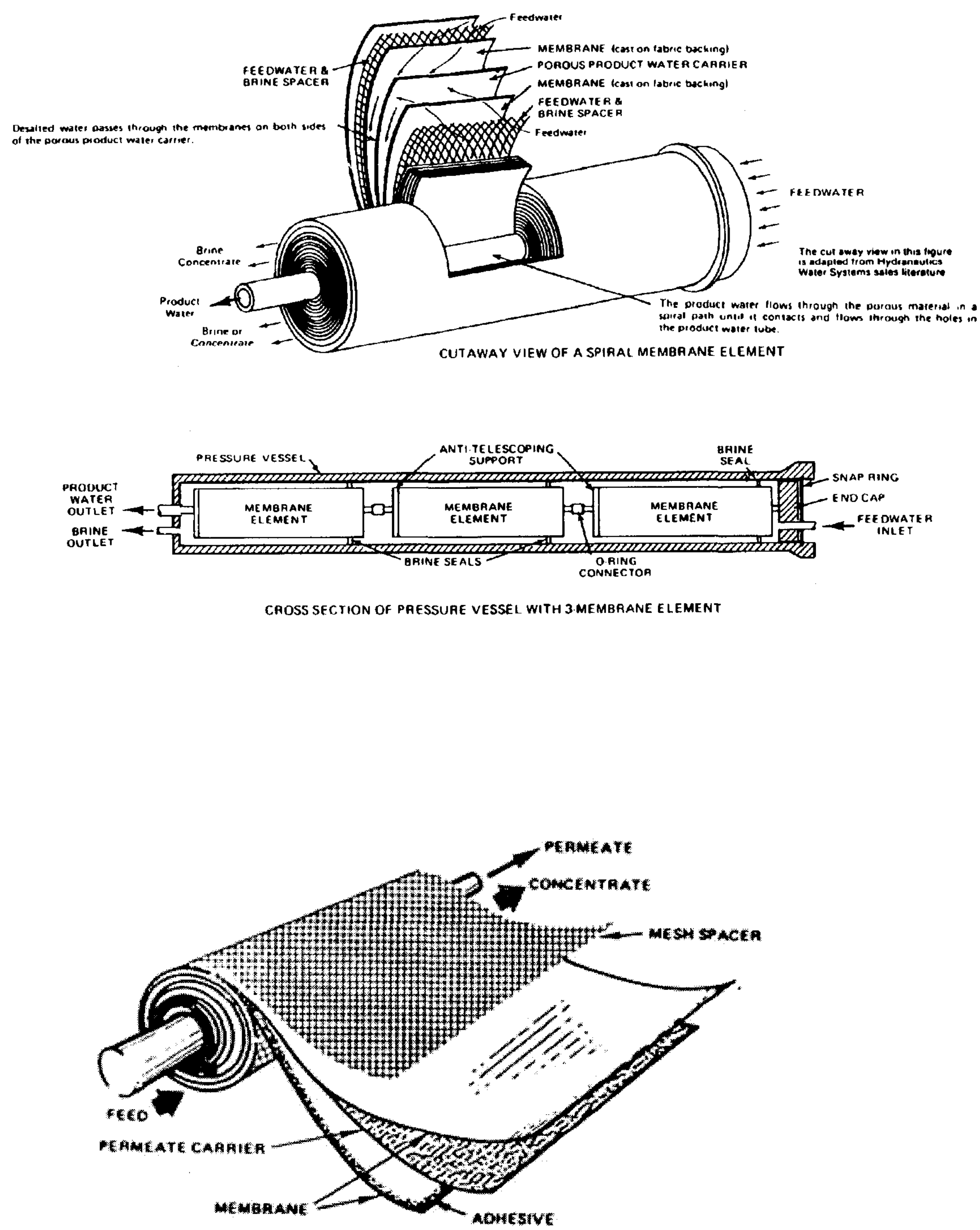

Table I.2. Membrane configurations.

Modules

Hollow Fiber-Capillary

- Very small diameter membranes(< 1mm).
- Consist large number of membranes in a module and self supporting.
- Density is about 600 to 1200 m^2/m^3.(for capillary membrane), up to 30000 m^2/m^3. (hollow fiber)
- Size is smaller than other module for given performance capacity.
- Process "inside-out", permeate is collected outside of membrane
- Process "outside-in", permeate passes into membrane bore.

Plate and Frame

- Structure is simple and the membrane replacement is easy.
- Similar to filter press
- Density is about 100 to 400 m^2/m^3.
- Membranes is placed in a sandwich style with feed sides facing each other.
- Feed flows from its sides and permeate comes out from the top and the bottom of the frame.
- Membranes are held apart by a corrugated spacer.

Spiral Wound

- Is formed from a plate and frame sheet wrapped around a center collection pipe
- Density is about 300 to 1000 m^2/m^3.
- Its diameter can up to 40cm.
- Feed flows axial on cylindrical module and permeate flow into the central pipe.
- Features:

1. High pressure durability.
2. Compactness.
3. Low permeate pressure drop and membrane contamination.
4. Minimum concentration polarisation.

- Ceramic membranes are usually monoliths of tubular capillaries.
- Channel sizes are in millimeter range.
- Becomes a module by attaching end fittings and a means of permeate collection.
- Many monoliths are usually incorporated into one modular housing.

- Not self supporting and normally are inserted in other materials' tubes with diameter more than 10mm.
- Density is not more than 300 m^2/m^3.
- Features:

1. Can operate with simple pre-treatment of feed liquid.
2. Membranes replacement is easy.
3. Easy to be washed.

Depending on the desired capacity of an RO system, one or more pressure vessels containing RO membranes are used to form a modular block. Pressure vessels within an RO block can be arranged in parallel, in series, or both, depending on the design requirements. Often this membrane-pressure-vessel arrangement is called a membrane array or a pressure-vessel array. For example, a 2:1 pressure-vessel array indicates a two-stage system with two pressure vessels in the first stage and one vessel in the second stage. In a reject-stage arrangement, the membranes in the second-stage vessel would treat the waste concentrate (reject) water from the first stage, thus recovering more product water from the feed-water supply.

I.5.4 Potential Water Sources

Although some locations have a shortage of water of any quality, the most common situation is a shortage of water of potable quality. Desalting processes can expand the availability of potable water supplies by converting previously unusable supplies to potable water. The potential sources of water for membrane desalting include brackish groundwater, brackish surface water, hard water, municipal waste water, high-nitrate groundwater, irrigation return flows, and seawater.

I.5.5 Feed Water Quality

The composition of raw water from the supply source must always be considered in the design of both conventional water treatment and desalting processes. However, the design of desalting systems and their operating economics are much more interrelated with feed-water composition and the required product composition than most conventional treatment processes. The composition of raw water is probably the most important component in desalting-process design. The typical water-quality parameters needed for the process design of membrane desalting systems are:

- Dissolved solids
- p^H
- Temperature
- Sparingly soluble salts
- Suspended solids
- Iron and manganese
- Microbial growth
- Organic

Feed water salinity and temperature are usually given parameters. Higher salinity increases the required feed water pressure, while higher temperature reduces the required feed water pressure and lowers the salt rejection. Fouling tendency also increases with temperature. Moreover, feed water fouling tendency is a function of the pretreatment. Table I.3 shows operating parameters for spiral wound (SW) and Dupont hollow fine fiber (HFF) membranes. Table I.4 shows average water chemistry data for spiral wound (SW) and Dupont hollow fine fiber (HFF) membranes.

Table I.3. Operating parameters for spiral wound (SW) and Dupont hollow fine fiber (HFF) membranes (Ebrahim et al., 2000).

Parameter	Spiral Wound Membrane (SW) (SW, 4820X12)	Dupont Hollow Fine Fiber Membrane (HFF) (HFF, SW-M-8540)
Total Dissolved Salt (TDS) Design range	Up to 30,000 ppm, designed for high salinity brackish water.	Up to 35,000 ppm and higher, designed for seawater
Productivity m^3/d	22.8	89
Salt Rejection, %	99.6	99.9
Max. Operating Pressure, bar	41	69
Max. Operating Temp., ^0C	< 45	35
Max. Recovery, %	65	66
SDI, %	< 5.0	< 4.0
p^H	4 - 11	4 - 9

Feed - Water entering an RO machine; **Permeate** – Portion of the feed that passes through the membrane and is collected for use. In water purification, this is the product; **Concentrate (reject)** – Portion of the feed which does not pass through the membrane, which exists as a separate stream containing concentrated impurities and is usually discharged to drain; **Rejection** – Percentage of dissolved material, which does not pass through the membrane; **Recovery** – Ratio of the permeate (product) rate to the feed rate; **SDI** – Percentage of silt density index.

Table I.4. Average water chemistry data for spiral wound (SW) and Dupont hollow fine fiber (HFF) membranes at Kifan site, Kuwait (Ebrahim et al., 2000).

Analytical Parameter	RAW	Product	
		Spiral Wound (SW) Membrane	Hollow Fine Fiber(HFF) Membrane
P^H	7.15	5.88	6.25
TDS, mg/l	10,786.60	152.00	139.32
T. alkalinity, mg/l	143.30	8.96	17.24
CO_3^{-2}, mg/l	< 0.10	< 0.01	< 0.10
HCO_3^-, mg/l	143.30	8.96	17.24
CO_2, mg/l	7.72	6.68	6.02
Na^+, mg/l	3045.00	34.80	28.00
K^+, mg/l	55.15	0.37	0.27
Mg^+, mg/l	432.40	0.67	0.10
Ca^{+2}, mg/l	869.87	1.18	0.18
Al^{+3}, mg/l	1.55	< 0.05	< 0.05
Pb^+, mg/l	< 0.03	< 0.03	< 0.03
Mn^+, mg/l	< 0.05	< 0.05	< 0.05
F^-, mg/l	1.95	0.16	0.10
Cl^-, mg/l	3983.80	43.20	30.60
SO_4^{-2}, mg/l	3018.90	30.30	20.72
Tot. Fe, mg/l	< 0.05	< 0.05	< 0.05
Silica, mg/l	5.45	2.10	1.94
Ba^{+2}, mg/l	< 0.05	< 0.05	< 0.05
Zn^{+2}, mg/l	< 0.05	< 0.05	< 0.05
PO_4^{-3}, mg/l	< 0.05	< 0.05	< 0.05
COD, mg/l	32.33	9.67	2.33
BOD, mg	1.60	0.80	0.73

I.5.6 Pre-treatment

Pre-treatment is usually required to protect the membrane system, to improve performance, or both. The type of pre-treatment required depends on the feed-water characteristics, membrane type, and system design parameters. Pre-treatment requirements can be minimal, such as cartridge filtration of well water, or extensive, such as conventional coagulation, sedimentation, and filtration of surface water supply.

An RO membrane is an effective "Depth" filter. Many of the suspended solids fed to it will be retained. This results in rapidly declining flow and shortens the membrane life. Hence, the membrane will retain almost all the dirt that is fed to it. Therefore, RO systems require a suspended solid load of less than 1 ppm to operate stably.

I.5.6.1 Turbidity

Turbidity is traditionally used to check for suspended solids. It is the only way to measure the performance of a media filter system on line. As a measurement, it is acceptable for traditional applications (Table I.5).

I.5.6.2 Silt Density Index (SDI)

The RO industry relies on SDI to check the feed water to an RO plant. SDI is a measure of the plugging potential of the water. It is measured by passing a sample through a 0.45 micron filter paper, and measuring the change in flow decay. SDI should be < 3 for stable RO operation. Each unit increase in the SDI almost certainly indicates an exponential increase in fouling. As a consequence, turbidity by itself is not a good enough measurement for RO stability because it is not related to SDI.

Table I.5. Typical turbidity data, (Chakravorty and Layson, 1997).

CONDITION	TURBIDITY, NTU
Normal Media Filter Operation	**0.05-0.5**
Typical Turbidity Blip from Media Filters	**2-5**
Typical Turbidity Alarm Set Point	**1**
Typical "Deadtime" before Alarm Becomes Active	**30-120 sec.**

I.5.6.3 Modified Fouling Index (MFI)

The Modified Fouling Index (MFI) is a recent refinement of the SDI test. It uses the same apparatus as the SDI test. Its difference is that it looks at the rate of change of the flow through filter paper, whereas the SDI uses the ratio of two flows at the start and end of the test. The result is a more accurate and meaningful parameter.

Unfortunately, there is not a lot of MFI data published, so it is hard to define a recommended value for RO feed water. Table I.6 shows some of the data that is available.

Table I.6. Modified Fouling Index (Chakravorty and Layson, 1997)

Process	MFI, s/l^2
Traditional Pretreatment	**14.5**
Microfilter Pretreatment	**5.5**

For RO systems, standard pre-treatment usually consists of adding chemicals for scale control, followed by cartridge filtration (usually 1, 5, 10, or 20-microm nominal rating) for membrane protection. The feed water is often acidified to lower its p^H; this step is nearly always required for cellulosic membranes. Scale inhibitors such as sodium hexametaphosphate or proprietary chemicals are also added to reduce carbonate and sulphate scale potential.

I.5.7 Pump System

The pump system raises the pressure of the pre-treated feed water to the level required for operation of the desalting system, which is primarily related to the salinity and temperature of the feed water. The higher the salt content (TDS), the higher the pressure; and the lower the temperature, the higher the pressure (Al-Wazzan et al., 2002). For RO, the pump system discharge pressure typically is 8.8-28.1 kg/cm² (125-400 psi) for low-TDS and brackish-water systems and 56.2-84.3 kg/cm² (800-1,200 psi) for seawater systems. The pump system for RO might also include energy recovery devices, particularly for seawater systems.

I.5.8 Post-treatment

Post-treatment to supply drinking water commonly includes product-water p^H adjustment for corrosion control and chemical addition for disinfection. Typically entrained gases such as carbon dioxide and hydrogen sulphide (if present) are removed before final p^H adjustment and disinfection.

Removal of these gases is normally accomplished by stripping in a forced draft packed column. In most cases, carbon dioxide must be removed to stabilize the RO product water. If hydrogen sulphide is present, degassing of the product water is usually done to control odor and minimize the amount of disinfectant (e.g., chlorine). The final product-water p^H is often adjusted by caustic soda, soda ash, or lime. Non-corrosive water can be produced by using these alkaline chemicals and, in some cases, other chemicals and blending with raw or other water supplies that may also feed the distribution system.

Post-treatment disinfection is normally accomplished with chlorine. However, if the desalting process allows the passage of trihalomethane (THM) precursors, chlorine dioxide, or chloramines, some additional post-treatment may be required to comply with THM drinking-water quality standards.

I.5.9 Factors Influencing the Performance of RO

I.5.9.1 Silt Density Index (SDI)

One of the most important parameters for raw water quality in RO plants is the silt density index (SDI). This parameter is an index for the degree to which the raw water is contaminated with suspended or colloidal impurities (Abdel-Jawad, 1998).

To obtain the SDI value, the reduction in filtration speed through a membrane filter with a specific pore size is measured. Membrane filters with an average pore size of 0.45 microns are utilized for the purpose. Initially, 500 ml of raw water are filtered through the membrane at a pressure of 2 bars. The filtering time recorded for this is entered as t_1 in the mathematical expression for the SDI given below. Following this, raw water is filtered for further period, e.g. 15 minutes, at constant pressure. This period represents the duration of the test T. Subsequently, a further 500 ml of raw water is filtered across the membrane and the time for filtration t_2 is also entered in the mathematical expression given below.

$$SDI_T = \frac{\left(1 - \frac{t_1}{t_2}\right) * 100}{T} \qquad [\% \text{ min}^{-1}]$$

SDI_T = Blocking index for duration of test T, e.g. SDI_{15} for T = 15 min.

t_1 = Filtration time for a defined volume, usually 100 or 500 ml, measured immediately at the beginning of filtration.

t_2 = Filtration time of the same volume as t_1, measured after duration on the test T.

T = Duration of test – length of filtration period from the start until commencement of measurement t_2; e.g. T_{15} = 15 min.; T_5 = 5 min.

I.5.9.2 Osmotic Pressure

Osmotic pressure is the head equivalent difference which arises when a dilute solution and a concentrated solution are separated by a semipermeable membrane, approximately equal to 1 psi per 100 mg/L total dissolved solids for water.

For the ideal solution, Van't Hoff's law applies as follows:

$$\pi = C * R * T$$

where $\boldsymbol{R}$ is the molar gas constant = 8.315 j/mole/K, $\boldsymbol{T}$ is the absolute temperature = 273 + °C (K) and $\boldsymbol{C}$ is the concentration of the solution (mole/l).

Then, the osmotic pressure π has the dimension of bar and is proportional to the concentration of the salt on the high pressure side of the semipermeable membrane (Abdel-Jawad, 1998). The form of Van't Hoff's equation cited here holds only for undissociated solutions. For dissociated solutions of ideally diluted electrolyses, the osmotic coefficient (*f*) must also be taken into account.

$$\pi = f * C * R * T$$

$$f = 1 + \alpha(\beta - 1)$$

where,

α = Degree of dissociation.

β = Stoichiometric equivalence no. (No. of the ions in the dissociated form).

I.5.10 Basic Transport Equations in RO

Water Flux equation (Helfferich, 1959)

$$Q_w = K_w * (A/\tau) * (\Delta p - \Delta\pi)$$

where,

Q_w = Water flow rate through the membrane.

Δp = Hydraulic pressure differential across the membrane.

$\Delta\pi$ = Osmotic pressure differential across the membrane.

K_w = Membrane permeability coefficient for water.

A = Membrane area.

τ = Membrane thickness.

Salt Flux equation (Helfferich, 1959)

$$Q_s = K_s * (A/\tau) * \Delta C$$

where,

Q_s = Flow rate of salt through the membrane.

ΔC = Salt concentration differential across the membrane.

$\boldsymbol{K_s}$ = Membrane permeability coefficient for salt.

The water flux through a membrane increases with increasing diffusion (Dw) and increasing water concentration (Cw) inside the membrane. In a similar way, the salt permeability coefficient can be detailed to:

$$\boldsymbol{K_s = D_s * K}$$

where,

$\boldsymbol{D_s}$ = Salt diffusion coefficient in the membrane.

$\boldsymbol{K}$ = Distribution coefficient for salt between the membrane and the external salt solution.

The lower the diffusion coefficient, and, the lower the salt concentration in the membrane are, the lower will be salt passage through the membrane and vice versa (M. Abdel-Jawad, 1998).

I.5.11 Salt Rejection and Salt Passage

The desalination ability of a membrane is usually characterized by the salt rejection (R) or the salt passage (SP) respectively:

$$R = \left(1 - \frac{C_p}{C_F} \right) * 100 \quad [\%]$$

$$SP = \left(\frac{C_p}{C_F} \right) * 100 \quad [\%]$$

where C_p and C_F are concentrations of permeate (product) and feed respectively. It turns out that the sum of R and SP is unity.

$$R + SP = 100 \quad [\%]$$

I.5.12 Basic Equations in RO

From flow balance:

$$Q_b = Q_f - Q_p$$

Conversion (Y):

$$Y = \frac{Q_p}{Q_f}$$

where,

Q = Flow.

b = Brine.

f = Feed.

p = Product.

Concentration factor (C_F):

$$C_F = \frac{Q_f}{Q_b}$$

Concentration factor (C_p):

$$C_p = \frac{Q_p}{Q_b}$$

Average feed-brine flow (Q_{fb}):

$$Q_{fb} = \frac{Q_f + Q_b}{2}$$

From pressure balance, bundle pressure drop (ΔP_{fb}):

$$\Delta P_{fb} = P_f - P_b$$

Average feed-brine pressure (P_{fb}):

$$P_{fb} = \frac{P_f - P_b}{2}$$

APPENDIX II

BACKGROUND

II.1 General Information about Kuwait and Wafra farms

Kuwait is an arid country with very few natural water resources (Figure II.1). The only water resource in Kuwait with limited natural replenishment is groundwater. Except for some isolated fresh water lenses in northern Kuwait at Raudhatain and Umm Al-Aish, the rest of the usable groundwater is mostly saline, with some brackish zones existing in the southwestern regions. Most of the brackish groundwater fields are located in the center and western regions of Kuwait. Groundwater from these fields is used for urban landscaping, gardening, building, road construction and blending with desalinated seawater. Abdally in the north and Wafra in the south are farming areas that depend on groundwater for irrigation. The remaining groundwater in Kuwait is highly saline with a maximum of total dissolved solids (TDS) of about 200,000 TDS. Most of the potable water comes from desalination plants (multi-stage flash distillation units) with a production cost of about \$1.5- \$3 per m^3. Fresh water is supplied to the domestic consumer at the rate of about \$0.67 per m^3 and for industrial consumers at the rate of \$0.21 per m^3 (Darwish et al., 1989; Bushnak, 1990). Supplying water at a highly subsidized price without

Figure II.1 Aerial photo for Kuwait and neighboring countries.

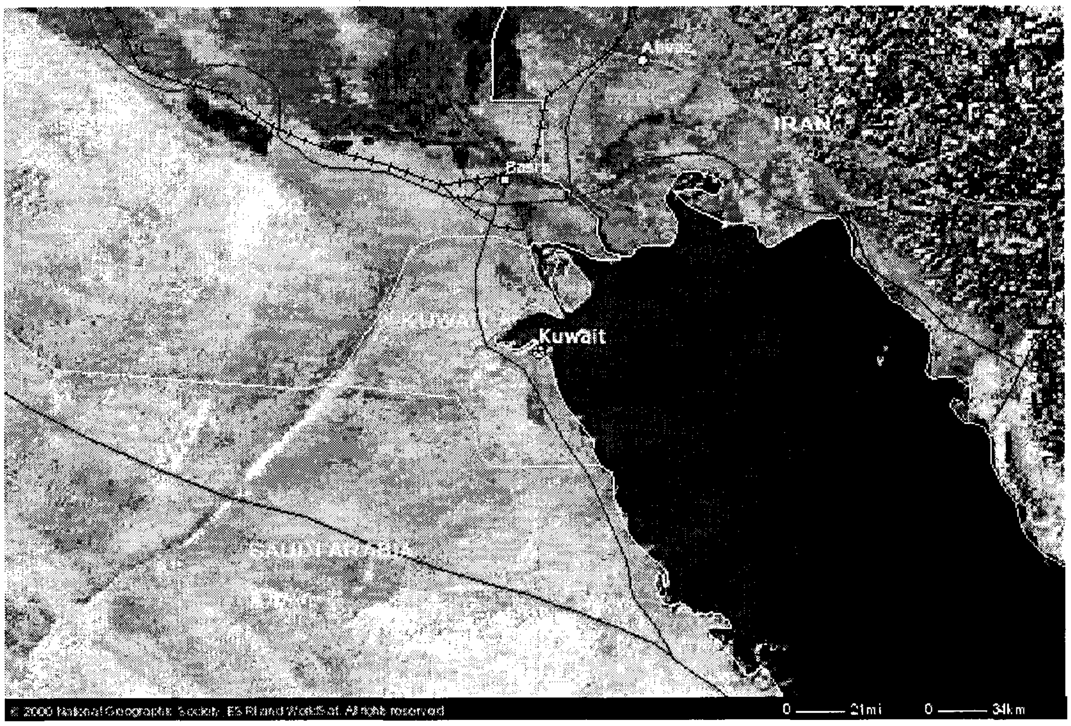

any limitations encourages waste. Farmers are allowed to pump groundwater without any limitations, for political reasons, which has resulted in several problems, such as a large decline in water table levels and deterioration of groundwater quality (Appendix III and VI), ultimately resulting in the abandonment of several farming areas.

Average annual rainfall and evapotranspiration is about 105 mm and 2270 mm respectively, so recharging of aquifers by rainfall is negligible. Low average rainfall within the region does not result in a significant direct recharge of aquifers. Extremely high evaporation rates owing to high ambient temperatures, low humidity and persistent wind action further reduce available moisture. Evaporation and transpiration produce a soil moisture deficiency that generally does not permit significant percolation or runoff to occur, except under exceptional conditions. Although runoff in the desert is low, several storms occasionally develop short duration flows in the area of integrated drainage (Bergstorm and Aten, 1964). Where surface runoff is concentrated in wadis (valley) and playa areas, there is sufficient infiltration and percolation to produce accumulations of fresh to brackish groundwater lenses. Beneath the wadis and basins where recharge occurs, the percolating water develops slight mounds of fresh to brackish water.

Water resources problem that are unique to the GCC countries (Saudi Arabia, Kuwait, Bahrain, Qatar, the United Arab Emirates and Oman) include the physical aspects of intermittent or no surface runoff, depletion of deep groundwater, over consumption, salinity, salt-water intrusion and pollution of shallow aquifers (Abdulrazzak, 1994). In Al-Wafra in the south, 50% of the wells pumped water with a salinity level higher than 7500 ppm in 1989. This figure is expected to reach 75-80% and 85-90% in the years 1997 and 2002 respectively. In Al-Abdally in the north, 55% of the deep drilled wells pumped water with a salinity level higher than 7500 ppm in 1989. This is expected to reach 75% and 90% after 5 and 10 years of operation respectively (FAO of the United Nations, Rome, 1997) (Figure II.2).

Groundwater quality deterioration in Kuwait is caused by two factors: one factor is the water quality in groundwater fields, where water is extracted for urban use could be affected by lateral flow of saline water. The other factor is that declining groundwater levels would accelerate the process of water quality deterioration. Hence, steps taken to reduce the rate of declining water levels would also reduce the risk of water deterioration. Water quality in the field where water is extracted for irrigation is affected by return of irrigation water with a higher TDS content, and aquifer mining will allow more lateral flow of saline water.

Figure II.2 The major water well fields of Kuwait.

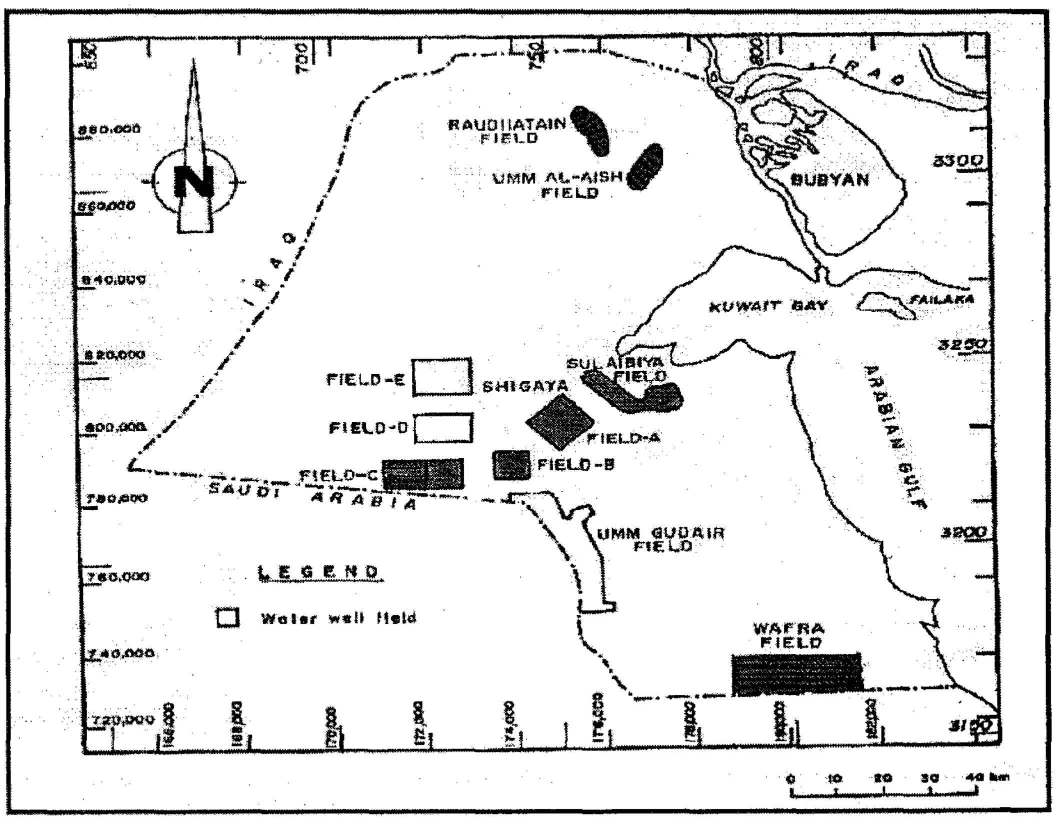

Kuwait Group Aquifer.

Dammam Lime Stone Aquifer.

The Wafra area is located in Kuwait near the southern border with Saudi Arabia between latitude 28 ° 30′ and 28 45′ N and longitudes 47° 45′ and 48° 15′ E, (Figure II.3). Wafra is generally a flat area, sloping very gently from west to east. Rainfall is restricted to winter and early spring (October-May), with a mean annual rainfall of 105 mm with great variability from one year to another and from one location to another. The average temperature ranges between 7 °C in January and 39.3 °C in July.

Figure II.3 Wafra area location map, Kuwait.

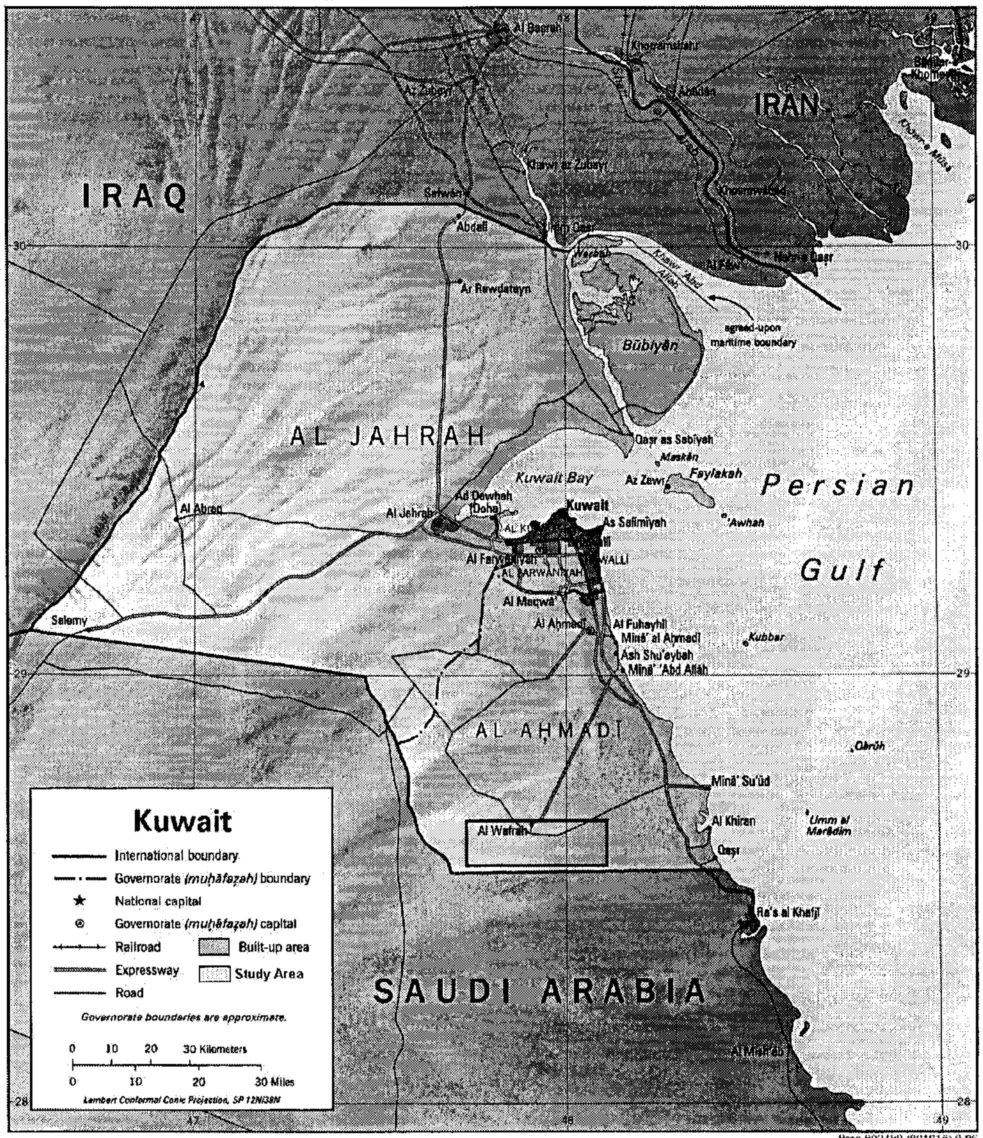

The maximum temperature ranges between 14.8 °C in January and 47.3 °C in July. The minimum temperature ranges between 2 °C in January and 31.5 °C in July. Relative humidity is highest in January (maximum 84 % and minimum 45 %) and lowest in June (maximum 40 % and minimum 13 %). The evaporation rate is very high and variable with a daily mean of 16.6 mm/d. It reaches 31 mm/d in summer and decreases to 5.2 mm/d in winter. Winds blow from the northwest and, to a lesser extent, from the southeast. The dry and hot northwestern winds that prevail in the early summer are mostly associated with dust storms and become particularly frequent in June and July (Omar et al., 1988). In winter and spring, dust storms and rising sand are mostly associated with strong southeasterly winds.

The soils in Kuwait are predominantly formed from Aeolian and alluvial deposits. A high percentage of the soils are sand and sandy loams. Loam to sandy clay loam exists in the subsoil layers of certain soils. A sand surface layer of 10-50 cm thick developed by deposition of wind-eroded materials is observed in many places. Depth of calcareous sandstone or gravelly bedrock and indurate layers are ranging from 0 to more than 2 m (Omar, et al., 1988). Significant piles of sand have accumulated along the shelterbelt and behind them inside the farms, particularly those located in the north and northwest boundaries in the prevailing wind direction (Al-Nakshabandi and El-Robee, 1988).

A large area in Wafra, in southern of Kuwait, was developed for crop production both in open fields and agriculture units under protected environmental conditions (Figure II.4). For more than a decade, farmers had been using groundwater and desalinated water for irrigation crops under both conditions. In irrigated desert lands, particularly when low quality water is used for irrigating crops, soil salinity build-up and erosion are prime factors causing land and vegetable degradation (Balachandran and Fisher, 1990). Salinization reduces the potential of land for crop production. The amount of annual precipitation is insufficient and scare water resources are the limiting factors to agricultural development. Consequently, farmers rely heavily on the groundwater resources, particularly in open field crop production, and on freshwater (desalinated) resources for crop production in protected environmental conditions. General observation of the Wafra area indicated a salinity build-up problem as well as sand encroachment on farms.

Figure II.4 Aerial photo for Wafra farms.

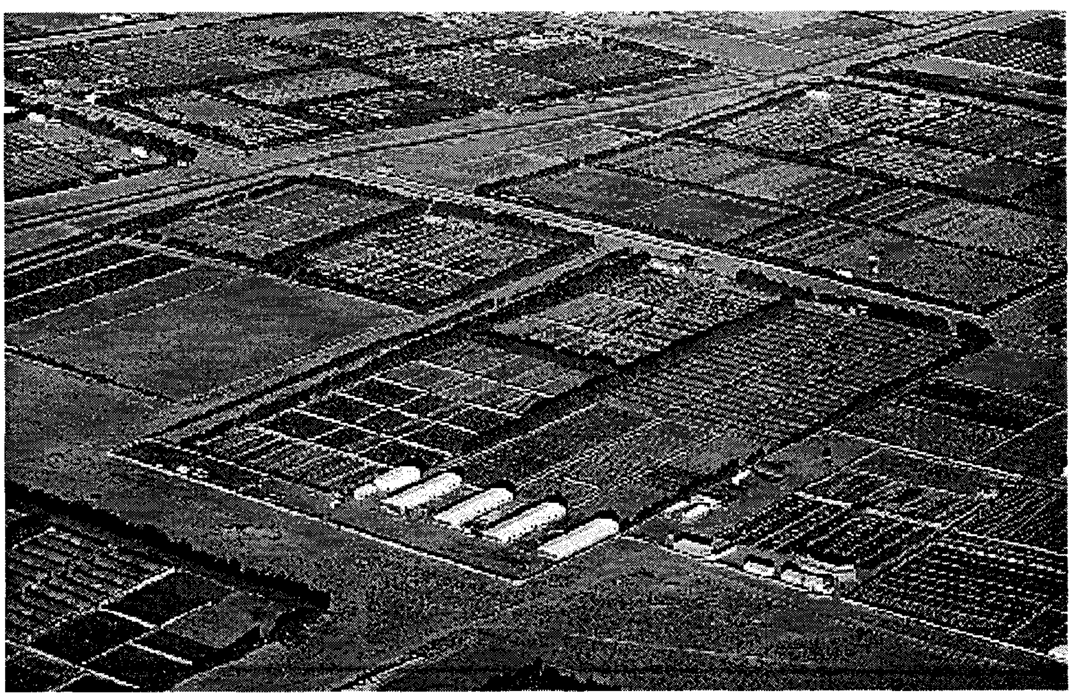

II.2 Sources of Water in Kuwait

For fresh water in earlier days Kuwaitis depended on a few artesian wells. Dhows manned by Kuwaiti seamen also brought fresh water from the Shatt Al-Arab in Iraq. With the rapid growth of population, however, the government of Kuwait built the first modern desalination plant in Kuwait city in 1953, followed by others. The Doha region had two desalination plants, whose capacity reached 138 million imperial gallons per day. A third plant was set up nearby for desalination through reverse osmosis. There are three main sources of water for agricultural uses; groundwater, treated wastewater and desalinated water (Akbar and Puskas, 1992). The general characteristics of water sources in Kuwait are as follows:

- **Groundwater (brackish).** The total available groundwater in Kuwait is 247 MIGD with TDS ranging between 3000 and 5000 mg/l. Presently, over 60% of the field irrigation and all the landscape irrigation in Kuwait are from groundwater (MEW, 1989; KISR, 1987: Abd Elhafez, 1990). Water pumping in Wafra was estimated in 1989 at about 42 MGD (KISR, 1994). The TDS of groundwater in the Kuwait group aquifer varies from about 4000 mg/l along the Saudi Arabian border to about 12000 mg/l along the northeastern corner.

- **Treated Wastewater.** Two sources of recycled water are used: municipal water and industrial wastewater. The quality of the municipal wastewater has markedly improved with the opening of the tertiary treatment plant in June 1985, making the water suitable for irrigation. The concentration of total dissolved solids was reported as 1000-1100 mg/l (Akbar and Puskas, 1992). The allocation of the treated wastewater is preferred for greenery irrigation.

- **Desalinated Water (fresh water).** Over 95 percent of the potable water is produced from seawater desalination. Prior to the Iraqi invasion of Kuwait, the total installed capacity was 254 MIGD (MEW, 1989). For agricultural production, desalinated water is used only in protected agriculture and the cost to the farmer is heavily subsidized. Irrigation with this water is not economically feasible without the present subsidy. The produced fresh water is distributed equally between agricultural productions and landscaping. About half of this amount can be considered waste due to uncontrolled irrigation (Abd Elhafez, 1990).

II.3 Topography and Geology of Kuwait

The topography of Kuwait is generally flat, broken only by occasional low hills and shallow depressions, with elevation ranges from sea level in the east to nearly 300 m in the southwestern corner of the country. Generally, the land surface of Kuwait slopes northeastward. The Jal Az-Zor escarpment forms one of the main topographic features in Kuwait (Fuches, 1968). Another elevation is the Al-Ahmadi Ridge of approximately 137 m, separating the plane of Burgan from the gulf coast, in addition to Wara hills. The major depression in Kuwait is in wadi (valley) Al-Batin, a broad shallow wadi marking the western boundary of Kuwait. The drainage pattern becomes obscure in the southwestern section of Kuwait, and the northeastern drainage trend tends to be visible in poorly developed wadies (Figure II.5).

Figure II.5 Topography and Drainage System of Kuwait.

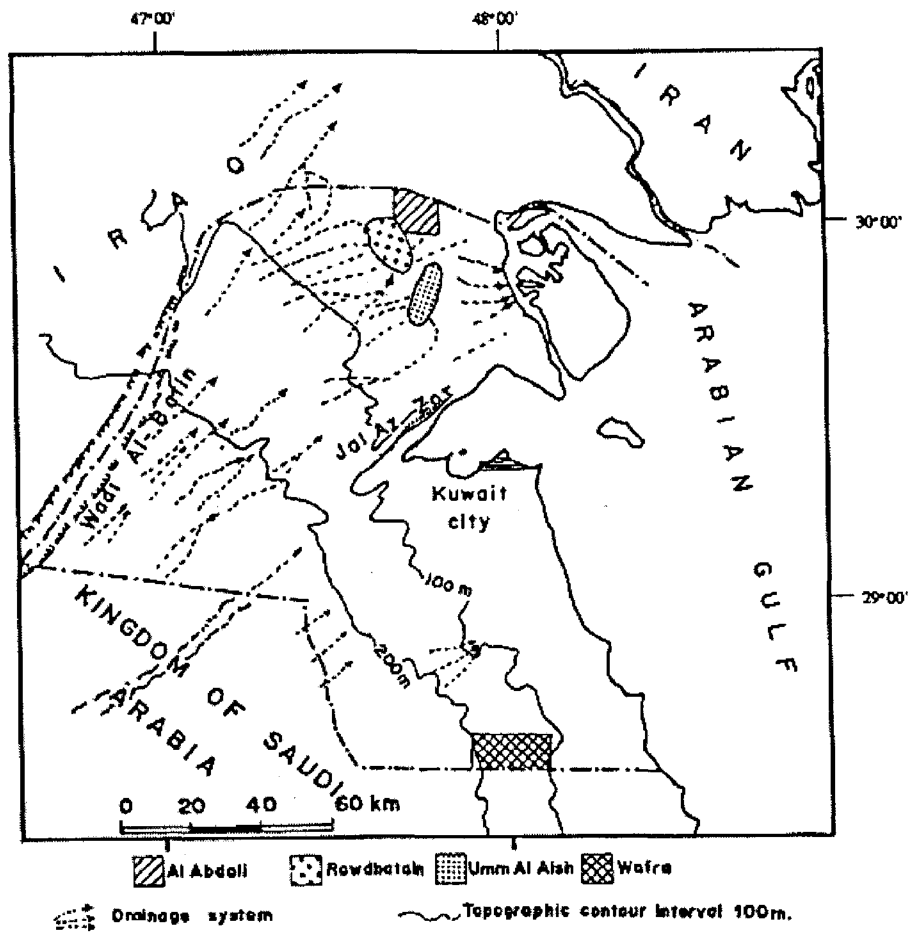

II.3.1 Surface Deposits

Satellite images, field trips and geological maps mainly studied the surface geology of Kuwait. The surface sediment of Kuwait consists of sedimentary deposits ranging in age from early Miocene to recent Figure (Table II.1). The correlation of deposits over long distances is difficult because of the lack of any fossil evidence and surface irregularities. The recent surface deposits may be classified into Aeolian deposits, residual deposits, playa deposits (inland deposits), desert plain deposits, and near shore sabkhas deposits (coastal deposits). Eolian sand is covers the scattered northwest to southwest topographic depressions.

The deposits were observed east of Al-Abdally farms and to the southeast in the Al-Jalaiah coastal zone. Desert plain deposits are another common feature in southern Kuwait. Recent fluvial deposits associated with northeast tending dry stream channels mainly consist of loose gravels and coarse-to-fine sand, derived from the eroded pre-existing deposits.

II.3.2 Kuwait Group

The Kuwait group underlies the unconsolidated recent and sub- recent sediments of various types, ranging from gravels and sand to fine grained coastal deposits, sandstone, clay, silts and limestone or marls covering the entire surface of Kuwait. Additionally, it extends down to the top of the underlying Dammam limestone formation (Figure II.6). The stratigraphic sequence consists of sediments ranging in age from Miocene to Holocene. It includes conglomerates, sandstones, sandy limestones, clay stones, sand and gravel. Owen and Nasr (1958) subdivided the Kuwait group in north Kuwait into three formations based on the presence of intermediate evaporite deposits as follows:

1. Dibdibba Formation	Sands and Gravels
2. Fars Formation	Evaporite sequence
3. Ghar Formation	Sands and Gravels

Table II.1 Stratigraphic column section of Kuwait.

Age	Group	Formation	Graphic	Lithology	Ground Water Conditions
Recent				Beach sands; sand; gravel; playa silts and wadi alluvium	Above ground water saturation or locally contain brackish to saline water
Pleistocene / Miocene	KUWAIT GROUP	Dibdibba		Coarse upland fluvial gravels Gravel and sand, mainly conglomeratic sandstone; siltstone shale; up to 120 m	Ground water locally fresh beneath wadis and depressions brackish at depth
Miocene	KUWAIT GROUP	Fars		Fine to conglomeratic calcareous sandstone; sand variegated shales; fossiliferous limestone; gypsiferous; 100 m thick	Ground water generally brackish
Miocene	KUWAIT GROUP	Undifferentiated Fars and Ghar		Quartzose sandstone; sand and conglomerate; some shale in lower parts; few meters to 250 m thick	Ground water generally brackish
Eocene	HASA GROUP	Dammam		Discontinuous chert cap; chalky and siliceous limestone; dolomite; 200 m thick	Moderately permeable; brackish water southwest of Kuwait; very brackish in east and north
Eocene	HASA GROUP	Rus		Anhydrite; limestone; marl; 70-120 m thick	Brackish/saline ground water?
Eocene	HASA GROUP	Umm Al-Radhuma		Marly limestone; dolomite anhydrite; 180-400 m thick	Brackish/saline ground water?

Figure II.6 The stratigraphic sequence of the Kuwait Group.

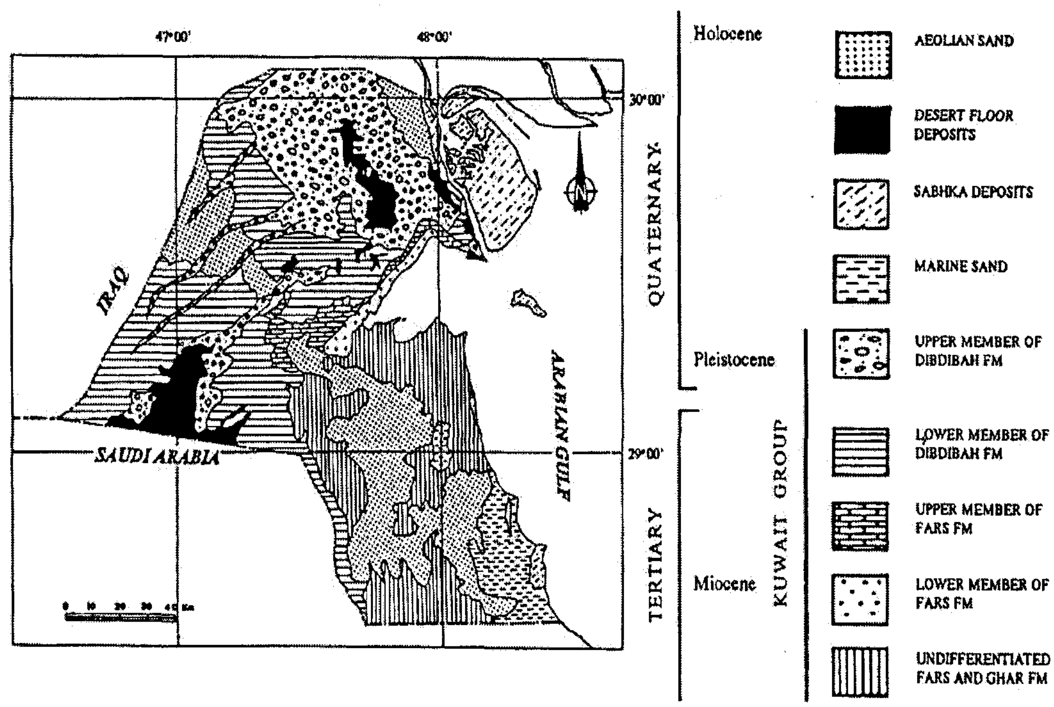

The thickness of the Kuwait Group increases from about 150 m in the southwest to about 400m in the northeast. The Kuwait Group is completely dry in the extreme southwest, and is almost saturated with water along the coast of the Arabian Gulf. Due to the absence of the Fars formation, the Kuwait Group is undifferentiated in southern Kuwait, i.e. the Wafra farms.

- **Dibdibba Formation**

The Dibdibba sequences lie between the top of the lower Fars formation and the base of the overlaid recent deposits. The Dibdibba term was used first by

Macfadyen (1938).

- **Upper Dibdibba Member.**

Sediments related to the upper Dibdibba member are present in the north and northeast Kuwait, where they underlie vast undulating gravel plains and ridges. The outcrop of this member extends from southeast Kuwait to the Saudi border to the northwestern plains. The base of this member is well-cemented, gritty calcareous sandstone. The member consists of sandy gravel, where the gravels are from lenses and thin banks, or are irregularly scattered within the sand matrix. The thickness of the upper Dibdibba member increases toward the northeast reaching about 30 m, near the Al-Raudhatain area.

- **Lower Dibdibba Member**

Sediments belonging to the lower member are exposed at the base of the Jal Az-Zor escarpment. The member is composed of medium to coarse sand with interbedded sand clay and sand limestone beds. The thickness of the member is unknown due to lack of fossils and the similarity of beds.

- **Fars Formations**

The Fars formation has been recognized in northern Kuwait, the name being adopted from exposure in the Fars province in southwest Iran. This formation is composed mainly of evaporite below the highest bedded anhydrite. In Kuwait, it consists of fine sediments, conglomeratic, calcareous sand stones, variegated shale (in the Raudhatain area) and thin fossiliferous limestone. The Fars formation is absent in the south, and its thickness ranges between 61 m to the west to 109 m to the north. It reaches the maximum thickness of about 182 m south of Bubiyan Island.

- **Ghar Formations**

This formation is named after its location in the Basra area of Iraq. It is composed of marine to terrestrial sand, silts and gravel. The dominant rock types are calcareous sandstone and clayey sand. The thickness of the Ghar formation increases from a southwesterly direction, reaching 182 m in the north and northeast of Kuwait. Considerable thickness of shale was indicated by drill cutting and by the electric and gamma ray logs over the lower Kuwait Group, encountered by wells drilled in the Al-Shigaya well field and some fields in the Al-Sulaibiya well field. A brown marly sandstone and fine crystalline limestone were recognized at the base of this formation, overlaying the erosional surface of the Dammam Formation.

II.3.3 Hasa Group

A marked erosional nonconformity separates the Kuwait Group from the underlying Hasa Group, which has a distinctive and widespread extent from Saudi

Arabia via Kuwait and Iraq to Iran. Aramco geologists working in Saudi Arabia named this group. It consists of the following formations:

1. Dammam formation	**limestone and dolomite limestone**
2. Rus formation	**anhydrite**
3. Umm-er-Rahduma formation	**limestone**

This group comprises the Paleocene to Eocene deposits, mainly carbonate sediments, partly dolomitizied at lower levels with anhydrite present in the middle part. The Umm-er- Rahduma consists mainly of lime stone, dolomite and anhydrite of the Paleocene age. The Rus formation consists of a massive anhydrate, unfossiliferous limestone with shale and marl beds which range in age from middle to lower Eocene. The Dammam Formation underlies the Kuwait Group in a nonconforming way, and it is the most widespread aquifer containing usable groundwater. It consists of nearly 182-212 m of porous chalky limestone and hard dolomite limestone with nummulitic green shale at the base. The top of the Dammam formation and the Husa Group is generally marked by the presence of a hard cherty layer with distinctive basal gray-green waxy shale. The piezometric head of the Dammam formation Group indicates that water levels were about 140 a.m.s.l. in the south western corner of Kuwait sloping towards the northeast. In addition, the head in the Dammam aquifer was 3 to 20 m higher than that in the Kuwait Group Aquifer (where piezometric head of the Kuwait Group at the same location was 120 a.m.s.l.). Hence, vertical leakage upward between aquifers is expected (Al-Ruwaih et al., 1998).

II.4 Hydrology of the Kuwait Group

The Kuwait Group hydrology was described in detail by Omar et al (1981). Barrat et al (1990, 1990a) have studied it further for the purpose of developing a regional aquifer flow model. The main features of the hydrology of the Kuwait Group as described in these sources are presented in the following sections.

II.4.1 Hydrostratigraphy

The clastic sequence of the Kuwait Group is hydrologically heterogeneous due to the uneven distribution of the clay lenses and variation in the degree of cementation both laterally and vertically. Lithological and geophysical studies show three recognizable zones of reduced hydraulic conductivity, caused by the preponderance of clayey ranges that can be correlated over large distances. Hence, these three zones act as aquitards and divide the Kuwait Group into three recognizable aquifer units. These aquitards and the aquifer sequence within the Kuwait Group, from top to bottom, are as follows:

-	**Dibdibba Aquifer (gravel sand).**
-	**Aquitard (silty sand).**
-	**Upper Kuwait Group Aquifer (sand and gravel).**
-	**Aquitard (clay and clay sand).**
-	**Lower Kuwait Group Aquifer (sand).**
-	**Aquitard (basal clay and cherty limestone at the top of Dammam formation).**

The unconfined Dibdibba aquifer is present only in north Kuwait, where some lenses of fresh water occupy the depression of Umm Al-Aish and the Raudhatain area. The upper Kuwait Group aquifer is underlies the whole of Kuwait, except in the north where the aquifer is semi-confined because of the presence of overlaying Dibdibba aquifer and the associated aquitard. However, in the Ahmadi area and in the southwestern corner of Kuwait the aquifer is dry, where the potentiometric head is below the base of the aquifer.

The lower Kuwait Group aquifer is present all over Kuwait and is mostly semi-confined due to the presence of the overlaying aquitard and the upper Kuwait Group aquifer. However, in the Ahmadi area and in the southwestern corner of Kuwait the aquifer is dry, due to the elevation of the aquifer base above the regional potentiometric head.

II.4.2 Potentiometry

All the subdivisions of the Kuwait Group, aquifers and aquitards, are connected with one another and with the underlying Dammam Formation. The regional potentiometric gradient is from southwest to northeast. Within the state of Kuwait, the Kuwait Group gains its water from the lateral inflow from Saudi Arabia and from the Dammam limestone through upward leakage (Figure II.7). The potentiometric head generally increases with depth giving rise to the upward component of the flow. The mean value of the head, however, decreases toward the northeast and east direction, toward the area of discharge, toward Kuwait Bay to be discharged by evapotranspiration at the marsh lands along the shoreline and ultimately into the bay and gulf by seepage. The piezometric head of the Kuwait Group indicates that water levels were about 120 a.m.s.l. in the southwestern corner of Kuwait (Al-Ruwaih et al., 1998), (Figure II.8).

Minor infiltration from rainfall occurs in Wadi and depression systems, mainly developed in northern Kuwait, where Dibdibba formation covers the surface. This has given rise to the freshwater lenses of the Raudhatain and Umm Al-Aish Fields.

II.4.3 Aquifer Parameters

The lithological heterogeneity and the variation in the saturation thickness have caused uneven distribution of transmissivity. Additionally, both upper and lower Kuwait Group aquifers are rarely tested individually for the determination of the aquifer parameters. Furthermore, all the available data refer to the composite system of these two aquifers. On the other hand, the Dibdibba aquifer was tested mainly in the areas of fresh water lenses occurrences.

Barrat et al (1990a) interpreted most of the available pumping test data and used the derived aquifer parameters in the development of the regional aquifer flow model. The parameters were adjusted within a reasonable limit during the calibration process. As suggested by Barrat et al (1990a) the Dibdibba aquifer has a transmissivity in the range of $0.1\text{-}2\text{x}10^{-3}$ m^2/s. The upper and the lower Kuwait Group aquifer together have variable transmissivities in the range of $1 - 0.02$ m^2/s.

Hence, lower and higher values may be present in isolated cases, and the transmissivity mostly decreases eastward.

Figure II.7 Schematic model of the groundwater flow system in Kuwait.

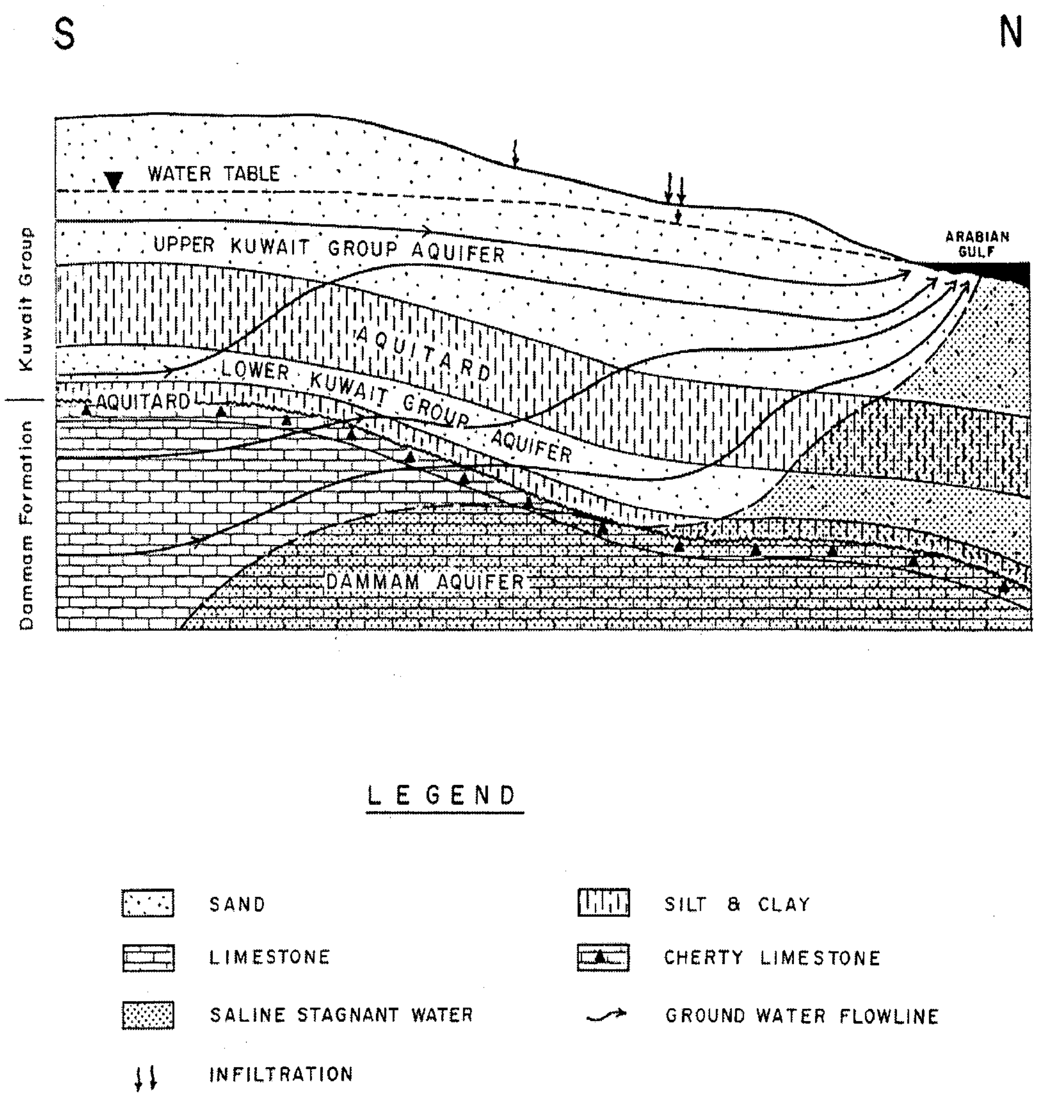

Figure II.8 Piezometric head of Kuwait Group.

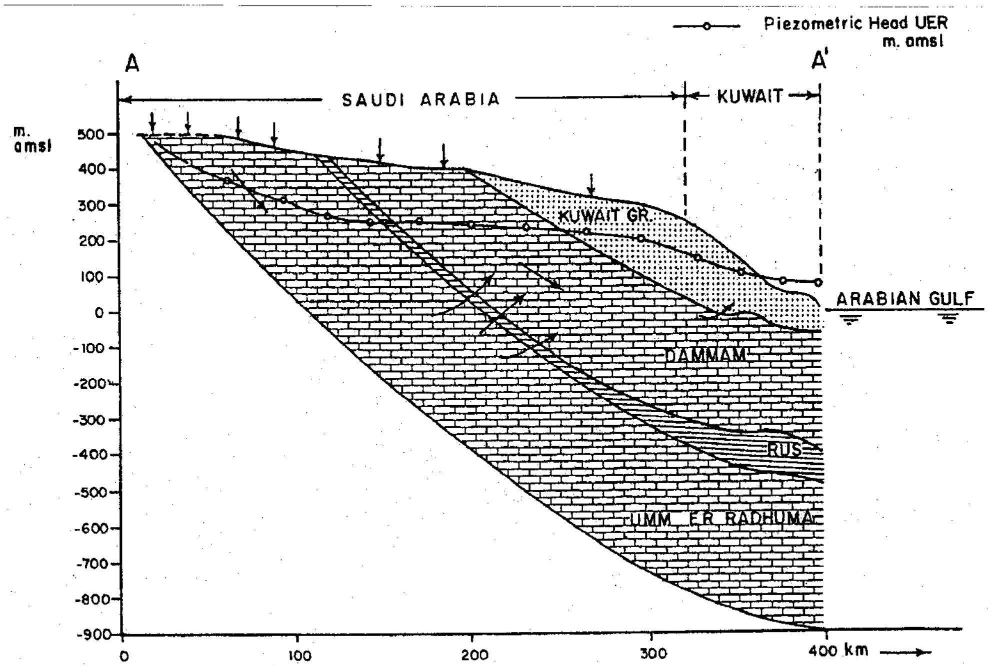

The storativity (storage coefficient) value used in the Barrat et al (1990a) study was in the range of 0.08 for the Dibdibba aquifer and for the combined upper and lower Kuwait Group aquifer in the Wafra and surrounding area in southern Kuwait, and in the range of 0.018 for the combined aquifer in the rest of the area, where the upper Kuwait Group is unconfined. For north Kuwait, where the upper Kuwait group is confined to semi-confined because of the presence of the overlying Dibdibba aquifer, storativity is in the range value of 1×10^{-4}.

A vertical hydraulic conductivity value in the range of 5×10^{-9} m/s was assigned by Barrat et al. (1990a) for the aquitard separating the Dibdibba aquifer from the upper Kuwait Group aquifer. A value in the range of 1.3×10^{-2} m/s was assigned for the combined aquifer in the rest of the area, where the upper Kuwait Group is unconfined.

For north Kuwait where the upper Kuwait Group is confined to semi-confined, due to the presence of the overlying Dibdibba aquifer, as evident in the Raudhtain and Umm Al-Aish field, a vertical hydraulic conductivity value of 5×10^{-9} m/s was assigned for the aquitard separating the Dibdibba aquifer from the upper Kuwait Group aquifer. A value in the range of 1.3×10^{-9} m/s was used for the aquitard separating the Dammam aquifer from the lower Kuwait Group, since the upper and lower Kuwait Group was considered a composite aquifer. In the Barrat et al. (1990a) study no vertical hydraulic conductivity value was assigned for the aquitard separating these two aquifers as evident in the Wafra area.

II.4.4 Hydrology of the Wafra Area

In the Al-Wafra area, the Kuwait group is undifferentiated, where there is no distinct or sharp boundary between the various layers of the formation. The total aquifer thickness ranges between 45 m in the west part to about 70 m in the east and northeast. Zonation of sediments sequence in the area is carried out on the basis of a mega-scopic description of the drill cutting supported by geophysical logging (Al-Sulaimi et al., 1993).

The petrographic study (Al-Sulaimi et al, 1993) of the drill cutting indicates the presence of four sediment types within the Kuwait Group aquifer, in addition to the topsoil (Figure II.9). The hydraulic conductivity of these soils is as follows:

Very coarse pebbly	10 m/d
Pebbly sand	9 m/d
Silty sand	0.1 m/d
Calcareous mud	0.001 m/d

Transmissivity of the aquifer in the Wafra area is unique and increasing from 150 m^2/d in the west to about 400 m^2/d in the east (Table II.2). Moreover, the specific yield (S_y) is estimated from simple trial and error of a subjective set of parameters using analytical pumping test software.

Table II.2 Wafra Agricultural Area Parameters, (personal communication with MEW, 2002).

LAND ELEVATION (M)	**120-140 MSL**
TOTAL DISSOLVED SOLIDS (TDS), (ppm)	**4000-9000** **Average 6000**
DEPTH TO WATER TABLE FROM GROUND SURFACE, (m)	**5-50**
TRANSMISSIVITY (m^2/day)	**150-400**
HYDRAULIC CONDUCTIVITY (m/day)	**3.5-7**

The studies showed that the potentiometric head is about 120m above mean sea level in the western part with a gradual decrease to the east to about 20 m above mean sea level. The lateral groundwater flow and transmissivity are known as the major controlling factors of the potentiometric head. On the other hand, the difference in potentiometric heads within the Kuwait Group aquifer in the Wafra is observed to be between a shallow sandy layer and deeper sandy layer. This suggests that silt and clay may occur at certain depth intervals to form a semi-pervious layer, separating the top and lower aquifer zones.

Figure II.9 The lithological cross section showing the heterogeneity in the study area.

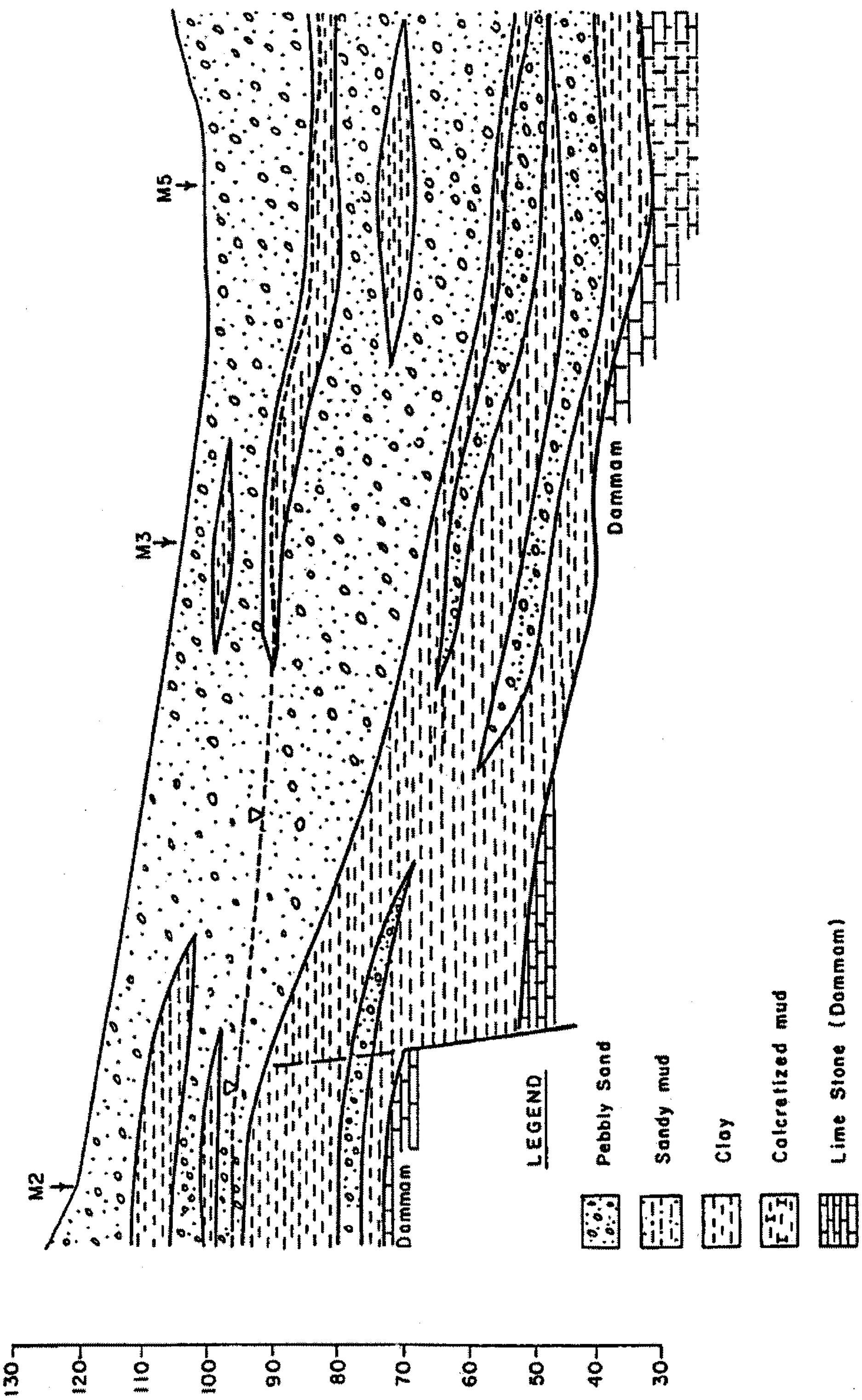

APPENDEXT III

DEPLETION

Figure III.1 Depletion of groundwater levels: the Kuwait Group 1960-90, (M. Al-Rashed et al.1998).

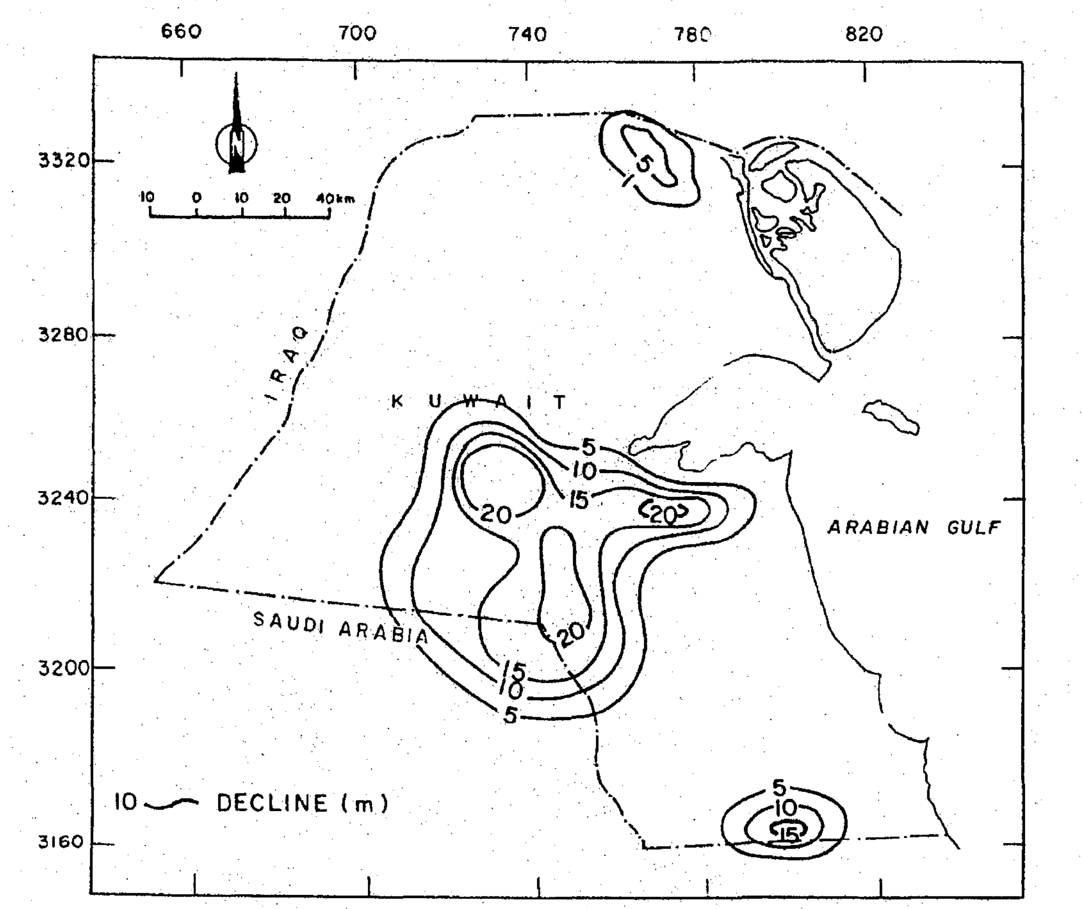

Figure III.2 Predicted decline in groundwater levels: the Kuwait Group 2010, (M. Al-Rashed et al.1998).

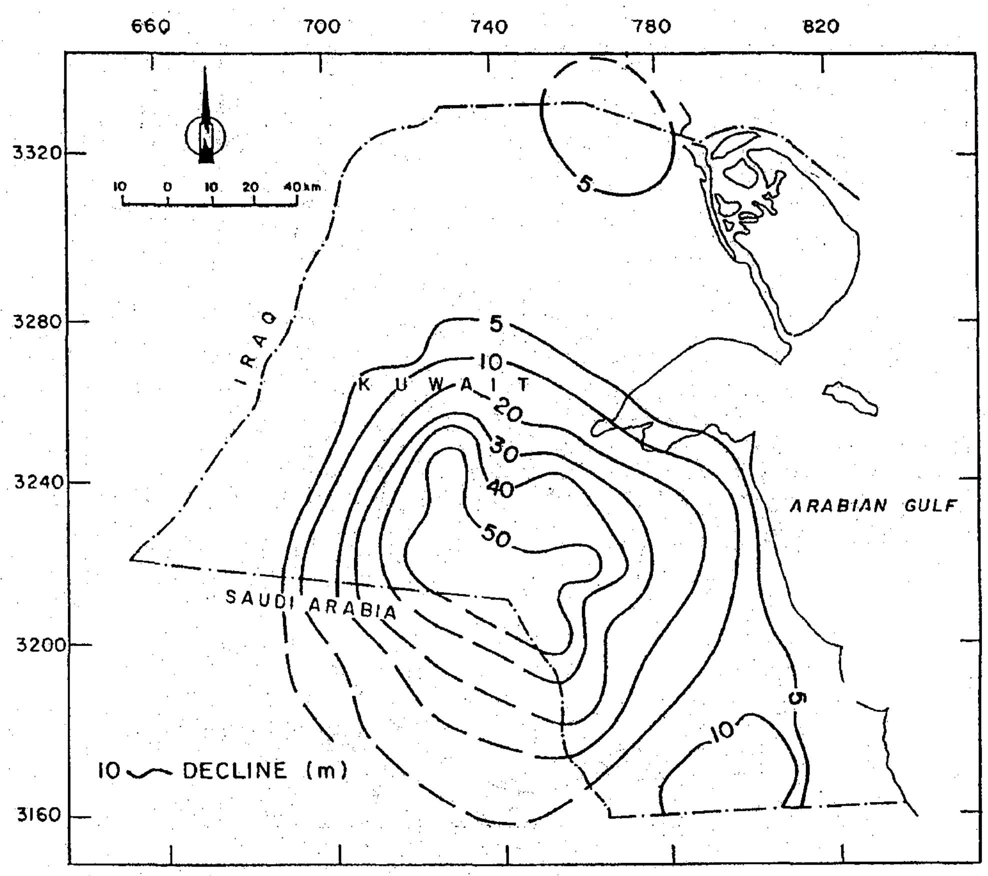

Figure III.3 Depletion of groundwater levels: the Dammam formation 1960-90, (M. Al-Rashed et al.1998).

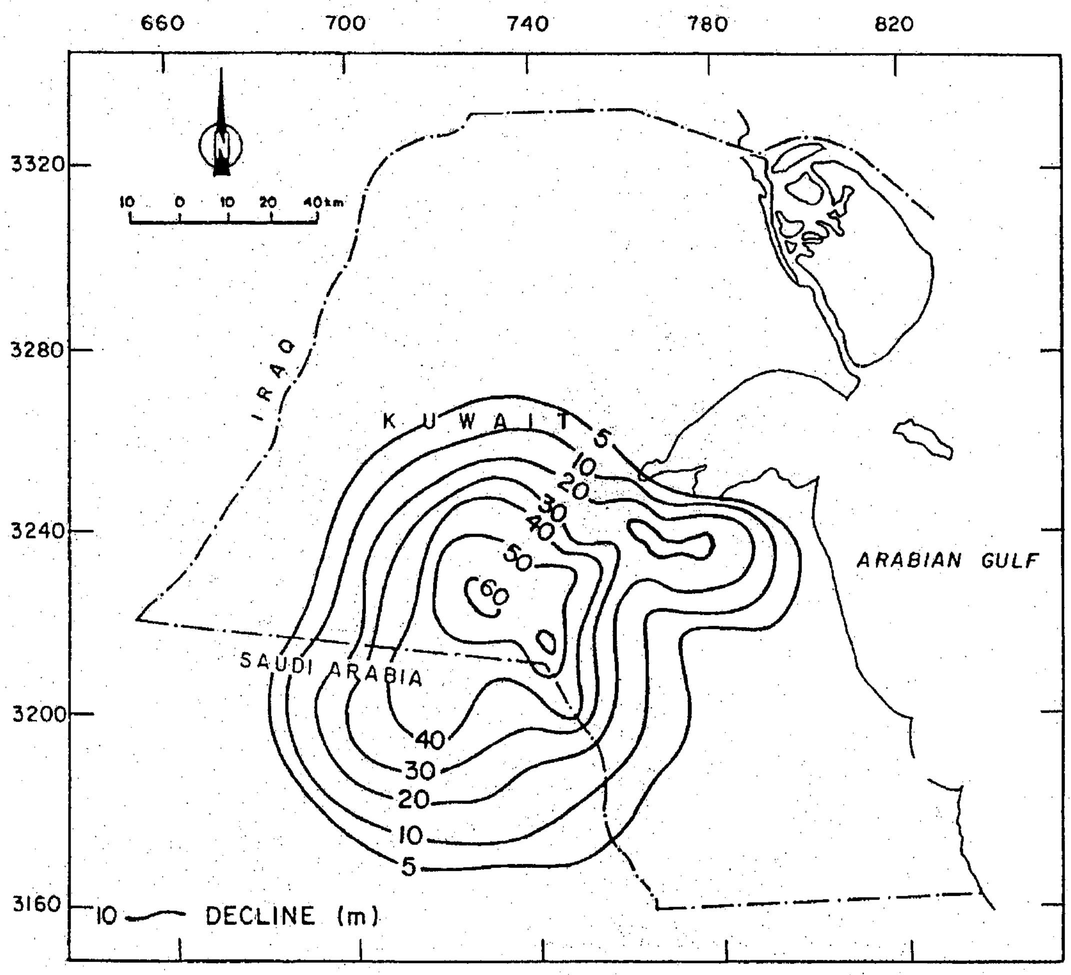

Figure III.4 Predicted decline in groundwater levels: the Dammam formation 2010, (M. Al-Rashed et al.1998).

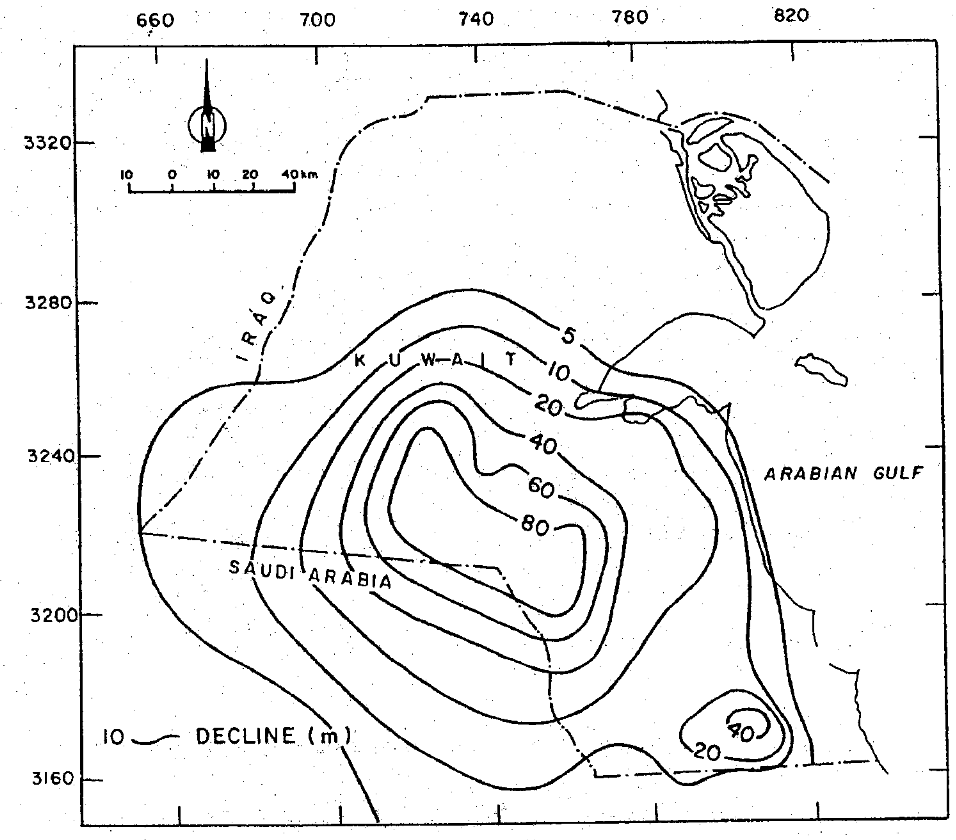

APPENDEXT IV

TDS CONTURES

Figure IV.1 TDS contours of the Wafra farms – Kuwait Group – upper horizon (ppm x 1000) – Initial.

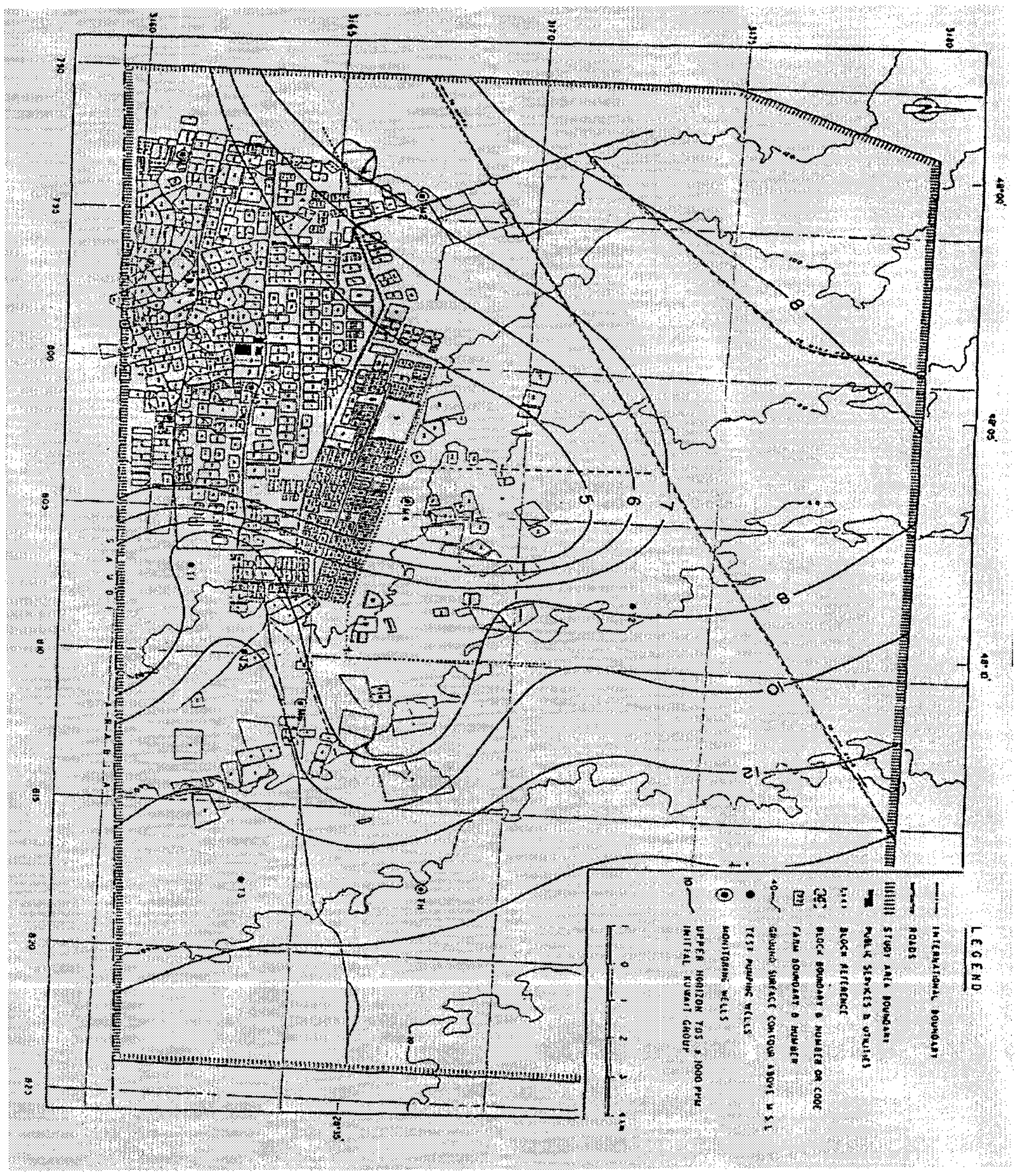

Figure IV.2 TDS contours of the Wafra farms – Kuwait Group – upper horizon (ppm x 1000) – 1993.

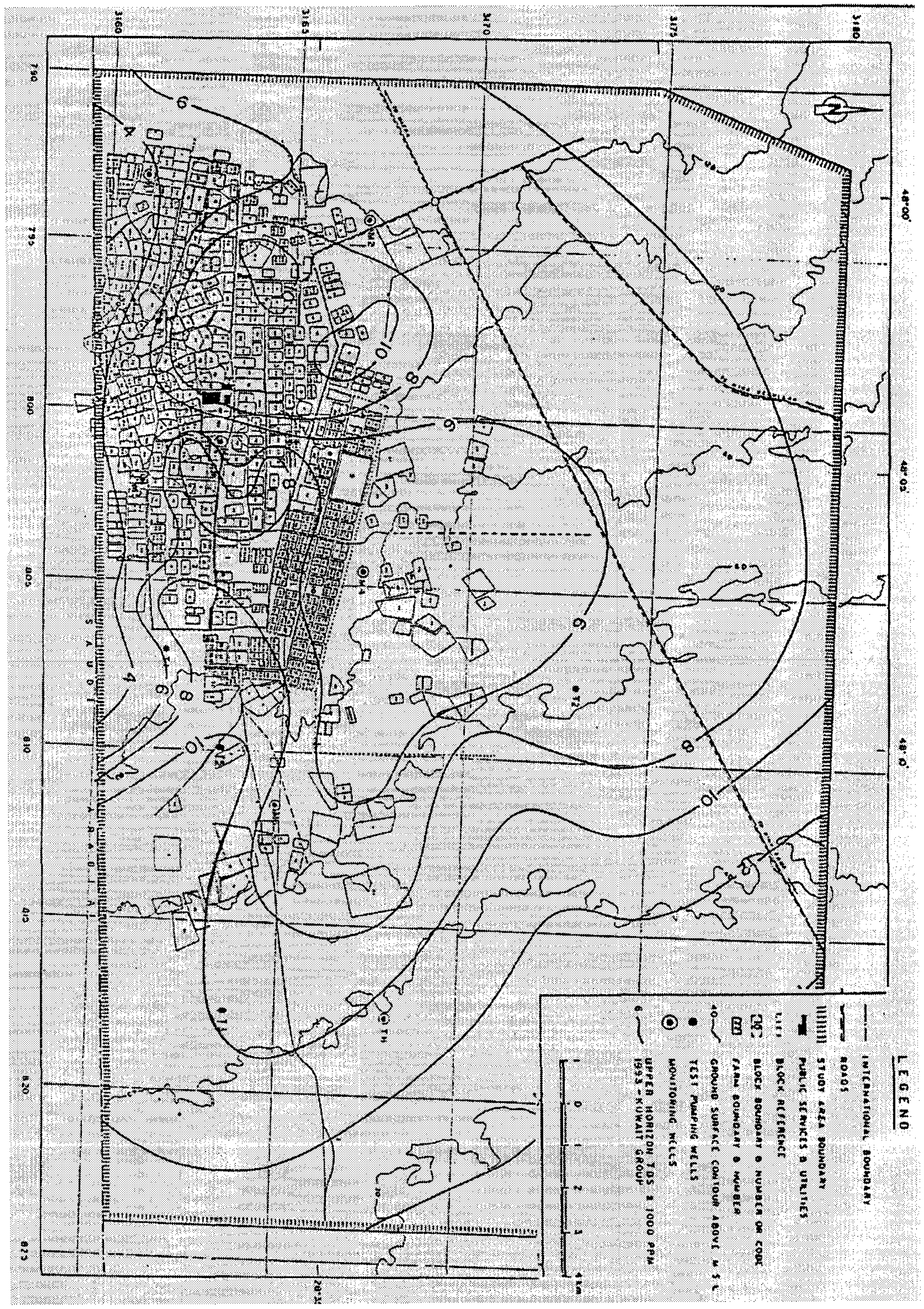

APPENDIX V

V.1 Evapotranspiration

Water from precipitation or irrigation can enter the soil where it comes into contact with the crop root system. Evapotranspiration is the water removed from soils and plant surface by evaporation and plant transpiration. Soil evaporation is a direct pathway for water to move from the soil to the atmosphere as water vapor. Over the course of an irrigation season, soil evaporation is 20-30 percent of total ***ET***. Soil evaporation rates are highest after irrigation or rainfall. At those times the soil surface is wet and the water readily evaporates. As the soil dries the soil evaporation rates will decline. Plant transpiration is evaporation of water from leaf and plant tissue, expressed as the total latent heat transfer per unit area or its equivalent depth of water per unit area. Transpiration is the last step in a continuous water pathway from the soil, into the plant roots, through the plant stems and leaves, and out into the atmosphere. Water conditions "drive" the system by pulling the water "uphill" through the entire pathway. Since water in this pathway also carries nutrients, transpiration is an essential process in plant life. The tremendous drying force that the atmosphere exerts drives both evaporation and transpiration on soil and plant surfaces. Water movement from higher to lower pressure shows the relative forces that exist in water as it is drawn through the plant or directly from the soil, where water is drawn or "pulled" by more negative tensions as it moves from the soil, through the plant and into the atmosphere.

V.1.1 Factors That Affect Evapotranspiration

- **Weather**

The power of the atmosphere to evaporate water is the driving force for soil evaporation and crop transpiration. Weather factors that have a major impact on this evaporative power include: air temperature, humidity, solar radiation, and wind. High air temperatures, low humidity, clear skies and high winds cause a large evaporative demand by the atmosphere. The crop may or may not be able to satisfy the atmosphere's evaporative demand, but the weather factors set the potential for ***ET***. This potential for ***ET***, governed by weather factors, is the starting point for estimating ***ET*** from weather data. Day-to-day variations in weather cause day-to-day variations in daily potential ***ET***. The actual crop ***ET*** (or crop water use) also responds to these weather variations.

- **Crop Type**

Different crops use different amounts of water over the course of the growing seasons. Crop planting times and water use patterns are somewhat different among the crops. Differences in water use among different crops are mainly due to planting time and days to maturity.

- **Crop Growth Stage**

During the course of the growing season, ***ET*** from a crop depends not only on the potential ***ET*** demand from the atmosphere, but also on the crop's stage of growth. ***ET*** is related to leaf surface area, so small plants transpire less water than large ones. Due to growth patterns of different crops, maximum ***ET*** occurs at different times during the calendar year. As crops continue through reproductive processes and approach maturity, ***ET*** decreases.

- **Crop Variety**

The relative maturity range of a particular variety has the most impact on seasonal crop ***ET***. At the same location, a crop variety with a maturity, as an example, of 120 days, will use more water than an 85 day variety. However, if both varieties are able to mature fully, the yield produced for each mm of ***ET*** is approximately equal. Longer season crop varieties use more water, but they also produce more yields if the heat units and water supply are available. The difference in water use is due to total days of water use, not a difference in daily water use.

- **Surface Cover and Tillage**

The amount of soil surface cover influences soil evaporation. When the soil surface is wet, evaporation depends on the amount of radiant energy at the soil surface. Lowest evaporation rates occur from shaded and mulched soil surfaces. Crops shade more and more of the soil as they grow, but soil evaporation continues. However, crop residues can reduce soil evaporation during the irrigation season.

- **Availability of Soil Water**

Research shows soil water content cannot be considered alone as the single factor controlling whether crop ***ET*** is reduced below its potential rate. The ability of soil to transmit water to plant roots and the actual evaporative demand for a given day also are important. For progressively drier soil, actual crop ***ET*** is below the demand rate. The drier soil is unable to transmit water to the roots fast enough to satisfy higher potential ***ET*** demand. When the soil is very dry, plants may not experience reductions in ***ET***, if the potential ***ET*** demand is low. Controlling factors are the potential ***ET*** demand and the soil's ability to transmit water to the roots. This transmitting ability is different for every soil, and for a given soil, it depends on the water content. When crops do not receive water to meet their ***ET*** demand, yields can be reduced. Limited water applications targeted to critical growth stages can be very effective for yield production.

V.1.2 Evapotranspiration and Crop Yield

Evapotranspiration is important to irrigation management because crop yield relates directly to ***ET***. Since yield increases linearly with ***ET***, maximum yield will not be reached unless the maximum ***ET*** level is reached. Irrigators who are working to achieve maximum yields need to apply water to meet the crop's ***ET*** demand. Applying extra water beyond ***ET*** demand will not translate into extra yield.

A particular crop variety responding to a particular climate has only so much capacity to transpire water. The goal for irrigation managers is to convert water to ***ET*** and ultimately to yield. It is not possible to convert all water into ***ET*** and yield. Furthermore, it takes more irrigation water to reach the same yield level from an inefficient system than a more efficient one. Crops, including corn, winter wheat, and determinate soybeans, need water during reproductive and grain filling growth stages. Indeterminate soybeans, which flower over a longer time, need water especially during grain filling. Little or no water was applied during vegetative growth. When crops do not receive water to meet their ***ET*** demand, yields can be reduced. Limited water applications targeted to critical growth stages can be very effective for grain production.

V.1.3 Estimating Evapotranspiration and Irrigation Water Requirements

Weather stations measure and record data, air temperature, relative humidity, incoming radiation, and wind speed. These data are used to calculate potential ***ET***, which estimates crop weather use for the region. The crop ***ET*** is calculated from potential ***ET***, reference evapotranspiration. Growth stages of crops are based on growing degree and days accumulated since crop emergence. The growth stages, crop density, and other cultural factors affecting ***ET*** combined with the potential ***ET***, from the weather data, give crop ***ET*** estimates. Moreover, irrigation water requirements will then be calculated from the crop ***ET***, and other essential factors like rainfall, runoff, deep percolation, etc. Thus, underprediction of evapotranspiration, ***ET***, introduces inaccuracies in water-balance irrigation scheduling procedures, which might lead to a significant reduction in the crop yield. Stockle et al. (1991) showed that yield reductions, ranging from 1 to 7% and from 8 to 27%, were predicted when daily evapotranspiration, ***ET***, was under predicted by 15% and 30%, respectively. Doorenbos and Pruitt (1977) defined the irrigation water requirements as "the depth of water needed to meet the water losses through evapotranspiration, ***ET***, of a disease-free crop, growing in a large field under non-restricting soil conditions including soil water and fertility and achieving full production potential under the given growing environment." Figure (V.1) shows a typical flow chart for estimating irrigation water requirements from climatic data using some selected evapotranspiration methods.

V.1.4 Evapotranspiration Calculation Method

The most recent methods of estimating evapotranspiration involve two essential steps. First, to estimate the potential or 'reference' evapotranspiration for a well-watered reference, alfalfa or grass, ET_r and ET_g respectively, a crop with standard canopy

Figure V.1 Typical flow chart for estimating irrigation water requirements from climatic data (Burman et al., 1980, 1983).

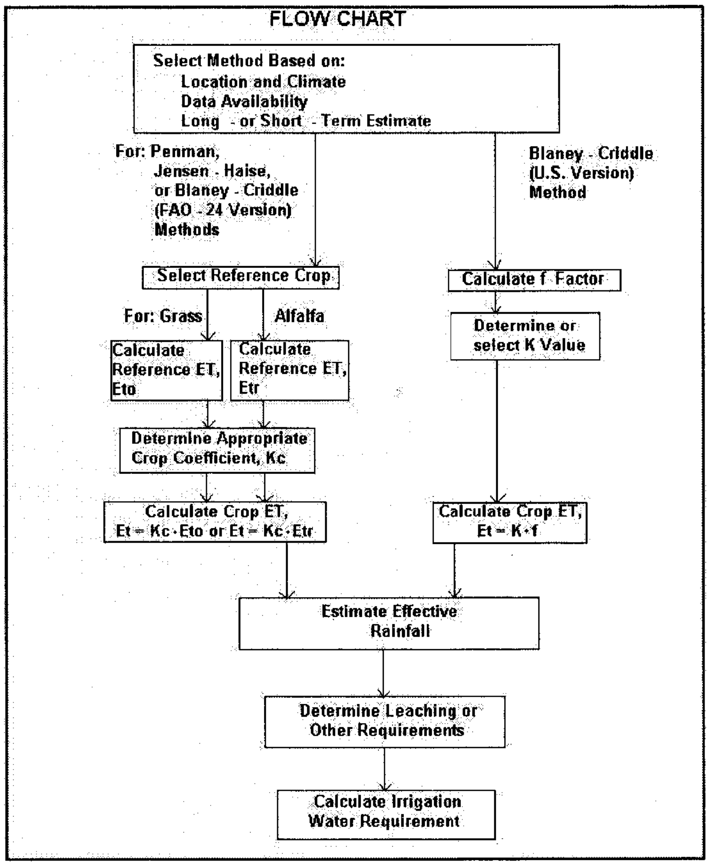

characteristics is considered. Second, to estimate the evapotranspiration, $\boldsymbol{ET_c}$, for the crop being considered multiply the evapotranspiration, $\boldsymbol{ET_g}$ or $\boldsymbol{ET_r}$, of the reference crop by a crop coefficient, "$\boldsymbol{K_c}$", which varies by the growth stage for each crop, Figure (V. 2). The distribution of the crop coefficient during the growing cycle of the crop is called "crop curves." Moreover, crop curves can be obtained experimentally and these curves represent the integrated effect of the changes of leaf area, degree of cover and canopy resistance, plant height, and albedo, α, on evapotranspiration, ET_g or ET_r, relative to the reference crop. Moreover, the correct reference crop ET must be used to obtain reliable estimates of ET_c. Thus, crop coefficients derived using a grass reference evapotranspitation, ET_g, should not be used with alfalfa reference evapotranspiration, ET_r, or vice versa,

where,

$$ET_c = ET_r \times K_c \qquad \text{(Alfalfa as a reference crop)} \quad \textbf{(V.1)}$$

$$ET_c = ET_g \times K_c \qquad \text{(Grass as a reference crop)} \quad \textbf{(V.2)}$$

and,

$$K_c = K_{cb} * K_a + K_s \qquad \text{(Basal crop coefficient)} \quad \textbf{(V.3)}$$

Or,

$$K_c = K_{cm} * K_a \qquad \text{(Mean crop coefficient)} \quad \textbf{(V.4)}$$

where,

K_{cb} = Curves represent basal crop coefficient for conditions when the soil surface is visually dry, so that evaporation is minimal but the availability of soil water does not limit plant growth or transpiration,

K_a = A dimensionless coefficient dependent on available soil water, the value of K_a =1 unless available soil water limits transpiration, in which case it has a value less than 1,

Figure V.2 Reference (ET_o), and crop evapotranspiration (ET_c).

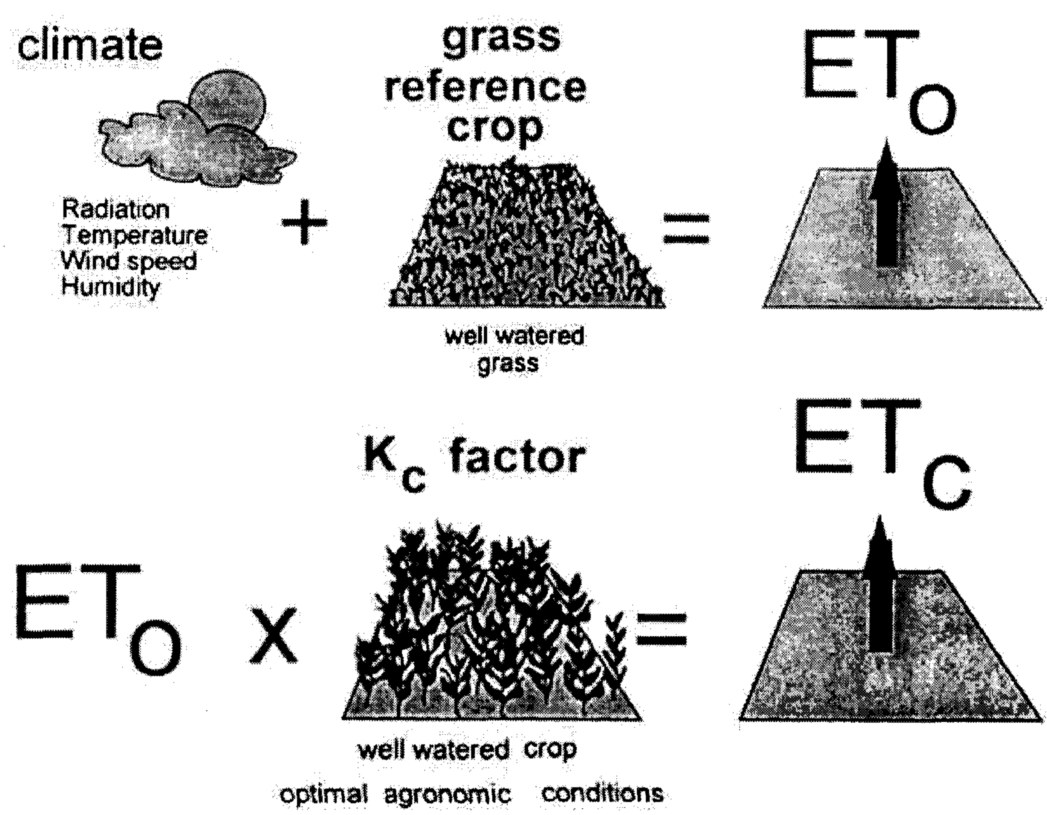

K_s = A coefficient to adjust for increased evaporation from wet soil immediately after rain and/or irrigation, and

K_{cm} = Mean crop coefficient, which includes wet soil effects

V.1.5 Types of Potential or 'Reference' Evapotranspiration, ET_g or ET_r, Methods

- **Combination methods**

Penman Combination Equation. Penman (1948, 1963) first derived the combination equation. He combined components to account for energy required to sustain evaporation and a mechanism required to remove the vapor, eliminating surface temperature and surface vapor pressure in the process. The energy source involved an estimate of net radiation from extraterrestrial radiation, percentage of sunshine, and humidity. From the sensible and latent heat equation,

$$\lambda E = (R_n - G)/(1+\beta) \qquad \textbf{(V.5)}$$

where,

λE = Latent heat flux (positive during evaporation),

R_n = Net radiation flux at the surface,

G = Sensible heat flux to the soil (positive if the soil is warming),

β = Bowen ratio, $\beta = H / \lambda E$, and

H = Sensible heat flux to the air (positive if the air is warming).

Penman developed the general form of the Penman combination equation as follows:

$$\lambda ET_g = \left(\frac{\Delta}{\Delta + \gamma'}\right) * (R_n - G) + \left(\frac{\gamma'}{\Delta + \gamma'}\right) * 6.43 * W_f (e^\circ_z - e_z) \quad \text{(V.6)}$$

$$\Delta = \frac{de^\circ}{dT} = 0.2 * (0.00738 * T + 0.8072)^7 - 0.000116 \;,$$

for $T \geq$ -23°C, Δ [kPa °C] **(V.7)**

$$\gamma' = \frac{c_p * P}{0.622 * \lambda} \;, \text{[kPa °C}^{-1}\text{]} \quad \text{(V.8)}$$

$$P = 101.3 - 0.01055 * EL \;, \text{[kPa]}, EL \text{ [m]} \quad \text{(V.9)}$$

$$\lambda = 2.501 - 2.361 \times 10^{-3} * T \text{, [MJ Kg}^{-1}\text{], } T \text{ [°C]} \qquad \textbf{(V.10)}$$

$$e^{\circ} = exp[\frac{16.78T - 116.9}{T + 237.3}] \qquad \textbf{(V.11)}$$

$$R_n = (1 - \alpha) * R_s \downarrow - R_b \uparrow \qquad \textbf{(V.12)}$$

$$R_s = (0.25 + 0.5 * n/N) * R_A \qquad \textbf{(V.13)}$$

$$R_b = [a * \frac{R_s}{R_{so}} + b] * R_{bo} \qquad \textbf{(V.14)}$$

$$R_{so} = \frac{R_s}{(0.35 + 0.61 * S)} \qquad \textbf{(V.15)}$$

$$R_{bo} = \acute{\varepsilon} * \sigma * T^4 = [a_1 + b_1\sqrt{e_d}] * \sigma * \left(\frac{T^4{}_{mean,max} + T^4{}_{mean,min}}{2}\right) \qquad \textbf{(V.16)}$$

$$G = 4.19 * \frac{(T_{i+1} - T_{i-1})}{\Delta t} \qquad \textbf{(V.17)}$$

$$W_f = a_w + b_w * u_2 \qquad \textbf{(V.18)}$$

where,

Δ = Slope of the saturation-vapor pressure temperature curve,

γ' = Psychometric constant for fully aspirated spectrometers,

W_f = Wind function,

T = Ambient air temperature,

P = Atmospheric pressure,

c_p = Specific heat of air at constant pressure,

λ = Latent heat of vaporization,

EL = Elevation,

e^o = Saturated vapor pressure,

e_d = Saturated vapor pressure at mean dew-point temperature,

R_A = Solar radiation above atmosphere (extraterrestrial radiation),

R_s = Solar radiation measured at earth's surface,

$\boldsymbol{R_b}$ = Net outgoing long-wave, thermal radiation,

$\boldsymbol{R_{so}}$ = Cloudless day solar radiation measured at earth's surface,

$\boldsymbol{R_{bo}}$ = Net outgoing long-wave, thermal radiation on a clear day,

$\boldsymbol{\alpha}$ = Short-wave reflectance or albedo,

$\boldsymbol{n/N}$ = Ratio between actual measured bright sunshine hours and maximum possible sunshine hours,

$\boldsymbol{a}$ = Experimental coefficient for net long-wave radiation equation,

$\boldsymbol{b}$ = Experimental coefficient for net long-wave radiation equation,

$\boldsymbol{a_1}$ = Experimental coefficient for net long-wave radiation equation,

$\boldsymbol{b_1}$ = Experimental coefficient for net long-wave radiation equation,

$\boldsymbol{\sigma}$ = Stefan-Boltzmann constant,

$\boldsymbol{\acute{\varepsilon}}$ = Net emissivity when using only screen height temperature,

S = Ratio of actual to possible sunshine,

a_w = Linear wind coefficient at height of 2 m,

b_w = Linear wind coefficient at height of 2 m,

Δt = Change in time, and

u_2 = Wind speed at height of 2 m.

Vapor Pressure Deficit, $d_a = (e^{\circ}_z - e_z)$, can be calculated in four different ways depending on the type of applied equation, where

Method 1,

$$d_a = (e^{\circ}_z - e_z) = e^{\circ}(T_{mean}) - e^{o}(T_{dew}) \tag{V.19}$$

Method 2,

$$d_a = (e^{\circ}_z - e_z) = e^{\circ}(T_{mean}) * \left(1 - \frac{RH_{max} + RH_{min}}{2}\right) \tag{V.20}$$

Method 3,

$$d_a = (e^\circ_z - e_z) = \frac{e^\circ(T_{max}) + e^\circ(T_{min})}{2} - e^\circ(T_{mean\,(dewpoint)}) \quad \textbf{(V.21)}$$

<u>Method 4,</u>

$$(e^\circ_z - e_z) = \frac{\left(e^\circ(T_{max}) - e^\circ(T_{mean-dew})\right) + \left(e^\circ(T_{min}) - e^\circ(T_{mean-dew})\right)}{2} \quad \textbf{(V.22)}$$

Penman-Monteith Combination Equation. Some other essential combination equations are widely available and useful like the Penman-Monteith Combination equation (Monteith, 1981), including the aerodynamic and surface resistance aspect terms, the aerodynamic resistance to sensible and vapor transfer, and surface resistance to vapor transfer into the combination equation,

where,

$$\lambda ET = (\frac{\Delta}{\Delta + \gamma^*}) * (R_n - G) + (\frac{\gamma'}{\Delta + \gamma^*}) * K_1 * \frac{0.622\lambda\rho}{P} * \frac{1}{r_a} * (e^\circ_z - e_z) \quad \textbf{(V.23)}$$

$$\gamma^* = \gamma * (1 + {}^{r_c}\!/_{r_a}) \quad \textbf{(V.24)}$$

$$K_1 * \frac{0.622\lambda\rho}{P} = 1710 - 6.85 * T,\ u_z\ [\mathrm{m\ s^{-1}}],\ T\ [^\circ\mathrm{C}] \quad \textbf{(V.25)}$$

$$K_1 * \frac{0.622\lambda\rho}{P} = 19.8 - 0.08 * T, \; u_z \text{ [km d}^{-1}\text{]}, \; T \text{ [}^{o}\text{C]} \tag{V.26}$$

$$r_a = \frac{ln[(z_w - d)/z_{om}] * ln[(z_p - d)/z_{ov}]}{(0.41)^2 * u_z} \tag{V.27}$$

$$\rho = 1.23 - 0.112 * EL \times 10^{-3} \;, \text{[kg m}^{-3}\text{]}, \; EL \text{ [m]} \tag{V.28}$$

$$\frac{h_c}{z_o} = 8.15 \tag{V.29}$$

$$z_{om} = \frac{h_c}{8.15} = 0.123 * h_c \tag{V.30}$$

$$z_{ov} = 0.1 * z_{om} \tag{V.31}$$

$$d = \frac{2}{3} * h_c \tag{V.32}$$

Allen et al. (1989) developed procedures for approximating the leaf-area index, ***LAI***, of grass and alfalfa reference crops as a function of canopy height as follows:

For clipped grass less than 15cm in height, then

$$LAI = 0.24 * h_c, \; h_c \text{[cm.]} \quad \text{(V.33)}$$

For non-clipped grass and alfalfa greater than 3 cm height and harvested only periodically, then

$$LAI = 1.5 * Ln(h_c) - 1.4, h_c \text{ [cm]} \quad \text{(V.34)}$$

Daily and monthly values of canopy resistance in cm^{-1} were estimated as,

$$r_c = \frac{100}{(0.5 * LAI)} \quad \text{(V.35)}$$

where,

K_1 = Dimension coefficient, insuring the term units,

ρ = Air density,

r_a = Aerodynamic resistance to sensible heat and vapor transfer,

r_c = Surface resistance to vapor transfer,

z_w = Height of the wind speed measurement,

z_{om} = Roughness length for momentum transfer,

z_p = Height of the humidity (psychrometer) and temperature measurement,

z_{ov} = Roughness length for vapor transfer,

z_o = Momentum transfer for bluff bodies,

u_z = Wind speed at height z_w,

d = Displacement height for a crop,

h_c = Mean height of a canopy, and

LAI = Leaf-area index.

From the original Penman-Monteith equation and the equations of the aerodynamic and canopy resistance, the FAO 56 Penman-Monteith, equation has been derived thus:

$$ET_o = \frac{0.408 * \Delta * (R_n - G) + \gamma * \frac{900}{T + 273} * u_2 * (e_s - e_a)}{\Delta + \gamma * (1 + 0.34 * u_2)} \quad \textbf{(V.36)}$$

where,

$\boldsymbol{ET_o}$ = Reference evapotranspiration [mm day^{-1}],

$\boldsymbol{R_n}$ = NET radiation at the crop surface [MJ m^{-2} day^{-1}],

$\boldsymbol{G}$ = Soil sensible heat flux density [MJ m^{-2} day^{-1}],

$\boldsymbol{T}$ = Mean air temperature at 2 m height [°C],

$\boldsymbol{u_2}$ = Wind speed at 2 m height [m s^{-1}],

$\boldsymbol{e_s}$ = Saturation vapor pressure [kPa],

$\boldsymbol{e_a}$ = Actual vapor pressure [kPa],

$\boldsymbol{e_s - e_a}$ = Saturation vapor pressure deficit [kPa],

Δ = Slope vapor pressure curve [kPa °C^{-1}],

γ' = Psychometric constant [kPa °C^{-1}].

$\boldsymbol{0.408 = \frac{1}{\lambda} = \frac{1}{2.54}}$, where λ = Latent heat of vaporization, to change from

[MJ/m2/day] to [mm/day].

The FAO Penman-Monteith equation determines the evapotranspiration from the hypothetical grass reference surface and provides a standard to which evapotranspiration in different periods of the year or in other regions can be compared and to which the evapotranspiration from other crops can be related.

Alfalfa-Reference combination equations

These equations are based on studies conducted in Kimberly, Idaho (Jensen et al., 1970, 1971; Wright, 1982; Wright and Jensen, 1972). Furthermore, these equations estimate the alfalfa reference evapotranspiration, ET_r, and can be used with either the basal or average type of crop coefficients. In all the cases, the vapor pressure deficit, d_a, is calculated by method 3.

$$\lambda ET_r = \left(\frac{\Delta}{\Delta+\gamma}\right) * (R_n - G) + \left(\frac{\gamma'}{\Delta+\gamma}\right) * 6.43 * W_f (e^\circ_z - e_z) \quad \textbf{(V.37)}$$

$$W_f = a_w + b_w * u_2 \quad \textbf{(V.38)}$$

Method 3.

$$d_a = (e_z^o - e_z) = \frac{e^o(T_{max}) + e^o(T_{min})}{2} - e^o(T_{dew}) \quad \textbf{(V.21)}$$

Kimberly Penman (1982) Equation. Wright (1982) presents a variable wind function coefficient for alfalfa reference evapotranspiration, ET_r, expressed as fifth-order polynomials with calendar day, D, as the independent variable.

$$a_w = 0.4 + 1.4 * exp\{-[\frac{(D-173)}{58}]^2\} \qquad \textbf{(V.39)}$$

$$b_w = 0.605 + 0.345 * exp\{-[\frac{(D-243)}{80}]^2\}\ , \quad u_2\ [\mathrm{m\ s^{-1}}] \qquad \textbf{(V.40)}$$

$$b_w = 0.007 + 0.004 * exp\{-[\frac{(D-243)}{80}]^2\}\ , u_2\ [\mathrm{km\ d^{-1}}] \qquad \textbf{(V.41)}$$

Kimberly Penman (1972) Equation. Kimberly Penman (1972) recommended for humid and arid areas with wind in ms^{-1} and for alfalfa –related combination equation with units of MJ m^{-2} d^{-1} as,

$$W_f = (1 + 0.0536 * u_2) \qquad \text{(Penman 1948)} \qquad \textbf{(V.42)}$$

$$W_f = (0.75 + 0.993 * u_2) \qquad \text{(Wright and Jensen, 1972)} \qquad \textbf{(V.43)}$$

Wright and Jensen (1972) Equation. Wright and Jensen (1972) recommended Equation (V.42) for alfalfa in coastal and humid climates and Equation (V.43) for arid and semiarid areas.

Grass-Reference combination equations

FAO Penman Equation. The FAO-24 presented by Doorenbos and Pruitt (1975, 1977) showed a modified Penman equation for estimating grass-reference evapotranspiration, ET_g. This modification involved a more sensitive wind function than used by Penman, an adjustment factor c which is based on local climate conditions. Moreover, they assumed that $G = 0$, the sensible heat flux to the soil, on a daily basis. The vapor pressure deficit, d_a, is calculated by Method 1 when dew-point temperatures are available, otherwise by Method 2.

$$\lambda ET_g = c * [(\frac{\Delta}{\Delta + \gamma'}) * (R_n - G) + (\frac{\gamma'}{\Delta + \gamma'}) * 2.7 * W_f(e^\circ_z - e_z)] \quad \textbf{(V.44)}$$

$$W_f = (1 + 0.864 u_2) \quad \textbf{(V.45)}$$

Where, the vapor pressure deficit is calculated when dew-point temperature is feasible by Method 1.

$$(e^\circ - e_z) = e^\circ(T_{mean}) - e^\circ(T_{dew}) \quad \textbf{(V.19)}$$

otherwise, by Method 2.

$$d_a = (e^\circ_z - e_z) = e^\circ(T_{mean}) * [1 - \frac{RH_{max} + RH_{min}}{2}] \qquad \textbf{(V.20)}$$

The adjustment factor, c, can be used from FAO tables, or can be used by

$$c = 0.68 + 0.0028 RH_{max} + 0.018 R_s - 0.068 U_2 + 0.013 \, {U_d}/{U_n} + 0.0097 U_d \, {U_d}/{U_n}$$
$$+ 0.430 \times 10^{-4} RH_{max} R_s U_d \qquad \textbf{(V.46)}$$

where,

RH_{max} = Maximum daily relative humidity in percentage,

RH_{min} = Minimum daily relative humidity in percentage,

U_d = Daytime wind speed, and

U_n = Nighttime wind speed.

Priestly-Taylor (1972) Equation. Priestly-Taylor (1972) proposed a simplified version of a grass reference combination equation for use when surface areas generally are wet. The aerodynamic component was deleted and the energy component was multiplied by a coefficient, α = 1.26, when the general surrounding area is wet or under humid conditions,

where,

$$\lambda E_p = \alpha * (\frac{\Delta}{\Delta + \gamma'}) * (R_n - G) \quad \textbf{(V.47)}$$

Other grass references include the 1963 Penman equation (Penman 1963) and the FAO-PPP-17 equation proposed by Frére and Popov (1979). Wind function coefficients for these grass reference combination equations as well as other alfalfa reference combination equations are presented in Table (V. 1).

- **Radiation methods**

Empirical radiation equations for estimating potential evapotranspiration are based generally on the energy balance variables from sensible and latent heat equation in the form of,

$$R_n = \lambda E + H + G \quad \textbf{(V.48)}$$

Most radiation methods take one of the following forms,

$$\lambda E = K_c * \phi_1 * R_n \quad \textbf{(V.49)}$$

and,

$$\lambda E = K_c * \phi_2 * R_s \quad \text{(V.50)}$$

Table V.1 Comparison of linear coefficient for use in the ET_r and ET_g combination equations, and associated methods of calculating vapor saturated deficit. (After ASCE-Manuals and Reports on Engineering Practice-No. 70).

Method and Reference saturation Surface method	Wind Coefficient at height of 2 m. $[W_f = a_w + b_w * u_2]$ u_2 in ms^{-1}		u_2 in kmd^{-1}		Vapor deficit
	a_w	b_w	a_w	b_w	$(e_z^o - e_z)$
Penman *(Penman 1948, 1963)*, **clipped grass**	1.0	0.537	1.0	0.0062	Method 1
1972 Kimberly Penman *(Wright & Jensen 1972)*, **alfalfa, 30-80 cm.**	0.75	0.993	0.75	0.75	Method 3
1982 Kimberly Penman *(Wright, 1982)*, **alfalfa**	Eq. (V.39)	Eq. (V.40)	Eq. (V.39)	Eq. (V.41)	Method 3
FAO-24 Penman *(Doorenbos & Pruitt, 1977)*, **clipped grass, 8-15 cm.**	1.0	0.864	1.0	0.0100	Method 1,2
FAO-PPP-17 Penman (*Frére and Popov ,1979)*					
$T_{max} - T_{min}$ °C					
‹ 12	1.0	0.54	1.0	0.00620	Method 1
12 - 13	1.0	0.60	1.0	0.00697	Method 1
13 - 14	1.0	0.67	1.0	0.00773	Method 1
14 - 15	1.0	0.73	1.0	0.00849	Method 1
15 - 16	1.0	0.80	1.0	0.00924	Method 1
› 16	1.0	0.86	1.0	0.01000	Method 1
Hourly value, $\lambda E_a = 0.268\, W_f (e_z^o - e_z)$ *(Doorenbos & Pruitt, 1977a)*, **then**					
$R_n > 0$	0.27	0.526			
$R_n \leq 0$	1.14	0.401			

Where α is albedo and H and G are positive if part of net radiation goes to heat the soil and air,

when $K_c = 1.0$

$$\phi_1 = \frac{\lambda E}{R_n} = 1 - \frac{(G + H)}{R_n} \qquad \text{(V.51)}$$

$$\phi_2 = \frac{\lambda E}{R_s} = 1 - \alpha - \frac{R_b}{R_s} - \frac{(G + H)}{R_s} \qquad \text{(V.52)}$$

Jensen-Haise Alfalfa-Reference Radiation Method Equation. Jensen and Haise (1963) established a linear relationship of ϕ_2. Mean air temperature was apparent, and the constants for the following linear equation were $C_T = 0.025$, and $T_x = -3$ for temperature in °C.

$$\lambda ET_r = C_T * (T - T_x) * R_s \qquad \text{(V.53)}$$

where,

C_T = Temperature coefficient,

T_x = Intercept of the temperature axis, and

T = Average maximum and minimum temperature for the warmest month of the year.

These coefficients were considered to be constant for a given area. Jensen (1966b) later defined C_T as,

$$C_T = \frac{1}{C_1 + C_2 * C_H} \tag{V.54}$$

$$C_H = \frac{5.0kPa}{(e^o{}_{mean-max} - e^o{}_{mean-min})} \tag{V.55}$$

Where, $e^o{}_{mean-max}, e^o{}_{mean-min}$ are the saturated vapor pressures at mean maximum and mean minimum temperatures, respectively, for the warmest month of the year in the area, and C_1 and C_2 are constants. Jensen et al. (1970) defined the coefficients in the equations (V.54) and (V.55) as,

$$C_1 = 38 - \frac{(2 * EL)}{305},\ C_2 = 7.3\ [^\circ\mathrm{C}] \tag{V.56}$$

$$T_x = -2.5 - 1.4(e^o{}_{mean-max} - e^o{}_{mean-min}) - \frac{EL}{550} \tag{V.57}$$

Hargreaves Grass-Related Radiation Method Equation. Hargreaves and Samani (1982, 1985) improved the Hargreaves (1975) equation for estimating grass – related radiation evapotranspiration, ET_g. Due to the frequent unavailability of solar radiation data, they recommended estimating the solar radiation, R_s, from the extraterrestrial radiation, R_A, and the difference between mean monthly maximum and mean monthly minimum temperatures, TD, in °C. The original equations with mean air temperature in °F and °C are,

$$ET_g = 0.0075 * R_s * T \text{, } T \text{ in } {}^oF \tag{V.58}$$

$$ET_g = 0.0135 * R_s * (T + 17.8) \text{, } T \text{ in } {}^oC \tag{V.59}$$

where,

$$R_s = KT * R_A * TD^{1/2} \tag{V.60}$$

$$KT = 0.035 * (100 - RH)^{1/3} \text{, } TD \text{ [°F], } RH > 54 \tag{V.61}$$

$$KT = 0.125 \text{, } RH < 54 \tag{V.62}$$

Hargreaves (1985) Method Radiation Equation. The Hargreaves et al. (1985) method combined equation (V.59), (V.60) and (V.61) or (V.62) with TD converted to °C and not limited by ***RH*** is,

$$ET_g = 0.0023 * R_A * TD^{1/2} * (T + 17.8) \qquad \textbf{(V.63)}$$

where,

TD = Difference between mean monthly maximum and mean monthly minimum temperatures,

KT = Temperature coefficient when ***TD*** is in ^oF, and

RH = Mean monthly relative humidity in percentage.

Doorenbos and Pruitt Grass-Related Radiation Method Equation.

Doorenbos and Pruitt (1977) established a radiation method for estimating ET_g using solar radiation. Their method was an adaptation of the Makkink (1957) method. This method is a good tool to estimate ET_g whenever measured wind and humidity were not available or could not be estimated.

$$ET_g = a + b * [\frac{\Delta}{\Delta + \gamma} * R_s] \qquad \textbf{(V.64)}$$

where,

a = -0.3 mm d^{-1}, and

b = an adjustment factor that varies with mean relative humidity and daytime wind speed.

The adjustment factor b was presented in graphic and tabular forms. Frevert et al. (1983) developed a polynomial equation for estimating b for use in computer calculations. Cuenca (1987) rounded the original coefficient so that the final values are within 0.01 of the original value.

$$b = 1.066 - 0.13 \times 10^{-2} RH_{mean} + 0.045 U_d - 0.2 \times 10^{-3} RH_{mean} U_d - 0.315 \times 10^{-4} RH^2_{mean} - 0.11 \times 10^{-2} U^2_d \qquad \textbf{(V.65)}$$

Turc (1961) simplified an earlier version of an equation for potential evaporation, ET_g, under the general climatic conditions of Western Europe and when expressed on a daily basis in mm d^{-1}, thus

For RH > 50%

$$ET_g = 0.013 * \frac{T}{T + 15} * (R_s + 50) \qquad \textbf{(V.66)}$$

For RH < 50%

$$ET_g = 0.013 * \frac{T}{T+15} * (R_s + 50) * (1 + \frac{(50 - RH)}{70}) \quad \textbf{(V.67)}$$

where T is the average temperature in °C and R_s is in cal cm $^{-2}$ d $^{-1}$.

- <u>**Temperature methods**</u>

Thornthwaite (1948) correlated mean monthly air temperature with potential evapotranspiration, ET_g, as determined by water balance studies in the valleys of east-central U.S.A.

SCS Blaney-Criddle Temperature Method Equation. SCS Blaney-Criddle (1945, 1950, and 1962) and Blaney et al. (1952) developed a method for estimating evapotranspiration which intended to estimate the seasonal estimation of evapotranspiration. This method for estimating potential evapotranspiration is well known in the western United States and has been used extensively throughout the world,

where,

$$U = KF = \sum k * f \quad \textbf{(V.68)}$$

$$f = {(t * p)}/{100} \quad \textbf{(V.69)}$$

where,

$\boldsymbol{U}$ = Estimated Evapotranspiration (consumptive use) in inches for a growing period or season,

$\boldsymbol{K}$ = Empirical consumptive use coefficient (irrigation season or growing period),

$\boldsymbol{F}$ = Sum of monthly use consumptive factors, $\boldsymbol{f}$, for the seasonal or growing period,

$\boldsymbol{t}$ = Mean monthly air temperature in $^o\boldsymbol{F}$,

$\boldsymbol{p}$ = Mean monthly percentage of annual daytime hours, and

$\boldsymbol{k}$ = Monthly consumptive use coefficient.

Tanner (1967) showed that most linear temperature methods are in the following general form:

$$ET_r = C_1 * L_d * T * (C_2 - C_3 * h) \qquad \textbf{(V.70)}$$

where,

C_1, C_2, C_3 = Constants,

L_d = Day length,

T = mean air temperature, and

h = Humidity term.

FAO-24 Blaney-Criddle Method Equation (SCS Modified Blaney-Criddle Method). Doorenbos and Pruitt (1977) introduced the most fundamental revision of the Blaney-Criddle method since its introduction; (SCS modified Blaney-Criddle method). The FAO-24 Blaney-Criddle Method is used to estimate a grass-related reference crop evapotranspiration, ET_g.

$$ET_g = (0.0043RH_{min} - n/N - 1.41) + (a_0 + a_1 RH_{min} + a_2\, n/N +$$

$$a_3 U_d + a_4 RH_{min}\, n/N + a_5 RH_{min} U_d) * p * (0.46T + 8.13) \quad \textbf{(V.71)}$$

where,

p = mean daily percent of annual daytime hours (***monthly p / (days / month)***),

T = mean air temperature [°C],

RH_{min} = Minimum daily relative humidity in percentage, and

U_d = Daytime wind speed at 2 m height [m / s].

- **Evaporation methods**

Pan evaporation data can be used to estimate reference evapotranspiration, ET, using a simple proportional relationship.

Where,

$$ET_g = k_p * E_{pan} \tag{V.72}$$

or,

$$ET_r = k_p * E_{pan} \tag{V.73}$$

where,

k_p= Type of pan used and other factors, and

E_{pan} = Pan evaporation.

Other pan evaporation equations are used to estimate potential evapotranspiration, like the **FAO-24 Pan Evaporation Method Equation** (Doorenbos and Pruitt, 1975), Table (V. 2). **Christiansen Pan Evaporation Method Equation.** Christiansen (1968) and Christiansen and Hargreaves (1969) developed an equation for estimating the reference crop evapotranspiration, ET_g, from USWB Class A pan evaporation and several weather parameters. Where,

$$ET_g = 0.755 * E_v C_{T2} * C_{W2} * C_{H2} * C_{S2} \qquad \textbf{(V.74)}$$

$$C_{T2} = 0.862 + 0.179 * (\frac{T_c}{T_{co}}) - 0.041 * (\frac{T_c}{T_{co}})^2 \qquad \textbf{(V.75)}$$

$$C_{W2} = 1.189 - 0.240 * (\frac{W}{W_o}) + 0.051 * (\frac{W}{W_o})^2 \qquad \textbf{(V.76)}$$

$$C_{H2} = 0.499 + 0.620 * (\frac{H_m}{H_{mo}}) - 0.119 * (\frac{H_m}{H_{mo}})^2 \qquad \textbf{(V.77)}$$

$$C_{S2} = 0.904 + 0.0080 * (\frac{S}{S_o}) + 0.088 * (\frac{S}{S_o})^2 \qquad \textbf{(V.78)}$$

where,

E_v = Measured Class A pan evaporation,

Table V.2 Suggested values of K_P for relating evaporation from a USA class A pan to evapotranspiration from 8-15 cm tall well watered grass turf (after Doorenbos and Pruitt, 1977)[1].

	Case A: Pan Surrounded by Short Green Crop				Case B: Pan Surrounded by Dray, Bare Area[3]			
	Mean relative Humidity (%)[2]				Mean relative Humidity (%)[2]			
Wind (km/d)	Upwind fetch of green crop(m)	Low < 40	Med 40-70	High >70	Upwind fetch of dry fallow(m)	Low < 40	Med 40-70	High >70
Light	0	0.55	0.65	0.75	0	0.7	0.8	0.85
< 175	10	0.65	0.75	0.85	10	0.6	0.7	0.8
km/d	100	0.7	0.8	0.85	100	0.55	0.65	0.75
(< m/s)	1000	0.75	0.85	0.85	1000	0.5	0.6	0.7
Moderate	0	0.5	0.6	0.65	0	0.65	0.75	0.8
175-425	10	0.6	0.7	0.75	10	0.55	0.65	0.7
km/d	100	0.65	0.75	0.8	100	0.5	0.6	0.65
(2-5 m/s)	1000	0.7	0.8	0.8	1000	0.45	0.55	0.6
Strong	0	0.45	0.5	0.6	0	0.6	0.65	0.7
425-700	10	0.55	0.6	0.65	10	0.5	0.55	0.65
km/d	100	0.6	0.65	0.7	100	0.45	0.5	0.6
(5-8 m/s)	1000	0.65	0.7	0.75	1000	0.4	0.45	0.55
V. Strong	0	0.4	0.45	0.5	0	0.5	0.6	0.65
> 700	10	0.45	0.55	0.6	10	0.45	0.5	0.55
km/d	100	0.5	0.6	0.65	100	0.4	0.45	0.5
(> 8 m/s)	1000	0.55	0.6	0.65	1000	0.35	0.4	0.45

[1] $ET_g = k_p * E_{pan}$

[2] Mean of maximum and minimum daily relative humidities.

[3] These coefficients apply only to conditions when the surface of the soil is indeed dry. Following rains for a day or two midsummers and for longer periods in fall, winter, and spring, such pans are essentially equivalent to Case A pans with large fetches. Rains also affect case A pans by essentially increasing the 0 – and 10 –m fetch to an effective moisture surface fetch of 1000 m or more. One large advantage of Case B pans is the minimal upkeep involved in such a sitting of the pan, i.e., only an effective weed control program is needed for the site.

T_c = mean temperature in ^oC, and $T_{co} = 20$ [^{o}C],

W = Mean wind velocity 2 m. above ground level in km per hour, and $Wo = 6.7$ km/hr,

H_m = Mean relative humidity in decimals, and $H_{mo} = 0.60$, and

S = Percentage of possible sunshine in decimals, and $S_o = 0.80$.

Table V.3 Data requirements of selected formula for computing potential or 'reference' evapotranspiration.

Method	T	R_s	e	u	Lat. /Day-L.	P.P.	T.R.I.D
Thoronthwaite	✓				✓		**Monthly**
Blaney-Criddle	✓				✓		**Monthly**
Hargreaves	✓		✓		✓		**Monthly**
Samani-Hargreaves	✓				✓		**Daily** [a]
Jensen-Hais	✓	✓					**Daily** [a]
Priestly-Taylor	✓	✓					**Daily**
Penmen	✓	✓	✓	✓			**Daily** [a, b]
Penman-Monteith	✓	✓	✓	✓		✓	**Daily** [a, b]

T, temperature; $\mathbf{R_s}$, solar radiation; **e**, humidity; **u**, wind.

Lat. /day-L., latitude/day-length; **P.P.**, plant parameters; **T.R.I.D.**, temporal resolution of input data.

[a] required daily minimum, maximum temperature.

[b] can be used with hourly input data.

APPENDIX VI

HYDRAULIC HEAD, GROUNDWATER CONCENTRATION AND BRINE WATER CONCENTRATION

Figure VI.1 Areal distribution, **orientation layout (1),** hydraulic head elevation distribution during the 5th simulation year.

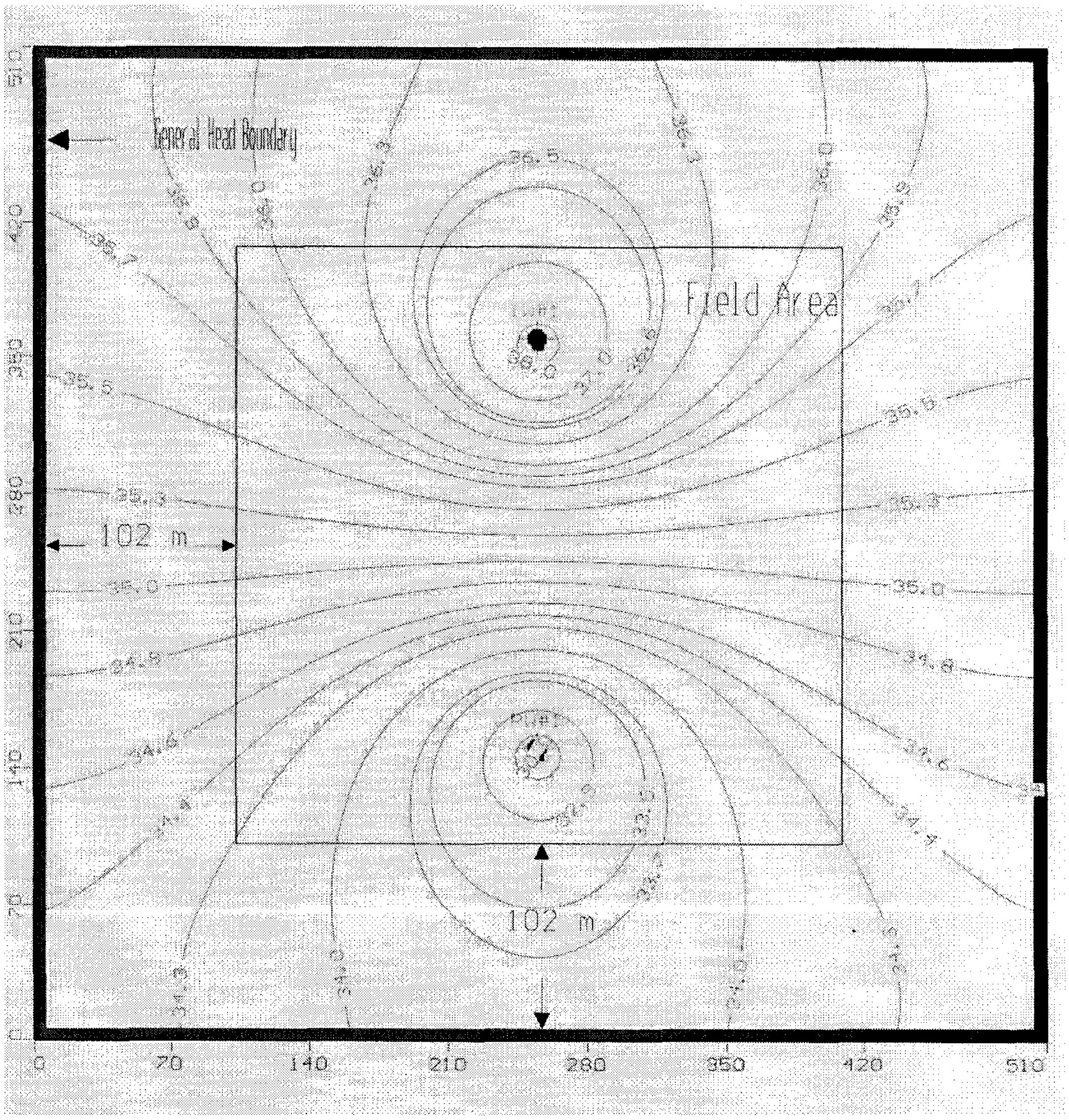

Figure VI.2 Areal distribution**, orientation layout (1),** groundwater salt concentration distribution during the 5th simulation year.

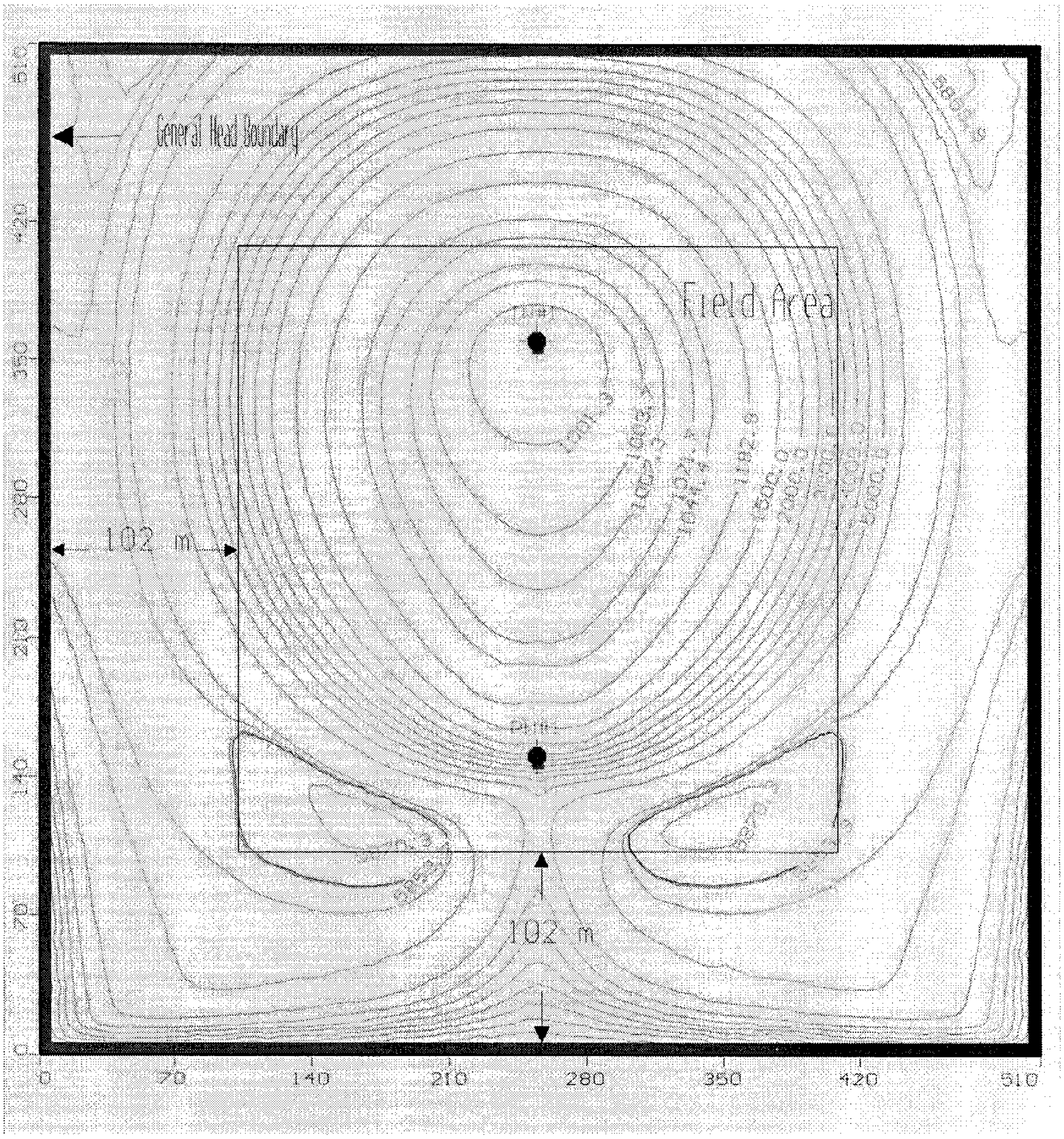

Figure VI.3 Areal distribution, **orientation layout (1),** hydraulic head elevation distribution during the10th simulation year.

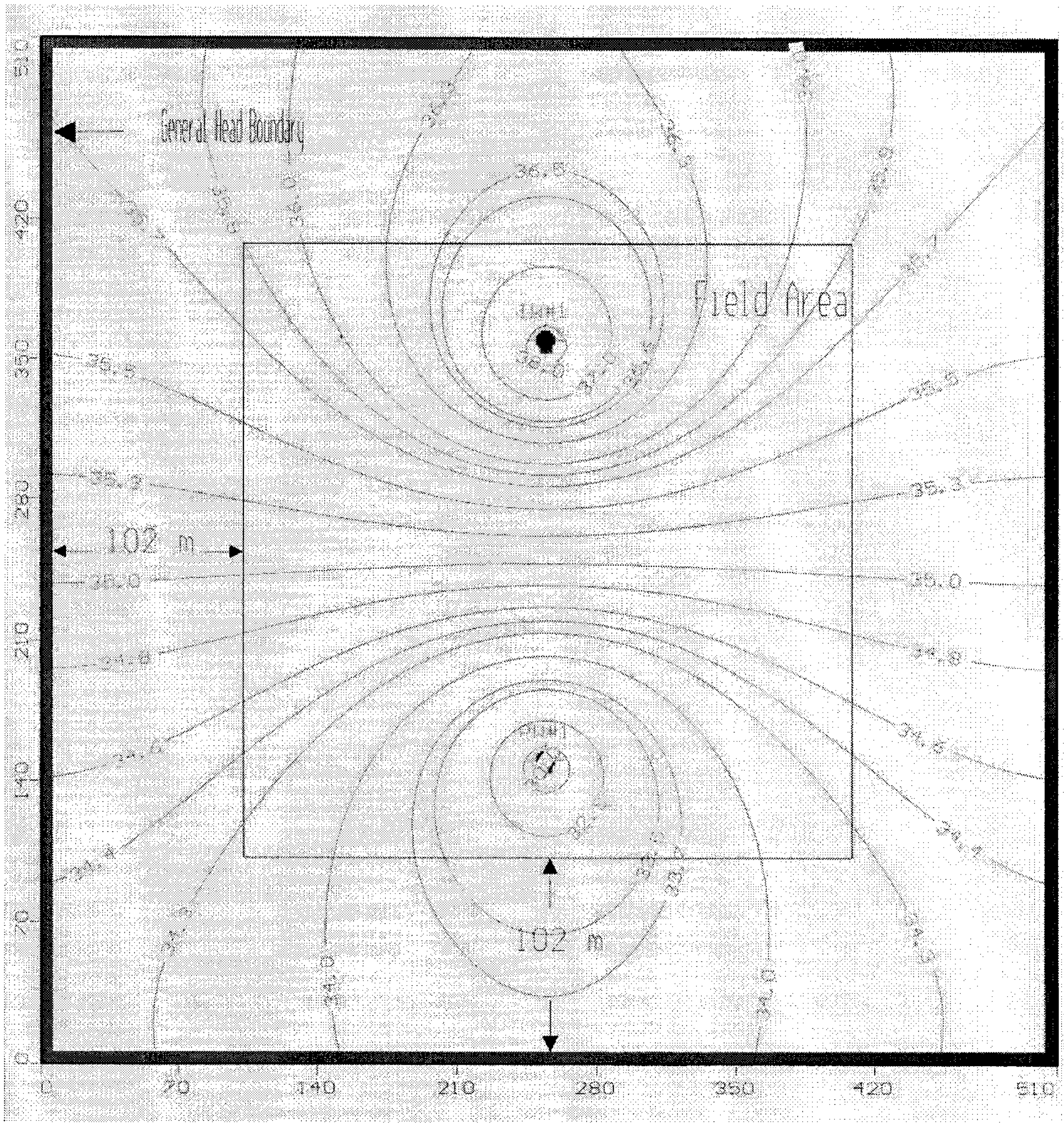

Emad H. AlAli

Figure VI.4 Areal distribution, **orientation layout (1),** groundwater salt concentration distribution during the10th simulation year.

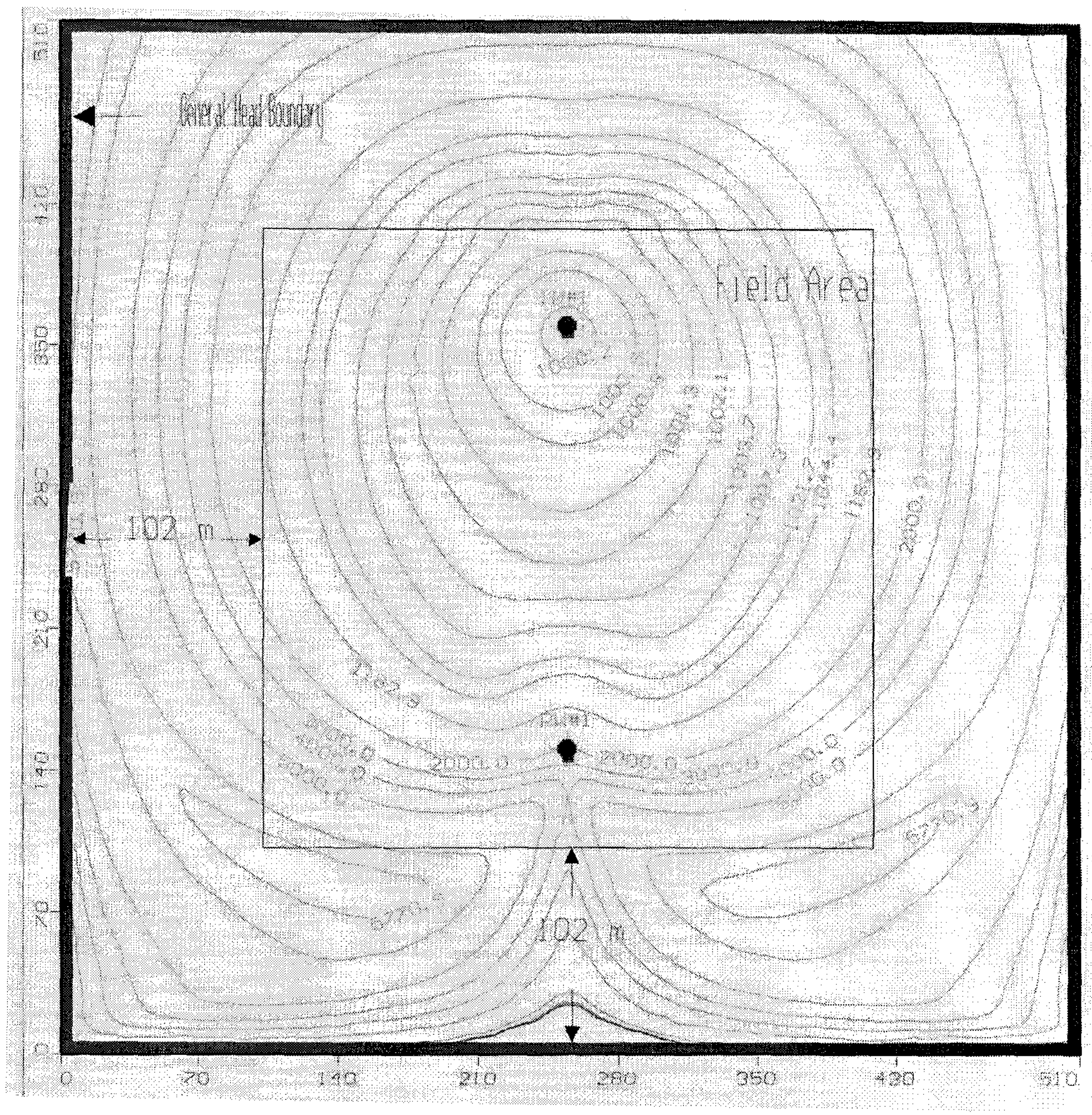

Figure VI.5 Areal distribution**, orientation layout (1),** hydraulic head elevation distribution during the 20th simulation year.

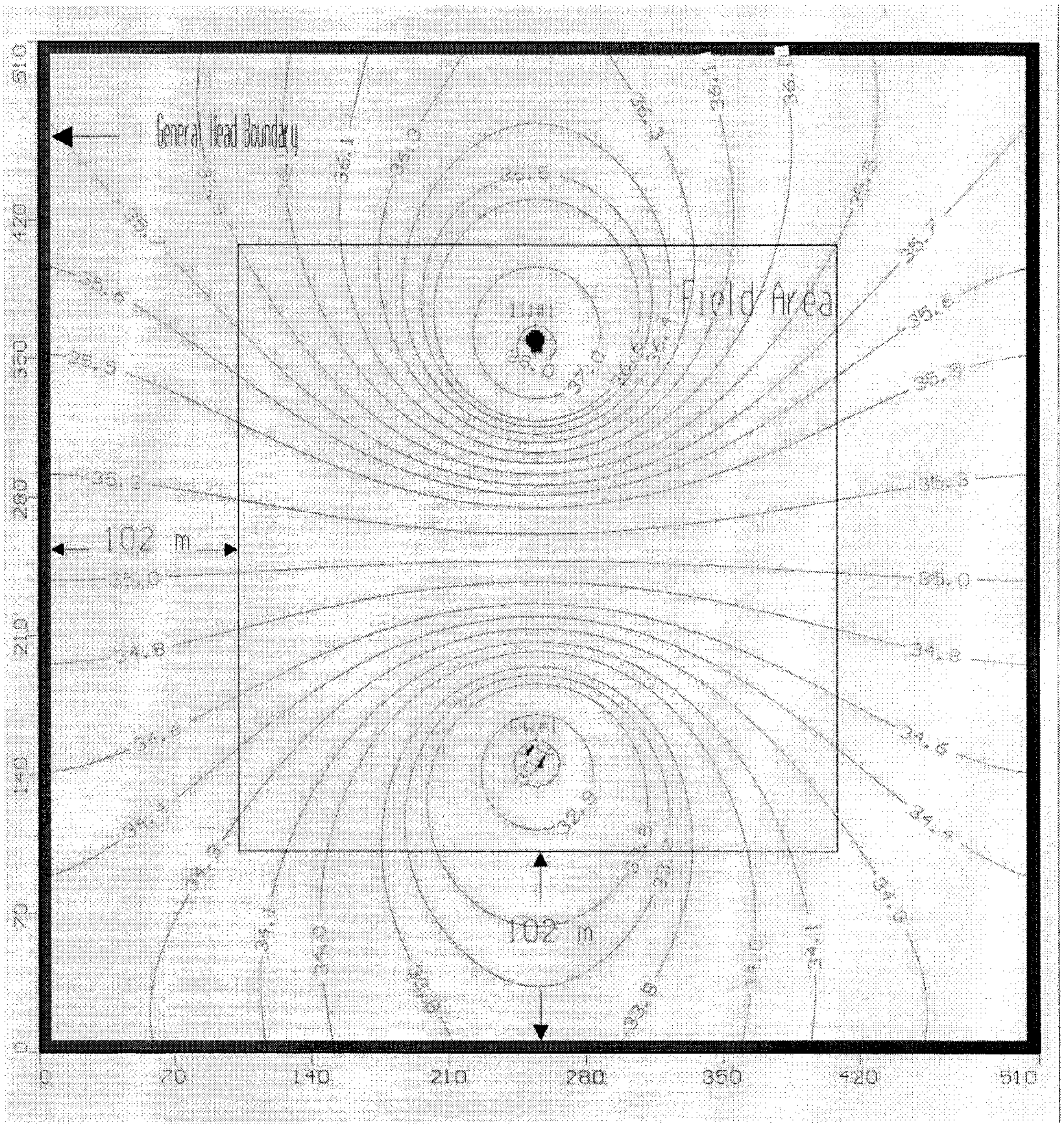

Figure VI.6 Areal distribution, **orientation layout (1),** groundwater salt concentration distribution during the 20th simulation year.

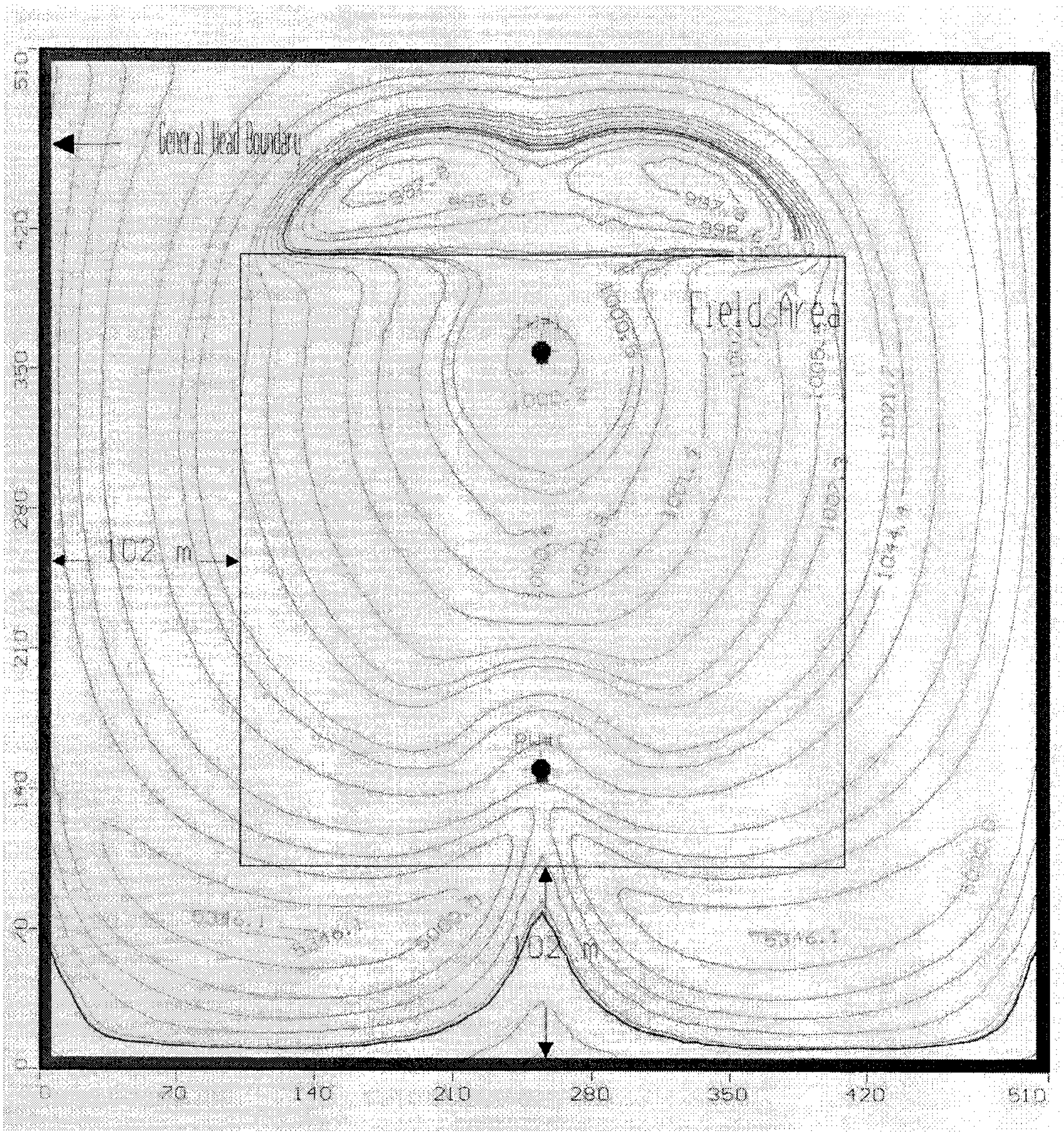

 Emad H. AlAli

Figure VI.7 Areal distribution**, orientation layout (1),** hydraulic head elevation distribution during the 40th simulation year.

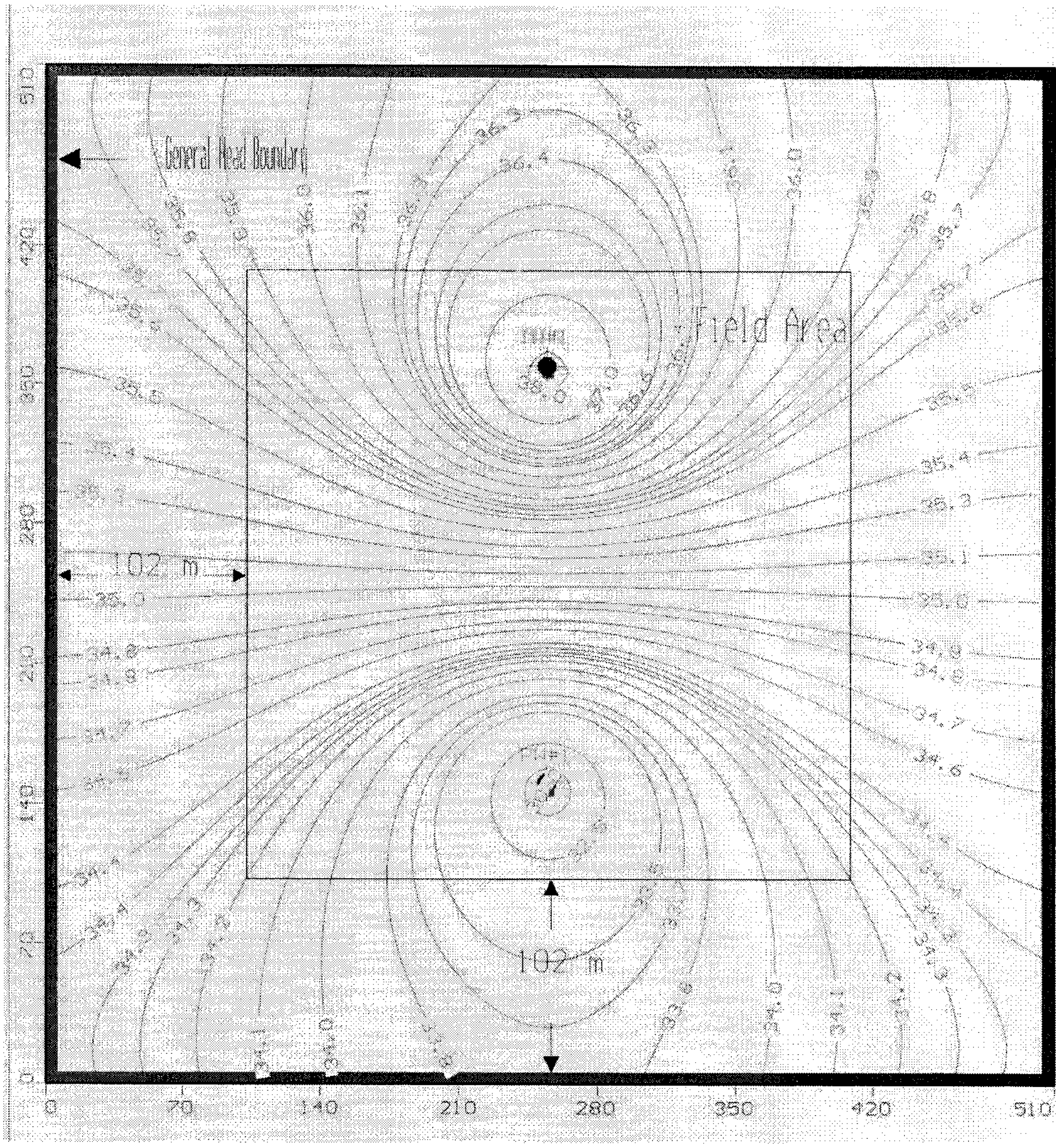

Emad H. AlAli

Figure VI.8 Areal distribution**, orientation layout (1),** groundwater salt concentration distribution during the 40th simulation year.

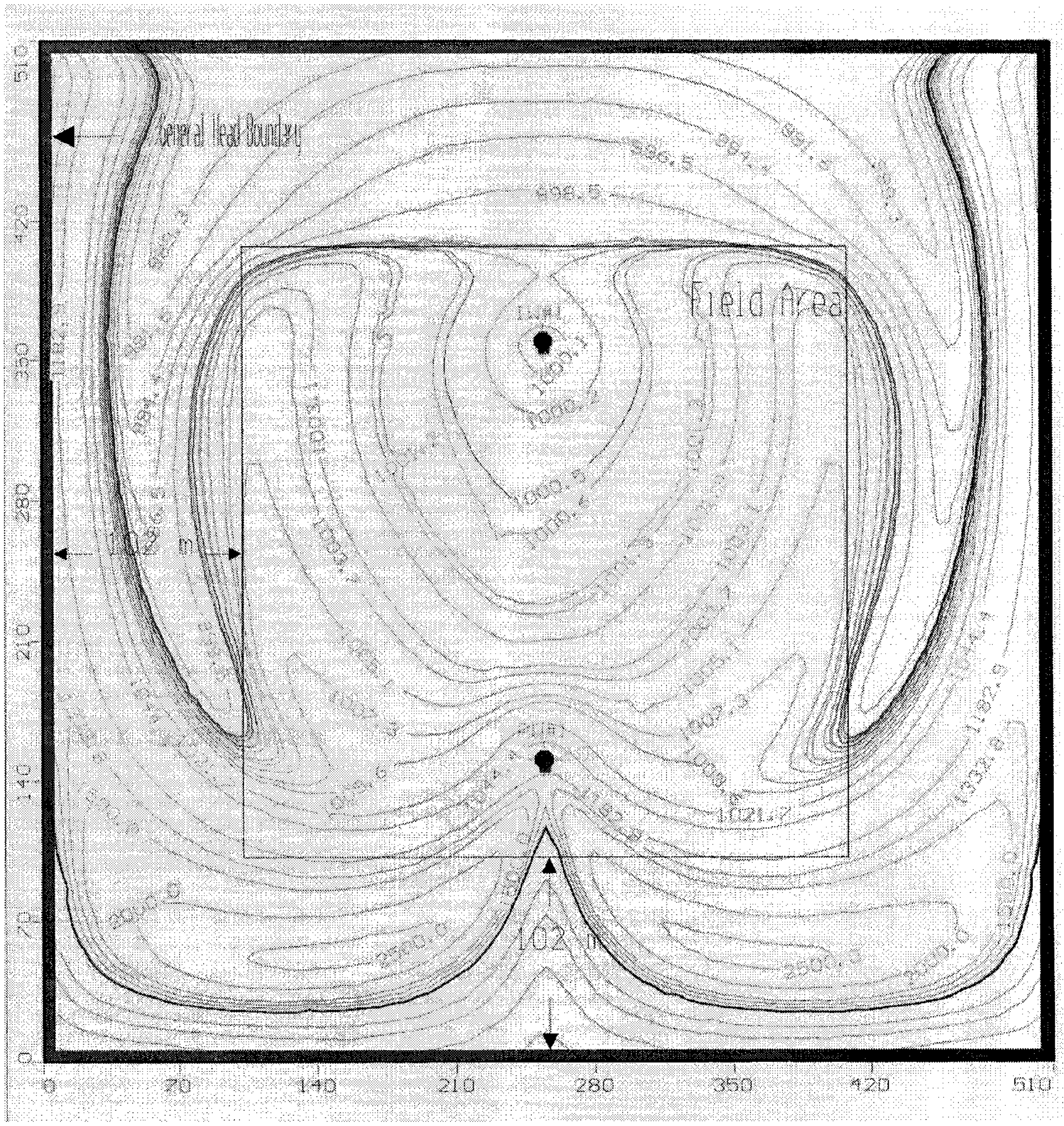

 Emad H. AlAli

Figure VI.9 Areal distribution, **orientation layout (2),** hydraulic head elevation distribution during the 5th simulation year.

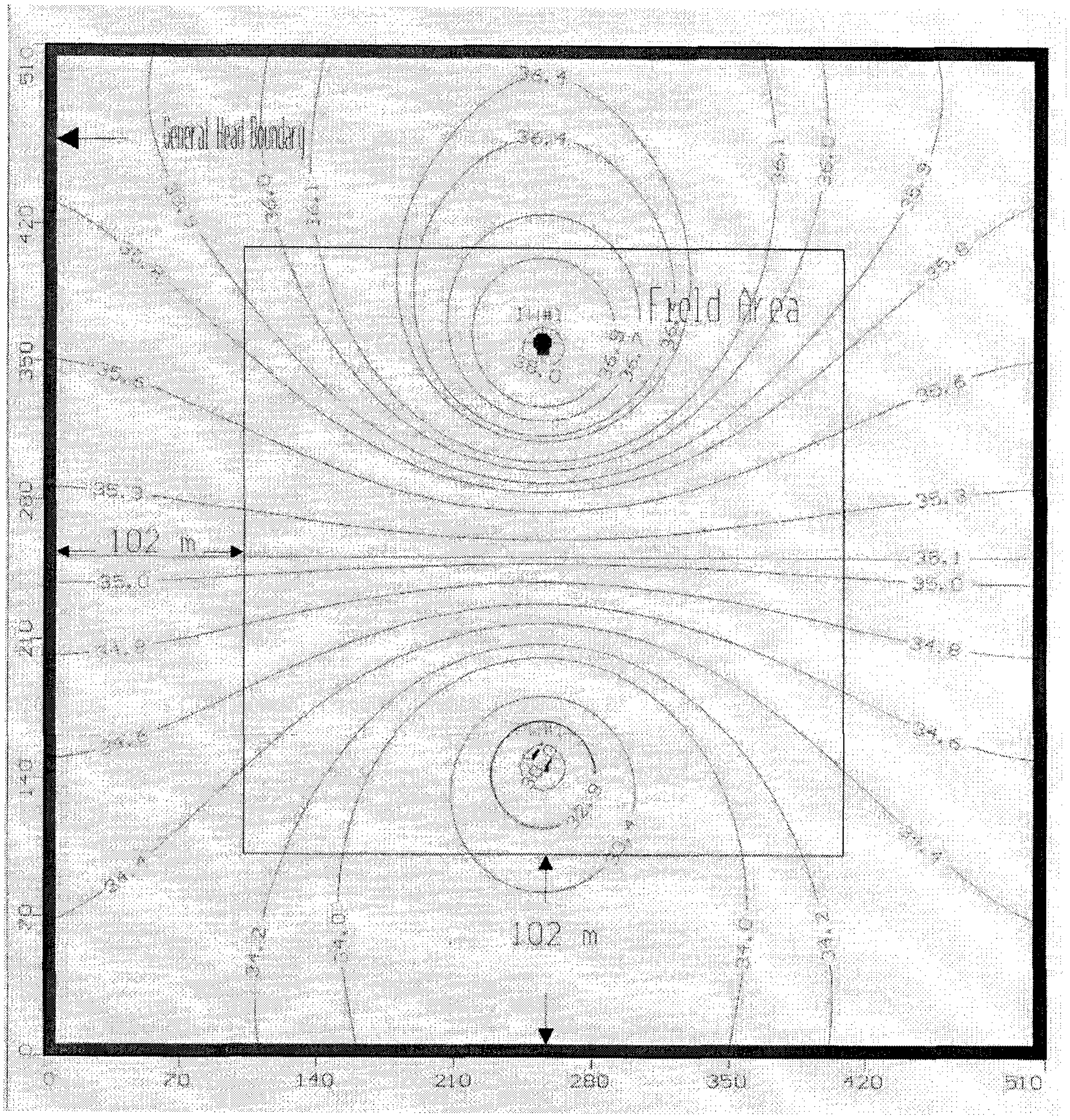

Emad H. AlAli

Figure VI.10 Areal distribution, **orientation layout (2),** groundwater salt concentration distribution during the 5th simulation year.

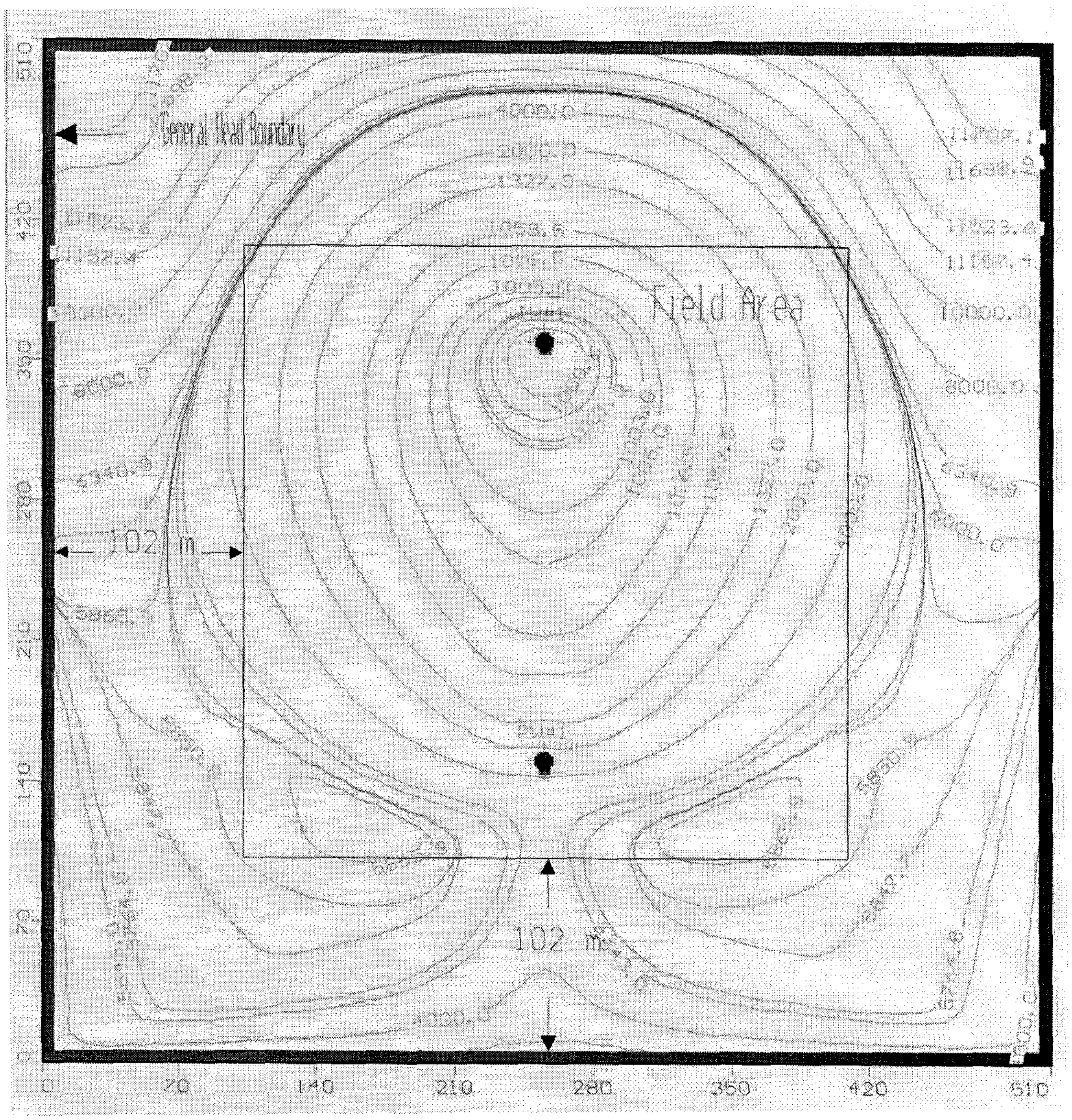

Figure VI.11 Areal distribution, **orientation layout (2),** hydraulic head elevation distribution during the 10th simulation year.

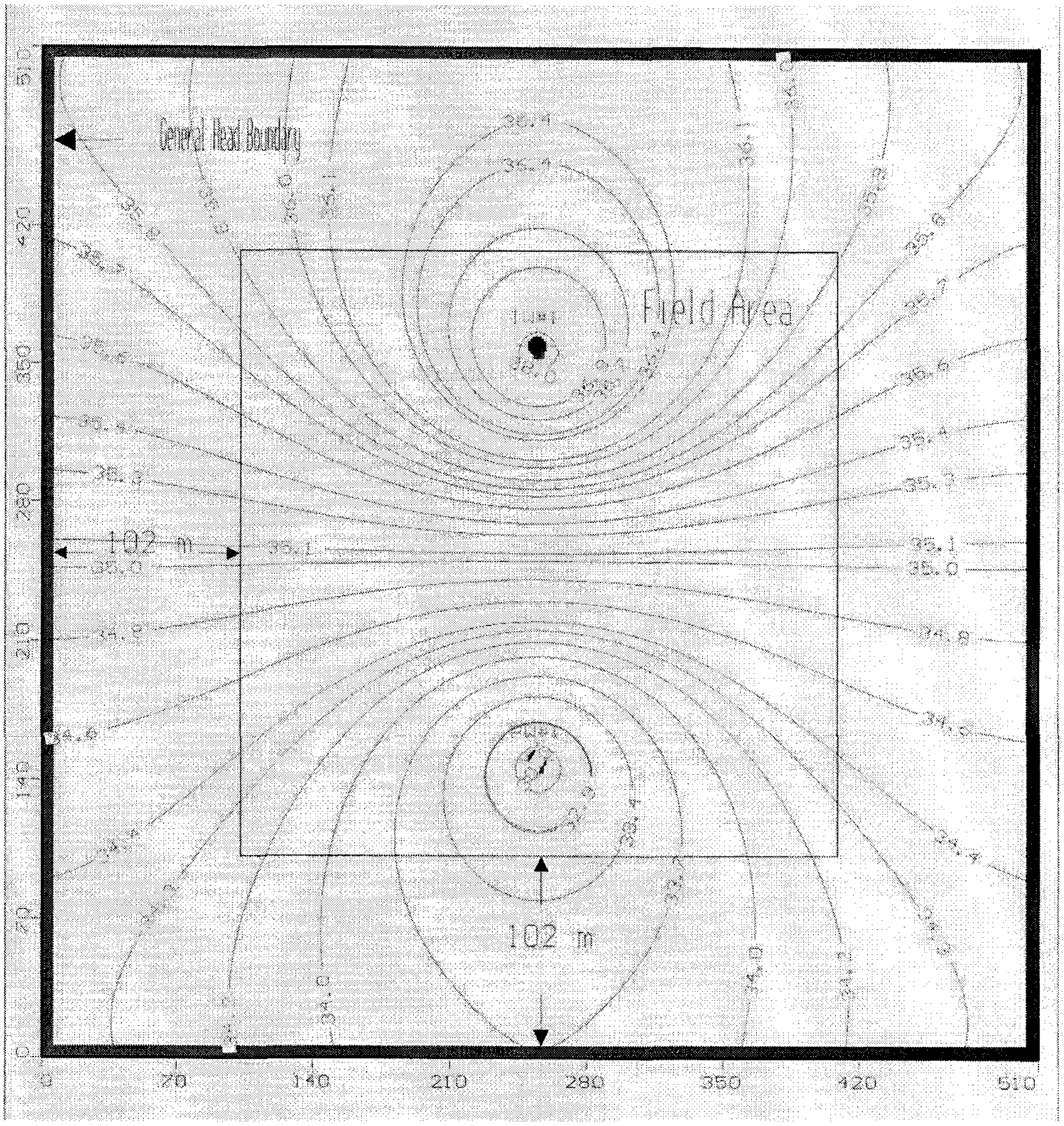

Figure VI.12 Areal distribution, **orientation layout (2),** groundwater salt concentration distribution during the 10th simulation year.

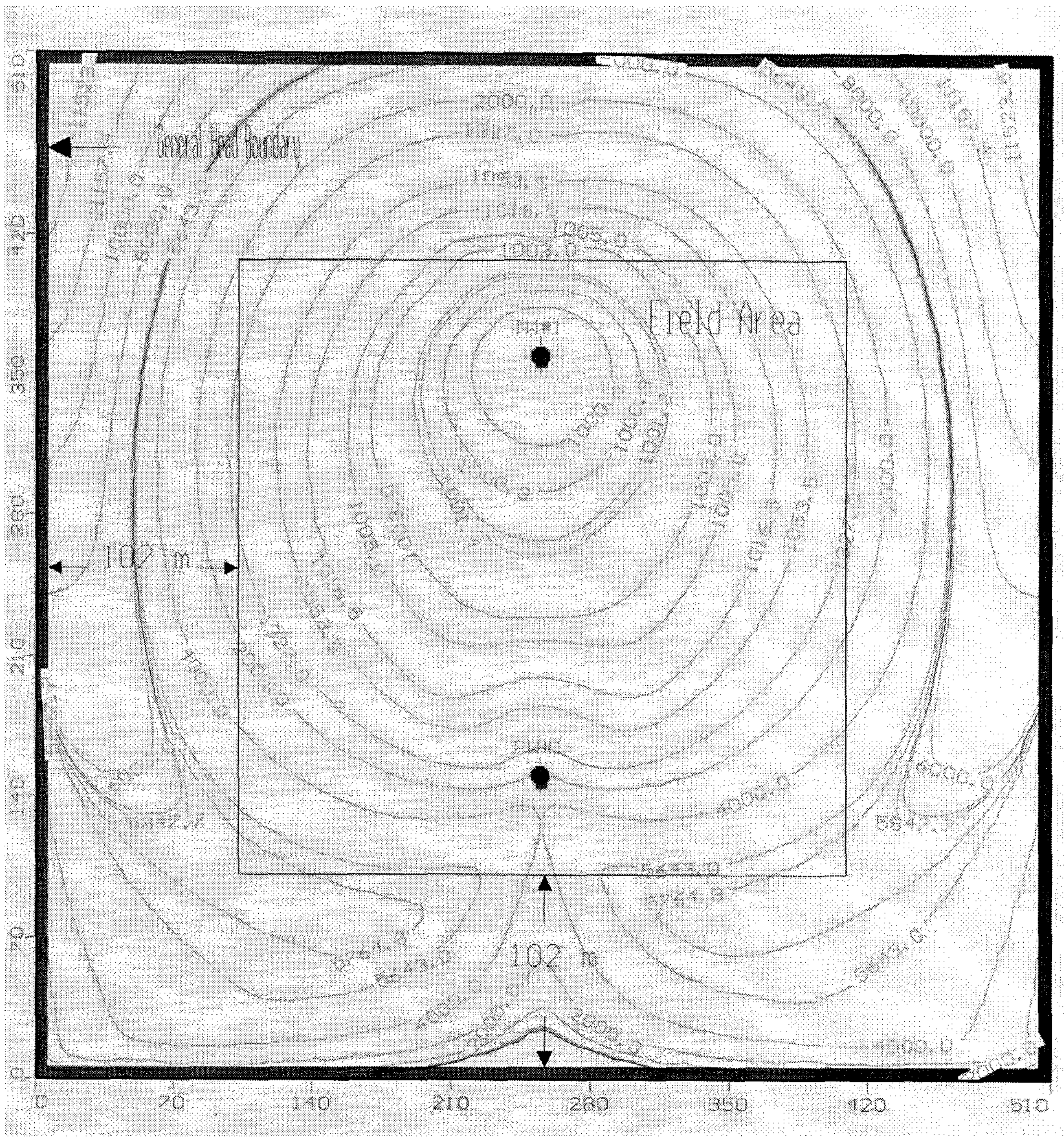

Figure VI.13 Areal distribution, **orientation layout (2),** hydraulic head elevation distribution during the 20th simulation year.

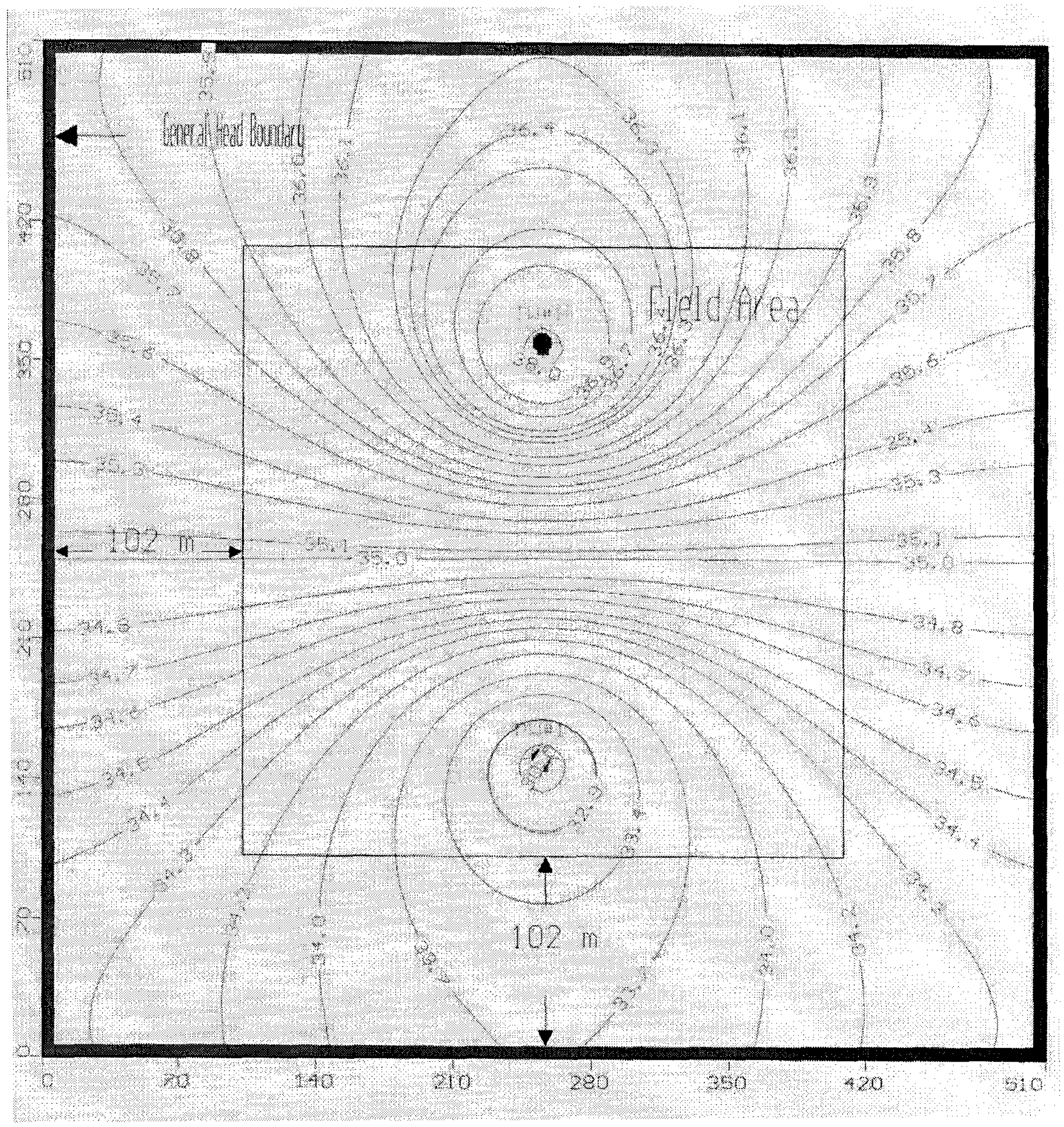

 Emad H. AlAli

Figure VI.14 Areal distribution**, orientation layout (2),** groundwater salt concentration distribution during the 20th simulation year.

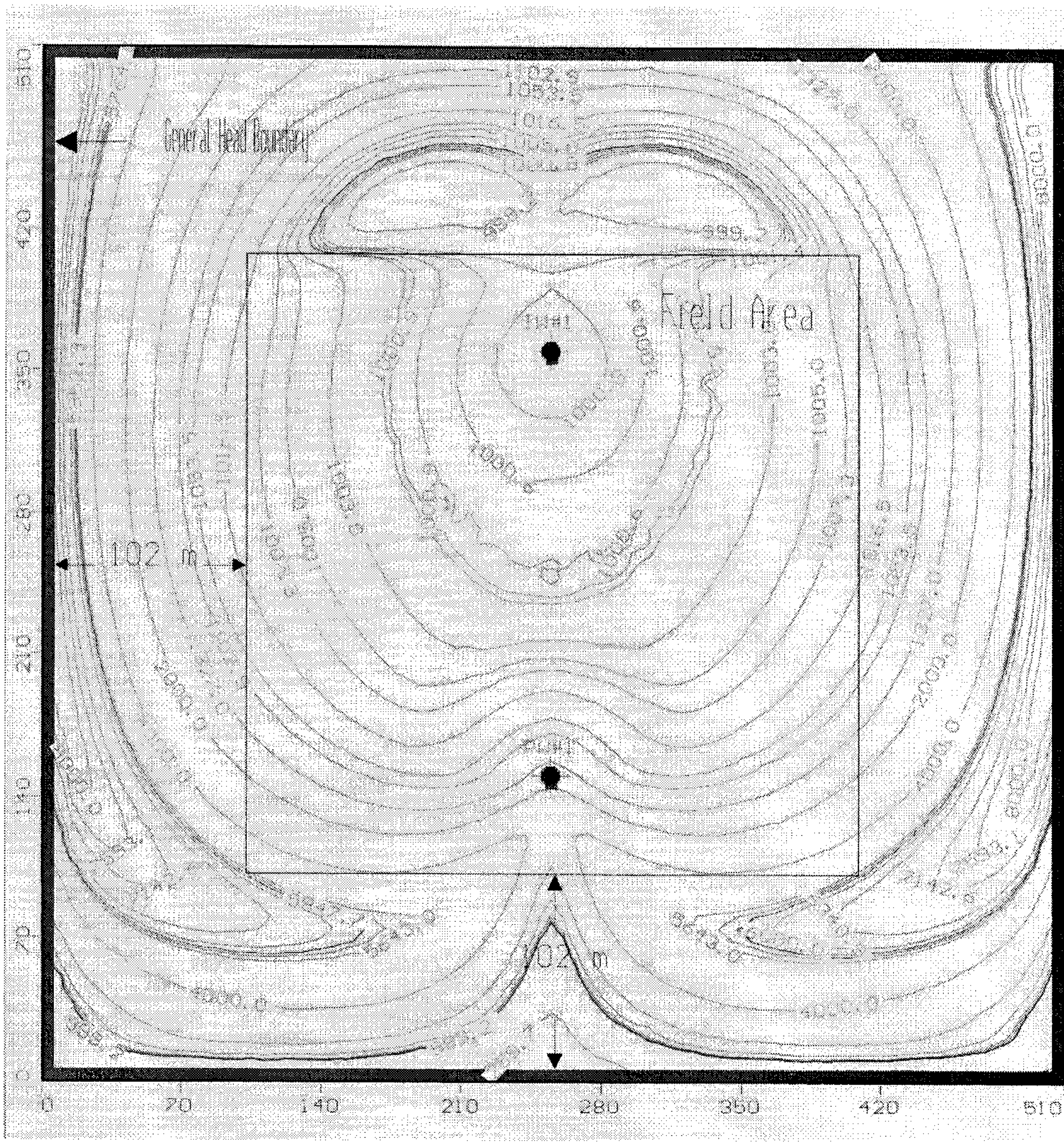

Figure VI.15 Areal distribution, **orientation layout (2),** hydraulic head elevation distribution during the 40th simulation year.

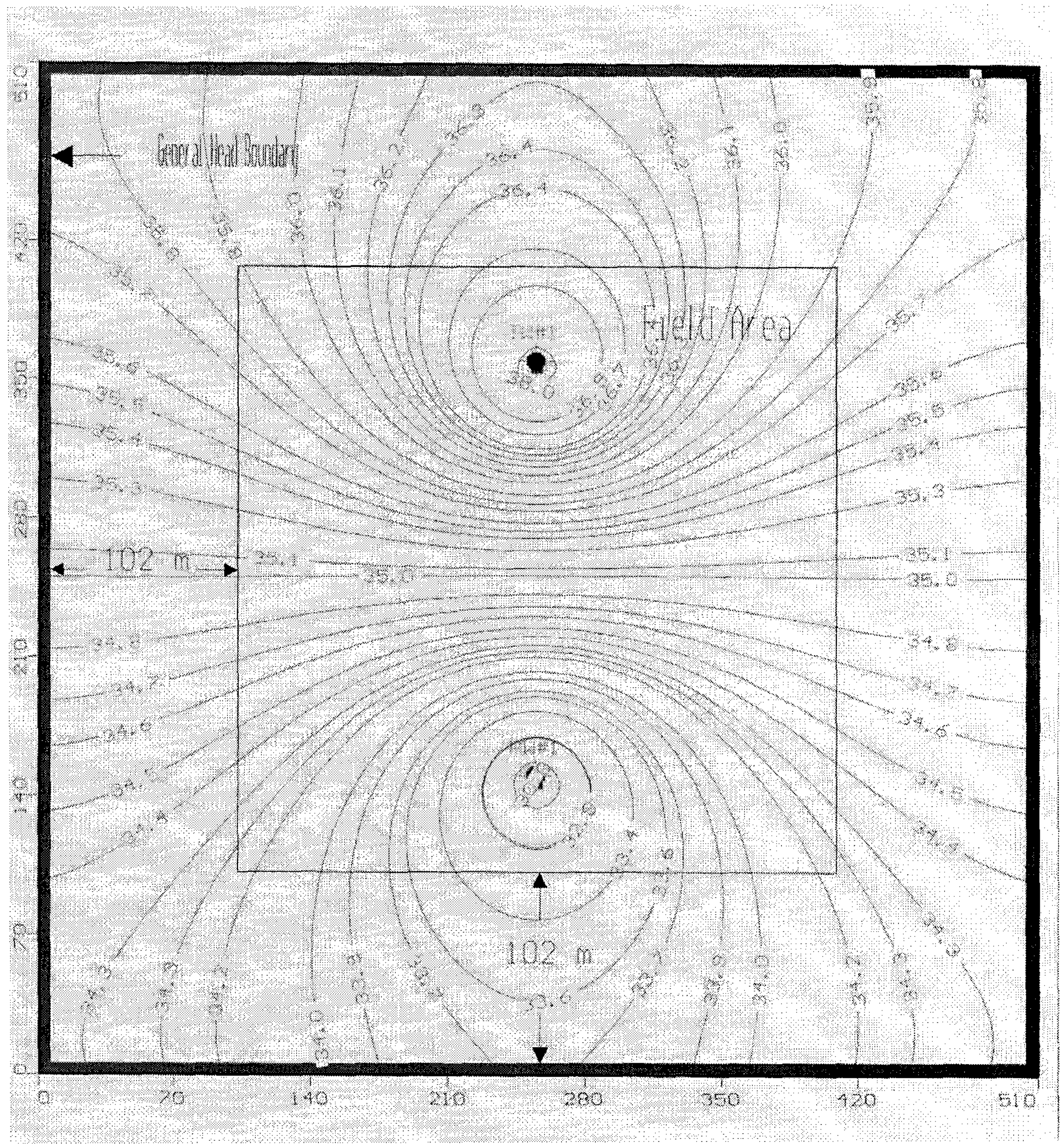

Figure VI.16 Areal distribution, **orientation layout (2),** groundwater salt concentration distribution during the 40th simulation year.

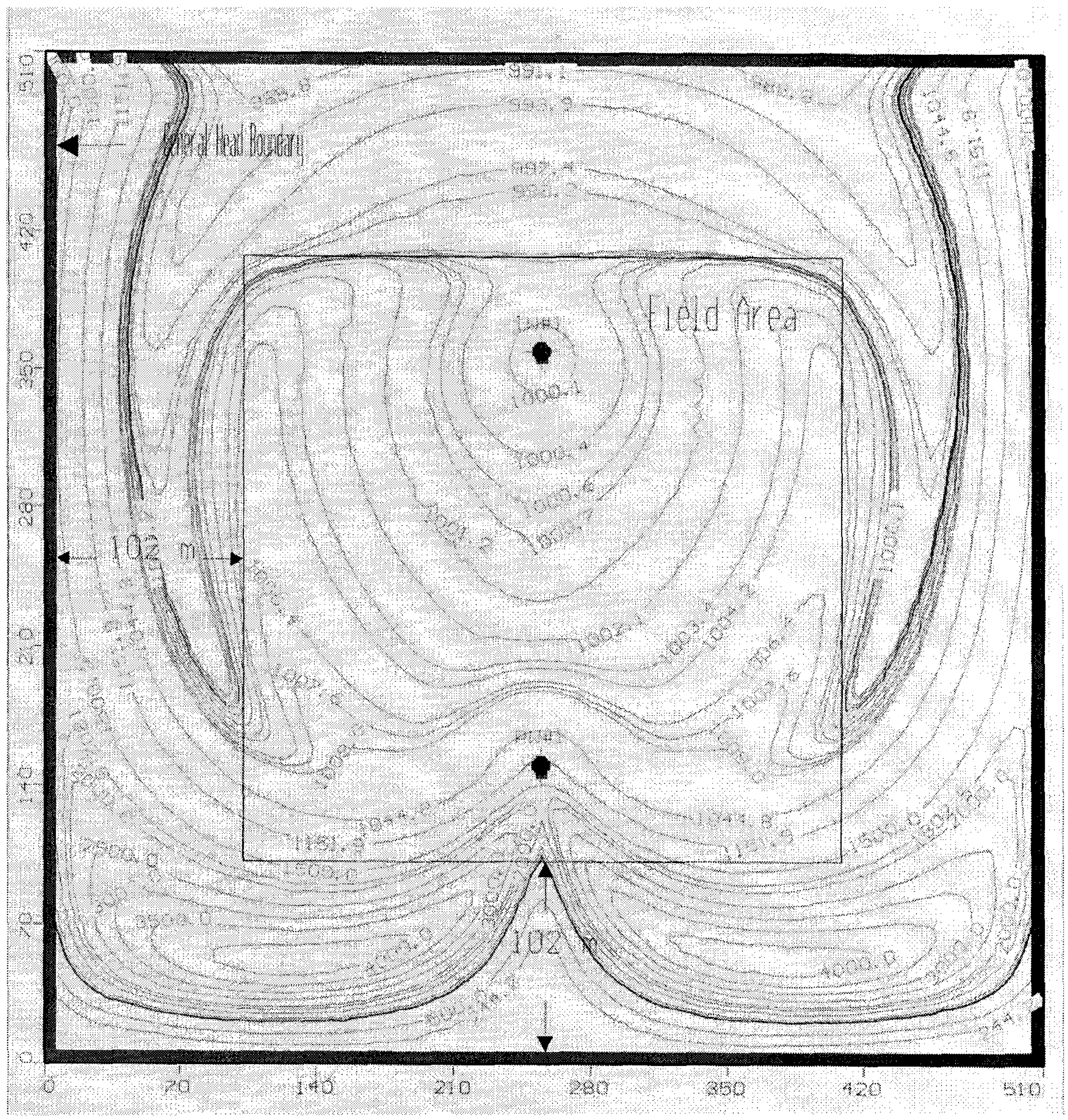

 Emad H. AlAli

Figure VI.17 Areal distribution, **orientation layout (3),** hydraulic head elevation distribution during the 5th simulation year.

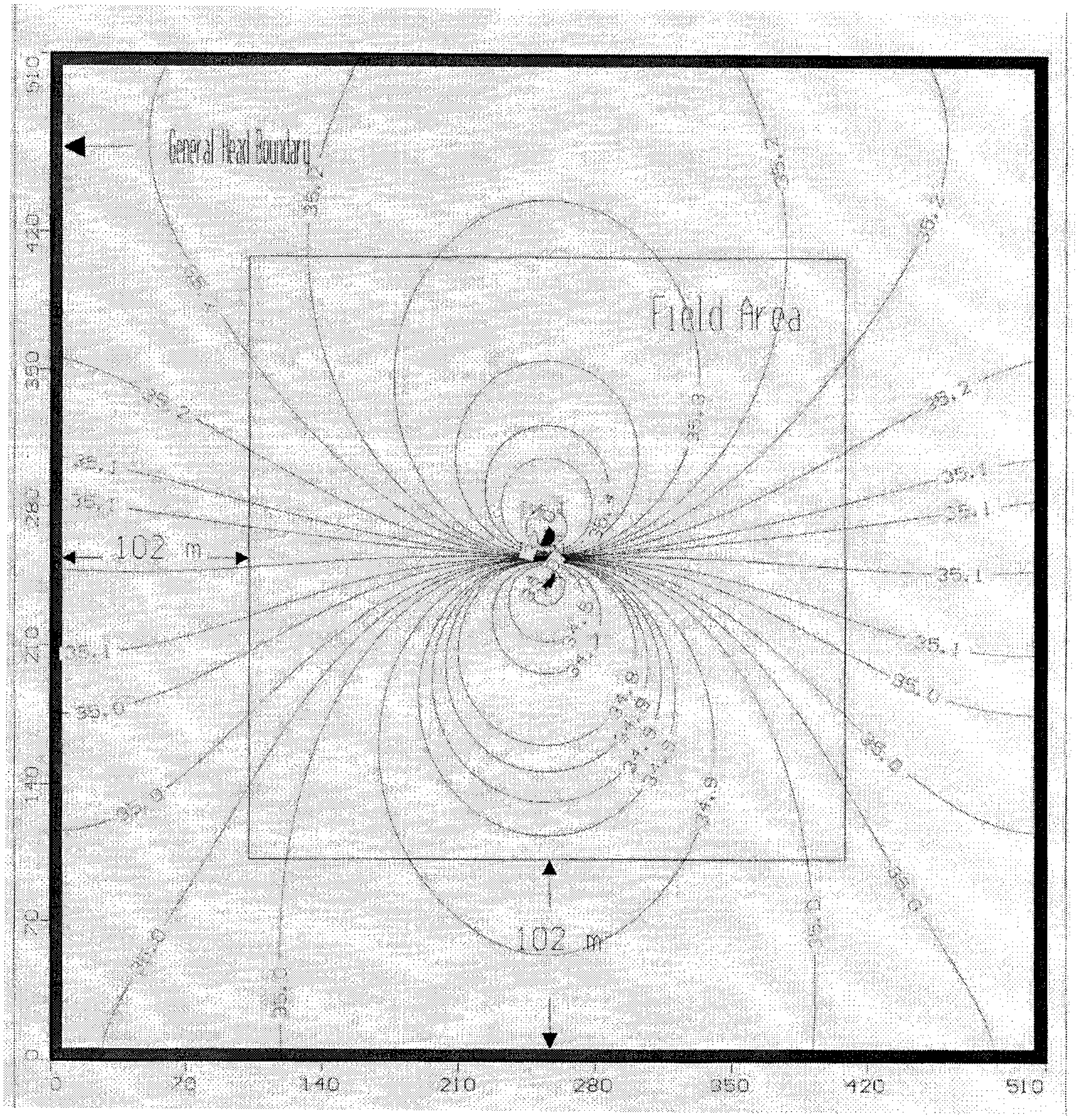

Figure VI.18 Areal distribution, **orientation layout (3),** groundwater salt concentration distribution during the 5th simulation year.

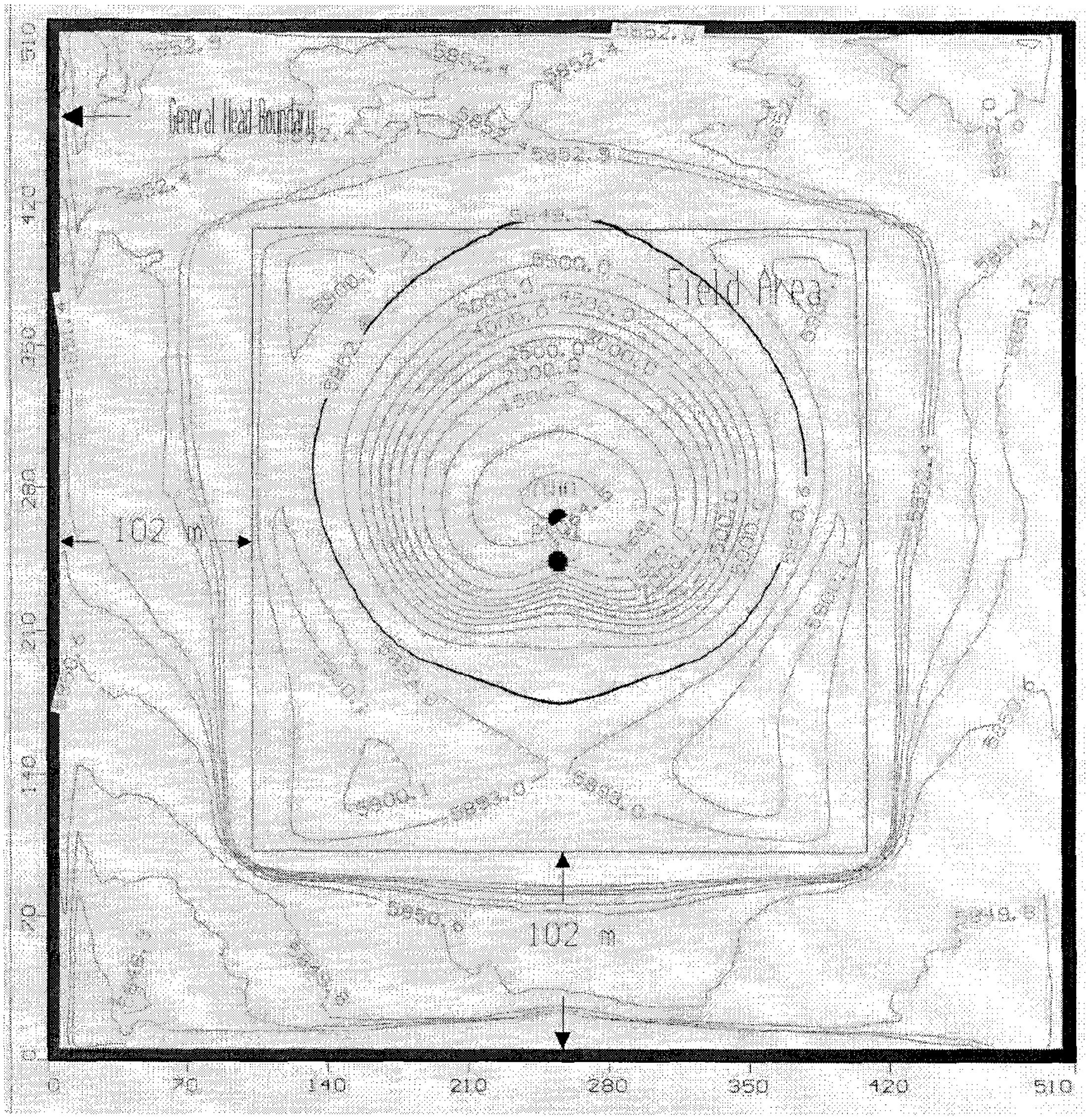

 Emad H. AlAli

Figure VI.19 Areal distribution, **orientation layout (3),** hydraulic head elevation distribution during the 10th simulation year.

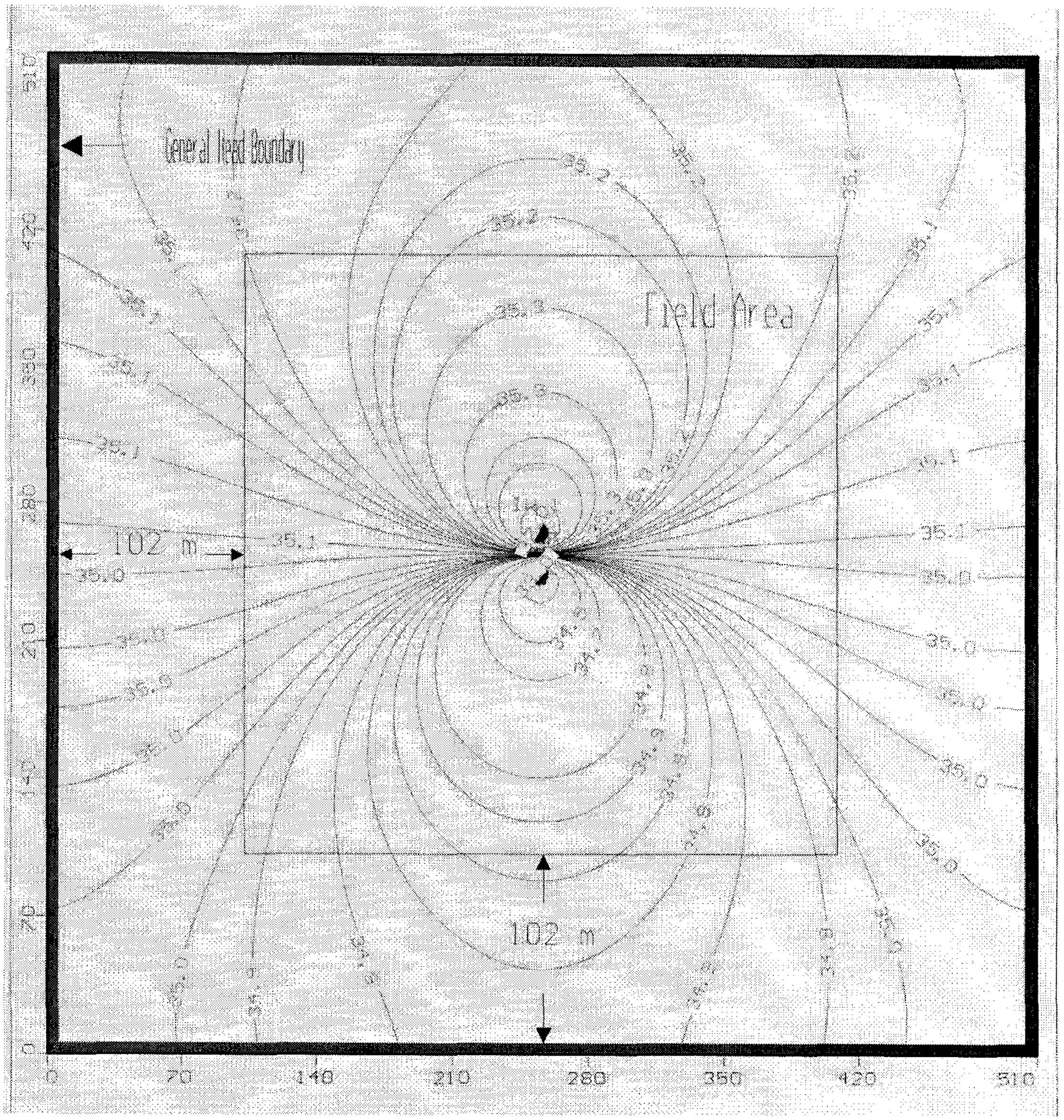

 Emad H. AlAli

Figure VI.20 Areal distribution**, orientation layout (3),** groundwater salt concentration distribution during the 10th simulation year.

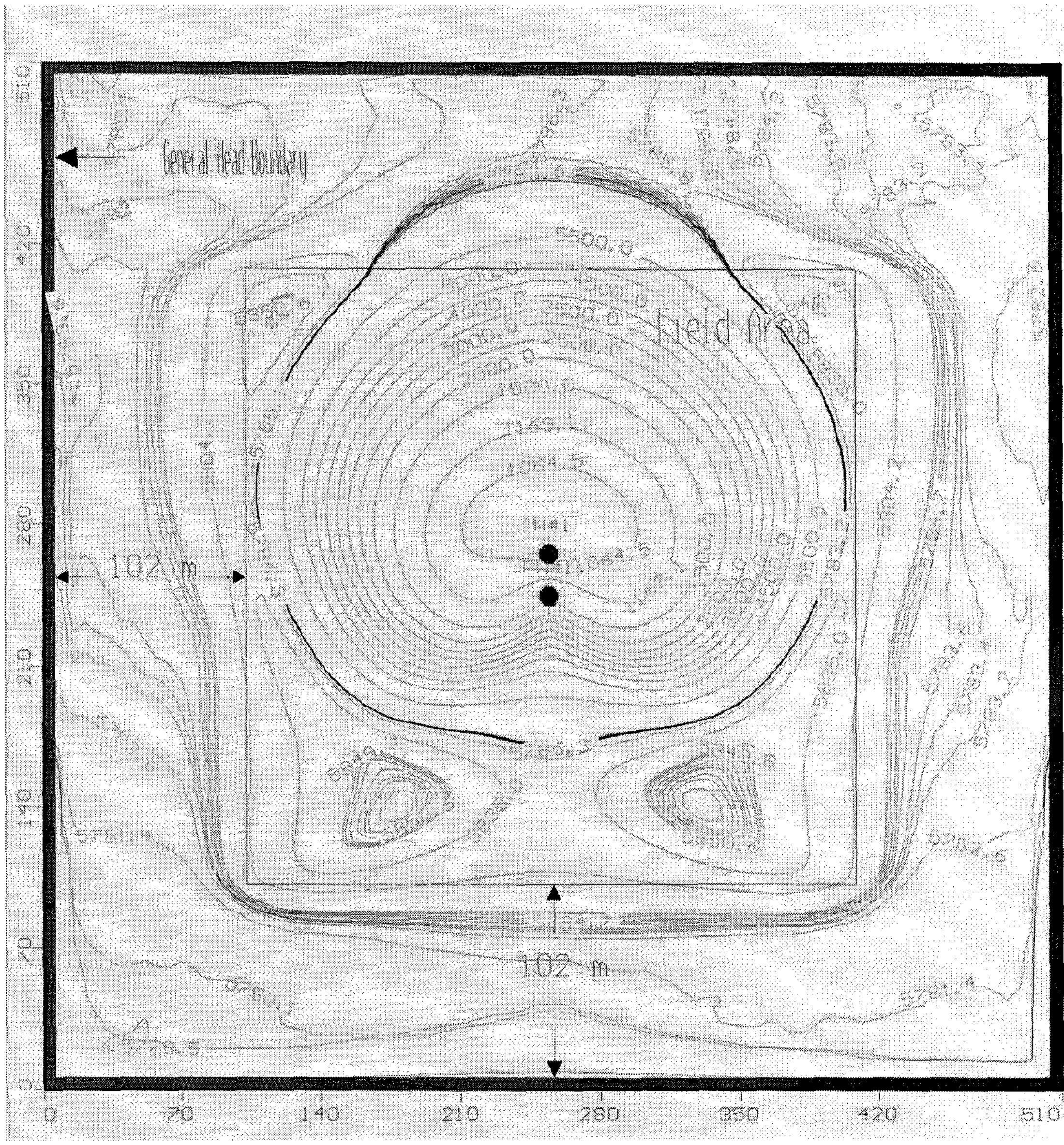

Emad H. AlAli

Figure VI.21 Areal distribution, **orientation layout (3),** hydraulic head elevation distribution during the 20th simulation year.

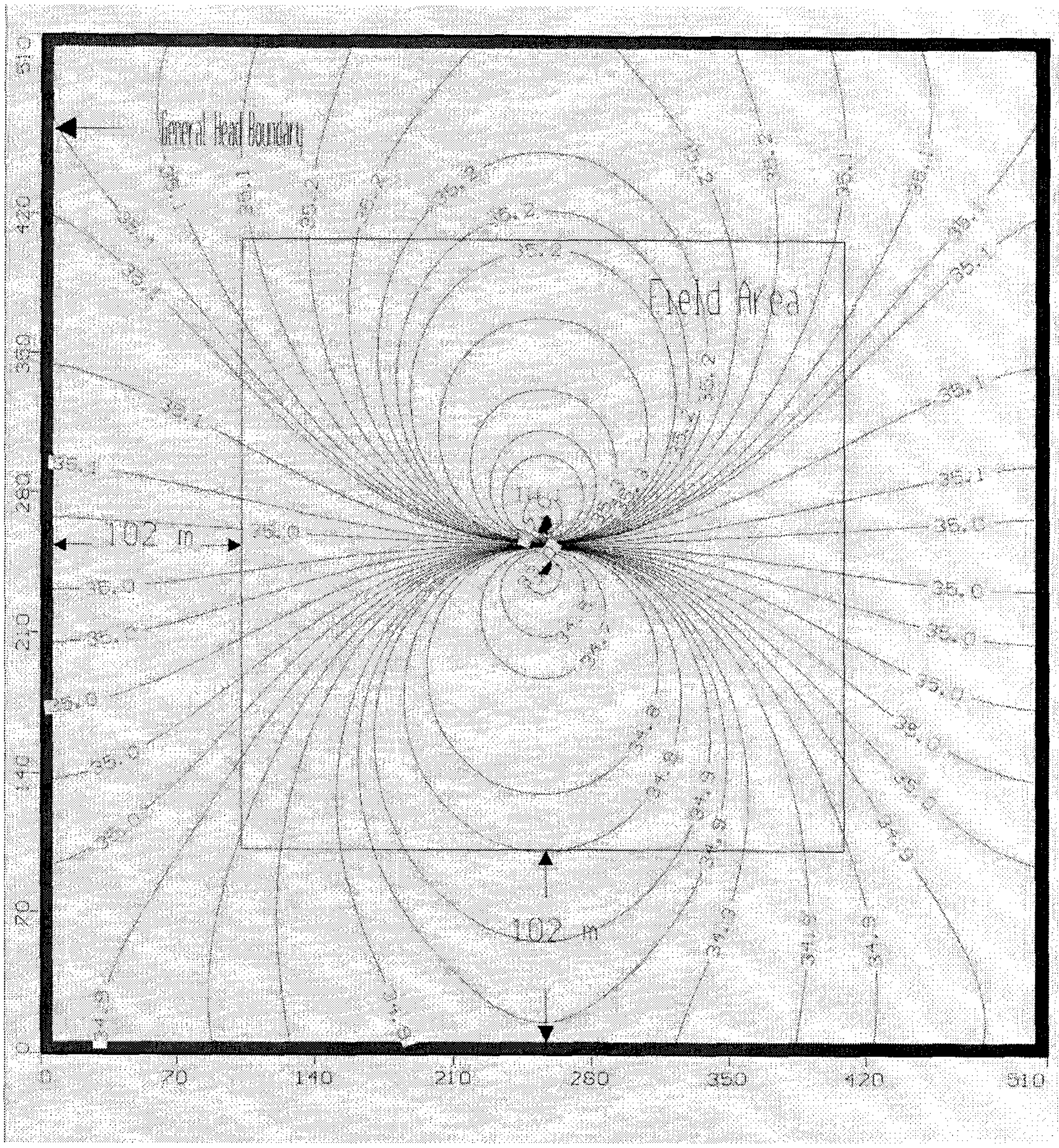

 Emad H. AlAli

Figure VI.22 Areal distribution, **orientation layout (3),** groundwater salt concentration distribution during the 20th simulation year.

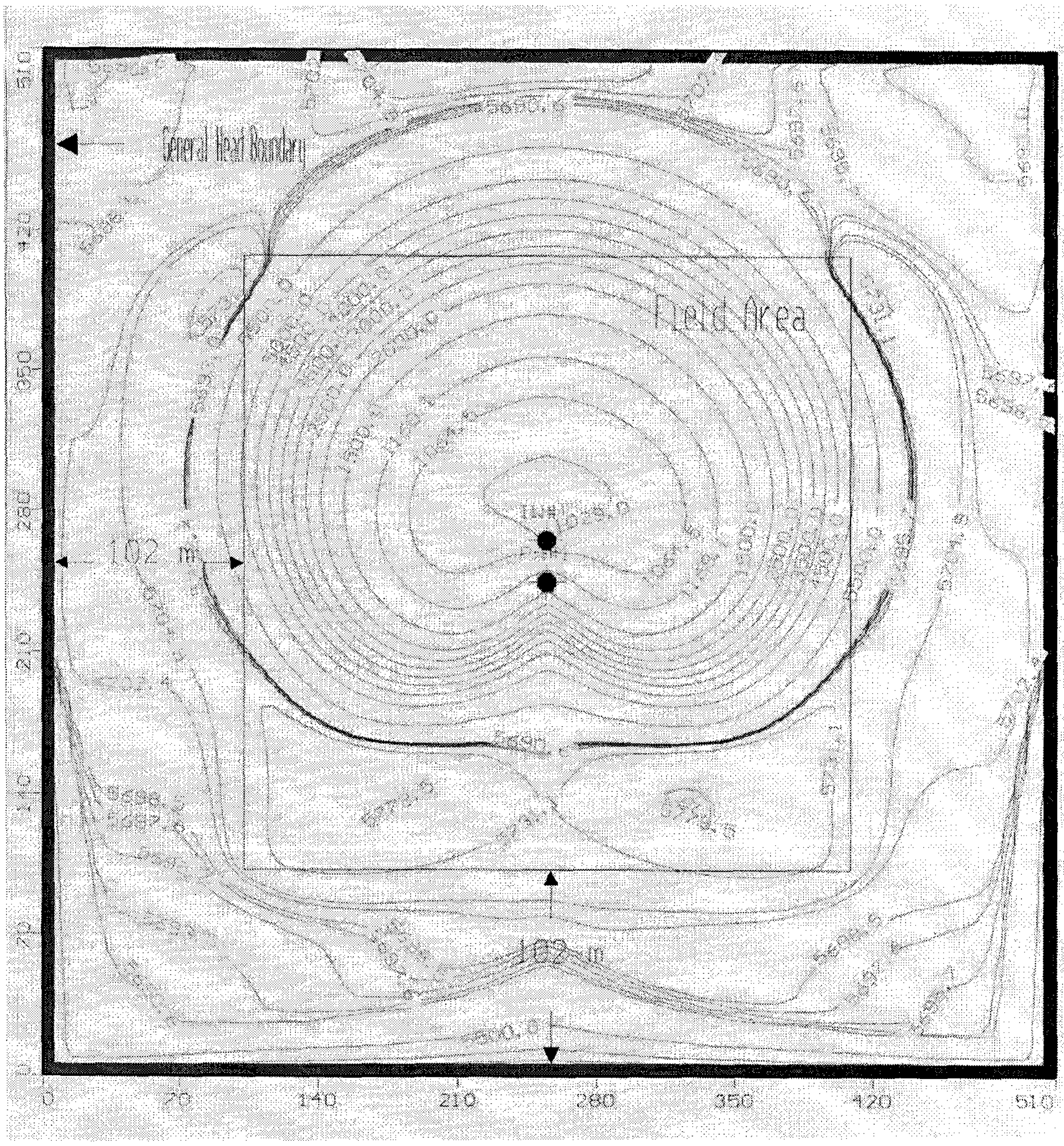

Figure VI.23 Areal distribution, **orientation layout (3),** hydraulic head elevation distribution during the 40th simulation year.

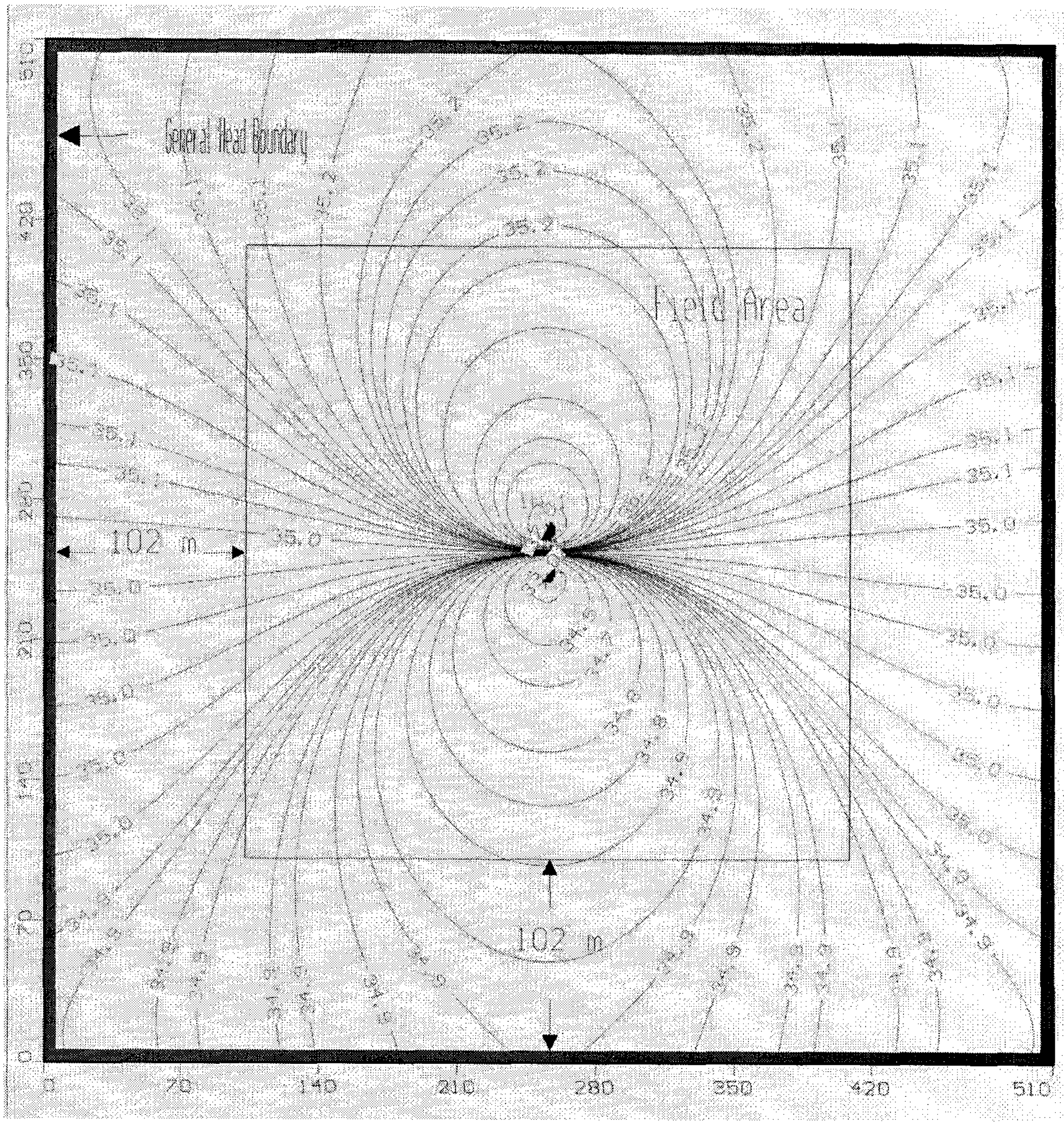

 Emad H. AlAli

Figure VI.24 Areal distribution, **orientation layout (3),** groundwater salt concentration distribution during the 40th simulation year.

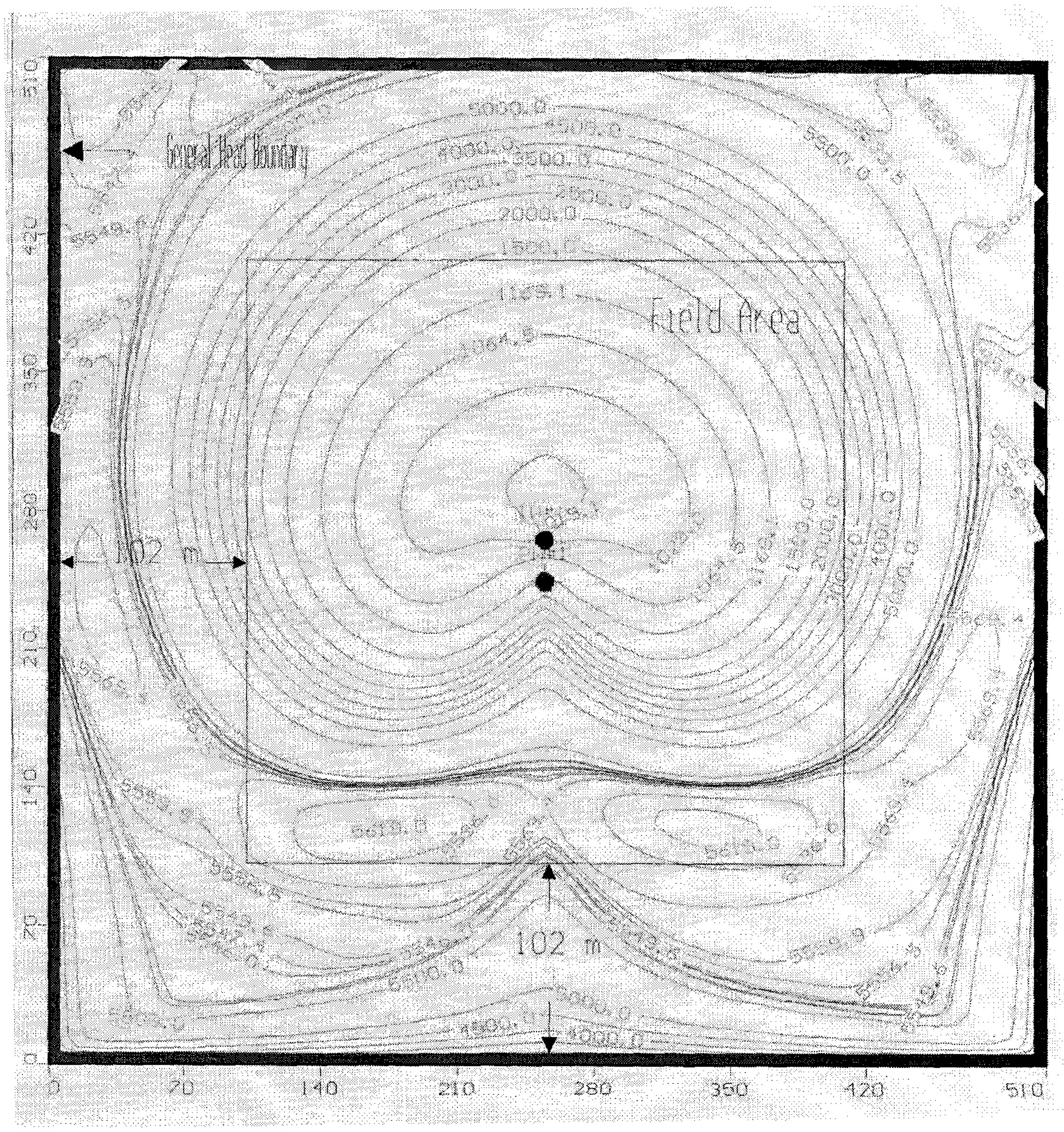

 Emad H. AlAli

Figure VI.25 Reverse osmosis brine water rejected for the base case of the general conceptual design system lump model and areal distribution model simulation approach vs. simulation periods.

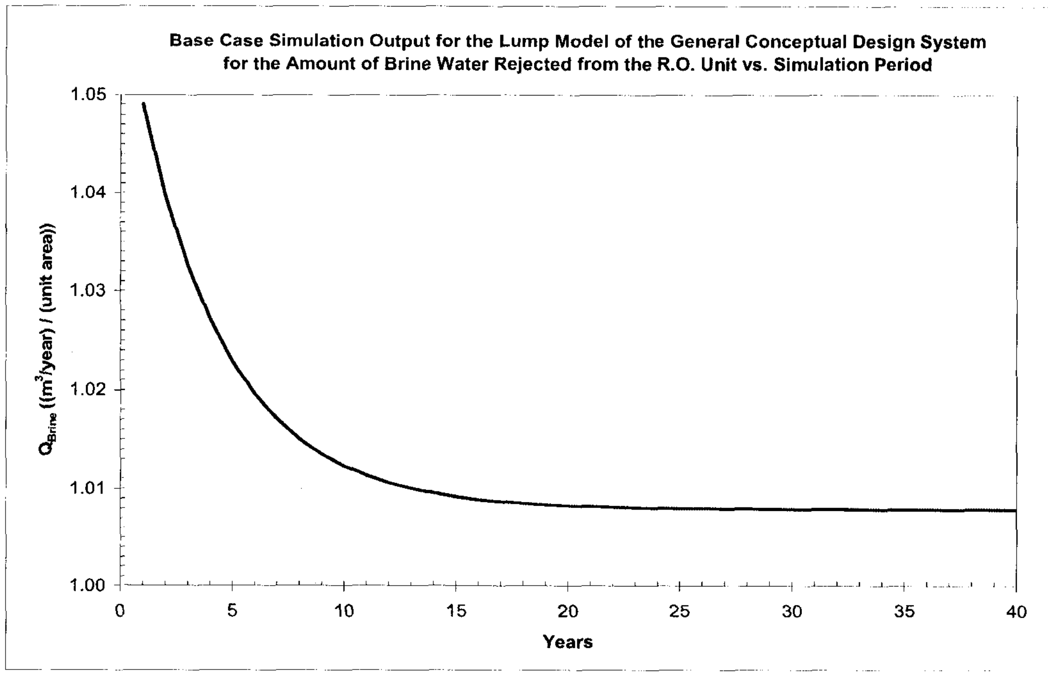

Figure VI.26 Reverse osmosis brine water rejected salt concentration for the base case of the general conceptual design system using lump model simulation approach vs. simulation periods.

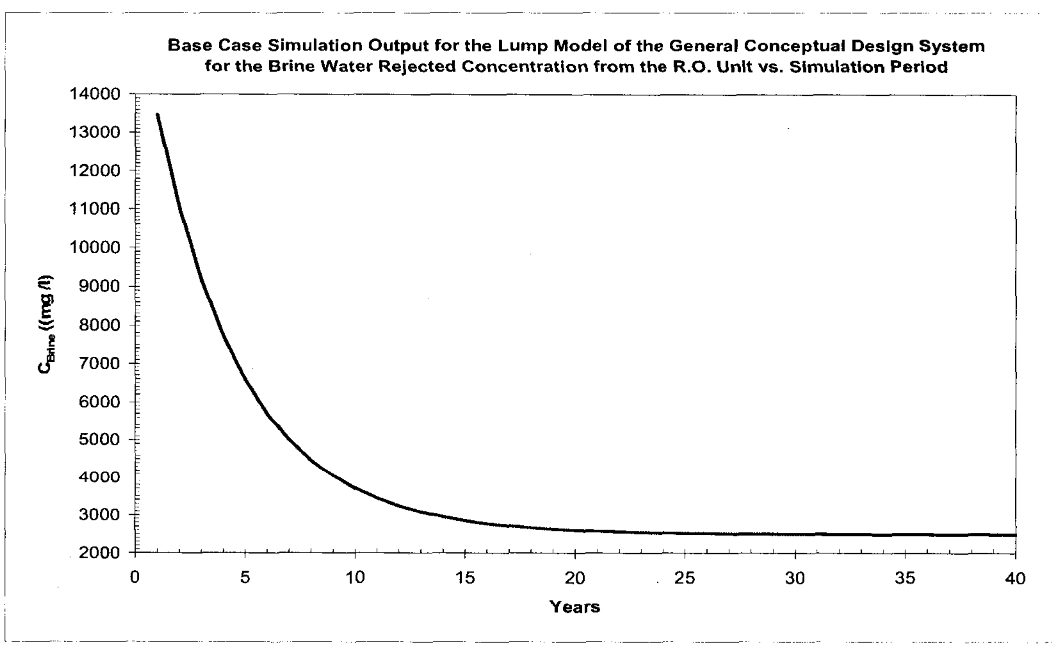

Figure VI.27 Reverse osmosis brine water rejected for the base case of the general conceptual design system using areal distribution simulation approach vs. simulation periods.

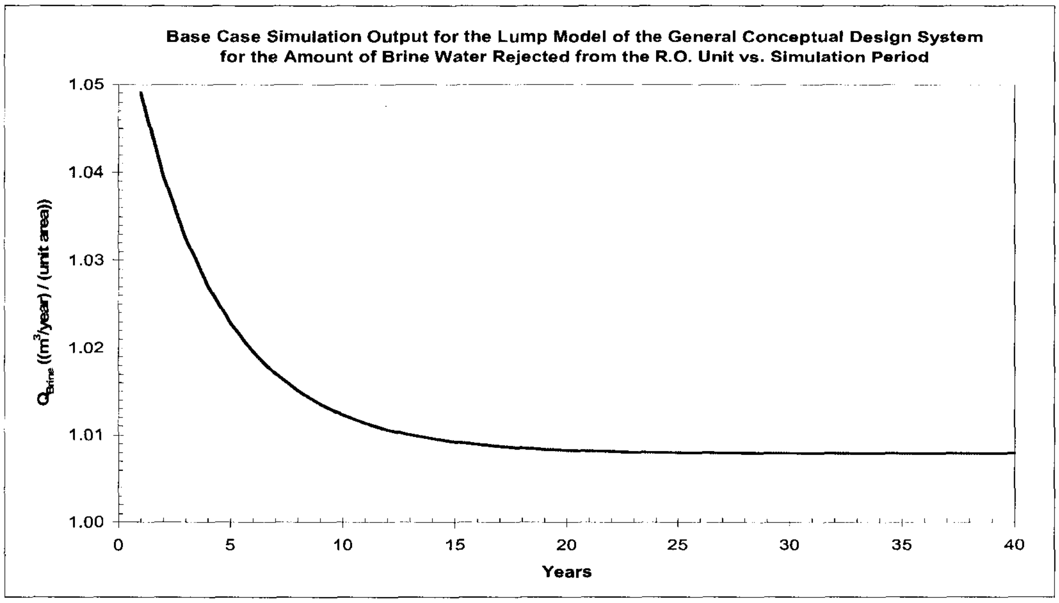

Figure VI.28 Reverse osmosis brine water rejected salt concentration for the base case of the general conceptual design system using areal distribution **(orientation layout (1))** model simulation approach vs. simulation periods.

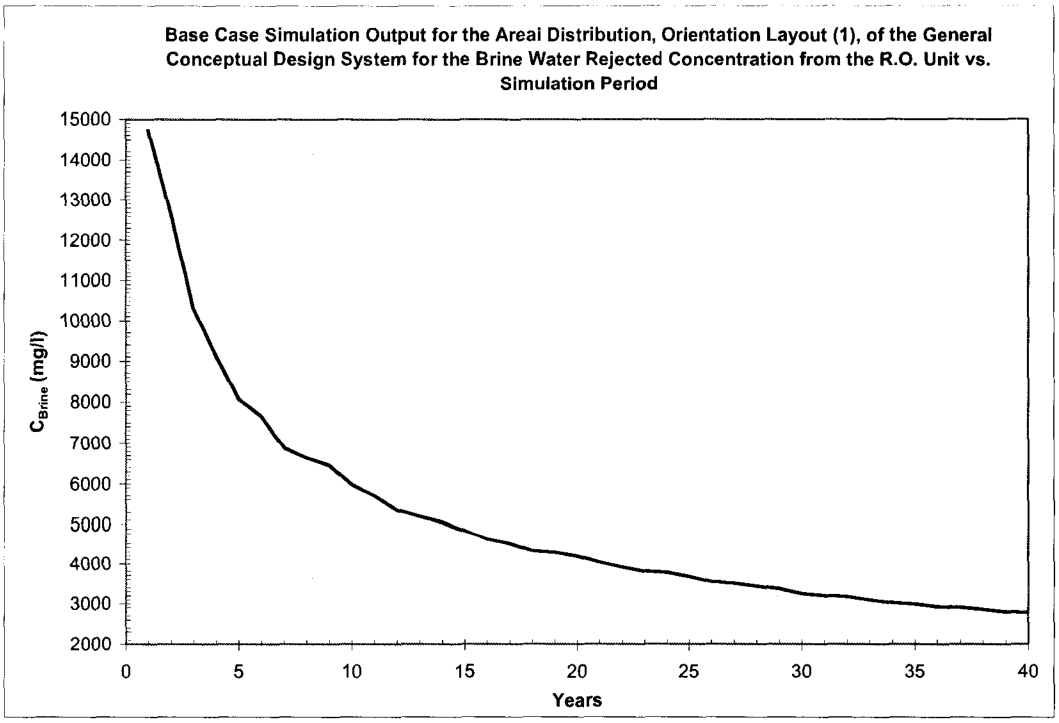

Figure VI.29 Reverse osmosis brine water rejected salt concentration for the base case of the general conceptual design system using areal distribution **(orientation layout (2))** model simulation approach vs. simulation periods.

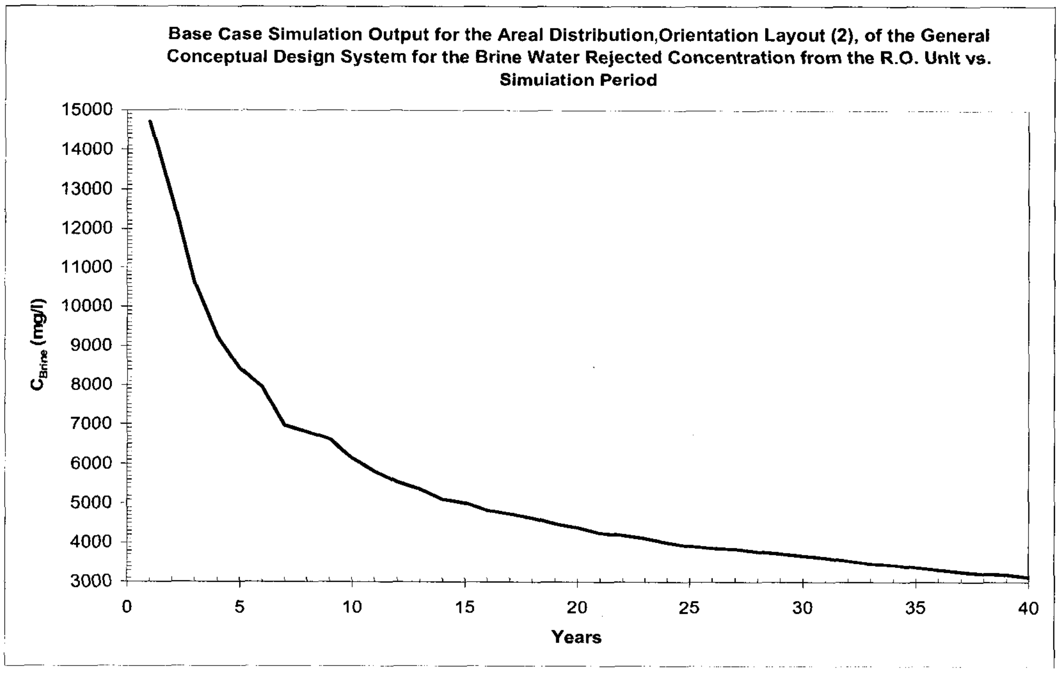

Figure VI.30 Reverse osmosis brine water rejected salt concentration for the base case of the general conceptual design system using areal distribution **(orientation layout (3))** model simulation approach vs. simulation periods.